

Assessment of in vivo kinematics of the normal  
and scapholunate instability wrist using  
dynamic CT scan

By

Jayalathge Dona Melanie Samanthi Amarasooriya

MBBS, MRCS (Eng.), MD (Orth)

Thesis

Submitted to Flinders University

for the degree of

Doctor of Philosophy by Research

College of Medicine and Public Health

30/11/2023

# TABLE OF CONTENTS

<b>Summary.....</b>	<b>7</b>
<b>Declaration by the student.....</b>	<b>9</b>
<b>Dedication .....</b>	<b>10</b>
<b>Acknowledgement.....</b>	<b>11</b>
<b>Publications.....</b>	<b>13</b>
<b>Chapter 01 .....</b>	<b>14</b>
<b>1. The literature review.....</b>	<b>14</b>
<b>1.1. Normal wrist.....</b>	<b>15</b>
1.1.1. Normal wrist anatomy.....	15
1.1.1.1. Carpal bones .....	16
1.1.1.2. The carpal ligaments.....	20
1.1.1.3. Kinematics of the normal wrist.....	30
<b>1.2. Scapholunate instability wrist.....</b>	<b>41</b>
1.2.1. Investigations for SLI.....	41
1.2.2. Classifications of SLI .....	46
1.2.3. Natural history.....	48
1.2.4. Pathoanatomy .....	48
1.2.5. Mechanism of injury .....	49
1.2.6. Kinematics of the SLI wrist.....	50
1.2.7. Kinetics of the SLI wrist.....	52
<b>1.3. Evolution of research techniques on carpal kinematics .....</b>	<b>54</b>
1.3.1. Plain radiography.....	54
1.3.2. Bi-planar radiography .....	54
1.3.3. Ligament sectioning studies .....	55



1.3.3.1.	Study designs .....	56
1.3.3.2.	Outcomes following sequential sectioning studies. ....	57
1.3.4.	Computed tomography .....	65
1.3.5.	MRI .....	69
1.3.6.	Biplanar video radiography.....	70
1.3.7.	Dynamic computed tomography (4D CT) .....	71
1.3.7.1.	History of dynamic CT.....	71
1.3.7.2.	Use of dynamic CT to assess hand and wrist pathology. ....	73
1.3.7.3.	Carpal motion quantification using dynamic CT.....	74
1.3.7.4.	Techniques of quantification of carpal bone motion using 4D CT.....	76
1.3.7.5.	Radiation.....	77
<b>1.4.</b>	<b>The gap in the literature .....</b>	<b>79</b>
<b>Chapter 02</b>	<b>.....</b>	<b>83</b>
<b>2.</b>	<b>Research methodology .....</b>	<b>83</b>
2.1.	Research questions.....	83
2.2.	Aims and Objectives .....	84
2.3.	Methodology .....	85
2.3.1.	Participant selection .....	85
2.3.2.	Power calculation .....	87
2.3.3.	Ethical considerations.....	87
2.3.4.	CT scanning.....	88
2.3.5.	Data archiving.....	90
2.3.6.	Radiation exposure .....	91
2.3.7.	Data management .....	91
2.3.8.	Segmentation and mesh generation .....	93
2.3.9.	Coordinate system.....	98
2.3.10.	Local coordinate system for carpal bones .....	99
2.3.11.	Radius stabilisation .....	102
2.3.12.	Carpal bone registration .....	105

2.3.13.	Calculations.....	106
2.3.14.	Euler's angle.....	106
2.4.	Validation.....	107
2.5.	Study 01- Radiocarpal kinematics.....	110
	Study aim .....	110
	Study objectives.....	110
	Hypothesis .....	110
	Materials and methods .....	111
	The outcome measures for this study .....	111
	Study method .....	111
2.6.	Study 02- Midcarpal kinematics .....	115
	Study aim.....	115
	Study objectives.....	115
	Hypothesis .....	115
	Materials and methods .....	115
	The outcome measures for this study were, .....	116
	Study method .....	116
2.7.	Study 03- Helical axis of motion .....	119
	Study aim.....	119
	Study objectives.....	119
	Hypothesis .....	119
	Materials and methods .....	120
	The outcome measures of this study were, .....	120
	Study method .....	120
<b>Chapter 03</b>	.....	<b>134</b>
<b>3.</b>	<b>Results.....</b>	<b>134</b>
3.1.	Validation.....	134
3.1.1.	Segment similarity (Similarity between 3D meshes of carpal bones).....	134
3.1.2.	Coordinate system placement.....	137

3.1.3.	Iterative closest point registration test and retest .....	139
3.2.	Patient demographics.....	140
3.2.1	Healthy participants.....	140
3.2.2.	SLI patients .....	141
3.2.3.	Range of motion (Normal Vs SLI wrist) .....	141
3.3.	Neutral position of the wrist (Normal Vs SLI wrist) .....	143
3.3.1.	Radioscaphoid angle .....	143
3.3.2.	Radiolunate angle .....	144
3.3.3.	Scaphoid and the lunate centroid positions .....	146
3.4.	Radiocarpal kinematics.....	148
3.4.1.	Wrist extension to flexion.....	148
3.4.2.	Wrist ulnar to radial deviation.....	168
3.4.3.	Radiocarpal kinematics (tables).....	188
3.4.4.	Important outcome measures-Radiocarpal kinematics.....	224
3.4.5.	Comparison between in-plane and out-of-plane motion .....	227
3.4.6.	Comparison of in-plane and out-of-plane motion (Tables) .....	231
3.5.	Midcarpal kinematics .....	235
3.5.1.	Wrist extension to flexion.....	235
3.5.2.	Wrist ulnar to radial deviation.....	241
3.5.3.	Midcarpal kinematics (Tables) .....	249
3.5.4.	Important outcome measures-Midcarpal kinematics .....	261
3.6.	Helical axis of motion .....	262
3.6.1.	Orientation of the helical axis.....	262
3.6.2.	Position of the helical axis .....	285
3.6.3.	Important outcome measures-Helical axis of motion .....	323
3.7.	Spectrum of kinematic changes seen in SLI .....	324
<b>Chapter 04</b>	.....	<b>333</b>
<b>4.</b>	<b>Discussion.....</b>	<b>333</b>
4.1.	Validation.....	335

4.2.	Patient demographics.....	337
4.3.	Neutral position of the wrist .....	338
4.4.	Radiocarpal kinematics.....	340
4.4.1.	Radiocarpal angular displacements during wrist motion .....	340
4.4.2.	Radiocarpal angles during wrist motion .....	350
4.4.3.	Radiocarpal centroid positions .....	358
4.5.	Midcarpal vs. Radiocarpal kinematics .....	362
4.6.	Helical axis of motion .....	366
4.7.	Spectrum of kinematic changes seen in SLI.....	374
4.8.	Statistics.....	375
4.9.	Limitations .....	378
<b>5.</b>	<b>Summary .....</b>	<b>380</b>
<b>6.</b>	<b>The original contribution to the literature.....</b>	<b>387</b>
<b>7.</b>	<b>Future directions .....</b>	<b>390</b>
<b>8.</b>	<b>References .....</b>	<b>392</b>

## SUMMARY

Scapholunate instability (SLI) remains the most common carpal instability, accounting for approximately 5% of the wrist sprains. The diagnosis of SLI is often missed. Even when diagnosed and treated, surgical outcomes remain less than ideal. In large joints such as the knee and the shoulder, the diagnosis of instability and surgical decision-making largely depends on dynamic clinical assessments. Despite a large amount of literature on carpal malalignment in SLI, the in vivo kinematics is poorly understood. Dynamic computed tomography (4D CT) enables an in vivo dynamic assessment of the wrist. The aim of this thesis was to define the objective dynamic changes of SLI compared to the healthy wrist using 4D CT, to better understand the in vivo kinematics in SLI.

Nineteen 4D CT scans of healthy wrists and 19 SLI wrists were assessed during wrist ulnar to radial deviation and extension to flexion. The radius, scaphoid, lunate, and capitate were segmented and converted to 3-dimensional (3D) models. The carpal displacements were calculated using a registration algorithm. The outcome measures were the radiocarpal angular and linear displacements, midcarpal angular displacements and the helical axis of motion (HAM) of the scaphoid and lunate.

Compared to the normal wrist, the SLI wrist had following significant findings in the arc of motion: The arc of radial angulation was greater, and the arc of flexion was less in the SLI scaphoid during wrist radial deviation beyond 10°. While the normal scaphoid had more out of plane motion during wrist radial deviation, the SLI scaphoid had more in-plane motion. The arc of flexion of the SLI lunate was less during wrist ulnar to radial deviation. During the wrist motion from 70° to 40° extension, the arc of flexion of the SLI scaphoid was greater; The arc of flexion of the SLI lunate was less.

Compared to the normal wrist, the SLI wrist had following significant findings in the radiocarpal angles: The radioscapoid angle was more flexed for the SLI wrist from wrist extension to flexion and from ulnar deviation to neutral position. The radiolunate angle was

more extended for the SLI wrist, during wrist flexion and radial deviation. The SLI scaphoid was more internally rotated in all wrist position.

Comparing the motion distribution between the radiocarpal and midcarpal joints, the scapho-capitate joint was found to be the dominant articulation in the normal wrist during radial deviation. In the SLI wrist, the dominant articulation was the radioscapoid joint. During wrist 70° to 40° extension, the radial column of the SLI wrist had more radiocarpal flexion than the normal wrist; the central column of the SLI wrist, had more midcarpal flexion than the normal wrist.

The HAM of the normal scaphoid and the lunate underwent sequential changes in the orientation and location as the wrist moved from ulnar to radial deviation. The SLI scaphoid HAM remained similar throughout. The SLI lunate had sequential changes in the orientation of the HAM but, of a lesser magnitude. The change in the orientation of the HAM from maximum ulnar to maximum radial deviation, was significantly greater in the normal wrist compared to the SLI wrist, in all three planes for the scaphoid and the lunate.

SLI result in increased 'in-plane' motion and reduced 'out-of-plane' motion of the scaphoid. There was an accompanying reduction of lunate 'out-of-plane' motion. The significant changes were evident mainly during wrist radial deviation. This is associated with multiple objectively measurable kinematic abnormalities in 3 dimensional radioscapoid and radiolunate angles, which supports a diagnosis of a 'kinematically abnormal wrist'. The kinematic changes may occur in a spectrum in SLI.

The clinical implications of the findings are partly diagnostic and enable understanding of the 3D kinematics of SLI. In addition, the sequential changes in the HAM of the scaphoid and the lunate are suggestive that a single-bundle tendon reconstructions are unlikely to recreate normal kinematics in SLI.

## DECLARATION BY THE STUDENT

"I certify that this thesis does not incorporate without acknowledgment any material previously submitted for a degree or diploma in any university and the research within will not be submitted for any other future degree or diploma without the permission of Flinders University; and to the best of my knowledge and belief, does not contain any material previously published or written by another person except where due reference is made in the text."

*JDMS Amarasooriya*

*30<sup>th</sup> November 2023*

## DEDICATION

*This thesis is dedicated to Prof. Gregory Bain for his commitment for advancing knowledge, dedication for teaching and passion for wrist kinematics.*



## **ACKNOWLEDGEMENT**

I am incredibly grateful for the opportunity to be a part of an exceptional research team that provides deep insights into wrist biomechanics at the Flinders University. I extend my heartfelt appreciation to my principal supervisor Prof. Gregory Bain, for generously sharing his extensive academic knowledge and playing a pivotal role in helping me establish myself within the academic community. I am truly thankful for his firm yet compassionate guidance, which not only facilitated significant contributions to publications during my PhD but also opened doors I never thought possible. I would also like to extend my appreciation to my associate supervisors Dr Rami Al-Dirini and Dr Kimberley Bryant, for providing exceptional guidance and unwavering support throughout this academic journey.

I am deeply grateful to Associate Prof John Troupis and Dr Marcus Crosset, from Monash Health Radiology Department for sharing their data, which was an integral part of this thesis. I am also grateful to Dr Pawel Skuza, statistical consultant at the Flinders University of South Australia, for his invaluable input on statistical methods.

I am indebted to the support I received from the Department of Orthopaedic Surgery at the Flinders Medical Centre, especially Prof. Ruurd Jaarsma for supporting my HDR and supporting me to be clinically involved as an orthopaedic surgical fellow. I extend my gratitude to Associate Prof. Chris Wilson for being the independent assessor for all the HDR milestones and for his constructive feedback.

I acknowledge the tuition fee offset provided by an “Australian Government Research Training Program Scholarship-RTPS” for the entire duration of the HDR and the Flinders University for providing financial support by offering the ‘Flinders University Research scholarship’ during the last year. Funding for this project was mainly facilitated by the principal supervisor Prof. Gregory Bain, with the support of the South Australian Hand Surgery Society. I would also like to thank The Australian Federation of University Women for providing me with a scholarship.

The lecturers and colleagues from the College of Engineering at the Flinders University have always been there to help with the difficult mathematical and engineering concepts. Prof. Mark Taylor, Prof. John Costi and my colleague Michael Russo have helped me upskill, take up engineering modules and learn computer programming. I would also like to thank Prof. Joseph Crisco, Director Bioengineering Laboratory, Department of Orthopaedics at The Warren Alpert Medical School of Brown University for generously sharing his work, time, and knowledge.

Southern Adelaide Local Health Network- Human Research Ethics Committee (SAHLN-HREC) have been instrumental in supporting all the ethics applications and enabling the project was continued up to highest ethical standards.

When I was facing challenges during this PhD journey, the HDR progression officers, the Office of Graduate Research and especially Prof. Diane Chamberlain, the former Dean of Graduate Research, have always been there, supporting, encouraging, and finding avenues to facilitate my progress.

Finally, I would like to thank my parents, my family for their unwavering support, and my son Senul, for being my inspiration, hope, and strength throughout challenging times.

## PUBLICATIONS

1. Amarasooriya M, Al Dirini R, Bryant K, Ian Bain G. Radiocarpal and midcarpal kinematics in scapholunate instability: a four-dimensional CT study in vivo. *J Hand Surg Eur Vol.* 2024 May 23;17531934241242676. doi: 10.1177/17531934241242676. Epub ahead of print. PMID: 38780127.
2. Amarasooriya M, Al-Dirini R, Bryant K, Bain GI. Scaphoid kinematics in scapholunate instability: a dynamic CT study. *Skeletal Radiol.* 2023 Aug;52(8):1557-1566. doi: 10.1007/s00256-023-04323-6. Epub 2023 Mar 23. PMID: 36951995; PMCID: PMC10276782.
3. Amarasooriya, M., MacLean, S., Bain, G.I. (2022). Clinical Biomechanics of the Wrist. In: Bhatia, D.N., Bain, G.I., Poehling, G.G., Graves, B.R. (eds) *Arthroscopy and Endoscopy of the Elbow, Wrist and Hand*. Springer, Cham.
4. Bain GI, Amarasooriya M. Scapholunate instability: why are the surgical outcomes still so far from ideal? *J Hand Surg Eur Vol.* 2023 Mar;48(3):257-268. doi: 10.1177/17531934221148009. Epub 2023 Feb 17. PMID: 36799288.
5. MacLean, S., Amarasooriya, M., & Bain, G. I. (2022). Functional Anatomy of the Wrist. *Arthroscopy and Endoscopy of the Elbow, Wrist and Hand: Surgical Anatomy and Techniques*, 553-561.

## **CHAPTER 01**

### **1. THE LITERATURE REVIEW**

The focus of this thesis is 'in vivo kinematics of scapholunate instability (SLI) compared to the healthy wrist, using dynamic CT (4D CT)'. Therefore, literature on the normal wrist, SLI wrist and also the evolution of the research techniques into SLI including 4D CT has been reviewed. The osseous and ligamental anatomy of the normal wrist has been added for better understand the normal variability of carpal kinematics and pathoanatomy of SLI.

The literature review is organised as three sections that include,

1. The normal wrist
2. The SLI wrist
3. Evolution of research techniques into scapholunate instability including dynamic (4D) CT

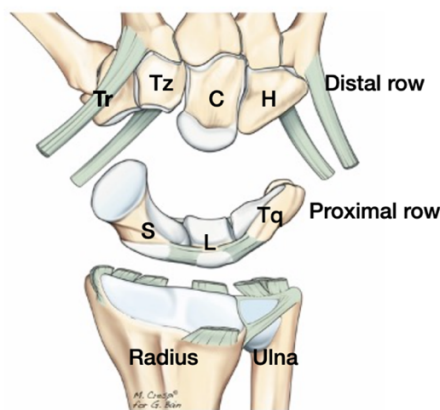
Findings of the research into SLI is discussed in the context of 'techniques used to study' in section 1.3 rather than under SLI, section 1.2 to avoid potential content overlap.

## 1.1. NORMAL WRIST

### 1.1.1. Normal wrist anatomy

The wrist facilitates the precision and power of the human hand. It is an intricate structure composed of eight carpal bones arranged in two rows. (Figure 1). The proximal row is an intercalated segment where no tendons attach. The distal carpal row bones are tightly bound to each other and function as a single unit. The scaphoid connects the distal and proximal rows.

The distal carpal row moves in response to the long wrist and finger tendons acting on the metacarpals. The only tendons attached to the distal carpal row are a slip of flexor carpi radialis (FCR) to the trapezium and a slip of flexor carpi ulnaris (FCU) to the hamate. The proximal row motion is directed by the moments transmitted from the distal row. The stability of this system depends largely on the ligamentous stabilisers. Dynamic muscular stabilisers are also important. A complex of intrinsic and extrinsic ligaments together with the dorsal capsule stabilises the carpal bones to the forearm and to one another.



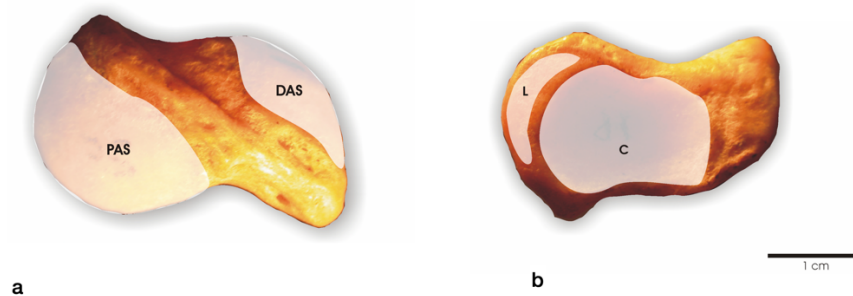
*Figure 1 Normal wrist anatomy. Dorsal view of the wrist demonstrating carpal rows. S-Scaphoid, L-Lunate, Tq-Triquetrum compose the proximal row. Tr-Trapezium, Tz-Trapezoid, C-Capitate and H-Hamate compose the distal row. Note the long wrist tendons pass distal to the carpal bones to attach onto the metacarpals. The proximal row has no tendon attachments and is a true intercalated segment. From "Scapholunate instability: why are the surgical outcomes still so far from ideal" by Bain et al., 2023, J Hand Surg Eur Vol. 2023 Mar;48(3):257-268. Copyright [2023] by SAGE Publications Ltd. Journals.*

#### 1.1.1.1. Carpal bones

The osseous anatomy of carpal bones is recognised to determine wrist kinematics (Bain et al., 2015; Fogg, 2004). Morphological variations of the scaphoid, lunate, triquetrum and capitate have been reported (Bain et al., 2015; Fogg, 2004; McLean et al., 2006; Tang et al., 2013).

##### ***The scaphoid***

The scaphoid is a 'boat-shaped' bone, strategically positioned between the proximal and the distal rows, acting as a mechanical linkage. Most of the scaphoid surface (approximately 80%) is covered with cartilage (Berger, 2001). The proximo-radial surface (Figure 2) is almost hemispherical and articulates proximally with the scaphoid facet of the radius. The medial surface of the proximal pole is flattened and crescent shaped to articulate with the lunate. Extending more distally, the medial surface of the waist creates the concavity for the head of the capitate to articulate. The distal pole in its entirety, articulates with the trapezium and trapezoid complex.



*Figure 2 Scaphoid articular surfaces a. The radial aspect of the scaphoid with proximal articular surface (PAS) and distal articular surface (DAS) for the trapezium and the trapezoid. From "Scaphoid variation and an anatomical basis for variable carpal mechanics," by Quentin Fogg, 2004, PhD Thesis, Adelaide University, p.18 Copyright [2004] by Dr Quentin Fogg. Reprinted with permission from the author.*

The vascular supply of the scaphoid is primarily derived by the radial artery, with three main sources (Gelberman et al., 1983; Taleisnik & Kelly, 1966). The distal pole is richly supplied by the nutrient arteries from the radial artery entering in close relation to scapho-trapezial ligaments. The dorso-radial vessels enter the scaphoid from the radiocarpal and intercarpal

arches of the dorsal wrist capsule at the level of the waist laterally and at the dorsal ridge. The 3<sup>rd</sup> source is via the scapholunate interosseous ligament.

Two morphological variations of the scaphoid have been identified and correlated to ligamental anatomy and kinematics (Fogg, 2004). Type one scaphoids are longer (Figure 3), has a more prominent tubercle and a single prominent dorsal crest. Type two scaphoids have a less distinct tubercle, less prominent three dorsal crests separated by shallow groves. The type 1 and 2 scaphoids have distinctly different ligament attachments to the dorsal crest. Type one scaphoid favours rotation about its longitudinal axis. Type two scaphoid flexes and extends around a transverse axis.

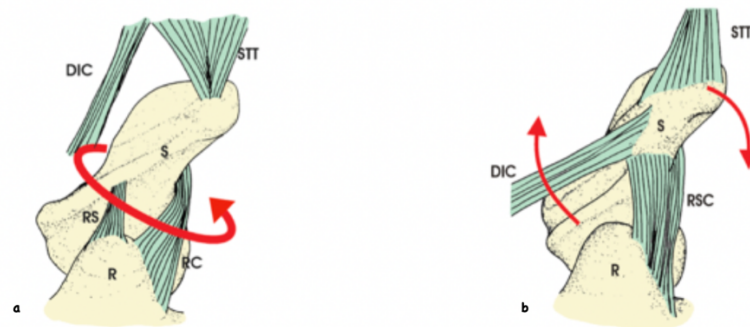
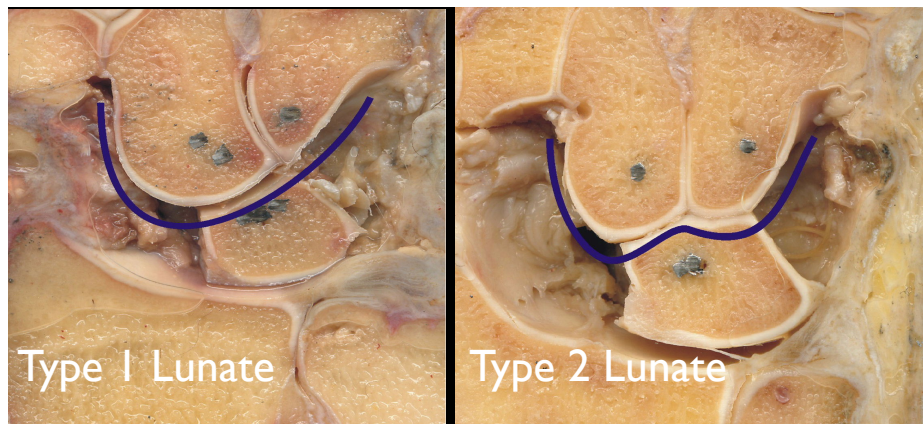


Figure 3. Two morphological types of scaphoids, a. Type 1 scaphoid having a single prominent dorsal crest and ligamental attachment favouring rotation of the scaphoid around its longitudinal axis. b. Type 2 has three less prominent dorsal crests separated by two shallow groves, resulting in flexion of the scaphoid around a transverse axis. From “Scaphoid variation and an anatomical basis for variable carpal mechanics,” by Quentin Fogg, 2004, PhD Thesis, Adelaide University, p. 243-6 Copyright [2004] by Dr Quentin Fogg. Reprinted with permission from the author.

### **The lunate**

The lunate is the intercalated bone of the intercalated segment. The lunate is a crescent shaped bone, proximally articulating with the lunate facet of the radius. A facet for the TFCC has been reported in some wrists (Lamas et al., 2007). The lunate is morphologically classified into two types. Type 1 has only one single articulation in the midcarpal joint, i.e., with capitate. The type 2 lunate has an additional articular facet for the hamate, medially (Viegas et al., 1990). Type 2 lunate articulates with a common ‘condyle’ formed by the capitate and hamate distally (Figure 4). A third ‘intermediate’ type is described, which does

not belong to either category (Sagerman et al., 1995). Morphological type of the lunate is correlated to variability of the kinematics of the normal wrist (Bain et al., 2015).



*Figure 4 Anatomical specimens demonstrating the hamate facet of the lunate. From “Scaphoid variation and an anatomical basis for variable carpal mechanics,” by Quentin Fogg, 2004, PhD Thesis, Adelaide University, p. 251 Copyright [2004] by Dr Quentin Fogg. Reprinted with permission from the author.*

### ***The triquetrum***

The triquetrum is the sensory hub of the wrist, providing the attachment sites to richly innervated dorsal wrist ligaments (Hagert et al., 2007). Adding to anatomical variability of the wrist, two morphological variations of triquetrum have been identified (McLean et al., 2006). The anatomic variations of the triquetrum are mainly seen in the triquetro-hamate articulation, which is in the dorso-radial surface.

### ***The capitate***

The capitate is part of the central column of the carpus. The centre of rotation of the wrist is in the proximal capitate (Youm, 1978; Youm et al., 1978). The capitate is tightly bound to the trapezoid on the radial side and hamate on the ulnar side. There are no ligaments restraining the capito-lunate joint. Capito-lunate joint has a ball and a socket configuration (Rohde et al., 2010), allowing a wide range of functional wrist motion. Three morphological types of capitates are described by Yazaki et al. (Yazaki et al., 2008). There is a 100% correlation of the V type with the lunate type II.



### ***The trapezium and trapezoid complex***

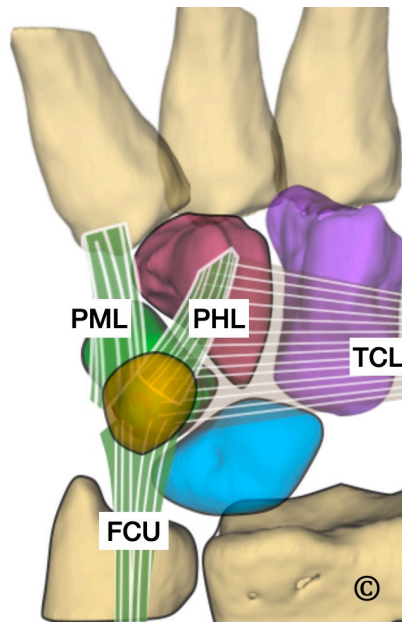
The trapezium and trapezoid are bound to each other with inter-carpal ligaments. It forms the roof of the scapho-trapezio-trapezoid (STT) joint and articulates with the distal pole of the scaphoid. Trapezoid ridge provides the attachment site to a slip of flexor carpi radialis (FCR) tendon, that dynamically stabilize the scaphoid against pronation reducing the strain on the scapholunate interosseous ligament (SLIL) (Salvà-Coll et al., 2011). Trapezium and trapezoid stabilize the scaphoid to the distal carpal row volarly via the STT ligaments and dorsally via the superficial limb of dorsal intercarpal ligament (DIC).

### ***The hamate***

The hamate articulates with the 4<sup>th</sup> and the 5<sup>th</sup> metacarpals distally, with the capitate radially, the triquetrum proximally and the lunate proximo-radially in the type II wrists. The distal articular surface of the hamate is bicondylar with a central ridge; the ulnar facet is convex, and the radial facet is concave (Drain et al., 2020). The hook of the hamate is an important landmark that separates the ulnar border of the carpal tunnel from the Guyon's canal. The height of the hook of the hamate is highly variable between individuals (Huang et al., 2019), adding to the variability of carpal morphology.

### ***The Pisiform***

The pisiform is a sesamoid bone within the flexor carpi ulnaris (FCU) tendon (Figure 5). The pisiform articulates with the triquetrum to form the piso-triquetral joint.



*Figure 5 The pisiform is a sesamoid bone with the flexor carpi ulnaris (FCR) tendon. It provides the attachment sites to the piso-metacarpal ligament (PML), the piso hamate ligament (PHL) and also to the transverse carpal ligament (TCL) From "Scapholunate instability why are the surgical outcomes still so far from ideal" by Bain et al., 2023, J Hand Surg Eur Vol. 2023 Mar;48(3):257-268. Copyright [2023] by SAGE Publications Ltd. Journals.*

#### **1.1.1.2. The carpal ligaments**

The carpal ligaments are classified as intrinsic and extrinsic based on their location and histological characteristics (Taleisnik, 1976). There is evidence that both intrinsic and extrinsic ligaments are important in scapholunate stability (Pérez et al., 2019; Short et al., 2005). Extrinsic ligaments extend between the distal radius or the metacarpals and the carpal bones, whereas the intrinsic ligaments have their origins and insertions within the carpal bones. Extrinsic ligaments are primarily capsular ligaments.

##### *Intrinsic ligaments*

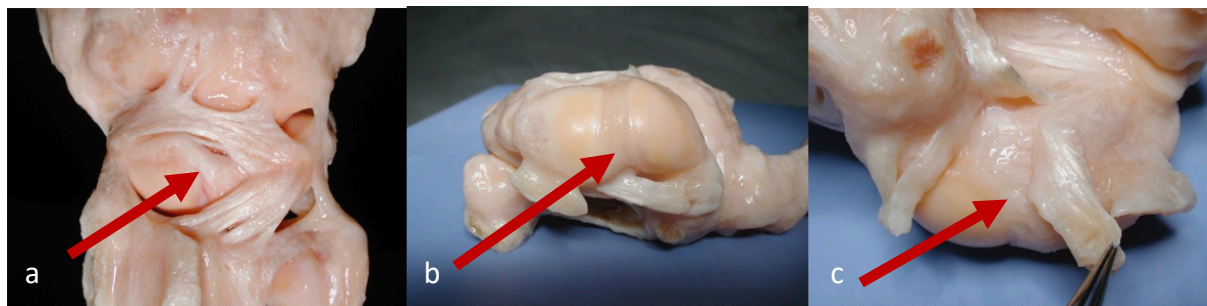
Intrinsic carpal ligaments include,

- Scapholunate interosseous ligament (SLIL)
- Lunotriquetral interosseous ligament (LTIL)
- Scapho trapezio trapezoid (STT) ligaments
- Dorsal intercarpal (DIC) ligament
- Triquetro hamate ligament (TqHL)

## Scapholunate Interosseous ligament (SLIL)

The SLIL is a C-shaped intrinsic ligament that attaches along the scapholunate joint's dorsal, proximal, and volar margins (Figure 6

*Figure 6*) (Berger, Blair, et al., 1982). The dorsal component is 3-4 mm thick with transversely arranged collagen fibres. The volar component is approximately 1 mm thick, and the proximal component consists of fenestrated fibrocartilage (Berger, Blair, et al., 1982). The SLIL is richly innervated with proprioceptive nerve endings, that are helpful in recruiting dynamic muscular stabilising mechanisms in injury (Mataliotakis et al., 2009).



*Figure 6 Components of the scapholunate interosseous ligament. a. Dorsal b. Proximal c. Palmar. Copyright [2023] by Dr Amit Gupta. Reprinted with permission.*

## The scapho-trapezio-trapezoid (STT) ligament

The STT ligaments stabilise the distal pole of the scaphoid to the distal carpal row. STT ligament anatomy was described by Drewniany et al. (Drewniany et al., 1985) as a V-shaped ligament complex extending from the distal pole of the scaphoid to the trapezium. The STT ligaments, together with the scapho-capitate (SC) ligament act as the collateral ligaments of the STT joint (Moritomo, Viegas, Nakamura, et al., 2000).

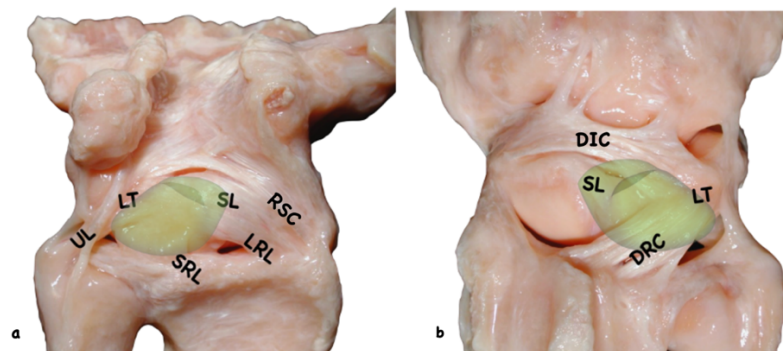
## Dorsal scapholunate septum

Dorsal capsule scapholunate septum (DCSS) is another anatomic structure that stabilises the scapho-lunate articulation (Tommasini Carrara de Sambuy et al., 2017). Anatomy and the

role of DCSS have been thoroughly studied and documented in the literature. The term “scapholunate ligament complex” is widely used to describe the dorsal capsuloligamentous structures that stabilise the scapholunate interval (Slutsky, 2013). The clinical syndrome and radiological pattern of scapholunate instability (SLI) develop following the disruption of the ‘scapholunate ligament complex’.

### *Extrinsic ligaments*

The extrinsic carpal ligaments include the dorsal radio carpal (DRC) ligament, radio-scapho-capitate (RSC) ligament, short radiolunate ligament (SRL), long radiolunate ligament (LRL), ulnocarpal ligaments (UCL) (Viegas et al., 1999). The volar extrinsic ligaments, the long and short radiolunate ligaments, stabilise the lunate, the keystone of the carpus to the radius (Figure 7). The ‘inverted V shaped’ medial and lateral limbs of the arcuate ligament stabilise the capitate to the radius and the ulna. On the dorsal aspect of the wrist DRC ligament stabilises the lunate and the triquetrum to the radius (Figure 7). The DIC ligament stabilises the bones of the proximal row to each other. The lunate has no ligaments attached to it spanning the midcarpal joint, allowing it to be freely mobile with the midcarpal joint.



*Figure 7 Ligaments stabilising the lunate. a. The volar carpal ligaments -The volar short and long radiolunate ligaments, ulno-lunate ligaments b. The dorsal carpal ligaments. The dorsal radio-carpal ligament are the extrinsic ligaments that stabilise the lunate to the forearm bones. (UL- ulno lunate ligament, LT -luno triquetral ligaments, SRL- Short radiolunate ligament, LRL- Long radiolunate ligament, RSC- radio-scapho- capitate ligament, SL-Scapholunate interosseous ligament (volar and dorsal components), DRC- dorsal radiocarpal ligament, DIC- dorsal intercarpal ligament. Copyright [2023] by Dr Amit Gupta. Reprinted with permission.*

DRC ligament spans from the radius to the proximal row; The DIC from the proximal row to the distal row; both, strengthening the dorsal capsule. While stabilising the proximal row,

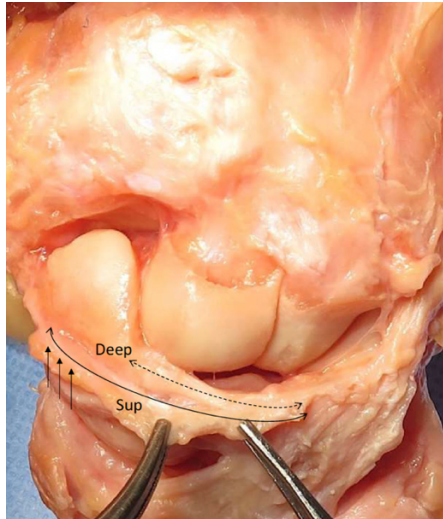
the DIC extends over the capitate stabilising the midcarpal joint (Wessel et al., 2022). Both DIC and DRC insert onto the dorsal tubercle of the triquetrum, as a combined footprint occupying a surface area of  $88.5 \pm 6.4 \text{ mm}^2$ .

#### Dorsal intercarpal (DIC) ligament

The DIC ligament extend from the dorsal tubercle of the triquetrum and passes radially as two bands, attaching to the dorsal surface of the lunate. The insertion of the DIC is to the dorsal ridge of the scaphoid proximally and the dorsal cortex of the trapezium distally (Wessel et al., 2022). The DIC deepens the proximal row acetabulum for the capitate and hamate to articulate with the proximal row (Figure 8).

The DIC was found to have deep and superficial layers. Their fiber orientation has been confirmed in high-resolution MRI scans and histologic sections. The superficial layer continued distally and radially to attach to the dorsal ridge of the scaphoid, then wrapping around the scaphoid radially and distally and to the trapezoid and trapezium. Wessel et al. reported that the deep component of the DIC, which extends from the triquetrum to the scaphoid ridge, has a distinct attachment to the lunate (Wessel et al., 2022). The footprint of the deep DIC on the lunate is distal to DRC insertion. This attachment can extend proximally to overhand the capitate creating a 'labrum' like structure containing the capitate (Figure 8). It was reported that the deep component is likely what has been previously described as the dorsal scapho triquetral ligament (DST), blending with the deep insertions of the DIC on the proximal row. This superficial distal component is almost a separate ligament named, dorsal ST ligament.

The importance of scaphoid and lunate insertions of the DIC and the DRC in maintaining carpal stability has been well recognized in the recent literature (Raja et al., 2022a). DIC is not merely a secondary stabilizer of the scapholunate articulation, but as a critical stabilizer of the wrist.



*Figure 8 The anatomy of the dorsal intercarpal (DIC) ligament. Superficial intercarpal fibres (Sup; solid arrow) is folded back proximally to expose the deep component (Deep; dotted arrow), inserting broadly on the distal dorsal borders of the triquetrum, lunate, and scaphoid and projecting distally as an extension of the proximal carpal row, providing dorso-palmar stability to the capitate and midcarpal joint. The straight arrow points to the superficial component's scaphoid ridge insertion. From "The Dorsal Ligament Complex: A Cadaveric, Histology, and Imaging Study" by Wessel et al. (2022). J Hand Surg Am, 47(5), 480.e1-480.e9. Copyright [2022] by Elsevier Science & Technology Journals. Reprinted with permission.*

#### Dorsal radiocarpal (DRC) ligament

The DRC ligament originates proximally from the dorsal rim of the distal radius from dorsal rim of the sigmoid notch to the level of Lister's tubercle. It inserts onto the dorsal cortices of the lunate and the triquetrum coursing distally and ulnarly. It is trapezoidal in shape, tapering as it passes obliquely toward the triquetrum. DRC was found to be uniformly inserted into the bare area of the lunate (Wessel et al., 2022).

DRC has been reported to have 4 subtypes (Viegas et al., 1999). The commonest variant is a single ligament with a broad attachment to the ulnar side of the Lister's tubercle of the distal radius, extending to the triquetrum with a robust attachment to the lunate midway. The other three types had an accessory band with varying configurations (Figure 9).

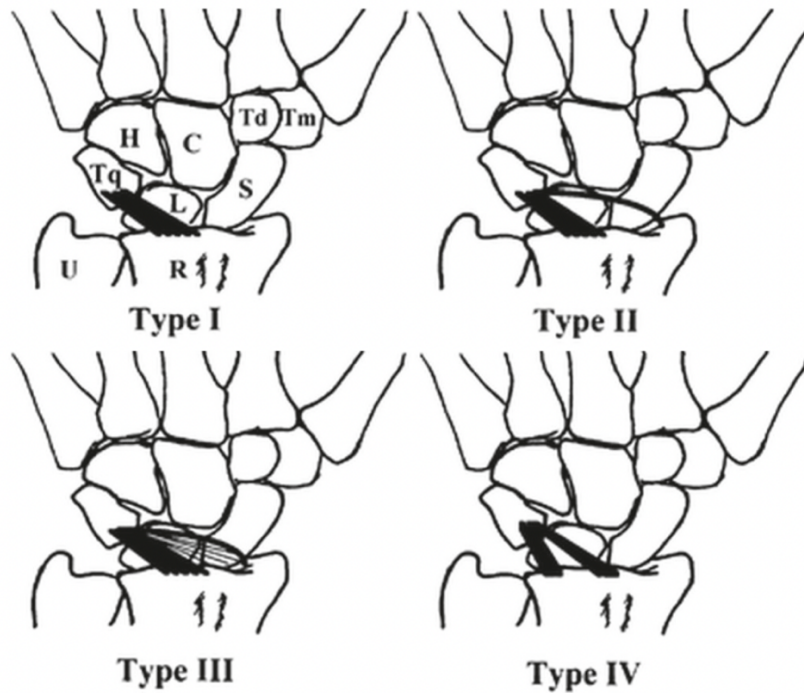


Figure 9 The four anatomical variants of the dorsal radio triquetral ligament (DRC). The commonest variant is a single ligament with a broad attachment to the ulnar side of the Lister's tubercle of the distal radius, extending to the triquetrum with a robust attachment to the lunate midway. The other three types had an accessory band with varying configurations. From "The dorsal ligaments of the wrist: anatomy, mechanical properties, and function." by Viegas, et al. (1999). *J Hand Surg Am*, 24(3), 456-468. Copyright [1999] by Elsevier Science & Technology Journals. Reprinted with permission.

However, not all authors agree on the anatomy of the DRC. Viegas et al. and Nagao et al. confirmed a lunate insertion in 89 of 90 and 4 of 8 of specimens, respectively (Viegas et al., 1999) (Nagao et al., 2005). Neither Horii et al. nor Ruby et al. describe an insertion of the DRC on the lunate (Horii et al., 1991) (Ruby, 1992). Wessel et al. reported that the DRC has robust and consistent lunate insertions on a dorsal "bare" area that is devoid of articular cartilage (Wessel et al., 2022). The lunate insertion of DIC and DRC is recognized to be important in maintaining the sagittal balance of the lunate (Raja et al., 2022b).

#### Radio scapho-capitate (RSC) ligament

The RSC ligament originates from a roughened area on the volar radial surface of the radial styloid (Berger, 1997). The RSC ligament spans distally and ulnarly from its origin and partially inserts on to the radial aspect of the waist and the distal pole of the scaphoid.

Majority of the fibres pass anterior to the scaphoid waist and interdigitate with the fibres from the medial limb of the arcuate ligament forming the volar capsule of the midcarpal joint. According to Berger et al. 10% of the fibres inserts to the capitate neck (Berger, 1997; Sennwald, 1987). However, some controversy exists on this fact; some authors have reported that most of the fibres attached the capitate neck (Buijze, Dvinskikh, et al., 2011; Buijze, Lozano-Calderon, et al., 2011).

#### Short radiolunate ligament (SRL)

The short radiolunate ligament (SRL) originates from the ulno-palmar edge of the distal radius and inserts at the junction between the proximal articular surface and the non-articular portion of the volar horn of the lunate, proximal to the ulno-lunate insertion (Apergis, 2013; Berger, 1997). Interestingly, the shape of this ligament changes from being fan shaped in flexion to longitudinal sheet during wrist extension.

#### Long radiolunate ligament (LRL)

The LRL is a robust capsular ligament, originating at the volar rim of the scaphoid facet of the distal radius just ulnar to the RSC ligament. It courses distally and ulnarly overlapping the volar SLIL and inserts onto the palmer horn of the lunate. Some researchers report that the LRL continues to insert onto the triquetrum, Berger et al confirms that fibres of the LRL do not insert onto the triquetrum, thus the terms volar radio-luno-triquetral and volar radio-triquetral ligaments are misleading (Berger, 1997).

#### Ulna-lunate (UL) ligament

Ulna-lunate (UL) ligament originates from the radial most region of the volar radioulnar ligament and inserts at the volar edge of the lunate. It is also known to change its shape during flexion-extension of the wrist (Moritomo, Murase, Arimitsu, et al., 2008). The relevance of the ulnocarpal ligaments to this thesis and scapholunate instability in general is



that ulnocarpal ligaments may be important in cases of SLI with ulnar translocation of the carpus (Viegas et al., 1995).

#### Ulna-triquetral (UT) ligament

The UT ligament originates from the volar radioulnar ligament and inserts distally onto the proximal and palmar surface of the triquetrum (Moritomo, 2013). There are two weak areas associated with this ligament, distally a perforation leading to piso-triquetral ligament and another perforation leading to pre-styloid recess proximally. The medial border of the UT ligament demarcates the ulnar and dorsal boundary of the ulnar carpal joint and forms the deep surface of the extensor carpi ulnaris (ECU) tendon sheath.

#### Ulna-capitate (UC) ligament

The UC ligament is the only ligament that has a clear attachment to the fovea of the ulna. From its origin, it spans superficial to UT and UL ligaments. It interdigitates with volar lunotriquetral (LT) ligament at the distal margin of the palmar horn of the lunate, interdigitating with fibres from the RSC ligament, forming an “arcuate” (deltoid) ligament (Berger, 1997; Moritomo, 2013). As with the RSC ligament, only approximately 10 % of the fibres of the UC ligament attach to the body of the capitate (Moritomo, 2013).

### *Material properties of ligaments*

The scapholunate interosseous ligament (SLIL) has historically been considered the primary stabiliser of the scapholunate articulation. The other critical stabilisers are the DIC, the DRC, LRL, SRL and STT ligaments. DCSS has also been recognised to be a stabilising factor in SL articulation. The material properties of the carpal ligaments implicated in SLI are important, to understand how they would fail and what we need to aim for, in the reconstructions. A summary of material properties of carpal ligaments implicated in SLI is shown in Table 1.

Table 1 Failure strength of carpal ligaments

Ligament	Tensile strength (N)	Loading rate	Number	Reference
<b>Dorsal SLIL</b>	260 (118)	5mm/s	8	(Berger et al., 1999)
	83	5mm/min	8	(F. Nikolopoulos et al., 2011)
	62	100mm/min	1	(Logan et al., 1986)
	141 (20)	6.4 mm/min	14	(Hofstede et al., 1999)
	93 (33)	10 mm/min	6	(Cuénod et al., 2002)
	270 (91)	10 mm/min	8	(Pang et al., 2018)
<b>Volar SLIL</b>	118 (21)	5mm/s	8	(Berger et al., 1999)
	86	5mm/min	8	(F. V. Nikolopoulos et al., 2011)
	125	100mm/min	1	(Logan et al., 1986)
<b>Proximal SLIL</b>	63 (32)	5mm/s	8	(Berger et al., 1999)
<b>Entire SLIL</b>	357 (110)	100mm/min	8	(Johnston et al., 2004)
	260 (73)	0.1mm/s	6	(Svoboda et al., 1995)
	170 (97)	10 mmm/min	7	(Harvey et al., 1999)
<b>LRL</b>	110(30)N	100mm/min	10	(Nowak, 1991)
<b>STT</b>	150N (30)	100mm/min	10	(Nowak, 1991)
<b>DRC</b>	143(41)	50mm/min	10	(Viegas et al., 1999)
<b>DIC</b>	82(49)	50mm/min	12	(Viegas et al., 1999)

*Note: Tensile strength of a ligament is defined as the ultimate load at failure divided by initial cross-sectional area. As the cross-sectional area is not measured in the above studies, the results presented are the load at failure. Mean values are provided with the standard deviation in parenthesis when it was provided in the referenced publication.*

Material properties of the scapholunate interosseous ligament (SLIL)

Out of the three components of the SLIL, the dSLL is reported to be the most functionally significant component for stability and has the highest tensile strength according to Berger et al (Berger et al., 1999). In the physiological wrist motion, the palmar component acts as a rotational constraint (Berger et al., 1999; Sokolow & Saffar, 2001). The tensile strength of the palmar component is reported to be 118 N. The proximal component has a tensile strength of 63 N.

The tensile strength of the dSLL however, varies between the studies from 140 N (Hofstede et al., 1999) to 260 N (Berger et al., 1999; Shin et al., 1998). Some researchers (F. V. Nikolopoulos et al., 2011; Viegas et al., 1999) propose that both dorsal and palmar SLIL have similar tensile strengths. Johnston et al reported that the load to failure for the entire SLIL was 357N (Johnston et al., 2004). However, study designs for each of these studies differ as follows.

Nikolopoulos et al (F. V. Nikolopoulos et al., 2011) loaded the pneumatic grip held scaphoid and the lunate in tension in a uniaxial plane and found the tensile strength of the dorsal SLIL to be 83 N; volar SLIL 86 N, with each group having 8 specimens. Berger et al. (Berger et al., 1999) studied the tensile strength during translational and rotational loading of the scaphoid and lunate fixed with K wires. He also included the palmar and dorsal portions of the same cadaveric wrist specimen for comparison, resulting in matched pairs of ligaments.

Loading rates were also different between the two studies with Berger et al. loading the SL articulation at 5mm/s and Nikolopoulos et al. loading at the rate of 5mm/min. Faster loading conditions may simulate clinical scenarios like falls, and explain the higher tensile strength reported by Berger et al. Johnston et al. applied a loading rate of 100mm/min, almost simulating that would be applied during a fall. He reported the tensile strength to be 357N (Johnston et al., 2004).

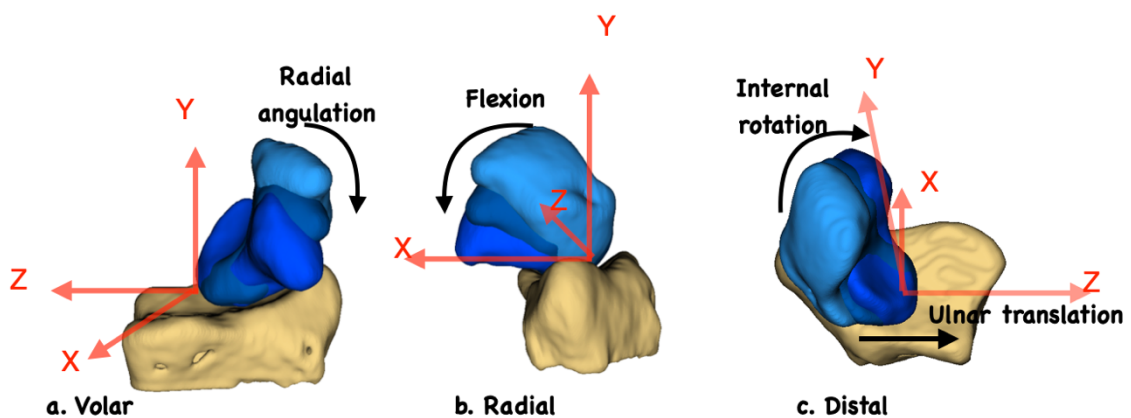
During unrestrained wrist motion, the average tensile forces in the SLIL is around 20N (Dimitris et al., 2015). The tensile forces are calculated to be higher during wrist extension than during flexion. The absolute maximum tensile force recorded in any wrist during unrestrained motion was 26 N. Being able to resist forces in the order of 50N are recommended to protect the scapholunate reduction, repair or reconstruction in normal daily activities (Werner, 2021). With strenuous activities, ability to withstand a tensile load of 110N is recommended to maintain SL stability. While during a fall, SL articulation needs to be able to sustain a 350N tensile load.

### 1.1.1.3. Kinematics of the normal wrist

#### *Normal wrist motion*

Anatomically, the wrist moves in two orthogonal planes, coronal and sagittal. In addition, there is carpal prono- supination relative to the radius. The planar wrist motions are named radioulnar deviation and flexion-extension. In real life, most of the human hand functions involve moving the wrist from radial extension to ulnar flexion, as in throwing a dart, casting a fishing rod or using a hammer. This motion is called the “Dart Throwers’ Motion” (DTM). The plane that the wrist moves during DTM is called “Dart Throwers’ plane” (DTP) (Crisco et al., 2005; Palmer et al., 1985).

Carpal bones have six degrees of freedom to result in the said wrist motions. Each carpal bone can rotate around X, Y and Z axes and translate along these axes (Figure 10). The carpal ligaments act sequentially, and neuromuscular feedback mechanisms help coordinate the synchronous carpal motion. This coordinated carpal bone motion, enables the hand to do functional tasks.



*Figure 10 Scaphoid has six degrees of freedom to move with the wrist motion. The scaphoid rotates around x, y and z axes and translates along the same. Image from segmented normal scaphoid bone during ulnar to radial deviation of the wrist using 4D CT scan shows the rotations of the scaphoid. Darker colour shows maximum radial deviation, the lighter colour maximum ulnar deviation. As the wrist radially deviates, the scaphoid radially angulate (a. volar view), flexes (b. radial view) and internally rotates and translates ulnarly (distal view). Image copyrights Melanie Amarasooriya and Gregory Bain.*

The normal wrist has an active radial deviation of  $28.8^{\circ} (\pm 10.8^{\circ})$  and ulnar deviation of  $39.4^{\circ} (\pm 11.8^{\circ})$  (Lendner et al., 2019). The normal flexion is  $74^{\circ} (\pm 13^{\circ})$  and the extension is  $66.7^{\circ} (\pm 14.1^{\circ})$ . While the wrist is anatomically considered to consist of two carpal rows or three columns, it functions as two main articulations, the radiocarpal and the midcarpal joint.

### *Functional articulations within the wrist*

The wrist broadly functions as two articulations, the radiocarpal and midcarpal joints. The STT joint, the capito-lunate (CL) and the triquetro-hamate (TqH) joints have unique functions during the wrist motion, although they function as a midcarpal joint collectively.

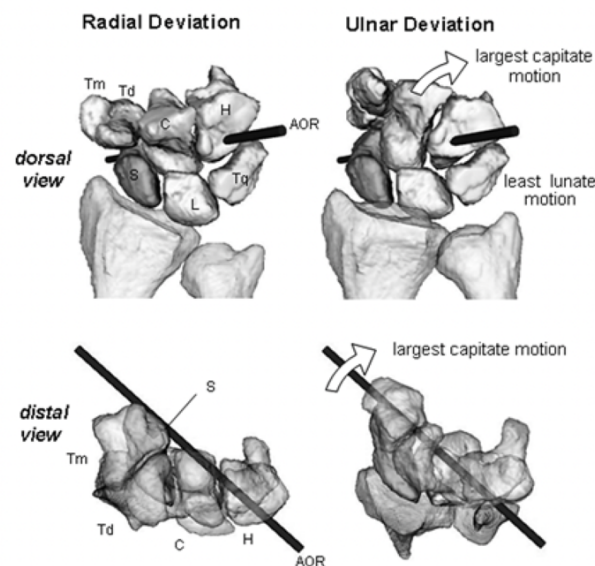
### *Radiocarpal joint*

The radiocarpal joint is the articulation between the radius and the proximal carpal row. Contribution of radiocarpal joint to the wrist motion varies in flexion-extension and radioulnar deviation. Seventy five percent (75%) of radial column flexion and extension occur through the radioscapoid joint, 50% of the central column flexion and extension through the capito-lunate joint (Kaufmann et al., 2006). During radial deviation, midcarpal motion accounts for 60% of the total carpal motion (Kaufmann et al., 2005). During ulnar deviation 86% of the motion occurred through the midcarpal joint.

Although it is considered that the dart throwers' motion (DTM) occurs through the midcarpal joint, radiocarpal joint does contribute to the DTM to a variable degree (Crisco et al., 2005; Goto et al., 2005; Moritomo et al., 2006; Werner et al., 2004). It is reported that the plane of wrist motion where the scaphoid motion is 'negligible' and plane of wrist motion where lunate motion is 'negligible' differs from one another by approximately  $10^{\circ}$  (Crisco et al., 2005). There is no consensus of the exact dart throwers' plane. It is likely that multiple planes exist to suit functional tasks, with varying degrees of scaphoid rotation (Garg et al., 2014; Werner et al., 2004). Hence, the proximal row changes its alignment, facilitating the distal row motion in the 'desired' 'dart thrower's plane'.

## Midcarpal joint

Midcarpal joint consists of the STT joint and luno-triquetrum-capitate-hamate (LT-CH) joint. The distal articular surface of lunate and triquetrum is a concave ellipsoid, whereas the distal scaphoid is convex and extend above the lunotriquetral plane (Moritomo et al., 2006). The anatomical axes of both midcarpal joint articulations (STT and LT-CH joint) aligns with the dart thrower plane (Figure 11) (Moritomo et al., 2004). Thus, the bony architecture provides the mechanically advantageous movement to radial extension to ulnar flexion, in the midcarpal joint. Scapho-capitate articulation links both joints (STT and CH-LT).



A. RUD

Figure 11 Dorsal and distal views of the scaphoid-based motions of the right wrist and the axes of rotation (AOR) of the capitate relative to the scaphoid during radioulnar deviation (RUD). S = scaphoid, L = lunate, Tq = triquetrum, Tm = trapezium, Td = trapezoid, C = capitate, and H = hamate. From "In vivo three-dimensional kinematics of the midcarpal joint of the wrist." by Moritomo et al. (2006). *J Bone Joint Surg Am*, 88(3), 611-621. Copyright [2006] by Wolters Kluwer Health, Inc. Reprinted with permission.

When the scaphoid is static, scapho capitate articulation would only allow the capitate to extend radially and flex ulnarly producing DTM (Moritomo et al., 2006). Regardless of the wrist motion, the scaphoid motion relative to capitate occurs through the scaphoid axial plane (Moritomo et al., 2004). Nonetheless, with changing wrist motion from radioulnar deviation, dart throwers to flexion extension, the magnitude of the scaphoid rotation

changes (Figure 12). The highest midcarpal scaphoid rotation occurs when the wrist is in radioulnar deviation and the lowest during opposite dart throwing motion inclined flexion and extension (Moritomo et al., 2006). Thus, the magnitude of the scaphoid rotation determines the plane of global wrist motion, with the scaphoid acting like a “gear lever” making changes to the plane of the capitate and the distal row.

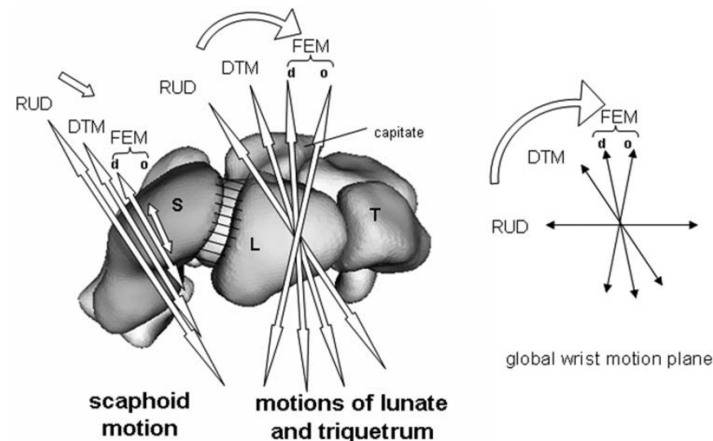


Figure 12 Proximal view of the right carpus, showing the direction and range of motions of the scaphoid (S), lunate (L), and triquetrum (T) relative to the capitate in radioulnar deviation (RUD), the dart-throwing motion (DTM), the dart-throwing-motion-inclined flexion-extension motion (FEM) (d), and the opposite dart-throwing-motion-inclined flexion-extension motion (o). The amount of motion is related to the length of the arrows. From “In vivo three-dimensional kinematics of the midcarpal joint of the wrist.” by Moritomo et al. (2006). *J Bone Joint Surg Am*, 88(3), 611-621. Copyright [2006] by Wolters Kluwer Health, Inc. Reprinted with permission.

### **Scapho Trapezio Trapezoid Joint (STT joint)**

The STT joint consists of the distal articular surface of the scaphoid and the proximal articular surfaces of the trapezium and the trapezoid. Regardless of the wrist motion, the STT joint moves in a single, oblique plane parallel to the trapezoid and trapezium articulation relative to the capitate (Moritomo et al., 2004; Moritomo, Viegas, Nakamura, et al., 2000). The dorsal ridge on the distal scaphoid is an anatomical landmark along which the STT joint moves and determine the plane of motion (Moritomo, Viegas, Nakamura, et al., 2000). The volar STT ligament and scapho capitate (SC) ligament are the two collateral ligaments of the STT joint. Thereby, they stabilise STT motion from radial extension to ulnar flexion.

Whilst the STT joint determines the plane of DTM in radial extension, the remaining articulations of the midcarpal joint synchronizes with it for the smooth transition into ulnar flexion, so that, DTM can be explained by the kinematics of the STT joint. During radioulnar deviation and flexion extension, a similar mechanism operates in the STT joint (Figure 13). While the direction of scaphoid motion relative to capitate remains the same throughout any motion sequence, the magnitude changes with the direction of global wrist motion (Figure 13).

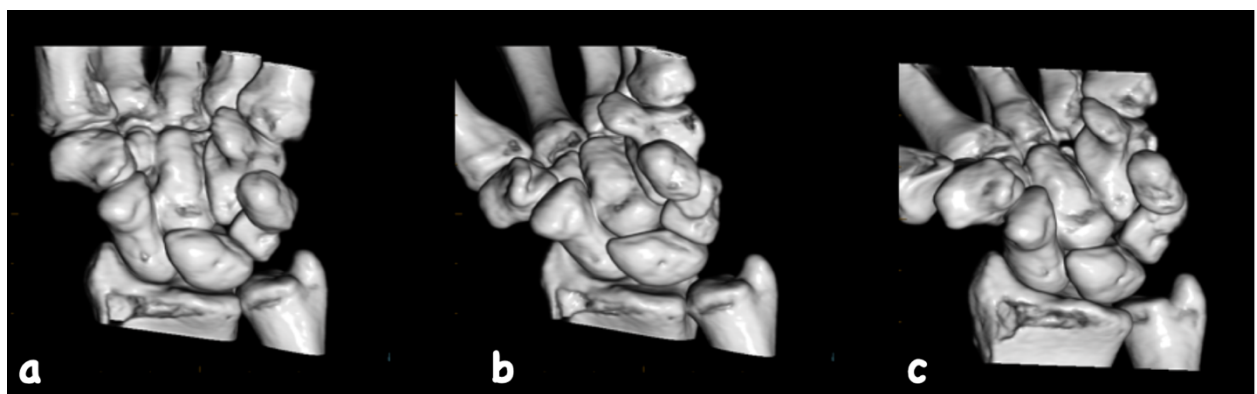


Figure 13. 3D CT scan images of the volar aspect of the wrist. (a) neutral position, (b) maximum radial extension in (DTM) and (c) maximum radial deviation. Note the scapho-capitate (SC) articulation and the difference in scaphoid flexion. The scaphoid in the neutral wrist position (a) and in DTM (b) appear similar with radial extension of the trapezium and trapezoid complex in (b). The scaphoid in the maximum radial deviation (c) appear comparatively flexed with radial angulation of the trapezium and trapezoid complex. Image copyrights Melanie Amarasooriya and Gregory Bain.

### *Contribution of the forearm and distal radioulnar joint*

The functional dart throwers motion (DTM) such as hammering occurs in pronation at the distal radioulnar joint (DRUJ). The contribution of the DRUJ to DTM has not been quantified. In a hammering task, the range of forearm prono-supination has been quantified to be  $12^{\circ} \pm 8^{\circ}$  (Leventhal et al., 2010).

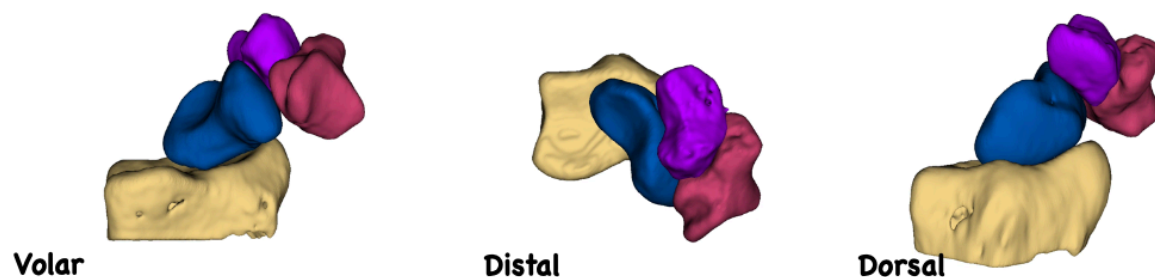


The following section is a review of kinematics of the radiocarpal and midcarpal joints of the normal wrist during wrist motion.

### *Radioulnar Deviation*

Radioulnar deviation of the wrist is represented by the radial or ulnar angulation of the 3<sup>rd</sup> metacarpal relative to the radius. Extensor carpi radialis longus (ECRL), FCR, abductor pollicis longus (APL) and extensor pollicis longus (EPL) are the wrist radial deviators. FCU, and ECU are the ulnar deviators of the wrist. None of these muscles have tendons attaching to the proximal carpal row.

The radial pull of the tendons triggers a sequential motion pattern in the carpus. The distal carpal row, together with the trapezium and trapezoid, angulate radially. Allowing for the distal row to radially angulate, the scaphoid then rotates out-of-plane, flexing and shortening the radial column height. During the normal wrist radial deviation, the predominant motion of the scaphoid is flexion (de Lange et al., 1985; Kobayashi, Berger, et al., 1997)(Table 2). With the intact scapholunate ligament complex, the lunate flexes with the scaphoid. On a lateral plane the scaphoid flexion and trapezium moving over the dorsal surface of the scaphoid, shortening the radial column can be seen (Figure 14).



*Figure 14 The position of the scapho-trapezio-trapezoid joint in extreme radial deviation. Note that the scaphoid has flexed allowing the trapezio-trapezoid complex to be positioned dorsal to the scaphoid, while radially angulating. Image copyrights Melanie Amarasooriya and Gregory Bain.*

*Table 2 In-Plane and Out-of-Plane Motion of the Scaphoid During Ulnar-Radial Deviation of the Wrist. From “In vivo analysis of carpal kinematics and comparative review of the literature.” by Moojen et al. (2003) J Hand Surg Am, 28(1), 81-87. Copyright [2004] by Elsevier Science & Technology Journals. Reprinted with permission.*

Wrist Posture	20° UD	RD 20°	20° UD	RD 20°
(Savelberg et al., 1993)	7°UD	3°RD	14°EX	14°FL
(Horii et al., 1991)	9°UD	7°RD	12°EX	8°FL
(Kobayashi, Berger, et al., 1997)	11°UD	7°RD	16°EX	9°FL
(Ritt et al., 1998)	9°UD	5°RD	11°EX	11°FL
(Moojen et al., 2003)	10°UD	5°RD	20°EX	15°FL

Moojen et al. assessed in vivo wrist kinematics using 3D CT and found that the out of plane motion of the scaphoid during wrist radial deviation is greater compared to the in vitro studies (Moojen et al., 2003). He used series of 3D CT scans performed at static wrist positions to arrive at his conclusions.

Assessing radiocarpal and midcarpal motions together, it is reported that during the wrist radial deviation the proximal row flexes, and the distal row extends; both rows also radially angulate (Kaufmann et al., 2005). During ulnar deviation, the proximal row extends and the distal row flexes, while both rows angulate ulnarly. Radioulnar deviation predominantly occurs through the midcarpal joint, with the midcarpal joint accounting for 60% of radial deviation and 86% of ulnar deviation of the wrist.

### *Flexion and Extension*

During flexion and extension both proximal and distal rows move in the same plane. Flexor tendons and extensor tendons exert a flexion and extension moments, on the distal row first. The proximal intercalated segment flexes in response. Flexion-extension angles of each proximal row bone differ according to their proximal convexity. Contribution of each bone to carpal flexion and extension is shown in (Table 3). During wrist flexion and extension, the scaphoid and lunate flexion and extension angles differ (Moojen, Snel, Ritt, Kauer, et al.,

2002; Rainbow et al., 2013). With 60° wrist flexion, the scaphoid flexes 19° more than the lunate (Moojen, Snel, Ritt, Venema, et al., 2002). With 60° wrist extension the scaphoid extends 13° more than the lunate. Due to the difference of flexion and extension of each bone, the SL and LT ligaments experience a rotatory a torque, which has been quantified to be the maximum during extreme extension (Werner, 2021).

*Table 3 Contribution of scaphoid and lunate rotation (flexion-extension) to wrist flexion-extension. From “In vivo analysis of carpal kinematics and comparative review of the literature.” by Moojen et al. (2003) J Hand Surg Am, 28(1), 81-87. Copyright [2004] by Elsevier Science & Technology Journals. Reprinted with permission.*

Study /Reference	Wrist extension 60°			Wrist flexion 60°		
	Scaphoid (%)	Lunate (%)	Scapho-lunate (°)	Scaphoid (%)	Lunate (%)	Scapho-lunate (°)
(Moojen et al., 2003)	87	66	13	62	31	19
(Savelberg et al., 1993)	92	58	20	62	39	14
(Kobayashi, Berger, et al., 1997)	87	50	22	63	36	16
(Patterson et al., 2007)	58	22	14	61	63	1
(Ishikawa et al., 1997)	NM	47	16	NM	53	10
(Werner et al., 1997)	95	38	34	88	51	22
(Ruby et al., 1988)	NM	45	13	NM	63	13
(Wolfe et al., 1997)	NM	43	NM	NM	43	NM
(Horii et al., 1991)	85	48	22	72	55	10
(Ritt et al., 1998)	87	49	23	66	38	17
(Wolfe et al., 2000)	99	68	19	73	46	16

*Scaphoid and lunate rotation as a percentage of capitate rotation is presented in the table. Scapho-lunate indicate the relative intercarpal rotation between the scaphoid and the lunate. NM- Not mentioned.*

In addition, it is reported that the magnitude of the scaphoid angulation differs between the wrist flexion and wrist extension (Moojen, Snel, Ritt, Kauer, et al., 2002; Rainbow et al., 2013). While the scaphoid extends 52° during 60° wrist extension, it only flexes 37° with 60° wrist flexion. The proximal row bones ulnar deviate with the wrist flexion (Moojen, Snel, Ritt, Kauer, et al., 2002). The scaphoid on average ulnar deviates 8.3° ( $\pm 1.1^\circ$ ) with wrist flexion; Internal and external rotation however is negligible.

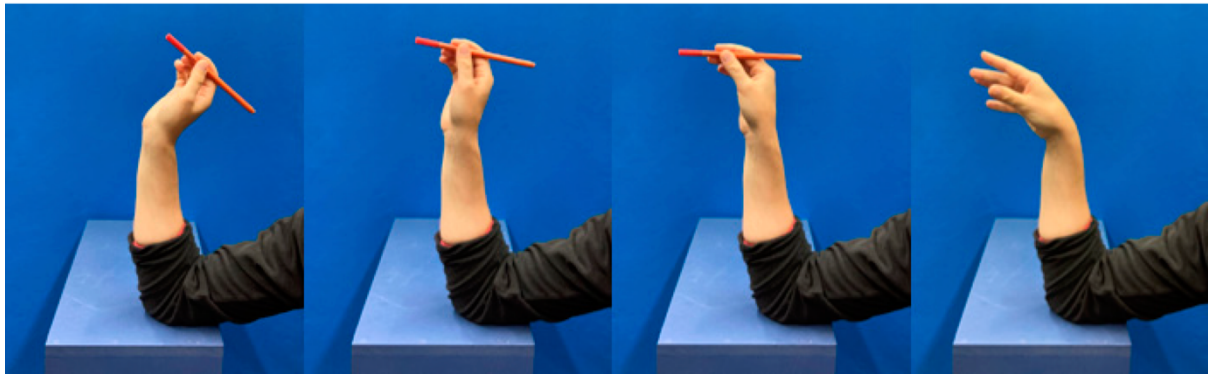
Contribution of the radiocarpal and midcarpal joints to wrist flexion and extension varies depending on the column (Kaufmann et al., 2006). In the radial column, 75% of the flexion

and 92% of the extension occurred at the radiocarpal (radioscaphoid) joint. The midcarpal joint accounted for remaining 25% flexion and 8% extension. In the central column, 50% of the flexion and 52% of the extension occurred through the radiocarpal (radiolunate) joint. The midcarpal joint contributed at nearly half of the flexion and extension of the central column. Bain et al. reported that the central column radiocarpal and midcarpal motion changes with the Lunate type; In type I lunate midcarpal extension dominates (predominantly 10:7) and in type 2 lunate radiocarpal extension dominates (Bain et al., 2015).

The normal scaphoid and lunate helical axis of motion (HAM) has been studied using 3D CT and 4D CT. Best et al. assessing the HAM for radioulnar deviation and flexion and extension using 3D CT scans of static wrist positions concluded that the normal scapholunate rotation axis is highly variable (Best et al., 2019). The conclusion from this study suggests that it is unlikely to be able to recreate a single scapholunate rotation axis. A 4D CT based study has concluded that the scapholunate rotation axis passes through the dorsal region of the proximal pole of the scaphoid (de Roo, Muurling, et al., 2019). The study by de Roo et al. concludes that the rotation axis can be recreated by reattaching the ligament to the dorsal proximal scaphoid.

### *Dart Throwers' Motion (DTM)*

Henke 150 years ago suggested that two axes of the radiocarpal and midcarpal joints are perpendicular to each other; Hence, there is no “pure” global wrist motion (Henke, 1859). Fisk in 1981, described this ‘conjoint axis’ of the whole carpus, as the true physiological axis, that is being used in hammering, throwing darts or conducting an orchestra using a baton (Fisk, 1983). Palmer et al, named this wrist motion occurring around an oblique axis, the “Dart Throwers’ Motion-DTM” (Palmer et al., 1985). Since then, it is commonly agreed that the dart thrower’s motion is the functional wrist motion.



*Figure 15 The sequence of dart throwers motion with the wrist moving from radial extension to ulnar flexion. From “In vivo measurement of wrist movements during the dart-throwing motion using inertial measurement units” by Fischer, G.; Wirth, M.A.; Balocco, S.; Calcagni, M. (2021) Sensors 2021, 21, 5623. [used under Creative Commons CC-BY license]*

Joseph Crisco in 2005, quantified this axis to be  $26.6^{\circ} \pm 4.4^{\circ}$  oblique to the sagittal plane. He proposed that it is the mechanical axis of the carpus (Crisco et al., 2005; Crisco et al., 2011). It is believed that the DTM is the most stable and controlled motion of the wrist (Rohde et al., 2010). It combines the power of the forearm muscles to the precision elicited by the thumb. The STT joint, hence, is the ‘steering’ mechanism; The FCU, ECRL and extensor carpi radialis brevis (ECRB) becomes ‘the wrist motor’ for DTM (Moritomo et al., 2007).

Midcarpal joint plays an important role in DTM. While it is considered that the DTM is a pure midcarpal motion, there is evidence that the radiocarpal joint and the forearm is actively moving during the functional tasks similar to DTM like hammering (Leventhal et al., 2010).

#### *Prono supination (Internal and external rotation)*

To achieve prono-supination of the hand for functional activities, proximal and distal radioulnar joints are crucial. It is an important observation that most of the functional tasks of the hand including power grip, occurs in relative DRUJ pronation. In addition to the radioulnar joints, internal and external rotation can occur in the radiocarpal and intercarpal joints. Pronation is defined as the counterclockwise motion of the hand relative to the forearm axis. Supination is the opposite. The carpus can also axially rotate relative to the radius, even if the radioulnar joints remain immobile. The primary axial rotational laxity of

the radiocarpal joint was approximately 20° (Ritt et al., 1996). Obliquity of the tendons enable the wrist to rotate around the longitudinal axis of the radius. The primary constraining ligament against radiocarpal pronation is the RSC ligament. The DRC and volar UL ligaments resist radiocarpal supination.

In addition to the radiocarpal prono-supination, there is a degree of inter-carpal prono-supination especially with axial loading. APL, FCU, and ECRL produce intercarpal supination. FCR and ECU produce intercarpal pronation (Salva-Coll et al., 2011). When the carpus is under isometric loading as in grip, there is an average of 1.9° of intercarpal pronation, which reverses with releasing the grip.

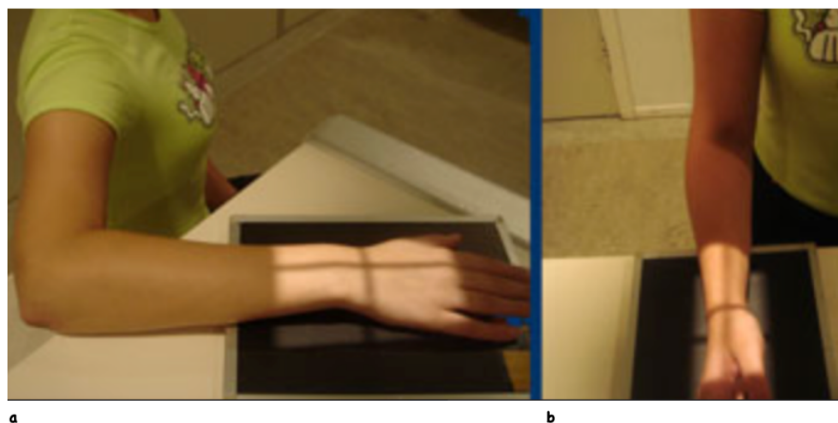
## 1.2. SCAPHOLUNATE INSTABILITY WRIST

Scapholunate instability (SLI) is defined as the clinical syndrome that occurs due the wrist dysfunction, abnormal kinematics and kinetics following partial or complete injury to the SLIL (Wessel & Wolfe, 2023). SLI was first described by Destot in 1926 (Destot, 2006). Linscheid and Dobyns in 1972, using radiographs, identified and described the kinematic changes that are of SLI (Linscheid et al., 1972).

Over the last 5 decades, there has been extensive research into the biomechanics, investigations, and treatment options for SLI. The SLI wrist is symptomatic during movement and load bearing activities and demonstrates abnormal kinematic patterns. The symptoms range from pain to sudden shifts or clunks during wrist motion.

### 1.2.1. Investigations for SLI

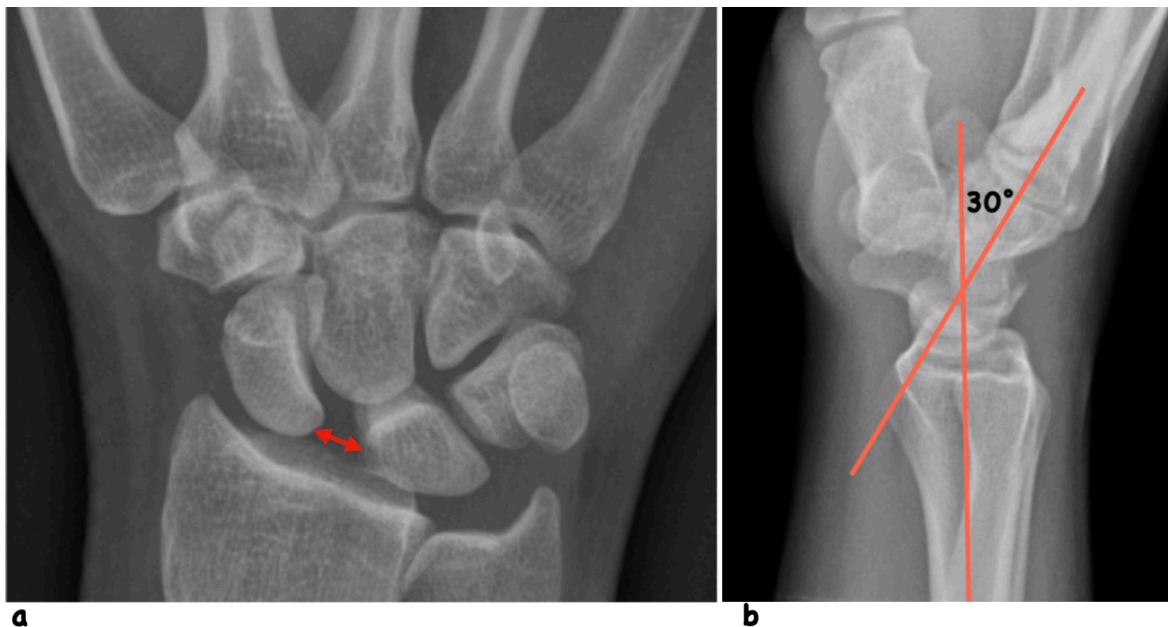
Despite being the most common carpal instability, SLI is often missed (Pietsch, 2019). A summary of diagnostic modalities, potential findings, sensitivities, and specificities in diagnosing SLI is presented in Table 4. The current preliminary diagnostic workup includes the standard postero-anterior and lateral radiographs (Dietrich et al., 2021) and contralateral wrist radiographs for comparison. Figure 16 shows how to perform a standard wrist radiograph.



*Figure 16 a. The standard postero-anterior view of the wrist. The shoulder is abducted, elbow is flexed to 90° with the wrist in pronation and the X ray beam projecting from posterior to anterior and the panel is placed anterior to the wrist. b. The standard lateral view of the wrist. The shoulder is abducted, elbow is flexed to 90°*

*with the wrist in neutral pronosupination and the X ray beam projecting from radial to ulnar and the panel is placed ulnar to the wrist. From “Carpal instability” by Louis A. Gilula and Ileana Chesaru. 2005. Radiology Assistant. <https://radiologyassistant.nl/musculoskeletal/wrist/carpal-instability>. Copy rights [Radiology Assistant]. Published with permission.*

The scapholunate diastasis demonstrating unilateral the SL gap more than the width of other intercarpal joints (2–3 mm) in a standard posteroanterior wrist radiograph or a clenched fist view is considered abnormal (Kitay & Wolfe, 2012; Schimmerl-Metz et al., 1999). The diastasis is measured at the proximo-distal midpoint at the scapholunate interval (Said et al., 2018) (Figure 17).



*Figure 17 Postero anterior-PA- (a) and lateral views of the wrist, demonstrating features of scapholunate instability. On the PA view, scapholunate diastasis can be observed (Red arrow). On the lateral view the lunate extension is seen as a radiolunate angle of 30°.*

The radioscapoid angle is measured according to the volar tangential method described by Larsen et al (Larsen, Mathiesen, et al., 1991). Scapholunate angle is the angle between the volar tangential line of the scaphoid and the axis of the lunate, defined as a perpendicular line to a tangential line along the cusps of the scaphoid (Figure 18).



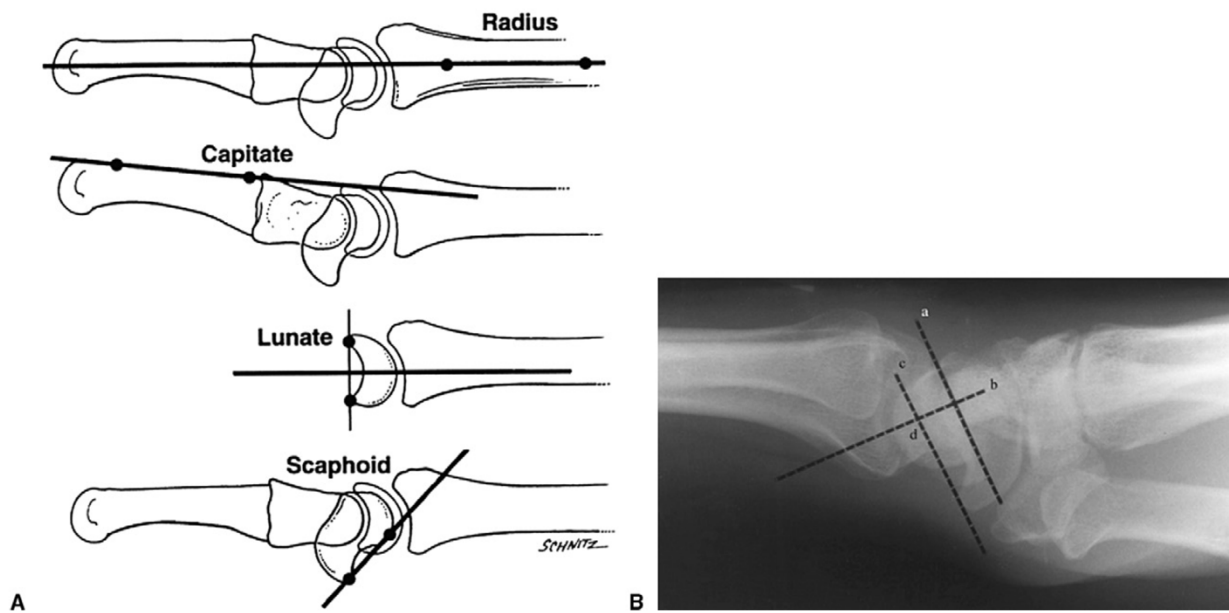


Figure 18 Reproducible measurement of intercarpal angles is facilitated by drawing tangents to the carpal contours. A Note that the lunate axis is perpendicular to the lunate tangent line. B Lunate tangent (a), lunate axis (b), scaphoid tangent (c). This lateral radiograph shows a 20° DISI posture of the lunate and a (d) 90° SL angle. From "Scapholunate instability: current concepts in diagnosis and management." by Kuo EC, Wolfe SW. (2008). *J Hand Surg Am J Hand Surg Am*, 33(6), 998-1013. Copyright [2008] by Elsevier Science & Technology Journals. Reprinted with permission.

The scaphoid flexion, lunate extension, scapholunate diastasis and dorsal scaphoid translation are common findings identified on plain radiographs (Wessel & Wolfe, 2023) (Linscheid et al., 1972). A scapholunate angle greater than 70°, radioscapoid angle greater than 70° and lunate extension greater than 15° are pathological and highly suggestive of SLI (Wessel & Wolfe, 2023).

Various stress views are helpful in the diagnosis of dynamic SLI. The twist X-ray, clenched fist, and pencil grip view are some of the common alternatives (Sikora et al., 2019). The stress views may unmask the features of instability when the wrist is under load.

Dynamic fluoroscopy enables the wrist to be moved through a range of motion and identify dynamic changes in real-time, unmasking the features of instability during wrist motion. Dynamic fluoroscopy has proven to have a sensitivity of 90%, a specificity of 97% and a diagnostic accuracy of 93% (Sulkers et al., 2013) in diagnosing SLI. Static computed

tomography (CT) scans are commonly used to diagnose wrist pathology. When combined with arthrography as in CT arthrogram (CTA), it can be very accurate (Dietrich et al., 2021). The diagnostic accuracy of CTA is found to be even better than conventional Magnetic Resonance Imaging (MRI) in detecting SLIL tears in a cadaveric model when using oblique and axial planar sections (Lee et al., 2017). CTA is recognized to have a sensitivity of 94% and specificity of 86% in detecting SLIL tears when arthroscopy is considered the gold standard diagnostic test (Bille et al., 2007). The chondral loss also can be assessed by CTA.

A meta-analysis comparing 3T MRI, MR Arthrogram (MRA) and 1.5T MRI for diagnostic accuracy of SLI found a sensitivity of 82% and specificity of 93% for MRA compared to arthroscopy or gross pathology as standard of reference. MRA had the best diagnostic accuracy and 3T MRI had the best specificity in detecting SLIL injuries (Hafezi-Nejad et al., 2016). With the available limited evidence on radiological evidence of DCSS, MRA is reported to provide the most accurate information on the integrity of the DCSS as well.

There is evidence to suggest that true and oblique sagittal cuts of MRI can identify extrinsic carpal ligaments (Adler et al., 1996). MRI in extremes of wrist radial and ulnar deviation change the width of the radiocarpal joint (Gheno et al., 2010) that lead to changes in visual conspicuity of the intrinsic carpal ligaments of the proximal row. This is used to visualise SLIL in extremes wrist positions. SLIL tears are more readily detectable on axial MRI sections than coronal (Greditzer et al., 2016). They also found that among wrists with SLI, 34% of cases had proximal pole dorsal subluxation. Of all the diagnostic parameters described only variable linked to patient outcome is the dorsal scaphoid translation (DST) (Gondim Teixeira et al., 2016).

Dynamic MRI and dynamic CT have created a lot of research interest in recent years. Nonetheless the place of these investigations in the diagnosis of SLI is not established due to limited availability in clinical setting and different study protocols used in the different centres (Dietrich et al., 2021). The technical details and the evolution of dynamic CT is described in detail in section 1.3.7.

*Table 4 Investigations used in diagnosing scapholunate instability.*

Investigation	Findings	Sensitivity/ specificity
Plain X-ray (posteroanterior and lateral)	Scaphoid flexion Dorsal intercalated segmental instability (DISI) Scapholunate diastasis Increased scapholunate angle (>70°) Dorsal subluxation of the proximal pole	Sensitivity 81% Specificity 80% (Sulkers et al., 2014)
Stress X rays (Clenched fist, pencil grip, twist x ray)	SL diastasis (over 3 mm) with stress	NA
Dynamic fluoroscopy	SL diastasis with stress and movement (SL gap increases in ulnar deviation) Dorsal subluxation of proximal pole with radial deviation	Sensitivity 90% Specificity 97% (Sulkers et al., 2014)
CTA-CT arthrogram	Visualisation of the intact SL ligament/ partial or full thickness tears Contrast leakage between compartments suggestive of SL injury Radiocarpal opacification-for cartilage assessment	Sensitivity 85–97 % Specificity 79–97 % (Bille et al., 2007)
Dynamic CT (4D CT)	Worsening SL gap (with movement and stress) Dynamic dorsal subluxation of the scaphoid	NA
Magnetic Resonance Imaging (MRI)	Partial or complete tears in SLIL Tears in DIC and DRC and other carpal ligament injuries Cartilage assessment	Sensitivity 75.7% Specificity 97.1% (Hafezi-Nejad et al., 2016)
Magnetic Resonance Arthrography (MRA)	In addition to features seen in MRI Better appreciation of ligament tears Granulation tissue associated with fibrous scar tissue infiltration of the injured ligament. Contrast extravasation from radiocarpal or midcarpal compartment	Sensitivity 82% and specificity 93% (Hafezi-Nejad et al., 2016)

### 1.2.2. Classifications of SLI

Since its identification in 1970s, SLI is recognised to be a spectrum of pathology. The instability may be classified as static or dynamic depending on whether carpal malignment is present in the standard radiographs or only in the stress radiographs. When scapholunate diastasis is not seen in posteroanterior wrist radiographs, but in stress views only, it is classified as dynamic SLI. When there is scapholunate diastasis in posteroanterior wrist radiographs but no arthritic changes, it is named static SLI (Salva-Coll et al., 2013). When arthritic changes are present, it is classified as scapholunate advanced collapse (SLAC) (Watson & Ballet, 1984).

A clinically applicable classification of SLI was first developed by William Geissler (Geissler, 2006). This classification is based on wrist arthroscopy findings, particularly the feasibility of passing a 2 mm probe through the scapholunate interval from the radiocarpal or midcarpal joints.

Dreant and Dautel developed another classification in 2003 based on wrist arthroscopy to quantify the arthroscopic grading of SLI (Dreant & Dautel, 2003). Currently, Garcia Elias's classification which is a stepwise algorithm of management is widely used in clinical practice and research settings (Table 5) (Garcia-Elias et al., 2006). The management algorithm is based on defining pathoanatomy. Stages 1-2 indicate either the SLIL is intact or easily repairable. Stage 3 indicates scaphoid malalignment. Stage 04 considers the lunate uncovering index. Stage 05 occurs in the presence of the scaphoid and lunate malalignment which is easily reducible. Stage 06 is when the malalignment is chronic so that the reduction is difficult but still the cartilage is normal. It is likely that in stage 02 dorsal SLIL is injured. However, with advanced staging, one or more other critical stabilisers are likely to be injured, such as DIC, DRC, STT or the volar radiolunate ligaments.

*Table 5 Garcia Elias classification of scapholunate instability. From “Three-ligament tenodesis for the treatment of scapholunate dissociation: indications and surgical technique.” by Garcia-Elias et al. (2006). J Hand Surg Am, 31(1), 125-134. Copyright [2006] by Elsevier Science & Technology Journals. Reprinted with permission.*

Scapholunate Dissociation stage	1	2	3	4	5	6
Is there a partial rupture with a normal dorsal SL ligament?	Yes	No	No	No	No	No
If ruptured, can the dorsal SL ligament be repaired?	Yes	Yes	No	No	No	No
Is the scaphoid normally aligned (radioscaphoid angle < 45°)?	Yes	Yes	Yes	No	No	No
Is the carpal malalignment easily reducible?	Yes	Yes	Yes	Yes	No	No
Are the cartilages at both RC and MC joints normal?	Yes	Yes	Yes	Yes	Yes	No

European Wrist Arthroscopy Society (EWAS) has developed a further classification system for scapholunate ligament injury and correlated each stage to anatomic-pathological cadaveric findings (Table 6). They observed that the complete widening of the scapholunate gap occurs with a complete tear of SLIL and one or more extrinsic carpal ligaments.

*Table 6 Arthroscopic EWAS (European Wrist Arthroscopy Society) Classification. From “The EWAS Classification of Scapholunate Tears: An Anatomical Arthroscopic Study.” by Messina et al. (2013). J Wrist Surg, 2(2), 105-109. Copyright [2013] by Thieme Medical Publishers, Inc. Reprinted with permission.*

Arthroscopic stage (EWAS)	Arthroscopic testing of SLIOL from MC joint
I	No passage of the probe
II lesion of membranous SLIOL	Passage of the tip of the probe in the SL space without widening (stable)
III A partial lesion involving the volar SLIOL	Volar widening on dynamic testing from MC joint (Anterior laxity)
III B partial lesion involving the dorsal SLIOL	Dorsal SL widening on dynamic testing. (Posterior laxity)
III C complete SLIOL tear, joint is reducible	Complete widening of SL space on dynamic testing, reducible with removal of probe
IV complete SLIOL with SL gap	SL gap with passage of the arthroscope from MC to RC joint No radiographic abnormalities

Arthroscopic stage (EWAS)	Arthroscopic testing of SLIOL from MC joint
V	Wide SL gap with passage of the arthroscope through SL joint Frequent X Ray abnormalities such as an increased SL gap, DISI deformity

### 1.2.3. Natural history

Despite the understanding of SLI over 5 decades the natural history remains elusive. Watson et al. has reported that untreated scapholunate instability progresses into a predictable pattern of arthritis ending in the SLAC wrist (Watson & Ballet, 1984). However, the natural history of dynamic SLI is less convincing (O'Meeghan et al., 2003). Later, Crisco et al. studied uninjured wrists of a cohort of SLI patients and reported that in the patients diagnosed with SLI in one wrist, the contralateral uninjured wrist also has radiological features of SLI. Whether the contralateral uninjured wrist develops arthritic changes is an unknown fact.

### 1.2.4. Pathoanatomy

The radiographic and the clinical features of SLI is considered a result of injury to multiple wrist ligaments that includes SLIL and other critical stabilisers (Raja et al., 2022b; Wessel & Wolfe, 2023). The above conclusion is drawn from cadaveric studies following sequential sectioning of carpal ligaments. There are not many in vivo studies correlating SLIL injury with presence of extrinsic ligament injuries. Van Overstaeten and Camu (Van Overstraeten & Camus, 2016) assessed 85 wrist arthroscopies, and correlated SLIL injury to extrinsic carpal ligament injuries. They found a significant correlation of SLIL injury with LRL injury. SLIL injury was also correlated to the number of lax extrinsic ligaments. While specifically looking at RSC, SRL, STT, DIC, they did not find any correlation of above ligament injuries to SLIL.

Imaging studies have confirmed that SLIL injuries are associated with in high number of extrinsic carpal ligament injuries. Ozkan et al reported that 58% of the SLIL injuries occur in association with either DIC or DRC injuries (Özkan et al., 2019). Studying 75 MRI scans of patients with wrist trauma Taneja et al. (Taneja et al., 2013) reported 50% of that cohort has combined intrinsic and extrinsic ligament injuries with the most common intrinsic being SLIL

injury (58%). The most common extrinsic ligament injuries were volar radio triquetral, DRC and RSC ligaments, each occurring at a rate of 40%. However, they have not correlated SLIL injury with extrinsic carpal ligament injuries.

#### 1.2.5. Mechanism of injury

SLI has been shown to develop as an early stage of peri-lunate instability, where carpal ligaments fail in sequence. The sequence of failure may depend not only on the material properties of the ligaments but also on the direction of the force.

Mayfield demonstrated that ligament instability of the wrist develops in a sequence of events following wrist extension, ulnar deviation and intercarpal supination (Figure 19) (Mayfield, 1980, 1984; Mayfield et al., 1980). SL ligament injury is described as stage 1 where the radial-sided ligaments including the SLIL fail in tension. In his cadaveric studies simulating this mechanism, the radio-scapho-capitate ligament (RSC) and SLIL were torn in stage 1.

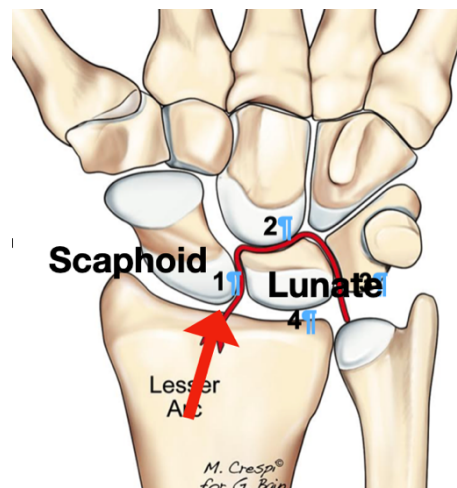


Figure 19 Scapholunate ligament is torn in stage 1 of progressive peri lunar instability Copyright [2021] Gregory Bain. Reprinted with permission.

There is biomechanical evidence that the ulnar-sided peri-lunate instability can lead to disruption of the dorsal scapho-triquetral ligament and the SLIL as the injury progresses onto stage 3 (Murray et al., 2012). However, this represents peri-lunate instability more

than SLI and is beyond the scope of this review. In major traumatic injuries the direction of force may be difficult to be defined.

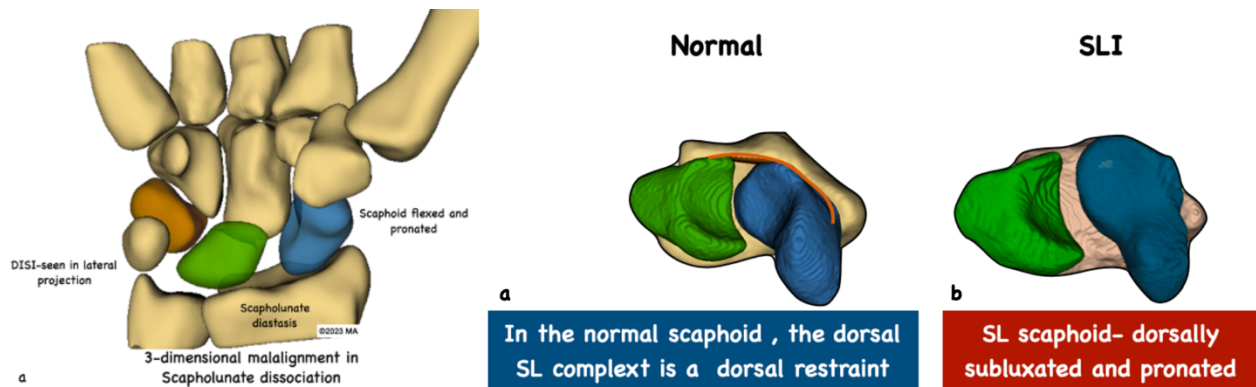
#### **1.2.6. Kinematics of the SLI wrist**

Static malalignment of SLI include scapholunate diastasis, scaphoid flexion (Linscheid et al., 1972), pronation, proximal scaphoid dorsal subluxation(Chan et al., 2019) and dorsal intercalated segmental instability (DISI) (Linscheid et al., 1972). Malalignment and instability, however, are distinctly different concepts (Garcia-Elias & Lluch, 2017). Malalignment is the abnormal carpal posture at a given time point; whereas instability is abnormal carpal posturing during load bearing, and not exhibiting normal kinematics during any portion of its arc of motion (Garcia-Elias, 1999). Dynamic studies including stress views and dynamic fluoroscopy can accentuate or unmask the instability (Bain et al., 1997).

Moritomo et al. in 2013 studied the DISI deformity occurring in the SL dissociation (SLD) compared to distal radius malunion (Omori et al., 2013). In SLD, he defined this 3-dimensional deformity as the scaphoid being translated dorsally and radially (Figure 20), with flexion and pronation(Omori et al., 2013). The lunate was extended and supinated. Contact area of the radioscapoid joint shifted dorso-radially with proximal pole dorsal subluxation. The radioscapoid joint was incongruent whereas radiolunate facet retained its congruity.

Crisco et al. (Crisco et al., 2003) studied the 3D CT scans of SLI wrists and the contralateral uninjured wrists and compared them with a normal sample of 3D CTs. His conclusion was that the uninjured wrist also had abnormal carpal postures. Furthermore, studying the scaphoid and the lunate postures in flexion and extension (two static positions), Crisco et al. described that the lunate in SLI extended less with wrist extension and the scaphoid in SLI flexed more with wrist flexion compared to normal wrist. Despite the limitation of studying only two extreme static positions of flexion and extension, this was the first in vivo 3D study reporting the flexion and extension arcs of the scaphoid and the lunate in SLI.





*Figure 20 The 3-dimensional malalignment in scapholunate instability. a. The SLI scaphoid is flexed and pronated. The scapholunate gap is wider. b. compared to the normal scapholunate articulation in a distal view the SLI scaphoid is pronated and dorsally subluxated. The lunate is extended and the scapholunate gap is wide. Note that normal and SLI wrists in figure 2. b is in radial deviation. Copyright [2023] Melanie Amarasooriya.*

More recently dynamic CT has been used to study the kinematics of SLI. Rauch et al. (Rauch et al., 2018) studied the variability of the radioscapoid and the radiolunate angles during radioulnar deviation of the wrist using the multiplanar reconstructions of dynamic CT scans. They reported that there is a significant reduction of the lunate flexion arc during radioulnar deviation, however, they did not find the scaphoid flexion arc to be different.

The same research group, using a similar technique studied the variability of the scapholunate diastasis during wrist radioulnar deviation and clenched fist (Abou Arab et al., 2018). They concluded that based on measurement of scapholunate diastasis, 4D CT in radioulnar deviation has excellent inter observer reliability and high diagnostic performance compared to the clenched fist motion. Furthermore, when SLI diagnosis was questionable on planar radiography as in 'dynamic SLI', 4D CT scanning has demonstrated increased 'range of scapholunate gap' compared to the normal wrist (Athlani et al., 2020). The researchers did not find any significant change in the minimum or the maximum SL gap between the normal and 'dynamic' SLI groups. A study using MRI showed that over 60% of the patients with SLIL injury do have concomitant DIC or DRC injury (Özkan et al., 2019). This confirms the fact that SLI is a multi-ligament injury.

The earlier studies using plane radiographs and static CTs report on the malalignment in SLI (Linscheid et al., 1972; Omori et al., 2013). Later studies using static CTs in extreme wrist positions extrapolate the kinematics based on the observation of the malalignment in two

static positions (Crisco et al., 2003). More recent studies using dynamic CT, has focussed more on diagnostic accuracy based on scapholunate gap and only quantifying the sagittal plane radiocarpal angles but not true 3-dimensional kinematics (Abou Arab et al., 2018; Athlani et al., 2021; Athlani et al., 2020).

While there was significant emphasis on the radiocarpal kinematics in SLI, there were no reports as to how the midcarpal kinematics change in SLI. While the helical axis of motion (HAM) of the normal scaphoid and the lunate has been studied there were no in vivo studies as to how HAM changes in SLI. A cadaveric study by Berger et al. have assessed the scaphoid HAM and concluded following SLIL sectioning the orientation of the scaphoid HAM changes (Berger, Crowninshield, et al., 1982). Lunate HAM however does not change following SLIL sectioning. The cadaveric sequential sectioning studies that assess the kinematic changes in scapholunate ligament deficient wrist is reviewed in section 1.3.3.2.

#### **1.2.7. Kinetics of the SLI wrist**

The wrist is known to load abnormally following ligament injuries or other pathological conditions such as Kienbock's disease (Kawanishi et al., 2015; Omori et al., 2013). Radiocarpal contact pressures are important in defining the loading patterns of the wrist. Blevens et al. observed that the isolated sectioning of SLIL reduced the radioscapoid contact area significantly and a 37% increase in the pressure across the radioscapoid joint compared to the intact stage (Blevens et al., 1989). The lunate contact area and pressure across the radiolunate joint increased by 20% compared to the intact stage. This stage of isolated SLIL sectioning is comparable to dynamic SLIL in a clinical case as shown in the study by Mitsuyasu (Mitsuyasu et al., 2004).

Daly et al. later studied the joint contact area and pressure in the radioscapoid and radiolunate joints in the neutral wrist and extended position following SLIL sectioning compared to the intact wrist (Daly et al., 2018). Their conclusion was that with the push up position in extension there is a significant increase in radioscapoid pressure but not the radiolunate pressure. They also observed that there is a radial translation of the radioscapoid contact area but no change in the lunate position following SLIL sectioning. In

another cadaveric study, it was reported that radiocarpal loading patterns are not affected following SLIL sectioning and axial loading in the neutral wrist position (Huddleston et al., 2021).

In an in vivo study, Omori et al. reported that the proximal pole of the scaphoid is dorsally and radially translated, leading to abnormal radioscapoid contact around the dorsal rim of the radius and the radial styloid (Omori et al., 2013). This explains the possibility of development of degenerative changes. Similar study by Johnson used MRI in vivo in neutral wrist position and functional grasp and studied the joint contact of the radiocarpal joint (Johnson et al., 2013). All joint contact parameters, such as mean and peak contact pressures and contact forces significantly increased, in the radioscapoid joint in SLIL during grip. Nonetheless, the radiolunate joint had only the peak contact pressures and peak contact area increased in SLI.

Hence the current literature is suggestive of abnormal loading patterns in SLI. However due to heterogeneity of the techniques, wrist positions and outcomes used, it is difficult to draw definite conclusions as to identify a pattern of change. From the two in vivo studies, it appears that the radioscapoid joint is more affected than the radiolunate joint (Johnson et al., 2013; Omori et al., 2013).

## **1.3. EVOLUTION OF RESEARCH TECHNIQUES ON CARPAL KINEMATICS**

Over the years abnormal in vivo kinematics of SLI have been studied using imaging modalities. Initially plain radiographs and then 3D CT and MRI in static positions have been used to understand the carpal malalignment in SLI. The following section is a review of the evolution of the research techniques and their findings on 'kinematics of SLI'.

### **1.3.1. Plain radiography**

The initial research into carpal kinematics used planar radiography (Bryce, 1896). Bryce, studying the radiographs of his own wrist in different positions, proposed that the wrist functions as two rows. Navarro proposed and Taleisnik modified, the column theory, describing the wrist as 3 columns of carpal bones, radial, ulnar and central (Taleisnik, 1976). The first study describing SLI using plane radiographs was published by Linscheid and Dobyns in 1972 (Linscheid et al., 1972). Since then, the plain radiography has been used to study SL ligament deficient wrist. Majority are cadaveric studies and will be discussed in section 1.3.3. (Elsaidi et al., 2004; Mitsuyasu et al., 2004; Pérez et al., 2019). In addition to these, other researchers used plain radiography in patients in cohort studies to describe the natural history of SLI (Watson & Ballet, 1984).

### **1.3.2. Bi-planar radiography**

Bi-planar radiography differs from planar radiographs as it uses two radiographic sources, positioned orthogonal to each other and obtaining simultaneous images (Garcia-Elias et al., 1991). This technique was the earliest used to study 3-dimensional carpal kinematics. Radio-opaque markers positioned on cadaveric carpal bones were imaged from 2 orthogonal planes; markers were digitised, and the spatial coordinates of each marker were calculated. Based on the 3-dimesional position of the markers, the carpal positions were estimated (Figure 21).

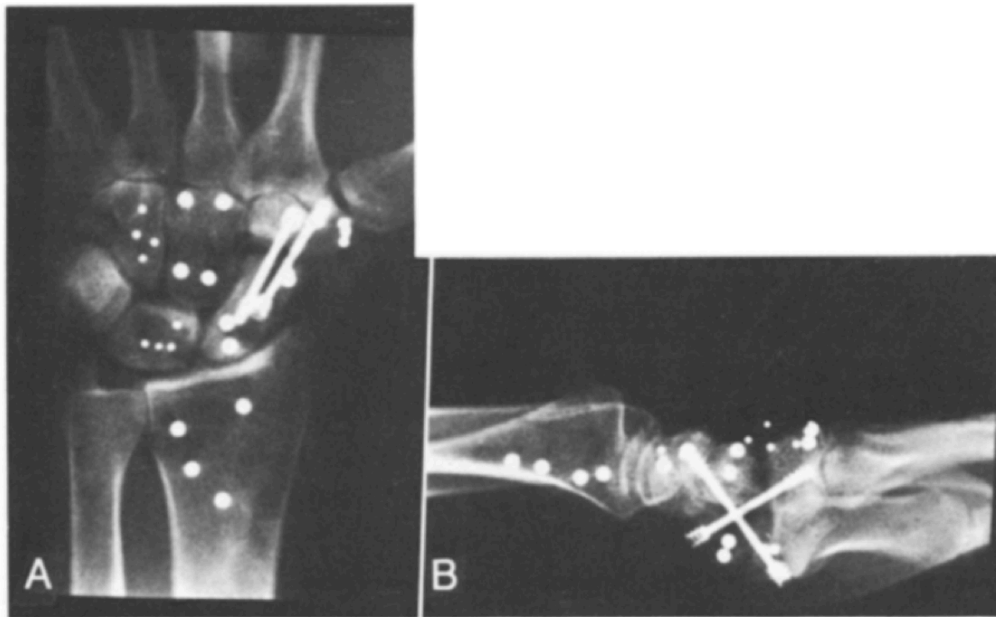


Figure 21. Radiographic images obtained using bi-planar radiography with radio-opaque markers. From “Wrist kinematics after limited intercarpal arthrodesis” by Garcia-Elias et al. (1989). *J Hand Surg Am*, 14(5), 791-799. Copyright [1989] by Elsevier Science & Technology Journals. Reprinted with permission. (Garcia-Elias et al., 1989)

Due to the radiation exposure and necessity for marker positioning, this technique was used in cadavers, (Meade et al., 1990; Ruby et al., 1987) until biplanar video radiography (BVR) with software support to create 3D models were developed (Akhbari et al., 2019a). Bi-planar radiography has contributed immensely to the understanding of the normal wrist (Kobayashi, Berger, et al., 1997; Kobayashi, Garcia-Elias, et al., 1997) and reconstruction techniques for SLI and other carpal pathology (Slater et al., 1999). The studies with the aim of understanding kinematic changes that occur in SLIL deficient wrist are included in the section 1.3.3.

### 1.3.3. Ligament sectioning studies

The scapholunate stability is maintained by multiple critical intrinsic and extrinsic ligaments. Disruption of each of these ligaments leading to ‘SLI’ has been studied using sequential ligament sectioning on cadavers. The literature on simulated SLI by resection of ligaments that were recognised to be important in maintaining scapholunate stability have been summarised in appendix 1.1 (Appendix table 01).

### 1.3.3.1. Study designs

There are several factors that should be considered in interpreting the published research on this topic. Firstly, the outcome measures are heterogeneous between studies. Most of the researchers used the radiocarpal angles (scaphoid and the lunate) and the centroid translations as their outcome measure to assess scapholunate dissociation (Short et al., 1995; Short et al., 2002b); Some researchers used scapholunate diastasis as seen on standard radiography (Mitsuyasu et al., 2004) and others used parameters like helical axis of motion and loading characteristics (Blevens et al., 1989; Viegas et al., 1987). Perez et al. (Pérez et al., 2019) defined their outcome measure as occurrence dorsal intercalated segment (DISI-radiolunate angle  $>15^\circ$ ) to define 'instability', whereas Padmore et al. considered a significant increase in the lunate extension compared to intact stage regardless of DISI as evidence of instability (Padmore et al., 2019). Therefore, the selection of outcome measures may influence the sensitivity of detecting SLI between these studies.

The second factor is the instrument that was used to measure the outcome. Some researchers used imaging modalities such as radiographs (Pérez et al., 2019) and some electromagnetic tracking (Werner et al., 1997) or optical marker based tracking (Padmore et al., 2019). Researchers that used plain radiographs, measured the carpal angles according to the method described by Larsen et al (Larsen, Mathiesen, et al., 1991). Some researchers modified this by creating loading conditions that simulate a clenched fist (Mitsuyasu et al., 2004). Electromagnetic tracking of markers attached to carpal bones and optical markers, both have been proven to have sub-degree and sub-millimetre accuracy for tracking carpal bones (Akhbari et al., 2019b; Short et al., 1995). However, sensitivity and specificity of each method are different and may affect the findings.

The third concern is the definition of instability, as it has been clearly stated instability and malignment are not synonymous (Garcia-Elias, 1999). Studies looking at dynamic aspects and 'change' in outcome measures with wrist movements and loading may have unmasked subtle instabilities. For instance, studies by Short et al. demonstrated that following certain ligament sectioning sequences, there was no additional flexion of the scaphoid but the wrist motion arc through which the scaphoid flexion occurred increased (Short et al., 2002a).

Lastly, the methods that were used to section the ligaments were of note, as some researchers used the dorsal approach as described by Berger et al (Berger & Bishop, 1997) which itself has been found to alter scapholunate kinematics (Loisel et al., 2021; Short et al., 2002a). Other researchers opted for minimally invasive techniques that limit the collateral damage (Elsaidi et al., 2004). Considering the above factors, the relative importance of carpal ligaments in maintaining scapholunate stability is discussed in the following section.

#### **1.3.3.2. Outcomes following sequential sectioning studies.**

With three elegant studies published, Short et al. concluded that the primary stabiliser of the scapholunate articulation is the scapholunate interosseous ligament (SLIL) (Short et al., 1995; Short et al., 2002b, 2005). For all three studies, they used cadaveric wrists fixed on a platform and simulated active wrist motion. They created flexion-extension moments and radioulnar deviation moments with the tendons attached to hydraulic servers. Markers attached to the carpal bones were used to track the carpal positions with electromagnetic tracking. The accuracy of their technique was reported as 0.1° for rotations and 0.5mm for translations.

In the initial study by short et al. (Short et al., 1995) reported that the scaphoid is significantly flexed and pronated and the lunate is extended in simulated SLI, compared to the intact wrist during wrist motion. Ruby et al. 1987 conducted a study using bi-planar radiography and arrived at the same conclusions (Ruby et al., 1987). Blevens et al.(Blevens et al., 1989), Dunn et al.(Dunn & Johnson, 2001), and Payet et al. (Payet et al., 2015) all agreed that SLIL sectioning leads to scaphoid flexion. Nonetheless, they were unable to quantify the pronation of the scaphoid as standard radiographs were used for measurements.

Berger et al. also had similar findings (Berger, Blair, et al., 1982), although his outcome measure was the helical axis of motion (HAM or screw displacement axis-SDA). He studied the changes of the HAM for the scaphoid and lunate tracking them with the sonic digitizer method before and after sectioning the SLIL during wrist motion in 08 cadaveric wrists

(Berger, Blair, et al., 1982). He reported that the orientation of the HAM of the scaphoid changes significantly following isolated SLIL sectioning, but the SDA for the lunate does not. These changes were only seen during certain parts of the wrist motion (neutral to ulnar deviation and neutral to extension) and not throughout the range.

All the above mentioned cadaveric studies including Short et al.(Short et al., 1995) had the limitation of approaching the wrist through dorsal capsulotomy and may have inadvertently violated the DRC during the procedure. In later studies, researchers have confirmed that violating DRC through dorsal capsulotomy alone can affect scapholunate kinematics (Loisel et al., 2021; Short et al., 2002a).

In subsequent studies, many researchers including Short et al. used a minimally invasive approach to preserve the DRC integrity (Short et al., 2002a). In subsequent studies Short et al. and others concluded that even after using a minimal access technique, isolated sectioning of SLIL alone would lead to a significant ‘change’ in at least one outcome measure (Loisel et al., 2021; Padmore et al., 2019; Short et al., 2005; Short et al., 2007). The outcome measures that reflected ‘SLI’ were,

- Scaphoid flexion (Short et al., 2005; Short et al., 2007)
- Scaphoid ulnar angulation (Short et al., 2002a; Short et al., 2005)
- Higher scapholunate angle (Padmore et al., 2019),
- Lunate extension(Padmore et al., 2019; Short et al., 2005)
- Increased scapholunate gap (Loisel et al., 2021)

Then, there was interest among the researchers to study how each component of SLIL affects scapholunate kinematics. Initial publication by Berger et al.(Berger, 1996) which reported that the dSLL has the highest tensile strength out of the 3 components may have led to the hypothesis that it is more important in SLI. Waters et al. (Waters et al., 2016) found that dSLL sectioning led to two thirds of scaphoid flexion that would be seen following complete SLIL sectioning during wrist radioulnar deviation and dart throwers motion. Interestingly, this study revealed dSLL sectioning also causes at least half of the lunate



extension that would be seen in a complete SLIL sectioning. Isolated volar SLIL sectioning caused insignificant kinematic changes.

Studies published after this contest these findings, reporting no significant changes occurred in scaphoid flexion, lunate extension or scapholunate diastasis with isolated dSLL sectioning (Padmore et al., 2019). Padmore et al. studied the carpal bone changes during wrist motion using optical markers and concluded that dSLL sectioning alone has negligible effect on scapholunate kinematics. Further to this, Perez et al. (Pérez et al., 2019) and Loisel et al. (Loisel et al., 2021) reported that they did not observe scaphoid flexion or lunate extension even with complete SLIL sectioning.

It is worth noting that the techniques used to measure carpal posture in these four studies were different, with both Perez and Loisel (Loisel et al., 2021; Pérez et al., 2019) using simulated stress radiographs in static positions; Padmore, using optical marker-based tracking during wrist motion (Padmore et al., 2019) and Waters, electromagnetic tracking during wrist motion (Waters et al., 2016).

One of the earliest reports suggesting that SLI is a multi-ligament injury was by Meade et al in 1990 (Meade et al., 1990). He assessed the scaphoid and lunate carpal postures after sequential sectioning of the radio-scapholunate ligament (RSL), SLIL and radio-capitate (RC) ligaments. Using plain radiography on cadaveric wrists he studied the radiocarpal angles for the scaphoid and the lunate at the neutral position, ulnar deviation and radial deviation and compared the values between the intact wrist and stages of ligament sectioning. He concluded that multiple ligaments including SLIL need to be sectioned before changes in carpal positions on radiographs are seen. However, the statistical significance of the changes occurring at each stage was not reported. He also concluded the scapholunate angle (SLA) best reflected the progressive nature of instability.

SLI as a multi-ligament wrist pathology continued to interest the researchers. The most common ligaments that have been studied in this regard are the DIC, DRC, STT, RSC, LRL and SRL ligaments. Some early researchers also evaluated the role of the radio-scapholunate (RSL) ligament, although currently this is not considered a true ligament. Many researchers

agree that isolated division of any of the ligaments other than SLIL does not cause significant changes in carpal postures (Elsaidi et al., 2004; Patterson et al., 2013; Short et al., 2005; Short et al., 2007).

Comparing several ligament sectioning sequences, Short et al. (Short et al., 2005) concluded that irrespective of the order of sectioning, no significant change in carpal positions occurred until SLIL was sectioned. Other studies attempting to demonstrate the importance of carpal ligaments other than SLIL, had the limitation of every sectioning sequence having the SLIL sectioned at the beginning. Therefore, effects of isolated sectioning of carpal ligaments other than SLIL could not be assessed (Pérez et al., 2019).

Almost all studies agree that instability worsens progressively as SLIL sectioning is compounded by other carpal ligament sectioning. Mitsuyasu et al. further evaluated the role of extrinsic carpal ligaments for SLI (Mitsuyasu et al., 2004). His assessment was based on carpal postures on plain posteroanterior and lateral radiographs and a three-dimensional evaluation of digitized metal marker positions with and without wrist loading. Both radiographic and digitized markers confirmed that the significant changes occurred with sectioning of dSLL and DIC resected off the scaphoid and loading (Figure 22 B). The scaphoid flexed, scapholunate diastasis occurred, without significant changes in the lunate. He proposed this stage is comparable to 'dynamic scapholunate instability' seen in the clinical setting. When the SLIL is completely sectioned, DIC was off the scaphoid and the lunate, the lunate showed signs of DISI in both loaded and unloaded states and 'static' deformity (Figure 22).

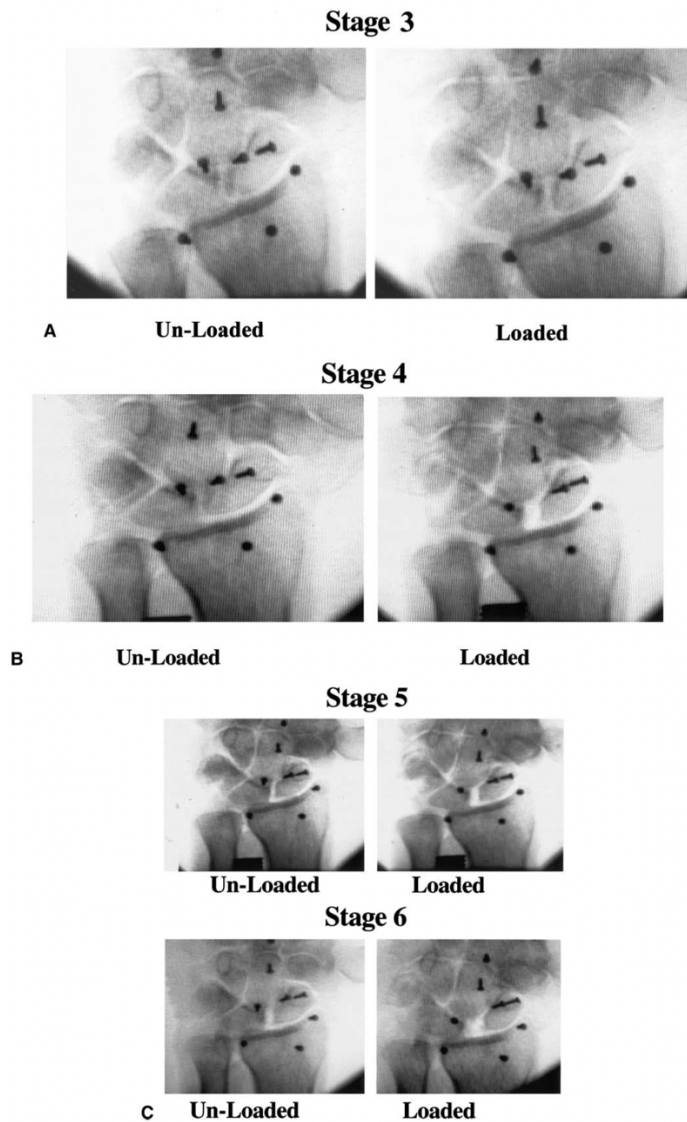


Figure 22 Posteroanterior radiographs (A) of one specimen in both unloaded and loaded conditions of stage 3 without scapholunate diastasis (B) The same specimen with scapholunate diastasis in the stage 4 sectioning with loaded condition compared with the unloaded condition, and (C) scapholunate diastasis both unloaded and loaded conditions in stages 5 and 6. The stages of section are as follows- stage 1, partial dorsal capsulectomy retaining both the DIC and DRC ligaments. Stage 2, sectioning the palmar portion of the SLIL and the membranous portion of the SLIL. stage 3, detaching the DIC ligament from its attachment on the scaphoid and trapezium; stage 4, sectioning the dorsal portion of the SLIL (dSLIO); stage 5, detaching the DIC ligament from its attachment on the lunate; stage 6, complete sectioning of the LTIO ligament. From "The role of the dorsal intercarpal ligament in dynamic and static scapholunate instability." by Mitsuyasu et al. (2004 J Hand Surg Am, 29(2), 279-288. Copyright [2004] by Elsevier Science & Technology Journals. Reprinted with permission.(Mitsuyasu et al., 2004)

Elsaidi et al (Elsaidi et al., 2004) added volar radiolunate ligaments into their sectioning sequence. They used arthroscopy for the resection of ligaments to minimize collateral

damage. Standard anteroposterior radiographs in static positions with a 30 lb traction load was used to measure carpal angles. He did not observe any significant change in diastasis or radiocarpal angles following palmar extrinsic ligament resection and complete SLIL resection. However, once the DIC was resected off the scaphoid, the scaphoid flexed. DISI developed only when DIC was resected from both the scaphoid and the lunate and DRC was resected off the lunate (Figure 23). Findings by both Elsaidi and Mitsuyasu confirm that, in sequential instability of the wrist, the scaphoid would be unstable early in the course, and is unmasked under load. However, Mitsuyasu and Elsaidi did not observe any kinematic changes until both SLIL and at least the DIC was resected off the scaphoid. This contrasts with previous studies (Padmore et al., 2019; Short et al., 1995; Short et al., 2002b, 2005).

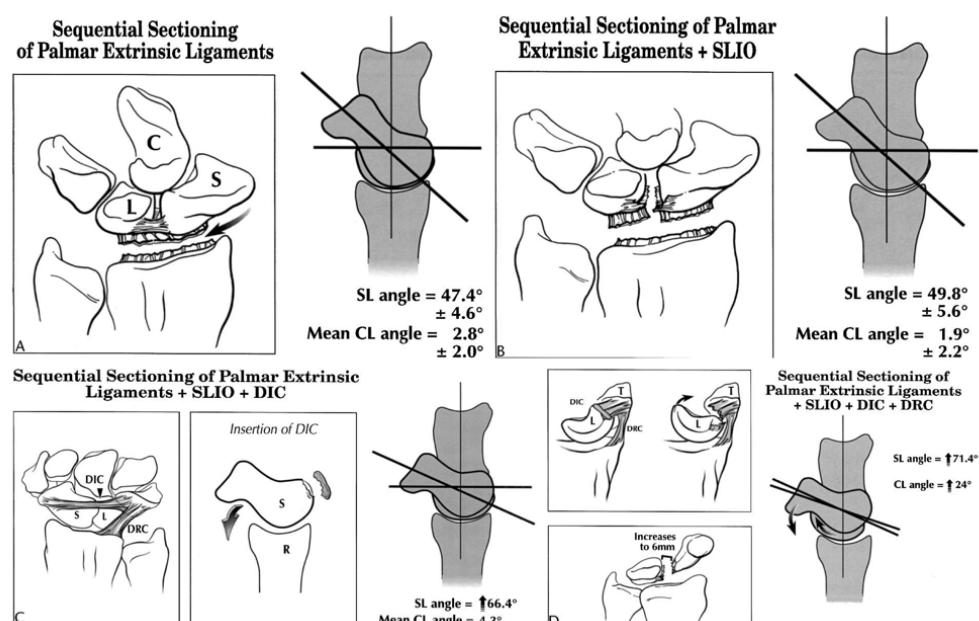


Figure 23 (A) Sectioning of the palmar extrinsic ligaments alone did not result in statistically significant change in radiographic parameters. (B) After sectioning of the palmar extrinsic ligaments and sequential sectioning of the components of the scapholunate interosseous ligament (SLIL), there was no significant change in scapholunate angle, capito-lunate angle, or scapholunate gap. (C) The addition of the release of the dorsal intercarpal (DIC) ligament and the dorsal capsule from the scaphoid resulted in rotatory subluxation of the scaphoid with an increase in the scapholunate angle. (D) Sectioning of the extrinsic ligaments, SLIL, DIC, and the dorsal radiocarpal ligament (DRC) from the lunate resulted in a static dorsal intercalated scapholunate instability collapse pattern. From "Dorsal wrist ligament insertions stabilize the scapholunate interval: cadaver study." by Elsaidi et al. (2004) *Clin Orthop Relat Res*(425), 152-157. Copyright [2004] by Wolters Kluwer Health, Inc. Reprinted with permission.

The studies that noted changes with isolated SLIL sectioning were based on optical marker and electromagnetic tracking during wrist motion that had a submillimeter and sub degree accuracy (Akhbari et al., 2019a; Short et al., 1995). Elsaidi and Mitsuyasu et al were based on radiographic parameters, which may have led to the difference in findings.

Perez et al. (Pérez et al., 2019) studied 30 cadaveric wrists and concluded none of the specimens developed DISI with isolated SLIL sectioning. Having randomised 30 wrists into 5 groups, he subjected each group to a sequence of ligament sectioning that included SLIL, LRL, STT, DIC (scaphoid insertion) and DIC (lunate insertion). Then he assessed the radiolunate angle (Figure 24), the scapholunate angle, the scapholunate gap and dorsal scaphoid translation in standard radiographic films under loading, simulating a clenched fist. Findings of Perez et al, Elsaidi et al, Mitsuyasu et al. and Short et el. taken together, confirm that DIC or DRC injury can worsen the scaphoid instability created by SLIL injury.

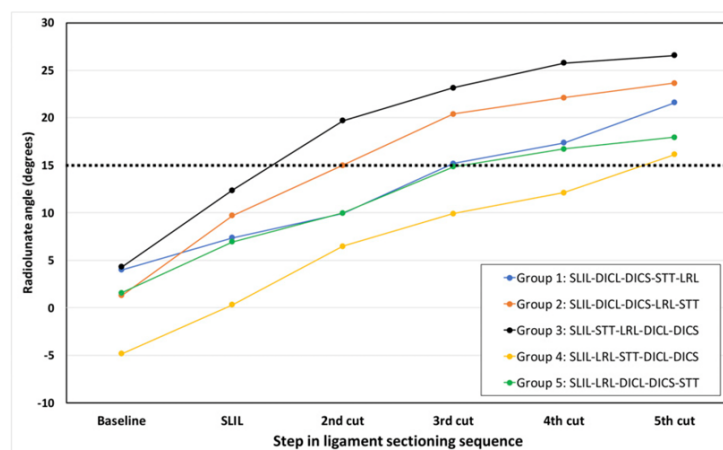


Figure 24 Mean radiolunate angles. The lines represent the 5 different groups (ligament section sequences), the x coordinate represents each step on the sequence, and the horizontal dotted line represents the IWIW limit for dorsal intercalated segment instability. From "Role of Ligament Stabilizers of the Proximal Carpal Row in Preventing Dorsal Intercalated Segment Instability: A Cadaveric Study." by Perez et al. (2019). *J Bone Joint Surg Am*, 101(15), 1388-1396. Copyright [2019] by Wolters Kluwer Health, Inc. Reprinted with permission. (Pérez et al., 2019)

Patterson et al.(Patterson et al., 2013) concluded that if the SLL is intact, the dorsal radiocarpal ligament and the DICL can be cut without altering SL kinematics in their study of 6 cadavers. Short et al.(Short et al., 2007) confirmed these findings, further reporting

sectioning of either one or both DIC and DRC would not cause significant scapholunate kinematic changes. Therefore, the current literature favours that DISI, or other kinematic changes are unlikely to occur with isolated DIC or DRC injury. Caveat to this argument however is, Short et al. (Short et al., 2002a) and Loisel (Loisel et al., 2021) reported that even with a dorsal approach to the wrist scaphoid and lunate kinematics were altered.

The importance of STT ligament is also difficult to assess with the existing literature. It is widely agreed STT ligament sectioning on its own would not result in any kinematic change in the scaphoid or the lunate (Short et al., 2005; Short et al., 2007). In one study, sectioning of STT after the SLIL ligament only increased the range through which scaphoid flexion was observed, during wrist flexion-extension, but did not affect the magnitude of scaphoid flexion, compared to isolated SLIL sectioning (Short et al., 2005). However, adding STT sectioning increased scaphoid flexion and lunate extension during wrist radioulnar deviation, indicating that the role of STT may differ with the type of wrist motion.

But a subsequent study by the same research group showed that sectioning STT with SLIL caused scaphoid flexion and lunate extension during flexion (Short et al., 2007). Interestingly cyclical loading created more angular changes, which were explained by the attenuation of intact ligaments with cyclical loading. Perez et al. noted that DISI was created when SLIL was compounded by sectioning LRL followed by STT. Interestingly, when the sequence is reversed, in the same study, to section SLIL, then STT and LRL, DISI was not observed. They consistently observed that the scapholunate angle increased with STT ligament sectioning.

Padmore et al (Padmore et al., 2019) noted that when the SLIL sectioning is compounded by STT and RSC the lunate extends during wrist flexion but it would not change the scaphoid posture. It appears that the STT ligament is an important stabilizer, but there is variability between studies and within studies on how STT sectioning would destabilise the scaphoid and the lunate. It has not been investigated whether importance of STT ligaments varies between lunate types or any other variable.

While radiocarpal angles during wrist motion appeared to change early in sequential instability, scapholunate diastasis was observed only after multiple ligaments were

sectioned (Meade et al., 2005; Mitsuyasu et al., 2004; Short et al., 2002b, 2005). Dunn et al. found no diastasis on radiographs while observing changes in radiocarpal angles (Dunn & Johnson, 2001). The scapholunate diastasis occurred only with SLIL sectioning plus both insertions of DIC resected and STT sectioned or when SLIL, DIC and either of LRL or STT were sectioned according to Perez (Pérez et al., 2019). This may be in part due to the low sensitivity of plain radiography to detect early changes in simulated SLI, even with loading.

Specifically studying translations of the carpals, Werner et al. reported that the scaphoid and the lunate translate radially with wrist ulnar deviation. The scaphoid translates volarly with the wrist flexion in the normal wrist and the lunate dorsally (Werner et al., 2011). Once the dorsal or volar ligaments sectioned with SLIL, the scaphoid translated radially and the lunate translated ulnarly, indicating the divergent directions of displacement, especially during wrist flexion and extension (Werner et al., 2005; Werner et al., 2011). However, Werner et al. concluded that the changes are exceedingly small in the range of 2 mm, these may not be discernible in clinical practice with standard radiography.

Importantly, additional cyclical loading of the carpus (Short et al., 2007) following ligament sectioning has consistently worsened scaphoid and lunate kinematics (Short et al., 2002b, 2005). The scaphoid flexion, ulnar deviation, lunate extension, scapholunate diastasis all have worsened in magnitude. There was an increase in the range of motion through which these changes occur, indicating that cyclic loading would unmask subtle changes by worsening them and by making them appear through a larger wrist motion arc.

#### **1.3.4. Computed tomography**

Invention of the CT scan enabled better appreciation of the 3D malalignment in scapholunate instability. In 1993, Viegas et al, studied the surface contours of carpal bones from CT scans to conduct 3-dimensional (3D) analysis (Viegas et al., 1993). They were able to create 3D rendered carpal bone models from CT scans, represent them graphically to visualise and rotate them to understand the 3D carpal morphology. They also quantified the lengths of inertial axes (principal axes of moment of inertia), the distances between carpal bones and volumes of carpal bones. The focus of their studies was to understand the 3D

anatomy and geometry of the carpus using CT (Patterson, Elder, et al., 1995; Patterson, Viegas, et al., 1995; Viegas et al., 1993).

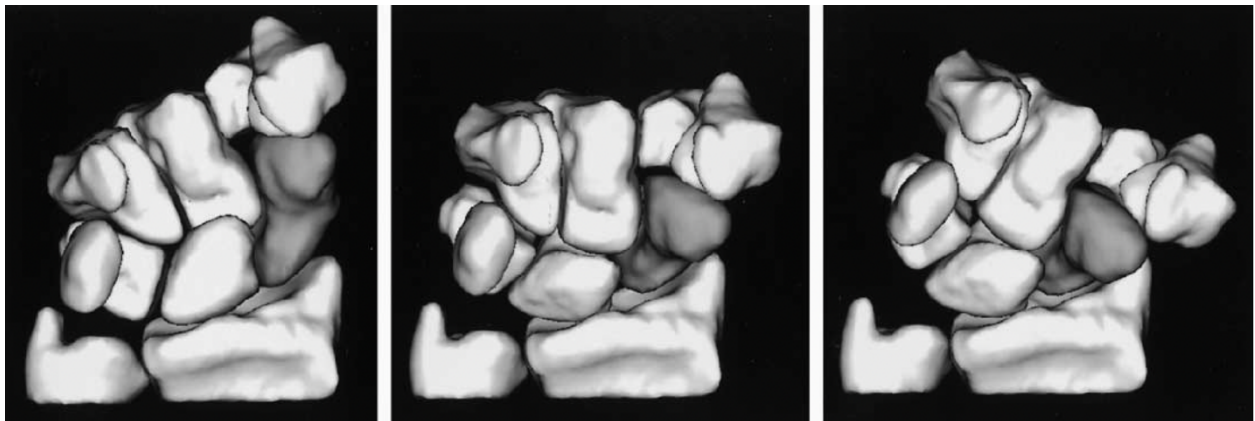
Using similar image segmentation and creation of 3D models of the scaphoid, the radius, and the lunate the researchers were able to compare the 3D malalignment of the SLI carpus to the normal (Omori et al., 2013). CT scans in various static wrist positions have been used to define the kinematic changes of the scaphoid and the lunate in the healthy wrist compared to SLI. The major advancement in this field occurred with Crisco et al. introducing marker-less 3D registration techniques for carpal bones using CT scans (Crisco et al., 1999; Crisco et al., 2001). In the proposed methodology Crisco et al. used CT scans with the pixel size of 0.2 X 0.8 and axial slice thickness of 1 mm conducted at various wrist positions. They created carpal bone segments or 3D surface contours of carpal bones from each CT using a technique similar to Patterson et al. (Patterson, Viegas, et al., 1995). They then used two approaches to calculate the carpal displacement. The 3D coordinates of the principal axes and centroid were matched between models and used to calculate the displacement field between carpal bone models in two wrist positions.

A custom registration algorithm by Pelizzari et al. was used to align the radius and the ulna (Pelizzari et al., 1991), because the radius and ulna were partially visualised and the principal axis would not be representative of the bone morphology. They also used the calculations published by Spoor et al. and Panjabi et al. to describe the helical axis of motion of the carpal bones (Panjabi & White, 1971; Spoor, 1984). Their accuracy was reported to be within 1 mm for linear displacements and 2° for angular displacements. Later another custom software was introduced for registration of carpal bones (Robb, 1985). Neu et al. compared all three registration techniques used in marker-less carpal kinematic studies, to assess the accuracy of quantifying carpal bone displacements and reported that the best rotational accuracy is within 0.5° for the scaphoid, lunate and the capitate and within 2° for other bones; The translational accuracy is within 1mm for all bones and 2 mm for the trapezium and the trapezoid (Neu et al., 2000).

Moojen et al. (Moojen et al., 2003) also studied carpal kinematics of the normal wrist using CT scans at various wrist positions (Figure 25) using a custom registration algorithm



published by Snel et al. (Snel et al., 2000). While the registration algorithms were different and customised for each study, the fundamental principles between them were similar, using segmented carpal bone models and a registration method to compute the displacement field between them in various wrist positions. The accuracy of Snel's algorithm was also reported to be similar to the accuracy reported in the study by Neu et al (Neu et al., 2000).



*Figure 25 An example of a wrist during ulnar–radial deviation. The palmar aspects of the carpal bones are shown. The scaphoid is presented in a different color. Using segmented carpal bone models and a custom registration algorithm Moojen computed the carpal displacement during wrist flexion-extension and radioulnar deviation. From “In vivo analysis of carpal kinematics and comparative review of the literature.” by Moojen et al. (2003) J Hand Surg Am, 28(1), 81-87. Copyright [2004] by Elsevier Science & Technology Journals. Reprinted with permission.*

In 1992, Paul J Besl (Besl & McKay, 1992), published on iterative closest point (ICP) algorithm for registration, in which a set of 3D volume points was registered by finding the best parameters, minimizing the sum of the distance from each 3D model point. Registration based on ICP algorithm for carpal kinematics has been validated and reported that errors are in the order of the voxel size of the acquired CT data ( $0.3 \times 0.3 \times 0.3 \text{ mm}^3$ ) (van de Giessen et al., 2009). Crisco et al. has used this technique and reported an angular error of  $0.3^\circ$  and a translation error of 0.9 mm. More recent publications have recommended the use of iterative closest point algorithm for carpal bones considering the uniformity of the results regardless of the bone shape (M. Beek et al., 2010). Over the years multiple researchers have used the ICP based registration for 3D CT, 4D CT, MRI and biplanar video radiography based carpal kinematics and also have validated reporting sub degree and

submillimeter accuracy (Abe et al., 2019; Akhbari et al., 2019a; Moritomo et al., 2003; Moritomo et al., 2004; Robinson et al., 2021; Wang et al., 2018; Zhao et al., 2015).

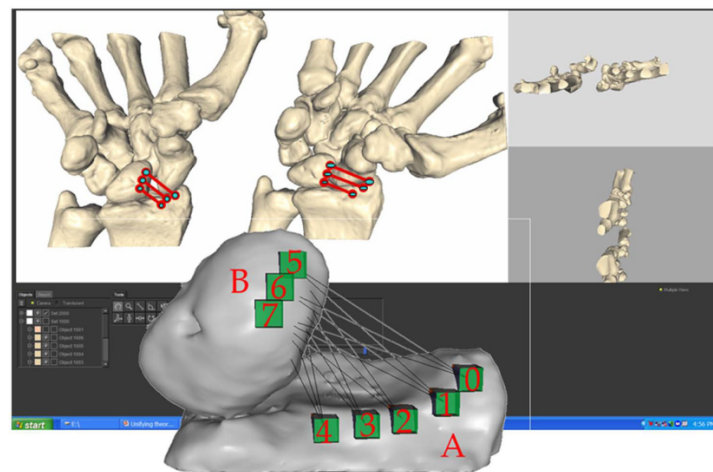
3D CT based 3D carpal models have also been used to measure SL ligament length and thereby, to predict the strain on SLIL with wrist motion and loading (Upal et al., 2006). These researchers indirectly measure the SL ligament length based on distance between SLIL footprint on the scaphoid and the lunate. Studying the length of the SLIL and its 3 components in wrist range of motion was a way to demonstrate the wrist positions where the SLIL is mostly at strain. Also, in the intact wrist this has shown that the 3 parts of SLIL function differently.

Upal et al. described that in the intact wrist from extension to flexion the palmar SLL lengthens and dSLL shortens (Upal et al., 2006). From wrist radial to ulnar deviation dSLL did not change but palmar SLL shortened. Tan et al. using a similar technique, demonstrated that during resisted ulnar deviation, the palmar subregion of the SLIL was significantly strained. During resisted radial deviation, the dorsal subregion of the SLIL was significantly strained. During DTM the ligaments did not have any length changes (Upal et al., 2006). This led to the idea that the 'DTM is safe' in post-surgical rehabilitation following SLI.

Chen et al. studied the length changes of SLIL at different wrist positions and forearm rotations without loading (Chen et al., 2015). The lengths of the palmar and proximal regions of SLIL increase substantially with full wrist extension with the mean percentage elongation being 43%, 36.8% 29.5%, respectively for distal, middle, and proximal portions of the palmar SLIL. However, the length of the dSLL did not change significantly. The clinical application would be that full wrist extension will place greater strain on the palmar SLIL and therefore should be avoided following injury or surgical stabilization.

Sandow et al. used a similar method to identify isometric points between the carpal bones using 3D CT during radioulnar deviation (Sandow, 2015; Sandow et al., 2014). While other researchers computed the length changes of SLIL (Upal et al., 2006), Sandow et al. utilised the same concept to predict where the intact ligament footprint would be, based on the concept of isometricity. He proposed, when the distance between two points on carpal

bones changes negligibly, that is because those two points are constrained by an intact ligament. According to this concept, He observed that there are distinct isometric connections between the radius and the lunate, the scaphoid and the lunate and the scaphoid and the trapezium (Figure 26). These isometric connections correspond to the LRL , dSLL and the STT ligaments, which was identified as three critical ligaments in SLI (Sandow & Fisher, 2020).



### **Lunate – Radius connection**

*Figure 26 . Example of a 3D wrist model, with the carpal bone segmented and measurement lines drawn between points on adjacent carpal bones in extremes of wrist motion. This example is of the assessment of isometricity on the volar aspect of the radius and lunate. From “Unifying model of carpal mechanics based on computationally derived isometric constraints and rules-based motion – the stable central column theory.” by Sandow et al., 2014 J Hand Surg Eur Vol, 39(4), 353-363. Copyright [2014] by SAGE Publications Ltd. Journals. Reprinted with permission.*

As described above, 3D imaging studies combined with marker-less registration techniques have been instrumental in kinematics in SLI. Nonetheless, the limitation is that it only allows a limited number of static positions to be studied and kinematics in between extrapolated (Best et al., 2019; Crisco et al., 2005). Therefore, true dynamic studies like dynamic CT or BVR have an advantage of understanding in vivo kinematics of the carpus during actual movement.

### **1.3.5. MRI**

MRI has been mainly important as a diagnostic tool, identifying the structural changes and pathoanatomy in SLI. MRI scans performed on static wrist positions have been used to

compute wrist kinematics (Goto et al., 2005; Moritomo et al., 2004, 2006). MRI scans conducted at the neutral wrist position and four extreme wrist positions (radial deviation, ulnar deviation, extension, and flexion) in healthy participants were studied. The initial post processing was similar to CT based studies involving carpal bone segmentation. The registration technique was based on the ICP algorithm and found to have rotational error rate of  $1.29^{\circ} \pm 1.03$  (Goto et al., 2005). There is also MRI evidence that during axial loading in the neutral wrist and the extended wrist, the palmar and proximal portion of the SLIL is strained (Lee et al., 2010). But the dorsal portion was not strained. The strain is calculated in this study as a function of length change. The limitation would be if the elastic properties of all three components are not equal length change cannot be extrapolated as a change in strain. If dorsal SLIL is less elastic than the palmer SLIL, under the same strain different length changes will occur.

More recently dynamic MRI has been used in carpal kinematic research. Scapho-trapezial motion and capito-triquetral distance has been quantified using dynamic MRI, although as observation by radiologists rather than a systematic automated method (Henrichon et al., 2020). While this is currently at the research stage it is an important development because an investigation without the risk of radiation for a dynamic study is highly advantageous. Radiation-less dynamic studies will be especially useful for patient subgroups like children or pregnant patients where even low dose radiation can be harmful.

#### **1.3.6. Biplanar video radiography**

Biplanar video radiography (BVR) is a good alternatives to static CT, because they combine the strengths of 3D CT with marker-less registration and representing true dynamic motion in vivo (Akhbari et al., 2021; R. Carr et al., 2019). BVR has previously been used as a low dose radiation method to study kinematics of other human joints such as knee (Miranda et al., 2013). BVR technology can capture high speed data (up to 1000 Hz) with a low radiation (e.g., 0.03 mSv/sec) for upper extremity studies. The possibility of studying functional activities of the wrist is an advantage. While the image acquisition occurs using two planar radiographic machines, the BVR software typically matches the carpal bone contours with

in-built models of the bones that are reconstructed from the CT images stored as grayscale volumes.

BVR has been proven to be accurate to define in vivo carpal kinematics. However, an inherent limitation is difficulty in tracking of carpal bones when they overlap (Akhbari et al., 2021). Other concerns with BVR are its limited availability and the time-consuming specialist post-processing assessment.

### **1.3.7. Dynamic computed tomography (4D CT)**

In the following section the history and technical aspects of dynamic CT is discussed.

#### **1.3.7.1. History of dynamic CT**

Computed tomography (CT) scanning has historically been a static imaging modality and has applicability in every anatomical region of human body. Use of static CT scans have been risen by a threefold between 1993- 2006 , to over a 70 million scans a year (Mettler Jr et al., 2008). In the recent years, CT scanning has advanced to image the dynamics of human physiology, such as joint movement and organ perfusion.

Introduction of dynamic CT scanning dates back to 1980s, with applications in cardiac medicine using the 'dynamic spatial reconstructor -DSR' (Ritman et al., 1980) and the Imatron electron beam scanner (Lipton et al., 1984). With the 28 x-ray tubes mounted in a semi-circle with opposing image intensifiers and video cameras, the DSR was a pioneer in dynamic imaging. It could image with longitudinal coverage of 24 cm with a 38 cm field of view. The DSR produced 60 frames per second using 28 views. Cost, radiation, and practicality were limitations.

The Imatron system used a different technique, substituting the X ray tube with an electron beam being swept across a large semicircular tungsten target array (Mather, 2013). This system could produce a temporal resolution of 50ms and covered 8 cm of anatomy with no

table motion for the first time. While these designs are not in current use, they pave the way to more sophisticated dynamic CT designs.

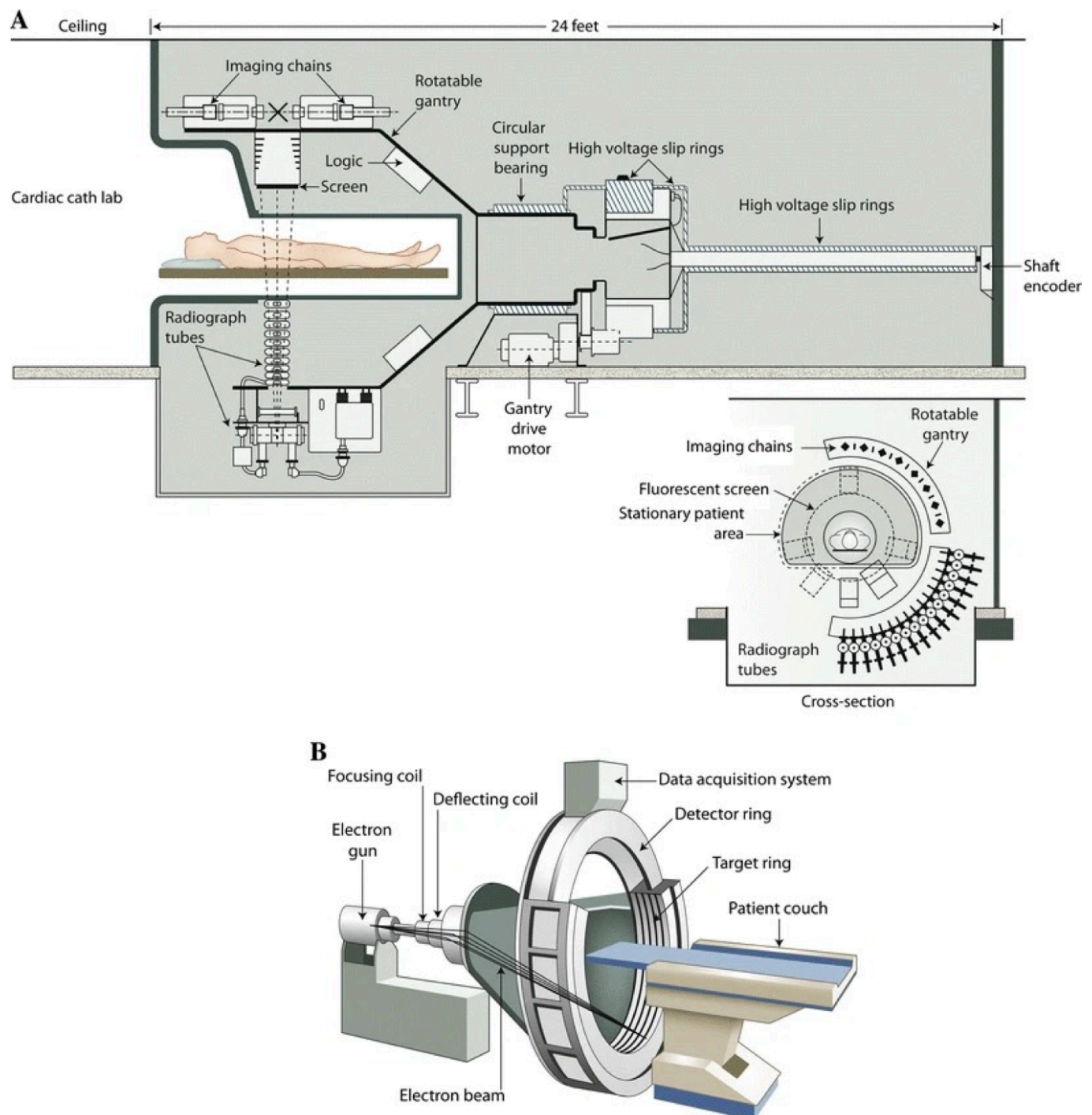


Figure 27 Early pioneers of dynamic imaging with CT. a The Dynamic Spatial Reconstructor (DSR) was built from 28 x-ray tubes and image intensifiers. b Imatron's electron beam scanner swept an electron beam across a large, semicircular tungsten target surrounding the patient. From "CT Dynamics: The Shift from Morphology to Function" by Mather, R, 2013, *Current Radiology Reports*, 1(1), 64-75. Copyright [2013] by Springer Nature BV. Reprinted with permission.

Among many techniques of dynamic CT scanning the currently accepted techniques is, acquiring images of dynamic motion by repeated scanning without table motion (Lipton et al., 1984). However, the craniocaudal distance that can be covered is a limitation, with most 64 row detector scanners can only cover about 5 cm of anatomy. There are other scanners that can cover 16 cm of longitudinal width (Ruíz et al., 2010). It is designed in a way that entire volume is scanned in one temporal phase (Ruíz et al., 2010).

While multiple static images can possibly be used to extrapolate the dynamic changes in joints, sudden changes in position which would be missed using a “stop-motion” technique (Bond & Berquist, 1991) . Earliest reports on 4D CT in the application of musculoskeletal medicine was on the knee and the patellar femoral joints using an electron beam scanner (Shapeero et al., 1988; Stanford et al., 1988).

#### **1.3.7.2. Use of dynamic CT to assess hand and wrist pathology.**

Fluoroscopy has a well-established role in hand and wrist conditions, unmasking instabilities that are not visible in static imaging (Bain et al., 1997). The limitation is the 2-dimensional nature of fluoroscopy which makes it difficult to assess overlapping structures. First reports on 4D CT on the wrists was in 2008 where researchers assessed feasibility of 4D CT in cadaveric wrist mounted on a motion device (Tay et al., 2008). They concluded that 4D is a feasible investigation for the wrist (Tay et al., 2007) but observed a linear relationship with the degree of image quality degradation and the speed of wrist motion.

Leng and colleagues in a subsequent publication concluded that carpal bones and joint spaces could be well delineated using 4D CT without motion blurring or banding artefacts at all time points (Leng et al., 2011). In addition, they reported that good quality images that would not compromise diagnostic confidence was achieved at a skin radiation dose of 33mGy. The technique had high spatial (0.6 mm) and temporal (75ms) resolution. While this scanner only had 3.8 cm longitudinal coverage, scanners with wider longitudinal coverage have been used later (Kalia et al., 2009). The first report on SLI using dynamic CT was published by Halpenny et al (Halpenny et al., 2012) using a 320-multidetector CT (a 320-

multidetector CT (320-MDCT) system (Aquilion ONE, Toshiba Medical Systems, Tochigi-ken, Japan) reporting they observed the scapholunate distance to increase up to 6mm in dynamic imaging while static images reported the distance to be normal.

Motion artefacts have been a concern in several other publications and the motion rate needed to minimise motion artefact has been extensively studied (Nakamura et al., 2009; Neo et al., 2013). Neo et al found that motion velocities do affect the spatial resolution mostly in the axial plane, and was reported to be 0.96mm at a velocity of 36mm/s (Neo et al., 2013). Banding artefacts (step ladder pattern artefacts that occur because of motion) occurred only in coronal plane and were however minimal even at that velocity.

4D CT enables kinematic assessment of active wrist motion, allowing for visualisation of slight bone positional changes with a high temporal and spatial resolution (Rauch et al., 2018). 4D CT scans are utilised as an alternative diagnostic modality, particularly for cases with inconclusive findings that may otherwise require invasive procedures such as wrist arthroscopy (Demehri et al., 2016). The utility of 4D CT in diagnosing scapholunate interosseous ligament injuries has already been published (Kakar et al., 2016).

Dynamic CT enables better diagnosis of hand and wrist pathology involving instability and impingement (Renee Carr et al., 2019; White et al., 2019). Demehri et al. first used dynamic CT in a comparative study between healthy and SLI wrists. He recommended when x rays are inclusive, dynamic CT can be used to diagnose SLI (Demehri et al., 2016). Other researchers concluded the 4D CT had excellent interobserver and intra observer reliability for diagnosing SLI using angular measurements for patients with SLI (Rauch et al., 2018).

Abou Arab et al. studied the SL diastasis in clenched fist and RUD comparing the normal and SLI. Their observation was that RUD shows better diagnostic value but both stress manoeuvres are effective in diagnosing SLD using 4D CT when distastes were considered the parameter (Abou Arab et al., 2018).

#### **1.3.7.3. Carpal motion quantification using dynamic CT.**

Until recently the diagnosis of carpal instabilities and pathologies was based on visual appreciation of the changes in carpal posture and subjective measurements (Garcia-Elias et



al., 2014). Quantification of carpal posture was an important concept as that would enable automated objective measures. Initial quantifications were based on multiplanar reconstructions (MPR) and manual or semiautomated measurements (Abou Arab et al., 2018; Demehri et al., 2016; Demehri et al., 2015; Rauch et al., 2018). While these studies have revealed important findings like dorsal scaphoid translation with wrist motion, they were not true 3-D studies and the findings were presented as individual patients and not correlated to the wrist motion (Teixeira et al., 2021). Later, Zhao et al validated a process of segmentation of carpal bones using 4D CT followed by quantification of carpal posture (Zhao et al., 2015).

Recently Dobbe et al. quantified accuracy and precision of the quantification process (Dobbe et al., 2019). Their technique is different from Zhao et al. as they only segmented one set of carpal bones from a 3D CT scan and used a registration technique to quantify carpal postures. This has the advantage of automation of the quantification process, compared to the method published by Zhao et al (Zhao et al., 2015). They did observe that their error rates are still sub degree and submillimeter, however scanner specifications, motion velocity and partial gantry rotations could affect the error rate (Dobbe et al., 2019).

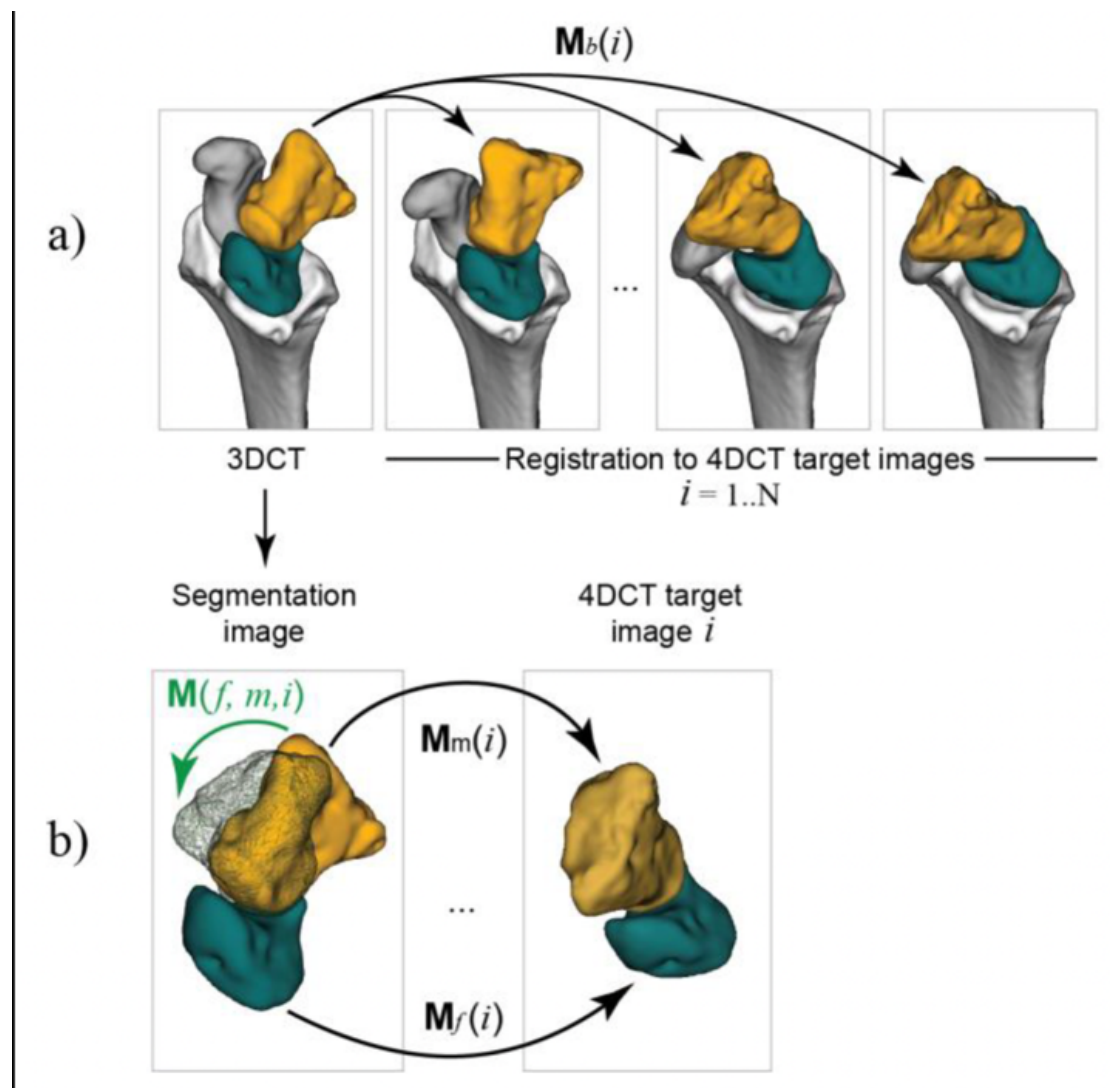


Figure 28 A high quality 3DCT image is used to segment the bones. An additional 4DCT scan containing 3D time frames is used for motion analysis. Each of the segmented bone objects is registered to the  $N$  time frames in the 4DCT scan. Registration results in a positioning matrix  $M_b(i)$  for each bone object  $b$  to a target image  $i$ . b) The moving bone  $m$  is shown in the same relative position with the fixed bone  $f$  (cyan) as in the segmentation image (orange) or as in the selected target image  $i$  (transparent) by repositioning  $m$  using matrix  $M(f, m, i)$ . From “Evaluation of a Quantitative Method for Carpal Motion Analysis Using Clinical 3-D and 4-D CT Protocols” by Dobbe et al, 2019, IEEE Trans Med Imaging, 38(4), 1048-1057. Copyright [2019] by The Institute of Electrical and Electronics Engineers, Incorporated (IEEE). Reprinted with permission.

#### 1.3.7.4. Techniques of quantification of carpal bone motion using 4D CT

Carpal bone segmentation of the wrist can be challenging due to the thin cortical bone, partial volume effects, and bone-to-bone proximity (Sebastian et al., 2003). It can be time consuming with some literature quoting 120 human hours for each thumb carpo-metacarpal

joint (Wang et al., 2018). Carpal bone segmentation and registration was previously validated in the wrist by Zhao et al. in 2015 (Zhao et al., 2015) and Mat Jais in 2014 (Mat Jais & Tay, 2017).

Iterative closest point (ICP) registration algorithm has been used and validated with an error rate less than a millimetre in both 3D CT and 4D CT data before. Using ICP registration for segmented carpal bones have yielded error rates less than 0.4 mm (M. Beek et al., 2010; van de Giessen et al., 2009). Tracking artificially inserted fiducial markers on a cadaver wrist, they have concluded that that mean fiducial localisation error was 0.054 (standard deviation: 0.018) mm, with a range of 0.023–0.139 mm. Mean rotational and translations errors after aggregating acquisition, segmentation, surface reconstruction, and registration errors are presented in Table 7.

*Table 7. Error rates for semiautomatic segmentation and ICP algorithm registration of carpal bones using 4D CT. Zhao et al 2014. Mean (SD) values for angular and translational errors of each bone. From “A technique for quantifying wrist motion using four-dimensional computed tomography: approach and validation.” by Zhao et al. (2015). J Biomech Eng, 137(7), 0745011-0745015. Copyright [2006] by American Society of Mechanical Engineers ASME. Reprinted with permission.*

Bone	Rotation (deg)			Translation (mm)		
	x	Y	Z	X	y	Z
Lunate	-0.002 (1.807)	-0.679 (1.150)	-0.538 (0.770)	-0.105 (0.282)	0.086 (0.201)	0.298 (0.380)
Radius	-0.137 (0.550)	0.314 (0.563)	-0.034 (0.334)	0.020 (0.106)	0.041 (0.103)	-0.132 (0.230)
Scaphoid	-0.224 (0.882)	0.400 (0.893)	0.046 (0.601)	-0.011 (0.127)	-0.020 (0.125)	0.038 (216)

#### 1.3.7.5. Radiation

There are several studies reporting on the radiation exposure of following 4D CT. The effective radiation dose (ERD) can be calculated by multiplying the dose length product (DLP) by a conversion factor of 0.0001, which is recommended for distal extremities (Biswas et al., 2009). Demehri et al. reported an effective radiation dose of 0.06 mSv ( $\pm 0.06$ ) for a wrist 4D

CT scan in a patient with SLI (Demehri et al., 2016). Carr et al. reported an effective radiation dose of 0.26 mSv per wrist 4D CT scan (R. Carr et al., 2019). Robinson et al. reported a DLP of 713.64 mGy-cm and a total skin dose of 0.067 Gy (Robinson et al., 2021). The threshold for skin erythema is considered 2Gy. The effective environmental radiation is for average person is considered 3mSv per year(Lin, 2010). The Table 8 provides the radiation doses of wrist 4D CT scans as reported by other researchers.

*Table 8 Dose length product and effective dose values for various 4DCT wrist motion studies. From “Evaluation of Four-Dimensional Computed Tomography as a Technique for Quantifying Carpal Motion.” by Robinson et al. (2021). Journal of Biomechanical Engineering, 143(6). Copyright [2021] by American Society of Mechanical Engineers ASME. Reprinted with permission.*

Study	DLP (mGy-cm)	Effective dose (mSv)	Total skin dose (Gy)
(Robinson et al., 2021)	713.64 total	0.013	0.067
(Zhao et al., 2015)	36 per scan	0.09	NA
(Leng et al., 2011)	NA	NA	0.2
(Garcia-Elias et al., 2014)	33	0.79	NA
(Troupis & Amis, 2013)	410.7 per scan	0.05 per scan, 0.18 total	NA
(Repse et al., 2015)	433.7	0.04 mSv	NA
(Demehri et al., 2015)	Patient 1: 378.3 Patient 2 (right): 63.9 Patient 2 (left): 64.5	Patient 1: 3026.4 Patient 2 (right): 671.8 Patient 2 (left): 685.6	Patient 1: 0.5 Patient 2 (right): 0.11 Patient 2 (left): 0.12
(Demehri et al., 2016)	Asymptomatic: 445.30 ± 122.04 Symptomatic: 606.46 ± 619.86	Asymptomatic: 0.06 ± 0.06 mSv Symptomatic: 0.05 ± 0.01 mSv	NA
(Edirisinghe et al., 2014)	NA	Did not exceed 0.15 mSv for three DTM	NA
(Shores et al., 2013)	84.3	NA	NA

*Note: The effective radiation dose (ERD) can be calculated by multiplying the dose length product(DLP) by a conversion factor of 0.0001, which is recommended for distal extremities (Biswas et al., 2009).NA: data not available.*

## 1.4. THE GAP IN THE LITERATURE

The literature review revealed that the dissociation between the scaphoid and the lunate can lead to carpal malalignment in scapholunate instability (SLI) (Crisco et al., 2003; Linscheid et al., 1972; Omori et al., 2013). The critical ligaments that are identified to be injured primarily or secondarily, are the scapholunate interosseous ligament (SLIL) (Short et al., 2005; Short et al., 2007) and dorsal intercarpal ligament (DIC) (Mitsuyasu et al., 2004; Raja et al., 2022b). It is also 'postulated' but not proven that dorsal radiocarpal ligament (DRC) and scapho-trapezio trapezoid ligament (STT) and volar carpal ligaments (long and short radiolunate ligaments) may be affected either primarily or secondarily. Therefore, the definite structural lesion that create SLI is an injury to SLIL, compounded by injury to one or more critical ligaments.

Hence, SLI has been identified as a spectrum of pathology (Garcia-Elias et al., 2006; Geissler, 2013; Messina et al., 2013). The hierarchy of pathology is based on carpal malalignment with the wrist in the neutral position. Correlation of the SLI spectrum to pathoanatomy or pathomechanics are based on subjective measures such as arthroscopy findings and reducibility of SL joint. The kinematic spectrum of scapholunate instability has not been considered in current classifications, prognostication, and surgical decision-making, partly due to lack of predefined objective, kinematic changes in SLI.

Extensive research has been conducted on normal wrists and SLI wrists in the neutral position. In vivo dynamic studies in SLI have primarily focused on improving diagnostic accuracy by examining the scapholunate diastasis and angle (Athlani et al., 2020). In vivo 3D kinematics of SLI during wrist motion is mostly described using static imaging modalities (Crisco et al., 2003) and dynamic cadaveric studies (Padmore et al., 2019; Short et al., 2005; Short et al., 2007). Therefore, in vivo kinematics in SLI has not been objectively described using true in vivo dynamic studies; Instead, extrapolated using static imaging and cadaveric ligament sectioning studies.

Clinical investigations and tools for diagnosis and surgical decision-making are static imaging modalities such as plain radiography, 3D CT, MRI with the arthroscopy being the gold standard (Dietrich et al., 2021). Unlike the large joints such as the shoulder or knee, clinical demonstration of carpal instability unique to each carpal bone is difficult due to complex anatomy of the wrist. Sensitivity and specificity of clinical signs of SLI are low (Easterling & Wolfe, 1994). Therefore, clinical features of instability do not form a major part of surgical decision making.

There is a myriad of surgical options for SLI. Some are based on restoration of scapholunate axis of rotation (Rosenwasser et al., 1997; Yao et al., 2016). However, a 3D CT based study has reported that axis of rotation of the scaphoid relative to lunate is highly variable (Best et al., 2019). While the knowledge of the rotation axis of the scaphoid and the lunate are important in surgical reconstruction there were no in-vivo studies on the rotation axis (helical axis of motion-HAM) of the scaphoid and the lunate in SLI compared to the normal wrist.

Once established it is known that SLI leads to degenerative arthritis of the wrist known as scapholunate advanced collapse (SLAC wrist) (Watson et al., 1997). However, it is not known whether every case leads to the same outcome. While it can be extrapolated that the kinematic changes may predict the outcome, the specific kinematic changes or their correlation to long term outcome is not known.

It was also evident that, the clinical outcomes following surgical management of SLI are suboptimum (Daly et al., 2020). The above gaps in the knowledge are likely have contributed the 'less-than ideal' outcome for SLI patients. The potential reasons for suboptimum outcome are,

- 1) Diagnostic

- a) Current diagnostic methods still use 2D angles and diastasis that has been described for planar radiography. SLI is a 3D carpal malalignment.
- b) Diagnosis and surgical decisions in SLI are based on demonstration of a structural ligament injury. Functional assessments and objective

measurements of instability do not comprise a major part of the assessment.

- c) Midcarpal kinematics in SLI is poorly understood.
- d) The spectrum of SLI is identified based on subjective parameters.

## 2) Therapeutic

- a) The aim of reconstruction is mainly to restore the 'alignment' in the neutral position.
- b) Scaphoid and lunate rotation axis and its implications in reconstruction surgery not clearly defined.
- c) The 3D kinematics of the SLI wrist in vivo and the normal wrist is not clearly understood. Hence, most current designs of reconstruction techniques aim to address 'pathoanatomy', not 'pathomechanics'.

The above gaps in the knowledge have been identified following the literature review.

Dynamic CT provides a unique advantage enabling objective measurement of the kinematics of SLI (R. Carr et al., 2019; White et al., 2019). This advantage is especially important to understand the in vivo kinematic changes that occur in the SLI wrist compared to the normal. It is expected that understanding of the 3D kinematic changes may help improving diagnosis. It is also expected that understanding the in vivo kinematic changes in SLI may facilitate surgical decision making, surgical technique design and prognostication.

Therefore, the aim of this thesis is to study the 3-dimensional kinematics of the SLI wrist compared to the healthy wrist. Thesis primarily aims to define the radiocarpal and midcarpal kinematic changes in SLI. The kinematic changes that have been identified in this thesis, may be important in objective diagnosis of SLI, classifying SLI based on pathomechanics and predicting the prognosis. More importantly, it is expected that the outcome measures considered in this thesis will help diagnosing a 'kinematically abnormal wrist' as opposed to a 'structurally abnormal wrist'. Moreover, it is expected that objective

identification of 3D patho-kinematics may help choosing and designing reconstruction techniques.



## **CHAPTER 02**

### **2. RESEARCH METHODOLOGY**

Following the literature review and identifying the knowledge gaps in literature, the research questions were developed.

#### **2.1. Research questions**

1. What are the measurable in vivo 3D kinematic changes that occur in SLI wrist compared to the healthy wrist, that potentially help
  - a. Diagnosis?
  - b. Classify SLI based on pathomechanics?
  - c. Understand the prognosis?
  - d. Surgical decision-making?
  - e. Selecting reconstruction techniques?

## **2.2. Aims and Objectives**

**The aim of the project was** to study the 3-dimensional (3D) kinematics of the carpus in SLI compared to the healthy wrist using dynamic CT.

To address the aim of the thesis, 3 objectives were defined.

Study the in vivo 3D kinematics of the SLI and normal wrist using dynamic 4D CT scans, and specifically assess the

1. Radiocarpal kinematics
2. Midcarpal kinematics
3. Helical axis of motion (HAM) of the scaphoid and the lunate during ulnar to radial deviation and extension to flexion in the SLI wrist, compared to the normal wrist.

**\*\*\*Three studies were designed to address the objectives.**

## **2.3. Methodology**

The methodology is arranged in sections; The first section describes the fundamental methodological concepts of the entire project. These include the participant selection, ethical considerations, the data collection (CT scanning procedure), the data storage and initial post processing concepts up to generation of 'materials' for the entire project. This first section is common to all three studies that were done for this thesis.

The second section is subdivided into 03 distinct studies conducted using the material generated as described in the first section. Each study was designed to answer a research question, has unique steps in methodology and distinct objective outcome measures.

### **2.3.1. Participant selection**

#### ***Scapholunate instability wrists***

All patients with SLI were identified from the database maintained at the Department of Orthopaedic Surgery at the Flinders Medical Centre (IRB number HREC/19/SAC/150-Appendix 1.6.1). Patients were assessed against the inclusion and exclusion criteria listed in Table 9. All patients with any stage of non-arthritis SLI, confirmed by arthroscopy performed by a fellowship-qualified upper limb surgeon, were included. Exclusion criteria were dynamic scans of patients under 18 years of age, pregnant patients, and patients with arthroscopic evidence of degenerative changes. Patients with concurrent fractures in the carpal bones or the distal radius were also excluded. Nineteen patients met the inclusion criteria.

*Table 9 Inclusion and exclusion criteria for selecting dynamic CT scans of scapholunate instability patients from the FMC database.*

<b>Inclusion criteria (SLI)</b>
1. Patients with symptomatic scapholunate instability (SLI) requiring operative management and diagnosis confirmed by wrist arthroscopy and has had 4D CT scan of the affected wrist prior to
<b>Exclusion criteria</b>
1. Degenerative changes observed in imaging or arthroscopy
2. Pregnant patients
3. Patients under the age of 18 years
4. Patients with distal radius or carpal bone fractures
5. Poor quality CT scans (E.g., Inadequate visibility of the radius throughout the scan)

### *Normal wrist*

The data for the healthy participants were obtained from Monash University, archived for a previous research project. Nineteen consecutive normal right wrist scans (n=19) were identified from the database maintained at the Monash Health Radiology Department. These scans were performed on healthy volunteer participants between the ages of 18 and 30 years, with no pre-existing wrist pathology. The data has been archived and anonymized, without demographic details, to comply with the ethics agreement. Therefore, case matching was not performed as demographic data was unavailable for the normal samples.

Poor-quality CT scans were retrospectively excluded from both groups. The criteria for poor quality were the radius being invisible for less than 1 cm at any point during the dynamic scan and scans with motion artefacts. Anatomical features of the radius, such as the radial styloid, distal articular surface, and ulnar border, were essential for understanding the

position of the radius. The radius was the reference bone for the study. Therefore, scans in which the radius was not adequately visualized were excluded.

### **2.3.2. Power calculation**

At the commencement of this project there were no comparative in vivo dynamic studies between normal and SLI wrists, that were available to guide a power calculation for the outcome measures that were planned to be addressed. Therefore, the sample size of 19 for every outcome measure was determined by the availability of data. The confidence intervals for the mean were included where comparisons were made, to support the reliability of conclusions drawn. While mean was used as the central tendency for normally distributed data. Median and interquartile ranges were presented when data were non-normally distributed. A post-hoc power analysis was not specifically conducted as there is evidence that the confidence intervals better inform about the conclusions drawn and post -hoc analysis are inferior to this (Levine & Ensom, 2001) (Further discussed in the discussion 4.7).

### **2.3.3. Ethical considerations**

Monash Health Radiology Department had archived data collected for a previous research project under institutional review board number RES-21-0000-266XL for study 14104B. The data were anonymized. A collaboration between Monash Health and Southern Adelaide Local Health Network (SALHN) enabled the transfer of dynamic CT data under the data transfer agreement (Appendix 1.6.6) These patients were incorporated as the control group of normal/healthy wrists.

Ethics approval for the patient database maintained at the Department of Orthopaedic Surgery at the Flinders Medical Centre was granted by the Southern Adelaide Local Health Network Human Resource Ethics Committee (SALHN HREC). The maintenance of a prospective database of all patients who underwent dynamic CT scanning (4D CT) was approved under the institutional review board number IRB number HREC/19/SAC/150 (Appendix 1.6.1).

The overall project for the quantification of carpal bone motion, incorporating the selected patients from the FMC database and healthy participants from Monash Health, was approved under IRB number HREC/20/SAC/7 (Appendix 1.6.4).

#### **2.3.4. CT scanning**

The CT scans of healthy participants and the SLI patients were done at different institutions. It was due to the healthy participant data being obtained as secondary data from a different institution (Monash Health) that had a different scanner. Although the scanning method was different, the data storage followed the standard DICOM protocol. Post processing and final assessment followed the same protocol described below.

CT scanning for both normal wrists and SLI patients followed the protocol previously published (R. Carr et al., 2019). Informed written consent was obtained from all participants. The CT scans were performed by a dedicated CT radiographer, under the supervision of a consultant radiologist. The radiographer positioned and directed the patient. Prior to the scanning procedure, participants were shown wrist motion sequences and asked to perform trial radioulnar deviation and flexion-extension sequences. They were instructed to keep the forearm still while performing wrist movements. Special dynamic movements such as the Dart thrower's motion and pronation-supination were only conducted in patients with wrist pathology relevant to clinical reasons. No restrictive devices or motion guiding devices were used to assist with wrist motion.

The patient was positioned standing beside the scanner table (Figure 29) with the carpus centred within the scan volume. A rubber rectangular block was provided to support the forearm for comfort and to minimize forearm motion. The scanning protocol involved moving the wrist from a neutral position to ulnar deviation, then to radial deviation, and back to neutral. During flexion and extension, patients moved the wrist from neutral to extension, then to flexion, and back to neutral.



*Figure 29 dynamic CT scan being performed on a patient with scapholunate instability. The patient is standing by the side of the scanner, with the wrist positioned within the gantry. The forearm is supported on rubber blocks for comfort and stability. Note that the radiographer or the clinician were not present in the scanner chamber during radiation exposure, images were taken prior to exposure. Copyright [2018] Prof Gregory Bain. Reprinted with permission.*

### ***Healthy participants***

The scanner used for scanning healthy participants was Toshiba Aquilion One Vision "320 slice" scanner (Toshiba, Tochigi, Japan). The table was centred at the +70 mm position. The volume range was set to 140 mm. The wrist was imaged 70 mm proximally and distally to the distal radioulnar joint (DRUJ). The slice thickness was set to 0.5 mm. The settings were 80 kV tube voltage, 0.275 seconds gantry rotation time, 50 mA current, and continuous X-ray. Each motion sequence occurred over 6-8 seconds. The radiographer monitoring the patient movements allowed the scan to be stopped and started on demand as each movement was completed.

### *SLI patients*

The scanner used was the Siemens Somatom Force scanner, which has a spatial resolution of 0.21 mm and a temporal resolution of up to 66 mS-1. The wrist was placed in the CT scanner gantry. A scout image was performed to centre the carpus in the gantry as the gantry width of this scanner is only 5.7 cm. Settings were 80 kV tube voltage, 0.25 seconds gantry rotation time, 50 mA current, and continuous X-ray. Each motion sequence occurred over 6-8 seconds. Images were acquired with an axial slice thickness of 0.4 mm, at 4 frames per second. The radiographer monitoring the patient movements allowed the scan to be stopped and started on demand as each movement was completed.

#### **2.3.5. Data archiving**

Healthy participants' data from Monash University were archived as thin slices with a slice thickness of 0.5 mm. The spatial resolution of the archived images was 0.8 mm. The SLI patients' data from the Flinders Medical Centre database were archived as raw data in Digital Imaging and Communications in Medicine (DICOM) format on external hard drives. All data were saved onto password-protected external hard drives.

Healthy participant scans had a voxel size of 0.82 x 0.82 x 0.5 mm. Voxel size represent the pixel size of the axial image (0.82 mm\*0.82 mm) and the slice thickness (0.5mm). SLI patients' scans had a voxel size of 0.21 x 0.21 x 0.4 mm (Figure 30). This resolution was sufficient for capturing the anatomical area of interest without significant noise. The scanning area was able to capture the carpal bones, proximal metacarpals, distal radius, and ulna.



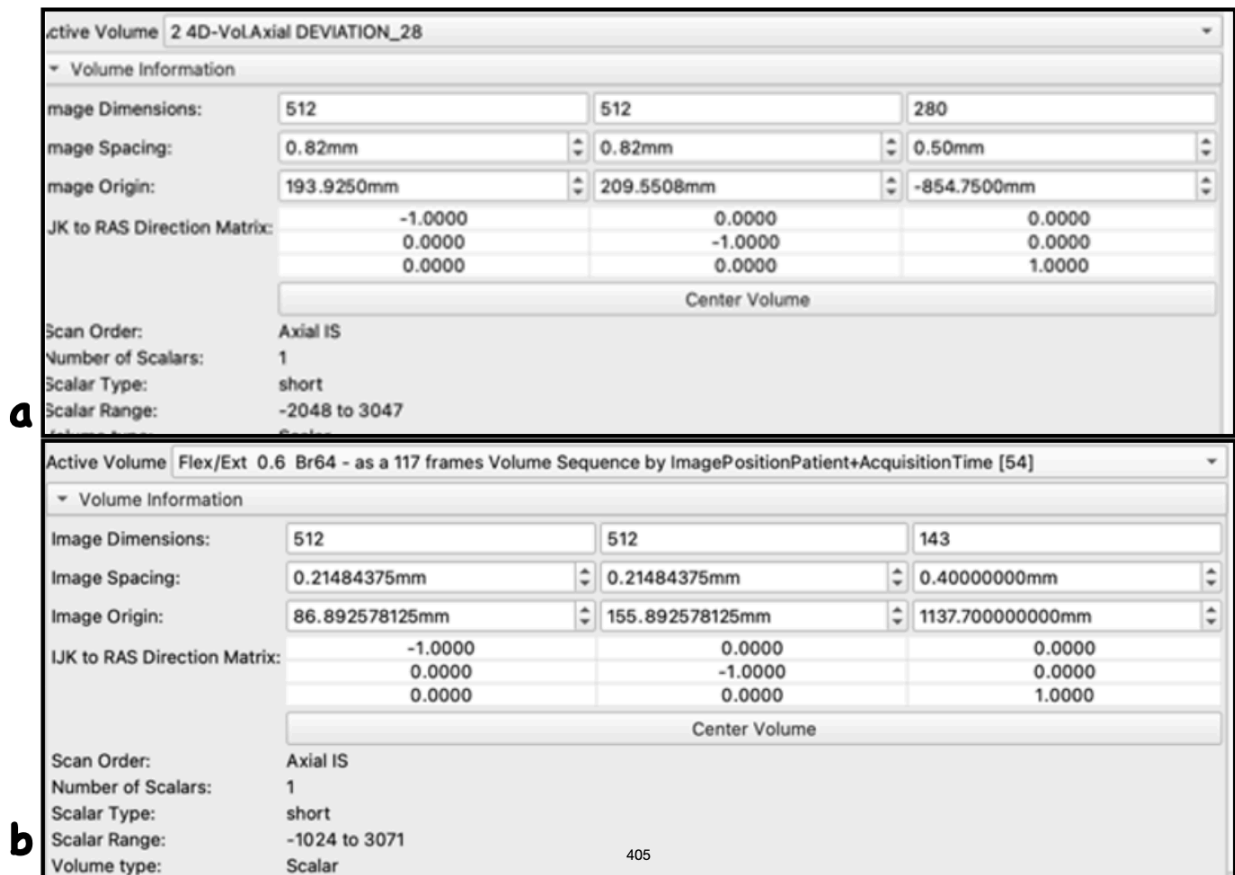


Figure 30 CT volume data indicating the spatial resolution and voxel size a. CT scan of a healthy participant (Toshiba Aquilion One Vision “320slice” scanner) b. CT scan of an SLI patient (Siemens Somatom Force scanner)

### 2.3.6. Radiation exposure

The total exposure time for each motion sequence varied between 6s and 8s. The total duration of the scan was determined by the clinical requirement for additional sequences. The effective radiation dose has been quantified as 0.231 mSv. This radiation data was prospectively collected at our institution using the method described by Biswas et al (Biswas et al., 2009). The calculated effective dosage is equivalent to 2 to 3 times of the effective radiation dose of a chest X ray (Mettler et al., 2008).

### 2.3.7. Data management

Post-processing for healthy and SLI wrists was conducted according to the protocol presented in Figure 31. Raw data from healthy wrists and SLI patients were transferred to an

open-source software, 3D Slicer (<http://www.slicer.org>) (Fedorov et al., 2012) for analysis. The DICOM data were converted to discrete 3D volumes for each acquisition time point. Each 3-dimensional (3D) volume (frame) was separately segmented to generate surface-rendered meshes in stereolithography (STL) format for each carpal bone. Further details are provided in the section " 2.3.8 Segmentation and Mesh Generation".

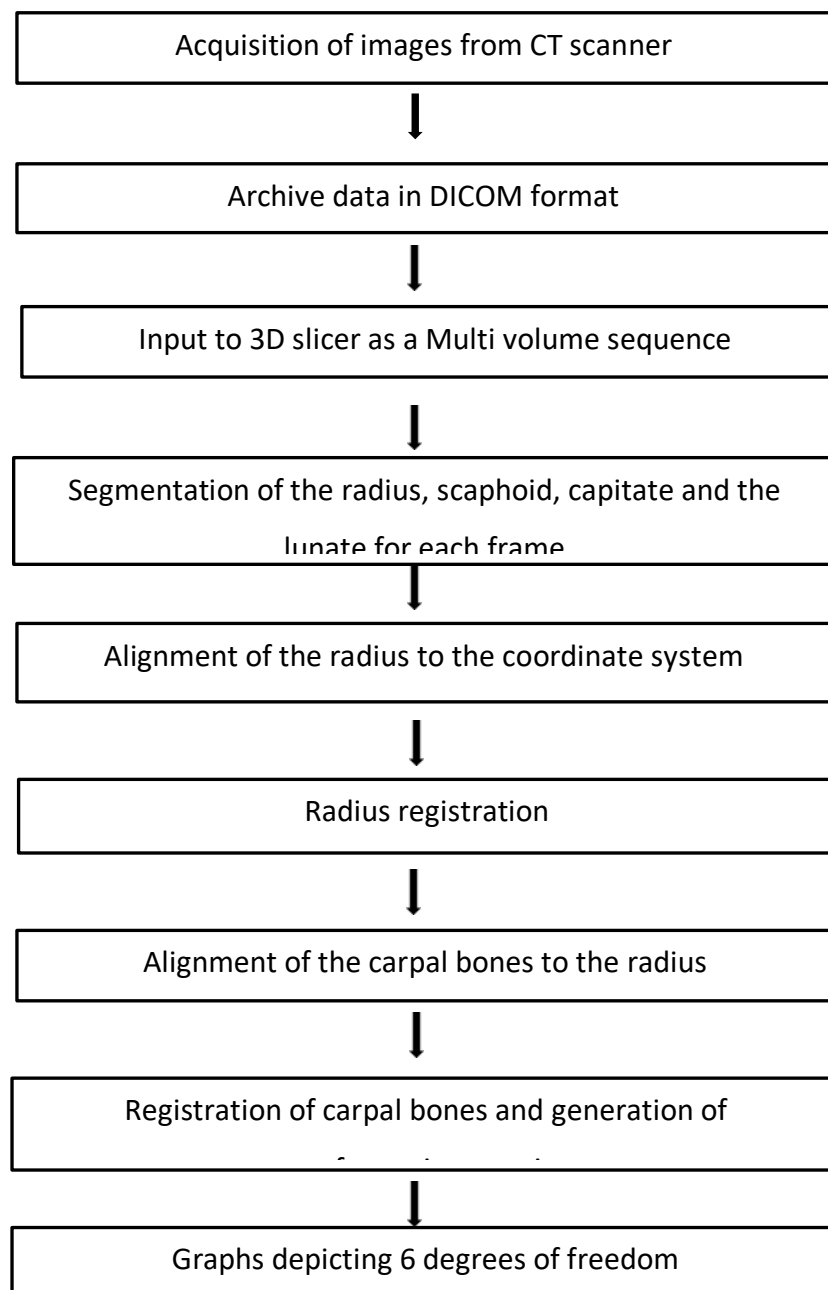


Figure 31 Flow chart on the CT scanning and post processing steps

### 2.3.8. Segmentation and mesh generation

First the neutral position of the wrist was identified as the wrist position where the longitudinal axis of the capitate (Lee et al., 2018) was aligned with the longitudinal axis of the radius. Two motion sequences were obtained. These were from maximum ulnar deviation to radial deviation and maximum extension to flexion. Images were saved as anonymized “.nrrd” (nearly raw raster data) files. The “.nrrd” is a file format that enable visualisation and processing of scientific imaging. They can be accessed using most medical image processing software like ‘3D slicer’, ‘Matlab Rb2022’ and ‘Image J’. The difference between the DICOM images and “.nrrd” is that DICOM format contains multiple images (thousands) per each 3D volume, whereas “.nrrd” is saved as a single file. In a single file, the 4D CT data is stored as a series of ‘frames’ with each frame representing a single 3D volume. When the “.nrrd” file is opened on the 3D slicer software, it can be played like a movie as the wrist moves, and each frame of the movie being a 3D volume (Figure 32). Also, “.nrrd” files do not contain any patient identifiers, whereas DICOM can contain patient identifiers as metadata. Using the saved “.nrrd” files, individual carpal bones were segmented semi-automatically from each frame using the segment editor module of the 3D slicer software (Fedorov et al., 2012)(Figure 32).

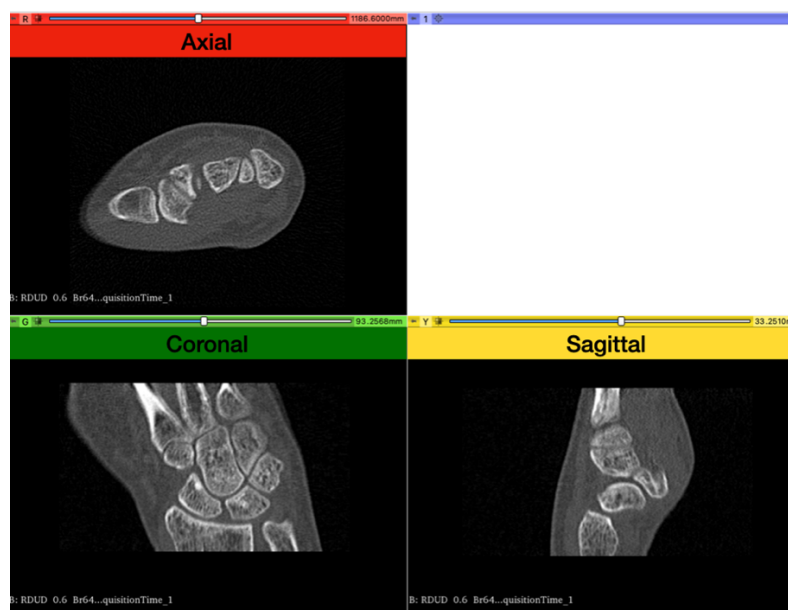


Figure 32. A single frame (3D volume) of raw data loaded onto 3d slicer. Each window shows the axial (red) coronal (green) and sagittal (yellow) sections of a single 3D volume. A single frame for each time point are generated.

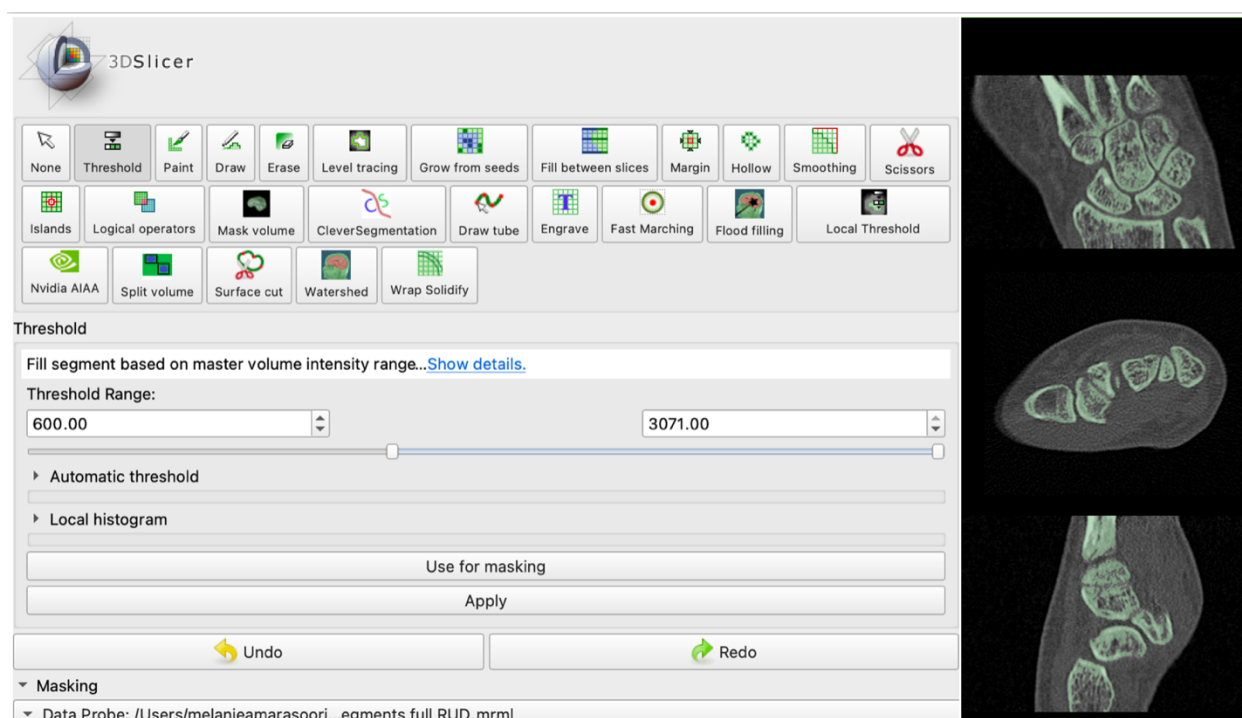
Raw CT data is comprised of 2-dimensional (2D) slices of grey scale images, each slice with 0.5 mm of depth, stacked on one another. Each slice has a regular number of pixels arranged in a regular pattern. Each 3D unit volume element is named a voxel and represented by a pixel and the slice thickness. The amount of data stored in this format for each CT is massive. With a dynamic CT, it is similar to obtaining one 3D CT scan/ volume for each time point as the patient moves the wrist. Therefore, considering the motions of ulnar to radial deviation, extension to flexion and other clinically relevant provocative manoeuvres, the amount of data is in the range of 30-40 GB per wrist.

Converting above data into a more manageable, visually recognizable, and quantifiable version was the first step. There are two methods in post-processing raw CT data, namely, 'volume rendering', and 'surface rendering'. Volume rendering is a process of converting this massive amount of data into a visually appealing and manageable image. It enables displaying a 2D projection of the 3D data, as seen from a camera angle. The process considers the camera angle and create the surface characteristics. Volume rendering is essentially a process for visualisation of data. Once the volume rendered images are saved onto a PACS (picture archiving and communication system), there is no real 3D data stored, but an image or a video file. More importantly, volume rendering does not allow to separate out carpal bones in a way that each carpal bone motion can be quantified independent of others.

Surface rendering is a process where the surface of the visualised structure is extracted as a point cloud with each point defined by its anatomical co-ordinates. The vertices are joined with faces in between which helps create a 'surface rendered model' for each carpal bone. The surface characteristic and colours of the original bones are not considered in this process. This enables the data to be more manageable and converted to a 'mathematic-friendly' format. It is stored as a point cloud of vertices and faces representing each individual carpal bone. The process of extracting the surface contour of the carpal bone and creating a surface rendered model is called 'segmentation'. Segmentation is an important post processing step in the methodology of this study and is validated and used with dynamic CT (4D CT) (Zhao et al., 2015).

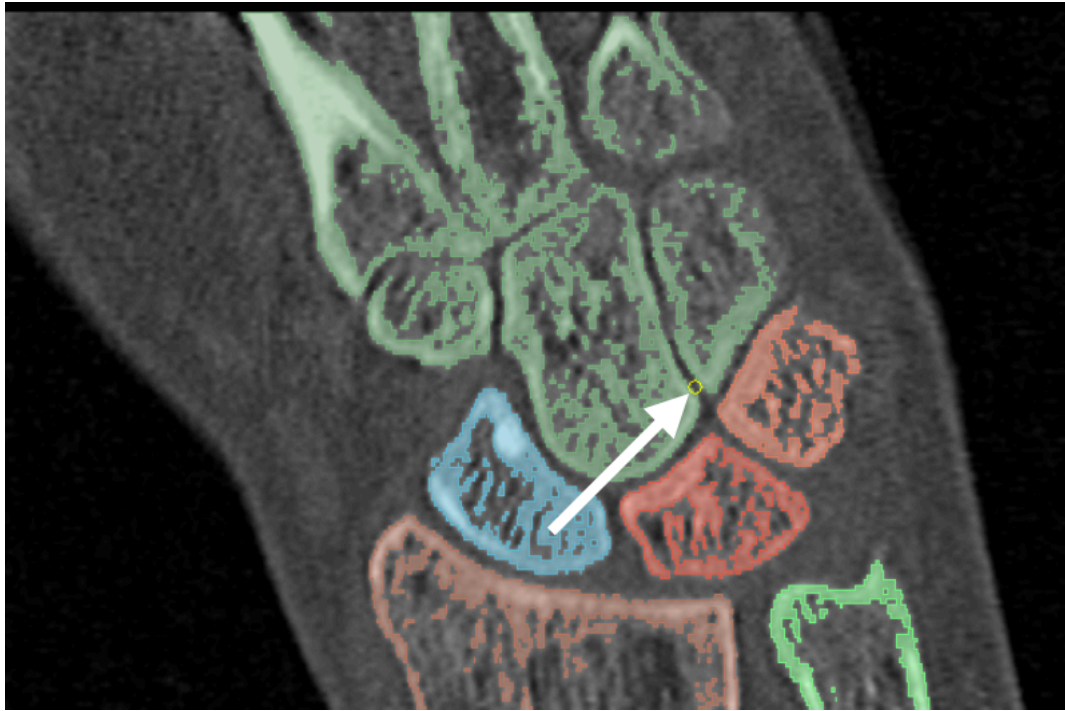
During the process of segmentation and assessment of the motion of the carpal bones, the scaphoid and lunate were both assessed in the normal and SLI wrist. The radius was also segmented as the reference bone and the capitate was segmented to be used as the indicator of the wrist motion. For the ease of explanation in this methods section, the description will be for the normal scaphoid, however the same methods were used for the lunate, radius, capitate and the SLI wrist.

To segment carpal bones from a 4D CT scan, a threshold of 600HU was applied to each CT frame consistently (Figure 33) (James et al., 1992; Weeks et al., 1985). This would eliminate most of the soft tissue from the segment and retain the carpal bones. Then a splitting algorithm was applied to define and separate the contours of the carpal bones (Kichenassamy et al., 1995).



*Figure 33 A threshold of 600 HU was used to define carpal bones in this example. This has excluded most of the soft tissue from the data field.*

In some cases where the carpal bones were inadequately separated, manual editing was required to erase the merged boundaries, using 3D eraser tool set at 1 mm (Figure 34) (minimum possible) level (Weidert et al., 2020).



*Figure 34 Manual editing using 1 mm eraser tool may be necessary to separate carpal bones as seen in this example (the 1 mm eraser tip between the capitate and the hamate indicated by the white arrow)*

Once bony contour is defined and inside of the contour is solidified, the image was converted into a surface rendered model and saved as a stereolithography (.STL) file (Figure 35 and Figure 36). A set of STL files were generated for scaphoid, lunate, capitate, and the radius for each frame resulting in series of carpal bone models pertaining to each frame or the time point representing the wrist position (Figure 37).

A stereolithography file (STL file) retains the spatial positional data as a point cloud of vertices with their spatial co-ordinates preserved. The segments were saved consistently with the name of the bone of interest followed by the frame number in two-digit format (e.g., Scaphoid 01, Capitate 04) in a folder specifying the patient index number and motion type). e.g., N01-RUD (Normal participant 01- Radioulnar deviation). The terms 'carpal bone segment', 'mesh' or 'model' is used interchangeably in this thesis to mean the generated surface rendered model of each carpal bone.

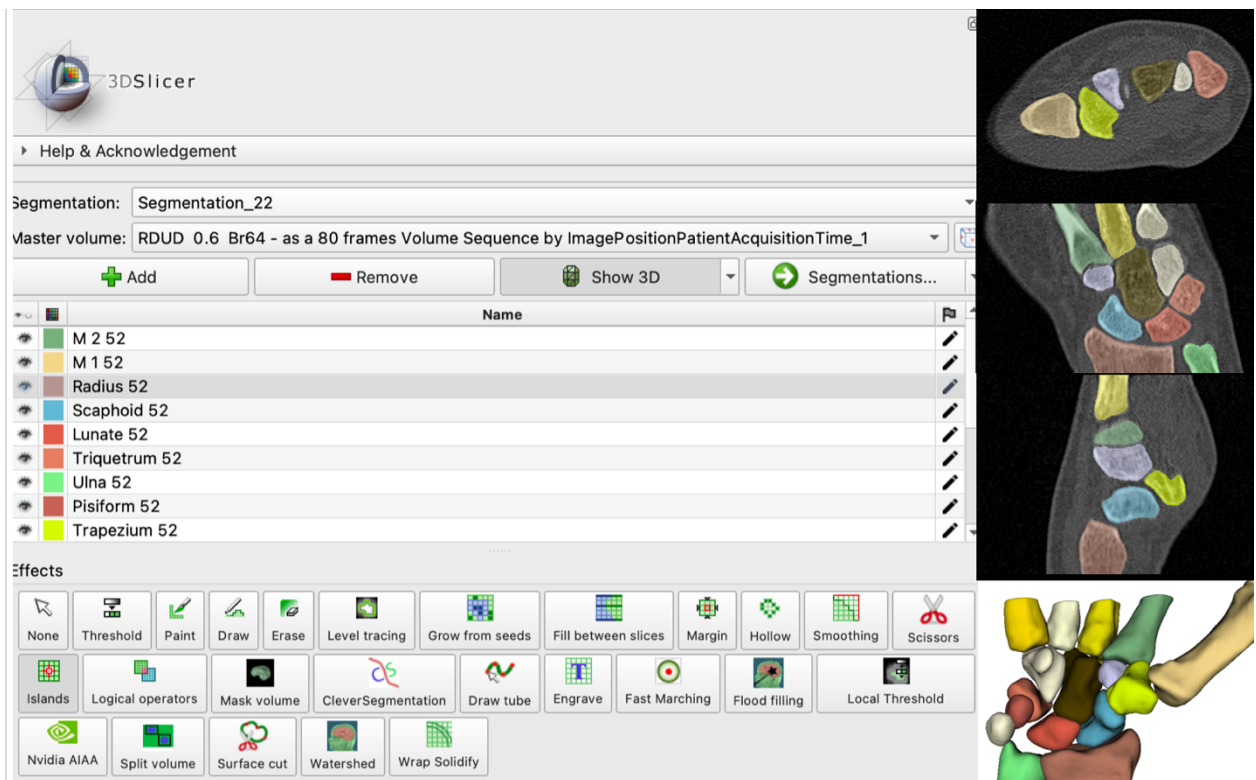


Figure 35 The complete segmentation of a single frame. The process involves separately identifying and segmenting carpal bones and solidifying them. They are then saved as stereolithography files with consistent labelling.

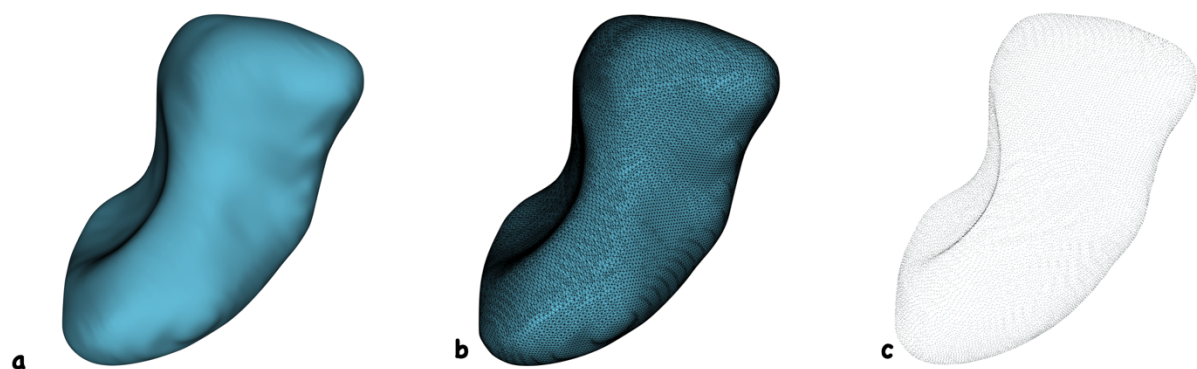
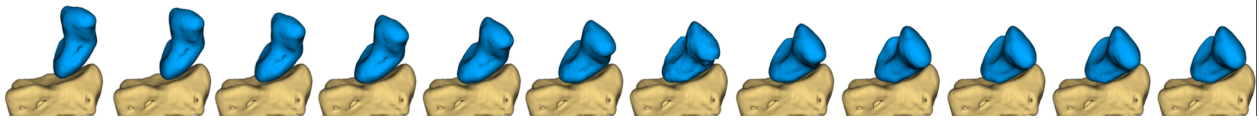


Figure 36 Graphic representation of a 3D mesh (model) of the scaphoid. a. The surface representation b. The 3-D mesh with vertices and triangles c. The point cloud representation of the mesh. Each point represents a vertex which preserves the spatial data of the x, y and z co-ordinates of its spatial position.





*Figure 37 Scaphoid positions during wrist ulnar to radial deviation, with its relation to the radius. The scaphoid is segmented in each time point and saved as a 3-dimensional mesh in the stereolithography (STL) format. The image shows the relationship of the scaphoid to the radius. Every 4<sup>th</sup> consecutive frame/ time point is depicted.*

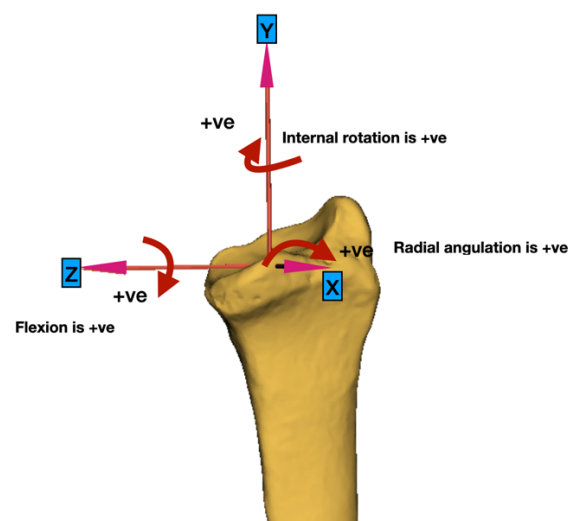
### **2.3.9. Coordinate system**

The radius was defined as the reference bone. The radius coordinate system was positioned following the International Society of Biomechanics (ISB) guidelines (de Roo et al., 2020; Wu et al., 2005) (Figure 38). The centreline of the radius was calculated by the method described by Crisco et al. (Bulstra et al., 2021; Crisco et al., 2003). This method calculates the centre of every section along the radius 1 mm apart and create centre line or y-axis of the radius. The z-axis is perpendicular to the centreline and passes through highest point of the radial styloid. The x-axis is perpendicular to y and z. Then the isocentre of this coordinate system was positioned at the midpoint of the ridge between the radioscapoid and the radiolunate facets of the radius. Ideally, the isocentre of the radius was recommended on a point midway between the centre of the proximal articular surface and the midpoint of the sagittal ridge between the radioscapoid and the radiolunate facets (Wu et al., 2005). However, none of the CT scanners capable of dynamic CT scans have a gantry width to cover the entire length of the radius to allow this method. Therefore, the isocentre was placed at the midpoint of the sagittal ridge between the radioscapoid and the radiolunate facets, which was the distal landmark of the ISB coordinate system. This was preferred as it is a reproducible and identifiable landmark even if there was restricted visualisation of the radius.

The directions of the coordinate system were assigned to indicate ulnar positive along the z-axis, distal positive along the y-axis and volar positive along the x-axis. Extension to flexion (flexion +ve) was defined as the rotation around the z-axis (Bulstra et al., 2021). The ulnar to radial deviation (radial +ve) was defined as the rotation around the x-axis. Internal to external rotation (internal rotation +ve) was defined as the rotation around the y-axis.



All patients' radii were finally checked manually for placement of the coordinate system and against the posteroanterior and lateral radiographs of the neutral wrist, that had a longer length of radius visible. When the left wrist was analysed, it was mirrored to reflect the right wrist, so that the defined axes and directions remained consistent. This enabled the assessment of all wrists, regardless of the side. Finally, a test and retest of the radius coordinate positioning was conducted to calculate the positioning error and the results were included in the results section 3.1.2.



*Figure 38 Radius coordinate system and definitions of directions of motion. The isocentre ('o') was located at the midpoint of the ridge between the scaphoid and the lunate facets. The y-axis is the longitudinal axis of the radius. The z-axis is the line perpendicular to the y-axis, passing from the radial styloid to the isocentre. The x-axis is orthogonal to z and y. Positive rotation is illustrated with curved arrows as flexion, radial angulation and internal rotation.*

### **2.3.10. Local coordinate system for carpal bones**

Local coordinate system (LCS) for individual carpal bone were defined using the International Society of Biomechanics (ISB) guidelines (Wu et al., 2005). The iso-center of the LCS was placed on the center of mass of each carpal bone in its neutral position. The x, y and z axes of the coordinate system remained parallel to the x, y and z axis of the radius coordinate system. This was used to calculate the change in the radiocarpal angle with wrist motion. The neutral wrist position radiocarpal angles were 'zero' with this method because

the coordinate system axes for radius and carpal bones were parallel to each other. Therefore, it was not possible to comment on the 3D radiocarpal angles in the neutral wrist position with this method.

While this method is suitable for calculation of angular displacements, the true radiocarpal angle is important for clinical translation of the findings. The commonly used tangential line method (Larsen, Mathiesen, et al., 1991) is for sagittal plane angles, hence defining 3D carpal posture was not possible. Therefore, it was necessary to use a unique coordinate system for the carpal bones defined by their shape, to calculate the radiocarpal angle at the neutral wrist position.

To achieve this purpose, moment of inertia based coordinate system (Figure 39) defined by Coburn et al. (Coburn et al., 2007) was used. The three principal axes of the carpal bone model were calculated using the moment of inertia with a custom script published by Crisco and McGovern, 1998 on Matlab® R2022b (Coburn et al., 2007; Crisco et al., 1999).

The principal inertial axes were arranged from the axis with the least moment of inertia to the highest, in the order of x, y and z axes. The isocenter of this system is considered the center of mass of the carpal bone model. The orientation of this axis system is unique to each carpal bone model. However, the direction or the sense is not (can appear as a mirrored version) (Figure 39). Therefore, each carpal model was manually checked and corrected for the consistency in the direction of the axis. The primary principal inertial axis is the axis with the least moment of inertia and is indicated in red; the tertiary principal inertial axis is the axis with highest moment of inertia and is indicated in blue. The secondary axis is orthogonal to the other two and is depicted in green (Figure 39).

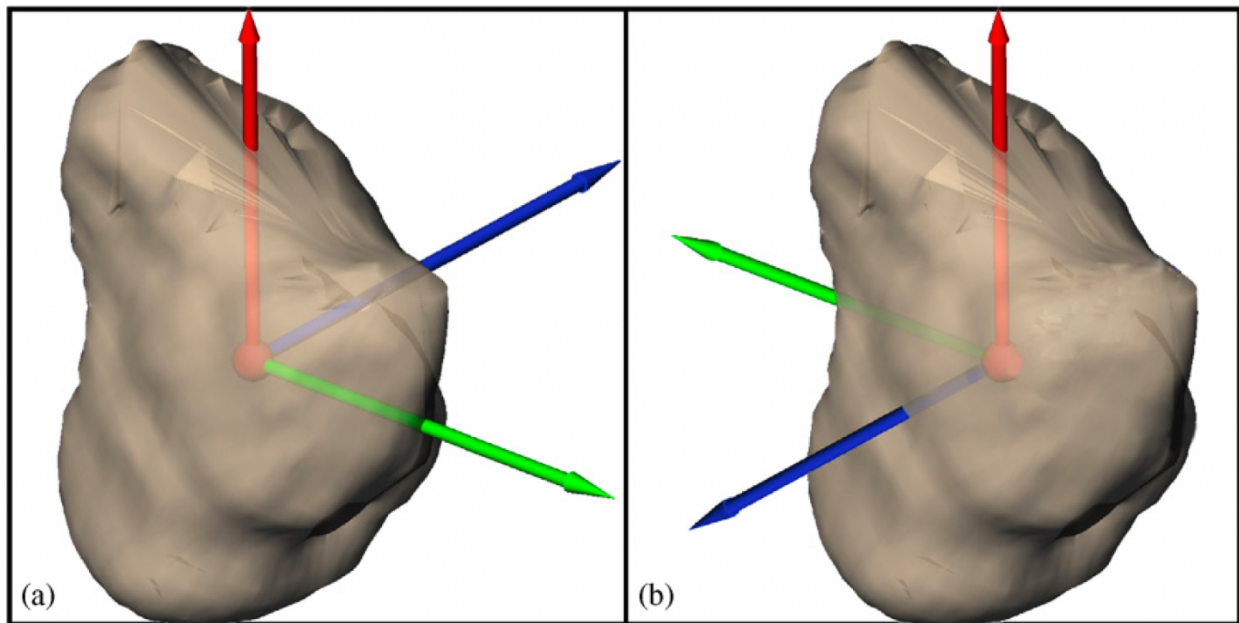


Figure 39 Local coordinate system of the capitate. The principal inertial axes of the capitate were arranged as orthogonal lines extending from the centre of mass in order of ascending inertial magnitude, X-axis (red), Y-axis (green), and Z-axis (blue). While inertia axes are unique for each bone surface model, the sense of the axes is not. The capitate bone is shown in the proposed, standardized inertial based coordinate system colored (X-red; Y-green; Z-blue) (a) and another possible version (b). From "Coordinate systems for the carpal bones of the wrist" by Coburn and Crisco. (2007). *J Biomech*, 40(1), 203-209. Copyright [2007] by Elsevier Science & Technology Journals. Reprinted with permission.

To calculate the radiocarpal angle, the primary principal axis is compared with the radius coordinate system and the angle formed with the x, y and z axes of the radius coordinate system was calculated. This method is previously described (Coburn et al., 2007; Crisco et al., 2003) and compared with the clinically used radiocarpal angles as described by Larsen (Larsen, Mathiesen, et al., 1991). They reported that the clinically used radiocarpal angles 'closely correlated' to the angles derived from the radiocarpal angles derived from the inertial axes.

Therefore, method by Crisco and Coburn (Coburn et al., 2007) was used in the current study to define the radiocarpal angles in 3 -planes for our data. More importantly, it has the advantage of a consistent and automated way of quantifying radiocarpal angle over the Larsen's method, which is manual, validated only for planar radiography, and has a variable inter and intra observer error rate (Larsen, Stigsby, et al., 1991). Also, this system facilitates

computing angles 3 dimensionally, which is not feasible with a tangential line drawn on 2-dimensional projection.

#### **2.3.11. Radius stabilisation**

Once the neutral position angles were defined, the carpal bone displacements were calculated with reference to the radius coordinate system. If the radius position was different at each time point, as the wrist moves, it would affect the angular displacement of the carpal bones. Therefore, any movement occurring at the radius had to be nullified, making all radii are correctly aligned to the coordinate system (Figure 42). The intention of this step was to minimise the effects of the movement of the radius /forearm on carpal bone motion. Once the radius of the neutral position was aligned to the coordinate system, all the radii at every time point was also aligned to the neutral radius. This alignment step was done using a 3D model registration plug-in on 3D slicer platform (Besl & McKay, 1992; Ma & Ellis, 2003; Ungi et al., 2016).

Registration of 3D models, radius or any other, is a process, where the spatial position of each vertex of one model (named as the '*fixed model*' in engineering terms) is matched against all the vertices of another model (named as the '*moving model*'). This process is iterated multiple times (usually 1000 or more), so that the data about the spatial difference between the two models is calculated. This spatial positional difference has two components, angular displacement, and linear displacement. In other words, moving model can be angulated or translated compared to the fixed model. This data on displacement is recorded in a linear transformation matrix that contains the 'sines' and 'cosines' of the angles and the translations as a negative or positive value depending on the direction (Figure 40 and Figure 41).

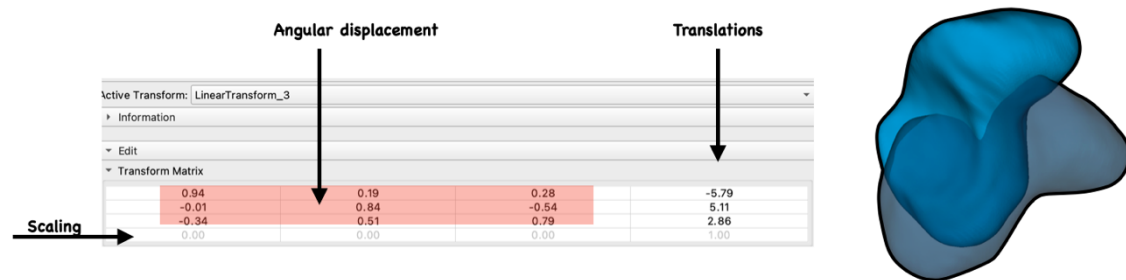


Figure 40 The transformation matrix resulted in following registration from the two scaphoid models. Rows 1 to 3 and columns 1 to 3 contains the data on angular displacements, in the form of sines and cosines of the angle in 3 -planes. These 9-cell matrix (3\*3) is also named the rotation matrix. The 4<sup>th</sup> column contains data on translations and the 4<sup>th</sup> row contains the scaling factor which is zero in this example. Note that the scaphoid is depicted here, but this concept is applied to any carpal model or radius to calculate the displacement.

The rows 1 to 3 and columns 1 to 3 of the transformation matrix is also named the rotation matrix. This is the nett result of the sequential multiplication of rotation matrices describing the rotation around x axis, y axis and then the z axis as seen is Figure 41. While the scaling factor of the matrix remains 0 on the 4<sup>th</sup> row. The 4<sup>th</sup> column contains the information of the translation.

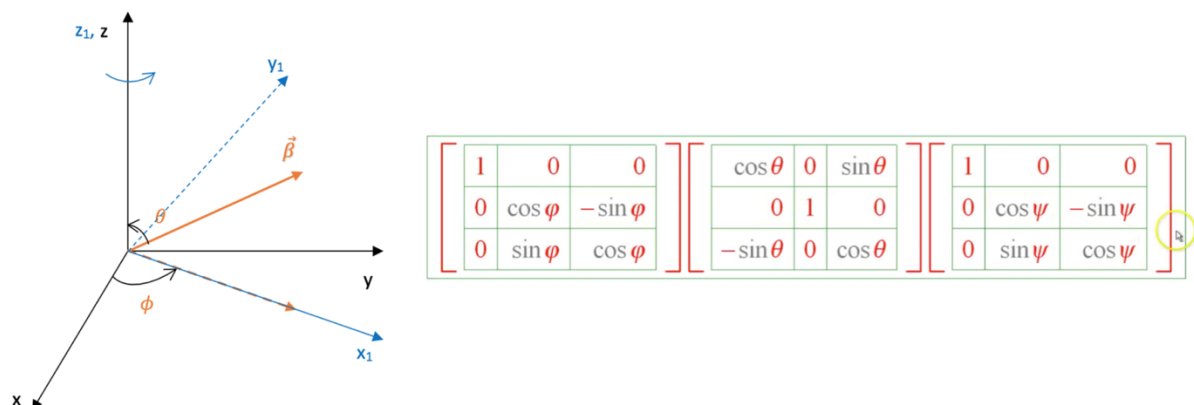
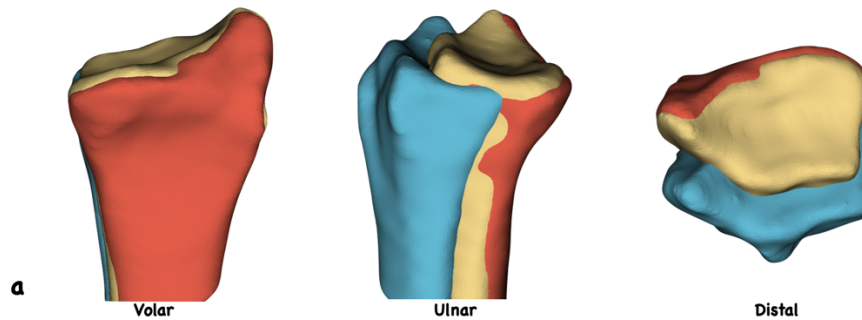


Figure 41 The rotation matrix in Figure 40 is the result of multiplication of the three rotation matrices similar to the image above. Each matrix defines angulation relative to each of the x, y and z axes. Multiplication of all three matrices sequentially, results in the total rotation matrix for the complete angular displacements around all three axes.

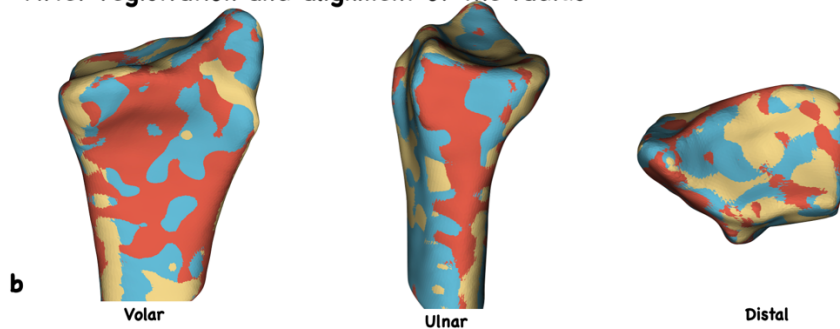
Similarly, once a radius (moving model) is registered to the radius of the neutral position (fixed model) a linear transformation matrix is generated. The transformation matrix is then

applied to the moving model or the registered radius, so the position of the moving radius is changed to match the fixed radius. This aligns moving radius aligned on to the fixed radius (Figure 42). This step is iterated for all the radii to align them with the radius of the neutral position. The 'model registration plug-in' on 3D slicer platform was used for this step and the registration result is observed for satisfactory alignment (Figure 42 b).

**Before registration and alignment of the radius**



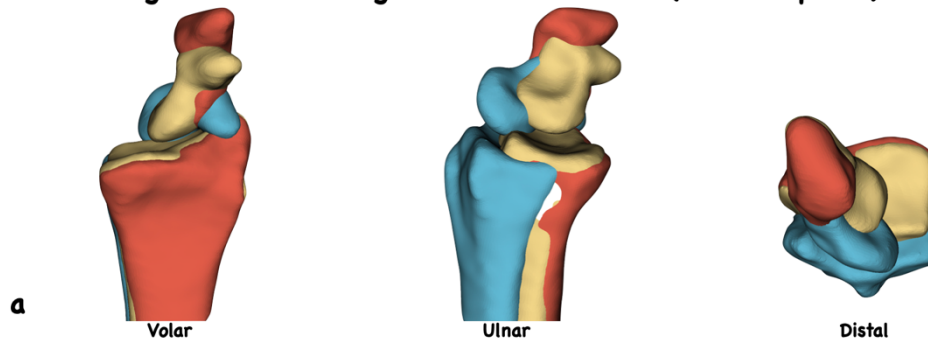
**After registration and alignment of the radius**



*Figure 42 Registration and alignment of the radius. This step is necessary to reorient the position of the radius to match the radius in the neutral wrist, thereby nullifying the effect of the radius motion during wrist radio ulnar deviation or flexion-extension.*

The individual carpal bone positions are dependent on the radius position. Therefore, the above transformation matrix was applied to relevant carpal bones pertaining to the same frame number as the radius. This enabled that all the radii are aligned to the neutral position radius. This process also ascertained that carpal bone that should be with a particular radius, retained their spatial relationship to their radius, while the radius position is corrected to match the reference position. Finally, this created a scene of moving carpal bones referenced to a stable static radius (Figure 43).

#### Before registration and alignment of the radius (With scaphoid)



#### After registration and alignment of the radius and aligning the scaphoid

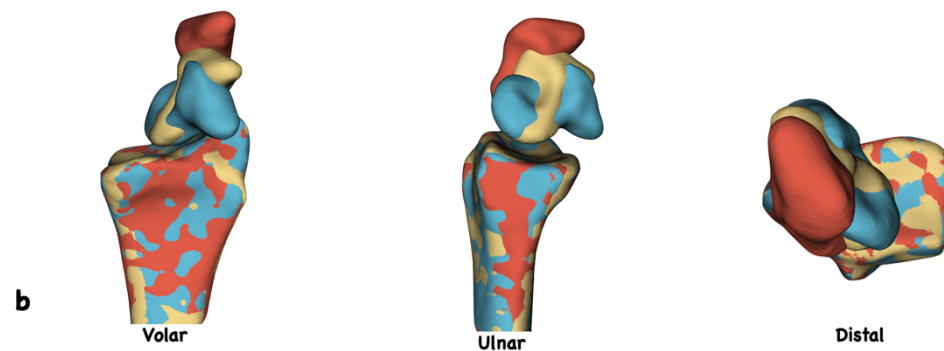


Figure 43 The radius of the neutral wrist position is considered the reference, and hence named the ‘fixed’ model. The radii of subsequent wrist positions may be slightly in a different spatial position due to patients moving the forearm. These subsequent radii are named the ‘moving’ radii. The moving radii was aligned to the ‘fixed radius’ and respective carpal bones that are aligned with the moving radius are corrected to the new position of the moving radius.

#### 2.3.12. Carpal bone registration

Individual carpal bones are known to be moving with 6 degrees of freedom, which includes three rotations and three translations with respect to the defined x, y and z axes. Rotations are defined as the change in angular displacement in coronal (radial angulation), sagittal (flexion) and axial (external rotation) planes. Translations are defined by the movement of the centre of mass (centroid) of each carpal bone (Werner et al., 2011). The linear displacement of the centroid is defined as the translation along the x, y and z axes as described in previous studies (Omori et al., 2013; Werner et al., 2011).

To calculate the angular and linear displacement, the individual carpal bone models pertaining to each time point (moving model) were registered to carpal bone model in the

neutral wrist position (fixed model). These models were also registered using the same technique described under radius stabilisation (2.3.11). The computer algorithm that's used for this step is named 'rigid iterative closest point (ICP) registration (Besl & McKay, 1992), and is basis of the 'model registration plug-in' in 3D Slicer platform (Ungi et al., 2016). The process generated a sequence of transformation matrices pertaining to sequential time points of the moving model. ICP registration is validated and used in point cloud registration of carpal bone models in multiple studies (Moritomo et al., 2004; van de Giessen et al., 2009; Wang et al., 2018). In the validation process it has been reported to have excellent precision and accuracy in calculating the displacement between carpal bone models with less than 0.4 mm error rate (M. Beek et al., 2010; van de Giessen et al., 2009). The ICP registration-based calculation has been the standard practice over 2 decades in multiple studies published on carpal kinematics (Beek et al., 2004; Crisco et al., 2005; Moritomo et al., 2004; Neu et al., 2000; Oki et al., 2019).

#### **2.3.13. Calculations**

Registration using the ICP algorithm generates a linear 4X4 transformation matrix, as described in Figure 40. The carpal angular and linear transformations were extracted from the linear transformation matrix using a custom script on MATLAB®2022b based on the function 'conversion of transformation matrices to Euler's angles.

#### **2.3.14. Euler's angle**

Euler's angles define the rotations of the carpal bones, i.e., the angular rotation around the x, y and z axes of the global coordinate system. The translation of the carpal bone is described as the change in the position of the centre of mass of the carpal bone with reference to the global coordinate system along the x and z-axis. Euler's angles can be sequence dependent, therefore the conventional sequence of rotations around z, x and y axes on a right-handed coordinate system as recommended by the ISB was used (Wu et al., 2002).



The sequence dependency occurs due to the technicalities of matrix multiplication. If the matrices are multiplied in the order of the rotation around the x axis, then y axis followed by z axis the result is different to matrix multiplication in the order of y, x z or z, x y order. For example, if a rigid body rotates 30° around the x axis and then rotates 60° around the y axis and reaches the position 'A'. If the same rigid body, rotates 60° around the y axis and then rotates 30° around the x axis, it will reach position 'B', which is different from A. While the rotation angles around each axis were similar the ultimate position A is different to B, due to the sequence of rotation. When the rotation angles are less than ' $\pi$ ', the difference is proven to be minimal (Panjabi et al., 1982). However, for larger rotation angles the change can be significant. This is applicable in a similar way to calculating the Euler's angles backwards from the rotation matrix. Hence, z, x and y sequence, is agreed upon by the International Society of biomechanics groups, which has been adhered to in the current thesis.

## **2.4. Validation**

Calculating the carpal bone angular and linear displacements using segmented CT or MRI data, registration using ICP algorithm and presenting as Euler's angles has been the standard practice in literature, especially for 3D CT or MRI based studies (Goto et al., 2014; Moritomo et al., 2006). This process has also been reported to be feasible and validated to be used dynamic CT (Mat Jais et al., 2014; Zhao et al., 2015). Multiple researchers later used this technique to understand carpal mechanics using dynamic CT (Robinson et al., 2021; Wang et al., 2018). However, there are few steps that can introduce variability into the results. One such challenge of the dynamic CT scan is that the motion artefacts and increased noise can lead to suboptimum segments being generated.

Theoretically, every scaphoid model created using the raw 4D CT data, at each time point of the motion should be identical. However, mainly due to motion artefacts there will be slight differences between each model. Creating consistent segments/ meshes are important to calculate the displacement of the bone of interest through the range of motion. Therefore, the structural consistency of the meshes for individual carpal bones were further assessed

using the Hausdorf distance, Dice similarity matrix and mesh volume for 05 cases of normal wrists and 05 cases of SLI randomly selected from the study cohort (Results section 3.1.1).

DICE similarity and Hausdorf distance have widely been used to calculate similarity between carpal bone model segmentations (Hendrix et al., 2021). The Dice coefficient is a statistic used to gauge the similarity of two samples. If one 3D model is considered a data set in the form of point cloud, it is compared with second point cloud and a similarity index was generated. If its 1 the samples are identical. Hausdorf distance is a similar indicator, calculating the distance between the vertices of 3D meshes, and then generating the mean distance between the two models. If two carpal bone models are structurally identical, when spatial positions are overlapped, the Hausdorf distance is 0, meaning there is 100% overlap of data points between two meshes. In addition, the mesh volume for each segment was also calculated and compared with each other. If the meshes are structurally similar the mesh volume also should be identical.

The second potential variability was due to positioning the coordinate system on the radius. Researchers have used the method described in this thesis with variable error rates of positioning (Crisco et al., 1999; de Roo et al., 2020). The reproducibility of positioning the coordinate system for the current study was also assessed as a step in the validation process. Five normal and five SLI radii were randomly selected. The radius coordinate system was positioned according to the method described above, then repeated, as a test and re-test. Then the difference in position of each radius between its first and second placement was calculated, by registering the first placement of the radius to the second. Ideally, if the placement is 100% correct, there will not be any change between the two positions of each radius and the expected transformation matrix would indicate zero change in position. Otherwise, the transformation matrix will indicate the change in angular and linear displacement of the second placement compared to the first. The difference of angular change in 3 planes and the translation in 3 directions were presented in the results section (3.1.2).

Following this step, the scaphoid, lunate and capitate were registered, and angular displacements were calculated repeatedly using ICP algorithm (described above in the

section 2.3.12). This was performed as a test and retest method. The Euler's angles for each bone for each time point was computed, as the wrist moves. This process was repeated, and the angles were obtained again. Process was conducted for five normal and five SLI wrists randomly selected from the study cohort. The values obtained in the first instance were compared to the values obtained in the second instance. The inter class correlation coefficient (ICC) was calculated for repeated measurements and presented in the section 3.1.3.

The statistical significance of the results was interpreted considering the error rates identified in the validation process. The results were considered to be not significant if the difference between the means of the normal and SLI groups were within the margin of error, even if the '*p-value*' was less than 0.05.

\*Above methodology will be common to all the studies for the participant recruitment, data acquisition, processing, initial data analysis and reference coordinate systems.

Methodological steps for each study from 1 to 3 are outlined below.

## **2.5. Study 01- Radiocarpal kinematics**

### **Radiocarpal kinematics of the normal and SLI wrist using dynamic CT.**

**The aim of the thesis** was to study the 3D kinematics of the carpus in SLI compared to the healthy wrist using dynamic CT.

#### **2.5.1. Study aim**

The primary aim of the study 01 was to assess the in vivo radiocarpal kinematics of the SLI wrist, compared to the normal wrist.

#### **2.5.2. Study objectives**

The objectives of the study 01 were,

- To define the radiocarpal angles and the centroid positions, in the neutral wrist in three anatomic planes
- To study the angular displacement of the carpal bones with the wrist motion
- To study the linear displacement of the carpal centroid position with the wrist motion
- To study the true angles (radiocarpal) of the scaphoid and the lunate with the wrist motion

In the SLI wrist compared to the normal relative to the radius

- To identify the spectrum of radiocarpal kinematic changes seen in SLI

#### **2.5.3. Hypothesis**

It was hypothesised that dynamic CT can be used to identify distinct kinematic patterns in SLI compared to the normal wrist in vivo during wrist motion.

#### **2.5.4. Materials and methods**

##### *Study Material – Sample*

The segmented carpal bone models (scaphoid, lunate, capitate, and radius from wrist extension to flexion and wrist ulnar to radial deviation) of 19 dynamic CT scans of healthy participants and 19 SLI patients were used. The radii of each scan were reoriented to be aligned to the coordinate system. Carpal bones were arranged on the stable radius as described in section 2.3.11.

#### **2.5.5. The outcome measures for this study**

The outcome measures for the study 01 study were,

1. Radio carpal angles in the neutral wrist position
2. Radio carpal angular displacement during the wrist motion
3. Radio carpal angles during the wrist motion
4. Radio carpal centroid positions during the wrist motion

#### **2.5.6. Study method**

**\*Detailed methodology common to all the studies for the participant recruitment, data acquisition, processing, analysis and reference to coordinate systems are described in the sections from 2.3.4 to 2.3.13.**

##### *Radio carpal angles in the neutral wrist position*

The radiocarpal angles in each plane were defined by the angle between the primary principal axis of the carpal bone and the x-, y- or z-axis of the radius coordinate system as described by Coburn et al. (Figure 44) (Coburn et al., 2007).

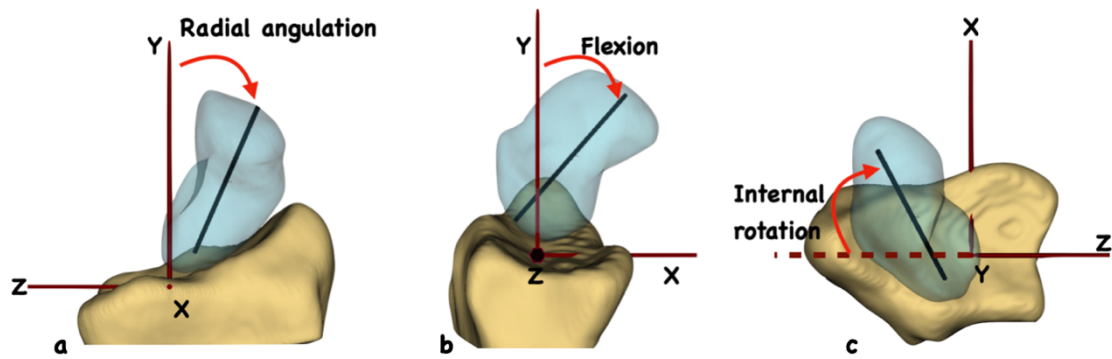


Figure 44 calculation of the individual carpal bone angles based on the primary principal axis. a. The radioscapoid angle -radial angulation (coronal plane) b. The radioscapoid angle -flexion (sagittal plane) c. The radioscapoid angle-internal rotation (axial plane)

The centroid of each carpal bone was defined as the centre of mass and was calculated as the mean of all the coordinate points of all vertices in the x, y and z axis. The x, y, z position of the centroid was defined with reference to the isocentre of the radius coordinate system. Then, the angular displacement was calculated as the Euler's angles compared to the neutral position using the linear transformation matrices as described in section 2.3.13. The radioscapoid angle with motion in each plane was the total of the radioscapoid angle in that plane in the neutral position and the angular displacement in that plane.

#### *Data representation and comparison*

The neutral position radiocarpal angles and centroid positions for each plane are presented in Table 20 to Table 25. The radiocarpal angular displacements and radiocarpal angles are graphed against the wrist angle. The angular displacements and radiocarpal angles in each plane for the scaphoid and the lunate were compared between the normal and SLI wrists. In addition, unique kinematic changes seen in specific cases were also identified to understand the spectrum of kinematic changes seen in SLI.

### *Statistical methods*

The data were first assessed for normality using Shapiro-Wilk test at the significance of 0.05. The unpaired T test was used once normality was established. The carpal angles of the neutral position of the wrist were compared using the unpaired t test. Statistical significance was set at 0.05 *p* value.

Generalised linear model (GLM) was used to assess and compare the angular displacements and radiocarpal angles between the normal and the SLI wrist. A 'GLM' is a statistical model that has the capability of comparing two data sets, generated from multiple participants in two groups (normal and SLI) and considering multiple observations are generated for each participant. This has previously been used to compare longitudinal data, specifically carpal motion patterns ("A Model for Longitudinal Data," 2000). The capitate angles were considered the repeated measurements occurring for each participant. There are dependent variables for each repeated measurement of capitate angles, which fits into the concept of longitudinal data belonging to each participant.

A challenging situation with dynamic CT data was that the wrist angle (dependent variable) remains a continuous variable with values unique to each participant wrist.

Therefore, to obtain comparable data points for the independent variable, the wrist angles had to be converted to a categorical variable before the GLM was applied. Linear interpolation was used to resample the capitate angle values for every 5° wrist motion, creating a categorical independent variable as described in a previous study (de Roo, Muurling, et al., 2019). Thereby, the carpal angles for every 5° increments of capitate angle were computed on Matlab R2022b.

The alternative approach where binning can be applied to create a categorical independent variable was also considered. Compared to the interpolation, binning process leads to clustering or grouping multiple dependent variable values on to single independent variable value. For example, all observations that occur between the wrist flexion of 35° to 45° were binned in to one clustered and 'assumed' that they occur the midpoint between 35° and

45°, which is 40° of wrist flexion. The results for 03 outcome measures according to this method has been calculated and included as a supplementary file (Appendix 1.3)

In the GLM, when capitate angles were considered as repeated measurement, they were correlated according to a first-order autoregressive moving average (ARMA (1,1) covariance structure. The first order autoregressive moving average covariance structure proposes that correlations between similar levels of capitate angle are higher than between capitate angle that are far apart. Considering the within-subject correlations, random intercepts and random slopes of capitate angle were also included in the GLM. This enabled the carpal bone motion patterns and its association with the capitate angle to be assumed to vary among the participants. The goodness of fit and the complexity of different possible model specifications were also considered before finalising all the parameters including the error covariance structure. The goodness of the fit of the model was assessed by checking the corrected Akaike information criterion and Bayesian criterion and examining the distribution of Pearson residuals.

All statistical tests were two-sided and a significance level of 5% was set.



## **2.6. Study 02- Midcarpal kinematics**

### **Midcarpal kinematics of the normal and SLI wrist using dynamic CT.**

**The aim of the thesis** was to study the 3D kinematics of the carpus in SLI compared to the healthy wrist using dynamic CT.

#### **2.6.1. Study aim**

The primary aim of the study 02 was to assess the in vivo midcarpal kinematics of the SLI wrist, compared to the normal wrist.

#### **2.6.2. Study objectives**

The objective of the study 2 was to assess the angular displacement of the carpal bones with the wrist motion, relative to the capitate in the midcarpal joint in the SLI wrist compared to the normal wrist.

#### **2.6.3. Hypothesis**

It was hypothesized that there is less midcarpal motion for the scaphoid and more midcarpal motion for the lunate in SLI compared to the healthy wrist.

#### **2.6.4. Materials and methods**

##### *Study Material – Sample*

The segmented carpal bone models (scaphoid, lunate, capitate, and radius from wrist extension to flexion and wrist ulnar to radial deviation) of 19 dynamic CT scans of healthy participants and 19 SLI patients were used.

### 2.6.5. The outcome measures for this study were,

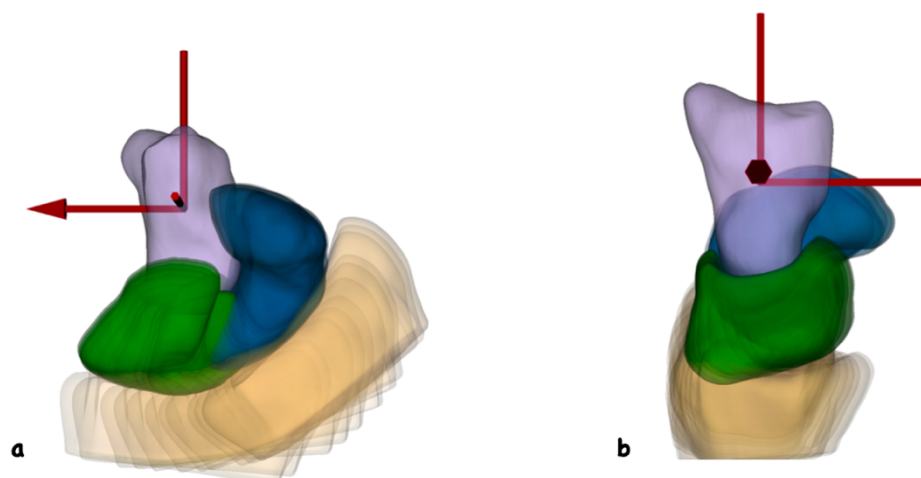
The outcome measures for this study were defined as midcarpal angular displacement during the wrist motion, from ulnar to radial deviation and extension to flexion.

### 2.6.6. Study method

#### *Midcarpal angular displacement during the wrist motion*

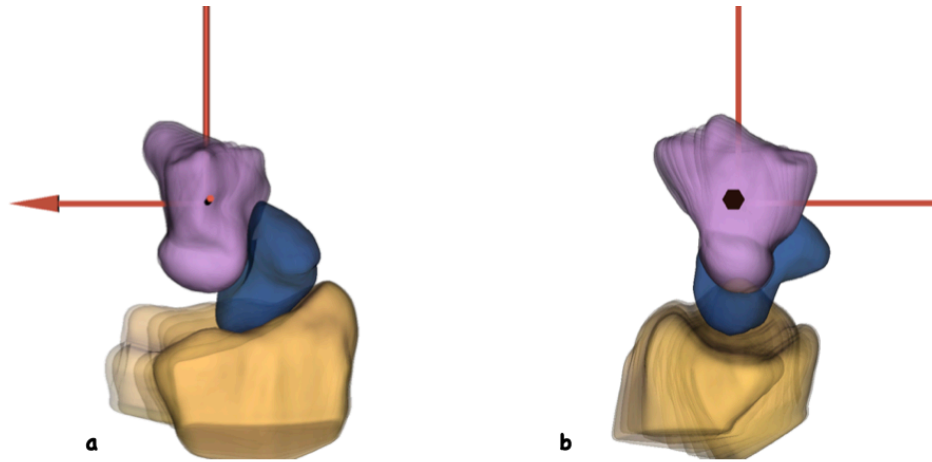
Midcarpal angular displacement for the scaphoid and lunate was calculated with referenced to the capitate (Bain et al., 2015; Kaufmann et al., 2006; Moritomo et al., 2006). It is essentially the motion of the scaphoid and the lunate if capitate was stabilised and considered the reference bone. In the inverse, it would represent the arithmetic inverse of the scapho-capitate or luno-capitate motion (Figure 45). The angular displacement would be the same in magnitude but inverse in direction, if the capitate motion was calculated with a still scaphoid (or lunate).

The x, y and z axis of the capitate coordinate system remained parallel to the radius coordinate system axis, as per ISB guidelines. This also enabled drawing comparisons between radiocarpal and midcarpal motions as the defined planes and axes remain parallel on both occasions. The isocentre was placed at the centre of mass of the capitate.



*Figure 45 Representation of the midcarpal motion of the scaphoid and the lunate. All bones are referenced to the capitate in the neutral wrist position, which was aligned to capitate coordinate system. The movement of the scaphoid and the*

*lunate relative to the capitate is presented. The radius is depicted for visual appreciation and depicts the radius motion relative to capitate, which is the inverse of radio-capitate motion. a. coronal view b. sagittal view.*



*Figure 46 Representation of the midcarpal motion relative to the scaphoid. All bones are referenced to the scaphoid in the neutral wrist position, which was aligned to capitate(midcarpal) coordinate system, which remains parallel to the radius coordinate system. The movement of the capitate and the radius relative to the scaphoid is presented. The image presents the scapho-capitate motion which is similar in magnitude but inverse in direction to capito-scaphoid motion depicted in Figure 45. The radius motion is the same in magnitude and inverse in direction to radioscapoid motion. in a. coronal view b. sagittal view.*

The capitate was registered using ICP algorithm and stabilised. The scaphoid and the lunate were aligned to the stable capitate using the generated linear transformation matrix (Figure 45). Then, the neutral wrist position scaphoid was registered to scaphoids in subsequent time points using the ICP algorithm. The angular displacements of the scaphoid relative to capitate were calculated. The same procedure was conducted for the lunate. The calculated carpal angular displacements were expressed as Euler's angles based on a right-handed coordinate system, using the conventional sequence of rotations around z, x, and y axes (Wang et al., 2018; Wu et al., 2002).

### ***Data representation and comparison***

The midcarpal angular displacements were graphed against the wrist angle. The angular displacements in each plane for the scaphoid and the lunate were compared between the normal and SLI wrists.

### *Statistical methods*

Generalised linear model was used to assess and compare the midcarpal angular displacements between the normal and the SLI wrist. The same protocol as study 01 was followed for study 02 with the midcarpal angular displacements as the dependent variable. All statistical tests were two-sided and a significance level of 5% was set.

## **2.7. Study 03- Helical axis of motion**

**The helical axis of motion of the scaphoid and the lunate in the normal wrist and the SLI wrist using dynamic CT**

**The aim of the thesis** was to study the 3D kinematics of the carpus in SLI compared to the healthy wrist using dynamic CT.

### **2.7.1. Study aim**

The primary aim of the study 03 was to assess the position and the orientation of the helical axis of motion of the scaphoid and the lunate with wrist motion in the SLI wrist, compared to the normal wrist.

### **2.7.2. Study objectives**

The objectives of the study 03 were,

- To calculate the helical axis of motion of the scaphoid and the lunate with wrist motion and
- To compare the orientation and the position of the helical axis of motion of the scaphoid and the lunate with wrists motion between the SLI and the healthy wrists.

### **2.7.3. Hypothesis**

It was hypothesised that the scaphoid and the lunate do not have a single axis of rotation, the axis of rotation changes with different wrist positions and is different between the normal and SLI wrists.

#### **2.7.4. Materials and methods**

##### *Study Material – Sample*

The segmented carpal bone models (scaphoid, lunate, capitate, and radius from wrist extension to flexion and wrist ulnar to radial deviation) of 19 dynamic CT scans of healthy participants and 19 SLI patients were used.

#### **2.7.5. The outcome measures of this study were,**

- The orientation of the helical axis of motion
- The position of the helical axis of motion of rotation of the scaphoid and the lunate with each incremental step of wrist motion.

#### **2.7.6. Study method**

##### *Helical axis of motion (Finite helical axis/ Finite screw axis)*

Helical axis of motion (HAM) is important as it provides insight into the carpal bone motion. While the Euler's angles remain one way of representing the motion patterns of carpal bones, helical axis of motion (HAM) method, is an alternative way. Prior to Spoor et al. (Spoor, 1984), the change in carpal position was described with the 6 degrees of freedom as Euler's angles and translations. HAM summarises the displacement of the rigid body into a unique axis around which the bone rotates and along which it translates.

The HAM has its own advantages. While the angular displacement describes how the carpal bone rotates, HAM method potentially informs about the how and 'around what' it rotates, defining an axis. The HAM combines the 3 angular displacements to a single angular displacement, around this axis. The HAM combines the 3 translations to a single translation along this axis. The HAM is a true axis of motion, with reference to the radius coordinate system.

Compared to HAM the Euler's angles are arbitrarily defined by the 3 individual components of vectors. In other words, although the scaphoid motion is described as scaphoid flexion, radial angulation and internal rotation, there are no such discrete motions in each plane. It is one single motion combined that is decomposed into 3 components for descriptive purposes. HAM presents the true motion of the carpal bone, the axis around which it rotates and the magnitude at which it rotates and translates along the axis.

The parameters that describe the helical axis are the

- Orientation of the HAM relative to the global coordinate system
- Position of the HAM relative to the global coordinate system
- Magnitude of the rotation of the rigid body around the screw axis
- Magnitude of the translation along the screw axis

There is various terminology for the HAM. Screw axis and helical axis are the similar in meaning and can be used interchangeably. Finite helical axis (FHA) of motion and Instantaneous helical axis (IHA) may be the same in value but conceptually different as the way of calculation is different.

In this thesis, finite HAM for each carpal bone at each time point during wrist extension to flexion and wrist ulnar to radial deviation was calculated. The calculation of the parameters of the screw axis are established according to the method described by Spoor et al.(Spoor, 1984). It is calculated using the 'pose' of the carpal bone of interest at two different time points and is based on the finite change in the 'pose'.

The displacement of a rigid body can be characterized by the rotation matrix "R" and the translation vector "v". The same displacement can also be described as the result of a rotation through an angle " $\phi$ " about the 'helical axis or screw axes and a translation "r" along this axis (Figure 47). The spatial position of a rigid body (Y) can be described by the following equation. (reproduced from Spoor et al. (Spoor, 1984))

$$\mathbf{Y} = \mathbf{R}\mathbf{w} + \mathbf{v}$$

(1)

( $\mathbf{Y}$  = Spatial position,  $\mathbf{R}$  = rotation matrix,  $\mathbf{v}$  = translation vector,  $\mathbf{w}$  = corresponding vector in the local coordinate system).

## Helical axis of motion

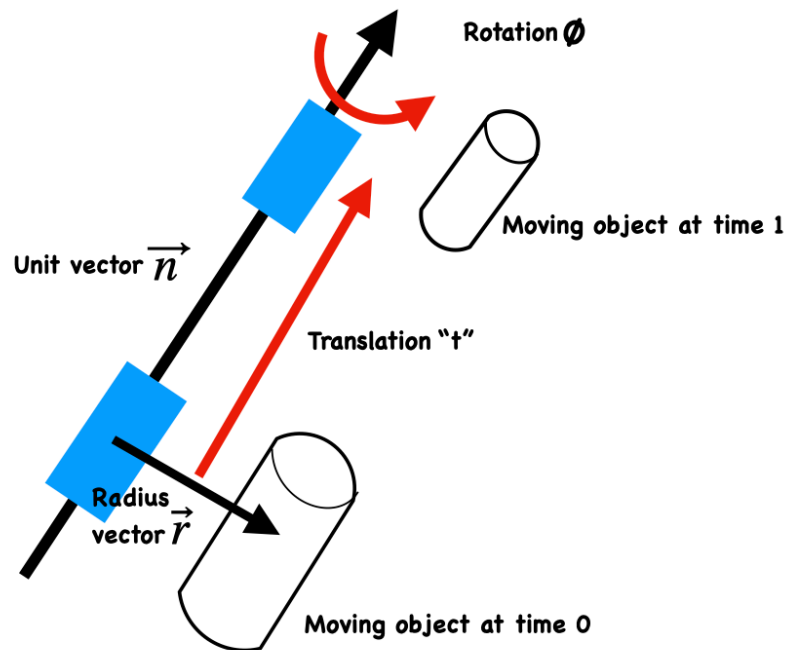


Figure 47 Schematic diagram of the helical axis representation of rigid body motion. The helical axis is the axis around which a rigid body rotates and along which it translates. The helical axis is calculated as a function of the unit vector of the moving rigid body compared to the reference radius vector.

The 3D rotation matrix 'R' is the results of sequential multiplication of three elementary orientation matrices. Each elementary orientation matrix represents the rotation of a carpal bone around each coordinate axis, x, y and z. Following sequential multiplication of each matrix result is a final matrix named R. The angle  $\phi$  in the following equations denotes a rotation of the rigid body of interest, about the  $i^{\text{th}}$  coordinate axis in the right-handed screw sense (Figure 48). The total rotation is represented by the rotation from the reference attitude in the order of i, j and k. (Reverse order is used for opposite signs but mirroring all lefts wrists to right avoids this problem).





Figure 48 The right-hand screw rule. According to the right-hand rule, right fingers curled in the direction of rotation and the right thumb pointing in the positive direction of the axis. Image reprinted from Right-hand rule on Wikimedia Foundation. Last updated 13 Oct 2023. [https://en.wikipedia.org/wiki/Right-hand\\_rule](https://en.wikipedia.org/wiki/Right-hand_rule). [used under Creative Commons CC-BY license]

If “ $\mathbf{n}$ ” is a unit vector along the helical axis and “ $\mathbf{s}$ ” is the radius vector of a point on this axis, so that  $\mathbf{n}$  and  $\mathbf{s}$  are orthogonal:

“

$$\mathbf{n}^T \mathbf{n} = 1; \quad \mathbf{n}^T \mathbf{s} = 0$$

(2)

The right-hand screw rule will determine the direction of “ $\mathbf{n}$ ” and the sense of rotation. Assuming that  $\varnothing$  is positive and less than or equal  $\pi$  rad, the connection between both descriptions of the movement of the body is given by the requirement that ( $\mathbf{R}$  = rotation matrix,  $\mathbf{v}$  = translation vector,  $\mathbf{w}$  = corresponding vector in the local coordinate system).

$$\mathbf{R}\mathbf{w} + \mathbf{v} = \mathbf{w} + t\mathbf{n} + (1 - \cos\varnothing)\mathbf{n} * (\mathbf{n} * (\mathbf{w} - \mathbf{s})) + \sin\varnothing\mathbf{n} * (\mathbf{w} - \mathbf{s})$$

(3)

must hold for every vector  $\mathbf{w}$ .

Consequently:

$$\mathbf{v} = t\mathbf{n} + (1 - \cos\varnothing)\mathbf{s} - \sin\varnothing\mathbf{n} * \mathbf{s}$$

(4)

$$Rw = \cos\theta w + (1 - \cos\theta)nn^T w + \sin\theta n * w \quad (5)$$

For every W, where the last equation is seen to be equivalent with:

$$\frac{1}{2}(R - R^T)w = \sin\theta n * w \quad (6)$$

For every W

$$\frac{1}{2}(R + R^T) = \cos\theta I + (1 - \cos\theta)nn^T \quad (7)$$

The matrix  $\frac{1}{2}(R - R^T)$  is skew-symmetric and it can be shown that  $\sin\theta n$  is given by:

$$\sin\theta n = \frac{1}{2} \begin{pmatrix} R_{32} - R_{23} \\ R_{13} - R_{31} \\ R_{21} - R_{12} \end{pmatrix} \quad (8)$$

With  $n^T n = 1$  and  $\sin\theta \geq 0$  this equation can be solved for  $\sin\theta$ , which results in:

$$\sin\theta = \frac{1}{2} (R_{32} - R_{23})^2 + (R_{13} - R_{31})^2 + (R_{21} - R_{12})^2 \quad (9)$$

Apart from this  $\cos\theta$  can be calculated from (7) by adding up the components on the principal diagonal of the matrices.

Then:

$$3\cos\theta + (1 - \cos\theta) \text{trace}(nn^T) = \text{trace}\left(\frac{1}{2}(R + R^T)\right) \quad (10)$$

and because of  $\text{trace}(nn^T) = n^T n = 1$  it follows:

$$\cos\theta = \frac{1}{2}(R_{11} + R_{22} + R_{33} - 1) \quad (11)$$

Both equations (9) and (11) can be used to calculate  $\phi$ . For numerical reasons it is preferred to use **(11)**

$$\text{if } \sin \phi \leq \frac{1}{2} \sqrt{2} \text{ and (34) } \sin \phi > \frac{1}{2} \sqrt{2}.$$

As soon as  $\sin \phi$  is known  $n$  can be determined from **(8)** if  $\sin \phi \neq 0$ .

From a numerical point of view this is not recommendable if  $\phi$  approaches  $\pi$ . With known  $\cos \phi$  it is preferred to use **(8)** if  $\phi > 3/4\pi$ .

While:

$$(1 - \cos \phi)nn^T = \frac{1}{2}(R + R^T) - \cos \phi 1 = [b_1 b_2 b_3] \quad (12)$$

it is seen that each of the columns  $b_1$ ,  $b_2$  and  $b_3$  of the matrix  $1/2(R + R^T) - \cos \phi 1$  is a vector in the same direction as  $n$ . Hence, apart from a factor,  $n$  is equal to  $b_1$ ,  $b_2$  and  $b_3$ . Let  $b_i$  ( $i = 1, 2$  or  $3$ ) be the column with the greatest length  $\sqrt{b_i^T b_i}$ . Then  $n$  is determined by:

$$b_i^T b_i = \max(b_1^T b_1, b_2^T b_2, b_3^T b_3); \quad n = \pm \frac{b_i}{\sqrt{b_i^T b_i}} \quad (13)$$

The sign of  $n$  must be chosen such that  $\sin \phi$  in **(8)** is positive. The translation  $t$  along the helical axis and the radius vector  $s$  of a point on this axis follow from **(3)** and **(4)**:

$$t = n^T V \quad (14)$$

$$s = -\frac{1}{2}n * (n * v) + \frac{\sin \phi}{2(1 - \cos \phi)}n * v \quad (15)$$

The relations **(11)**, **(12)** and **(13)** hold if  $\phi \neq 0$ . If  $\phi \neq 0$  there is no rotation at all. In that case the helical axis is not defined and therefore  $n$ ,  $s$  and  $1$  are not unique. If  $\phi = 0$  and  $v \neq 0$  then one can use:

$$t = \sqrt{V^T V}; \quad n = \frac{1}{t} v \quad s = 0 \quad (16)$$

If  $\phi = 0$  and  $v = 0$  there is no movement at all. This case is of no interest. Sufficient for the computation of  $n$ ,  $\phi$ ,  $s$  and  $t$  are (9) and (11) for  $\phi$ , (8) and (12) to (15) for  $n$ ,  $t$  and  $s$  if  $\phi \neq 0$  and (16) if  $\phi = 0$ .

The calculation of the position, orientation of the helical axis and the rotation about and the translation along the helical axis  $s$  calculated using a MATLAB®2022b, based on the above calculation.

#### *Data representation and comparison*

In this study, the position of the scaphoid in the initial wrist position (Time point 0, or extreme extension or extreme ulnar deviation for each participant) was recorded. It was then compared to the subsequent wrist position, with each position of scaphoid  $n^{\text{th}}$  scaphoid being registered to the  $1+n^{\text{th}}$  scaphoid. This process generated a sequence of linear transformation matrices, which captured the displacement data of the scaphoid throughout each incremental wrist motion. Using these matrices, the HAM for the scaphoid between each incremental wrist position was calculated. The same procedure was repeated for the lunate as well.

The various participants did not reach the matching wrist angles, at comparable time points. This was due to variability in the range of motion between participants, rate of motion of the wrist while the scan being conducted and time points at which each frame was obtained. Hence, pooling data between patients for comparison between the normal and SLI groups was challenging. For example, the first time point (T1) or frame 1 of the patient x was with the wrist in extension of 72°; same for the patient y was 63° wrist extension, which is not comparable.

To overcome this problem, a binning process was used, as described by Best (Best et al., 2019). This concept groups capitate angles that are close to each other into a single “bin”. Bins were created to cover 10° increments of wrist angles, ranging from ulnar to radial deviation and from extension to flexion. The transformation matrices determined were then grouped into their respective bins based on the wrist position at which they were calculated. For instance, all participants’ rotation axes falling between 5° of wrist extension and 15° of wrist flexion were assigned to the 10° bin. These rotation axes were visually presented in graphical form, and all relevant outcome measures were computed for each occurrence and for each patient within the corresponding bin.

*Calculation of mean helical axis of motion and the variability of the orientation and position (outcome measures)*

The orientation of the mean helical axis and variability

The linear transformation matrices in each bin were converted into their vectors. The vectors were normalised by a process call normalisation which calculate the unit length of the vector. This is similar to converting a vector that 3,4,5, as x, y and z coordinate position into a vector that has x value as 1 and the other values relative to that, such that the direction of the vector remains unchanged, but the magnitude remains a “unit”. If the vectors with different lengths were averaged the result becomes incorrect. Then the mean vector was calculated by averaging the normalised vectors. This defined the orientation of the mean vector.

The alternative approach to calculate the mean rotation axis was using normalised quaternion representations of the rotation matrices, which were derived from the linear transformation matrices. The results obtained from both methods were found to be identical (Figure 49 ).

### Finite helical axis of the scaphoid relative to radius (Wrist 15° radial deviation to 25° radial deviation)

Mean axis (calc with quaternions) — Mean axis (calc with vectors) —

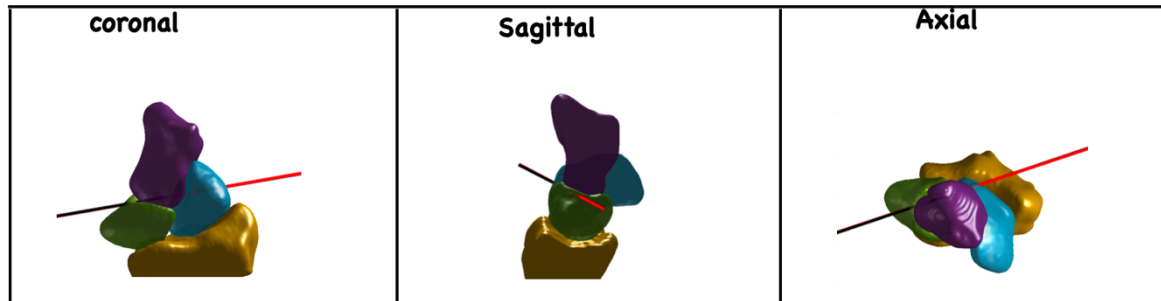


Figure 49 Mean rotation axis can be calculated using normalised vectors or using quaternions. The line depicted in this image is the mean vector or the mean axis of rotation for 19 patients within the wrist range of 15° radial deviation to 25° radial deviation. In the given example the mean rotation axis was calculated with quaternion mean and vector averaging, which confirms the result obtained by both methods are similar.

Then the difference between each vector and the mean vector was calculated, resulting in the variability of each vector from the mean. By summing the squares of all the individual values and then dividing the sum by the frequency (number of values), the variance was obtained. The standard deviation was subsequently determined as the square root of the variance (Figure 50).

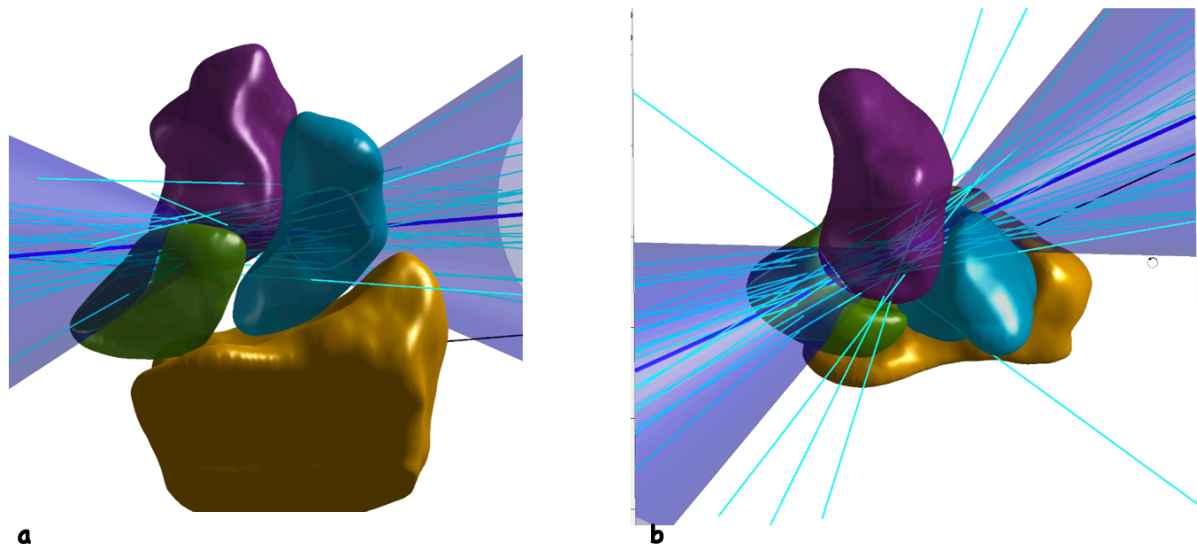


Figure 50 Graphic representation of the results from a single bin at 10° of radial deviation. The helical axis of motion of the scaphoid for all healthy wrists, in the wrist of 10°(bin) of radial deviation is indicated by thin lines in cyan. The mean axis of rotation is indicated by the thick dark blue line. The variance is indicated by the shaded area. a. coronal view b. axial view

While the orientation of the helical axis of motion can be described as a vector, it is useful to describe the orientation of the mean axis and its variability in relation to the anatomic planes as it helps visualising the direction relative to a known plane (Figure 51). The inverse tangent (ATAN) of the ratio between components of mean and the individual vectors were used to calculate the angle of the helical axis in three anatomic planes.

If the individual components of a vector- $v$ , (either mean or individual) are  $x$ ,  $y$  and  $z$  the angle that ' $v$ ' forms in each anatomical plane ( $\emptyset$ ,  $\Omega$  and  $\psi$  in Figure 51) can be calculated by the following equations.

$$\emptyset = \tan^{-1} \frac{y}{z}$$

$$\Omega = \tan^{-1} \frac{y}{z}$$

$$\psi = \tan^{-1} \frac{x}{z}$$

Angle of the mean axis within each anatomic plane was first calculated. Additionally, the angles of the individual axes in the same plane were also computed. This approach provided valuable insights into the dispersion or variability of individual axes around the mean axis within each anatomic plane (Figure 51).

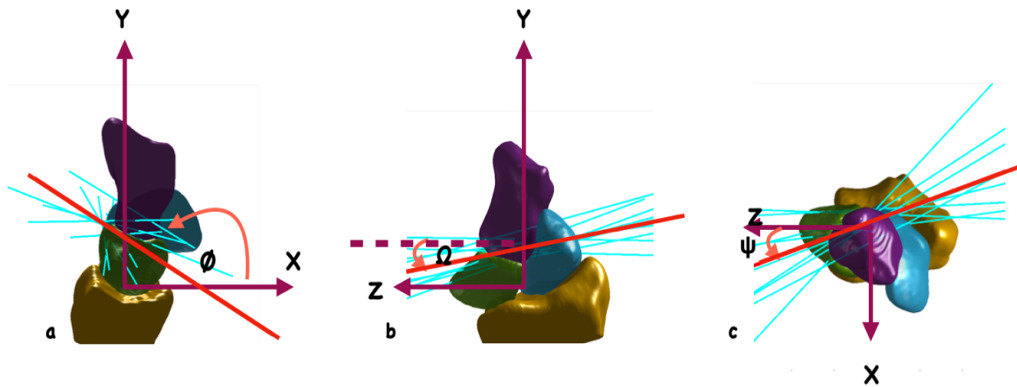


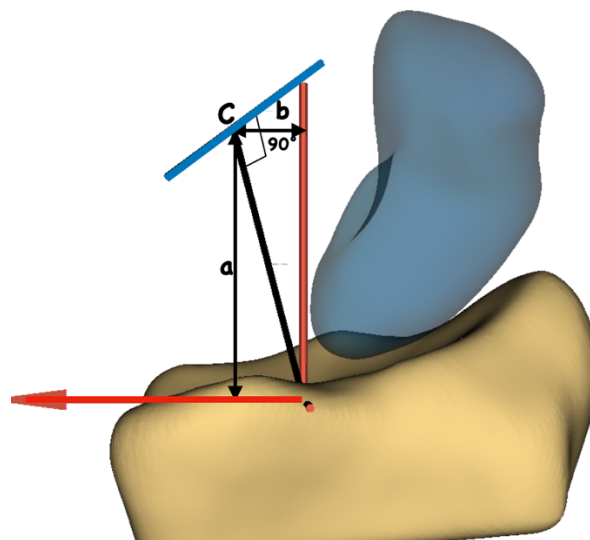
Figure 51 The angle of the rotation axis with reference to the anatomic planes.  $\phi$ ,  $\Omega$ ,  $\psi$  the angles between the helical axis of motion and the X-Y(sagittal), Y-Z (coronal), and X-Z(axial) planes respectively. Positive angle is indicated by the direction of the curved arrow; The counterclockwise angle formed from the positive horizontal axis remains positive angle up to  $180^\circ$  according to the right-hand rule. Red line depicts the mean axis and the lines in cyan depict the individual axes. The angles were only demonstrated on the mean axis for easier reading but calculated for the mean and all individual axes.

When calculating the inverse tangent as described above can lead to a confusion in the interpretation of the direction of the vector. For example, in vector 'v' if the x and y components are both positive values the resultant ' $\phi$ ' is a positive angle. If the x and y and both negative values, the vector is pointing in the opposite direction to 'v', however the resultant ' $\phi$ ' is still a positive angle. It is not possible to determine the direction based on the resultant ' $\phi$ '. Therefore to overcome this confusion, the four quadrant arc tangent function on MATLAB Rb2022 was used (Marghitu, 2009). This function adds an adjustment to generate angles from  $-180^\circ$  to  $+180^\circ$  covering the entire  $360^\circ$  circle, so that the value of the angle reflects the direction of the vector.



The position of the helical axis and variability

The location of the mean axis was calculated as the length of a straight line perpendicular to the mean axis from the isocentre of the reference coordinate system (Best et al., 2019), in this study, the radius. The co-ordinates of the intersection points (Figure 52) between this perpendicular line and the helical axis were recorded. The process was repeated to calculate the location of each individual axis in radioulnar, dorso-volar and proximo distal directions. All the outcome measures were recorded for each individual instance as well as the mean for a specific bin (Figure 50).



*Figure 52 The calculation of the position of the helical axis of motion. The helical axis of motion of the scaphoid is represented by the thick blue line. "C" is the intersection point between the HAM and a line representing the shortest Euclidian distance between the HAM and the isocentre of the radius coordinate system. The point co-ordinates of the "C" represent the radioulnar (b), proximodistal (a) and dorso-volar distances to the HAM from the isocentre of the radius coordinate system. Only a and b are represented in the figure.*

Comparisons were made between.

- Each bin for the normal wrist (From extension to flexion and ulnar to radial deviation)
- Each bin for the SLI wrist (From extension to flexion and ulnar to radial deviation)

- The change in the orientation of the HAM between the normal and SLI wrists from maximum ulnar to maximum radial deviation

### *Statistical methods*

While t test can be applied to normally distributed data, non-parametric tests are recommended for non-normally distributed data. Therefore, the 'position of the HAM' data was first assessed for normality using the Shapiro Wilks test. The sample size for certain bins were less than 20 and data were not normally distributed.

Therefore, the position of the helical axis was compared between the bins using the Mann-Whitney U test, with the significance set at 0.05. Each bin was compared to the subsequent bin. This enabled identifying the point at which a significant change in the position of the helical axis would occur. The normal and SLI wrists were compared to identify the patterns of change between the 2 groups.

Orientation of the HAM with reference to an anatomic plane, is a description of a direction, in a 360° circle in the plane considered. This represented a set of angles arranged around a 360° in the coronal, sagittal and axial planes. It was necessary to calculate the difference between the orientation of the HAM of the scaphoid between wrist positions. As the axis is part of "circular data", and it can't just simply be averaged arithmetically, to calculate a mean and a standard deviation. Therefore, statistical analysis of this data had be conducted using the principals of circular statistics (Mardia et al., 2000; Watson, 1983). The direction must be considered. The tests conducted to assess the normality or circular uniformity in circular statistic were,

- Rayleigh test (Fisher, 1953; Zar, 1999)
- Omnibus test (Zar, 1999)
- Rao's spacing test (Watson, 1982)

As our data did not show circular uniformity, comparable to linear statistics, the data analysis was conducted using the non-parametric equivalent of circular statistics tests. It is a

circular analogue to the Kruskal-Wallis's test and was described by Fisher et al (Fisher, 1953) and implemented in circular statistics toolbox as described by Berens et al (Berens, 2009). MATLAB Rb2022® has developed a 'circular statistic toolbox' which is designed specifically for this purpose (Berens, 2009; Jammalamadaka & SenGupta, 2001). The orientation of the HAM was computed for each 'bin' and compared between 'bins' using the non-parametric equivalent circular statistics tests on the 'circular statistic toolbox' on MATLAB Rb2022® platform with the significance set at 0.5.

## CHAPTER 03

### 3. RESULTS

#### 3.1. Validation

##### 3.1.1. Segment similarity (Similarity between 3D meshes of carpal bones)

Five normal and 5 SLI wrists were randomly selected from the study cohort. The scaphoid, the lunate and the capitate were included in the assessment. Segment similarity was assessed by comparing the 3D model of a carpal bone at time point 0 (segment 00) with the carpal bone models of the same bone in subsequent time points (segment 00 + n).

The outcome measures were,

- Hausdorf distance
- Dice coefficient
- Segment volume as a percentage of the segment 00

The results are presented in Table 10 to Table 12.

#### *Hausdorf distance*

The mean Hausdorf distance between the carpal bone model at the time point 0 and the subsequent time points, was always less than 0.2mm for the scaphoid, the lunate, and the capitate (Table 10). The results are indicative of excellent structural similarity between carpal bone models when compared across the time series.

*Table 10 Mean Hausdorf distance between the carpal bone model at time point 0 and subsequent time points for the scaphoid, the lunate, and the capitate for 10 randomly selected wrists.*

<b>Carpal bone</b>	<b>Scaphoid</b>		<b>Lunate</b>		<b>Capitate</b>	
<b>Wrist</b>	<b>Mean (mm)</b>	<b>SD</b>	<b>Mean (mm)</b>	<b>SD</b>	<b>Mean (mm)</b>	<b>SD</b>
N 00	0.15	0.02	0.12	0.02	0.12	0.03
N 01	0.06	0.01	0.05	0.01	0.07	0.01
N 04	0.06	0.01	0.05	0.01	0.17	0.04
N 11	0.05	0.02	0.08	0.01	0.06	0.04
N 18	0.13	0.03	0.11	0.02	0.14	0.04
SLI 01	0.12	0.01	0.10	0.02	0.17	0.02
SLI 03	0.14	0.03	0.12	0.03	0.14	0.03
SLI 10	0.14	0.02	0.09	0.02	0.15	0.07
SLI 11	0.10	0.01	0.09	0.01	0.12	0.01
SLI 19	0.07	0.01	0.06	0.01	0.08	0.01
<b>Mean</b>	<b>0.10</b>	<b>0.04</b>	<b>0.09</b>	<b>0.03</b>	<b>0.12</b>	<b>0.05</b>

*Hausdorf distance of '0' indicates that the segments are similar. SD-Standard Deviation N-Normal SLI-Scapholunate instability. The index number of the wrist is indicated in the first column (e.g., N 00 is the Normal wrist numbered 00). Raw data files with individual data points for all frames are included in Appendix 1.2.*

### *Dice coefficient*

The Dice similarity coefficient between the carpal bone model at the time point 0 and the subsequent time points, always remained above 0.97 for all carpal bones (Table 11).

The results are indicative of excellent structural similarity between carpal bone models when compared across the time series.

Table 11 Mean Dice coefficient between the carpal bone model at time point 0 and subsequent time points for 10 randomly selected wrists.

Carpal bone	Scaphoid		Lunate		Capitate	
Wrist	Mean	SD	Mean	SD	Mean	SD
<b>N 00</b>	0.97	0.00	0.97	0.00	0.98	0.01
<b>N 01</b>	0.99	0.00	0.99	0.00	0.99	0.00
<b>N 04</b>	0.99	0.00	0.99	0.00	0.97	0.01
<b>N 11</b>	0.99	0.01	0.98	0.00	0.99	0.01
<b>N 18</b>	0.97	0.01	0.97	0.01	0.97	0.01
<b>SLI 01</b>	0.97	0.00	0.98	0.00	0.97	0.01
<b>SLI 03</b>	0.97	0.01	0.97	0.01	0.97	0.01
<b>SLI 10</b>	0.97	0.00	0.98	0.01	0.97	0.01
<b>SLI 11</b>	0.98	0.00	0.98	0.00	0.98	0.00
<b>SLI 19</b>	0.99	0.00	0.99	0.00	0.99	0.00
<b>Mean</b>	0.98	0.01	0.98	0.01	0.98	0.01

Dice coefficient of '1' indicates that the segments are similar. SD-Standard Deviation. N-Normal SLI-Scapholunate instability. The index number of the wrist is indicated in the first column (e.g., N 00 is the Normal wrist numbered 00). Raw data files with individual data points for all frames are included in Appendix 1.2. Segment volume as a percentage of segment 00.

Mesh volume between the carpal bone model at the time point 0 and the subsequent time points always remained above 95% and below 105%. In an ideal situation if the segments are identical between time point 0 and subsequent time points, the volume of each model should be similar. In the current study, the variability of the mesh volume between the models were within 5%.

Table 12 Mean percentage volume between the carpal bone model at time point 0 and subsequent time points for 10 randomly selected wrists.

Carpal bone	Scaphoid		Lunate		Capitate	
Wrist	Mean	SD	Mean	SD	Mean	SD
N 00	100.2	0.5	101.6	1.5	99.9	0.5
N 01	103.7	2.6	103.9	2.1	104.5	2.1
N 04	99.8	1.7	98.8	1.5	100.6	2.4
N 11	98.4	2.5	99.0	3.3	99.9	3.0
N 18	98.4	1.9	100.4	3.1	104.7	3.7
SLI 01	98.5	0.4	99.6	0.5	99.4	0.9
SLI 03	105.0	1.5	105.1	0.8	102.5	1.3
SLI 10	101.6	0.7	100.0	0.4	100.8	0.7
SLI 11	99.1	0.6	99.9	0.2	100.4	0.6
SLI 19	99.4	1.7	99.0	1.4	99.0	0.9
Mean	100.4	2.7	100.7	2.7	101.2	2.7

100% volume indicates that the segments are similar in volume. SD-Standard Deviation. N-Normal SLI-Scapholunate instability. The index number of the wrist is indicated in the first column (e.g., N 00 is the Normal wrist numbered 00). Raw data files with individual data points for all frames are included in Appendix 1.2)

### 3.1.2. Coordinate system placement

The reproducibility of coordinate system placement was assessed using test and retest repeatability (Figure 53). The rotational and translational differences between the first and the second placement are presented in Table 13 and Table 14.

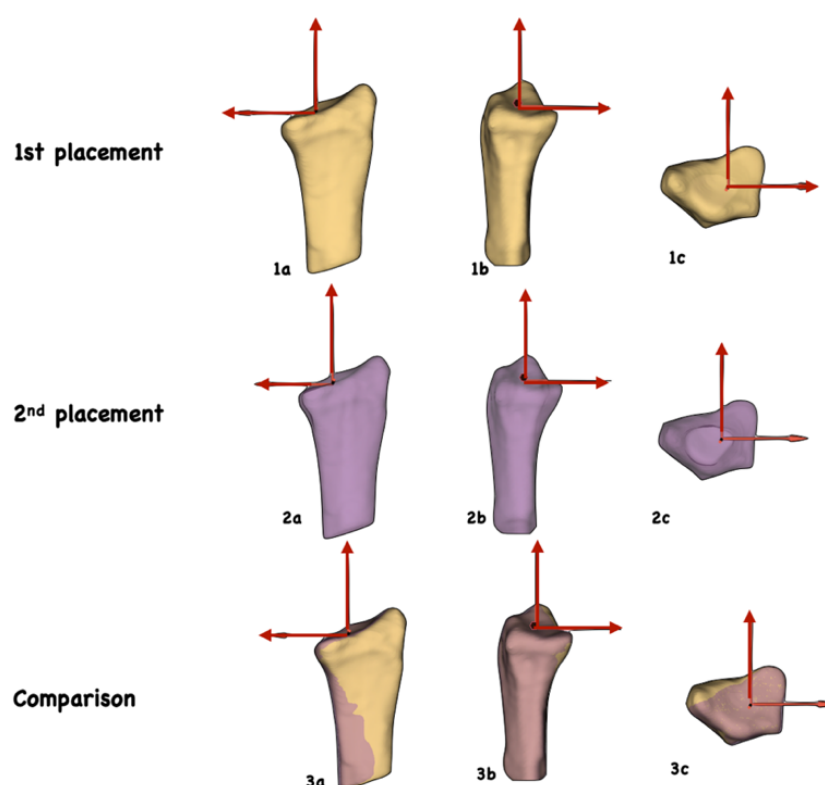


Figure 53 Reproducibility of the radius coordinate system placement. The coordinate system was placed on the radius of a randomly selected wrist in the neutral position according to the method described in section (2.3.9). This is the first placement. 1.a, 1.b and 1.c depicts the coronal, sagittal and axial projections of the first placement. Then the process was repeated for the same radius, independent of the first placement. This is named the second placement. The second placement is depicted in 2a, 2b and 2c. The first and second placement positions were compared to assess the reproducibility. The comparison is shown in 3a, 3b and 3c, depicting the two placements in two colours-first Brown, second- purple. If the coordinate system placement was 100% reproducible at every attempt, the result would be identical. The positioning reproducibility was calculated by registering the first placement radius to the second placement radius and calculating the angular and linear changes between the two.

Table 13 Reproducibility of radius coordinate system placement -rotational error

Axis	Mean	Standard deviation
Rotation around z-axis (flexion-extension)	1.47°	0.96°
Rotation around-x-axis (radioulnar angulation)	1.25°	1.26°
Rotation around y-axis (Internal- external rotation)	2.10°	1.48°

The mean rotational error of the positioning the radius coordinate system around 3 axes is presented in degrees. Raw data files are included in Appendix 1.2.



The rotational error was  $2.1^{\circ} (\pm 1.48^{\circ})$  and was detected around the y-axis, indicating internal-external rotation (Table 13).

*Table 14 Reproducibility of radius coordinate system placement -translational error*

Direction	Mean (mm)	Standard deviation
Translation along the z-axis (radioulnar translation)	0.49	0.23
Translation along the x-axis (dorso-volar translation)	0.41	0.31
Translation along the y-axis (proximo-distal translation)	0.22	0.21

*The mean translational error of the positioning coordinate system along 3 axes are presented in mm. Raw data files are included in Appendix 1.2.*

The translational error was 0.49 mm ( $\pm 0.23$  mm) and was detected along the z-axis, indicating radioulnar direction (Table 14)

### **3.1.3. Iterative closest point registration test and retest**

Scaphoid, lunate, and capitate in five randomly selected healthy wrists and five SLI wrists, from the study cohort, were registered using iterative closest point (ICP) algorithm. Then, Euler's angles were calculated. This procedure was considered the first observation. A re-test was done repeating the same steps and the results obtained were considered the second observation. This was a test-retest repeatability assessment of the Euler's angles calculated after ICP registration. The interclass correlation coefficient (ICC) was calculated between the first and the second observation. The results are presented in Table 15.

Table 15 Reproducibility of iterative closest point (ICP) registration of carpal bone models (Interclass correlation coefficient between the first and the second observation)

Wrist	ICC for z-axis (flexion-extension)	ICC for x-axis (radioulnar angulation)	ICC for y-axis (Internal-external rotation)
N 00	1.000	1.000	1.000
N 01	1.000	1.000	0.997
N 04	0.999	0.999	0.978
N 11	1.000	1.000	0.984
N 18	0.999	1.000	0.995
SLI 01	1.000	1.000	0.986
SLI 03	1.000	1.000	0.997
SLI 10	0.999	1.000	0.993
SLI 11	1.000	1.000	0.999
SLI 19	1.000	1.000	0.994
Average	0.99	0.99	0.99

Note -ICC (Interclass correlation coefficient) was assessed between repeated registrations and Euler's angle calculation as test-retest repeatability. Raw data files are included in Appendix 1.2. The average has been calculated comparing the first set of observations for the scaphoid in all wrists with the second set of observations for the scaphoid in all wrists; Similarly for the lunate and the capitate.

Euler's angles calculated repeatedly by registration using the ICP algorithm demonstrated excellent correlation, indicated by ICC of over 0.99 between the first and the second observation.

## 3.2. Patient demographics

### 3.2.1 Healthy participants

Nineteen normal right wrist scans were performed on healthy volunteer participants between the ages of 18-30 years with no pre-existing wrist pathology. The data was archived and anonymized to comply with the ethics agreement, hence no demographic data was available for this cohort.

### 3.2.2. SLI patients

Nineteen scapholunate instability (SLI) patients fulfilled the inclusion criteria described in the methodology section. Demographic data are presented in Table 16. There were 16 males and 3 females. Twelve SLI patients had their right wrist affected and 7 had left wrist affected. The mean age of the SLI patients at the time of the scan was  $36 \pm 13.6$  years.

Table 16 Demographic data for the scapholunate instability (SLI) patients

Gender	Mean age in years (SD)	Right wrist (n)	Left wrist (n)
Male	35.3 (14.8)	10	6
Female	40 (3.6)	2	1
Total	36 (13.6)	12	7

SD – Standard deviation, n - number

### 3.2.3. Range of motion (Normal Vs SLI wrist)

The normal distribution of data was confirmed by the Shapiro-Wilk test (Table 17). The mean range of motion was less for the SLI wrist than the normal wrist, in both extension to flexion and in ulnar to radial deviation (Table 18). This was statistically significant with extension to flexion (*mean  $\pm$  standard deviation, SLI  $92^\circ \pm 31.4^\circ$  vs normal  $122^\circ \pm 24.6^\circ$ ;  $p=0.002$ ).*

Table 17 Shapiro-Wilk test results for normality for wrist ranges of motion

Direction of motion	p-value
Extension to flexion (Normal)	0.410
Ulnar to radial deviation (Normal)	0.252
Extension to flexion (SLI)	0.602
Ulnar to radial deviation (SLI)	0.832

*\*Results are considered statistically significantly deviated from the normal distribution if the p-value is less than 0.05.*

Table 18 The mean (standard deviation) wrist ranges of motion.

Wrist motion	Normal	SLI	Two-sided p-value
Wrist extension to flexion	122° (24.6°)	92° (31.4°*)	0.002
Wrist ulnar to radial deviation	53.6° (7.1°)	47° (12.6°)	0.055

\*Indicates statistical significance at a p-value of 0.05.

The kinematic changes are presented as three subsections representing study 01, study 02 and study 03. Each section presents the changes that were identified in the SLI wrist, in the scaphoid and the lunate with regard to

- Radiocarpal kinematics (study 01)
  - Angular and linear displacement of the scaphoid and the lunate (the change in the angle from the neutral wrist position)
  - Radiocarpal angles (e.g., radioscapoid and the radiolunate angle)
  - Centroid position of the scaphoid and the lunate
- Midcarpal kinematics (study 02)
  - Angular displacement of the scaphoid and the lunate
- Helical axis of motion (HAM) of the scaphoid and the lunate (study 03)
  - The position and the orientation of the HAM

### 3.3. NEUTRAL POSITION OF THE WRIST (NORMAL VS SLI WRIST)

#### 3.3.1. Radioscaphoid angle

The normal distribution of data was confirmed by the Shapiro-Wilk test (Table 19). The SLI scaphoid was more flexed ( $66.1^{\circ} \pm 12.9^{\circ}$  Vs  $47.9^{\circ} \pm 12.6^{\circ}$ ;  $p < 0.001$ ) and internally rotated ( $70.2^{\circ} \pm 10.7^{\circ}$  Vs  $60.4^{\circ} \pm 9^{\circ}$ ;  $p = 0.004$ ) than the normal scaphoid (Table 20, Figure 54). There was no significant difference in the radial angulation between the two groups.

Table 19 Shapiro-Wilk test results for normality for radioscaphoid angle in the neutral wrist position

Direction	p-value	
	Normal	SLI
Flexion	0.923	0.144
Radial angulation	0.225	0.346
Internal rotation	0.496	0.268

\*Results are considered statistically significantly deviated from the normal distribution if the p-value is less than 0.05.

Table 20 The radioscaphoid angles in the wrist neutral position

Rotation	Normal mean (SD)	SLI mean (SD)	Two- Sided p	Mean Difference	Std. Error of Difference	95% Confidence Interval of the Difference	
						Lower	Upper
Radial angulation (Coronal)	32.4° (12.9°)	39.4°±21.6°	0.237	-6.9°	5.8°	-18.7°	4.8°
Flexion (Sagittal)	47.9° (12.6°)	66.1° (12.9°)*	<0.001	-18.2°	4.1°	-26.6°	-9.9°
Internal Rotation (Axial)	60.4° (9°)	70.2° (10.7°)*	0.004	-9.8°	3.2°	-16.4°	-3.3°

\*Indicates statistical significance at a p-value of 0.05. The results presented are the mean (SD-standard deviation) for 19 wrists in each group. Negative mean difference indicates that the SLI mean is higher than the normal.

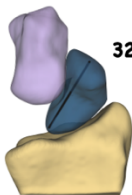
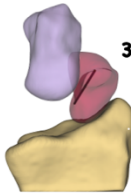

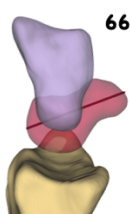
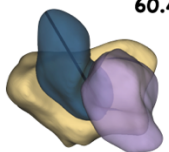
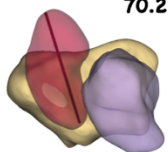
Normal		SLI	
Ia	 $32.4^{\circ} \pm 12.9^{\circ}$	IIa	 $39.4^{\circ} \pm 21.6^{\circ}$
Coronal			
Ib	 $47.9^{\circ} \pm 12.6^{\circ}$	IIb	 $66.1^{\circ} \pm 12.9^{**}$
Sagittal			
Ic	 $60.4^{\circ} \pm 9^{\circ}$	IId	 $70.2^{\circ} \pm 10.7^{**}$
Axial			

Figure 54 The radioscaphoid angles in the neutral wrist position. \*Indicates statistical significance at a p-value of 0.05. The results presented are the mean  $\pm$  standard deviation for 19 wrists. Note that a single representative wrist is depicted.

### 3.3.2. Radiolunate angle

The normal distribution of data for the radiolunate angle was confirmed by the Shapiro-Wilk test (Table 21).

Table 21 Shapiro-Wilk test results for normality for radiolunate angle in the neutral wrist position

Direction	p-value	
	Normal	SLI
Flexion	0.561	0.313
Radial angulation	0.211	0.227
Internal rotation	0.785	0.763

\*Results are considered statistically significantly deviated from the normal distribution if the p-value is less than 0.05.

The SLI lunate was more extended than the normal lunate ( $-22^{\circ} \pm 13^{\circ}$  Vs  $11^{\circ} \pm 5.8^{\circ}$ ;  $p=0.002$ , Table 22, Figure 55). There were no significant differences in the radial angulation and internal rotation between the two groups.

Table 22 The radiolunate angles in the neutral wrist position.

Rotation	Normal mean (SD)	SLI mean (SD)	Two- Sided p	Mean Difference	Std. Error of Difference	95% Confidence Interval of the Difference	
						Lower	Upper
Radial angulation (Coronal)	57.6° (16.5°)	55.2° (0.2°)	0.677	2.5°	5.9°	-9.6°	14.6°
<b>Flexion (Sagittal)</b>	<b>-11° (5.8°)</b>	<b>-22° (13°)*</b>	<b>0.002</b>	<b>10.9°</b>	<b>3.3°</b>	<b>4.3°</b>	<b>17.6°</b>
Internal Rotation (Axial)	64.5° (9°)	61.4° (14°)	0.420	3.1°	3.8°	-4.6°	10.8°

\*Indicates statistical significance at a p-value of 0.05. Note that the negative direction indicate extension. The results presented are the mean (SD- standard deviation) for 19 wrists in each group. Negative mean difference indicates that the SLI mean is higher than the normal.

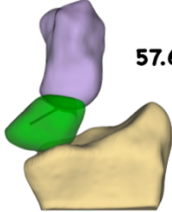



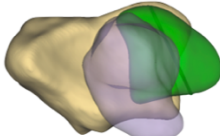
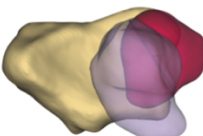
Normal		SLI	
Coronal	Ia		
		$57.6^{\circ} \pm 16.5^{\circ}$	$55.2^{\circ} \pm 20.2^{\circ}$
	Ib		
Sagittal		$-11^{\circ} \pm 5.8^{\circ}$	$-22^{\circ} \pm 13^{**}$
	Ic		
		$64.5^{\circ} \pm 9^{\circ}$	$61.4^{\circ} \pm 14^{\circ}$
Axial		Ic	IIf

Figure 55 The radiolunate angles in the neutral wrist position. \*Indicates statistical significance at a p-value of 0.05. The results presented are the mean  $\pm$  standard deviation for 19 wrists in each group. Note that a single representative wrist is depicted.

### 3.3.3. Scaphoid and the lunate centroid positions

The data were first assessed for normality using the Shapiro-Wilk's test (Table 23).

Table 23 Shapiro-Wilk test results for scaphoid and the lunate centroid positions in the neutral wrist position.

Direction	p-value	
	Normal	SLI
Scaphoid radioulnar translation	0.185	0.947
Scaphoid dorso-volar translation	0.579	0.084
Scaphoid proximo-distal translation	0.914	0.249
Lunate radioulnar translation	0.489	0.799
Lunate dorso-volar translation	0.516	0.185
Lunate proximo-distal translation	0.592	0.255

\*Results are considered statistically significantly deviated from the normal distribution if the p-value is less than 0.05.



The SLI scaphoid centroid position was more radial than the normal scaphoid ( $-7.3\text{mm} \pm 1.2$  Vs  $-6.4\text{ mm} \pm 1.2$   $p=0.03$ , Table 24).

Table 24 The scaphoid centroid position in the neutral wrist position.

Direction	Normal mean (SD)	SLI mean (SD)	Two-Sided p	Mean Difference	Std. Error of Difference	95% Confidence Interval of the Difference	
						Lower	Upper
Radioulnar direction (ulnar +ve)	-6.4 (1.2)	-7.3 (1.2)*	0.036	0.8	0.4	0.1	1.6
Dorso-volar direction (volar +ve)	3.6 (1.3)	3.8 (1.1)	0.709	-0.1	0.4	-0.9	0.6
Proximodistal translation (distal +ve)	13.5 (1.6)	14 (2)	0.483	-0.4	0.6	-1.6	0.8

\*Indicates statistical significance at a p-value of 0.05. Units are in mm. The results presented are the mean (SD-standard deviation) for 19 wrists in each group. Negative mean difference indicates that the SLI mean is higher than the normal.

The SLI lunate centroid position was more ulnar than the normal lunate ( $8.3\text{ mm} \pm 1.3$  Vs  $7\text{ mm} \pm 1.3$ ;  $p=0.004$ , Table 25)

Table 25 The lunate centroid position in the wrist neutral position

Direction	Normal mean (SD)	SLI mean (SD)	Two-Sided p	Mean Difference	Std. Error of Difference	95% Confidence Interval of the Difference	
						Lower	Upper
Radioulnar direction (ulnar +ve)	7 (1.3)	8.3 (1.3)	0.004	-1.3	0.4	-2.2	-0.4
Dorso-volar direction (volar +ve)	3.3 (1)	3.6 (1.5)	0.516	-0.3	0.4	-1.1	0.6
Proximodistal translation (distal +ve)	6.1 (0.8)	5.9 (0.8)	0.541	0.2	0.3	-0.4	0.7

\*Indicates statistical significance at a p-value of 0.05. Units are in mm. The results presented are the mean (SD-standard deviation) for 19 wrists in each group. Negative mean difference indicates that the SLI mean is higher than the normal.

## 3.4. RADIOCARPAL KINEMATICS

### 3.4.1. Wrist extension to flexion

#### *Scaphoid and lunate angular displacements*

In this section, the angular displacements of the scaphoid and the lunate are presented. Angular displacement was measured as the change in the carpal angle from the neutral wrist position, as the wrist moved. All tables (Table 26 to Table 61) containing the detailed results of radiocarpal kinematics are presented at the end of this section.

#### Scaphoid flexion

From 70° to 40° wrist extension, the SLI scaphoid flexed more than the normal scaphoid (Figure 56). The statistical significance at each incremental step of 5° is presented in the Table 26. From 35° wrist extension to 30° wrist flexion, there was no significant difference between the SLI scaphoid and the normal scaphoid flexion. From 35° flexion to 50° flexion, there was less flexion in the SLI scaphoid than the normal scaphoid.

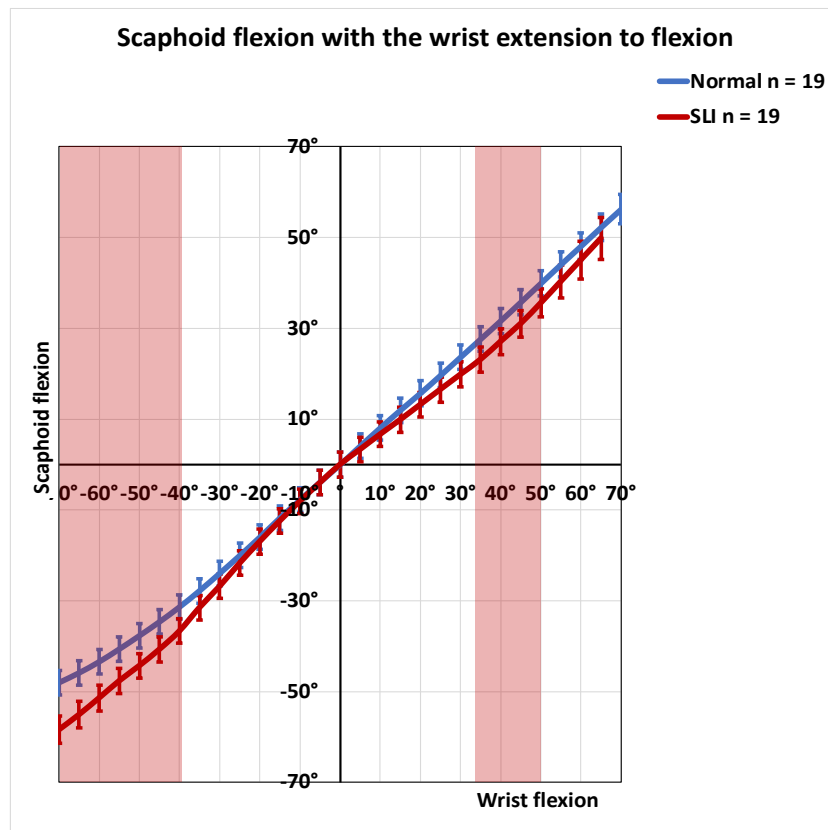


Figure 56 Scaphoid flexion with the wrist extension to flexion (95% confidence intervals are marked by the error bars). Note that the both the SLI and the normal scaphoids flexed with the wrist flexion. The red highlighted zones indicate the wrist range of motion where a statistically significant difference exists between the normal and the SLI wrist.

#### Scaphoid radial angulation

With the wrist extension to flexion, there was no significant difference in the radial angulation of the scaphoid between the two groups, until the wrist reached 60° flexion (Figure 57, Table 27). However, at 65° of wrist flexion, where there was a significant difference, the confidence intervals of mean overlapped.

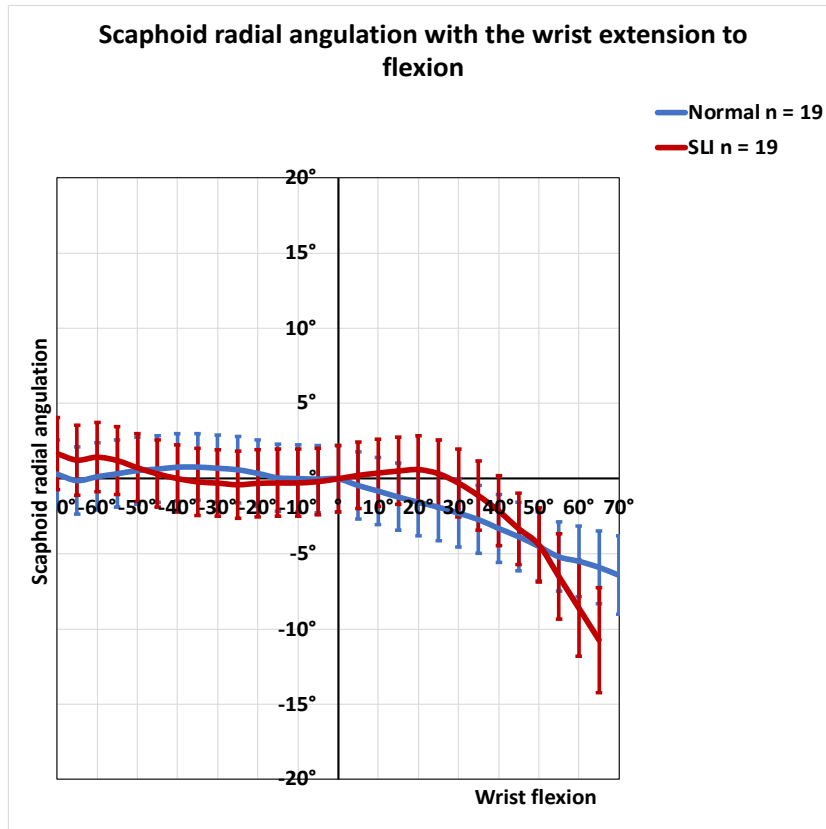


Figure 57 Scaphoid radial angulation with the wrist extension to flexion (95% confidence intervals are marked by the error bars). Note that with the wrist extension to flexion the scaphoid angulated ulnarly but less than 5° until the wrist reached 50° flexion.

#### Scaphoid internal rotation

As the wrist moved from extension to flexion, both the SLI and the normal scaphoids externally rotated. With the wrist extension to flexion, there was no significant difference in the internal/external rotation of the scaphoid between the two groups until the wrist reached 60° flexion (Figure 58). However, at this point, the confidence intervals of mean overlapped, and the mean difference was within the margin of error of the method (Table 28).

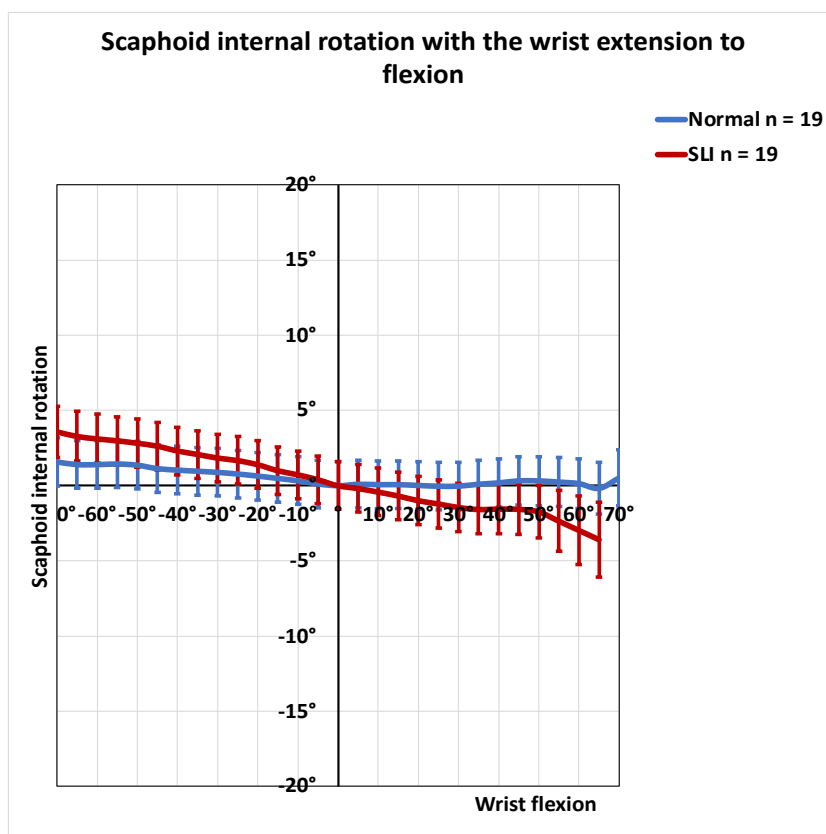


Figure 58 Scaphoid internal rotation with the wrist extension to flexion (95% confidence intervals are marked by the error bars). Note that there was no statistically significant difference between the two groups.

## Lunate flexion

With the wrist extension to flexion both the SLI and the normal lunate flexed. From 70° wrist extension to 30° wrist extension, the SLI lunate flexed less than the normal lunate (Figure 59, Table 29). From 25° extension of the wrist to 65° flexion, there was no significant difference in flexion of the lunate between the SLI and the normal groups.

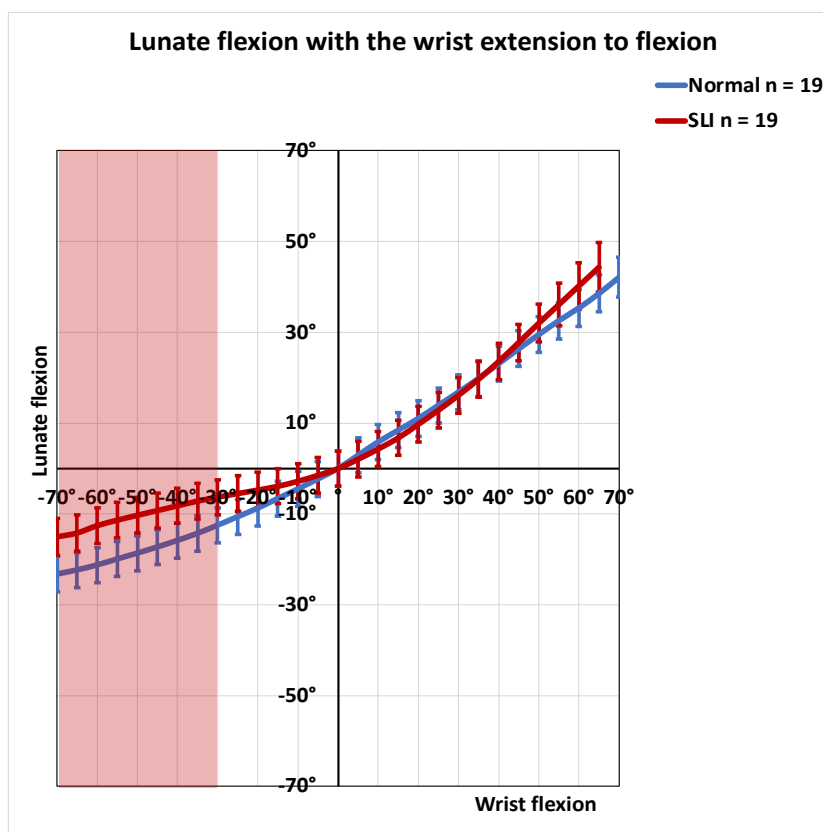


Figure 59 Lunate flexion with the wrist extension to flexion (95% confidence intervals are marked by the error bars). Note The SLI lunate flexed significantly less than the normal lunate from 70 to 30° wrist extension. The red highlighted zones indicate the wrist range of motion where a statistically significant difference exists between the normal and the SLI wrist.

## Lunate radial angulation

With wrist extension to flexion, both the SLI and the normal lunates angulated ulnarly. There was no significant difference in radioulnar angulation of the lunate between the SLI and the normal groups except when the wrist is in extension beyond 55° (Figure 60, Table 30). Nonetheless, the statistically significant difference seen in extreme extension between the two groups were within the margin of error of the method.

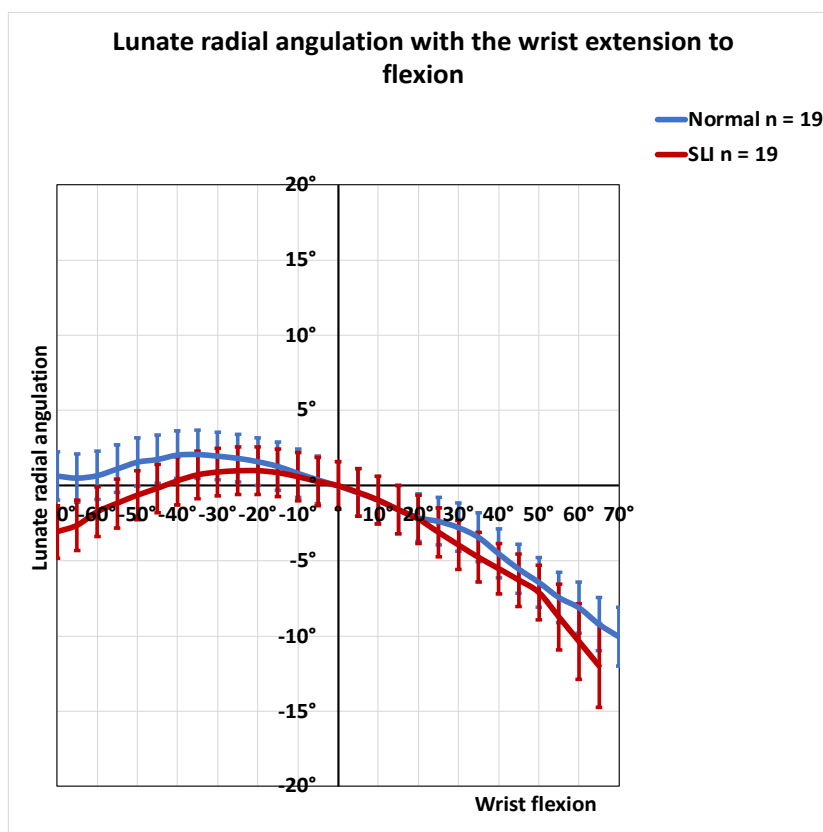


Figure 60 Lunate radial angulation with the wrist extension to flexion (95% confidence intervals are marked by the error bars). With the wrist moving from extension to flexion, both the SLI and the normal lunates angulated ulnarly however, there was no statistically significant difference between the two groups.

## Lunate internal rotation

With wrist extension to flexion, the SLI lunate has more external rotation (negative internal rotation) than the normal lunate, either when the wrist is extended beyond 50° or the when the wrist is flexed beyond 60° (Figure 61). However, the mean difference is within the error rate of the method, hence this significance was considered negligible (Table 31).

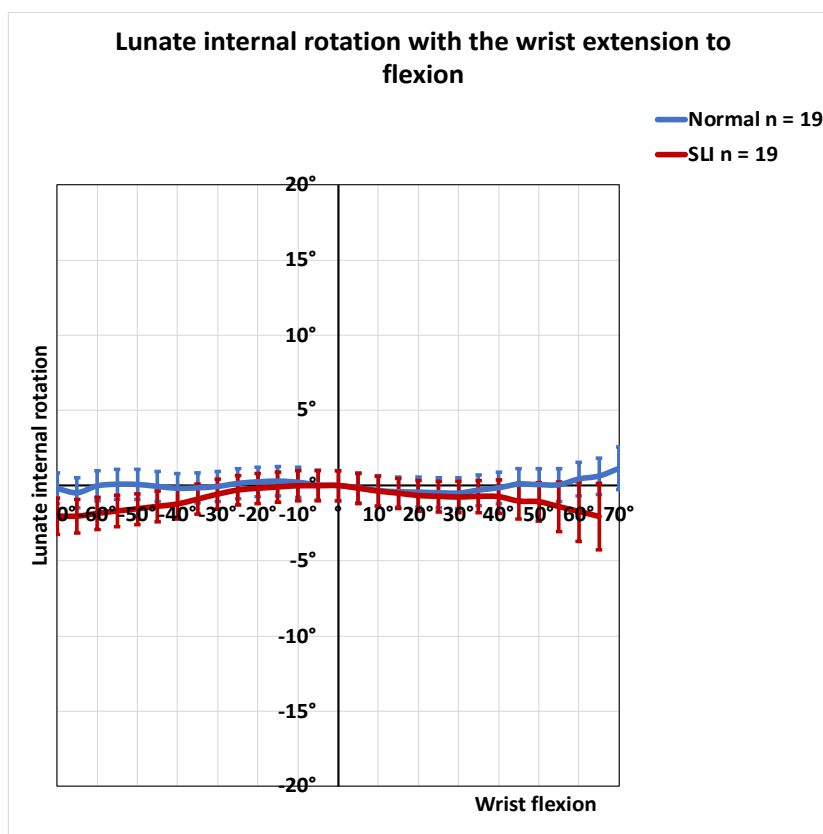


Figure 61 Lunate internal rotation with the wrist extension to flexion (95% confidence intervals are marked by the error bars). SLI lunate appeared to have more external rotation than the normal lunate in the extremes of wrist motion, i.e., when the wrist was extended beyond 50° or flexed beyond 65°. Nonetheless, this significance is not a true significance as the values were within the error rate of the method.

### Radioscaphoid and radiolunate angulations

In this section, the radioscaphoid angle, and the radiolunate angle, in the coronal, sagittal and axial planes, as the wrist moves from extension to flexion are presented. The sagittal plane radioscaphoid angle is the 'radioscaphoid angle (flexion)', the coronal plane radioscaphoid angle is the 'radioscaphoid angle (radial angulation)' and the axial plane radioscaphoid angle is the 'radioscaphoid angle (internal rotation)'. This is a true angle of the scaphoid relative to the radius compared to the previous section that presented the angular displacement.



## Radioscaphoid angle (flexion)

With wrist extension to flexion, the SLI scaphoid remains more flexed than the normal scaphoid, throughout the range of motion (Figure 62, Figure 63). Statistical significance at each incremental step of 5° is presented in the Table 32. At the neutral position the Radioscaphoid angle differs by 18.9° between the two groups. At 50° wrist extension, this difference is 11.6°; At 50° wrist flexion the difference is 13.7°.

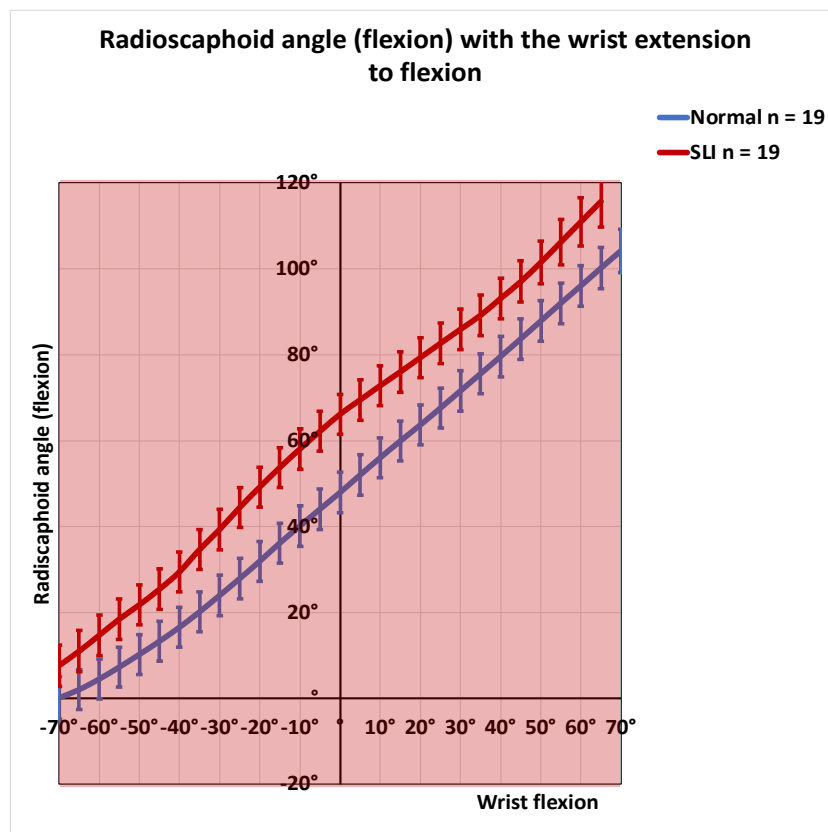


Figure 62 Radioscaphoid angle (flexion) with the wrist extension to flexion (95% confidence intervals are marked by the error bars). Note that the difference in the radioscaphoid flexion angle varies from 11.6° at 50° wrist extension to 13.7° at 50° wrist flexion. The red highlighted zones indicate the wrist range of motion where a statistically significant difference exists between the normal and the SLI wrist.

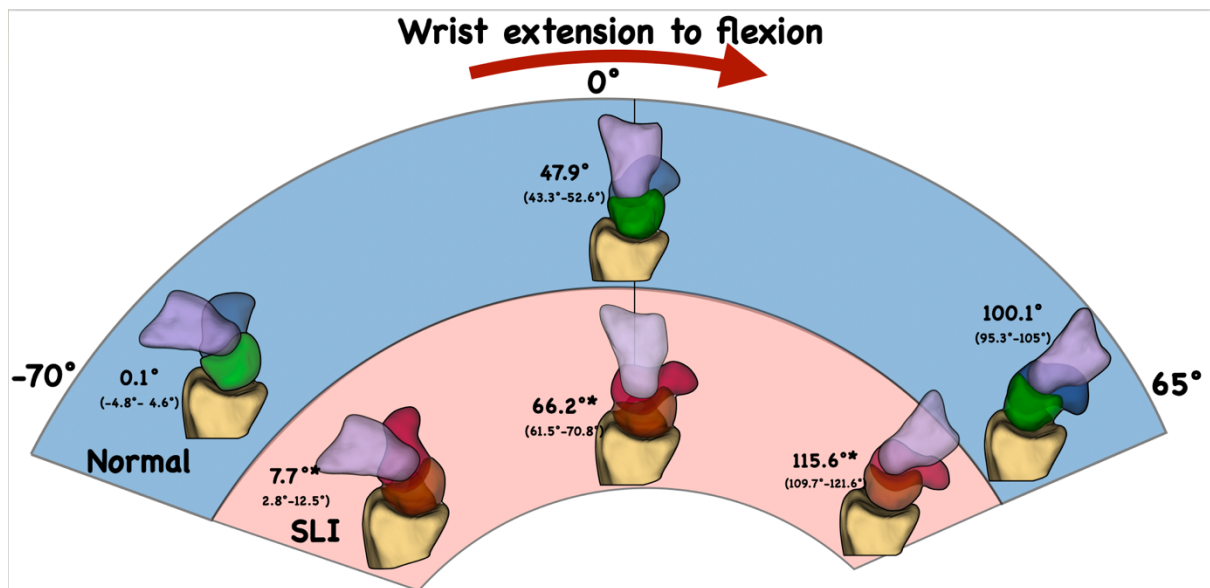


Figure 63 Graphic representation of the radioscapoid angle (flexion) in scapholunate instability (SLI). The radioscapoid angle in SLI remain significantly flexed compared to the normal wrist throughout extension to flexion. Note that “\*” indicate statistical significance at p value of 0.05 level. The results presented are the mean (95% confidence interval).

#### Radioscapoid angle (radial angulation)

With the wrist extension to flexion, there was no statistically significant difference between the radioscapoid angles (radial angulation) of the normal scaphoid and the SLI scaphoid (Figure 64, Table 33). While it appeared that the SLI scaphoid remained radially angulated throughout the range a significant difference was not observed between the two groups due to the variability.

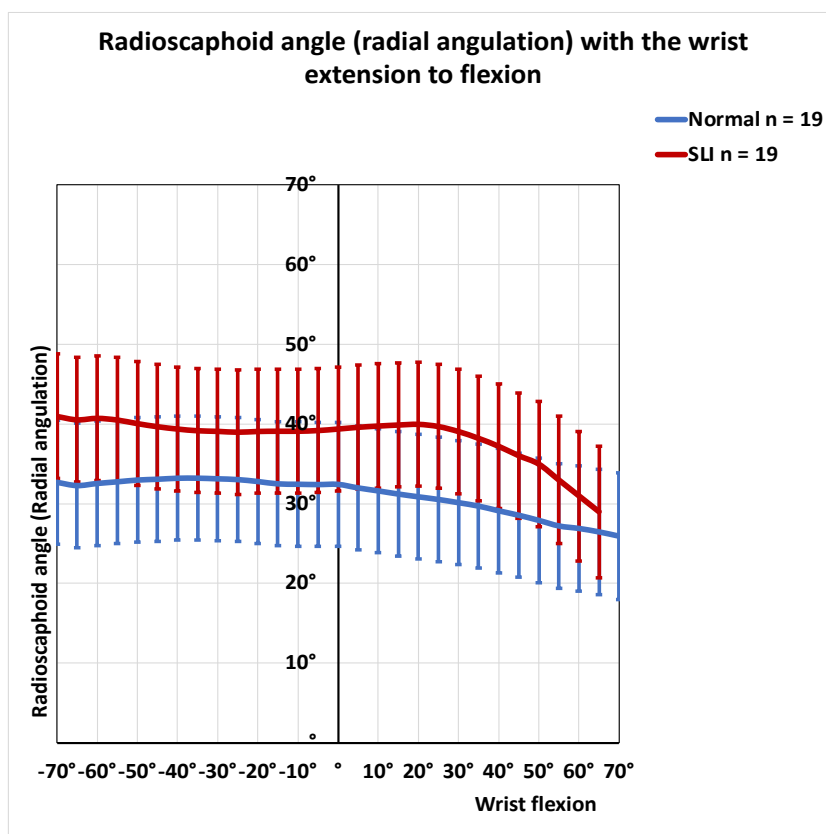


Figure 64 Radioscaphoid angle (radial angulation) with the wrist extension to flexion (95% confidence intervals are marked by the error bars). Note that with the wrist moving from extension to flexion, the SLI scaphoid appeared radially angulated more than the normal scaphoid but there was no significant difference between the two groups.

Radioscaphoid angle (internal rotation)

With wrist extension to flexion, the SLI scaphoid remains more internally rotated than the normal scaphoid, up to 55° of wrist flexion (Figure 65, Table 34).

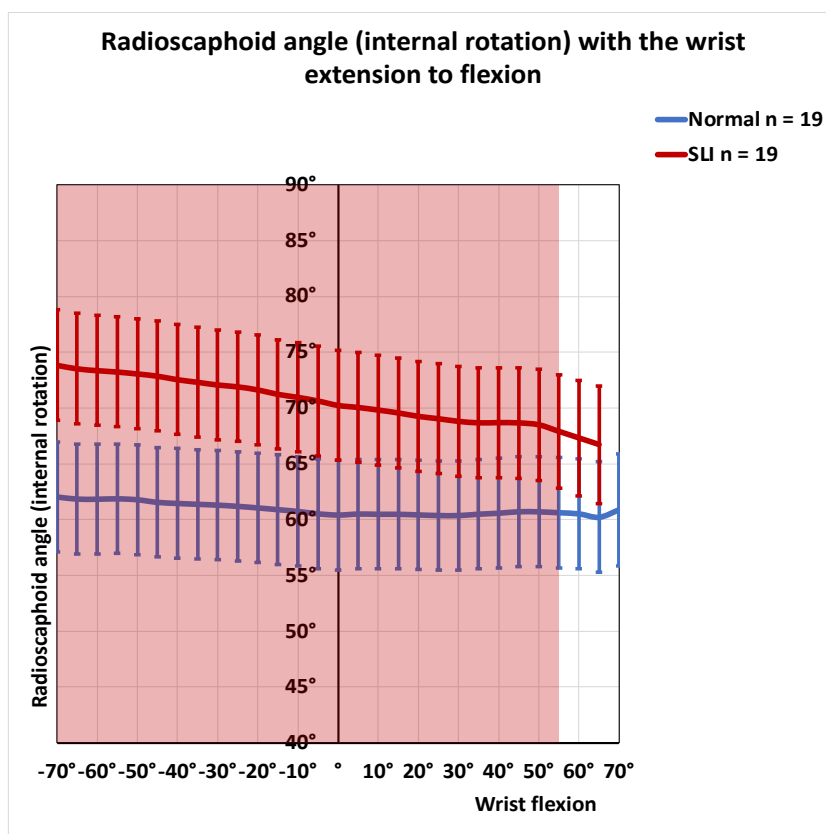


Figure 65 Radioscaphoid angle (internal rotation) with the wrist extension to flexion (95% confidence intervals are marked by the error bars). Note that the SLI scaphoid was significantly more internally rotated than the normal scaphoid until the wrist reached 60° flexion. The red highlighted zones indicate the wrist range of motion where a statistically significant difference exists between the normal and the SLI wrist.

#### Radiolunate angle (flexion)

With wrist extension to flexion, the radiolunate angle increased (from negative, i.e., lunate extension to positive, flexion). From the wrist 70° extension to 20° extension, there was no statistically significant change in the radiolunate angle (flexion) between the SLI and the normal wrists (Figure 66, Table 35). From 20° wrist extension to 55° flexion, the SLI radiolunate angle remains lower (more extended and less flexed) than the normal lunate (Figure 67).

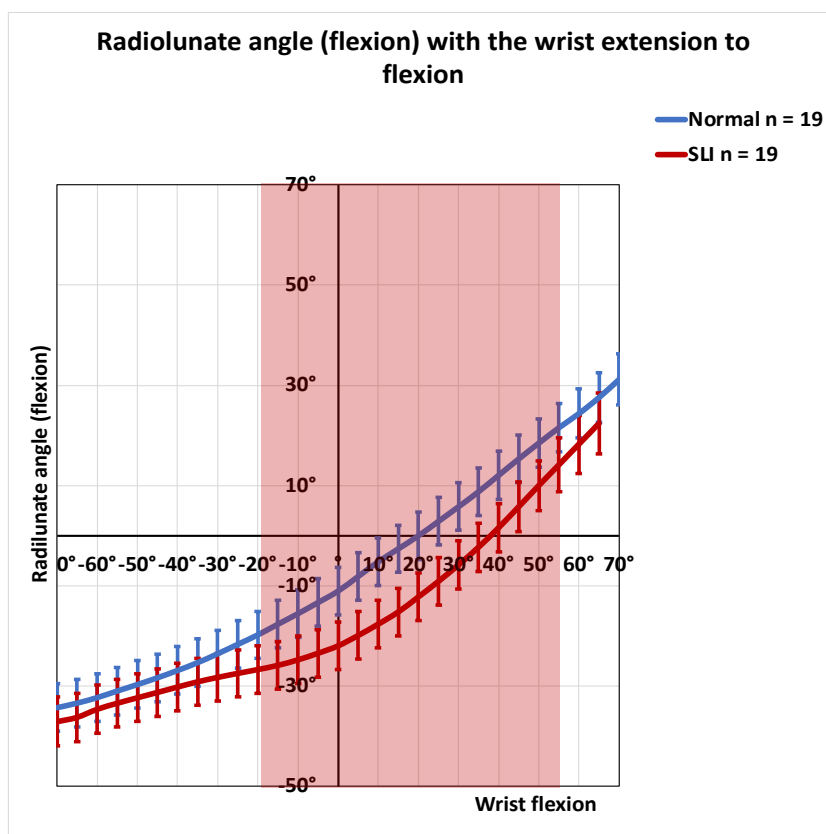


Figure 66 Radiolunate angle (flexion) with the wrist extension to flexion (95% confidence intervals are marked by the error bars). Note that a statistically significant difference of the radiolunate angle (flexion) between the SLI and the normal wrists was observed from 20° wrist extension to flexion. The red highlighted zones indicate the wrist range of motion where a statistically significant difference exists between the normal and the SLI wrist.

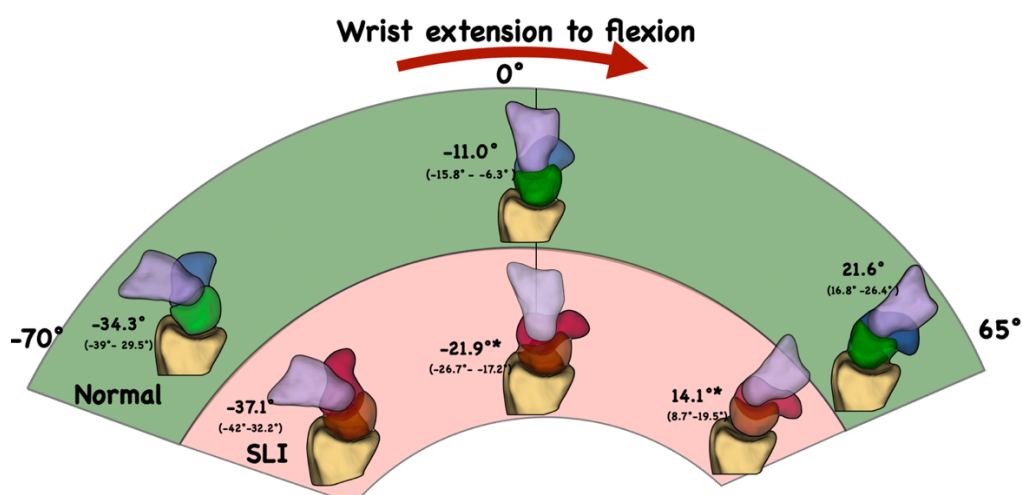


Figure 67 Graphic representation of the radiolunate angle (flexion) in scapholunate instability (SLI). The radiolunate angle was similar between the SLI and the normal wrists when the wrist was in extension but significantly different when the wrist was neutral or in flexion. Note that “\*” indicate statistical significance at  $p$  value of 0.05 level. The results presented are the mean (95% confidence interval).

## Radiolunate angle (radial angulation)

As the wrist moved from extension to flexion, there was no statistically significant difference in the radiolunate angles (radial angulation) between normal and SLI wrists (Figure 68, Table 36).

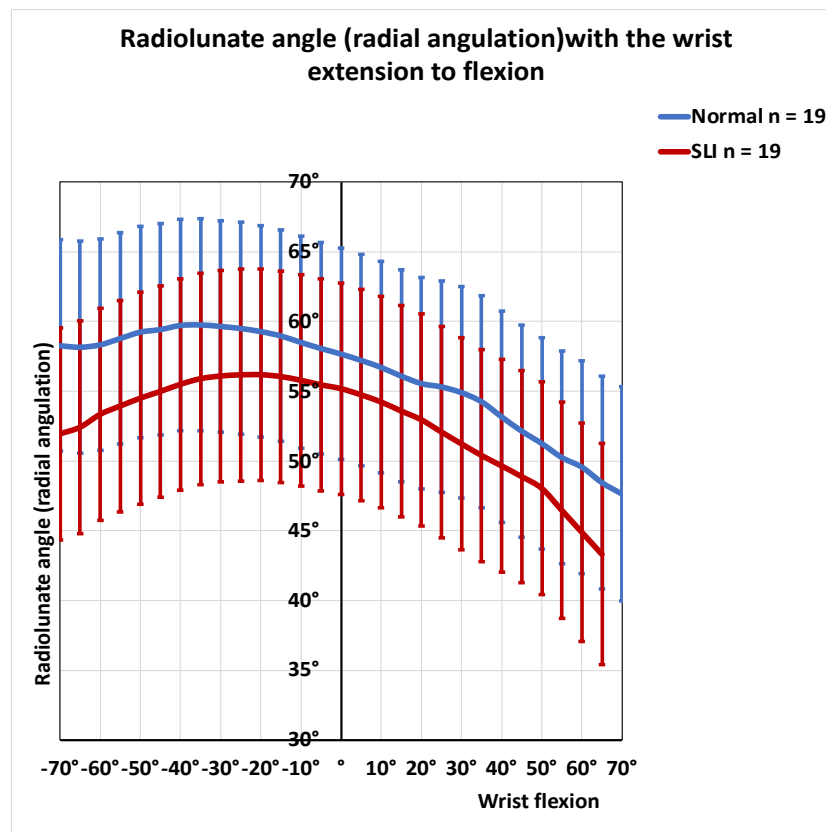


Figure 68 Radiolunate angle (radial angulation) with the wrist extension to flexion (95% confidence intervals are marked by the error bars). There was no statistically significant difference in the radiolunate angle (radial angulation) between the two groups.

## Radiolunate angle (internal rotation)

With wrist extension to flexion, there was no statistically significant difference between the radiolunate angles (internal rotation) of normal and SLI wrists (Figure 69, Table 37). It appeared that throughout the range of motion the SLI lunate remained externally rotated compared to the normal, however there was no significant difference between the two groups.

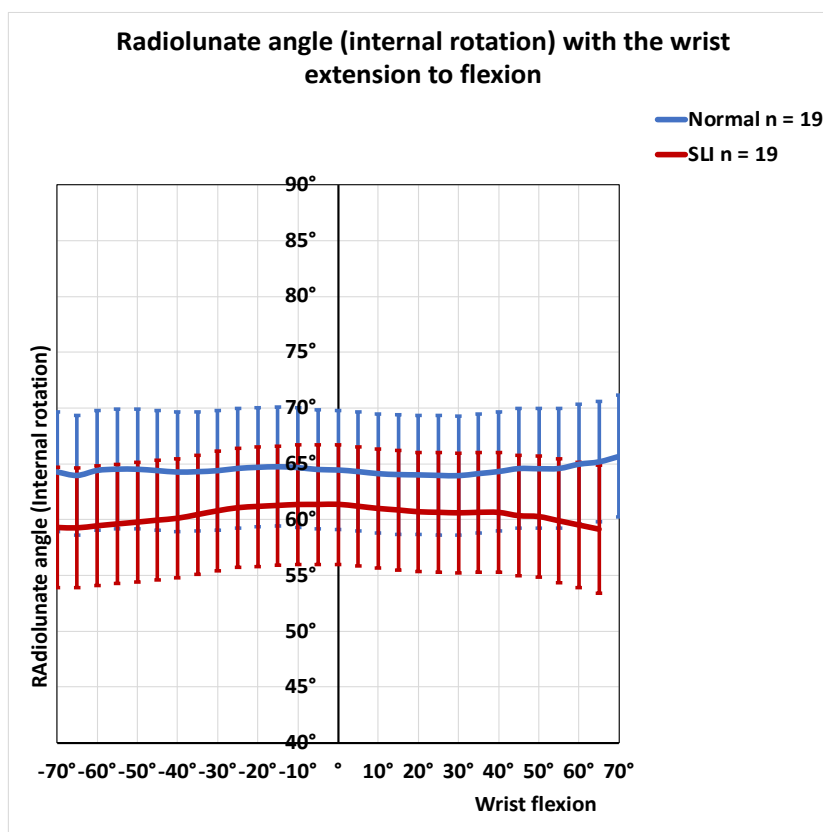


Figure 69 Radiolunate angle (internal rotation) with the wrist extension to flexion (95% confidence intervals are marked by the error bars). Throughout the range of motion there was no statistically significant difference in the radiolunate angle (internal rotation) between the two groups.

### Scaphoid and lunate centroid position

In this section, the scaphoid and lunate centroid position changes with the wrist moving from the extension to flexion, are presented.

Scaphoid centroid position (radio-ulnar direction)

With wrist moving from 70° extension to 15° flexion, the SLI scaphoid centroid position remained more radial than the normal scaphoid centroid position (Figure 70, Table 38). With wrist flexion from 20° to 50° there was no statistically significant difference in the scaphoid centroid position between the two groups.

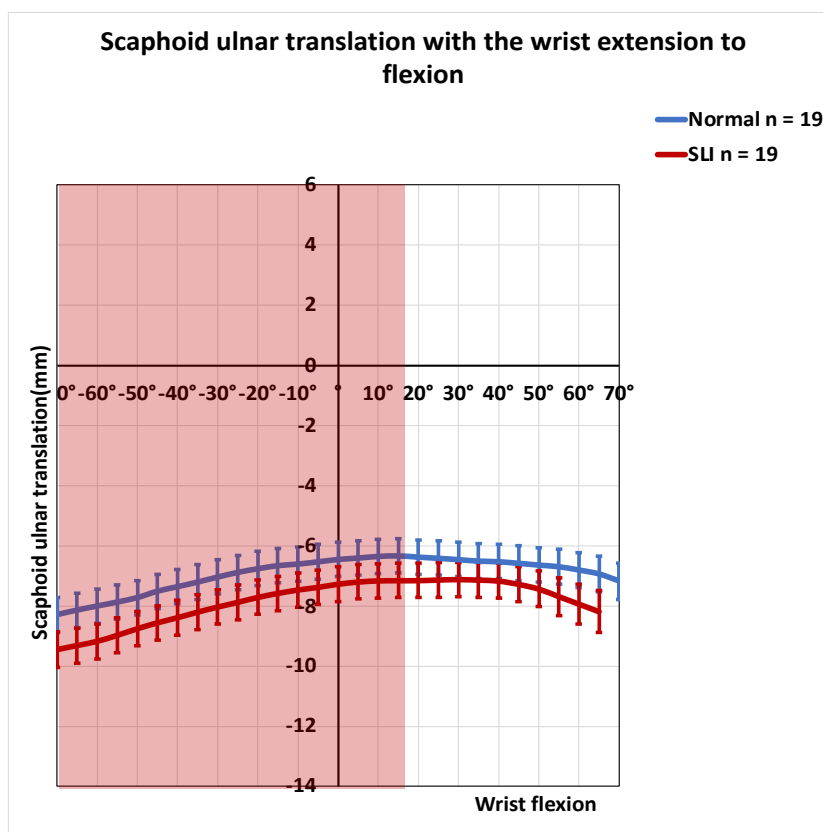


Figure 70 Scaphoid ulnar translation with the wrist extension to flexion (95% confidence intervals are marked by the error bars). The SLI scaphoid centroid position remained more radial than the normal scaphoid centroid position, however a statistically significant difference is observed from 70° wrist extension to 15° flexion. The red highlighted zones indicate the wrist range of motion where a statistically significant difference exists between the normal and the SLI wrist.

Scaphoid centroid position (dorso-volar direction)

With wrist extension to flexion, the centroid position of the normal and the SLI scaphoid both translated volarly. There was no statistically significant difference in the scaphoid centroid positions between the normal and the SLI wrists, along the dorso-volar direction (Figure 71, Table 39)



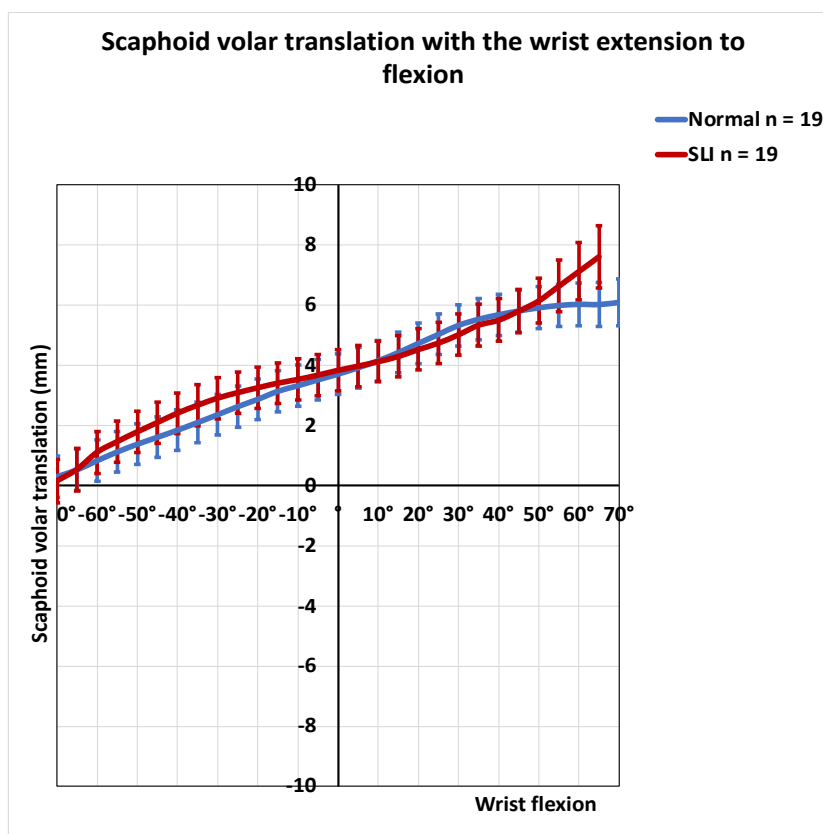


Figure 71 Scaphoid volar translation with the wrist extension to flexion (95% confidence intervals are marked by the error bars). Note that there was no statistically significant difference between the scaphoid centroid positions of normal and SLI wrists along the dorso-volar direction.

Scaphoid centroid position (proximo-distal direction)

From wrist 70° extension to 30° extension, the SLI scaphoid centroid remained more distal than the normal scaphoid (Figure 72, Table 40). From 30° wrist extension to 70° flexion, there was no statistically significant difference between the scaphoid centroid positions of normal and SLI wrists along the proximo distal direction.

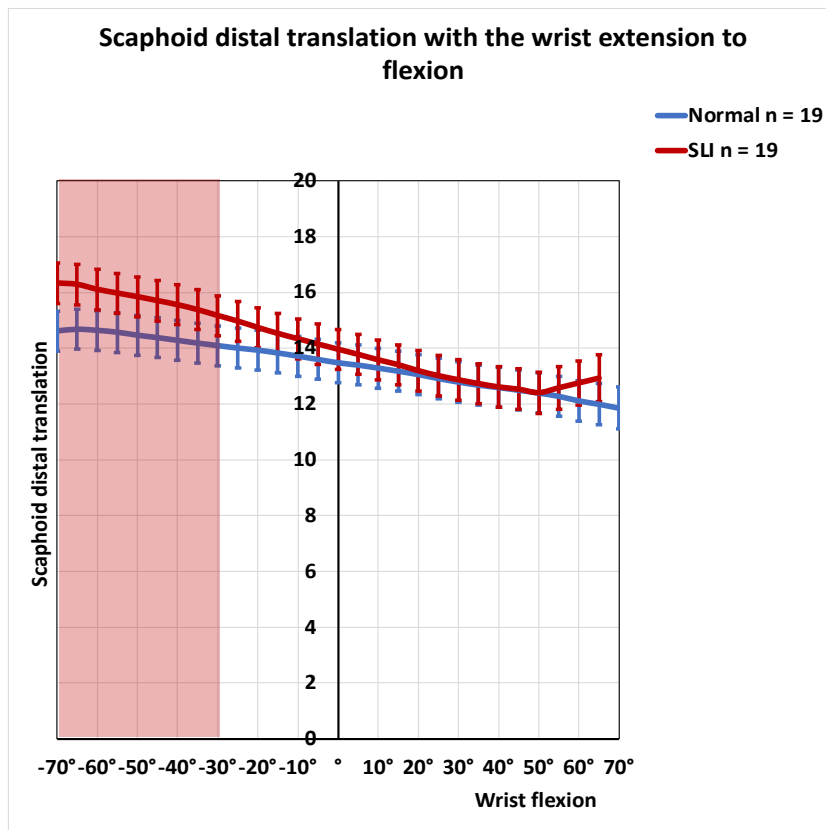


Figure 72 Scaphoid distal translation with the wrist extension to flexion (95% confidence intervals are marked by the error bars). Note that the SLI scaphoid centroid remained more distal than the normal centroid when the wrist is in extension more than 30°. The red highlighted zones indicate the wrist range of motion where a statistically significant difference exists between the normal and the SLI wrist.

Lunate centroid position (radio-ulnar direction)

With wrist 70° extension to 50° flexion, the SLI lunate centroid position remained more ulnar than the normal lunate centroid position (Figure 73, Table 41).

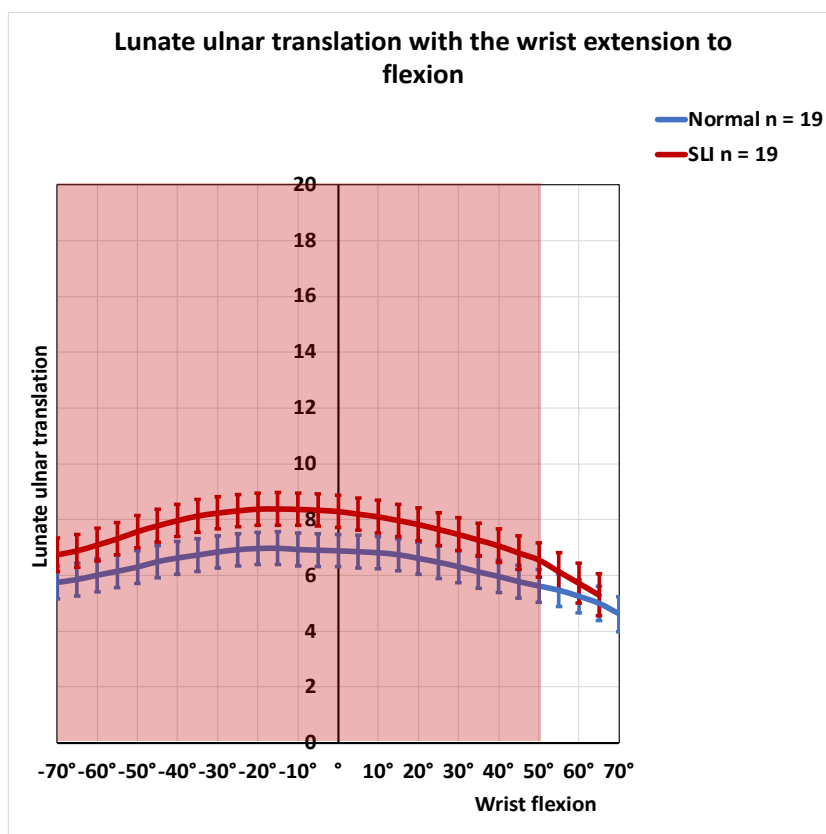


Figure 73 Lunate ulnar translation with the wrist extension to flexion (95% confidence intervals are marked by the error bars). Note that the SLI lunate centroid position remained more ulnar than the normal lunate centroid position and the difference is statistically significant throughout the range of motion, until the wrist reached 55° flexion. The red highlighted zones indicate the wrist range of motion where a statistically significant difference exists between the normal and the SLI wrist.

Lunate centroid position (dorso-volar direction)

With wrist extension to flexion, there was no statistically significant difference between the lunate centroid positions of normal and SLI wrists along the dorso-volar direction (Figure 74, Table 42).

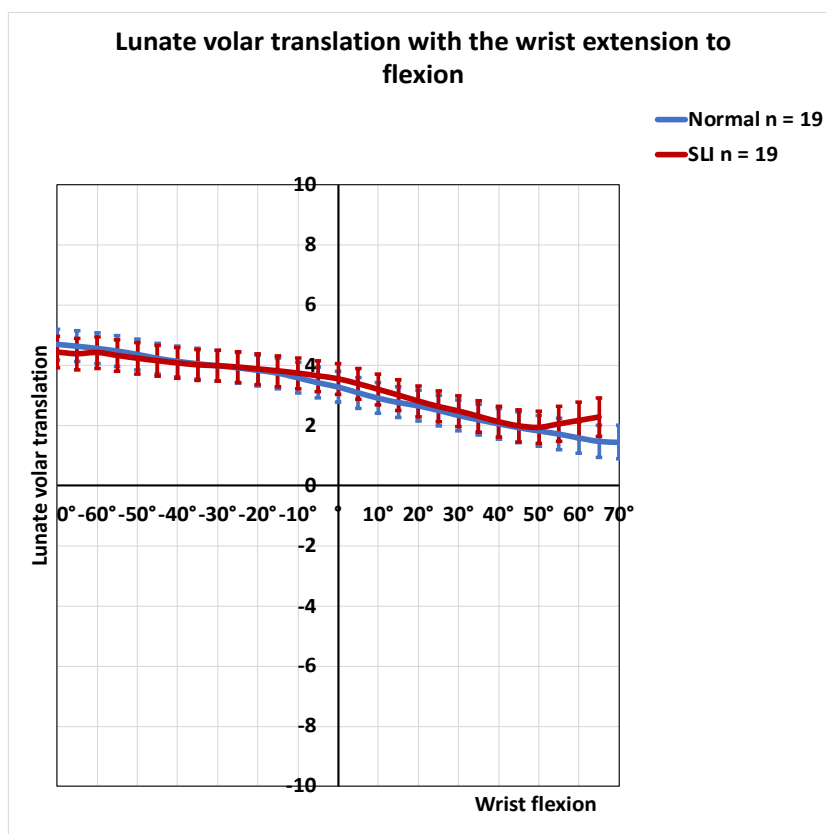


Figure 74 Lunate volar translation with the wrist extension to flexion (95% confidence intervals are marked by the error bars). Note that there was no statistically significant difference in the lunate centroid positions between the two groups.

Lunate centroid position (proximo-distal direction)

With wrist extension to flexion, there was no statistically significant difference in the lunate centroid positions between normal and SLI wrists along the proximo-distal direction (Figure 75, Statistical significance at each incremental step of 5° is presented in the Table 43).

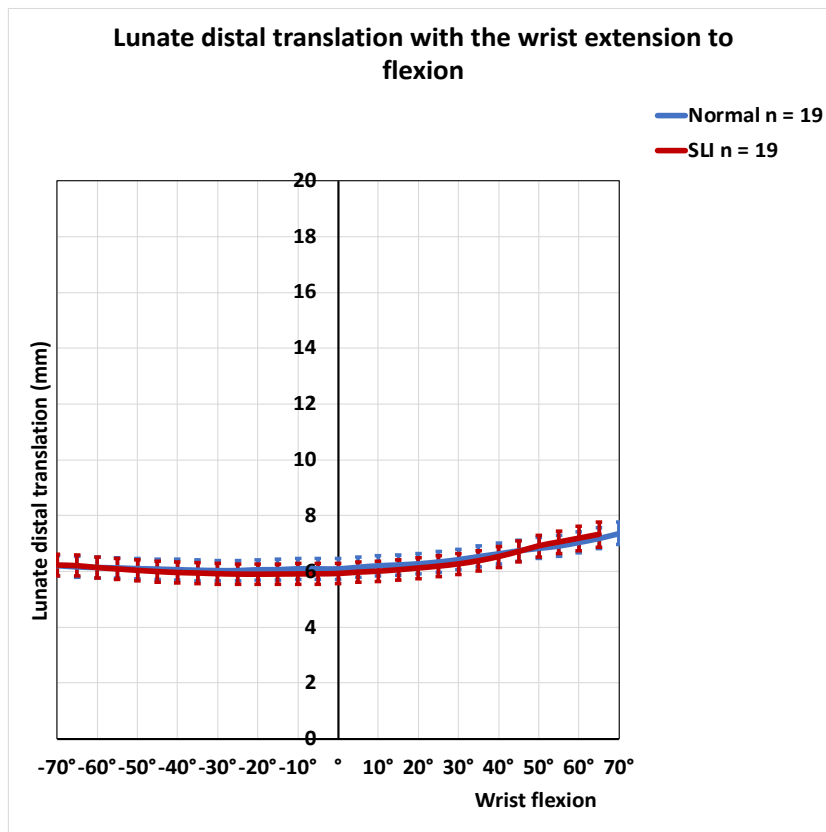


Figure 75 Lunate distal translation with the wrist extension to flexion (95% confidence intervals are marked by the error bars). Note that there was no statistically significant difference in the lunate centroid positions between the two groups.

### 3.4.2. Wrist ulnar to radial deviation

#### *scaphoid and lunate angular displacements*

In this section the angular displacements of the scaphoid and the lunate during the wrist ulnar to radial deviation is presented.

#### Scaphoid flexion

During wrist ulnar to radial deviation, both the SLI and the normal scaphoids flexed (Figure 76, Figure 77, Table 44). From 10° of radial deviation, as the wrist radially deviated more, there was less flexion in the SLI scaphoid than the normal scaphoid.

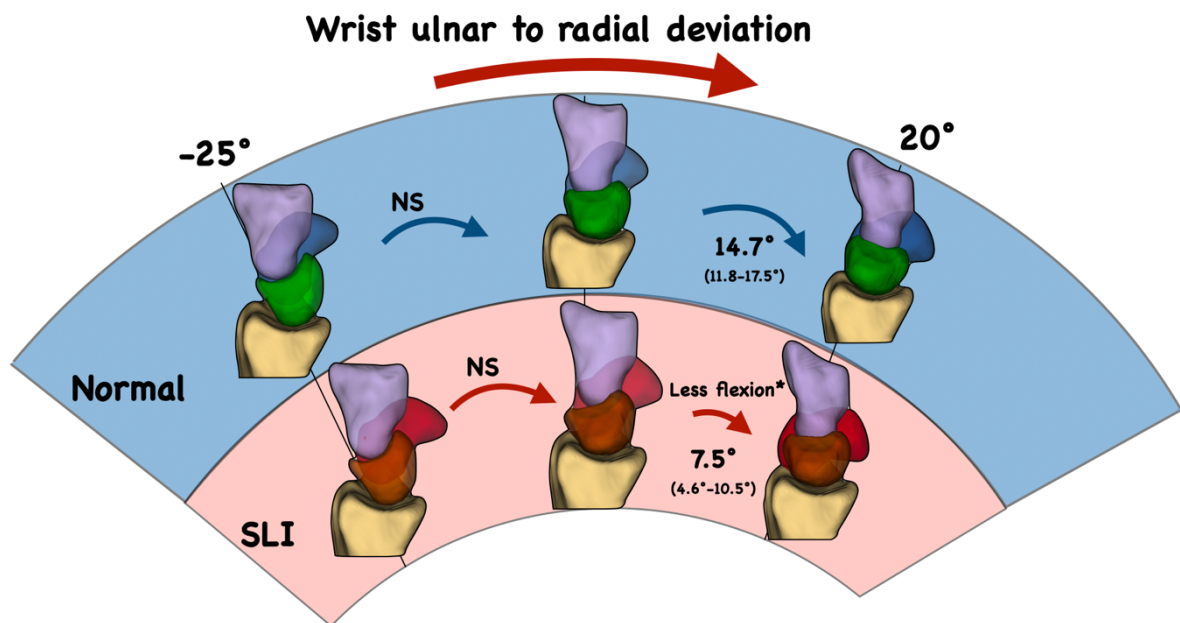


Figure 76 Graphic representation of the decreased flexion (out-of-plane motion) of the scaphoid in scapholunate instability (SLI). Note that “\*” indicate statistical significance at *p* value of 0.05 level. The results presented are the mean (95% confidence interval). NS-No statistically significant difference between the SLI and normal wrists.

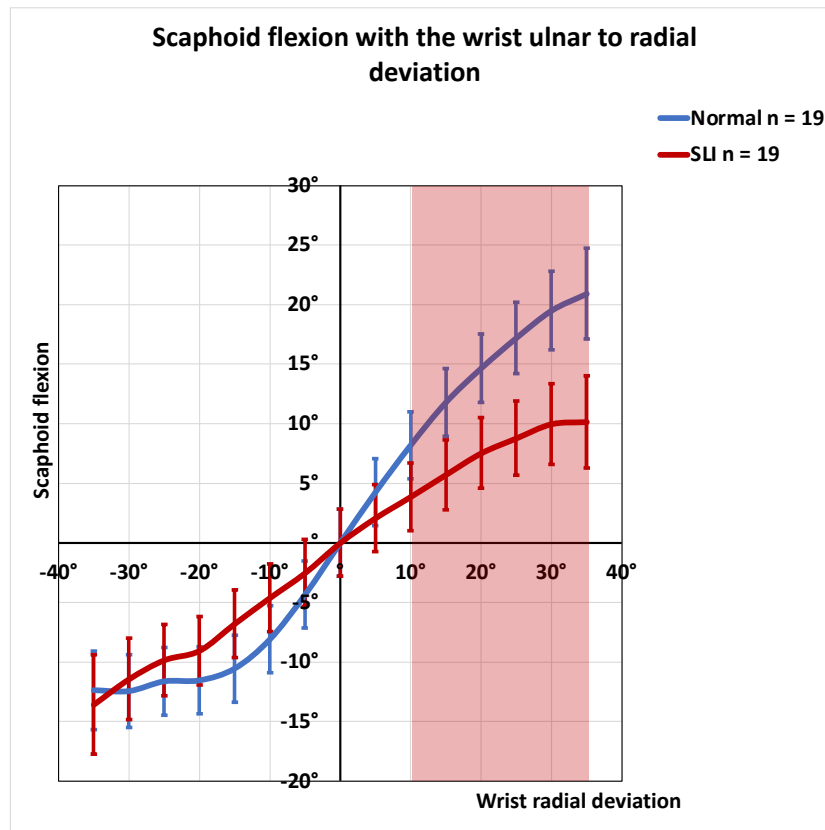


Figure 77 Scaphoid flexion with the wrist ulnar to radial deviation (95% confidence intervals are marked by the error bars). From wrist 10° radial deviation onwards the SLI scaphoid had less flexion than the normal scaphoid. The red highlighted zones indicate the wrist range of motion where a statistically significant difference exists between the normal and the SLI wrist.

### Scaphoid radial angulation

With wrist moving from ulnar to radial deviation, both the SLI and the normal scaphoids radially angulated (Figure 78, Figure 79, Table 45). From 10° of radial deviation, as the wrist radially deviated more, the SLI scaphoid had more radial angulation than the normal scaphoid.

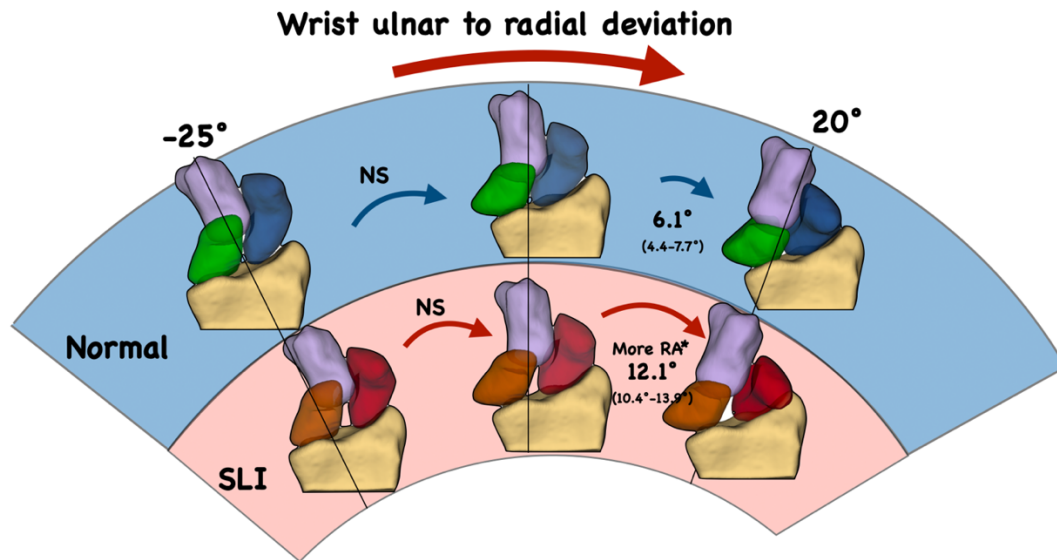


Figure 78 Graphic representation of the increased radial angulation (in-plane motion) of the scaphoid in scapholunate instability (SLI). Note that “\*” indicate statistical significance at  $p$  value of 0.05 level. The results presented are the mean (95% confidence interval). NS-No statistically significant difference between the SLI and normal wrists.

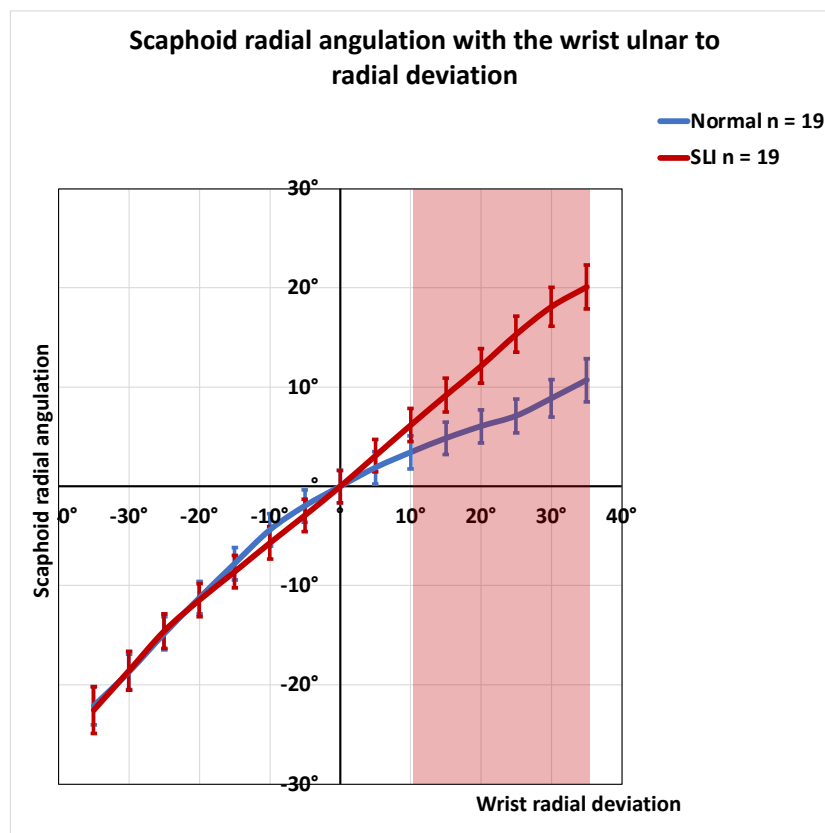


Figure 79 Scaphoid radial angulation with the wrist ulnar to radial deviation (95% confidence intervals are marked by the error bars). From wrist 10° radial deviation onwards the SLI scaphoid had more radial angulation



than the normal scaphoid. The red highlighted zones indicate the wrist range of motion where a statistically significant difference exists between the normal and the SLI wrist.

## Scaphoid internal rotation

From 10° of radial deviation, as the wrist radially deviated more, the normal scaphoid had more external rotation than the SLI scaphoid (Figure 80). Nonetheless, difference seen in the range of 10° to 25° of wrist radial deviation, between the two groups were within the margin of error of the method. Therefore, it is not considered to be significant (Table 46).

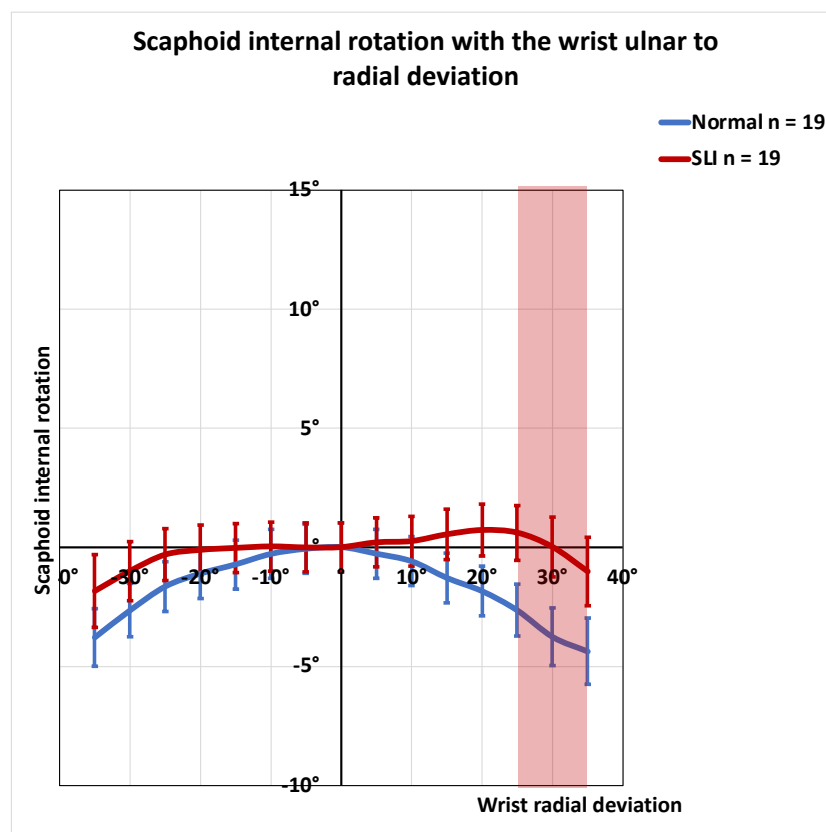


Figure 80 Scaphoid internal rotation with the wrist ulnar to radial deviation (95% confidence intervals are marked by the error bars). The red highlighted zones indicate the wrist range of motion where a statistically significant difference exists between the normal and the SLI wrist.

## Lunate flexion

With wrist ulnar to radial deviation, both the SLI and the normal lunates flexed (Figure 81, Figure 82, Table 47). Throughout the range of wrist motion from ulnar to radial deviation,

the SLI lunate exhibited less flexion than the normal lunate, except between 5° of ulnar deviation and 10° of radial deviation.

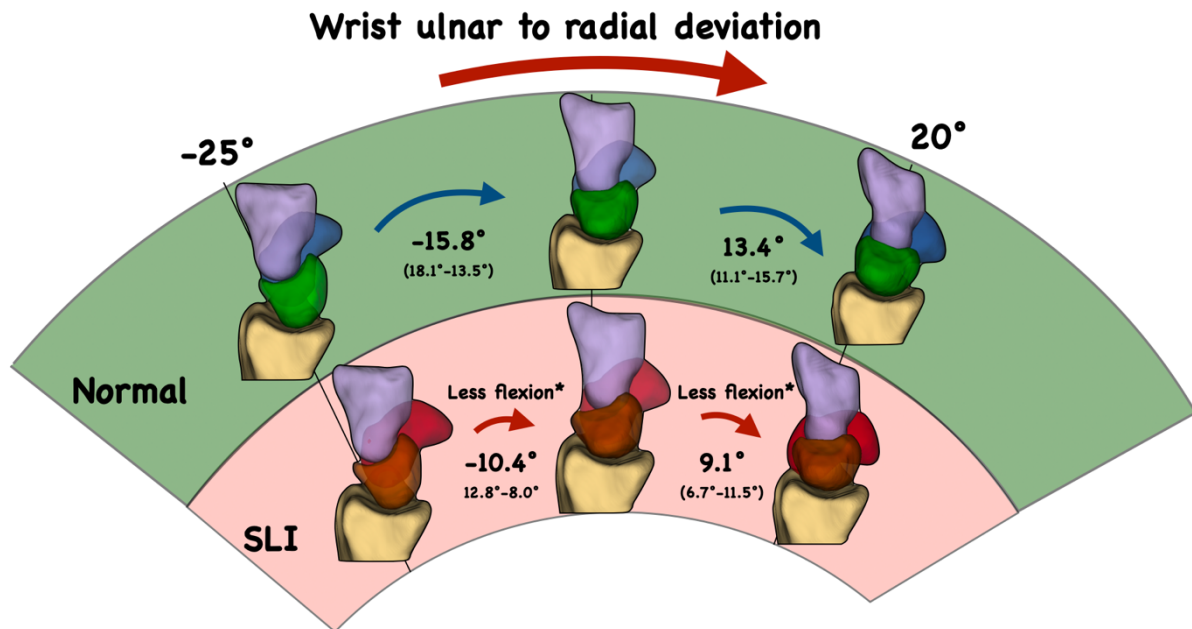


Figure 81 Graphic representation of the decreased flexion (out-of-plane motion) of the lunate in scapholunate instability (SLI). Note that “\*” indicate statistical significance at p value of 0.05 level. The results presented are the mean (95% confidence interval).

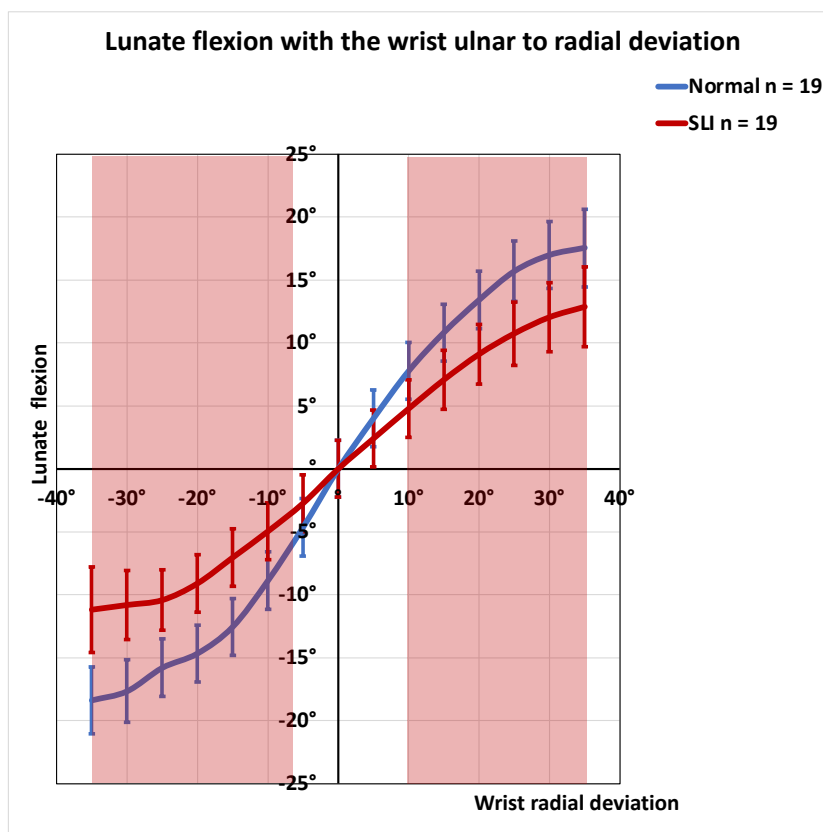


Figure 82 Lunate flexion with the wrist ulnar to radial deviation (95% confidence intervals are marked by the error bars). Note that throughout the range from ulnar to radial deviation of the wrist, the SLI lunate had less flexion than the normal lunate, except between 5° ulnar deviation to 10° radial deviation of the wrist. The red highlighted zones indicate the wrist range of motion where a statistically significant difference exists between the normal and the SLI wrist.

#### Lunate radial angulation

With wrist ulnar to radial deviation, there was no statistically significant difference between the radial angulation of the normal lunate and the SLI lunate (Figure 83, Table 48).

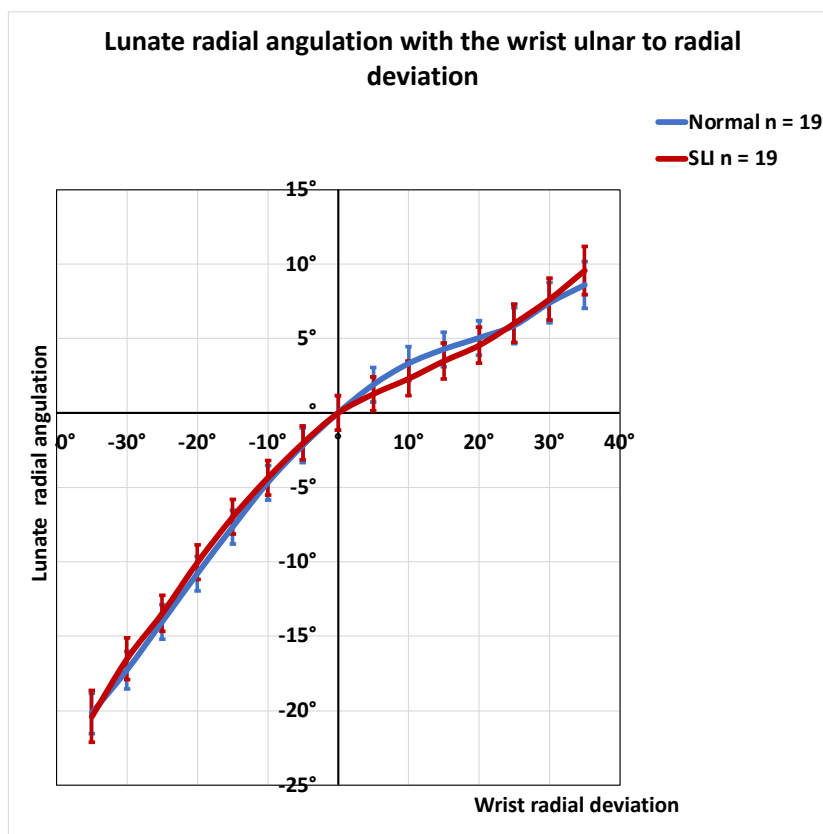


Figure 83 Lunate radial angulation with the wrist ulnar to radial deviation (95% confidence intervals are marked by the error bars). Note that there was no statistically significant difference between the radial angulation of the normal lunate and the SLI lunate.

#### Lunate internal rotation

With the wrist moving from 35° ulnar deviation to 25° ulnar deviation, the SLI lunate had more internal rotation than the normal lunate (Figure 83, Table 48). The statistically significant difference seen in extreme ulnar deviation between the two groups were within the margin of error of the method. From 25° ulnar deviation to 35° radial deviation, there was no statistically significant difference between the internal rotation of the normal lunate and the SLI lunate.

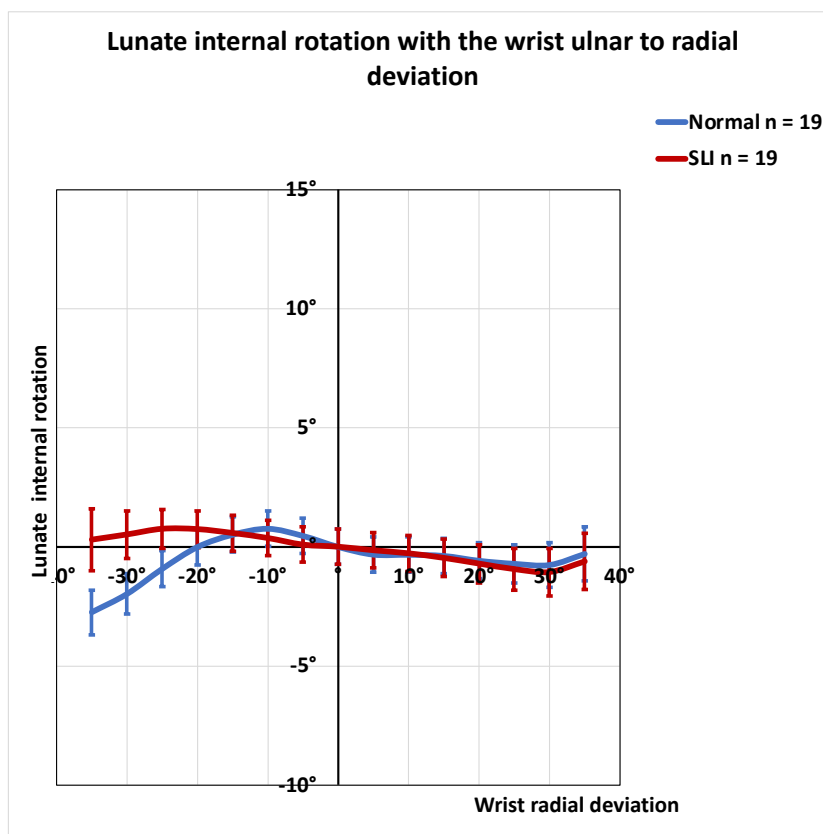


Figure 84 Lunate internal rotation with the wrist ulnar to radial deviation (95% confidence intervals are marked by the error bars). Note that there was a statistically significant difference in the lunate internal rotation between the two groups only during the extreme ulnar deviation. It was not considered significant as the values were within the margin of error.

### Radioscaphoid and radiolunate angulations

In this section, the radioscaphoid angle and the radiolunate angle, in the coronal, sagittal and axial planes, during the wrist ulnar to radial deviation are presented. The sagittal plane radioscaphoid angle is the 'radioscaphoid angle (flexion); the coronal plane angle is the 'radioscaphoid angle (radial angulation) and the axial plane angle is the 'radioscaphoid angle (internal rotation).

#### Radioscaphoid angle (flexion)

With wrist 30° ulnar deviation to the neutral position, the SLI scaphoid remained more flexed than the normal scaphoid (Figure 85, Table 50). With the wrist moving from the neutral

position to 35° radial deviation, there was no statistically significant difference between the radioscapoid angles (flexion) of the normal and the SLI wrists.

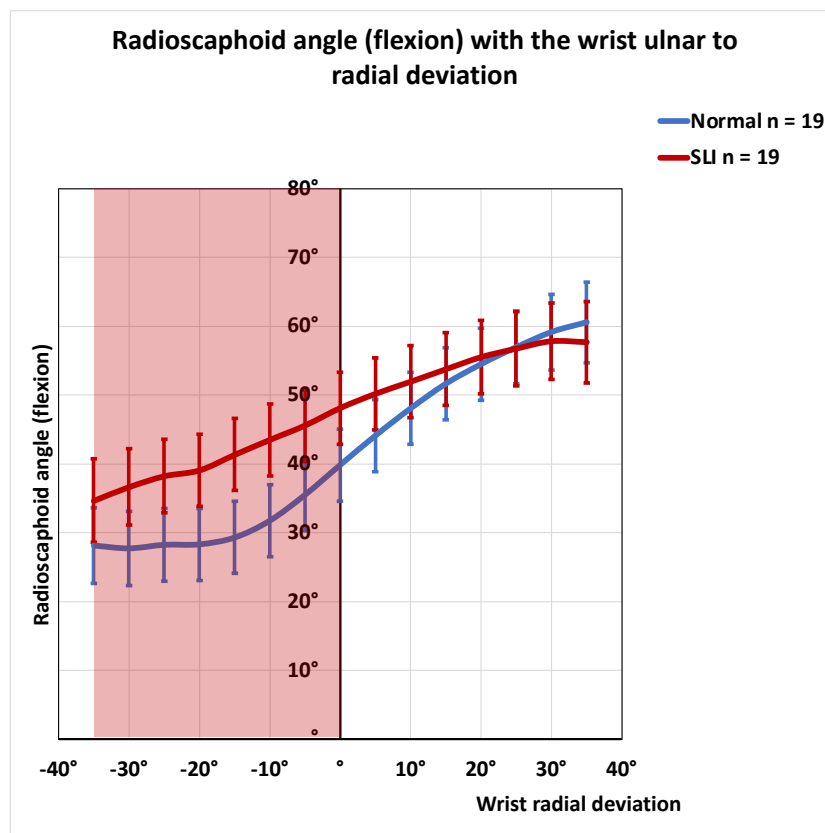


Figure 85 Radioscapoid angle (flexion) with the wrist ulnar to radial deviation (95% confidence intervals are marked by the error bars). The SLI scaphoid was significantly more flexed from 30° ulnar deviation of the wrist to the neutral position. This difference was not significant as the wrist radially deviated. The red highlighted zones indicate the wrist range of motion where a statistically significant difference exists between the normal and the SLI wrist.

#### Radioscapoid angle (radial angulation)

With wrist ulnar to radial deviation, there was no statistically significant difference between the radioscapoid angles (radial angulation) between normal and SLI wrists (Figure 86, Table 51).

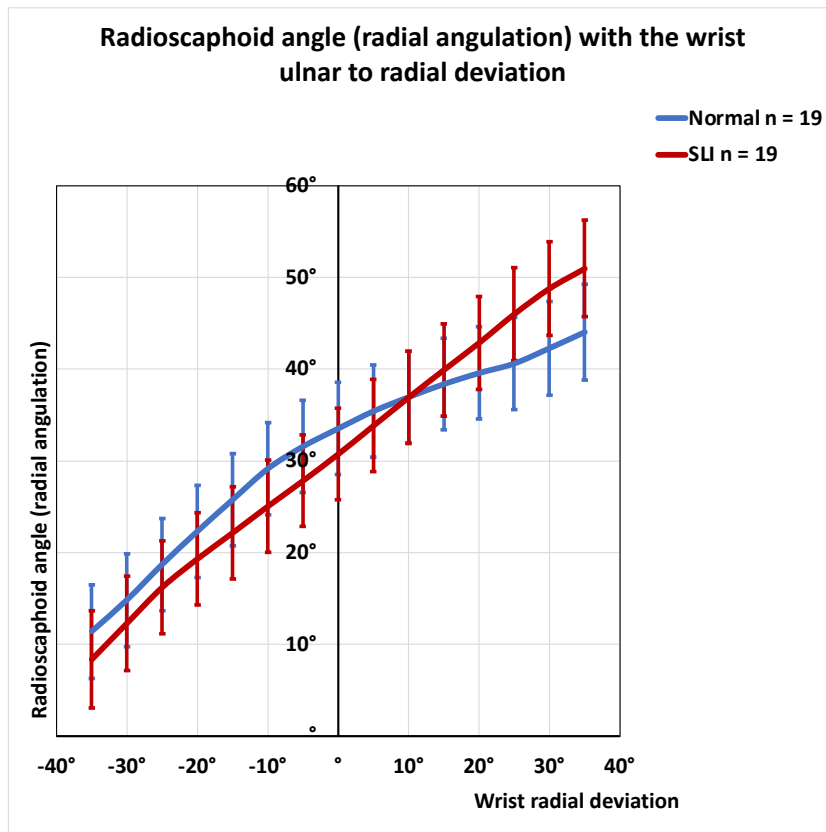


Figure 86 Radioscaphoid angle (radial angulation) with the wrist ulnar to radial deviation (95% confidence intervals are marked by the error bars). Note that, there was no statistically significant difference between the radioscaphoid angles (radial angulation) between the normal and the SLI wrists.

Radioscaphoid angle (internal rotation)

With the wrist moving from ulnar to radial deviation, throughout the range, the SLI scaphoid remained internally rotated than the normal scaphoid (Figure 87, Table 52).

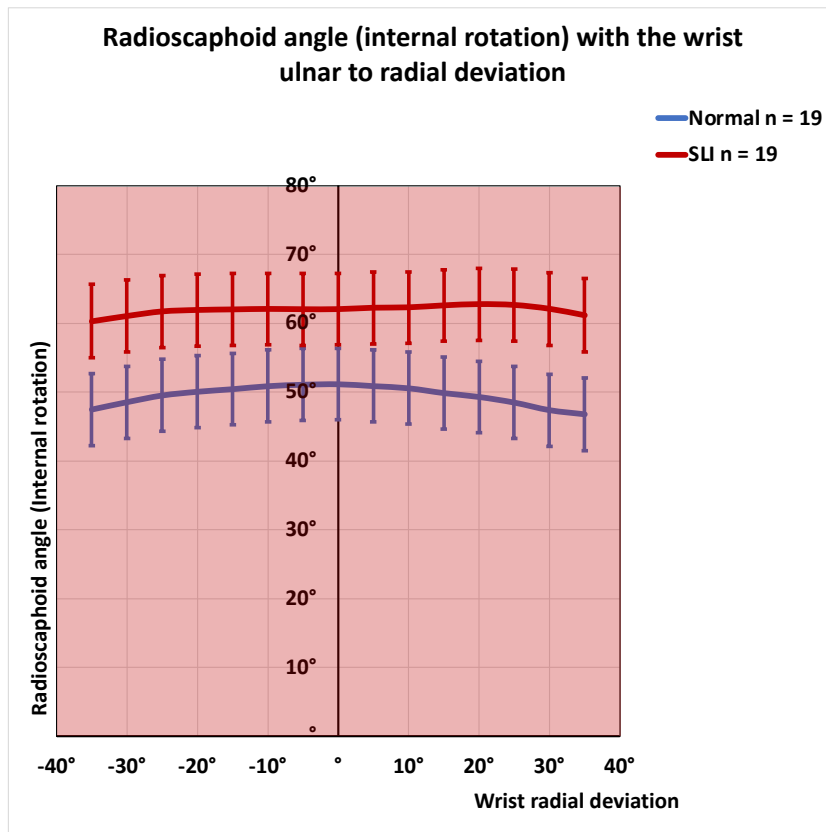


Figure 87 Radioscaphoid angle (internal rotation) with the wrist ulnar to radial deviation (95% confidence intervals are marked by the error bars). Note that the SLI scaphoid remained internally rotated than the normal scaphoid. The red highlighted zones indicate the wrist range of motion where a statistically significant difference exists between the normal and the SLI wrist.

#### Radiolunate angle (flexion)

With the wrist moving from 35° ulnar deviation to the neutral position there was no statistically significant difference between the radiolunate angles (flexion) of normal and SLI wrists (Figure 88, Table 53). From the neutral wrist position to 35° of radial deviation the radiolunate angle (flexion) of the SLI wrist was lower (lunate extended) than the normal wrist.



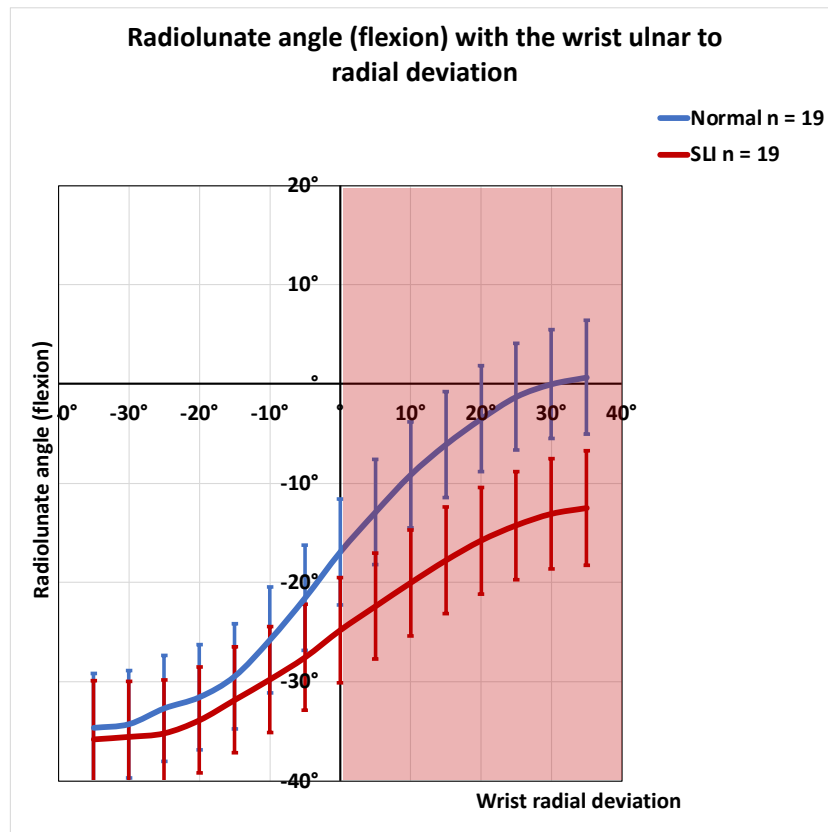


Figure 88 Radiolunate angle (flexion) with the wrist ulnar to radial deviation (95% confidence intervals are marked by the error bars). Note that from the neutral wrist position to 35° of radial deviation the radiolunate angle (flexion) of the SLI wrist was lower (lunate extended) than the normal wrist. The red highlighted zones indicate the wrist range of motion where a statistically significant difference exists between the normal and the SLI wrist.

Radiolunate angle (radial angulation)

With wrist ulnar to radial deviation, there was no statistically significant difference between the radiolunate angles (radial angulation) between normal and SLI wrists (Figure 89, Table 54).

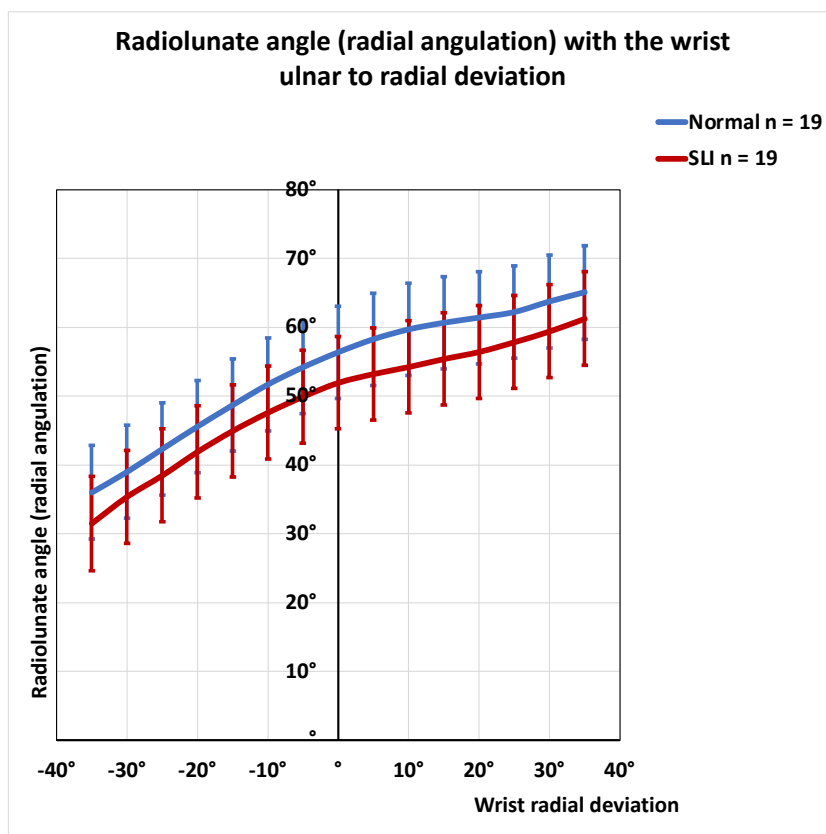


Figure 89 Radiolunate angle (radial angulation) with the wrist ulnar to radial deviation (95% confidence intervals are marked by the error bars). Note that there was no statistically significant difference between the radiolunate angles (radial angulation) between the normal and the SLI wrists.

Radiolunate angle (internal rotation)

With wrist ulnar to radial deviation, there was no statistically significant difference between the radiolunate angles (internal rotation) between normal and SLI wrists (Figure 90, Table 55).

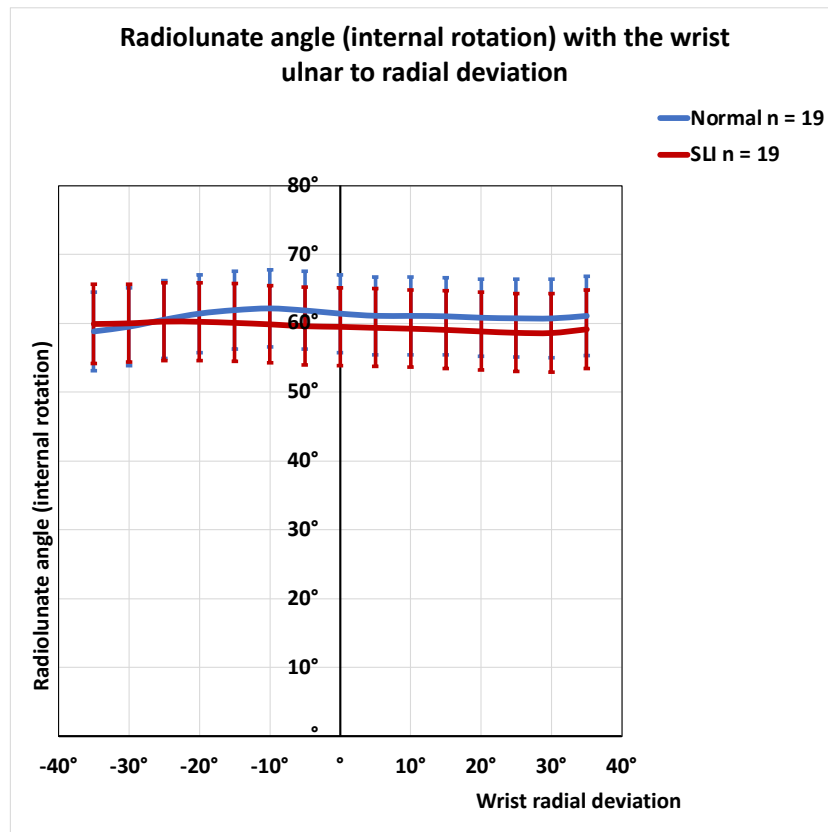


Figure 90 Radiolunate angle (Internal rotation) with the wrist ulnar to radial deviation (95% confidence intervals are marked by the error bars). Note that there was no statistically significant difference between the radiolunate angles (internal rotation) between the normal and the SLI wrists.

### Scaphoid and lunate centroid positions

In this section, the changes in the centroid positions of the scaphoid and lunate during wrist ulnar to radial deviation are presented.

Scaphoid centroid position (radio-ulnar direction)

Between 15° of ulnar deviation and 5° of radial deviation, the SLI scaphoid centroid position was more radial than the normal scaphoid (Figure 91, Table 56).

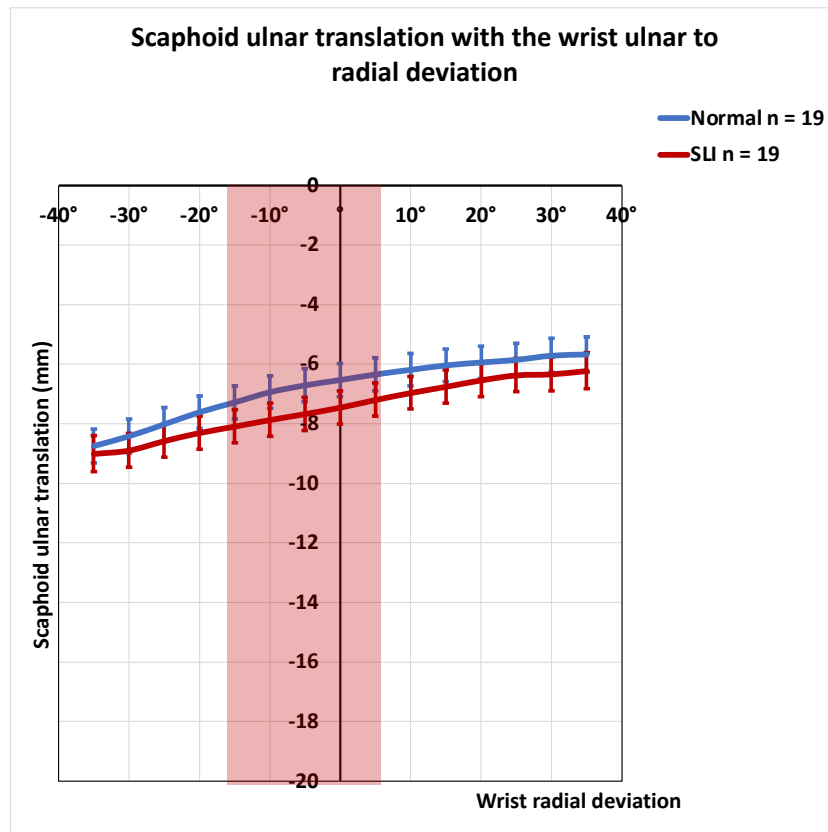


Figure 91 Scaphoid ulnar translation with the wrist ulnar to radial deviation (95% confidence intervals are marked by the error bars). Note that during the wrist range between 15° of ulnar deviation and 5° of radial deviation, the SLI scaphoid centroid position remains significantly more radial than the normal scaphoid. The red highlighted zones indicate the wrist range of motion where a statistically significant difference exists between the normal and the SLI wrist.

Scaphoid centroid position (dorso-volar direction)

During wrist movement from ulnar to radial deviation, the scaphoid centroid in both groups translated volarly. However, there was no statistically significant difference in the scaphoid centroid positions between the normal and SLI wrists along the dorso-volar direction. (Figure 92, Table 56).

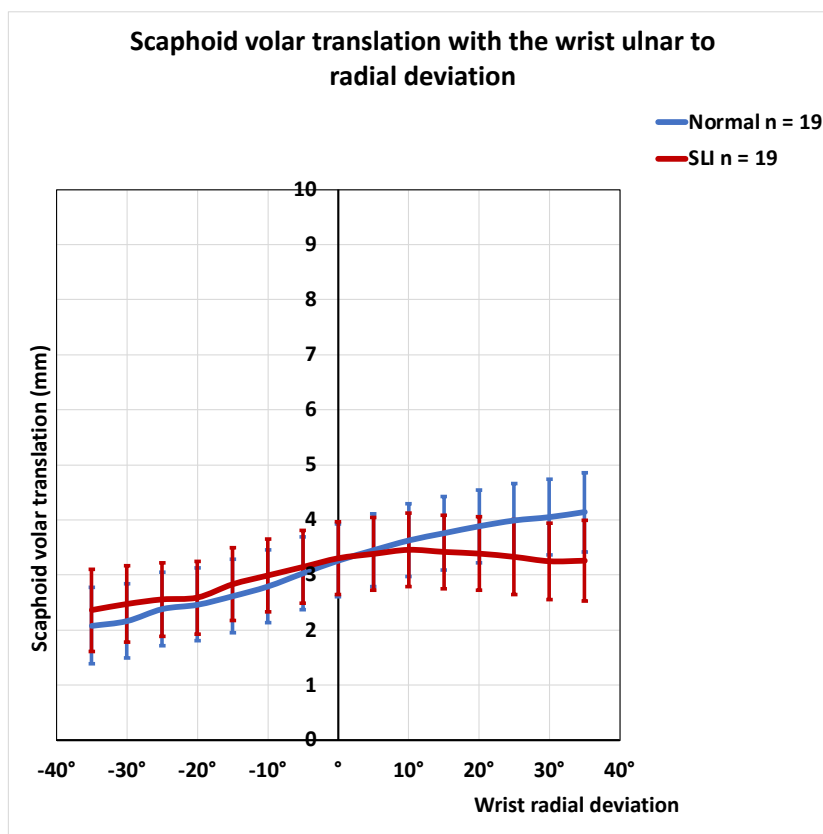


Figure 92 Scaphoid volar translation with the wrist ulnar to radial deviation (95% confidence intervals are marked by the error bars). Note that there was no statistically significant difference in the scaphoid centroid positions between normal and SLI wrists.

Scaphoid centroid position (proximo-distal direction)

From wrist 35° ulnar deviation to 5° radial deviation, the SLI scaphoid centroid remained more distal than the normal scaphoid (Figure 93, Table 58). From 5° radial deviation to 25° radial deviation, there was no statistically significant difference in the scaphoid centroid positions between normal and SLI wrists along the proximo distal direction.

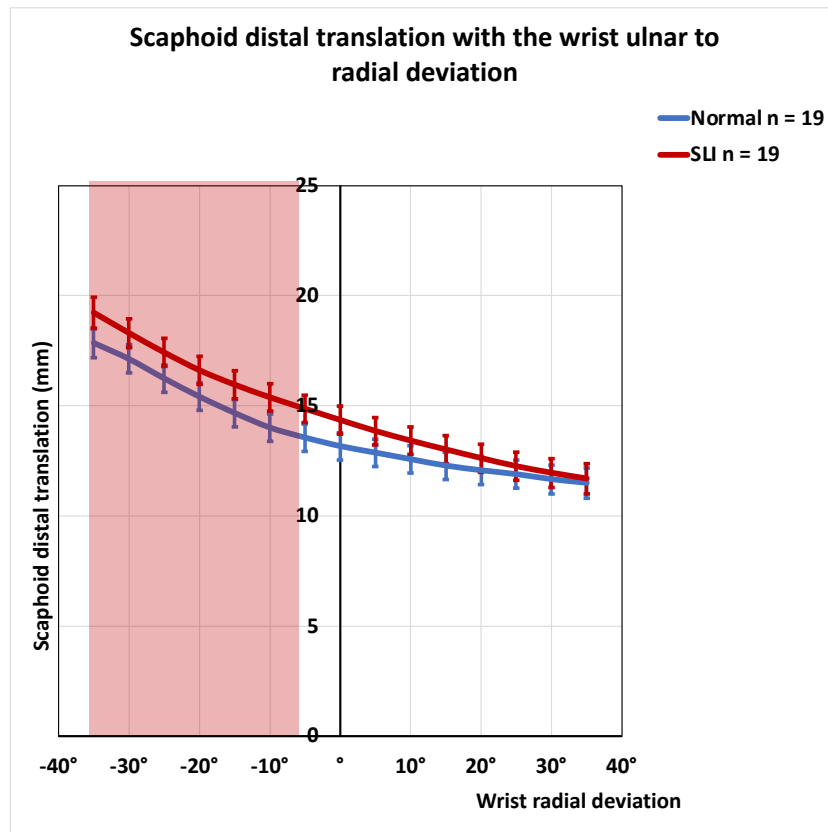


Figure 93 Scaphoid distal translation with the wrist ulnar to radial deviation (95% confidence intervals are marked by the error bars). Note that from wrist 35° ulnar deviation to 5° radial deviation, the SLI scaphoid centroid remained more distal than the normal scaphoid. The red highlighted zones indicate the wrist range of motion where a statistically significant difference exists between the normal and the SLI wrist.

Lunate centroid position (radio-ulnar direction)

With wrist ulnar to radial deviation, both the SLI and the normal lunate centroid positions moved ulnarly (Figure 94, Table 59). From 35° to 15° of wrist ulnar deviation, the SLI lunate centroid remained more ulnar than the normal lunate. From 15° ulnar deviation to 35° radial deviation there was no statistically significant difference in the lunate centroid positions between normal and SLI wrists along the radioulnar direction.

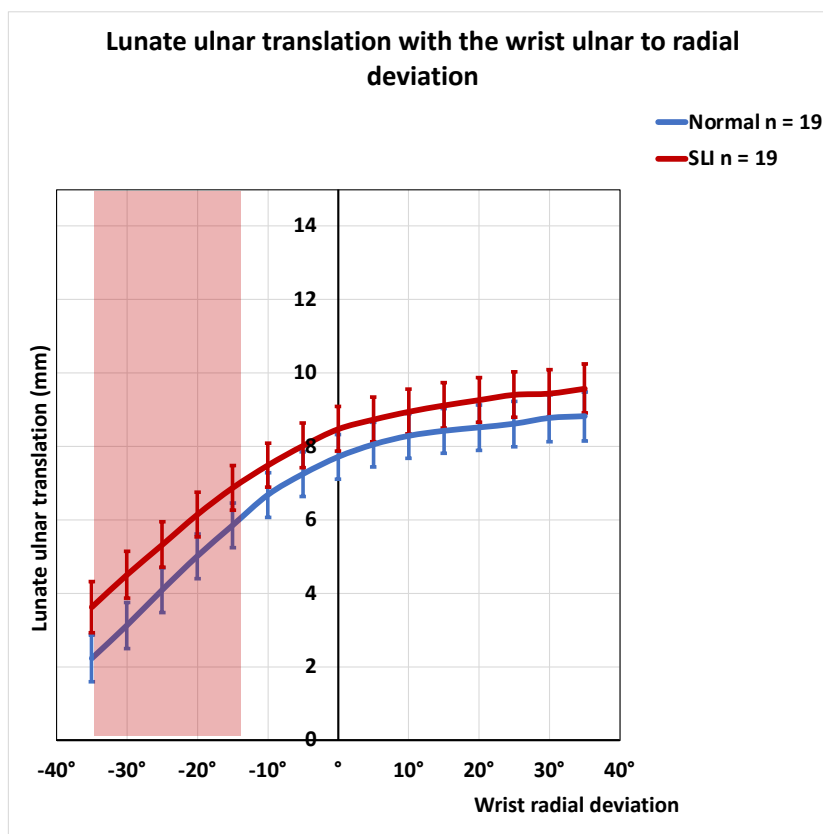


Figure 94 Lunate ulnar translation with the wrist ulnar to radial deviation (95% confidence intervals are marked by the error bars). From 35° to 15° of wrist ulnar deviation, the SLI lunate centroid remained more ulnar than the normal lunate. The red highlighted zones indicate the wrist range of motion where a statistically significant difference exists between the normal and the SLI wrist.

Lunate centroid position (dorso-volar direction)

With the wrist moving from ulnar to radial deviation, there was no statistically significant difference in the lunate centroid positions between normal and SLI wrists along the dorso-volar direction (Figure 95, Table 60).

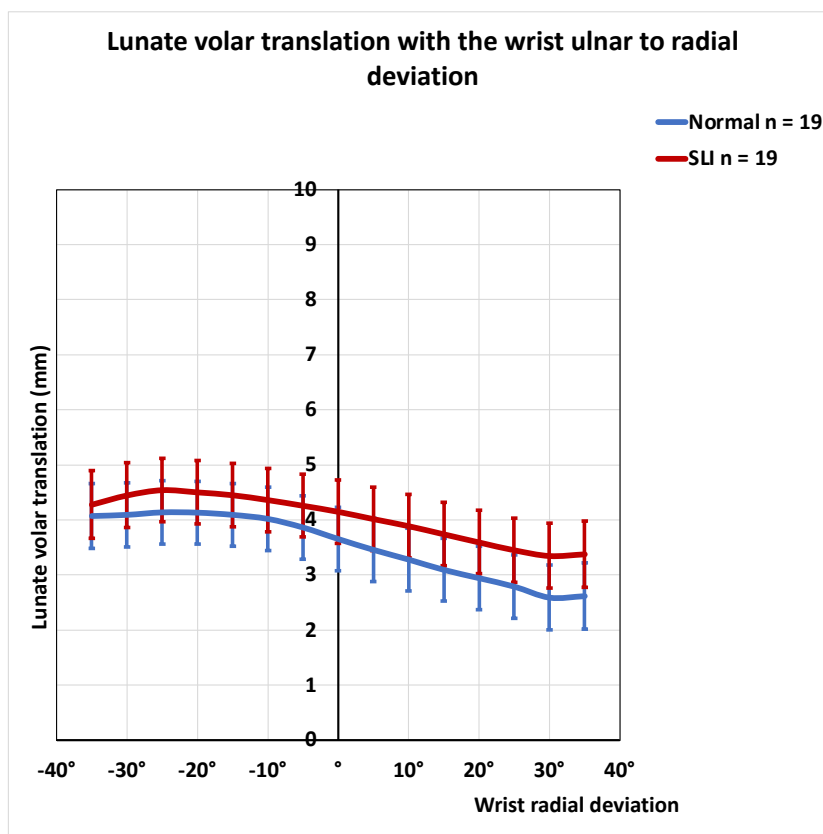


Figure 95 Lunate volar translation with the wrist ulnar to radial deviation (95% confidence intervals are marked by the error bars). Note that there was no statistically significant difference between the lunate centroid positions of normal and SLI wrists along the dorso-volar direction.

Lunate centroid position (proximo-distal direction)

With the wrist moving from ulnar to radial deviation, there was no statistically significant difference between the lunate centroid positions of normal and SLI wrists along the proximo-distal direction (Figure 96, Table 61).



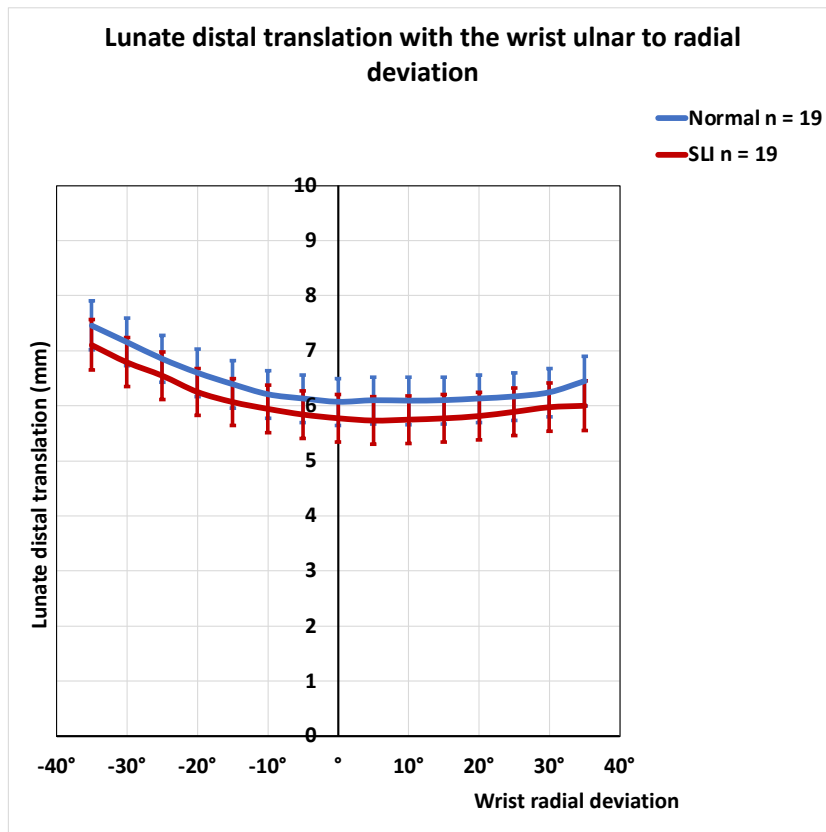


Figure 96 Lunate distal translation with the wrist ulnar to radial deviation (95% confidence intervals are marked by the error bars). Note that there was no statistically significant difference between the lunate centroid positions of normal and SLI wrists along the proximo-distal direction.

### 3.4.3. Radiocarpal kinematics (tables)

Table 26 Scaphoid flexion with the wrist extension to flexion

Wrist angle from extension to flexion (degrees)	Normal				SLI				p value
	Mean	Std. Error	Lower CI	Upper CI	Mean	Std. Error	Lower CI	Upper CI	
-70°	-48.0°	1.4°	-50.7°	-45.3°	-58.4°*	1.5°	-61.3°	-55.4°	<.001
-65°	-45.9°	1.4°	-48.6°	-43.1°	-55.0°*	1.5°	-57.9°	-52.2°	<.001
-60°	-43.4°	1.4°	-46.1°	-40.7°	-51.4°*	1.4°	-54.2°	-48.6°	<.001
-55°	-40.6°	1.4°	-43.3°	-37.9°	-47.6°*	1.4°	-50.4°	-44.9°	<.001
-50°	-37.7°	1.4°	-40.4°	-35.0°	-44.3°*	1.4°	-47.0°	-41.6°	<.001
-45°	-34.6°	1.4°	-37.3°	-31.9°	-40.7°*	1.4°	-43.4°	-38.0°	0.002
-40°	-31.4°	1.4°	-34.1°	-28.6°	-36.7°*	1.4°	-39.4°	-33.9°	0.007
-35°	-27.8°	1.4°	-30.5°	-25.1°	-31.5°	1.4°	-34.2°	-28.8°	0.057
-30°	-24.0°	1.4°	-26.7°	-21.3°	-26.8°	1.4°	-29.5°	-24.1°	0.142
-25°	-20.0°	1.4°	-22.7°	-17.3°	-21.7°	1.4°	-24.4°	-19.0°	0.386
-20°	-16.0°	1.4°	-18.7°	-13.3°	-17.0°	1.4°	-19.7°	-14.3°	0.621
-15°	-11.8°	1.4°	-14.5°	-9.1°	-12.4°	1.4°	-15.1°	-9.7°	0.738
-10°	-7.8°	1.4°	-10.5°	-5.1°	-8.1°	1.4°	-10.8°	-5.4°	0.877
-5°	-3.9°	1.4°	-6.6°	-1.2°	-4.0°	1.4°	-6.7°	-1.3°	0.946
0°	0.0°	1.4°	-2.7°	2.7°	0.0°	1.4°	-2.7°	2.7°	1.000
5°	4.1°	1.4°	1.4°	6.8°	3.3°	1.4°	0.6°	6.0°	0.699
10°	8.1°	1.4°	5.4°	10.8°	6.6°	1.4°	3.9°	9.4°	0.463
15°	12.0°	1.4°	9.3°	14.7°	9.9°	1.4°	7.1°	12.6°	0.281
20°	15.7°	1.4°	13.0°	18.4°	13.2°	1.4°	10.5°	15.9°	0.200
25°	19.6°	1.4°	16.9°	22.4°	16.5°	1.4°	13.8°	19.3°	0.114
30°	23.7°	1.4°	20.9°	26.4°	19.8°	1.4°	17.0°	22.6°	0.054
35°	27.6°	1.4°	24.9°	30.4°	23.1°*	1.4°	20.3°	25.9°	0.024
40°	31.7°	1.4°	28.9°	34.4°	27.1°*	1.5°	24.2°	29.9°	0.024
45°	35.8°	1.4°	33.0°	38.6°	31.0°*	1.5°	28.1°	34.0°	0.021
50°	39.9°	1.4°	37.1°	42.7°	35.5°*	1.6°	32.5°	38.6°	0.039
55°	44.1°	1.4°	41.2°	46.9°	40.3°	1.9°	36.6°	44.0°	0.109
60°	48.1°	1.5°	45.2°	51.0°	45.0°	2.1°	40.9°	49.2°	0.232
65°	52.3°	1.5°	49.3°	55.2°	49.8°	2.3°	45.2°	54.4°	0.377
70°	56.3°	1.7°	53.0°	59.5°	NA	NA	NA	NA	NA

“\*” and bold font Indicate statistical significance at a p-value of 0.05. NA-data not available beyond 65° of flexion for SLI wrist

Table 27 Scaphoid radial angulation with the wrist extension to flexion

Wrist angle from extension to flexion (degrees)	Normal				SLI				p value
	Mean	Std. Error	Lower CI	Upper CI	Mean	Std. Error	Lower CI	Upper CI	
-70°	0.3°	1.1°	-1.9°	2.6°	1.7°	1.2°	-0.7°	4.1°	0.414
-65°	-0.1°	1.1°	-2.4°	2.1°	1.2°	1.2°	-1.1°	3.6°	0.409
-60°	0.1°	1.1°	-2.1°	2.4°	1.4°	1.2°	-0.9°	3.7°	0.426
-55°	0.3°	1.1°	-1.9°	2.6°	1.2°	1.2°	-1.1°	3.5°	0.589
-50°	0.5°	1.1°	-1.7°	2.8°	0.7°	1.1°	-1.5°	3.0°	0.907
-45°	0.6°	1.1°	-1.6°	2.9°	0.3°	1.1°	-1.9°	2.6°	0.844
-40°	0.8°	1.1°	-1.5°	3.0°	0.0°	1.1°	-2.2°	2.3°	0.638
-35°	0.8°	1.1°	-1.4°	3.0°	-0.2°	1.1°	-2.4°	2.0°	0.540
-30°	0.7°	1.1°	-1.5°	2.9°	-0.3°	1.1°	-2.5°	1.9°	0.539
-25°	0.6°	1.1°	-1.6°	2.8°	-0.4°	1.1°	-2.6°	1.8°	0.533
-20°	0.4°	1.1°	-1.9°	2.6°	-0.3°	1.1°	-2.5°	1.9°	0.678
-15°	0.1°	1.1°	-2.2°	2.3°	-0.3°	1.1°	-2.5°	2.0°	0.830
-10°	0.0°	1.1°	-2.2°	2.2°	-0.3°	1.1°	-2.5°	2.0°	0.855
-5°	0.0°	1.1°	-2.3°	2.2°	-0.2°	1.1°	-2.4°	2.0°	0.917
0°	0.0°	1.1°	-2.2°	2.2°	0.0°	1.1°	-2.2°	2.2°	1.000
5°	-0.4°	1.1°	-2.7°	1.8°	0.2°	1.1°	-2.0°	2.5°	0.678
10°	-0.8°	1.1°	-3.0°	1.4°	0.4°	1.1°	-1.9°	2.6°	0.456
15°	-1.2°	1.1°	-3.4°	1.0°	0.5°	1.1°	-1.7°	2.8°	0.284
20°	-1.6°	1.1°	-3.8°	0.7°	0.6°	1.1°	-1.6°	2.9°	0.180
25°	-1.9°	1.1°	-4.1°	0.4°	0.3°	1.2°	-1.9°	2.6°	0.169
30°	-2.3°	1.1°	-4.5°	0.0°	-0.3°	1.2°	-2.6°	2.0°	0.219
35°	-2.7°	1.1°	-5.0°	-0.5°	-1.1°	1.2°	-3.4°	1.2°	0.332
40°	-3.3°	1.2°	-5.6°	-1.0°	-2.1°	1.2°	-4.5°	0.2°	0.482
45°	-3.9°	1.2°	-6.1°	-1.6°	-3.3°	1.2°	-5.7°	-0.9°	0.754
50°	-4.5°	1.2°	-6.8°	-2.2°	-4.4°	1.3°	-6.9°	-1.9°	0.951
55°	-5.2°	1.2°	-7.5°	-2.9°	-6.5°	1.5°	-9.4°	-3.6°	0.482
60°	-5.5°	1.2°	-7.8°	-3.1°	-8.6°	1.6°	-11.8°	-5.4°	0.121
<b>65°</b>	<b>-5.9°</b>	<b>1.2°</b>	<b>-8.3°</b>	<b>-3.5°</b>	<b>-10.7°*</b>	<b>1.8°</b>	<b>-14.2°</b>	<b>-7.2°</b>	<b>0.025</b>
70°	-6.4°	1.3°	-9.0°	-3.8°	NA	NA	NA	NA	NA

“\*” and bold font Indicate statistical significance at a p-value of 0.05. NA-data not available beyond 65° of flexion for SLI wrists.

Table 28 Scaphoid internal rotation with the wrist extension to flexion

Wrist angle from extension to flexion (degrees)	Normal				SLI				<i>p</i> value
	Mean	Std. Error	Lower CI	Upper CI	Mean	Std. Error	Lower CI	Upper CI	
-70°	1.6°	0.8°	0.0°	3.2°	3.6°	0.9°	1.9°	5.3°	0.092
-65°	1.4°	0.8°	-0.2°	3.0°	3.3°	0.8°	1.6°	4.9°	0.109
-60°	1.4°	0.8°	-0.2°	3.0°	3.1°	0.8°	1.5°	4.7°	0.139
-55°	1.4°	0.8°	-0.1°	3.0°	3.0°	0.8°	1.4°	4.6°	0.180
-50°	1.4°	0.8°	-0.2°	2.9°	2.8°	0.8°	1.2°	4.4°	0.203
-45°	1.1°	0.8°	-0.4°	2.7°	2.6°	0.8°	1.0°	4.2°	0.191
-40°	1.0°	0.8°	-0.5°	2.6°	2.3°	0.8°	0.7°	3.9°	0.263
-35°	1.0°	0.8°	-0.6°	2.5°	2.1°	0.8°	0.5°	3.7°	0.325
-30°	0.9°	0.8°	-0.7°	2.5°	1.8°	0.8°	0.3°	3.4°	0.402
-25°	0.8°	0.8°	-0.8°	2.4°	1.7°	0.8°	0.1°	3.3°	0.431
-20°	0.6°	0.8°	-0.9°	2.2°	1.4°	0.8°	-0.2°	3.0°	0.505
-15°	0.5°	0.8°	-1.1°	2.1°	1.0°	0.8°	-0.6°	2.6°	0.650
-10°	0.3°	0.8°	-1.3°	1.9°	0.7°	0.8°	-0.9°	2.3°	0.723
-5°	0.1°	0.8°	-1.5°	1.7°	0.4°	0.8°	-1.2°	2.0°	0.799
0°	0.0°	0.8°	-1.6°	1.6°	0.0°	0.8°	-1.6°	1.6°	1.000
5°	0.1°	0.8°	-1.5°	1.7°	-0.2°	0.8°	-1.8°	1.4°	0.809
10°	0.1°	0.8°	-1.5°	1.6°	-0.4°	0.8°	-2.0°	1.2°	0.669
15°	0.1°	0.8°	-1.5°	1.7°	-0.7°	0.8°	-2.3°	0.9°	0.511
20°	0.0°	0.8°	-1.6°	1.6°	-1.0°	0.8°	-2.6°	0.6°	0.379
25°	0.0°	0.8°	-1.6°	1.6°	-1.2°	0.8°	-2.8°	0.4°	0.308
30°	0.0°	0.8°	-1.6°	1.6°	-1.4°	0.8°	-3.1°	0.2°	0.221
35°	0.1°	0.8°	-1.5°	1.7°	-1.6°	0.8°	-3.2°	0.0°	0.149
40°	0.2°	0.8°	-1.4°	1.8°	-1.6°	0.8°	-3.2°	0.1°	0.140
45°	0.3°	0.8°	-1.3°	1.9°	-1.6°	0.9°	-3.3°	0.1°	0.112
50°	0.3°	0.8°	-1.3°	1.9°	-1.7°	0.9°	-3.5°	0.0°	0.093
55°	0.2°	0.8°	-1.4°	1.9°	-2.4°	1.0°	-4.4°	-0.3°	0.052
<b>60°</b>	<b>0.1°</b>	<b>0.8°</b>	<b>-1.5°</b>	<b>1.8°</b>	<b>-3.0°*</b>	<b>1.2°</b>	<b>-5.2°</b>	<b>-0.7°</b>	<b>0.031</b>
<b>65°</b>	<b>-0.2°</b>	<b>0.9°</b>	<b>-1.9°</b>	<b>1.5°</b>	<b>-3.6°*</b>	<b>1.3°</b>	<b>-6.1°</b>	<b>-1.1°</b>	<b>0.027</b>
70°	0.5°	0.9°	-1.3°	2.4°	NA	NA	NA	NA	NA

“\*” and bold font Indicate statistical significance at a *p*-value of 0.05. NA-data not available beyond 65° of flexion for SLI wrists.

Table 29 Lunate flexion with the wrist extension to flexion

Wrist angle from extension to flexion (degrees)	Normal				SLI				<i>p</i> value
	Mean	Std. Error	Lower CI	Upper CI	Mean	Std. Error	Lower CI	Upper CI	
-70°	-23.2°	2.0°	-27.1°	-19.4°	-15.0°*	2.1°	-19.1°	-11.0°	0.004
-65°	-22.3°	2.0°	-26.2°	-18.5°	-14.2°*	2.0°	-18.2°	-10.2°	0.004
-60°	-21.2°	2.0°	-25.1°	-17.4°	-12.6°*	2.0°	-16.5°	-8.6°	0.002
-55°	-19.9°	2.0°	-23.8°	-16.1°	-11.4°*	2.0°	-15.3°	-7.4°	0.002
-50°	-18.6°	2.0°	-22.5°	-14.8°	-10.3°*	2.0°	-14.2°	-6.4°	0.003
-45°	-17.3°	2.0°	-21.2°	-13.4°	-9.2°*	2.0°	-13.1°	-5.3°	0.004
-40°	-15.8°	2.0°	-19.7°	-12.0°	-8.2°*	2.0°	-12.1°	-4.3°	0.006
-35°	-14.3°	2.0°	-18.1°	-10.4°	-7.2°*	2.0°	-11.0°	-3.3°	0.011
-30°	-12.5°	2.0°	-16.4°	-8.6°	-6.3°*	2.0°	-10.2°	-2.4°	0.026
-25°	-10.6°	2.0°	-14.5°	-6.8°	-5.5°	2.0°	-9.4°	-1.6°	0.066
-20°	-8.7°	2.0°	-12.6°	-4.9°	-4.7°	2.0°	-8.6°	-0.8°	0.151
-15°	-6.6°	2.0°	-10.5°	-2.7°	-3.9°	2.0°	-7.8°	0.0°	0.330
-10°	-4.5°	2.0°	-8.4°	-0.6°	-2.8°	2.0°	-6.7°	1.1°	0.539
-5°	-2.3°	2.0°	-6.2°	1.6°	-1.5°	2.0°	-5.3°	2.4°	0.771
0°	0.0°	2.0°	-3.9°	3.9°	0.0°	2.0°	-3.9°	3.9°	1.000
5°	2.9°	2.0°	-1.0°	6.8°	2.1°	2.0°	-1.8°	5.9°	0.760
10°	5.9°	2.0°	2.0°	9.7°	4.3°	2.0°	0.4°	8.2°	0.585
15°	8.4°	2.0°	4.6°	12.3°	6.8°	2.0°	2.9°	10.6°	0.551
20°	11.0°	2.0°	7.2°	14.9°	9.8°	2.0°	5.9°	13.7°	0.652
25°	13.9°	2.0°	10.0°	17.8°	12.9°	2.0°	9.0°	16.8°	0.710
30°	16.8°	2.0°	12.9°	20.7°	16.2°	2.0°	12.2°	20.1°	0.813
35°	19.8°	2.0°	15.9°	23.7°	19.7°	2.0°	15.8°	23.7°	0.961
40°	23.1°	2.0°	19.2°	27.0°	23.6°	2.0°	19.6°	27.6°	0.866
45°	26.4°	2.0°	22.4°	30.3°	27.8°	2.1°	23.7°	31.8°	0.628
50°	29.5°	2.0°	25.6°	33.5°	32.0°	2.1°	27.9°	36.2°	0.390
55°	32.6°	2.0°	28.6°	36.5°	36.1°	2.4°	31.5°	40.8°	0.252
60°	35.4°	2.1°	31.4°	39.4°	40.3°	2.6°	35.2°	45.4°	0.141
65°	38.6°	2.1°	34.5°	42.7°	44.4°	2.8°	38.9°	49.9°	0.097
70°	42.1°	2.2°	37.8°	46.5°	NA	NA	NA	NA	NA

“\*” and bold font Indicate statistical significance at a *p*-value of 0.05. NA-data not available beyond 65° of flexion for SLI wrists.

Table 30 Lunate radial angulation with the wrist extension to flexion

Wrist angle from extension to flexion (degrees)	Normal				SLI				<i>p</i> value
	Mean	Std. Error	Lower CI	Upper CI	Mean	Std. Error	Lower CI	Upper CI	
-70°	<b>0.7°</b>	<b>0.8°</b>	<b>-1.0°</b>	<b>2.3°</b>	<b>-3.1°*</b>	<b>0.9°</b>	<b>-4.8°</b>	<b>-1.3°</b>	<b>0.002</b>
-65°	<b>0.5°</b>	<b>0.8°</b>	<b>-1.1°</b>	<b>2.1°</b>	<b>-2.6°*</b>	<b>0.9°</b>	<b>-4.3°</b>	<b>-1.0°</b>	<b>0.008</b>
-60°	<b>0.7°</b>	<b>0.8°</b>	<b>-0.9°</b>	<b>2.3°</b>	<b>-1.7°*</b>	<b>0.8°</b>	<b>-3.4°</b>	<b>-0.1°</b>	<b>0.039</b>
-55°	<b>1.1°</b>	<b>0.8°</b>	<b>-0.5°</b>	<b>2.7°</b>	<b>-1.2°*</b>	<b>0.8°</b>	<b>-2.8°</b>	<b>0.5°</b>	<b>0.048</b>
-50°	1.6°	0.8°	0.0°	3.2°	-0.6°	0.8°	-2.2°	1.0°	0.055
-45°	1.8°	0.8°	0.2°	3.3°	-0.2°	0.8°	-1.8°	1.4°	0.093
-40°	2.1°	0.8°	0.5°	3.6°	0.3°	0.8°	-1.3°	1.9°	0.132
-35°	2.1°	0.8°	0.5°	3.7°	0.7°	0.8°	-0.9°	2.3°	0.231
-30°	2.0°	0.8°	0.4°	3.6°	0.9°	0.8°	-0.7°	2.5°	0.348
-25°	1.8°	0.8°	0.2°	3.4°	1.0°	0.8°	-0.6°	2.6°	0.458
-20°	1.6°	0.8°	0.0°	3.2°	1.0°	0.8°	-0.6°	2.6°	0.590
-15°	1.3°	0.8°	-0.3°	2.9°	0.9°	0.8°	-0.7°	2.5°	0.702
-10°	0.8°	0.8°	-0.8°	2.4°	0.6°	0.8°	-1.0°	2.2°	0.834
-5°	0.4°	0.8°	-1.2°	2.0°	0.3°	0.8°	-1.3°	1.9°	0.912
0°	0.0°	0.8°	-1.6°	1.6°	0.0°	0.8°	-1.6°	1.6°	1.000
5°	-0.5°	0.8°	-2.0°	1.1°	-0.4°	0.8°	-2.0°	1.1°	0.993
10°	-1.0°	0.8°	-2.5°	0.6°	-1.0°	0.8°	-2.5°	0.6°	0.997
15°	-1.6°	0.8°	-3.2°	0.0°	-1.6°	0.8°	-3.2°	0.0°	0.989
20°	-2.1°	0.8°	-3.7°	-0.5°	-2.2°	0.8°	-3.8°	-0.6°	0.928
25°	-2.4°	0.8°	-4.0°	-0.8°	-3.1°	0.8°	-4.7°	-1.5°	0.525
30°	-2.8°	0.8°	-4.4°	-1.2°	-3.9°	0.8°	-5.6°	-2.3°	0.315
35°	-3.4°	0.8°	-5.0°	-1.8°	-4.8°	0.8°	-6.4°	-3.1°	0.252
40°	-4.5°	0.8°	-6.1°	-2.9°	-5.5°	0.9°	-7.2°	-3.8°	0.398
45°	-5.5°	0.8°	-7.2°	-3.9°	-6.3°	0.9°	-8.0°	-4.5°	0.539
50°	-6.4°	0.8°	-8.1°	-4.8°	-7.1°	0.9°	-8.9°	-5.3°	0.583
55°	-7.4°	0.9°	-9.1°	-5.8°	-8.7°	1.1°	-10.9°	-6.5°	0.350
60°	-8.1°	0.9°	-9.8°	-6.4°	-10.4°	1.3°	-12.9°	-7.9°	0.144
65°	-9.2°	0.9°	-11.0°	-7.4°	-12.0°	1.4°	-14.8°	-9.2°	0.096
70°	-10.0°	1.0°	-12.0°	-8.1°	NA	NA	NA	NA	NA

“\*” and bold font Indicate statistical significance at a *p*-value of 0.05. NA-data not available beyond 65° of flexion for SLI wrists.

Table 31 Lunate internal rotation with the wrist extension to flexion

Wrist angle from extension to flexion (degrees)	Normal				SLI				<i>p</i> value
	Mean	Std. Error	Lower CI	Upper CI	Mean	Std. Error	Lower CI	Upper CI	
-70°	-0.2°	0.5°	-1.2°	0.8°	-2.0°	0.6°	-3.2°	-0.8°	0.021
-65°	-0.5°	0.5°	-1.5°	0.5°	-2.0°	0.6°	-3.2°	-0.9°	0.041
-60°	0.0°	0.5°	-1.0°	1.0°	-1.9°	0.5°	-2.9°	-0.8°	0.014
-55°	0.1°	0.5°	-0.9°	1.1°	-1.7°	0.5°	-2.7°	-0.7°	0.016
-50°	0.1°	0.5°	-0.9°	1.1°	-1.5°	0.5°	-2.6°	-0.5°	0.026
-45°	-0.1°	0.5°	-1.0°	0.9°	-1.4°	0.5°	-2.4°	-0.4°	0.066
-40°	-0.2°	0.5°	-1.2°	0.8°	-1.2°	0.5°	-2.2°	-0.2°	0.145
-35°	-0.2°	0.5°	-1.1°	0.8°	-0.9°	0.5°	-1.9°	0.1°	0.291
-30°	-0.1°	0.5°	-1.1°	0.9°	-0.6°	0.5°	-1.6°	0.4°	0.469
-25°	0.1°	0.5°	-0.9°	1.1°	-0.3°	0.5°	-1.3°	0.7°	0.532
-20°	0.2°	0.5°	-0.7°	1.2°	-0.2°	0.5°	-1.2°	0.8°	0.546
-15°	0.3°	0.5°	-0.7°	1.3°	-0.1°	0.5°	-1.1°	0.9°	0.580
-10°	0.2°	0.5°	-0.8°	1.2°	0.0°	0.5°	-1.0°	1.0°	0.740
-5°	0.0°	0.5°	-0.9°	1.0°	0.0°	0.5°	-1.0°	1.0°	0.934
0°	0.0°	0.5°	-1.0°	1.0°	0.0°	0.5°	-1.0°	1.0°	1.000
5°	-0.1°	0.5°	-1.1°	0.8°	-0.2°	0.5°	-1.2°	0.8°	0.966
10°	-0.3°	0.5°	-1.3°	0.7°	-0.4°	0.5°	-1.4°	0.6°	0.954
15°	-0.4°	0.5°	-1.4°	0.6°	-0.5°	0.5°	-1.5°	0.5°	0.891
20°	-0.4°	0.5°	-1.4°	0.6°	-0.7°	0.5°	-1.7°	0.3°	0.747
25°	-0.5°	0.5°	-1.5°	0.5°	-0.7°	0.5°	-1.8°	0.3°	0.740
30°	-0.5°	0.5°	-1.5°	0.5°	-0.8°	0.5°	-1.8°	0.3°	0.712
35°	-0.3°	0.5°	-1.3°	0.7°	-0.7°	0.5°	-1.8°	0.3°	0.577
40°	-0.1°	0.5°	-1.2°	0.9°	-0.7°	0.6°	-1.9°	0.4°	0.442
45°	0.1°	0.5°	-1.0°	1.2°	-1.0°	0.6°	-2.2°	0.1°	0.159
50°	0.1°	0.5°	-1.0°	1.1°	-1.1°	0.6°	-2.3°	0.2°	0.178
55°	0.1°	0.6°	-1.0°	1.1°	-1.4°	0.9°	-3.1°	0.3°	0.151
60°	0.4°	0.6°	-0.7°	1.6°	-1.7°	1.0°	-3.7°	0.2°	0.062
65°	0.6°	0.6°	-0.6°	1.8°	-2.1°	1.1°	-4.3°	0.2°	0.037
70°	1.1°	0.7°	-0.3°	2.6°	NA	NA	NA	NA	NA

NA-data not available beyond 65° of flexion for SLI wrists.

Table 32 Radioscaphoid angle (flexion) with the wrist extension to flexion

Wrist angle from extension to flexion (degrees)	Normal				SLI				p value
	Mean	Std. Error	Lower CI	Upper CI	Mean	Std. Error	Lower CI	Upper CI	
-70°	0.1°	2.4°	-4.8°	4.6°	7.7°*	2.5°	2.8°	12.5°	0.02
-65°	2.1°	2.4°	-2.6°	6.7°	11.0°*	2.4°	6.3°	15.8°	0.01
-60°	4.5°	2.4°	-0.2°	9.2°	14.7°*	2.4°	10.0°	19.4°	0.00
-55°	7.3°	2.4°	2.6°	12.0°	18.5°*	2.4°	13.8°	23.2°	<.001
-50°	10.2°	2.4°	5.6°	14.9°	21.8°*	2.4°	17.1°	26.5°	<.001
-45°	13.3°	2.4°	8.6°	18.0°	25.4°*	2.4°	20.7°	30.1°	<.001
-40°	16.6°	2.4°	11.9°	21.2°	29.5°*	2.4°	24.8°	34.2°	<.001
-35°	20.1°	2.4°	15.5°	24.8°	34.7°*	2.4°	30.0°	39.3°	<.001
-30°	24.0°	2.4°	19.3°	28.6°	39.3°*	2.4°	34.7°	44.0°	<.001
-25°	27.9°	2.4°	23.2°	32.6°	44.4°*	2.4°	39.8°	49.1°	<.001
-20°	31.9°	2.4°	27.3°	36.6°	49.2°*	2.4°	44.5°	53.9°	<.001
-15°	36.2°	2.4°	31.5°	40.8°	53.7°*	2.4°	49.1°	58.4°	<.001
-10°	40.1°	2.4°	35.5°	44.8°	58.1°*	2.4°	53.4°	62.7°	<.001
-5°	44.0°	2.4°	39.4°	48.7°	62.2°*	2.4°	57.5°	66.8°	<.001
0°	47.9°	2.4°	43.3°	52.6°	66.2°*	2.4°	61.5°	70.8°	<.001
5°	52.0°	2.4°	47.3°	56.7°	69.5°*	2.4°	64.8°	74.1°	<.001
10°	56.0°	2.4°	51.3°	60.7°	72.8°*	2.4°	68.1°	77.5°	<.001
15°	59.9°	2.4°	55.2°	64.6°	76.0°*	2.4°	71.3°	80.7°	<.001
20°	63.6°	2.4°	59.0°	68.3°	79.3°*	2.4°	74.6°	84.0°	<.001
25°	67.6°	2.4°	62.9°	72.2°	82.6°*	2.4°	77.9°	87.3°	<.001
30°	71.6°	2.4°	66.9°	76.3°	85.9°*	2.4°	81.2°	90.6°	<.001
35°	75.6°	2.4°	70.9°	80.2°	89.2°*	2.4°	84.4°	93.9°	<.001
40°	79.6°	2.4°	74.9°	84.3°	93.1°*	2.4°	88.3°	97.9°	<.001
45°	83.7°	2.4°	79.0°	88.4°	97.0°	2.5°	92.2°	101.8°	<.001
50°	87.8°	2.4°	83.1°	92.5°	101.5°*	2.5°	96.6°	106.4°	<.001
55°	92.0°	2.4°	87.2°	96.7°	106.2°*	2.7°	100.9°	111.5°	<.001
60°	96.0°	2.4°	91.2°	100.8°	110.9°*	2.9°	105.3°	116.6°	<.001
65°	100.1°	2.5°	95.3°	105.0°	115.6°*	3.0°	109.7°	121.6°	<.001
70°	104.2°	2.6°	99.1°	109.2°	NA	NA	NA	NA	NA

Note: The radioscaphoid angle in SLI remain significantly flexed compared to the normal wrist throughout extension to flexion. “\*” and bold font Indicate statistical significance at a p-value of 0.05. NA-data not available beyond 65° of flexion for SLI wrists.



Table 33 Radioscaphoid angle (radial angulation) with the wrist extension to flexion

Wrist angle from extension to flexion (degrees)	Normal				SLI				p- value
	Mean	Std. Error	Lower CI	Upper CI	Mean	Std. Error	Lower CI	Upper CI	
-70°	32.7°	4.0°	24.9°	40.5°	41.0°	4.0°	33.1°	48.8°	0.142
-65°	32.3°	4.0°	24.5°	40.1°	40.5°	4.0°	32.7°	48.4°	0.142
-60°	32.6°	4.0°	24.8°	40.3°	40.7°	4.0°	32.9°	48.5°	0.146
-55°	32.8°	4.0°	25.0°	40.6°	40.5°	4.0°	32.7°	48.3°	0.167
-50°	33.0°	4.0°	25.2°	40.8°	40.1°	4.0°	32.3°	47.9°	0.207
-45°	33.1°	4.0°	25.3°	40.9°	39.7°	4.0°	31.9°	47.5°	0.240
-40°	33.2°	4.0°	25.4°	41.0°	39.4°	4.0°	31.6°	47.2°	0.271
-35°	33.2°	4.0°	25.4°	41.0°	39.2°	4.0°	31.4°	47.0°	0.289
-30°	33.1°	4.0°	25.3°	40.9°	39.1°	4.0°	31.3°	46.9°	0.289
-25°	33.0°	4.0°	25.2°	40.8°	39.0°	4.0°	31.2°	46.8°	0.290
-20°	32.8°	4.0°	25.0°	40.6°	39.1°	4.0°	31.3°	46.9°	0.263
-15°	32.5°	4.0°	24.7°	40.3°	39.1°	4.0°	31.3°	46.9°	0.240
-10°	32.5°	4.0°	24.7°	40.2°	39.1°	4.0°	31.3°	46.9°	0.236
-5°	32.4°	4.0°	24.6°	40.2°	39.2°	4.0°	31.4°	47.0°	0.227
0°	32.4°	4.0°	24.6°	40.2°	39.4°	4.0°	31.6°	47.2°	0.216
5°	32.0°	4.0°	24.2°	39.8°	39.6°	4.0°	31.8°	47.4°	0.175
10°	31.6°	4.0°	23.8°	39.4°	39.8°	4.0°	32.0°	47.6°	0.147
15°	31.2°	4.0°	23.4°	39.0°	39.9°	4.0°	32.1°	47.7°	0.123
20°	30.9°	4.0°	23.1°	38.7°	40.0°	4.0°	32.2°	47.8°	0.105
25°	30.5°	4.0°	22.7°	38.3°	39.7°	4.0°	31.9°	47.5°	0.103
30°	30.1°	4.0°	22.3°	37.9°	39.1°	4.0°	31.3°	46.9°	0.112
35°	29.7°	4.0°	21.9°	37.5°	38.2°	4.0°	30.4°	46.0°	0.131
40°	29.1°	4.0°	21.3°	36.9°	37.2°	4.0°	29.4°	45.0°	0.151
45°	28.6°	4.0°	20.7°	36.4°	36.0°	4.0°	28.2°	43.9°	0.186
50°	27.9°	4.0°	20.1°	35.7°	35.0°	4.0°	27.1°	42.8°	0.212
55°	27.2°	4.0°	19.4°	35.0°	33.0°	4.1°	25.0°	41.0°	0.313
60°	26.9°	4.0°	19.1°	34.7°	31.0°	4.1°	22.8°	39.1°	0.480
65°	26.5°	4.0°	18.6°	34.3°	29.0°	4.2°	20.7°	37.2°	0.667
70°	25.9°	4.0°	18.0°	33.8°	NA	NA	NA	NA	NA

“\*” and bold font Indicate statistical significance at a p-value of 0.05. NA-data not available beyond 65° of flexion for SLI wrists.

Table 34 Radioscaphoid angle (internal rotation) with the wrist extension to flexion

Wrist angle from extension to flexion (degrees)	Normal				SLI				p- value
	Mean	Std. Error	Lower CI	Upper CI	Mean	Std. Error	Lower CI	Upper CI	
-70°	62.0°	2.5°	57.1°	67.0°	73.9°*	2.5°	68.9°	78.8°	<.001
-65°	61.8°	2.5°	56.9°	66.8°	73.5°*	2.5°	68.6°	78.5°	0.001
-60°	61.8°	2.5°	56.9°	66.7°	73.4°*	2.5°	68.4°	78.3°	0.001
-55°	61.9°	2.5°	57.0°	66.8°	73.2°*	2.5°	68.3°	78.2°	0.001
-50°	61.8°	2.5°	56.9°	66.7°	73.1°*	2.5°	68.2°	78.0°	0.001
-45°	61.6°	2.5°	56.6°	66.5°	72.9°*	2.5°	68.0°	77.8°	0.001
-40°	61.5°	2.5°	56.5°	66.4°	72.6°*	2.5°	67.6°	77.5°	0.002
-35°	61.4°	2.5°	56.5°	66.3°	72.3°*	2.5°	67.4°	77.2°	0.002
-30°	61.3°	2.5°	56.4°	66.2°	72.1°*	2.5°	67.2°	77.0°	0.002
-25°	61.2°	2.5°	56.3°	66.1°	71.9°*	2.5°	67.0°	76.8°	0.003
-20°	61.1°	2.5°	56.1°	66.0°	71.6°*	2.5°	66.7°	76.5°	0.003
-15°	60.9°	2.5°	56.0°	65.8°	71.2°*	2.5°	66.3°	76.1°	0.004
-10°	60.7°	2.5°	55.8°	65.7°	71.0°*	2.5°	66.1°	75.9°	0.004
-5°	60.5°	2.5°	55.6°	65.4°	70.6°*	2.5°	65.7°	75.5°	0.004
0°	60.4°	2.5°	55.5°	65.3°	70.2°*	2.5°	65.3°	75.1°	0.006
5°	60.5°	2.5°	55.6°	65.4°	70.1°*	2.5°	65.1°	75.0°	0.007
10°	60.5°	2.5°	55.6°	65.4°	69.8°*	2.5°	64.9°	74.7°	0.009
15°	60.5°	2.5°	55.6°	65.4°	69.6°*	2.5°	64.6°	74.5°	0.011
20°	60.4°	2.5°	55.5°	65.3°	69.2°*	2.5°	64.3°	74.2°	0.013
25°	60.4°	2.5°	55.5°	65.3°	69.0°*	2.5°	64.1°	74.0°	0.015
30°	60.4°	2.5°	55.5°	65.3°	68.8°*	2.5°	63.9°	73.7°	0.018
35°	60.5°	2.5°	55.6°	65.4°	68.7°*	2.5°	63.7°	73.6°	0.022
40°	60.6°	2.5°	55.7°	65.5°	68.7°*	2.5°	63.7°	73.6°	0.023
45°	60.7°	2.5°	55.8°	65.6°	68.7°*	2.5°	63.7°	73.6°	0.026
50°	60.7°	2.5°	55.8°	65.6°	68.5°*	2.5°	63.5°	73.5°	0.029
55°	60.6°	2.5°	55.7°	65.6°	67.9°*	2.6°	62.8°	73.0°	0.044
60°	60.5°	2.5°	55.6°	65.5°	67.3°	2.6°	62.1°	72.5°	0.063
65°	60.2°	2.5°	55.3°	65.2°	66.7°	2.7°	61.4°	72.0°	0.079
70°	60.9°	2.6°	55.9°	65.9°	NA	NA	NA	NA	NA

“\*” and bold font Indicate statistical significance at a p-value of 0.05. NA-data not available beyond 65° of flexion for SLI wrists.

Table 35 Radiolunate angle (flexion) with the wrist extension to flexion

Wrist angle from extension to flexion (degrees)	Normal				SLI				p- value
	Mean	Std. Error	Lower CI	Upper CI	Mean	Std. Error	Lower CI	Upper CI	
-70°	-34.3°	2.4°	-39.0°	-29.5°	-37.1°	2.5°	-42.0°	-32.2°	0.423
-65°	-33.4°	2.4°	-38.1°	-28.6°	-36.2°	2.5°	-41.0°	-31.4°	0.412
-60°	-32.3°	2.4°	-37.0°	-27.5°	-34.6°	2.4°	-39.4°	-29.8°	0.499
-55°	-31.0°	2.4°	-35.7°	-26.2°	-33.4°	2.4°	-38.2°	-28.6°	0.477
-50°	-29.7°	2.4°	-34.4°	-24.9°	-32.3°	2.4°	-37.1°	-27.5°	0.442
-45°	-28.3°	2.4°	-33.0°	-23.6°	-31.2°	2.4°	-36.0°	-26.5°	0.393
-40°	-26.9°	2.4°	-31.6°	-22.1°	-30.2°	2.4°	-34.9°	-25.4°	0.334
-35°	-25.3°	2.4°	-30.0°	-20.6°	-29.1°	2.4°	-33.9°	-24.4°	0.264
-30°	-23.5°	2.4°	-28.3°	-18.8°	-28.2°	2.4°	-33.0°	-23.5°	0.168
-25°	-21.6°	2.4°	-26.4°	-16.9°	-27.4°	2.4°	-32.2°	-22.7°	0.090
-20°	<b>-19.8°</b>	<b>2.4°</b>	<b>-24.5°</b>	<b>-15.0°</b>	<b>-26.7°*</b>	<b>2.4°</b>	<b>-31.4°</b>	<b>-21.9°</b>	<b>0.043</b>
-15°	<b>-17.6°</b>	<b>2.4°</b>	<b>-22.4°</b>	<b>-12.9°</b>	<b>-25.8°*</b>	<b>2.4°</b>	<b>-30.6°</b>	<b>-21.1°</b>	<b>0.016</b>
-10°	<b>-15.5°</b>	<b>2.4°</b>	<b>-20.3°</b>	<b>-10.8°</b>	<b>-24.7°*</b>	<b>2.4°</b>	<b>-29.5°</b>	<b>-20.0°</b>	<b>0.007</b>
-5°	<b>-13.3°</b>	<b>2.4°</b>	<b>-18.0°</b>	<b>-8.6°</b>	<b>-23.4°*</b>	<b>2.4°</b>	<b>-28.2°</b>	<b>-18.7°</b>	<b>0.003</b>
0°	<b>-11.0°</b>	<b>2.4°</b>	<b>-15.8°</b>	<b>-6.3°</b>	<b>-21.9°*</b>	<b>2.4°</b>	<b>-26.7°</b>	<b>-17.2°</b>	<b>0.001</b>
5°	<b>-8.1°</b>	<b>2.4°</b>	<b>-12.8°</b>	<b>-3.4°</b>	<b>-19.9°*</b>	<b>2.4°</b>	<b>-24.6°</b>	<b>-15.1°</b>	<b>&lt;.001</b>
10°	<b>-5.2°</b>	<b>2.4°</b>	<b>-9.9°</b>	<b>-0.4°</b>	<b>-17.6°*</b>	<b>2.4°</b>	<b>-22.4°</b>	<b>-12.9°</b>	<b>&lt;.001</b>
15°	<b>-2.6°</b>	<b>2.4°</b>	<b>-7.3°</b>	<b>2.1°</b>	<b>-15.2°*</b>	<b>2.4°</b>	<b>-19.9°</b>	<b>-10.4°</b>	<b>&lt;.001</b>
20°	<b>0.0°</b>	<b>2.4°</b>	<b>-4.7°</b>	<b>4.7°</b>	<b>-12.2°*</b>	<b>2.4°</b>	<b>-16.9°</b>	<b>-7.4°</b>	<b>&lt;.001</b>
25°	<b>2.9°</b>	<b>2.4°</b>	<b>-1.9°</b>	<b>7.6°</b>	<b>-9.1°*</b>	<b>2.4°</b>	<b>-13.9°</b>	<b>-4.3°</b>	<b>&lt;.001</b>
30°	<b>5.8°</b>	<b>2.4°</b>	<b>1.1°</b>	<b>10.6°</b>	<b>-5.8°*</b>	<b>2.4°</b>	<b>-10.6°</b>	<b>-1.0°</b>	<b>&lt;.001</b>
35°	<b>8.8°</b>	<b>2.4°</b>	<b>4.1°</b>	<b>13.6°</b>	<b>-2.3°*</b>	<b>2.4°</b>	<b>-7.1°</b>	<b>2.5°</b>	<b>0.001</b>
40°	<b>12.1°</b>	<b>2.4°</b>	<b>7.3°</b>	<b>16.9°</b>	<b>1.6°*</b>	<b>2.5°</b>	<b>-3.2°</b>	<b>6.5°</b>	<b>0.003</b>
45°	<b>15.3°</b>	<b>2.4°</b>	<b>10.6°</b>	<b>20.1°</b>	<b>5.8°*</b>	<b>2.5°</b>	<b>0.9°</b>	<b>10.7°</b>	<b>0.006</b>
50°	<b>18.5°</b>	<b>2.4°</b>	<b>13.7°</b>	<b>23.3°</b>	<b>10.0°*</b>	<b>2.5°</b>	<b>5.0°</b>	<b>15.0°</b>	<b>0.016</b>
55°	<b>21.6°</b>	<b>2.5°</b>	<b>16.8°</b>	<b>26.4°</b>	<b>14.1°*</b>	<b>2.8°</b>	<b>8.7°</b>	<b>19.5°</b>	<b>0.044</b>
60°	24.4°	2.5°	19.5°	29.3°	18.3°	2.9°	12.5°	24.1°	0.112
65°	27.6°	2.5°	22.7°	32.5°	22.4°	3.1°	16.3°	28.6°	0.196
70°	31.2°	2.6°	26.1°	36.3°	NA	NA	NA	NA	NA

“\*” and bold font Indicate statistical significance at a p-value of 0.05. NA-data not available beyond 65° of flexion for SLI wrists.

Table 36 Radiolunate angle (radial angulation) with the wrist extension to flexion

Wrist angle from extension to flexion (degrees)	Normal				SLI				p- value
	Mean	Std. Error	Lower CI	Upper CI	Mean	Std. Error	Lower CI	Upper CI	
-70°	58.3°	3.9°	50.7°	65.9°	51.9°	3.9°	44.3°	59.6°	0.248
-65°	58.2°	3.9°	50.6°	65.8°	52.4°	3.9°	44.8°	60.0°	0.293
-60°	58.3°	3.9°	50.8°	65.9°	53.3°	3.9°	45.7°	60.9°	0.360
-55°	58.8°	3.9°	51.2°	66.4°	53.9°	3.9°	46.3°	61.5°	0.374
-50°	59.3°	3.9°	51.7°	66.8°	54.5°	3.9°	46.9°	62.1°	0.384
-45°	59.4°	3.9°	51.9°	67.0°	55.0°	3.9°	47.4°	62.6°	0.414
-40°	59.7°	3.9°	52.1°	67.3°	55.5°	3.9°	47.9°	63.1°	0.437
-35°	59.8°	3.9°	52.2°	67.4°	55.9°	3.9°	48.3°	63.5°	0.477
-30°	59.7°	3.9°	52.1°	67.3°	56.1°	3.9°	48.5°	63.7°	0.512
-25°	59.5°	3.9°	51.9°	67.1°	56.2°	3.9°	48.6°	63.8°	0.539
-20°	59.3°	3.9°	51.7°	66.9°	56.2°	3.9°	48.6°	63.8°	0.568
-15°	59.0°	3.9°	51.4°	66.6°	56.0°	3.9°	48.5°	63.6°	0.590
-10°	58.5°	3.9°	50.9°	66.1°	55.8°	3.9°	48.2°	63.4°	0.615
-5°	58.1°	3.9°	50.5°	65.7°	55.5°	3.9°	47.9°	63.0°	0.630
0°	57.7°	3.9°	50.1°	65.3°	55.2°	3.9°	47.6°	62.8°	0.647
5°	57.2°	3.9°	49.6°	64.8°	54.7°	3.9°	47.1°	62.3°	0.648
10°	56.7°	3.9°	49.1°	64.3°	54.2°	3.9°	46.6°	61.8°	0.647
15°	56.1°	3.9°	48.5°	63.7°	53.6°	3.9°	46.0°	61.2°	0.644
20°	55.6°	3.9°	48.0°	63.2°	53.0°	3.9°	45.4°	60.5°	0.632
25°	55.3°	3.9°	47.7°	62.9°	52.1°	3.9°	44.5°	59.7°	0.552
30°	54.9°	3.9°	47.3°	62.5°	51.2°	3.9°	43.6°	58.8°	0.501
35°	54.3°	3.9°	46.7°	61.9°	50.4°	3.9°	42.8°	58.0°	0.481
40°	53.2°	3.9°	45.6°	60.8°	49.7°	3.9°	42.0°	57.3°	0.520
45°	52.2°	3.9°	44.6°	59.8°	48.9°	3.9°	41.3°	56.5°	0.551
50°	51.3°	3.9°	43.7°	58.9°	48.0°	3.9°	40.4°	55.7°	0.558
55°	50.3°	3.9°	42.7°	57.9°	46.5°	3.9°	38.7°	54.2°	0.493
60°	49.6°	3.9°	42.0°	57.2°	44.9°	4.0°	37.1°	52.7°	0.402
65°	48.5°	3.9°	40.8°	56.1°	43.3°	4.0°	35.4°	51.3°	0.360
70°	47.6°	3.9°	40.0°	55.3°	NA	NA	NA	NA	NA

NA-data not available beyond 65° of flexion for SLI wrists.

Table 37 Radiolunate angle (internal rotation) with the wrist extension to flexion

Wrist angle from extension to flexion (degrees)	Normal				SLI				p- value
	Mean	Std. Error	Lower CI	Upper CI	Mean	Std. Error	Lower CI	Upper CI	
-70°	64.3°	2.7°	58.9°	69.6°	59.3°	2.7°	53.9°	64.7°	0.198
-65°	64.0°	2.7°	58.6°	69.3°	59.3°	2.7°	53.9°	64.6°	0.224
-60°	64.4°	2.7°	59.1°	69.8°	59.4°	2.7°	54.1°	64.8°	0.198
-55°	64.5°	2.7°	59.2°	69.9°	59.6°	2.7°	54.3°	65.0°	0.202
-50°	64.5°	2.7°	59.2°	69.9°	59.8°	2.7°	54.4°	65.1°	0.218
-45°	64.4°	2.7°	59.1°	69.8°	59.9°	2.7°	54.6°	65.3°	0.248
-40°	64.3°	2.7°	58.9°	69.6°	60.1°	2.7°	54.8°	65.5°	0.281
-35°	64.3°	2.7°	59.0°	69.7°	60.4°	2.7°	55.1°	65.8°	0.316
-30°	64.4°	2.7°	59.1°	69.8°	60.8°	2.7°	55.4°	66.1°	0.348
-25°	64.6°	2.7°	59.3°	70.0°	61.1°	2.7°	55.7°	66.4°	0.357
-20°	64.7°	2.7°	59.4°	70.1°	61.2°	2.7°	55.8°	66.5°	0.359
-15°	64.8°	2.7°	59.4°	70.1°	61.3°	2.7°	55.9°	66.6°	0.364
-10°	64.7°	2.7°	59.3°	70.0°	61.3°	2.7°	56.0°	66.7°	0.386
-5°	64.5°	2.7°	59.2°	69.9°	61.3°	2.7°	56.0°	66.7°	0.412
0°	64.5°	2.7°	59.1°	69.8°	61.4°	2.7°	56.0°	66.7°	0.421
5°	64.3°	2.7°	59.0°	69.7°	61.2°	2.7°	55.8°	66.5°	0.416
10°	64.1°	2.7°	58.8°	69.5°	61.0°	2.7°	55.6°	66.3°	0.415
15°	64.0°	2.7°	58.7°	69.4°	60.9°	2.7°	55.5°	66.2°	0.408
20°	64.0°	2.7°	58.7°	69.4°	60.7°	2.7°	55.3°	66.0°	0.389
25°	64.0°	2.7°	58.6°	69.3°	60.6°	2.7°	55.3°	66.0°	0.389
30°	63.9°	2.7°	58.6°	69.3°	60.6°	2.7°	55.2°	66.0°	0.386
35°	64.1°	2.7°	58.8°	69.5°	60.6°	2.7°	55.3°	66.0°	0.366
40°	64.3°	2.7°	59.0°	69.7°	60.6°	2.7°	55.3°	66.0°	0.341
45°	64.6°	2.7°	59.2°	70.0°	60.3°	2.7°	55.0°	65.7°	0.273
50°	64.6°	2.7°	59.2°	69.9°	60.3°	2.8°	54.9°	65.7°	0.267
55°	64.6°	2.7°	59.2°	70.0°	59.9°	2.8°	54.4°	65.4°	0.231
60°	65.0°	2.7°	59.6°	70.4°	59.5°	2.9°	53.9°	65.2°	0.169
65°	65.2°	2.8°	59.8°	70.6°	59.1°	2.9°	53.4°	64.9°	0.132
70°	65.7°	2.8°	60.2°	71.2°	NA	NA	NA	NA	NA

NA-data not available beyond 65° of flexion for SLI wrists.

Table 38 Scaphoid ulnar translation with the wrist extension to flexion

Wrist angle from extension to flexion (degrees)	Normal				SLI				p- value
	Mean	Std. Error	Lower CI	Upper CI	Mean	Std. Error	Lower CI	Upper CI	
-70°	-8.3	0.3	-8.9	-7.7	-9.5*	0.3	-10.0	-8.9	0.006
-65°	-8.1	0.3	-8.7	-7.6	-9.3*	0.3	-9.9	-8.7	0.005
-60°	-8.0	0.3	-8.6	-7.4	-9.2*	0.3	-9.8	-8.6	0.005
-55°	-7.9	0.3	-8.4	-7.3	-9.0*	0.3	-9.6	-8.4	0.008
-50°	-7.7	0.3	-8.3	-7.2	-8.8*	0.3	-9.3	-8.2	0.013
-45°	-7.5	0.3	-8.1	-6.9	-8.6*	0.3	-9.1	-8.0	0.011
-40°	-7.4	0.3	-7.9	-6.8	-8.4*	0.3	-9.0	-7.8	0.013
-35°	-7.2	0.3	-7.8	-6.6	-8.2*	0.3	-8.8	-7.6	0.016
-30°	-7.0	0.3	-7.6	-6.5	-8.0*	0.3	-8.6	-7.5	0.016
-25°	-6.9	0.3	-7.5	-6.3	-7.9*	0.3	-8.5	-7.3	0.016
-20°	-6.8	0.3	-7.3	-6.2	-7.7*	0.3	-8.3	-7.1	0.021
-15°	-6.7	0.3	-7.2	-6.1	-7.6*	0.3	-8.2	-7.0	0.025
-10°	-6.6	0.3	-7.2	-6.0	-7.5*	0.3	-8.0	-6.9	0.037
-5°	-6.5	0.3	-7.1	-6.0	-7.4*	0.3	-7.9	-6.8	0.039
0°	-6.4	0.3	-7.0	-5.9	-7.3*	0.3	-7.8	-6.7	0.046
5°	-6.4	0.3	-7.0	-5.8	-7.2	0.3	-7.8	-6.6	0.053
10°	-6.3	0.3	-6.9	-5.8	-7.2	0.3	-7.7	-6.6	0.048
15°	-6.3	0.3	-6.9	-5.8	-7.2	0.3	-7.7	-6.6	0.046
20°	-6.4	0.3	-6.9	-5.8	-7.2	0.3	-7.7	-6.6	0.058
25°	-6.4	0.3	-7.0	-5.8	-7.1	0.3	-7.7	-6.6	0.081
30°	-6.5	0.3	-7.0	-5.9	-7.1	0.3	-7.7	-6.5	0.109
35°	-6.5	0.3	-7.1	-5.9	-7.1	0.3	-7.7	-6.6	0.128
40°	-6.5	0.3	-7.1	-5.9	-7.2	0.3	-7.7	-6.6	0.123
45°	-6.6	0.3	-7.2	-6.0	-7.3	0.3	-7.9	-6.7	0.095
50°	-6.6	0.3	-7.2	-6.1	-7.4	0.3	-8.0	-6.8	0.059
55°	-6.7	0.3	-7.3	-6.1	-7.7*	0.3	-8.3	-7.1	0.023
60°	-6.8	0.3	-7.4	-6.2	-7.9*	0.3	-8.6	-7.3	0.012
65°	-6.9	0.3	-7.5	-6.3	-8.2*	0.4	-8.9	-7.5	0.007
70°	-7.2	0.3	-7.8	-6.6	NA	NA	NA	NA	NA

“\*” and bold font Indicate statistical significance at a p-value of 0.05. NA-data not available beyond 65° of flexion for SLI wrists.

Table 39 Scaphoid volar translation with the wrist extension to flexion

Wrist angle from extension to flexion (degrees)	Normal				SLI				p- value
	Mean	Std. Error	Lower CI	Upper CI	Mean	Std. Error	Lower CI	Upper CI	
-70°	0.3	0.3	-0.4	1.0	0.2	0.4	-0.6	0.9	0.767
-65°	0.5	0.3	-0.2	1.2	0.5	0.4	-0.2	1.2	0.986
-60°	0.8	0.3	0.2	1.5	1.1	0.4	0.4	1.8	0.584
-55°	1.1	0.3	0.4	1.8	1.5	0.4	0.8	2.2	0.496
-50°	1.4	0.3	0.7	2.1	1.8	0.4	1.1	2.5	0.410
-45°	1.6	0.3	0.9	2.3	2.1	0.3	1.4	2.8	0.325
-40°	1.8	0.3	1.2	2.5	2.4	0.3	1.7	3.1	0.253
-35°	2.1	0.3	1.4	2.8	2.7	0.3	2.0	3.4	0.246
-30°	2.4	0.3	1.7	3.0	2.9	0.3	2.2	3.6	0.264
-25°	2.6	0.3	2.0	3.3	3.1	0.3	2.4	3.8	0.345
-20°	2.9	0.3	2.2	3.6	3.3	0.3	2.6	3.9	0.436
-15°	3.1	0.3	2.5	3.8	3.4	0.3	2.7	4.1	0.583
-10°	3.3	0.3	2.6	4.0	3.5	0.3	2.9	4.2	0.672
-5°	3.5	0.3	2.8	4.2	3.7	0.3	3.0	4.4	0.751
0°	3.7	0.3	3.0	4.4	3.8	0.3	3.2	4.5	0.800
5°	3.9	0.3	3.2	4.6	4.0	0.3	3.3	4.7	0.914
10°	4.2	0.3	3.5	4.8	4.1	0.3	3.4	4.8	0.949
15°	4.4	0.3	3.7	5.1	4.3	0.3	3.6	5.0	0.790
20°	4.7	0.3	4.1	5.4	4.5	0.3	3.8	5.2	0.681
25°	5.0	0.3	4.4	5.7	4.7	0.4	4.1	5.4	0.559
30°	5.3	0.3	4.6	6.0	5.0	0.4	4.3	5.7	0.530
35°	5.5	0.4	4.8	6.2	5.3	0.4	4.6	6.0	0.697
40°	5.7	0.4	5.0	6.4	5.5	0.4	4.8	6.2	0.726
45°	5.8	0.4	5.1	6.5	5.8	0.4	5.1	6.5	0.996
50°	5.9	0.4	5.2	6.6	6.1	0.4	5.4	6.9	0.655
55°	6.0	0.4	5.3	6.7	6.6	0.4	5.8	7.5	0.253
60°	6.0	0.4	5.3	6.7	7.1	0.5	6.2	8.1	0.071
65°	6.0	0.4	5.3	6.8	7.6	0.5	6.6	8.7	0.014
70°	6.1	0.4	5.3	6.9	NA	NA	NA	NA	NA

NA-data not available beyond 65° of flexion for SLI wrists.

Table 40 Scaphoid distal translation with the wrist extension to flexion

Wrist angle from extension to flexion (degrees)	Normal				SLI				p- value
	Mean	Std. Error	Lower CI	Upper CI	Mean	Std. Error	Lower CI	Upper CI	
-70°	14.6	0.4	13.9	15.3	16.3*	0.4	15.6	17.1	0.001
-65°	14.7	0.4	14.0	15.4	16.3*	0.4	15.6	17.0	0.002
-60°	14.6	0.4	13.9	15.4	16.1*	0.4	15.4	16.8	0.005
-55°	14.6	0.4	13.9	15.3	16.0*	0.4	15.3	16.7	0.007
-50°	14.5	0.4	13.8	15.2	15.8*	0.4	15.1	16.6	0.008
-45°	14.4	0.4	13.7	15.1	15.7*	0.4	15.0	16.4	0.011
-40°	14.3	0.4	13.6	15.0	15.6*	0.4	14.8	16.3	0.014
-35°	14.2	0.4	13.5	14.9	15.4*	0.4	14.7	16.1	0.021
-30°	14.1	0.4	13.4	14.8	15.2*	0.4	14.5	15.9	0.037
-25°	14.0	0.4	13.3	14.7	15.0	0.4	14.3	15.7	0.062
-20°	13.9	0.4	13.2	14.6	14.7	0.4	14.0	15.5	0.117
-15°	13.8	0.4	13.1	14.5	14.5	0.4	13.8	15.2	0.179
-10°	13.7	0.4	13.0	14.4	14.3	0.4	13.6	15.1	0.230
-5°	13.6	0.4	12.9	14.3	14.1	0.4	13.4	14.9	0.289
0°	13.5	0.4	12.8	14.2	14.0	0.4	13.2	14.7	0.353
5°	13.4	0.4	12.7	14.1	13.8	0.4	13.1	14.5	0.459
10°	13.3	0.4	12.6	14.0	13.6	0.4	12.9	14.3	0.572
15°	13.2	0.4	12.5	13.9	13.4	0.4	12.7	14.1	0.658
20°	13.1	0.4	12.3	13.8	13.2	0.4	12.5	13.9	0.795
25°	12.9	0.4	12.2	13.6	13.0	0.4	12.3	13.7	0.851
30°	12.8	0.4	12.1	13.5	12.9	0.4	12.1	13.6	0.881
35°	12.7	0.4	12.0	13.4	12.7	0.4	12.0	13.5	0.922
40°	12.6	0.4	11.9	13.3	12.6	0.4	11.9	13.3	0.975
45°	12.5	0.4	11.8	13.2	12.5	0.4	11.8	13.3	0.954
50°	12.4	0.4	11.7	13.1	12.4	0.4	11.7	13.1	0.987
55°	12.3	0.4	11.6	13.0	12.6	0.4	11.8	13.3	0.579
60°	12.1	0.4	11.4	12.8	12.8	0.4	12.0	13.6	0.250
65°	12.0	0.4	11.3	12.7	12.9	0.4	12.1	13.8	0.100
70°	11.9	0.4	11.1	12.6	NA	NA	NA	NA	NA

“\*” and bold font Indicate statistical significance at a p-value of 0.05. NA-data not available beyond 65° of flexion for SLI wrists.



Table 41 Lunate ulnar translation with the wrist extension to flexion

Wrist angle from extension to flexion (degrees)	Normal				SLI				p- value
	Mean	Std. Error	Lower CI	Upper CI	Mean	Std. Error	Lower CI	Upper CI	
-70°	5.7	0.3	5.2	6.3	6.7*	0.3	6.1	7.4	0.020
-65°	5.9	0.3	5.3	6.4	6.9*	0.3	6.3	7.5	0.015
-60°	6.0	0.3	5.4	6.6	7.1*	0.3	6.5	7.7	0.010
-55°	6.1	0.3	5.6	6.7	7.3*	0.3	6.7	7.9	0.006
-50°	6.3	0.3	5.7	6.9	7.6*	0.3	7.0	8.2	0.003
-45°	6.5	0.3	5.9	7.1	7.8*	0.3	7.2	8.4	0.002
-40°	6.6	0.3	6.0	7.2	8.0*	0.3	7.4	8.6	0.001
-35°	6.7	0.3	6.2	7.3	8.1*	0.3	7.6	8.7	<.001
-30°	6.8	0.3	6.3	7.4	8.2*	0.3	7.7	8.8	<.001
-25°	6.9	0.3	6.3	7.5	8.3*	0.3	7.7	8.9	<.001
-20°	7.0	0.3	6.4	7.5	8.4*	0.3	7.8	9.0	<.001
-15°	7.0	0.3	6.4	7.6	8.4*	0.3	7.8	9.0	<.001
-10°	6.9	0.3	6.4	7.5	8.4*	0.3	7.8	9.0	<.001
-5°	6.9	0.3	6.3	7.5	8.3*	0.3	7.8	8.9	<.001
0°	6.9	0.3	6.3	7.5	8.3*	0.3	7.7	8.9	<.001
5°	6.9	0.3	6.3	7.4	8.2*	0.3	7.6	8.8	0.001
10°	6.8	0.3	6.2	7.4	8.1*	0.3	7.5	8.7	0.002
15°	6.7	0.3	6.2	7.3	8.0*	0.3	7.4	8.6	0.004
20°	6.6	0.3	6.0	7.2	7.8*	0.3	7.2	8.4	0.004
25°	6.5	0.3	5.9	7.1	7.7*	0.3	7.1	8.2	0.005
30°	6.3	0.3	5.7	6.9	7.5*	0.3	6.9	8.1	0.006
35°	6.1	0.3	5.5	6.7	7.3*	0.3	6.7	7.9	0.007
40°	6.0	0.3	5.4	6.5	7.1*	0.3	6.5	7.7	0.010
45°	5.8	0.3	5.2	6.4	6.8*	0.3	6.2	7.4	0.016
50°	5.6	0.3	5.0	6.2	6.6*	0.3	5.9	7.2	0.030
55°	5.5	0.3	4.9	6.1	6.1	0.3	5.5	6.8	0.136
60°	5.2	0.3	4.7	5.8	5.7	0.4	5.0	6.4	0.315
65°	5.0	0.3	4.4	5.6	5.3	0.4	4.5	6.1	0.529
70°	4.6	0.3	4.0	5.2	NA	NA	NA	NA	NA

“\*” and bold font Indicate statistical significance at a p-value of 0.05. NA-data not available beyond 65° of flexion for SLI wrists.

Table 42 Lunate volar translation with the wrist extension to flexion

Wrist angle from extension to flexion (degrees)	Normal				SLI				p- value
	Mean	Std. Error	Lower CI	Upper CI	Mean	Std. Error	Lower CI	Upper CI	
-70°	4.7	0.3	4.2	5.2	4.4	0.3	3.9	5.0	0.491
-65°	4.6	0.3	4.1	5.1	4.4	0.3	3.9	4.9	0.502
-60°	4.6	0.3	4.0	5.1	4.4	0.3	3.9	4.9	0.715
-55°	4.5	0.3	4.0	5.0	4.3	0.3	3.8	4.8	0.688
-50°	4.4	0.3	3.9	4.9	4.2	0.3	3.7	4.7	0.723
-45°	4.2	0.3	3.7	4.7	4.1	0.3	3.6	4.7	0.825
-40°	4.1	0.3	3.6	4.6	4.1	0.3	3.6	4.6	0.881
-35°	4.1	0.3	3.5	4.6	4.0	0.3	3.5	4.5	0.911
-30°	4.0	0.3	3.5	4.5	4.0	0.3	3.5	4.5	0.998
-25°	3.9	0.3	3.4	4.4	3.9	0.3	3.4	4.5	0.952
-20°	3.8	0.3	3.3	4.3	3.9	0.3	3.4	4.4	0.901
-15°	3.7	0.3	3.2	4.3	3.8	0.3	3.3	4.3	0.847
-10°	3.6	0.3	3.1	4.1	3.7	0.3	3.2	4.3	0.676
-5°	3.4	0.3	2.9	3.9	3.6	0.3	3.1	4.2	0.541
0°	3.3	0.3	2.8	3.8	3.6	0.3	3.0	4.1	0.467
5°	3.1	0.3	2.6	3.6	3.4	0.3	2.9	3.9	0.424
10°	2.9	0.3	2.4	3.4	3.2	0.3	2.7	3.7	0.435
15°	2.8	0.3	2.3	3.3	3.0	0.3	2.5	3.5	0.517
20°	2.7	0.3	2.1	3.2	2.8	0.3	2.3	3.3	0.674
25°	2.5	0.3	2.0	3.0	2.6	0.3	2.1	3.1	0.736
30°	2.3	0.3	1.8	2.9	2.5	0.3	2.0	3.0	0.699
35°	2.2	0.3	1.7	2.7	2.3	0.3	1.8	2.8	0.769
40°	2.1	0.3	1.6	2.6	2.1	0.3	1.6	2.6	0.873
45°	1.9	0.3	1.4	2.5	2.0	0.3	1.5	2.5	0.886
50°	1.8	0.3	1.3	2.3	1.9	0.3	1.4	2.5	0.770
55°	1.7	0.3	1.2	2.2	2.1	0.3	1.5	2.6	0.405
60°	1.6	0.3	1.1	2.1	2.2	0.3	1.6	2.8	0.163
65°	1.5	0.3	1.0	2.0	2.3	0.3	1.6	2.9	0.060
70°	1.5	0.3	0.9	2.0	NA	NA	NA	NA	NA

NA-data not available beyond 65° of flexion for SLI wrists.

Table 43 Lunate distal translation with the wrist extension to flexion

Wrist angle from extension to flexion (degrees)	Normal				SLI				p- value
	Mean	Std. Error	Lower CI	Upper CI	Mean	Std. Error	Lower CI	Upper CI	
-70°	6.2	0.2	5.8	6.6	6.2	0.2	5.8	6.6	0.945
-65°	6.2	0.2	5.8	6.5	6.2	0.2	5.8	6.6	0.869
-60°	6.1	0.2	5.8	6.5	6.1	0.2	5.8	6.5	0.995
-55°	6.1	0.2	5.8	6.5	6.1	0.2	5.7	6.5	0.890
-50°	6.1	0.2	5.7	6.5	6.0	0.2	5.7	6.4	0.819
-45°	6.1	0.2	5.7	6.5	6.0	0.2	5.6	6.4	0.741
-40°	6.1	0.2	5.7	6.4	6.0	0.2	5.6	6.3	0.707
-35°	6.0	0.2	5.7	6.4	5.9	0.2	5.6	6.3	0.711
-30°	6.0	0.2	5.7	6.4	5.9	0.2	5.5	6.3	0.680
-25°	6.0	0.2	5.7	6.4	5.9	0.2	5.5	6.3	0.641
-20°	6.1	0.2	5.7	6.4	5.9	0.2	5.5	6.3	0.556
-15°	6.1	0.2	5.7	6.4	5.9	0.2	5.5	6.3	0.560
-10°	6.1	0.2	5.7	6.5	5.9	0.2	5.5	6.3	0.492
-5°	6.1	0.2	5.7	6.5	5.9	0.2	5.5	6.3	0.505
0°	6.1	0.2	5.7	6.5	5.9	0.2	5.6	6.3	0.541
5°	6.1	0.2	5.8	6.5	6.0	0.2	5.6	6.3	0.508
10°	6.2	0.2	5.8	6.6	6.0	0.2	5.6	6.4	0.471
15°	6.2	0.2	5.9	6.6	6.1	0.2	5.7	6.4	0.511
20°	6.3	0.2	5.9	6.6	6.1	0.2	5.7	6.5	0.567
25°	6.3	0.2	6.0	6.7	6.2	0.2	5.8	6.6	0.567
30°	6.4	0.2	6.1	6.8	6.3	0.2	5.9	6.6	0.554
35°	6.5	0.2	6.2	6.9	6.4	0.2	6.0	6.8	0.561
40°	6.6	0.2	6.3	7.0	6.5	0.2	6.2	6.9	0.690
45°	6.7	0.2	6.4	7.1	6.7	0.2	6.3	7.1	0.896
50°	6.8	0.2	6.5	7.2	6.9	0.2	6.5	7.3	0.776
55°	6.9	0.2	6.5	7.3	7.0	0.2	6.6	7.5	0.642
60°	7.0	0.2	6.7	7.4	7.2	0.2	6.8	7.6	0.640
65°	7.2	0.2	6.8	7.6	7.3	0.2	6.9	7.8	0.673
70°	7.4	0.2	7.0	7.8	NA	NA	NA	NA	NA

NA-data not available beyond 65° of flexion for SLI wrists.

Table 44 Scaphoid flexion with the wrist from ulnar to radial deviation

Wrist angle from ulnar to radial deviation (degrees)	Normal				SLI				<i>p- value</i>
	Mean	Std. Error	Lower CI	Upper CI	Mean	Std. Error	Lower CI	Upper CI	
-35°	-12.4°	1.7°	-15.7°	-9.1°	-13.6°	2.1°	-17.8°	-9.4°	0.66
-30°	-12.4°	1.6°	-15.5°	-9.4°	-11.4°	1.7°	-14.8°	-8.0°	0.67
-25°	-11.6°	1.5°	-14.5°	-8.8°	-9.8°	1.5°	-12.8°	-6.8°	0.40
-20°	-11.5°	1.4°	-14.4°	-8.7°	-9.1°	1.5°	-11.9°	-6.2°	0.23
-15°	-10.5°	1.4°	-13.4°	-7.7°	-6.8°	1.4°	-9.6°	-4.0°	0.07
-10°	-8.1°	1.4°	-10.9°	-5.3°	-4.6°	1.4°	-7.4°	-1.8°	0.09
-5°	-4.3°	1.4°	-7.2°	-1.5°	-2.5°	1.4°	-5.3°	0.3°	0.37
0°	0.0°	1.4°	-2.8°	2.8°	0.0°	1.4°	-2.8°	2.8°	1.00
5°	4.3°	1.4°	1.4°	7.1°	2.1°	1.4°	-0.7°	4.9°	0.28
<b>10°</b>	<b>8.2°</b>	<b>1.4°</b>	<b>5.4°</b>	<b>11.0°</b>	<b>3.9°*</b>	<b>1.5°</b>	<b>1.0°</b>	<b>6.7°</b>	<b>0.03</b>
<b>15°</b>	<b>11.8°</b>	<b>1.4°</b>	<b>9.0°</b>	<b>14.6°</b>	<b>5.7°*</b>	<b>1.5°</b>	<b>2.8°</b>	<b>8.6°</b>	<b>0.00</b>
<b>20°</b>	<b>14.7°</b>	<b>1.5°</b>	<b>11.8°</b>	<b>17.5°</b>	<b>7.5°*</b>	<b>1.5°</b>	<b>4.6°</b>	<b>10.5°</b>	<b>&lt;.001</b>
<b>25°</b>	<b>17.2°</b>	<b>1.5°</b>	<b>14.2°</b>	<b>20.2°</b>	<b>8.8°*</b>	<b>1.6°</b>	<b>5.7°</b>	<b>11.9°</b>	<b>&lt;.001</b>
<b>30°</b>	<b>19.5°</b>	<b>1.7°</b>	<b>16.2°</b>	<b>22.8°</b>	<b>10.0°*</b>	<b>1.7°</b>	<b>6.6°</b>	<b>13.4°</b>	<b>&lt;.001</b>
<b>35°</b>	<b>20.9°</b>	<b>1.9°</b>	<b>17.1°</b>	<b>24.7°</b>	<b>10.2°*</b>	<b>2.0°</b>	<b>6.3°</b>	<b>14.1°</b>	<b>&lt;.001</b>

“\*” and bold font Indicate statistical significance at a p-value of 0.05.

Table 45 Scaphoid radial angulation with the wrist from ulnar to radial deviation

Wrist angle from ulnar to radial deviation (degrees)	Normal				SLI				p- value
	Mean	Std. Error	Lower CI	Upper CI	Mean	Std. Error	Lower CI	Upper CI	
-35°	-22.1°	1.0°	-24.0°	-20.2°	-22.5°	1.2°	-24.9°	-20.2°	0.768
-30°	-18.7°	0.9°	-20.4°	-16.9°	-18.6°	1.0°	-20.5°	-16.6°	0.94
-25°	-14.8°	0.8°	-16.5°	-13.2°	-14.6°	0.9°	-16.3°	-12.8°	0.84
-20°	-11.2°	0.8°	-12.9°	-9.6°	-11.4°	0.8°	-13.1°	-9.8°	0.85
-15°	-7.8°	0.8°	-9.4°	-6.1°	-8.6°	0.8°	-10.3°	-6.9°	0.48
-10°	-4.4°	0.8°	-6.0°	-2.7°	-5.7°	0.8°	-7.3°	-4.1°	0.27
-5°	-2.0°	0.8°	-3.6°	-0.3°	-2.9°	0.8°	-4.5°	-1.3°	0.43
0°	0.0°	0.8°	-1.6°	1.6°	0.0°	0.8°	-1.6°	1.6°	1.00
5°	1.9°	0.8°	0.2°	3.5°	3.1°	0.8°	1.4°	4.7°	0.31
<b>10°</b>	<b>3.4°</b>	<b>0.8°</b>	<b>1.8°</b>	<b>5.1°</b>	<b>6.2°*</b>	<b>0.8°</b>	<b>4.5°</b>	<b>7.8°</b>	<b>0.02</b>
<b>15°</b>	<b>4.8°</b>	<b>0.8°</b>	<b>3.2°</b>	<b>6.5°</b>	<b>9.2°*</b>	<b>0.9°</b>	<b>7.5°</b>	<b>10.9°</b>	<b>&lt;.001</b>
<b>20°</b>	<b>6.1°</b>	<b>0.8°</b>	<b>4.4°</b>	<b>7.7°</b>	<b>12.1°*</b>	<b>0.9°</b>	<b>10.4°</b>	<b>13.9°</b>	<b>&lt;.001</b>
<b>25°</b>	<b>7.1°</b>	<b>0.9°</b>	<b>5.4°</b>	<b>8.8°</b>	<b>15.3°*</b>	<b>0.9°</b>	<b>13.5°</b>	<b>17.1°</b>	<b>&lt;.001</b>
<b>30°</b>	<b>8.9°</b>	<b>1.0°</b>	<b>7.0°</b>	<b>10.8°</b>	<b>18.1°*</b>	<b>1.0°</b>	<b>16.2°</b>	<b>20.1°</b>	<b>&lt;.001</b>
<b>35°</b>	<b>10.7°</b>	<b>1.1°</b>	<b>8.5°</b>	<b>12.9°</b>	<b>20.1°*</b>	<b>1.1°</b>	<b>17.9°</b>	<b>22.3°</b>	<b>&lt;.001</b>

“\*” and bold font Indicate statistical significance at a p-value of 0.05.

Table 46 Scaphoid Internal rotation with the wrist from ulnar to radial deviation

Wrist angle from ulnar to radial deviation (degrees)	Normal				SLI				<i>p</i> value
	Mean	Std. Error	Lower CI	Upper CI	Mean	Std. Error	Lower CI	Upper CI	
-35°	-3.8°	0.6°	-5.0°	-2.6°	-1.8°	0.8°	-3.4°	-0.3°	0.050
-30°	-2.6°	0.6°	-3.8°	-1.5°	-1.0°	0.6°	-2.2°	0.3°	0.05
-25°	-1.6°	0.5°	-2.7°	-0.6°	-0.3°	0.6°	-1.4°	0.8°	0.08
-20°	-1.1°	0.5°	-2.1°	-0.1°	-0.1°	0.5°	-1.2°	0.9°	0.19
-15°	-0.7°	0.5°	-1.8°	0.3°	0.0°	0.5°	-1.1°	1.0°	0.36
-10°	-0.3°	0.5°	-1.3°	0.7°	0.0°	0.5°	-1.0°	1.1°	0.67
-5°	-0.1°	0.5°	-1.1°	1.0°	0.0°	0.5°	-1.0°	1.0°	0.94
0°	0.0°	0.5°	-1.0°	1.0°	0.0°	0.5°	-1.0°	1.0°	1.00
5°	-0.3°	0.5°	-1.3°	0.8°	0.2°	0.5°	-0.8°	1.2°	0.52
10°	-0.6°	0.5°	-1.6°	0.4°	0.3°	0.5°	-0.8°	1.3°	0.26
15°	<b>-1.3°</b>	<b>0.5°</b>	<b>-2.3°</b>	<b>-0.3°</b>	<b>0.5°*</b>	<b>0.5°</b>	<b>-0.5°</b>	<b>1.6°</b>	<b>0.02</b>
20°	<b>-1.8°</b>	<b>0.5°</b>	<b>-2.9°</b>	<b>-0.8°</b>	<b>0.7°*</b>	<b>0.6°</b>	<b>-0.4°</b>	<b>1.8°</b>	<b>&lt;.001</b>
25°	<b>-2.6°</b>	<b>0.6°</b>	<b>-3.7°</b>	<b>-1.6°</b>	<b>0.6°*</b>	<b>0.6°</b>	<b>-0.5°</b>	<b>1.7°</b>	<b>&lt;.001</b>
30°	<b>-3.8°</b>	<b>0.6°</b>	<b>-5.0°</b>	<b>-2.6°</b>	<b>0.0°*</b>	<b>0.6°</b>	<b>-1.2°</b>	<b>1.3°</b>	<b>&lt;.001</b>
35°	<b>-4.4°</b>	<b>0.7°</b>	<b>-5.8°</b>	<b>-3.0°</b>	<b>-1.0°*</b>	<b>0.7°</b>	<b>-2.4°</b>	<b>0.4°</b>	<b>0.00</b>

“\*” and bold font Indicate statistical significance at a *p*-value of 0.05.

Table 47 Lunate flexion with the wrist from ulnar to radial deviation

Wrist angle from ulnar to radial deviation (degrees)	Normal				SLI				<i>p</i> - value
	Mean	Std. Error	Lower CI	Upper CI	Mean	Std. Error	Lower CI	Upper CI	
-35°	-18.4°	1.4°	-21.0°	-15.7°	-11.2°*	1.7°	-14.6°	-7.8°	0.001
-30°	-17.6°	1.3°	-20.1°	-15.2°	-10.8°*	1.4°	-13.6°	-8.1°	<.001
-25°	-15.8°	1.2°	-18.1°	-13.5°	-10.4°*	1.2°	-12.8°	-8.0°	0.0
-20°	-14.6°	1.2°	-16.9°	-12.4°	-9.1°*	1.2°	-11.4°	-6.8°	<.001
-15°	-12.5°	1.2°	-14.8°	-10.3°	-7.0°*	1.2°	-9.3°	-4.8°	<.001
-10°	-8.9°	1.2°	-11.1°	-6.6°	-5.0°*	1.2°	-7.2°	-2.7°	0.0
-5°	-4.6°	1.2°	-6.9°	-2.4°	-2.7°	1.2°	-5.0°	-0.5°	0.2
0°	0.0°	1.2°	-2.3°	2.3°	0.0°	1.2°	-2.3°	2.3°	1.0
5°	4.0°	1.2°	1.7°	6.3°	2.4°	1.2°	0.1°	4.7°	0.3
10°	7.8°	1.2°	5.5°	10.0°	4.8°	1.2°	2.5°	7.1°	0.1
15°	10.8°	1.2°	8.5°	13.1°	7.1°*	1.2°	4.7°	9.4°	0.0
20°	13.4°	1.2°	11.1°	15.7°	9.1°*	1.2°	6.7°	11.5°	0.0
25°	15.7°	1.2°	13.3°	18.1°	10.7°*	1.3°	8.2°	13.3°	0.0
30°	17.0°	1.4°	14.3°	19.6°	12.0°*	1.4°	9.3°	14.8°	0.0
35°	17.5°	1.6°	14.5°	20.6°	12.9°*	1.6°	9.7°	16.0°	0.0

“\*” and bold font Indicate statistical significance at a *p*-value of 0.05.

Table 48 Lunate radial angulation with the wrist from ulnar to radial deviation

Wrist angle from ulnar to radial deviation (degrees)	Normal				SLI				<i>p- value</i>
	Mean	Std. Error	Lower CI	Upper CI	Mean	Std. Error	Lower CI	Upper CI	
-35°	-20.2°	0.7°	-21.5°	-18.8°	-20.4°	0.9°	-22.1°	-18.6°	0.85
-30°	-17.3°	0.6°	-18.5°	-16.0°	-16.5°	0.7°	-17.9°	-15.1°	0.43
-25°	-14.0°	0.6°	-15.2°	-12.9°	-13.5°	0.6°	-14.7°	-12.2°	0.50
-20°	-10.8°	0.6°	-11.9°	-9.6°	-10.0°	0.6°	-11.2°	-8.9°	0.37
-15°	-7.7°	0.6°	-8.8°	-6.5°	-7.0°	0.6°	-8.2°	-5.8°	0.42
-10°	-4.7°	0.6°	-5.8°	-3.5°	-4.4°	0.6°	-5.5°	-3.2°	0.69
-5°	-2.2°	0.6°	-3.3°	-1.0°	-2.0°	0.6°	-3.2°	-0.9°	0.85
0°	0.0°	0.6°	-1.2°	1.2°	0.0°	0.6°	-1.2°	1.2°	1.00
5°	1.9°	0.6°	0.7°	3.0°	1.3°	0.6°	0.1°	2.4°	0.46
10°	3.3°	0.6°	2.2°	4.5°	2.3°	0.6°	1.1°	3.5°	0.23
15°	4.3°	0.6°	3.1°	5.4°	3.5°	0.6°	2.3°	4.7°	0.36
20°	5.0°	0.6°	3.9°	6.2°	4.5°	0.6°	3.3°	5.7°	0.57
25°	5.9°	0.6°	4.6°	7.1°	6.0°	0.7°	4.7°	7.3°	0.86
30°	7.4°	0.7°	6.0°	8.7°	7.6°	0.7°	6.2°	9.0°	0.80
35°	8.6°	0.8°	7.0°	10.2°	9.6°	0.8°	7.9°	11.2°	0.39

“\*” and bold font Indicate statistical significance at a *p*-value of 0.05.



Table 49 Lunate internal rotation with the wrist ulnar to radial deviation

Wrist angle from ulnar to radial deviation (degrees)	Normal				SLI				<i>p</i> - value
	Mean	Std. Error	Lower CI	Upper CI	Mean	Std. Error	Lower CI	Upper CI	
-35°	-2.75	<b>0.48</b>	<b>-3.69</b>	<b>-1.80</b>	<b>0.30*</b>	<b>0.66</b>	<b>-1.00</b>	<b>1.59</b>	<b>&lt;.001</b>
-30°	-1.98	<b>0.43</b>	<b>-2.83</b>	<b>-1.13</b>	<b>0.52*</b>	<b>0.51</b>	<b>-0.48</b>	<b>1.51</b>	<b>&lt;.001</b>
-25°	-0.92	<b>0.39</b>	<b>-1.68</b>	<b>-0.16</b>	<b>0.75*</b>	<b>0.42</b>	<b>-0.07</b>	<b>1.57</b>	<b>0.00</b>
-20°	0.00	0.38	-0.75	0.74	0.74	0.39	-0.02	1.50	0.17
-15°	0.52	0.38	-0.23	1.26	0.58	0.38	-0.18	1.33	0.91
-10°	0.77	0.38	0.03	1.51	0.37	0.38	-0.38	1.11	0.45
-5°	0.46	0.38	-0.28	1.21	0.09	0.38	-0.65	0.83	0.48
0°	0.00	0.38	-0.74	0.74	0.00	0.38	-0.74	0.74	1.00
5°	-0.32	0.38	-1.06	0.42	-0.15	0.38	-0.89	0.60	0.74
10°	-0.33	0.38	-1.07	0.41	-0.28	0.39	-1.04	0.48	0.92
15°	-0.38	0.38	-1.13	0.37	-0.47	0.40	-1.25	0.31	0.87
20°	-0.58	0.39	-1.35	0.18	-0.71	0.41	-1.51	0.10	0.82
25°	-0.71	0.41	-1.52	0.10	-0.94	0.44	-1.81	-0.07	0.71
30°	-0.76	0.48	-1.70	0.18	-1.06	0.50	-2.05	-0.08	0.66
35°	-0.29	0.58	-1.44	0.85	-0.62	0.60	-1.79	0.56	0.70

“\*” and bold font Indicate statistical significance at a *p*-value of 0.05.

Table 50 Radioscaphoid angle (flexion) with the wrist ulnar to radial deviation

Wrist angle from ulnar to radial deviation (degrees)	Normal				SLI				<i>p</i> - value
	Mean	Std. Error	Lower CI	Upper CI	Mean	Std. Error	Lower CI	Upper CI	
-35°	28.1°	2.8°	22.6°	33.6°	34.7°	3.1°	28.5°	40.8°	0.119
-30°	<b>27.7°</b>	<b>2.7°</b>	<b>22.3°</b>	<b>33.1°</b>	<b>36.6°*</b>	<b>2.8°</b>	<b>31.1°</b>	<b>42.2°</b>	<b>0.024</b>
-25°	<b>28.2°</b>	<b>2.7°</b>	<b>23.0°</b>	<b>33.5°</b>	<b>38.2°*</b>	<b>2.7°</b>	<b>32.9°</b>	<b>43.6°</b>	<b>0.009</b>
-20°	<b>28.3°</b>	<b>2.7°</b>	<b>23.1°</b>	<b>33.5°</b>	<b>39.1°*</b>	<b>2.7°</b>	<b>33.8°</b>	<b>44.3°</b>	<b>0.005</b>
-15°	<b>29.3°</b>	<b>2.7°</b>	<b>24.1°</b>	<b>34.5°</b>	<b>41.3°*</b>	<b>2.7°</b>	<b>36.1°</b>	<b>46.6°</b>	<b>0.002</b>
-10°	<b>31.7°</b>	<b>2.7°</b>	<b>26.5°</b>	<b>37.0°</b>	<b>43.5°*</b>	<b>2.7°</b>	<b>38.3°</b>	<b>48.7°</b>	<b>0.002</b>
-5°	<b>35.5°</b>	<b>2.7°</b>	<b>30.3°</b>	<b>40.7°</b>	<b>45.6°*</b>	<b>2.7°</b>	<b>40.4°</b>	<b>50.8°</b>	<b>0.008</b>
0°	<b>39.8°</b>	<b>2.7°</b>	<b>34.6°</b>	<b>45.1°</b>	<b>48.1°*</b>	<b>2.7°</b>	<b>42.9°</b>	<b>53.3°</b>	<b>0.028</b>
5°	44.1°	2.7°	38.9°	49.3°	50.2°	2.7°	44.9°	55.4°	0.107
10°	48.0°	2.7°	42.8°	53.3°	51.9°	2.7°	46.7°	57.2°	0.303
15°	51.6°	2.7°	46.4°	56.9°	53.7°	2.7°	48.4°	59.0°	0.577
20°	54.5°	2.7°	49.2°	59.7°	55.5°	2.7°	50.2°	60.8°	0.785
25°	56.9°	2.7°	51.6°	62.3°	56.7°	2.8°	51.3°	62.1°	0.958
30°	59.1°	2.8°	53.6°	64.6°	57.8°	2.8°	52.2°	63.4°	0.741
35°	60.6°	3.0°	54.7°	66.4°	57.7°	3.0°	51.7°	63.6°	0.495

“\*” and bold font Indicate statistical significance at a *p*-value of 0.05.

Table 51 Radioscaphoid angle (radial angulation) with the wrist ulnar to radial deviation

Wrist angle from ulnar to radial deviation (degrees)	Normal				SLI				<i>p- value</i>
	Mean	Std. Error	Lower CI	Upper CI	Mean	Std. Error	Lower CI	Upper CI	
-35°	11.4°	2.6°	6.3°	16.5°	8.4°	2.7°	3.1°	13.7°	<i>0.42</i>
-30°	14.8°	2.6°	9.8°	19.9°	12.3°	2.6°	7.2°	17.4°	<i>0.49</i>
-25°	18.7°	2.6°	13.7°	23.7°	16.2°	2.6°	11.2°	21.3°	<i>0.49</i>
-20°	22.3°	2.6°	17.3°	27.3°	19.3°	2.6°	14.3°	24.3°	<i>0.41</i>
-15°	25.8°	2.6°	20.7°	30.8°	22.2°	2.6°	17.1°	27.2°	<i>0.32</i>
-10°	29.1°	2.6°	24.1°	34.2°	25.0°	2.6°	20.0°	30.1°	<i>0.26</i>
-5°	31.6°	2.6°	26.6°	36.6°	27.8°	2.6°	22.8°	32.9°	<i>0.30</i>
0°	33.5°	2.6°	28.5°	38.5°	30.7°	2.6°	25.7°	35.8°	<i>0.44</i>
5°	35.4°	2.6°	30.4°	40.4°	33.8°	2.6°	28.8°	38.8°	<i>0.66</i>
10°	37.0°	2.6°	31.9°	42.0°	36.9°	2.6°	31.9°	41.9°	<i>0.99</i>
15°	38.4°	2.6°	33.4°	43.4°	39.9°	2.6°	34.9°	44.9°	<i>0.67</i>
20°	39.6°	2.6°	34.6°	44.6°	42.9°	2.6°	37.8°	47.9°	<i>0.37</i>
25°	40.6°	2.6°	35.6°	45.7°	46.0°	2.6°	40.9°	51.1°	<i>0.14</i>
30°	42.3°	2.6°	37.2°	47.4°	48.8°	2.6°	43.6°	53.9°	<i>0.08</i>
35°	44.0°	2.7°	38.8°	49.3°	50.9°	2.7°	45.7°	56.2°	<i>0.07</i>

“\*” and bold font Indicate statistical significance at a p-value of 0.05.

Table 52 Radioscaphoid angle (internal rotation) with the wrist ulnar to radial deviation

Wrist angle from ulnar to radial deviation (degrees)	Normal				SLI				<i>p</i> - value
	Mean	Std. Error	Lower CI	Upper CI	Mean	Std. Error	Lower CI	Upper CI	
-35°	47.5°	2.7°	42.2°	52.7°	60.3°*	2.7°	55.0°	65.6°	<.001
-30°	48.5°	2.7°	43.3°	53.8°	61.1°*	2.7°	55.8°	66.3°	<.001
-25°	49.5°	2.7°	44.3°	54.7°	61.7°*	2.7°	56.5°	66.9°	0.001
-20°	50.1°	2.7°	44.8°	55.3°	61.9°*	2.7°	56.7°	67.1°	0.002
-15°	50.4°	2.7°	45.2°	55.6°	62.0°*	2.7°	56.8°	67.2°	0.002
-10°	50.9°	2.7°	45.7°	56.1°	62.1°*	2.7°	56.8°	67.3°	0.003
-5°	51.1°	2.7°	45.9°	56.3°	62.0°*	2.7°	56.8°	67.2°	0.004
0°	51.2°	2.7°	45.9°	56.4°	62.0°*	2.7°	56.8°	67.2°	0.004
5°	50.9°	2.7°	45.7°	56.1°	62.2°*	2.7°	57.0°	67.4°	0.003
10°	50.6°	2.7°	45.3°	55.8°	62.3°*	2.7°	57.1°	67.5°	0.002
15°	49.9°	2.7°	44.6°	55.1°	62.6°*	2.7°	57.3°	67.8°	<.001
20°	49.3°	2.7°	44.1°	54.5°	62.7°*	2.7°	57.5°	67.9°	<.001
25°	48.5°	2.7°	43.2°	53.7°	62.6°*	2.7°	57.4°	67.8°	<.001
30°	47.4°	2.7°	42.1°	52.6°	62.1°*	2.7°	56.8°	67.3°	<.001
35°	46.8°	2.7°	41.5°	52.1°	61.2°*	2.7°	55.8°	66.5°	<.001

“\*” and bold font Indicate statistical significance at a *p*-value of 0.05.

Table 53 Radiolunate angle (flexion) with the wrist ulnar to radial deviation

Wrist angle from ulnar to radial deviation (degrees)	Normal				SLI				p- value
	Mean	Std. Error	Lower CI	Upper CI	Mean	Std. Error	Lower CI	Upper CI	
-35°	-34.6°	2.8°	-40.1°	-29.1°	-35.8°	3.0°	-41.7°	-29.8°	0.783
-30°	-34.3°	2.8°	-39.7°	-28.8°	-35.5°	2.8°	-41.1°	-30.0°	0.751
-25°	-32.7°	2.7°	-38.0°	-27.3°	-35.2°	2.7°	-40.6°	-29.8°	0.519
-20°	-31.5°	2.7°	-36.9°	-26.2°	-33.8°	2.7°	-39.2°	-28.5°	0.549
-15°	-29.4°	2.7°	-34.8°	-24.1°	-31.8°	2.7°	-37.1°	-26.5°	0.537
-10°	-25.8°	2.7°	-31.1°	-20.5°	-29.8°	2.7°	-35.1°	-24.4°	0.300
-5°	-21.5°	2.7°	-26.9°	-16.2°	-27.5°	2.7°	-32.8°	-22.2°	0.119
0°	-16.9°	2.7°	-22.2°	-11.6°	-24.8°*	2.7°	-30.1°	-19.5°	<b>0.040</b>
5°	-12.9°	2.7°	-18.2°	-7.6°	-22.4°*	2.7°	-27.7°	-17.1°	<b>0.014</b>
10°	-9.1°	2.7°	-14.5°	-3.8°	-20.0°*	2.7°	-25.4°	-14.7°	<b>0.005</b>
15°	-6.1°	2.7°	-11.4°	-0.8°	-17.8°*	2.7°	-23.1°	-12.4°	<b>0.003</b>
20°	-3.5°	2.7°	-8.8°	1.8°	-15.8°*	2.7°	-21.2°	-10.4°	<b>0.002</b>
25°	-1.3°	2.7°	-6.7°	4.1°	-14.2°*	2.8°	-19.7°	-8.8°	<b>&lt;.001</b>
30°	0.0°	2.8°	-5.5°	5.5°	-13.1°*	2.8°	-18.6°	-7.5°	<b>0.001</b>
35°	0.7°	2.9°	-5.1°	6.4°	-12.5°*	2.9°	-18.3°	-6.7°	<b>0.002</b>

“\*” and bold font Indicate statistical significance at a p-value of 0.05.

Table 54 Radiolunate angle (radial angulation) with the wrist ulnar to radial deviation

Wrist angle from ulnar to radial deviation (degrees)	Normal				SLI				<i>p- value</i>
	Mean	Std. Error	Lower CI	Upper CI	Mean	Std. Error	Lower CI	Upper CI	
-35°	36.0°	3.4°	29.3°	42.8°	31.5°	3.5°	24.6°	38.3°	0.355
-30°	39.0°	3.4°	32.3°	45.8°	35.4°	3.4°	28.6°	42.1°	0.453
-25°	42.3°	3.4°	35.6°	49.0°	38.5°	3.4°	31.7°	45.2°	0.425
-20°	45.6°	3.4°	38.9°	52.3°	41.9°	3.4°	35.2°	48.6°	0.447
-15°	48.7°	3.4°	42.0°	55.4°	44.9°	3.4°	38.2°	51.7°	0.438
-10°	51.7°	3.4°	45.0°	58.4°	47.6°	3.4°	40.9°	54.3°	0.399
-5°	54.2°	3.4°	47.5°	60.9°	49.9°	3.4°	43.2°	56.6°	0.379
0°	56.4°	3.4°	49.6°	63.1°	51.9°	3.4°	45.2°	58.7°	0.361
5°	58.2°	3.4°	51.5°	65.0°	53.2°	3.4°	46.5°	59.9°	0.298
10°	59.7°	3.4°	52.9°	66.4°	54.2°	3.4°	47.5°	61.0°	0.262
15°	60.6°	3.4°	53.9°	67.4°	55.4°	3.4°	48.7°	62.1°	0.280
20°	61.4°	3.4°	54.7°	68.1°	56.4°	3.4°	49.7°	63.2°	0.307
25°	62.2°	3.4°	55.5°	68.9°	57.8°	3.4°	51.1°	64.6°	0.371
30°	63.7°	3.4°	57.0°	70.5°	59.4°	3.4°	52.6°	66.2°	0.377
35°	65.1°	3.5°	58.2°	71.9°	61.3°	3.5°	54.4°	68.1°	0.438

“\*” and bold font Indicate statistical significance at a p-value of 0.05.

Table 55 Radiolunate angle (Internal rotation) with the wrist ulnar to radial deviation

Wrist angle from ulnar to radial deviation (degrees)	Normal				SLI				<i>p- value</i>
	Mean	Std. Error	Lower CI	Upper CI	Mean	Std. Error	Lower CI	Upper CI	
-35°	58.8°	2.9°	53.1°	64.5°	59.9°	2.9°	54.2°	65.7°	0.783
-30°	59.5°	2.9°	53.8°	65.1°	60.0°	2.9°	54.3°	65.7°	0.90
-25°	60.5°	2.9°	54.9°	66.1°	60.3°	2.9°	54.6°	65.9°	0.95
-20°	61.4°	2.9°	55.8°	67.0°	60.2°	2.9°	54.6°	65.9°	0.77
-15°	61.9°	2.9°	56.3°	67.6°	60.1°	2.9°	54.4°	65.7°	0.65
-10°	62.2°	2.9°	56.5°	67.8°	59.9°	2.9°	54.2°	65.5°	0.57
-5°	61.9°	2.9°	56.2°	67.5°	59.6°	2.9°	53.9°	65.2°	0.58
0°	61.4°	2.9°	55.7°	67.0°	59.5°	2.9°	53.9°	65.1°	0.64
5°	61.1°	2.9°	55.4°	66.7°	59.3°	2.9°	53.7°	65.0°	0.67
10°	61.1°	2.9°	55.4°	66.7°	59.2°	2.9°	53.6°	64.9°	0.65
15°	61.0°	2.9°	55.4°	66.6°	59.0°	2.9°	53.4°	64.7°	0.63
20°	60.8°	2.9°	55.1°	66.4°	58.8°	2.9°	53.2°	64.5°	0.63
25°	60.7°	2.9°	55.0°	66.4°	58.6°	2.9°	53.0°	64.3°	0.61
30°	60.7°	2.9°	55.0°	66.4°	58.6°	2.9°	52.9°	64.3°	0.61
35°	61.1°	2.9°	55.3°	66.8°	59.1°	2.9°	53.4°	64.9°	0.64

“\*” and bold font Indicate statistical significance at a *p*-value of 0.05.

Table 56 Scaphoid ulnar translation with the wrist ulnar to radial deviation

Wrist angle from ulnar to radial deviation (degrees)	Normal				SLI				<i>p</i> - value
	Mean	Std. Error	Lower CI	Upper CI	Mean	Std. Error	Lower CI	Upper CI	
-35°	-8.7	0.3	-9.3	-8.2	-9.0	0.3	-9.6	-8.4	0.533
-30°	-8.4	0.3	-9.0	-7.8	-8.9	0.3	-9.5	-8.3	0.239
-25°	-8.0	0.3	-8.6	-7.5	-8.6	0.3	-9.1	-8.0	0.160
-20°	-7.6	0.3	-8.2	-7.1	-8.3	0.3	-8.9	-7.8	0.081
-15°	-7.3	0.3	-7.8	-6.7	-8.1	0.3	-8.6	-7.5	0.042
-10°	-6.9	0.3	-7.5	-6.4	-7.9	0.3	-8.4	-7.3	0.020
-5°	-6.7	0.3	-7.3	-6.2	-7.7	0.3	-8.2	-7.1	0.016
0°	-6.5	0.3	-7.1	-6.0	-7.5	0.3	-8.0	-6.9	0.021
5°	-6.3	0.3	-6.9	-5.8	-7.2	0.3	-7.7	-6.6	0.032
10°	-6.2	0.3	-6.7	-5.6	-7.0	0.3	-7.5	-6.4	0.052
15°	-6.0	0.3	-6.6	-5.5	-6.8	0.3	-7.3	-6.2	0.074
20°	-5.9	0.3	-6.5	-5.4	-6.5	0.3	-7.1	-6.0	0.136
25°	-5.9	0.3	-6.4	-5.3	-6.4	0.3	-6.9	-5.8	0.201
30°	-5.7	0.3	-6.3	-5.1	-6.3	0.3	-6.9	-5.8	0.131
35°	-5.7	0.3	-6.3	-5.1	-6.2	0.3	-6.8	-5.6	0.197

“\*” and bold font Indicate statistical significance at a *p*-value of 0.05.



Table 57 Scaphoid volar translation with the wrist ulnar to radial deviation

Wrist angle from ulnar to radial deviation (degrees)	Normal				SLI				<i>p</i> - value
	Mean	Std. Error	Lower CI	Upper CI	Mean	Std. Error	Lower CI	Upper CI	
-35°	2.1	0.4	1.4	2.8	2.4	0.4	1.6	3.1	0.590
-30°	2.2	0.3	1.5	2.8	2.5	0.4	1.8	3.2	0.539
-25°	2.4	0.3	1.7	3.0	2.6	0.3	1.9	3.2	0.725
-20°	2.5	0.3	1.8	3.1	2.6	0.3	1.9	3.3	0.793
-15°	2.6	0.3	2.0	3.3	2.8	0.3	2.2	3.5	0.657
-10°	2.8	0.3	2.1	3.5	3.0	0.3	2.3	3.7	0.681
-5°	3.0	0.3	2.4	3.7	3.1	0.3	2.5	3.8	0.814
0°	3.3	0.3	2.6	3.9	3.3	0.3	2.6	4.0	0.929
5°	3.5	0.3	2.8	4.1	3.4	0.3	2.7	4.0	0.888
10°	3.6	0.3	3.0	4.3	3.5	0.3	2.8	4.1	0.722
15°	3.8	0.3	3.1	4.4	3.4	0.3	2.8	4.1	0.478
20°	3.9	0.3	3.2	4.5	3.4	0.3	2.7	4.1	0.302
25°	4.0	0.3	3.3	4.7	3.3	0.3	2.6	4.0	0.174
30°	4.1	0.4	3.4	4.7	3.2	0.4	2.6	3.9	0.109
35°	4.1	0.4	3.4	4.9	3.3	0.4	2.5	4.0	0.091

“\*” and bold font Indicate statistical significance at a *p*-value of 0.05.

Table 58 Scaphoid distal translation with the wrist ulnar to radial deviation

Wrist angle from ulnar to radial deviation (degrees)	Normal				SLI				<i>p</i> value
	Mean	Std. Error	Upper CI	Lower CI	Mean	Std. Error	Upper CI	Lower CI	
-35°	17.8	0.3	17.2	18.5	19.2*	0.4	18.5	19.9	0.005
-30°	17.1	0.3	16.5	17.8	18.3*	0.3	17.6	19.0	0.012
-25°	16.2	0.3	15.6	16.9	17.4*	0.3	16.8	18.0	0.010
-20°	15.4	0.3	14.8	16.0	16.6*	0.3	16.0	17.2	0.009
-15°	14.7	0.3	14.0	15.3	16.0*	0.3	15.3	16.6	0.005
-10°	14.0	0.3	13.4	14.6	15.4*	0.3	14.8	16.0	0.003
-5°	13.5	0.3	12.9	14.2	14.9*	0.3	14.2	15.5	0.004
0°	13.2	0.3	12.5	13.8	14.4*	0.3	13.7	15.0	0.009
5°	12.9	0.3	12.2	13.5	13.9*	0.3	13.2	14.5	0.030
10°	12.6	0.3	11.9	13.2	13.4	0.3	12.8	14.0	0.062
15°	12.3	0.3	11.6	12.9	13.0	0.3	12.4	13.6	0.105
20°	12.1	0.3	11.4	12.7	12.6	0.3	12.0	13.3	0.221
25°	11.9	0.3	11.3	12.5	12.3	0.3	11.6	12.9	0.424
30°	11.7	0.3	11.0	12.3	12.0	0.3	11.3	12.6	0.529
35°	11.5	0.3	10.8	12.2	11.7	0.3	11.0	12.4	0.682

“\*” and bold font Indicate statistical significance at a *p*-value of 0.05.

Table 59 Lunate ulnar translation with the wrist ulnar to radial deviation

Wrist angle from ulnar to radial deviation (degrees)	Normal				SLI				<i>p</i> - value
	Mean	Std. Error	Lower CI	Upper CI	Mean	Std. Error	Lower CI	Upper CI	
-35°	2.2	0.3	1.6	2.9	3.6*	0.4	2.9	4.3	<b>0.004</b>
-30°	3.1	0.3	2.5	3.7	4.5*	0.3	3.9	5.2	<b>0.003</b>
-25°	4.1	0.3	3.5	4.7	5.3*	0.3	4.7	5.9	<b>0.005</b>
-20°	5.0	0.3	4.4	5.6	6.2*	0.3	5.5	6.8	<b>0.010</b>
-15°	5.8	0.3	5.2	6.5	6.9*	0.3	6.3	7.5	<b>0.019</b>
-10°	6.7	0.3	6.1	7.3	7.5	0.3	6.9	8.1	0.063
-5°	7.2	0.3	6.6	7.9	8.0	0.3	7.4	8.6	0.076
0°	7.7	0.3	7.1	8.3	8.5	0.3	7.9	9.1	0.080
5°	8.0	0.3	7.4	8.7	8.7	0.3	8.1	9.3	0.116
10°	8.3	0.3	7.7	8.9	9.0	0.3	8.3	9.6	0.127
15°	8.4	0.3	7.8	9.0	9.1	0.3	8.5	9.7	0.110
20°	8.5	0.3	7.9	9.1	9.3	0.3	8.7	9.9	0.086
25°	8.6	0.3	8.0	9.2	9.4	0.3	8.8	10.0	0.073
30°	8.8	0.3	8.1	9.4	9.4	0.3	8.8	10.1	0.141
35°	8.8	0.3	8.2	9.5	9.6	0.3	8.9	10.3	0.115

“\*” and bold font Indicate statistical significance at a *p*-value of 0.05.

Table 60 Lunate volar translation with the wrist ulnar to radial deviation

Wrist angle from ulnar to radial deviation (degrees)	Normal				SLI				<i>p- value</i>
	Mean	Std. Error	Lower CI	Upper CI	Mean	Std. Error	Lower CI	Upper CI	
-35°	4.1	0.3	3.5	4.7	4.3	0.3	3.7	4.9	0.629
-30°	4.1	0.3	3.5	4.7	4.4	0.3	3.9	5.0	0.398
-25°	4.1	0.3	3.6	4.7	4.5	0.3	4.0	5.1	0.328
-20°	4.1	0.3	3.6	4.7	4.5	0.3	3.9	5.1	0.368
-15°	4.1	0.3	3.5	4.7	4.5	0.3	3.9	5.0	0.384
-10°	4.0	0.3	3.4	4.6	4.4	0.3	3.8	4.9	0.403
-5°	3.9	0.3	3.3	4.4	4.3	0.3	3.7	4.8	0.335
0°	3.7	0.3	3.1	4.2	4.2	0.3	3.6	4.7	0.230
5°	3.5	0.3	2.9	4.0	4.0	0.3	3.4	4.6	0.176
10°	3.3	0.3	2.7	3.9	3.9	0.3	3.3	4.5	0.142
15°	3.1	0.3	2.5	3.7	3.7	0.3	3.2	4.3	0.119
20°	2.9	0.3	2.4	3.5	3.6	0.3	3.0	4.2	0.119
25°	2.8	0.3	2.2	3.4	3.5	0.3	2.9	4.0	0.114
30°	2.6	0.3	2.0	3.2	3.3	0.3	2.8	3.9	0.075
35°	2.6	0.3	2.0	3.2	3.4	0.3	2.8	4.0	0.082

“\*” and bold font Indicate statistical significance at a *p*-value of 0.05.

Table 61 Lunate distal translation with the wrist ulnar to radial deviation

Wrist angle from ulnar to radial deviation (degrees)	Normal				SLI				p- value
	Mean	Std. Error	Lower CI	Upper CI	Mean	Std. Error	Lower CI	Upper CI	
-35°	7.5	0.2	7.0	7.9	7.1	0.2	6.6	7.6	0.277
-30°	7.2	0.2	6.7	7.6	6.8	0.2	6.4	7.2	0.246
-25°	6.9	0.2	6.4	7.3	6.5	0.2	6.1	7.0	0.328
-20°	6.6	0.2	6.2	7.0	6.3	0.2	5.8	6.7	0.264
-15°	6.4	0.2	6.0	6.8	6.1	0.2	5.6	6.5	0.301
-10°	6.2	0.2	5.8	6.6	5.9	0.2	5.5	6.4	0.400
-5°	6.1	0.2	5.7	6.6	5.8	0.2	5.4	6.3	0.355
0°	6.1	0.2	5.6	6.5	5.8	0.2	5.3	6.2	0.342
5°	6.1	0.2	5.7	6.5	5.7	0.2	5.3	6.2	0.239
10°	6.1	0.2	5.7	6.5	5.7	0.2	5.3	6.2	0.272
15°	6.1	0.2	5.7	6.5	5.8	0.2	5.3	6.2	0.294
20°	6.1	0.2	5.7	6.6	5.8	0.2	5.4	6.2	0.314
25°	6.2	0.2	5.7	6.6	5.9	0.2	5.5	6.3	0.382
30°	6.2	0.2	5.8	6.7	6.0	0.2	5.5	6.4	0.402
35°	6.4	0.2	6.0	6.9	6.0	0.2	5.5	6.5	0.174

“\*” and bold font Indicate statistical significance at a p-value of 0.05.

### 3.4.4. Important outcome measures-Radiocarpal kinematics

Figure 97 and Figure 98 present a summary of important outcome measures in radiocarpal kinematics of the scaphoid and the lunate.

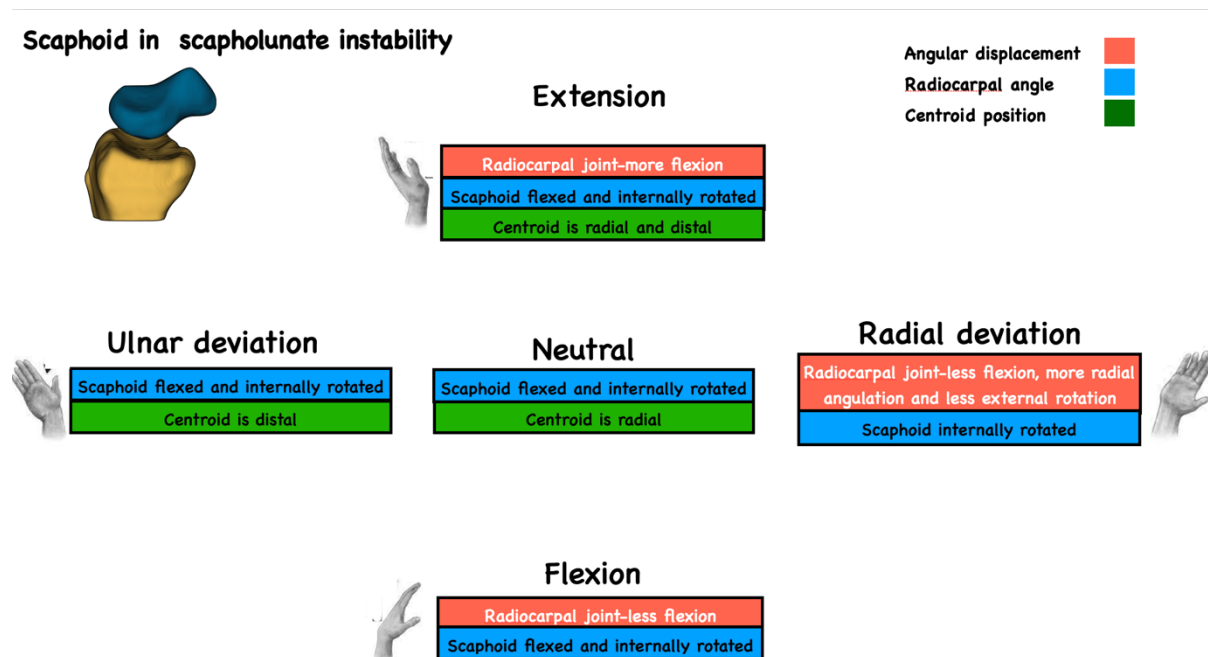


Figure 97 Summary of radiocarpal kinematic changes that occurred in the SLI scaphoid compared to the normal scaphoid. This includes radiocarpal angular displacement from the neutral position (pink background), the radiocarpal angles (in blue background) and centroid position (green background). Note that only the significant changes are mentioned. The changes that were observed only during 10° of wrist motion or less and values that were within the error rate of the method were excluded to prevent over-generalisation of the results.

The SLI scaphoid was more flexed compared to the normal scaphoid throughout wrist extension to flexion and during wrist ulnar deviation to neutral. There was no significant difference in the radioscapoid angle (flexion) when the wrist was moving from neutral to radial deviation. The SLI scaphoid was internally rotated compared to the normal, in all wrist positions.

During wrist 70° to 40° extension, the flexion arc of the SLI scaphoid was greater than the normal scaphoid. During wrist 35° flexion to 50° flexion, the flexion arc of the SLI scaphoid was less than the normal. There were no significant changes when the wrist was in mid-

range between 40° extension to 35° flexion. When the wrist was radially deviating beyond 10°, the flexion arc of the SLI scaphoid was less and the radial angulation arc was greater than that of the normal. When the wrist radially deviated beyond 25°, there was more external rotation of the normal scaphoid.

The SLI scaphoid centroid was more radial when the wrist was moving from 70° extension to 15° flexion and from 15° ulnar deviation to 5° radial deviation. It was more distal when the wrist was moving from 70° extension to 30° extension and 35° to 5° ulnar deviation. While the scaphoid centroid in both wrists moved volarly with wrist flexion and wrist radial deviation, there was no significant difference in between the two groups.

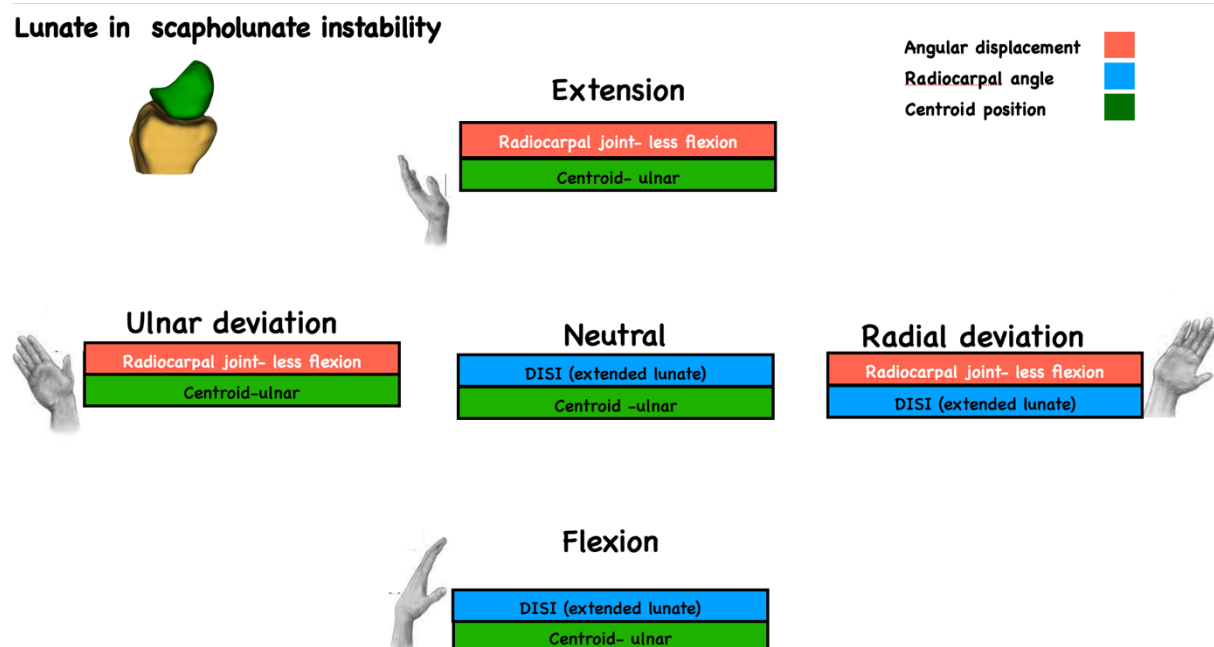


Figure 98 Summary of radiocarpal kinematic changes that occurred in the SLI lunate compared to the normal lunate. This includes radiocarpal angular displacement from the neutral position (pink background), the radiocarpal angles (in blue background), and centroid position (green background). Note that only the significant changes are mentioned. The changes that were observed only during 10° of wrist motion or less and values that were within the error rate of the method were excluded to prevent over-generalisation of the results.

The radiolunate angle was significantly extended in the SLI wrist from 20° wrist extension to 55° flexion and from neutral wrist position to radial deviation. The radiolunate angle

(flexion) was not different between the two group when the wrist was extended beyond 20° or ulnar deviated.

During 70° to 30° wrist extension, the flexion arc of the SLI lunate was less than the normal. The flexion arc of the SLI lunate was also less than that of the normal throughout ulnar to radial deviation of the wrist, except in the midrange from 5° of ulnar to 10° of radial deviation. No significant changes were observed in other planes.

The SLI lunate centroid was more ulnar when the wrist was moving from 70° extension to 50° flexion and from 35° ulnar deviation to 15° ulnar deviation. While the lunate centroid in both wrists moved dorsally with wrist flexion and radial deviation, there was no significant difference between the two groups.



### 3.4.5. Comparison between in-plane and out-of-plane motion

All tables containing the detailed comparison between the 'in-plane' and 'out-of-plane' motion results (Table 62 to Table 65) are included at the end of this section as 3.4.6.

One fundamental difference that was observed in SLI scaphoid was a reversal in the kinematic pattern during wrist ulnar to radial deviation. The normal scaphoid had more flexion than radial angulation when the wrist was radially angulating more than 10°. It also had more radial angulation when the wrist was ulnar deviated 25° or more. Hence, in the normal wrist three clear zones could be identified, with regard to scaphoid motion (Figure 99).

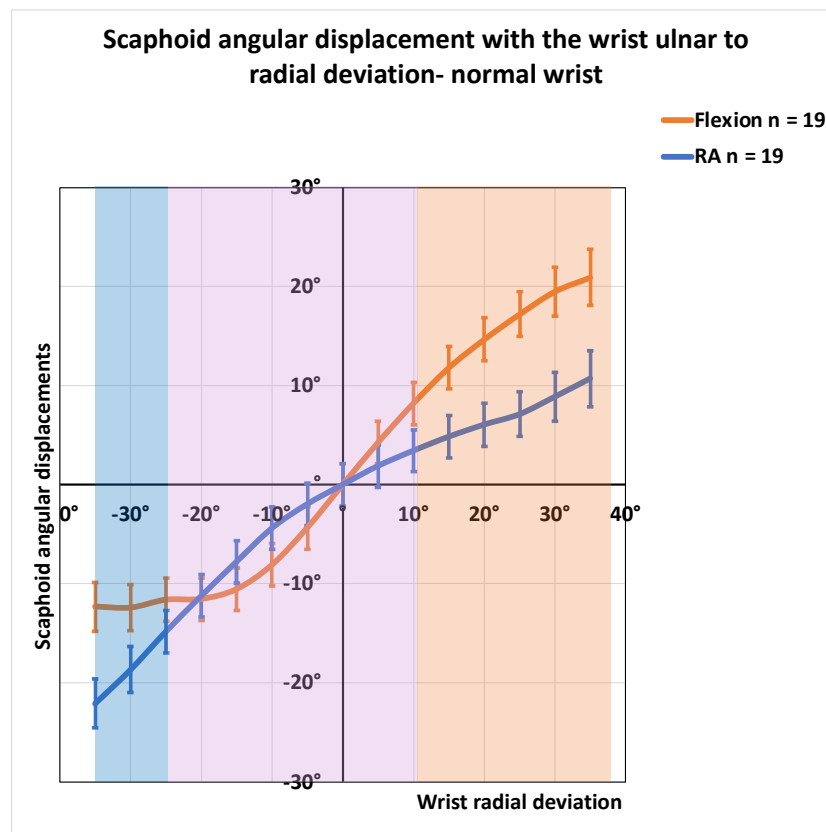


Figure 99 The scaphoid angular displacements (flexion and radial angulation) of the normal wrist during ulnar to radial deviation. Note that 3 zones could be identified i. blue- more radial angulation ii-purple -no difference iii-orange-more flexion (significantly more out-of-plane motion). RA-Radial angulation

In contrast, the SLI scaphoid had more radial angulation when the wrist was moving from 35° to 25° ulnar deviation as well as when radially deviating more than 15° (Figure 100).

When the wrist was in between 20° ulnar deviation and 15° radial deviation, there was no difference between radial angulation and flexion of the scaphoid. This was a fundamental difference observed even in early stage or ‘dynamic’ stage of SLI.

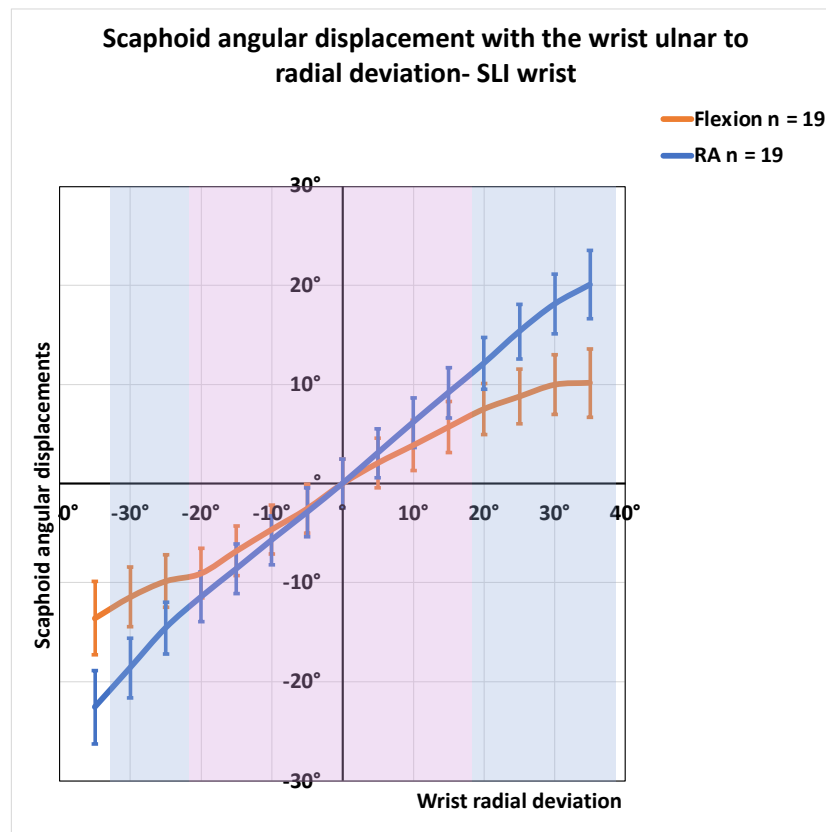


Figure 100 The scaphoid angular displacements (flexion and radial angulation) of the SLI wrist during ulnar to radial deviation Note that there was no zone where flexion (out-of-plane motion) exceeded radial angulation (motion) i. blue- More ulnar angulation ii-purple -no difference iii-blue-more radial angulation. RA-Radial angulation

Interestingly, the normal lunate had a very similar kinematic pattern to the scaphoid, where the lunate had more flexion than radial angulation when the wrist was radially deviating more than 10° (Figure 101)

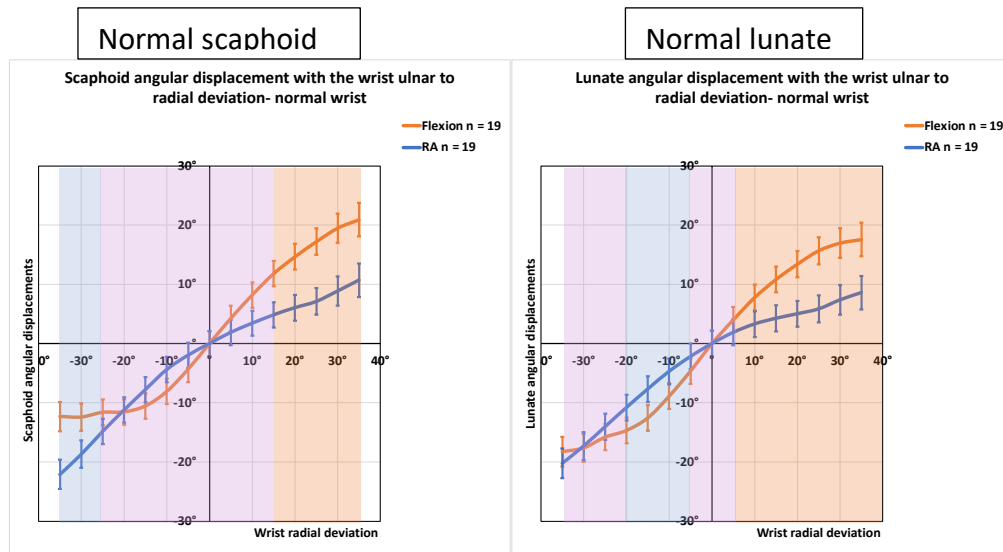


Figure 101 The scaphoid and lunate angular displacements (flexion and radial angulation) of the normal wrist during ulnar to radial deviation. Note that 3 zones could be identified i. blue- more radial angulation ii-purple - no difference iii-orange-more radial angulation (more out-of-plane motion). RA-Radial angulation. Note the similarity of the scaphoid and lunate graphs.

The SLI lunate, in contrast to SLI scaphoid, maintained more flexion (out-of-plane motion) when the wrist was radially deviating (Figure 102). While the magnitude of flexion in SLI lunate was less compared to the normal lunate, it was still the dominant motion in wrist radial deviation. Compared to the scaphoid the change that occurred in the lunate was a reduction of the magnitude of the out-of-plane motion. There was no reversal of the kinematic pattern as seen between the normal and SLI scaphoid.

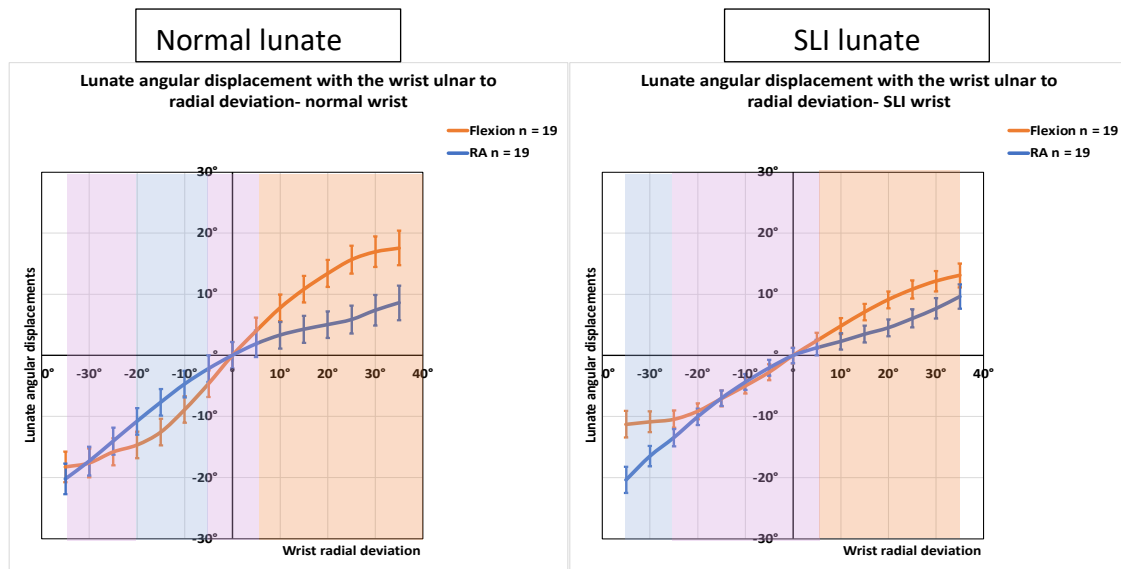


Figure 102 The Lunate angular displacements (flexion and radial angulation) of the normal and SLI wrists during ulnar to radial deviation. Note that in both the normal and SLI lunates three zones could be identified i. blue- more radial angulation) ii-purple -no difference iii-orange-more flexion (more out-of-plane motion). RA- Radial angulation. While the magnitude of flexion in SLI lunate was less, it was still the dominant motion in wrist radial deviation.

The angular displacement in the axial plane (internal and external rotation) of the scaphoid and the lunate were presented in the results section (3.4) but not in this section. While the axial rotation is considered a part of the out-of-plane motion, the mean differences observed between the normal and SLI scaphoid were between 2° to 4°. Considering that the error rate of coordinate system positioning in the axial plane was 2.1°, the axial rotation was not discussed as a significant contribution to out-of-plane motion.

### 3.4.6. Comparison of in-plane and out-of-plane motion (Tables)

Table 62 The scaphoid angular displacements (flexion and radial angulation) of the normal wrist during ulnar to radial deviation.

Wrist angle from ulnar to radial deviation (degrees)	Flexion				Radial angulation				p- value
	Mean	Std. Error	Lower CI	Upper CI	Mean	Std. Error	Lower CI	Upper CI	
-35°	<b>-12.3°</b>	<b>1.3°</b>	<b>-14.8°</b>	<b>-9.8°</b>	<b>-22.1°*</b>	<b>1.3°</b>	<b>-24.6°</b>	<b>-19.6°</b>	<b>&lt;.001</b>
-30°	<b>-12.4°</b>	<b>1.2°</b>	<b>-14.7°</b>	<b>-10.1°</b>	<b>-18.7°*</b>	<b>1.2°</b>	<b>-21.0°</b>	<b>-16.4°</b>	<b>&lt;.001</b>
-25°	<b>-11.6°</b>	<b>1.1°</b>	<b>-13.8°</b>	<b>-9.4°</b>	<b>-14.8°*</b>	<b>1.1°</b>	<b>-17.0°</b>	<b>-12.7°</b>	<b>0.04</b>
-20°	-11.5°	1.1°	-13.7°	-9.4°	-11.2°	1.1°	-13.4°	-9.1°	0.837
-15°	-10.5°	1.1°	-12.7°	-8.4°	-7.8°	1.1°	-9.9°	-5.6°	0.072
-10°	-8.1°	1.1°	-10.2°	-6.0°	-4.4°	1.1°	-6.5°	-2.3°	0.017
-5°	-4.3°	1.1°	-6.5°	-2.2°	-2.0°	1.1°	-4.1°	0.2°	0.122
0°	0.0°	1.1°	-2.1°	2.1°	0.0°	1.1°	-2.1°	2.1°	1
5°	4.3°	1.1°	2.1°	6.4°	1.9°	1.1°	-0.3°	4.0°	0.125
<b>10°</b>	<b>8.2°</b>	<b>1.1°</b>	<b>6.1°</b>	<b>10.3°</b>	<b>3.4°*</b>	<b>1.1°</b>	<b>1.3°</b>	<b>5.6°</b>	<b>0.002</b>
<b>15°</b>	<b>11.8°</b>	<b>1.1°</b>	<b>9.6°</b>	<b>13.9°</b>	<b>4.8°*</b>	<b>1.1°</b>	<b>2.7°</b>	<b>7.0°</b>	<b>&lt;.001</b>
<b>20°</b>	<b>14.7°</b>	<b>1.1°</b>	<b>12.5°</b>	<b>16.8°</b>	<b>6.1°*</b>	<b>1.1°</b>	<b>3.9°</b>	<b>8.2°</b>	<b>&lt;.001</b>
<b>25°</b>	<b>17.2°</b>	<b>1.1°</b>	<b>15.0°</b>	<b>19.4°</b>	<b>7.1°*</b>	<b>1.1°</b>	<b>4.9°</b>	<b>9.3°</b>	<b>&lt;.001</b>
<b>30°</b>	<b>19.5°</b>	<b>1.3°</b>	<b>17.0°</b>	<b>22.0°</b>	<b>8.9°*</b>	<b>1.3°</b>	<b>6.4°</b>	<b>11.3°</b>	<b>&lt;.001</b>
<b>35°</b>	<b>20.9°</b>	<b>1.4°</b>	<b>18.1°</b>	<b>23.8°</b>	<b>10.7°*</b>	<b>1.4°</b>	<b>7.9°</b>	<b>13.5°</b>	<b>&lt;.001</b>

“\*” and bold font Indicate statistical significance at a p-value of 0.05.

Table 63 The scaphoid angular displacements (flexion and radial angulation) of the SLI wrist during ulnar to radial deviation.

Wrist angle from ulnar to radial deviation (degrees)	Flexion				Radial angulation				p- value
	Mean	Std. Error	Lower CI	Upper CI	Mean	Std. Error	Lower CI	Upper CI	
-35°	<b>-13.6°</b>	<b>1.9°</b>	<b>-17.3°</b>	<b>-9.9°</b>	<b>-22.6°*</b>	<b>1.9°</b>	<b>-26.3°</b>	<b>-18.8°</b>	<b>&lt;.001</b>
-30°	<b>-11.4°</b>	<b>1.5°</b>	<b>-14.4°</b>	<b>-8.4°</b>	<b>-18.6°*</b>	<b>1.5°</b>	<b>-21.6°</b>	<b>-15.6°</b>	<b>0.001</b>
-25°	<b>-9.8°</b>	<b>1.3°</b>	<b>-12.5°</b>	<b>-7.2°</b>	<b>-14.6°*</b>	<b>1.3°</b>	<b>-17.2°</b>	<b>-11.9°</b>	<b>0.013</b>
-20°	-9.0°	1.3°	-11.6°	-6.5°	-11.4°	1.3°	-14.0°	-8.9°	0.185
-15°	-6.8°	1.3°	-9.3°	-4.3°	-8.6°	1.3°	-11.1°	-6.1°	0.314
-10°	-4.6°	1.3°	-7.1°	-2.1°	-5.7°	1.3°	-8.2°	-3.2°	0.544
-5°	-2.5°	1.3°	-5.0°	-0.1°	-2.9°	1.3°	-5.4°	-0.4°	0.833
0°	0.0°	1.3°	-2.5°	2.5°	0.0°	1.3°	-2.5°	2.5°	1
5°	2.1°	1.3°	-0.4°	4.6°	3.1°	1.3°	0.6°	5.6°	0.57
10°	3.9°	1.3°	1.4°	6.4°	6.2°	1.3°	3.7°	8.7°	0.201
15°	5.7°	1.3°	3.2°	8.3°	9.2°	1.3°	6.6°	11.7°	0.061
<b>20°</b>	<b>7.5°</b>	<b>1.3°</b>	<b>4.9°</b>	<b>10.1°</b>	<b>12.1°*</b>	<b>1.3°</b>	<b>9.5°</b>	<b>14.7°</b>	<b>0.014</b>
<b>25°</b>	<b>8.8°</b>	<b>1.4°</b>	<b>6.0°</b>	<b>11.5°</b>	<b>15.3°*</b>	<b>1.4°</b>	<b>12.6°</b>	<b>18.1°</b>	<b>&lt;.001</b>
<b>30°</b>	<b>10.0°</b>	<b>1.5°</b>	<b>7.0°</b>	<b>13.0°</b>	<b>18.1°*</b>	<b>1.5°</b>	<b>15.1°</b>	<b>21.1°</b>	<b>&lt;.001</b>
<b>35°</b>	<b>10.2°</b>	<b>1.8°</b>	<b>6.7°</b>	<b>13.6°</b>	<b>20.1°*</b>	<b>1.8°</b>	<b>16.6°</b>	<b>23.5°</b>	<b>&lt;.001</b>

“\*” and bold font Indicate statistical significance at a p-value of 0.05.

Table 64 The lunate angular displacements (flexion and radial angulation) of the normal wrist during ulnar to radial deviation.

Wrist angle from ulnar to radial deviation (degrees)	Flexion				Radial angulation				p- value
	Mean	Std. Error	Lower CI	Upper CI	Mean	Std. Error	Lower CI	Upper CI	
-35°	-18.2°	1.3°	-20.7°	-15.7°	-20.2°	1.3°	-22.7°	-17.7°	0.272
-30°	-17.6°	1.2°	-19.9°	-15.2°	-17.3°	1.2°	-19.6°	-14.9°	0.861
-25°	-15.8°	1.1°	-18.0°	-13.6°	-14.0°	1.1°	-16.2°	-11.8°	0.272
-20°	-14.6°	1.1°	-16.8°	-12.5°	-10.8°	1.1°	-13.0°	-8.6°	0.015
-15°	-12.5°	1.1°	-14.7°	-10.4°	-7.7°	1.1°	-9.9°	-5.5°	0.002
-10°	-8.9°	1.1°	-11.1°	-6.7°	-4.7°	1.1°	-6.9°	-2.5°	0.008
-5°	-4.6°	1.1°	-6.8°	-2.5°	-2.2°	1.1°	-4.4°	0.0°	0.118
0°	0.0°	1.1°	-2.2°	2.2°	0.0°	1.1°	-2.2°	2.2°	1
5°	4.0°	1.1°	1.8°	6.2°	1.9°	1.1°	-0.3°	4.1°	0.177
<b>10°</b>	<b>7.8°</b>	<b>1.1°</b>	<b>5.6°</b>	<b>10.0°</b>	<b>3.3°*</b>	<b>1.1°</b>	<b>1.1°</b>	<b>5.5°</b>	<b>0.005</b>
<b>15°</b>	<b>10.8°</b>	<b>1.1°</b>	<b>8.6°</b>	<b>13.0°</b>	<b>4.3°*</b>	<b>1.1°</b>	<b>2.1°</b>	<b>6.5°</b>	<b>&lt;.001</b>
<b>20°</b>	<b>13.4°</b>	<b>1.1°</b>	<b>11.2°</b>	<b>15.6°</b>	<b>5.0°*</b>	<b>1.1°</b>	<b>2.8°</b>	<b>7.2°</b>	<b>&lt;.001</b>
<b>25°</b>	<b>15.7°</b>	<b>1.2°</b>	<b>13.4°</b>	<b>18.0°</b>	<b>5.9°*</b>	<b>1.2°</b>	<b>3.6°</b>	<b>8.1°</b>	<b>&lt;.001</b>
<b>30°</b>	<b>17.0°</b>	<b>1.3°</b>	<b>14.5°</b>	<b>19.5°</b>	<b>7.4°*</b>	<b>1.3°</b>	<b>4.9°</b>	<b>9.9°</b>	<b>&lt;.001</b>
<b>35°</b>	<b>17.6°</b>	<b>1.4°</b>	<b>14.7°</b>	<b>20.4°</b>	<b>8.6°*</b>	<b>1.4°</b>	<b>5.8°</b>	<b>11.4°</b>	<b>&lt;.001</b>

“\*” and bold font Indicate statistical significance at a p-value of 0.05.

Table 65 The lunate angular displacements (flexion and radial angulation) of the SLI wrist during ulnar to radial deviation.

Wrist angle from ulnar to radial deviation (degrees)	Flexion				Radial angulation				p- value
	Mean	Std. Error	Lower CI	Upper CI	Mean	Std. Error	Lower CI	Upper CI	
-35°	-11.2°	1.1°	-13.4°	-9.1°	-20.3°*	1.1°	-22.5°	-18.2°	<.001
-30°	-10.8°	0.9°	-12.5°	-9.2°	-16.5°*	0.9°	-18.2°	-14.8°	<.001
-25°	-10.4°	0.7°	-11.8°	-9.0°	-13.4°*	0.7°	-14.8°	-12.0°	0.003
-20°	-9.1°	0.7°	-10.4°	-7.8°	-10.0°	0.7°	-11.3°	-8.7°	0.332
-15°	-7.0°	0.7°	-8.4°	-5.7°	-7.0°	0.7°	-8.3°	-5.7°	0.947
-10°	-5.0°	0.7°	-6.3°	-3.7°	-4.4°	0.7°	-5.6°	-3.1°	0.507
-5°	-2.7°	0.7°	-4.0°	-1.4°	-2.0°	0.7°	-3.3°	-0.7°	0.44
0°	0.0°	0.7°	-1.3°	1.3°	0.0°	0.7°	-1.3°	1.3°	1
5°	2.4°	0.7°	1.1°	3.7°	1.3°	0.7°	0.0°	2.6°	0.223
10°	4.8°	0.7°	3.5°	6.1°	2.3°*	0.7°	1.0°	3.6°	0.009
15°	7.1°	0.7°	5.7°	8.4°	3.5°*	0.7°	2.1°	4.8°	<.001
20°	9.1°	0.7°	7.7°	10.5°	4.6°*	0.7°	3.2°	5.9°	<.001
25°	10.8°	0.8°	9.3°	12.3°	6.1°*	0.8°	4.6°	7.5°	<.001
30°	12.2°	0.9°	10.5°	13.8°	7.7°*	0.9°	6.0°	9.4°	<.001
35°	13.1°	1.0°	11.1°	15.1°	9.7°*	1.0°	7.7°	11.6°	0.016

“\*” and bold font Indicate statistical significance at a p-value of 0.05.



## 3.5. MIDCARPAL KINEMATICS

### 3.5.1. Wrist extension to flexion

All tables containing detailed results of midcarpal kinematics (Table 66 to Table 77) are presented at the end of this section (3.5.4). The midcarpal angular displacements were calculated as scapho-capitate and luno-capitate angulations.

#### *Scapho-capitate flexion*

**3.5.2. During wrist extension to flexion, there was scapho-capitate flexion in both the normal and the SLI wrists. With the wrist moving from 70° to 40° extension, there was less scapho-capitate flexion in the SLI wrist than the normal (Figure 103). Statistical significance at each incremental step of 5° is presented in Table 66**

Table 66. From 40° extension to 30° flexion, scapho-capitate flexion was not significantly different between the SLI and normal wrists. From wrist 35° to 50° flexion, there was more scapho-capitate flexion in the SLI wrist than the normal.

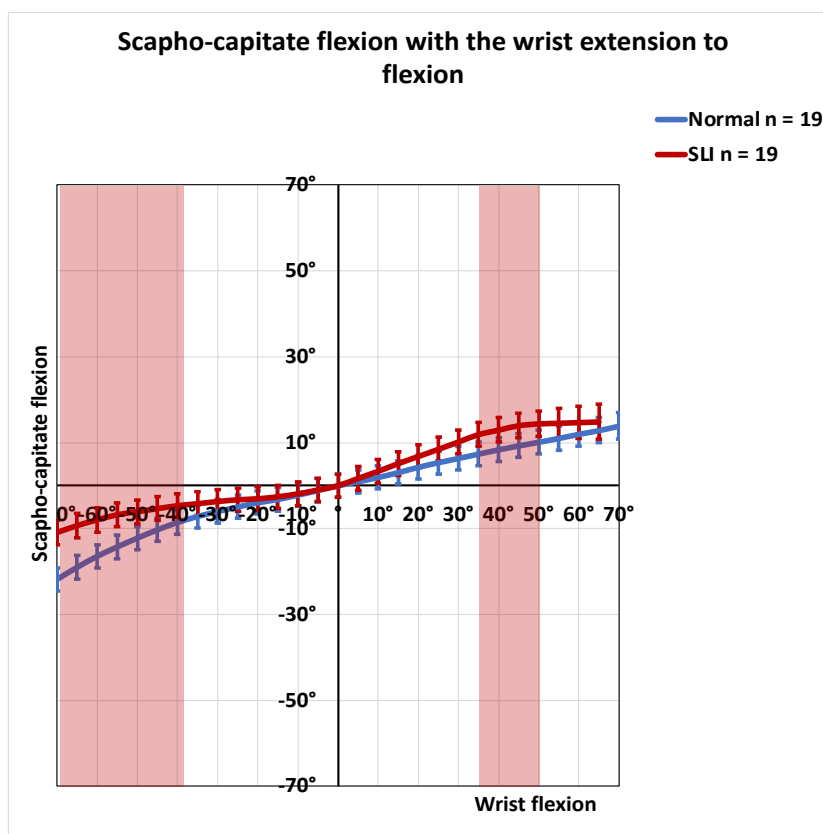


Figure 103 Scapho-capitate flexion with the wrist extension to flexion (95% confidence intervals are marked by the error bars). With the wrist moving from 70 to 40° extension there was less scapho-capitate flexion in the SLI wrist compared to the normal. From 35° to 50° flexion, the SLI wrist had more scapho-capitate flexion. The red highlighted zones indicate the wrist range of motion where a statistically significant difference exists between the normal and the SLI wrist.

### Scapho-capitate radial angulation

With the wrist moving from 70 to 45° extension the, there was less scapho-capitate radial angulation in the SLI wrist compared to the normal (Figure 104, Table 67). From 40° extension to 65° flexion, there was no statistically significant difference in scapho-capitate radial angulation between the SLI and normal wrists.

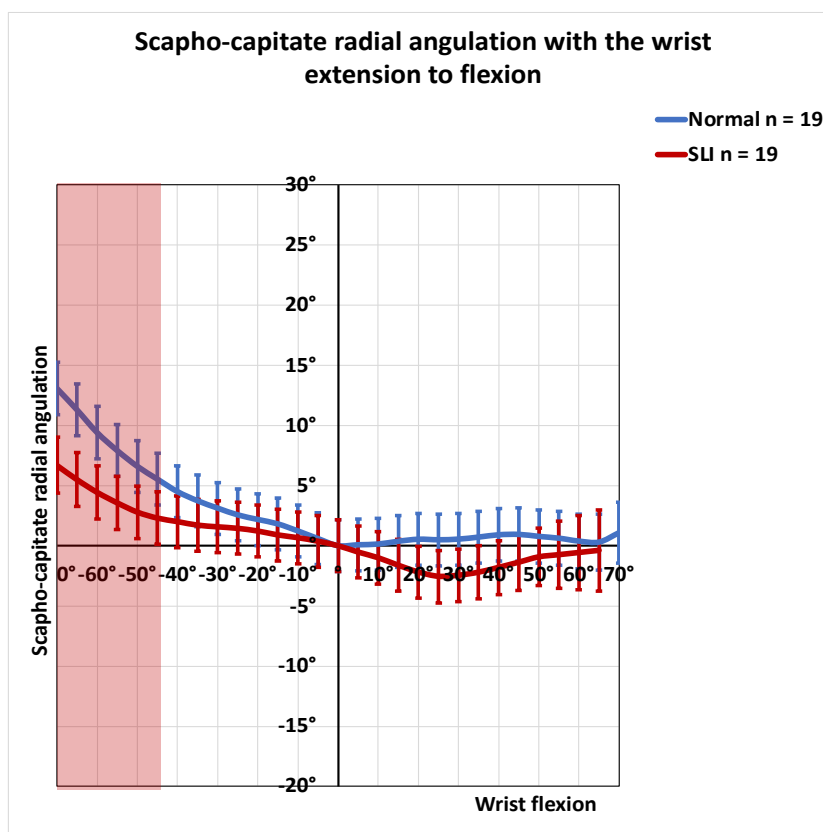


Figure 104 Scapho-capitate radial angulation with the wrist extension to flexion (95% confidence intervals are marked by the error bars). With the wrist moving from 70 to 45° extension, the SLI wrist had less scapho-capitate radial angulation. The red highlighted zones indicate the wrist range of motion where a statistically significant difference exists between the normal and the SLI wrist.

### Scapho-capitate internal rotation

With the wrist from 70° extension to 60° flexion, there was no statistically significant difference in the scapho-capitate internal rotation between the SLI and the normal wrists (Figure 105, Table 68). When the wrist flexed from 60° to 65° there was more scapho-capitate internal rotation in the normal wrist than the SLI wrist. Nonetheless, there was an overlap in the confidence intervals at this point.

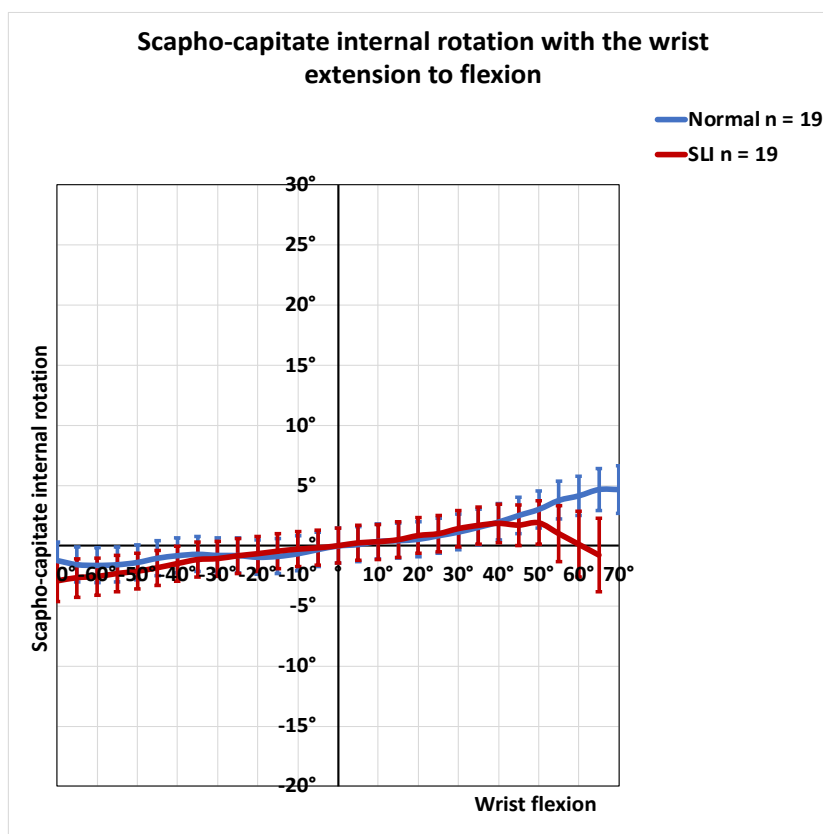


Figure 105 Scapho-capitate internal rotation with the wrist extension to flexion (95% confidence intervals are marked by the error bars). There was no statistically significant difference in the scapho-capitate internal rotation between the SLI and the normal wrists.

### Luno-capitate flexion

With the wrist moving from extension to flexion, there was luno-capitate flexion in both the SLI and the normal wrists. With the wrist moving from 70° extension to 30° extension, there was more luno-capitate flexion in the SLI the wrist than the normal wrist (Figure 106, Table 69). From 25° wrist extension to 65° flexion, there was no statistically significant difference in luno-capitate flexion between the SLI and normal wrists.

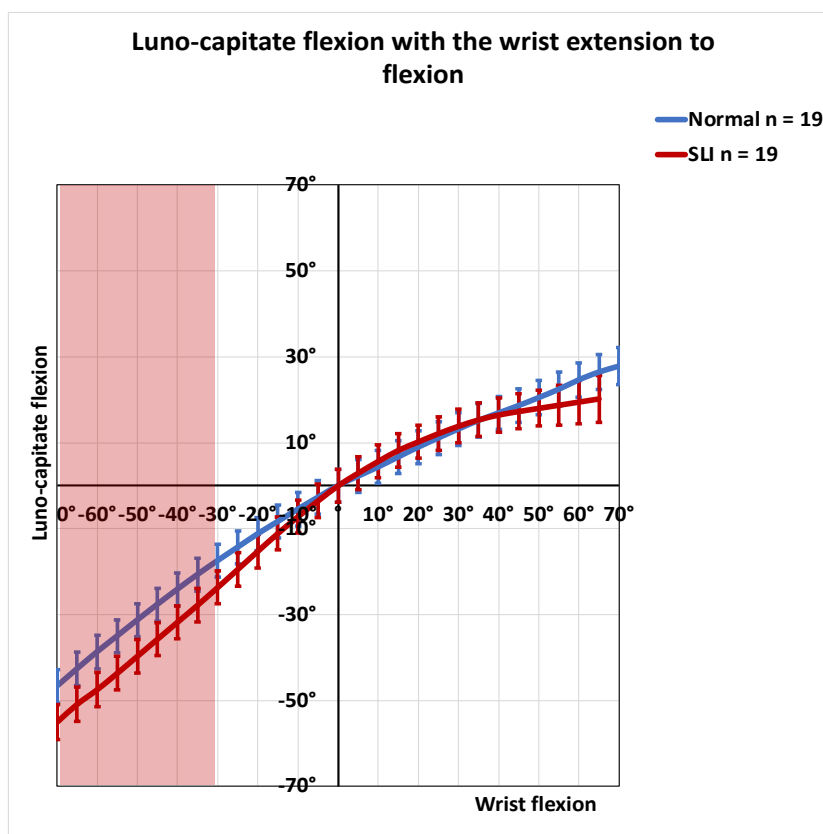


Figure 106 Luno-capitate flexion with the wrist extension to flexion. With the wrist from 70° extension to 30° extension, SLI the wrist had more luno-capitate flexion than the normal wrist. The red highlighted zones indicate the wrist range of motion where a statistically significant difference exists between the normal and the SLI wrist.

### *Luno-capitate radial angulation*

With the wrist moving from 70° to 60° extension, the SLI wrist had less luno-capitate radial angulation than the normal wrist (Figure 107, Table 70). From 55° extension to 65° flexion, there was no statistically significant difference in luno-capitate radial angulation between the SLI and normal wrists.

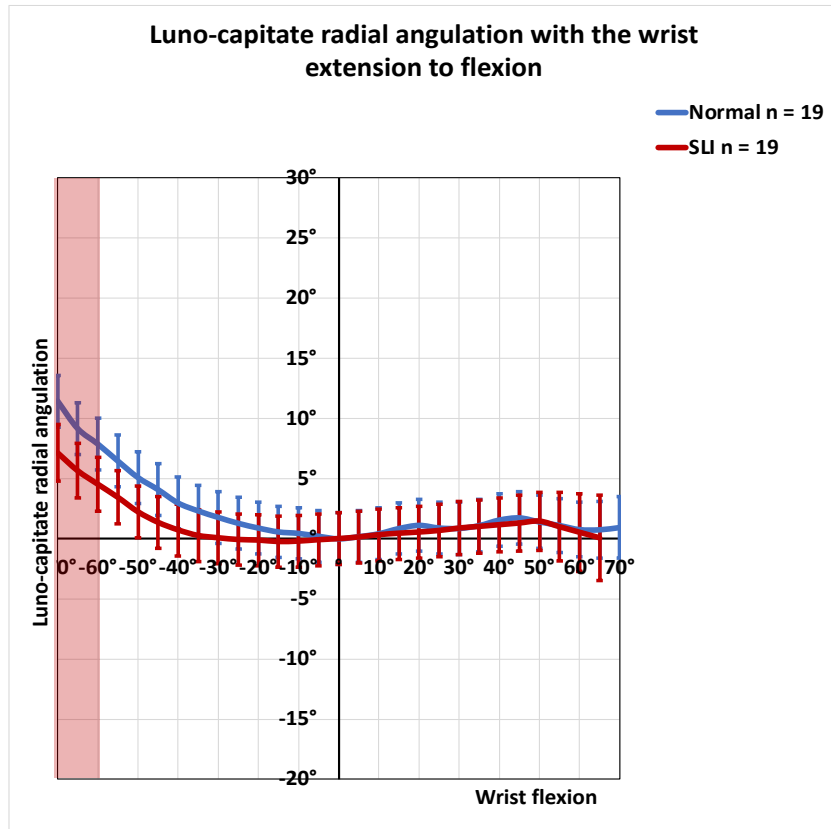


Figure 107 Luno-capitate radial angulation with the wrist extension to flexion (95% confidence intervals are marked by the error bars). A statistically significant difference in the luno-capitate radial angulation was observed only during extreme extension, from 70° to 60° extension. The red highlighted zones indicate the wrist range of motion where a statistically significant difference exists between the normal and the SLI wrist.

### Luno-capitate internal rotation

Between the wrist positions from 45° extension to 50° flexion, there was no statistically significant difference in the luno-capitate internal rotation between the SLI and the normal wrists (Figure 108, Table 71). However, when the wrist was in extension beyond 50°, the SLI wrist had more luno-capitate internal rotation; when the wrist was in 50° or more flexion the SLI wrist had less luno-capitate internal rotation than the normal wrist.

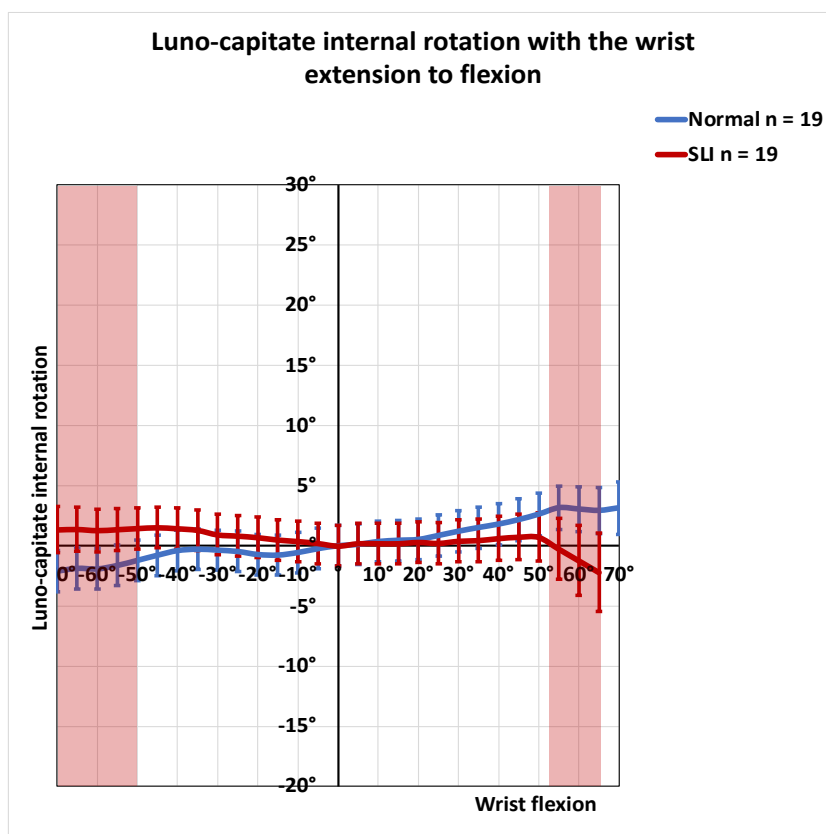


Figure 108 Luno-capitate internal rotation with the wrist extension to flexion (95% confidence intervals are marked by the error bars). When the wrist is in extension beyond 50°, the SLI wrist had more luno-capitate internal rotation; when the wrist is beyond 50° flexion the SLI wrist had less luno-capitate internal rotation than the normal wrist. The red highlighted zones indicate the wrist range of motion where a statistically significant difference exists between the normal and the SLI wrist.

### 3.5.3. Wrist ulnar to radial deviation

The scapho-capitate angular displacements for the normal wrist are presented in the Figure 109 . During wrist neutral to radial deviation, there was more midcarpal radial angulation (in-plane motion) than when the wrist was moving from ulnar deviation to neutral (Table 73). The midcarpal scapho-capitate flexion (out-of-plane motion) was similar between the wrist ulnar to neutral position and neutral to radial deviation (Table 72).

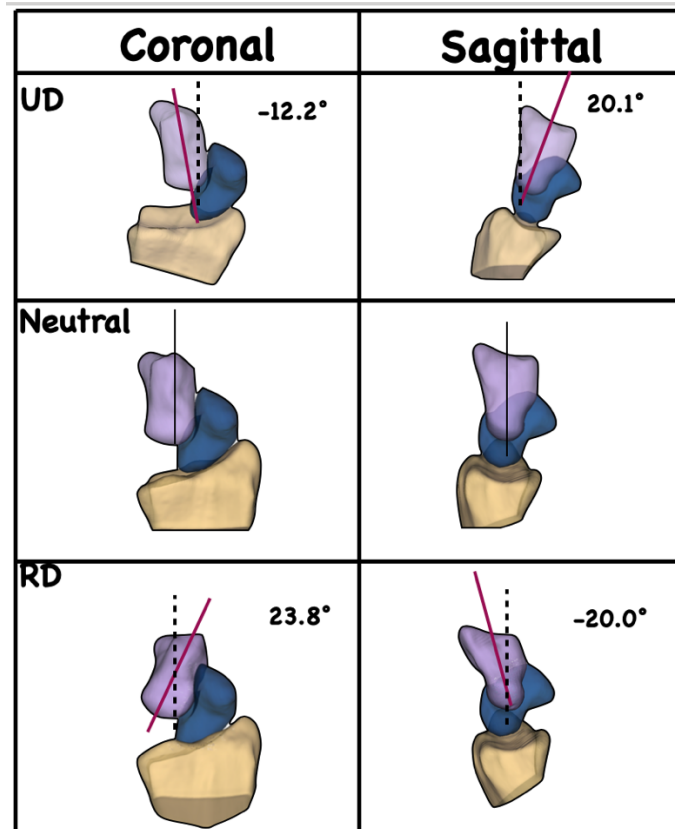


Figure 109 The scapho-capitate angulation of the normal wrist during the ulnar (35°) to radial deviation (35°). The coronal plane images depict the in-plane motion or the radial angulation. The sagittal plane images depict the out-of-plane motion or the flexion. Radial angulation and flexion are positive. Midcarpal in-plane motion was more in neutral to radial deviation, compared to ulnar deviation to neutral. Midcarpal out-of-plane motion remained similar between two phases, ulnar to neutral and neutral to radial deviation. Note that the confidence intervals were not included in the figure for easier reading but were included in Table 72 and Table 73. The black line indicates the principal axis of the capitate in the neutral position. The dotted black line indicates the principal axis of the capitate in the neutral position, depicted on ulnarly (UD) and radially deviated (RD) wrist. The red line indicates the principal axis of the capitate in UD and RD wrists.

### Scapho-capitate flexion

With the wrist moving from ulnar to radial deviation, both the SLI and the normal wrist had scapho-capitate extension (negative flexion) (Figure 110, Table 72). The SLI scapho-capitate flexion was significantly less than the normal scapho-capitate flexion when the wrist was ulnar deviated more than 10° or radially deviated more than 10°. In the mid-range between 5° of ulnar deviation to 5° of radial deviation, there was no statistically significant difference in the scapho-capitate flexion between the two groups.



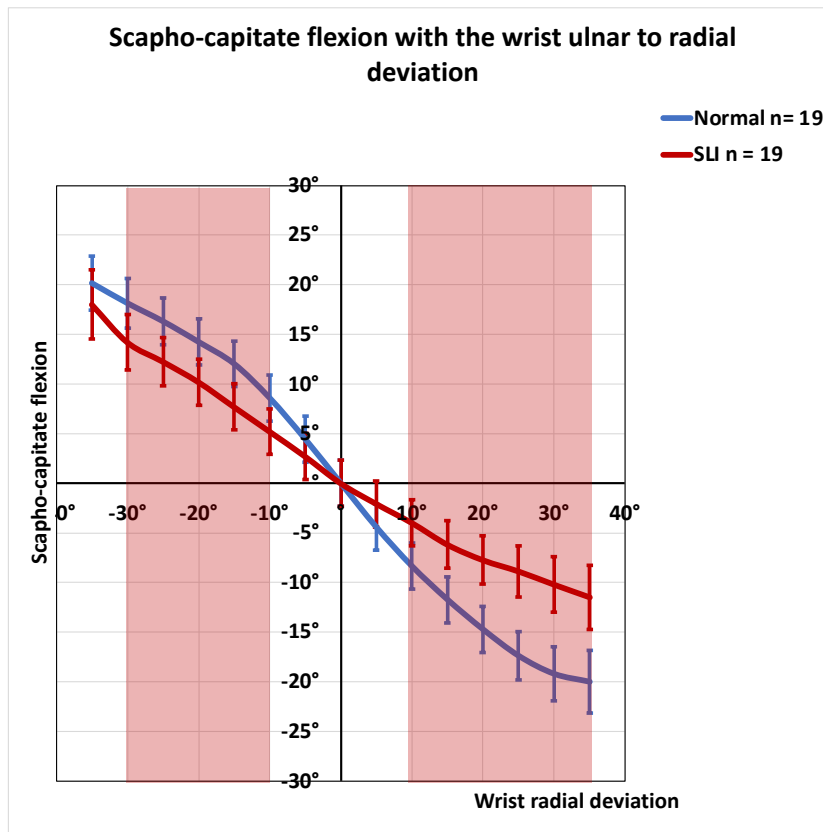


Figure 110 Scapho-capitate flexion with the wrist ulnar to radial deviation (95% confidence intervals are marked by the error bars). When the wrist is ulnar deviated beyond 10° or radially deviated beyond 10°, the SLI scapho-capitate flexion was significantly less than the normal scapho-capitate flexion. The red highlighted zones indicate the wrist range of motion where a statistically significant difference exists between the normal and the SLI wrist.

### Scapho-capitate radial angulation

With the wrist moving from ulnar to radial deviation, there was scapho-capitate radial angulation in both the SLI and the normal wrists (Figure 111, Table 73). When the wrist radially deviated beyond 10°, the SLI scapho-capitate radial angulation was significantly less than the normal scapho-capitate radial angulation.

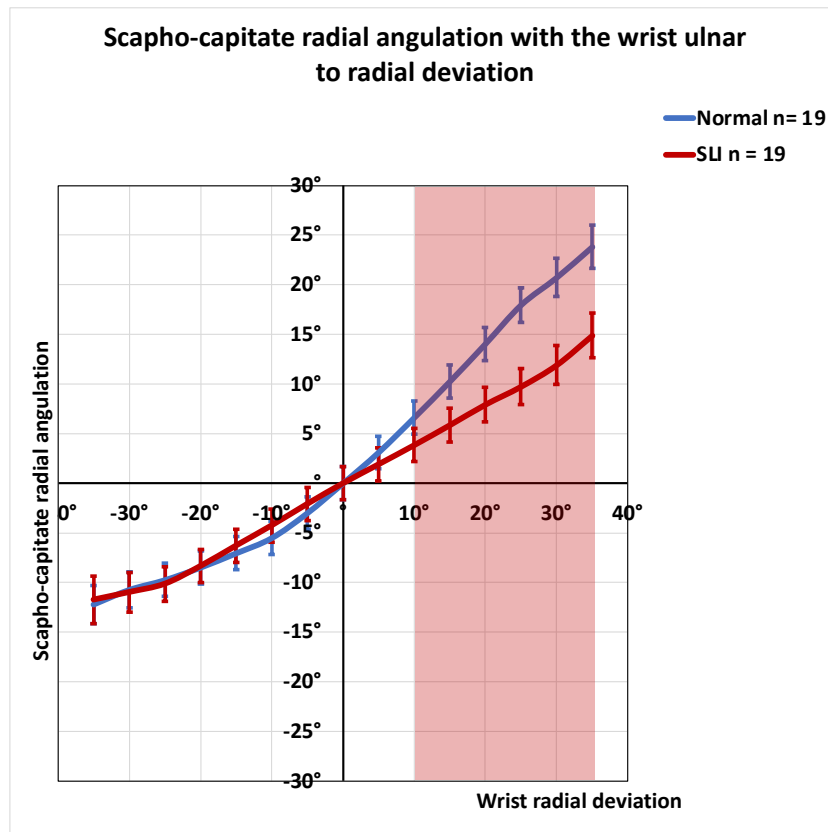


Figure 111 Scapho-capitate radial angulation with the wrist ulnar to radial deviation (95% confidence intervals are marked by the error bars). When the wrist radially deviated beyond 10°, the SLI scapho-capitate radial angulation was significantly less than the normal scapho-capitate radial angulation. The red highlighted zones indicate the wrist range of motion where a statistically significant difference exists between the normal and the SLI wrist.

### Scapho-capitate internal rotation

With the wrist moving from ulnar to radial deviation there was no statistically significant difference in the scapho-capitate internal rotation between the SLI and the normal wrists until it reached 30° radial deviation (Figure 112, Table 74). At the 30° wrist radial deviation, there is a statistically significant difference between the two groups, however, confidence intervals demonstrated overlap.

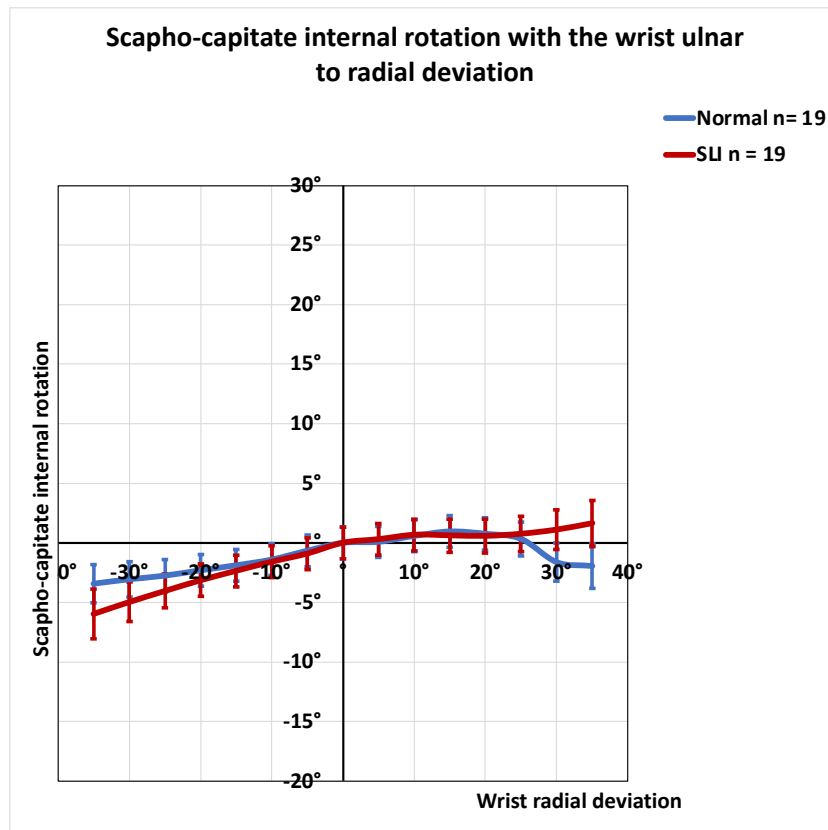


Figure 112 Scapho-capitate internal rotation with the wrist ulnar to radial deviation (95% confidence intervals are marked by the error bars). With the wrist moving from ulnar to radial deviation there was no statistically significant difference in the scapho-capitate internal rotations between the SLI and the normal wrists until it reached 30° radial deviation.

### Luno-capitate flexion

The luno-capitate flexion was significantly less in the SLI wrist than the normal lunate when the wrist is ulnar deviated beyond 15° (Figure 113, Table 75). From the wrist ulnar deviation of 15°, as the wrist radially deviated, there was no statistically significant difference in the luno-capitate flexion of the lunate between the two groups.

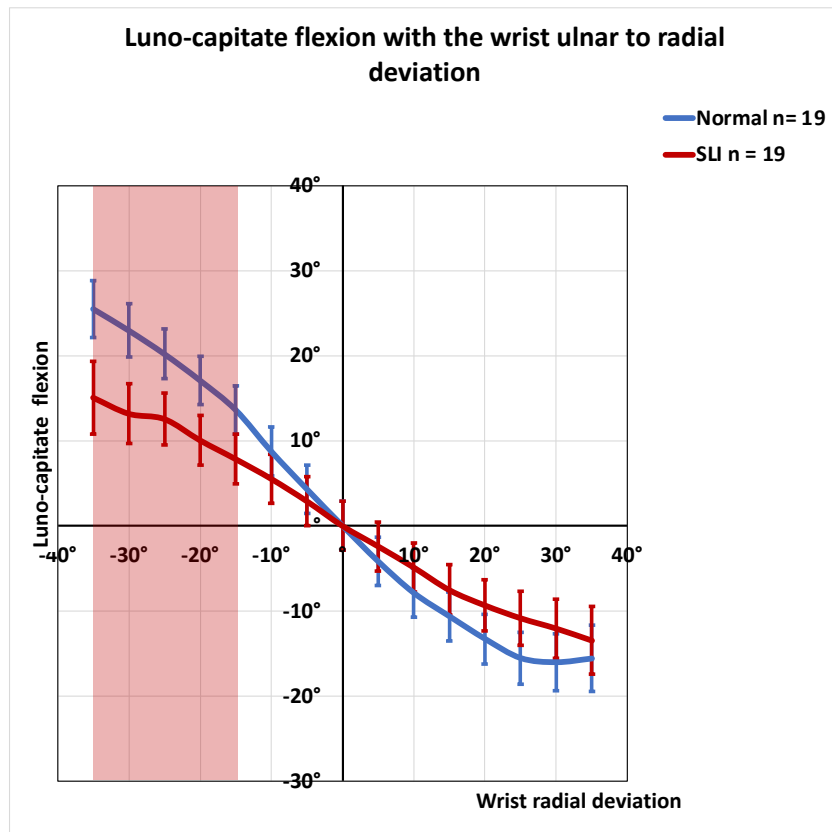


Figure 113 Luno-capitate flexion with the wrist ulnar to radial deviation (95% confidence intervals are marked by the error bars). The SLI luno-capitate flexion was significantly less than the normal lunate when the wrist was ulnar deviated beyond 15°. The red highlighted zones indicate the wrist range of motion where a statistically significant difference exists between the normal and the SLI wrist.

### *Luno-capitate radial angulation*

With the wrist moving from ulnar to radial deviation there was no statistically significant difference in the luno-capitate radial angulations between the two groups (Figure 114, Table 75).

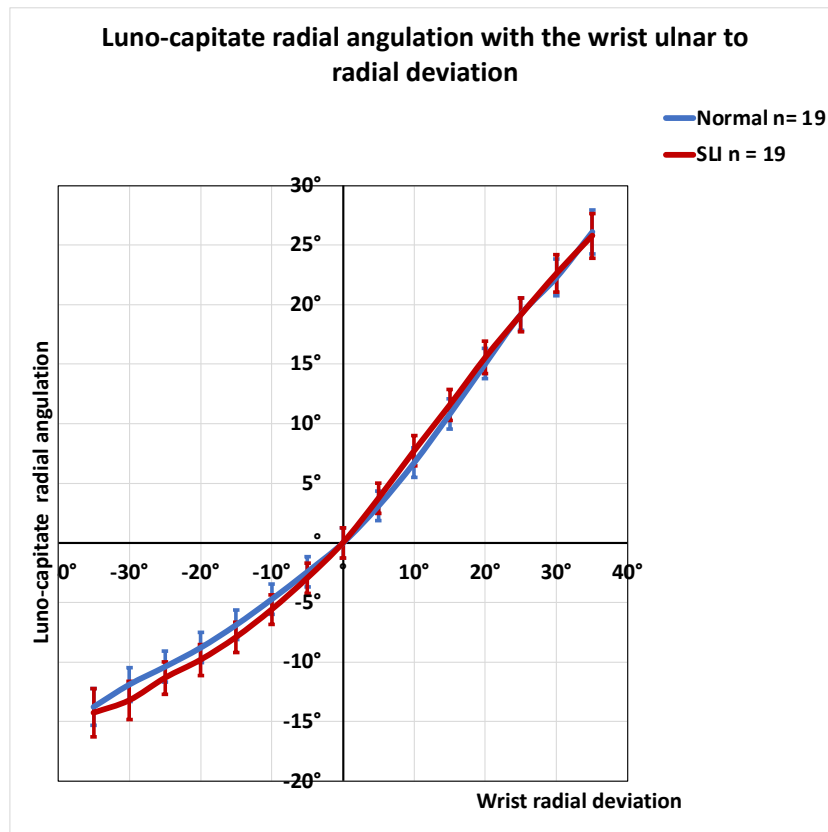


Figure 114 Luno-capitate radial angulation with the wrist ulnar to radial deviation (95% confidence intervals are marked by the error bars). There was no statistically significant difference in the luno-capitate radial angulations between the two groups.

### *Luno-capitate internal rotation*

With the wrist moving from ulnar to radial deviation there was no statistically significant difference in the luno-capitate internal rotation between the SLI and the normal wrist until the wrist reached 20° radial deviation (Figure 115, Table 77). Beyond 25° radial deviation there is a statistically significant difference between the two groups, however, the confidence intervals demonstrated overlap.

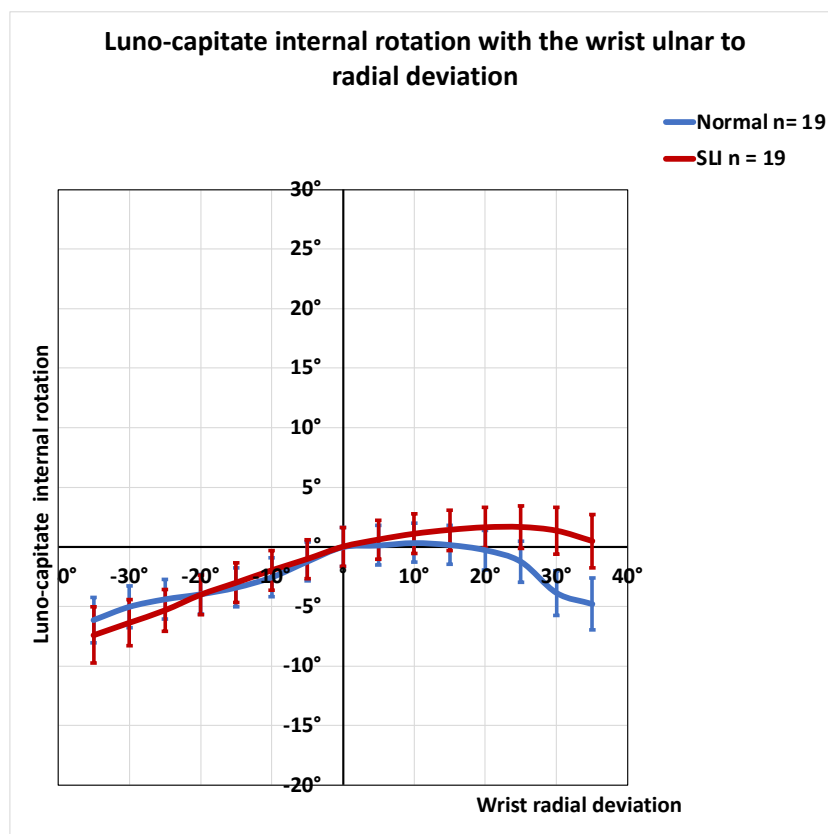


Figure 115 Luno-capitate internal rotation with the wrist ulnar to radial deviation (95% confidence intervals are marked by the error bars). There was no statistically significant difference in the luno-capitate internal rotation between the SLI and the normal wrist until the wrist reached 20° radial deviation.

### 3.5.4. Midcarpal kinematics (Tables)

Table 66 Scapho-capitate flexion with the wrist extension to flexion

Wrist angle from extension to flexion (degrees)	Normal				SLI				p- value
	Mean	Std. Error	Lower CI	Upper CI	Mean	Std. Error	Lower CI	Upper CI	
-70°	-21.8°	1.4°	-24.6°	-19.1°	-11.0°*	1.5°	-13.9°	-8.1°	<.001
-65°	-19.0°	1.4°	-21.7°	-16.3°	-9.3°*	1.4°	-12.2°	-6.5°	<.001
-60°	-16.5°	1.4°	-19.2°	-13.7°	-8.0°*	1.4°	-10.8°	-5.2°	<.001
-55°	-14.2°	1.4°	-17.0°	-11.5°	-6.8°*	1.4°	-9.6°	-4.0°	<.001
-50°	-12.2°	1.4°	-14.9°	-9.5°	-6.1°*	1.4°	-8.8°	-3.3°	0.002
-45°	-10.3°	1.4°	-13.0°	-7.5°	-5.4°*	1.4°	-8.1°	-2.6°	0.013
-40°	-8.6°	1.4°	-11.3°	-5.8°	-4.7°*	1.4°	-7.4°	-2.0°	0.049
-35°	-7.2°	1.4°	-9.9°	-4.4°	-4.2°	1.4°	-6.9°	-1.5°	0.134
-30°	-6.0°	1.4°	-8.7°	-3.3°	-3.7°	1.4°	-6.4°	-1.0°	0.242
-25°	-4.9°	1.4°	-7.7°	-2.2°	-3.3°	1.4°	-6.0°	-0.6°	0.403
-20°	-4.0°	1.4°	-6.7°	-1.2°	-3.1°	1.4°	-5.8°	-0.3°	0.646
-15°	-3.2°	1.4°	-5.9°	-0.5°	-2.6°	1.4°	-5.3°	0.1°	0.764
-10°	-2.2°	1.4°	-4.9°	0.6°	-1.9°	1.4°	-4.6°	0.8°	0.895
-5°	-1.1°	1.4°	-3.8°	1.6°	-1.0°	1.4°	-3.7°	1.7°	0.955
0°	0.0°	1.4°	-2.7°	2.7°	0.0°	1.4°	-2.7°	2.7°	1
5°	0.9°	1.4°	-1.8°	3.7°	1.7°	1.4°	-1.0°	4.4°	0.705
10°	1.9°	1.4°	-0.8°	4.7°	3.4°	1.4°	0.6°	6.1°	0.475
15°	3.1°	1.4°	0.3°	5.8°	5.1°	1.4°	2.4°	7.9°	0.29
20°	4.3°	1.4°	1.6°	7.0°	6.8°	1.4°	4.1°	9.6°	0.206
25°	5.4°	1.4°	2.7°	8.1°	8.5°	1.4°	5.7°	11.2°	0.118
30°	6.4°	1.4°	3.6°	9.1°	10.2°	1.4°	7.4°	13.0°	0.055
35°	7.4°	1.4°	4.6°	10.1°	11.9°*	1.4°	9.1°	14.7°	0.023
40°	8.4°	1.4°	5.6°	11.1°	13.0°*	1.4°	10.1°	15.8°	0.024
45°	9.3°	1.4°	6.5°	12.1°	14.0°*	1.5°	11.1°	16.9°	0.021
50°	10.2°	1.4°	7.4°	12.9°	14.4°*	1.5°	11.4°	17.4°	0.041
55°	11.0°	1.4°	8.2°	13.9°	14.6°	1.7°	11.2°	18.0°	0.117
60°	12.0°	1.5°	9.1°	14.9°	14.7°	1.9°	11.0°	18.5°	0.259
65°	12.9°	1.5°	9.9°	15.8°	14.9°	2.1°	10.8°	19.0°	0.434
70°	13.9°	1.6°	10.8°	17.0°	NA	NA	NA	NA	NA

“\*” and bold font Indicate statistical significance at a p-value of 0.05. NA-data not available beyond 65° of flexion for SLI wrists.

Table 67 Scapho-capitate radial angulation with the wrist extension to flexion

Wrist angle from extension to flexion (degrees)	Normal				SLI				p- value
	Mean	Std. Error	Lower CI	Upper CI	Mean	Std. Error	Lower CI	Upper CI	
-70°	<b>13.1°</b>	<b>1.1°</b>	<b>10.9°</b>	<b>15.3°</b>	<b>6.7°*</b>	<b>1.2°</b>	<b>4.4°</b>	<b>9.0°</b>	<b>&lt;0.001</b>
-65°	<b>11.3°</b>	<b>1.1°</b>	<b>9.1°</b>	<b>13.5°</b>	<b>5.5°*</b>	<b>1.1°</b>	<b>3.3°</b>	<b>7.8°</b>	<b>&lt;0.001</b>
-60°	<b>9.4°</b>	<b>1.1°</b>	<b>7.2°</b>	<b>11.6°</b>	<b>4.5°*</b>	<b>1.1°</b>	<b>2.2°</b>	<b>6.7°</b>	<b>0.002</b>
-55°	<b>7.9°</b>	<b>1.1°</b>	<b>5.8°</b>	<b>10.1°</b>	<b>3.6°*</b>	<b>1.1°</b>	<b>1.4°</b>	<b>5.8°</b>	<b>0.006</b>
-50°	<b>6.6°</b>	<b>1.1°</b>	<b>4.4°</b>	<b>8.8°</b>	<b>2.8°*</b>	<b>1.1°</b>	<b>0.6°</b>	<b>5.0°</b>	<b>0.015</b>
-45°	<b>5.5°</b>	<b>1.1°</b>	<b>3.4°</b>	<b>7.7°</b>	<b>2.3°*</b>	<b>1.1°</b>	<b>0.1°</b>	<b>4.5°</b>	<b>0.038</b>
-40°	4.5°	1.1°	2.3°	6.7°	2.0°	1.1°	-0.2°	4.2°	0.110
-35°	3.7°	1.1°	1.6°	5.9°	1.7°	1.1°	-0.4°	3.9°	0.193
-30°	3.1°	1.1°	1.0°	5.3°	1.6°	1.1°	-0.6°	3.7°	0.318
-25°	2.6°	1.1°	0.4°	4.7°	1.4°	1.1°	-0.7°	3.6°	0.472
-20°	2.2°	1.1°	0.0°	4.3°	1.2°	1.1°	-0.9°	3.4°	0.538
-15°	1.8°	1.1°	-0.3°	4.0°	0.9°	1.1°	-1.3°	3.1°	0.557
-10°	1.2°	1.1°	-0.9°	3.4°	0.7°	1.1°	-1.5°	2.8°	0.721
-5°	0.6°	1.1°	-1.6°	2.7°	0.4°	1.1°	-1.8°	2.5°	0.891
0°	0.0°	1.1°	-2.2°	2.2°	0.0°	1.1°	-2.2°	2.2°	1.000
5°	0.1°	1.1°	-2.1°	2.2°	-0.5°	1.1°	-2.7°	1.6°	0.698
10°	0.1°	1.1°	-2.0°	2.3°	-1.0°	1.1°	-3.2°	1.2°	0.464
15°	0.4°	1.1°	-1.8°	2.5°	-1.6°	1.1°	-3.8°	0.5°	0.200
20°	0.5°	1.1°	-1.6°	2.7°	-2.2°	1.1°	-4.4°	0.0°	0.081
25°	0.5°	1.1°	-1.7°	2.7°	-2.6°	1.1°	-4.7°	-0.4°	0.053
30°	0.5°	1.1°	-1.6°	2.7°	-2.5°	1.1°	-4.7°	-0.3°	0.056
35°	0.7°	1.1°	-1.5°	2.9°	-2.2°	1.1°	-4.4°	0.0°	0.065
40°	0.9°	1.1°	-1.3°	3.1°	-1.8°	1.2°	-4.1°	0.4°	0.091
45°	0.9°	1.1°	-1.3°	3.1°	-1.4°	1.2°	-3.7°	0.9°	0.155
50°	0.8°	1.1°	-1.4°	3.0°	-0.9°	1.2°	-3.3°	1.5°	0.307
55°	0.6°	1.1°	-1.6°	2.9°	-0.7°	1.4°	-3.5°	2.0°	0.451
60°	0.4°	1.2°	-1.9°	2.7°	-0.6°	1.6°	-3.7°	2.5°	0.630
65°	0.3°	1.2°	-2.0°	2.6°	-0.4°	1.7°	-3.8°	3.0°	0.744
70°	1.1°	1.3°	-1.4°	3.6°	NA	NA	NA	NA	NA

“\*” and bold font Indicate statistical significance at a p-value of 0.05. NA-data not available beyond 65° of flexion for SLI wrists.



Table 68 Scapho-capitate internal rotation with the wrist extension to flexion

Wrist angle from extension to flexion (degrees)	Normal				SLI				p-value
	Mean	Std. Error	Lower CI	Upper CI	Mean	Std. Error	Lower CI	Upper CI	
-70°	-1.2°	0.8°	-2.7°	0.3°	-2.9°	0.9°	-4.6°	-1.2°	0.131
-65°	-1.5°	0.7°	-3.0°	-0.1°	-2.7°	0.8°	-4.3°	-1.1°	0.314
-60°	-1.6°	0.7°	-3.1°	-0.2°	-2.6°	0.8°	-4.1°	-1.0°	0.377
-55°	-1.6°	0.7°	-3.0°	-0.1°	-2.3°	0.8°	-3.8°	-0.8°	0.479
-50°	-1.4°	0.7°	-2.8°	0.1°	-2.1°	0.8°	-3.6°	-0.6°	0.471
-45°	-1.0°	0.7°	-2.5°	0.4°	-1.8°	0.7°	-3.3°	-0.4°	0.436
-40°	-0.8°	0.7°	-2.3°	0.6°	-1.5°	0.7°	-2.9°	0.0°	0.516
-35°	-0.7°	0.7°	-2.1°	0.8°	-1.2°	0.7°	-2.6°	0.3°	0.658
-30°	-0.8°	0.7°	-2.2°	0.7°	-1.1°	0.7°	-2.5°	0.4°	0.782
-25°	-0.8°	0.7°	-2.2°	0.7°	-0.8°	0.7°	-2.3°	0.6°	0.966
-20°	-0.9°	0.7°	-2.4°	0.5°	-0.7°	0.7°	-2.1°	0.8°	0.793
-15°	-0.9°	0.7°	-2.3°	0.6°	-0.5°	0.7°	-1.9°	1.0°	0.696
-10°	-0.6°	0.7°	-2.1°	0.8°	-0.3°	0.7°	-1.7°	1.2°	0.73
-5°	-0.3°	0.7°	-1.7°	1.1°	-0.2°	0.7°	-1.6°	1.3°	0.904
0°	0.0°	0.7°	-1.4°	1.4°	0.0°	0.7°	-1.4°	1.4°	1
5°	0.1°	0.7°	-1.3°	1.6°	0.2°	0.7°	-1.2°	1.7°	0.902
10°	0.4°	0.7°	-1.1°	1.8°	0.3°	0.7°	-1.1°	1.8°	0.966
15°	0.4°	0.7°	-1.0°	1.9°	0.5°	0.7°	-1.0°	2.0°	0.949
20°	0.6°	0.7°	-0.9°	2.0°	0.9°	0.8°	-0.6°	2.3°	0.777
25°	0.8°	0.7°	-0.6°	2.3°	1.0°	0.8°	-0.5°	2.5°	0.882
30°	1.2°	0.8°	-0.3°	2.6°	1.4°	0.8°	-0.1°	2.9°	0.795
35°	1.6°	0.8°	0.1°	3.0°	1.7°	0.8°	0.2°	3.2°	0.891
40°	2.0°	0.8°	0.5°	3.5°	1.9°	0.8°	0.3°	3.5°	0.921
45°	2.5°	0.8°	1.0°	4.1°	1.7°	0.9°	0.0°	3.4°	0.486
50°	3.0°	0.8°	1.5°	4.6°	1.9°	0.9°	0.1°	3.7°	0.354
55°	3.8°	0.8°	2.2°	5.3°	1.0°	1.2°	-1.3°	3.3°	0.053
60°	<b>4.2°</b>	<b>0.8°</b>	<b>2.5°</b>	<b>5.8°</b>	<b>0.1°*</b>	<b>1.4°</b>	<b>-2.6°</b>	<b>2.8°</b>	<b>0.013</b>
65°	<b>4.7°</b>	<b>0.9°</b>	<b>3.0°</b>	<b>6.4°</b>	<b>-0.8°*</b>	<b>1.6°</b>	<b>-3.8°</b>	<b>2.3°</b>	<b>0.002</b>
70°	4.7°	1.0°	2.7°	6.7°	NA	NA	NA	NA	NA

“\*” and bold font Indicate statistical significance at a p-value of 0.05. NA-data not available beyond 65° of flexion for SLI wrists.

Table 69 Luno-capitate flexion with the wrist extension to flexion

Wrist angle from extension to flexion (degrees)	Normal				SLI				p- value
	Mean	Std. Error	Lower CI	Upper CI	Mean	Std. Error	Lower CI	Upper CI	
-70°	-46.7°	2.0°	-50.6°	-42.8°	-55.0°*	2.1°	-59.1°	-51.0°	<b>0.004</b>
-65°	-42.7°	2.0°	-46.5°	-38.8°	-50.9°*	2.0°	-54.8°	-46.9°	<b>0.004</b>
-60°	-38.7°	2.0°	-42.6°	-34.8°	-47.4°*	2.0°	-51.4°	-43.5°	<b>0.002</b>
-55°	-35.0°	2.0°	-38.9°	-31.2°	-43.6°*	2.0°	-47.5°	-39.7°	<b>0.002</b>
-50°	-31.3°	2.0°	-35.2°	-27.5°	-39.7°*	2.0°	-43.6°	-35.8°	<b>0.003</b>
-45°	-27.7°	2.0°	-31.5°	-23.8°	-35.7°*	2.0°	-39.6°	-31.8°	<b>0.004</b>
-40°	-24.1°	2.0°	-28.0°	-20.3°	-31.8°*	2.0°	-35.6°	-27.9°	<b>0.006</b>
-35°	-20.7°	2.0°	-24.5°	-16.8°	-27.8°*	2.0°	-31.6°	-23.9°	<b>0.011</b>
-30°	-17.5°	2.0°	-21.3°	-13.6°	-23.7°*	2.0°	-27.5°	-19.8°	<b>0.026</b>
-25°	-14.3°	2.0°	-18.2°	-10.5°	-19.5°	2.0°	-23.3°	-15.6°	0.064
-20°	-11.2°	2.0°	-15.1°	-7.4°	-15.3°	2.0°	-19.1°	-11.4°	0.146
-15°	-8.4°	2.0°	-12.2°	-4.5°	-11.1°	2.0°	-15.0°	-7.3°	0.322
-10°	-5.5°	2.0°	-9.3°	-1.6°	-7.2°	2.0°	-11.1°	-3.4°	0.533
-5°	-2.7°	2.0°	-6.6°	1.1°	-3.5°	2.0°	-7.4°	0.3°	0.768
0°	0.0°	2.0°	-3.8°	3.8°	0.0°	2.0°	-3.8°	3.8°	1.00
5°	2.2°	2.0°	-1.6°	6.1°	2.9°	2.0°	-0.9°	6.8°	0.792
10°	4.4°	2.0°	0.5°	8.2°	5.7°	2.0°	1.8°	9.5°	0.634
15°	6.7°	2.0°	2.8°	10.5°	8.2°	2.0°	4.4°	12.1°	0.575
20°	9.0°	2.0°	5.1°	12.8°	10.2°	2.0°	6.4°	14.1°	0.652
25°	11.1°	2.0°	7.2°	15.0°	12.1°	2.0°	8.3°	16.0°	0.708
30°	13.2°	2.0°	9.3°	17.1°	13.9°	2.0°	10.0°	17.8°	0.808
35°	15.2°	2.0°	11.3°	19.1°	15.3°	2.0°	11.4°	19.3°	0.952
40°	16.9°	2.0°	13.0°	20.8°	16.5°	2.0°	12.5°	20.5°	0.879
45°	18.7°	2.0°	14.7°	22.6°	17.3°	2.1°	13.3°	21.3°	0.637
50°	20.5°	2.0°	16.6°	24.4°	18.0°	2.1°	13.9°	22.2°	0.398
55°	22.5°	2.0°	18.5°	26.4°	18.8°	2.4°	14.2°	23.4°	0.235
60°	24.6°	2.0°	20.6°	28.6°	19.5°	2.6°	14.5°	24.6°	0.118
65°	26.4°	2.1°	22.4°	30.5°	20.2°	2.8°	14.8°	25.7°	0.073
70°	27.8°	2.2°	23.5°	32.1°	NA	NA	NA	NA	NA

“\*” and bold font Indicate statistical significance at a p-value of 0.05. NA-data not available beyond 65° of flexion for SLI wrists.

Table 70 Luno-capitate radial angulation with the wrist extension to flexion

Wrist angle from extension to flexion (degrees)	Normal				SLI				p- value
	Mean	Std. Error	Lower CI	Upper CI	Mean	Std. Error	Lower CI	Upper CI	
-70°	<b>11.4°</b>	<b>1.1°</b>	<b>9.3°</b>	<b>13.6°</b>	<b>7.1°*</b>	<b>1.2°</b>	<b>4.8°</b>	<b>9.5°</b>	<b>0.008</b>
-65°	<b>9.1°</b>	<b>1.1°</b>	<b>7.0°</b>	<b>11.3°</b>	<b>5.7°*</b>	<b>1.2°</b>	<b>3.4°</b>	<b>7.9°</b>	<b>0.029</b>
-60°	<b>7.9°</b>	<b>1.1°</b>	<b>5.7°</b>	<b>10.0°</b>	<b>4.5°*</b>	<b>1.1°</b>	<b>2.3°</b>	<b>6.8°</b>	<b>0.035</b>
-55°	6.5°	1.1°	4.3°	8.6°	3.4°	1.1°	1.3°	5.6°	0.054
-50°	5.1°	1.1°	2.9°	7.2°	2.2°	1.1°	0.1°	4.4°	0.067
-45°	4.1°	1.1°	1.9°	6.2°	1.4°	1.1°	-0.8°	3.5°	0.079
-40°	3.0°	1.1°	0.8°	5.1°	0.7°	1.1°	-1.4°	2.9°	0.147
-35°	2.3°	1.1°	0.2°	4.5°	0.3°	1.1°	-1.9°	2.4°	0.184
-30°	1.8°	1.1°	-0.4°	3.9°	0.1°	1.1°	-2.1°	2.2°	0.269
-25°	1.3°	1.1°	-0.9°	3.4°	-0.1°	1.1°	-2.2°	2.1°	0.377
-20°	0.9°	1.1°	-1.3°	3.0°	-0.1°	1.1°	-2.3°	2.0°	0.511
-15°	0.6°	1.1°	-1.6°	2.7°	-0.2°	1.1°	-2.4°	1.9°	0.597
-10°	0.5°	1.1°	-1.7°	2.6°	-0.2°	1.1°	-2.4°	1.9°	0.67
-5°	0.2°	1.1°	-1.9°	2.4°	-0.1°	1.1°	-2.2°	2.1°	0.846
0°	0.0°	1.1°	-2.1°	2.1°	0.0°	1.1°	-2.1°	2.1°	1.00
5°	0.2°	1.1°	-2.0°	2.3°	0.1°	1.1°	-2.0°	2.3°	0.98
10°	0.4°	1.1°	-1.7°	2.6°	0.3°	1.1°	-1.8°	2.5°	0.951
15°	0.9°	1.1°	-1.3°	3.0°	0.4°	1.1°	-1.7°	2.6°	0.795
20°	1.1°	1.1°	-1.0°	3.3°	0.5°	1.1°	-1.6°	2.7°	0.715
25°	0.9°	1.1°	-1.3°	3.1°	0.7°	1.1°	-1.5°	2.9°	0.888
30°	0.9°	1.1°	-1.3°	3.0°	0.9°	1.1°	-1.3°	3.1°	0.99
35°	1.1°	1.1°	-1.1°	3.3°	1.0°	1.1°	-1.2°	3.2°	0.96
40°	1.6°	1.1°	-0.6°	3.7°	1.2°	1.2°	-1.1°	3.4°	0.803
45°	1.7°	1.1°	-0.5°	3.9°	1.3°	1.2°	-1.0°	3.6°	0.789
50°	1.4°	1.1°	-0.8°	3.6°	1.5°	1.2°	-1.0°	3.9°	0.972
55°	1.1°	1.1°	-1.1°	3.3°	1.0°	1.5°	-1.9°	3.8°	0.953
60°	0.8°	1.2°	-1.5°	3.0°	0.5°	1.6°	-2.7°	3.7°	0.907
65°	0.7°	1.2°	-1.6°	3.1°	0.1°	1.8°	-3.5°	3.6°	0.753
70°	0.9°	1.3°	-1.6°	3.5°	NA	NA	NA	NA	NA

“\*” and bold font Indicate statistical significance at a p-value of 0.05. NA-data not available beyond 65° of flexion for SLI wrists.

Table 71 Luno-capitate internal rotation with the wrist extension to flexion

Wrist angle from extension to flexion (degrees)	Normal				SLI				p- value
	Mean	Std. Error	Lower CI	Upper CI	Mean	Std. Error	Lower CI	Upper CI	
-70°	-2.1°	0.9°	-3.8°	-0.4°	1.3°*	1.0°	-0.6°	3.3°	0.009
-65°	-1.9°	0.9°	-3.6°	-0.2°	1.4°*	0.9°	-0.4°	3.2°	0.011
-60°	-1.9°	0.9°	-3.6°	-0.2°	1.3°*	0.9°	-0.5°	3.1°	0.011
-55°	-1.6°	0.9°	-3.3°	0.1°	1.4°*	0.9°	-0.4°	3.1°	0.016
-50°	-1.2°	0.9°	-2.9°	0.5°	1.5°*	0.9°	-0.3°	3.2°	0.03
-45°	-0.8°	0.9°	-2.5°	0.9°	1.5°	0.9°	-0.2°	3.2°	0.059
-40°	-0.4°	0.9°	-2.1°	1.3°	1.4°	0.9°	-0.3°	3.1°	0.13
-35°	-0.3°	0.9°	-2.0°	1.4°	1.3°	0.9°	-0.4°	3.0°	0.19
-30°	-0.4°	0.9°	-2.0°	1.3°	0.9°	0.9°	-0.8°	2.6°	0.286
-25°	-0.5°	0.9°	-2.2°	1.2°	0.8°	0.9°	-0.9°	2.5°	0.282
-20°	-0.7°	0.9°	-2.4°	1.0°	0.7°	0.9°	-1.0°	2.4°	0.24
-15°	-0.8°	0.9°	-2.5°	0.9°	0.5°	0.9°	-1.2°	2.2°	0.293
-10°	-0.6°	0.9°	-2.2°	1.1°	0.4°	0.9°	-1.3°	2.1°	0.438
-5°	-0.2°	0.9°	-1.9°	1.4°	0.2°	0.9°	-1.5°	1.9°	0.708
0°	0.0°	0.9°	-1.7°	1.7°	0.0°	0.9°	-1.7°	1.7°	1
5°	0.1°	0.9°	-1.6°	1.8°	0.2°	0.9°	-1.5°	1.9°	0.945
10°	0.3°	0.9°	-1.3°	2.0°	0.2°	0.9°	-1.5°	1.9°	0.903
15°	0.5°	0.9°	-1.2°	2.1°	0.2°	0.9°	-1.5°	1.9°	0.835
20°	0.5°	0.9°	-1.2°	2.2°	0.3°	0.9°	-1.4°	2.0°	0.858
25°	0.9°	0.9°	-0.8°	2.6°	0.2°	0.9°	-1.5°	2.0°	0.612
30°	1.2°	0.9°	-0.5°	2.9°	0.4°	0.9°	-1.3°	2.2°	0.521
35°	1.5°	0.9°	-0.2°	3.2°	0.5°	0.9°	-1.3°	2.2°	0.402
40°	1.8°	0.9°	0.1°	3.5°	0.6°	0.9°	-1.2°	2.5°	0.363
45°	2.2°	0.9°	0.4°	3.9°	0.7°	1.0°	-1.2°	2.6°	0.279
50°	2.6°	0.9°	0.8°	4.4°	0.7°	1.0°	-1.3°	2.7°	0.166
55°	3.1°	0.9°	1.4°	4.9°	-0.3°*	1.3°	-2.8°	2.3°	0.031
60°	3.0°	0.9°	1.2°	4.9°	-1.2°*	1.5°	-4.1°	1.7°	0.016
65°	2.9°	1.0°	1.0°	4.9°	-2.2°*	1.7°	-5.4°	1.1°	0.008
70°	3.1°	1.1°	0.9°	5.3°	NA	NA	NA	NA	NA

“\*” and bold font Indicate statistical significance at a p-value of 0.05. NA-data not available beyond 65° of flexion for SLI wrists.

Table 72 Scapho-capitate flexion with the wrist ulnar to radial deviation

Wrist angle-value from ulnar to radial deviation (degrees)	Normal				SLI				p- value
	Mean	Std. Error	Lower CI	Upper CI	Mean	Std. Error	Lower CI	Upper CI	
-35°	20.1°	1.4°	17.4°	22.9°	18.0°	1.8°	14.5°	21.5°	0.342
-30°	<b>18.1°</b>	<b>1.3°</b>	<b>15.6°</b>	<b>20.6°</b>	<b>14.2°*</b>	<b>1.4°</b>	<b>11.4°</b>	<b>17.0°</b>	<b>0.042</b>
-25°	<b>16.3°</b>	<b>1.2°</b>	<b>14.0°</b>	<b>18.6°</b>	<b>12.3°*</b>	<b>1.3°</b>	<b>9.8°</b>	<b>14.7°</b>	<b>0.02</b>
-20°	<b>14.2°</b>	<b>1.2°</b>	<b>11.9°</b>	<b>16.5°</b>	<b>10.2°*</b>	<b>1.2°</b>	<b>7.9°</b>	<b>12.5°</b>	<b>0.016</b>
-15°	<b>12.0°</b>	<b>1.2°</b>	<b>9.7°</b>	<b>14.3°</b>	<b>7.7°*</b>	<b>1.2°</b>	<b>5.4°</b>	<b>10.0°</b>	<b>0.01</b>
-10°	<b>8.6°</b>	<b>1.2°</b>	<b>6.3°</b>	<b>10.9°</b>	<b>5.2°*</b>	<b>1.2°</b>	<b>2.9°</b>	<b>7.5°</b>	<b>0.043</b>
-5°	4.4°	1.2°	2.1°	6.7°	2.7°	1.2°	0.4°	5.0°	0.294
0°	0.0°	1.2°	-2.3°	2.3°	0.0°	1.2°	-2.3°	2.3°	1.00
5°	-4.4°	1.2°	-6.7°	-2.1°	-2.1°	1.2°	-4.4°	0.2°	0.157
10°	<b>-8.3°</b>	<b>1.2°</b>	<b>-10.7°</b>	<b>-6.0°</b>	<b>-4.0°*</b>	<b>1.2°</b>	<b>-6.3°</b>	<b>-1.6°</b>	<b>0.009</b>
15°	<b>-11.7°</b>	<b>1.2°</b>	<b>-14.0°</b>	<b>-9.4°</b>	<b>-6.2°*</b>	<b>1.2°</b>	<b>-8.6°</b>	<b>-3.8°</b>	<b>0.001</b>
20°	<b>-14.7°</b>	<b>1.2°</b>	<b>-17.1°</b>	<b>-12.4°</b>	<b>-7.7°*</b>	<b>1.2°</b>	<b>-10.2°</b>	<b>-5.3°</b>	<b>&lt;.001</b>
25°	<b>-17.4°</b>	<b>1.2°</b>	<b>-19.8°</b>	<b>-14.9°</b>	<b>-8.9°*</b>	<b>1.3°</b>	<b>-11.4°</b>	<b>-6.3°</b>	<b>&lt;.001</b>
30°	<b>-19.2°</b>	<b>1.4°</b>	<b>-21.9°</b>	<b>-16.5°</b>	<b>-10.2°*</b>	<b>1.4°</b>	<b>-13.0°</b>	<b>-7.4°</b>	<b>&lt;.001</b>
35°	<b>-20.0°</b>	<b>1.6°</b>	<b>-23.1°</b>	<b>-16.8°</b>	<b>-11.5°*</b>	<b>1.6°</b>	<b>-14.7°</b>	<b>-8.2°</b>	<b>&lt;.001</b>

“\*” and bold font Indicate statistical significance at a p-value of 0.05.

Table 73 Scapho-capitate radial angulation with the wrist ulnar to radial deviation

Wrist angle from ulnar to radial deviation (degrees)	Normal				SLI				p- value
	Mean	Std. Error	Lower CI	Upper CI	Mean	Std. Error	Lower CI	Upper CI	
-35°	-12.2°	1.0°	-14.1°	-10.3°	-11.7°	1.2°	-14.1°	-9.3°	0.774
-30°	-10.7°	0.9°	-12.5°	-8.9°	-11.0°	1.0°	-13.0°	-9.0°	0.851
-25°	-9.7°	0.9°	-11.4°	-8.1°	-10.1°	0.9°	-11.9°	-8.4°	0.745
-20°	-8.5°	0.8°	-10.1°	-6.8°	-8.3°	0.9°	-10.0°	-6.7°	0.913
-15°	-7.0°	0.8°	-8.7°	-5.4°	-6.3°	0.8°	-8.0°	-4.6°	0.528
-10°	-5.5°	0.8°	-7.2°	-3.8°	-4.2°	0.8°	-5.9°	-2.6°	0.293
-5°	-3.0°	0.8°	-4.7°	-1.3°	-2.1°	0.8°	-3.7°	-0.4°	0.44
0°	0.0°	0.8°	-1.7°	1.7°	0.0°	0.8°	-1.7°	1.7°	1
5°	3.1°	0.8°	1.5°	4.8°	1.9°	0.8°	0.3°	3.6°	0.317
<b>10°</b>	<b>6.6°</b>	<b>0.8°</b>	<b>5.0°</b>	<b>8.3°</b>	<b>3.8°*</b>	<b>0.9°</b>	<b>2.2°</b>	<b>5.5°</b>	<b>0.022</b>
<b>15°</b>	<b>10.3°</b>	<b>0.8°</b>	<b>8.6°</b>	<b>11.9°</b>	<b>5.9°*</b>	<b>0.9°</b>	<b>4.1°</b>	<b>7.6°</b>	<b>&lt;.001</b>
<b>20°</b>	<b>14.1°</b>	<b>0.9°</b>	<b>12.4°</b>	<b>15.7°</b>	<b>7.9°*</b>	<b>0.9°</b>	<b>6.2°</b>	<b>9.7°</b>	<b>&lt;.001</b>
<b>25°</b>	<b>18.0°</b>	<b>0.9°</b>	<b>16.2°</b>	<b>19.7°</b>	<b>9.7°*</b>	<b>0.9°</b>	<b>7.9°</b>	<b>11.6°</b>	<b>&lt;.001</b>
<b>30°</b>	<b>20.7°</b>	<b>1.0°</b>	<b>18.8°</b>	<b>22.6°</b>	<b>11.9°*</b>	<b>1.0°</b>	<b>9.9°</b>	<b>13.9°</b>	<b>&lt;.001</b>
<b>35°</b>	<b>23.8°</b>	<b>1.1°</b>	<b>21.6°</b>	<b>26.0°</b>	<b>14.9°*</b>	<b>1.1°</b>	<b>12.6°</b>	<b>17.1°</b>	<b>&lt;.001</b>

“\*” and bold font Indicate statistical significance at a p-value of 0.05.

Table 74 Scapho-capitate internal rotation with the wrist ulnar to radial deviation

Wrist angle from ulnar to radial deviation (degrees)	Normal				SLI				p- value
	Mean	Std. Error	Lower CI	Upper CI	Mean	Std. Error	Lower CI	Upper CI	
-35°	-3.4°	0.8°	-5.0°	-1.8°	-6.0°	1.1°	-8.0°	-3.9°	0.059
-30°	-3.1°	0.7°	-4.5°	-1.6°	-5.0°	0.8°	-6.6°	-3.3°	0.092
-25°	-2.8°	0.7°	-4.1°	-1.4°	-4.0°	0.7°	-5.5°	-2.6°	0.199
-20°	-2.3°	0.7°	-3.6°	-1.0°	-3.1°	0.7°	-4.5°	-1.8°	0.384
-15°	-1.9°	0.7°	-3.2°	-0.6°	-2.4°	0.7°	-3.7°	-1.0°	0.626
-10°	-1.4°	0.7°	-2.7°	-0.1°	-1.6°	0.7°	-2.9°	-0.3°	0.846
-5°	-0.7°	0.7°	-2.0°	0.7°	-0.9°	0.7°	-2.2°	0.4°	0.799
0°	0.0°	0.7°	-1.3°	1.3°	0.0°	0.7°	-1.3°	1.3°	1
5°	0.1°	0.7°	-1.2°	1.4°	0.3°	0.7°	-1.0°	1.6°	0.822
10°	0.6°	0.7°	-0.8°	1.9°	0.7°	0.7°	-0.7°	2.0°	0.925
15°	1.0°	0.7°	-0.4°	2.3°	0.6°	0.7°	-0.8°	2.0°	0.732
20°	0.8°	0.7°	-0.6°	2.1°	0.6°	0.7°	-0.8°	2.0°	0.855
25°	0.3°	0.7°	-1.1°	1.7°	0.8°	0.8°	-0.7°	2.2°	0.688
<b>30°</b>	<b>-1.6°</b>	<b>0.8°</b>	<b>-3.2°</b>	<b>0.0°</b>	<b>1.1°*</b>	<b>0.8°</b>	<b>-0.6°</b>	<b>2.8°</b>	<b>0.02</b>
<b>35°</b>	<b>-1.9°</b>	<b>1.0°</b>	<b>-3.8°</b>	<b>-0.1°</b>	<b>1.6°*</b>	<b>1.0°</b>	<b>-0.3°</b>	<b>3.6°</b>	<b>0.009</b>

“\*” and bold font Indicate statistical significance at a p-value of 0.05.

Table 75 Luno-capitate flexion with the wrist ulnar to radial deviation

Wrist angle from ulnar to radial deviation (degrees)	Normal				SLI				<i>p</i> - value
	Mean	Std. Error	Lower CI	Upper CI	Mean	Std. Error	Lower CI	Upper CI	
-35°	25.5°	1.7°	22.1°	28.9°	15.1°*	2.2°	10.8°	19.4°	<.001
-30°	23.0°	1.6°	19.8°	26.1°	13.2°*	1.8°	9.7°	16.7°	<.001
-25°	20.2°	1.5°	17.3°	23.1°	12.6°*	1.6°	9.5°	15.6°	<.001
-20°	17.1°	1.5°	14.2°	20.0°	10.1°*	1.5°	7.2°	13.0°	<.001
-15°	13.6°	1.5°	10.8°	16.5°	7.9°*	1.5°	5.0°	10.8°	<b>0.006</b>
-10°	8.8°	1.5°	5.9°	11.6°	5.5°	1.5°	2.7°	8.4°	0.120
-5°	4.3°	1.5°	1.4°	7.2°	2.9°	1.5°	0.0°	5.8°	0.497
0°	0.0°	1.5°	-2.9°	2.9°	0.0°	1.5°	-2.9°	2.9°	1.000
5°	-4.2°	1.5°	-7.0°	-1.3°	-2.4°	1.5°	-5.3°	0.5°	0.391
10°	-7.9°	1.5°	-10.8°	-5.0°	-4.9°	1.5°	-7.8°	-2.0°	0.150
15°	-10.6°	1.5°	-13.5°	-7.8°	-7.5°	1.5°	-10.5°	-4.6°	0.143
20°	-13.3°	1.5°	-16.2°	-10.4°	-9.3°	1.5°	-12.4°	-6.3°	0.066
25°	-15.5°	1.5°	-18.6°	-12.5°	-10.8°	1.6°	-14.0°	-7.7°	0.036
30°	-16.0°	1.7°	-19.4°	-12.7°	-12.1°	1.8°	-15.5°	-8.6°	0.108
35°	-15.6°	2.0°	-19.5°	-11.7°	-13.5°	2.0°	-17.5°	-9.5°	0.455

“\*” and bold font Indicate statistical significance at a *p*-value of 0.05.



Table 76 Luno-capitate radial angulation with the wrist ulnar to radial deviation

Wrist angle from ulnar to radial deviation (degrees)	Normal				SLI				<i>P- value</i>
	Mean	Std. Error	Lower CI	Upper CI	Mean	Std. Error	Lower CI	Upper CI	
-35°	-13.8°	0.8°	-15.3°	-12.2°	-14.3°	1.0°	-16.3°	-12.2°	0.690
-30°	-11.9°	0.7°	-13.3°	-10.5°	-13.2°	0.8°	-14.8°	-11.6°	0.216
-25°	-10.4°	0.7°	-11.7°	-9.1°	-11.3°	0.7°	-12.7°	-10.0°	0.315
-20°	-8.8°	0.6°	-10.1°	-7.5°	-9.8°	0.7°	-11.1°	-8.5°	0.260
-15°	-6.9°	0.6°	-8.1°	-5.6°	-7.9°	0.6°	-9.2°	-6.7°	0.254
-10°	-4.7°	0.6°	-6.0°	-3.5°	-5.6°	0.6°	-6.9°	-4.3°	0.333
-5°	-2.4°	0.6°	-3.7°	-1.2°	-3.0°	0.6°	-4.2°	-1.7°	0.555
0°	0.0°	0.6°	-1.3°	1.3°	0.0°	0.6°	-1.3°	1.3°	1.000
5°	3.1°	0.6°	1.9°	4.4°	3.7°	0.6°	2.5°	5.0°	0.492
10°	6.7°	0.6°	5.5°	8.0°	7.7°	0.7°	6.4°	9.0°	0.278
15°	10.8°	0.6°	9.5°	12.1°	11.6°	0.7°	10.3°	12.9°	0.415
20°	15.1°	0.7°	13.8°	16.3°	15.6°	0.7°	14.2°	16.9°	0.587
25°	19.2°	0.7°	17.9°	20.6°	19.2°	0.7°	17.7°	20.6°	0.964
30°	22.3°	0.8°	20.8°	23.8°	22.6°	0.8°	21.0°	24.2°	0.778
35°	26.1°	0.9°	24.3°	27.9°	25.8°	1.0°	23.9°	27.6°	0.812

“\*” and bold font Indicate statistical significance at a p-value of 0.05.

Table 77 Luno-capitate internal rotation with the wrist ulnar to radial deviation

Wrist angle from ulnar to radial deviation (degrees)	Normal				SL				<i>p</i> value
	Mean	Std. Error	Lower CI	Upper CI	Mean	Std. Error	Lower CI	Upper CI	
-35°	-6.2°	1.0°	-8.0°	-4.3°	-7.4°	1.2°	-9.8°	-5.0°	0.418
-30°	-5.0°	0.9°	-6.8°	-3.3°	-6.4°	1.0°	-8.3°	-4.4°	0.323
-25°	-4.4°	0.8°	-6.1°	-2.7°	-5.3°	0.9°	-7.1°	-3.6°	0.453
-20°	-4.0°	0.8°	-5.6°	-2.3°	-4.0°	0.8°	-5.7°	-2.4°	0.970
-15°	-3.4°	0.8°	-5.1°	-1.8°	-3.0°	0.8°	-4.7°	-1.4°	0.732
-10°	-2.5°	0.8°	-4.2°	-0.9°	-2.0°	0.8°	-3.6°	-0.3°	0.628
-5°	-1.2°	0.8°	-2.9°	0.4°	-1.0°	0.8°	-2.7°	0.6°	0.866
0°	0.0°	0.8°	-1.6°	1.6°	0.0°	0.8°	-1.6°	1.6°	1.000
5°	0.1°	0.8°	-1.5°	1.8°	0.6°	0.8°	-1.0°	2.2°	0.699
10°	0.3°	0.8°	-1.3°	2.0°	1.1°	0.8°	-0.6°	2.7°	0.535
15°	0.2°	0.8°	-1.5°	1.8°	1.4°	0.9°	-0.3°	3.1°	0.305
20°	-0.3°	0.8°	-1.9°	1.4°	1.6°	0.9°	-0.1°	3.3°	0.122
<b>25°</b>	<b>-1.2°</b>	<b>0.9°</b>	<b>-3.0°</b>	<b>0.5°</b>	<b>1.6°*</b>	<b>0.9°</b>	<b>-0.2°</b>	<b>3.4°</b>	<b>0.024</b>
<b>30°</b>	<b>-3.9°</b>	<b>1.0°</b>	<b>-5.8°</b>	<b>-2.0°</b>	<b>1.3°*</b>	<b>1.0°</b>	<b>-0.6°</b>	<b>3.3°</b>	<b>&lt;.001</b>
<b>35°</b>	<b>-4.8°</b>	<b>1.1°</b>	<b>-7.0°</b>	<b>-2.6°</b>	<b>0.5°*</b>	<b>1.1°</b>	<b>-1.7°</b>	<b>2.7°</b>	<b>&lt;.001</b>

“\*” and bold font Indicate statistical significance at a *p*-value of 0.05.

### **3.5.5. Important outcome measures-Midcarpal kinematics**

#### **Wrist extension to flexion**

There were no significant changes in the midcarpal flexion between the SLI and the normal scaphoid, when the wrist was in mid-range between 40° extension 35° flexion. During wrist 70° to 40° extension there was less midcarpal flexion in the SLI scaphoid. During 35° flexion to 50° flexion there was more midcarpal flexion in the SLI scaphoid. During wrist 70°extension to 45° extension there was less midcarpal radial angulation in the SLI scaphoid than the normal. No significant changes were observed in the axial plane.

During wrist 70°extension to 30° extension there was more midcarpal flexion of the SLI lunate than the normal. There was more midcarpal internal rotation of the SLI lunate when the wrist was extended more than 50°. There was less midcarpal internal rotation of the SLI lunate when the wrist was flexed more than 50°.

#### **Wrist ulnar to radial deviation**

When the wrist was ulnar deviated more than 10° or radially deviated beyond 10° there was less midcarpal flexion of the SLI scaphoid compared to the normal. There was less midcarpal radial angulation of the SLI scaphoid when the wrist was radially deviated beyond 10°.

There was less midcarpal flexion of the SLI lunate than the normal when the wrist was moving from 35° to 15° of ulnar deviation. No significant changes were observed in other planes.

## 3.6. HELICAL AXIS OF MOTION

### 3.6.1. Orientation of the helical axis

The results of the orientation of the helical axis of motion (HAM) are described in the sagittal, coronal, and axial planes according to the right-hand rule. The counterclockwise rotation measured from the positive horizontal axis remains positive up to  $180^\circ$  and the clockwise rotation from the horizontal axis remains negative (Figure 116). The mean HAM expressed as a 3D vector and the variability around it is included in the Appendix 1.5.

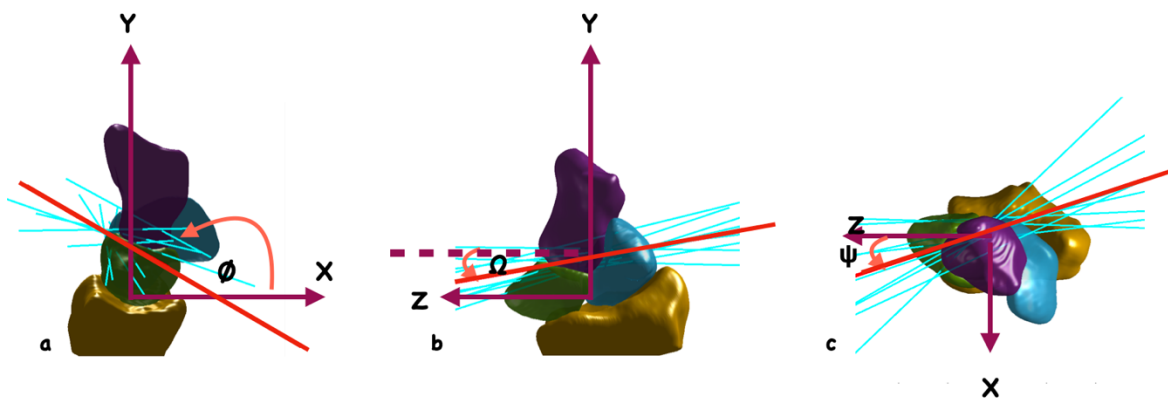


Figure 116 The orientation of the helical axis of motion (HAM) in the sagittal (a), coronal (b) and axial (c) planes. The Positive angle is indicated by the direction of the curved arrow; The counterclockwise angle formed from the positive horizontal axis remains positive up to  $180^\circ$ . The axes of the radius coordinate system are labelled as x, y and z. The dotted line in 'b' is a line parallel to the z-axis of the radius coordinate system.  $\phi$ : angle of the HAM in the sagittal plane, measured from the x-axis.  $\Omega$ : angle of the HAM in the coronal plane, measured from the z-axis.  $\psi$ : angle of the HAM in the axial plane, measured from the z-axis.

In Figure 117 to Figure 120, the results of the orientation of the HAM are presented as follows; The wrist position (also referred to as a 'bin') is presented in  $10^\circ$  increments, from wrist ulnar deviation ( $-20^\circ$ ) to radial deviation ( $+20^\circ$ ). The curved arrow indicates the direction of the wrist motion. The HAM for each wrist position is calculated as a 3-dimensional vector and presented in the three anatomical projections. The scaphoid HAM is represented by blue lines and the lunate HAM is represented by green lines. The mean HAM for each wrist position is reported adjacent to the axis. The mean and median angles

presented in the table were calculated as a circular mean and circular median of all the individual axes in each bin.

In the tables (Table 78 to Table 103) the results of the orientation of the HAM are presented as follows; The reference bin (R) indicates the starting wrist position. For example, 20° ulnar deviation in the first row of table 65 is the reference bin(R) and hence represents the starting wrist position. The comparison bin (C) indicates the subsequent wrist position which is being compared to the reference. The ‘number’ represents the instances being considered in each bin. For each reference (R) and the comparison (C) bin, the mean orientation of the HAM in the given anatomical plane is presented. Since the statistical significance was determined using nonparametric tests, given the sample size of less than 20 and the non-normal distribution of the sample, the median angle for each bin is also provided, along with the p-value. A complete statistical analysis, including an assessment of circular normality of the data, is presented in Appendix 1.4.

### 3.6.1.1. Normal Scaphoid with wrist ulnar to radial deviation

The orientation of the HAM of the normal scaphoid in the 3 anatomical planes is presented in the Figure 117. The orientation of the HAM of the normal scaphoid changed with incremental wrist motions from ulnar to radial deviation in sagittal, coronal and axial planes (Table 78 to Table 80). The change was seen as a sequential increase or decrease of the angle that the HAM formed in the respective plane (Figure 117). The statistically significant changes occurred at distinct wrist positions, in the axial plane.

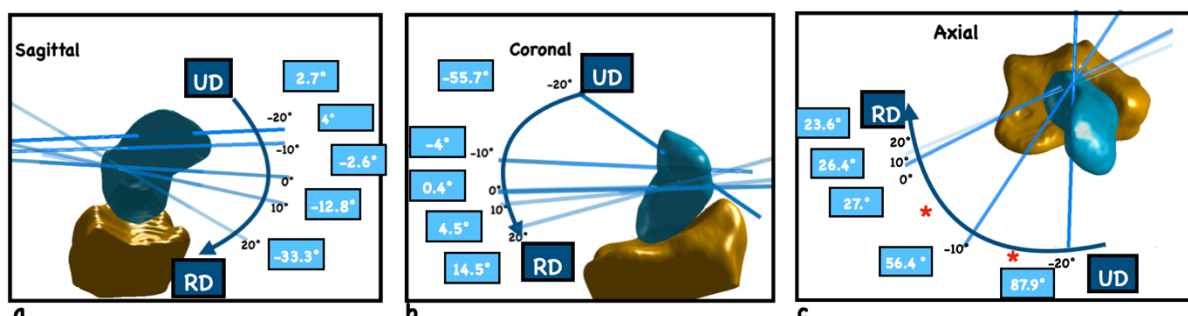
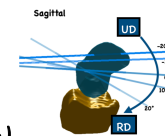


Figure 117 The orientation of the helical axis of motion (HAM) of the normal scaphoid changed sequentially with incremental wrist motions from ulnar to radial deviation in (a)sagittal, (b)coronal, and (c)axial planes. The

straight blue lines represent the mean axis of rotation at each wrist position. The wrist ulnar to radial deviation is represented by wrist positions at 10° intervals from -20° ulnar deviation to 20° radial deviation. The angle that the HAM forms in the corresponding plane is also mentioned in the blue text box. The significant changes in the orientation of HAM occurred between 20° ulnar deviation and 10° ulnar deviation, and then, between 10° ulnar deviation and the neutral position, in the axial plane. “\*” indicates statistical significance at *p* value of 0.05. The curved arrow indicates the direction of wrist ulnar to radial deviation.

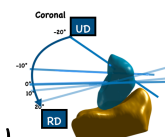


### Orientation of the helical axis of the normal scaphoid (sagittal plane)

Table 78 The orientation of the mean helical axis of motion of the normal scaphoid in the sagittal plane during wrist ulnar to radial deviation.

Reference bin (R)	Comparison bin (C)	Number		Mean angle (R)	Mean angle (C)	Median angle (R)	Median angle (C)	<i>p</i> value
		R	C					
20 ° UD	10° UD	22	24	2.7°	4°	3.2°	4.8°	0.555
10° UD	0° (Neutral)	24	29	4°	-2.6°	4.8°	0.3°	0.126
0° (Neutral)	10° RD	29	27	-2.6°	-12.8°	0.3°	-7.2°	0.181
10° RD	20° RD	27	19	-12.8°	-33.3°	-7.2°	-19.6°	0.134

The orientation of the helical axis of motion (HAM) of the scaphoid in the sagittal plane changed sequentially from positive to negative direction, as the wrist moved from ulnar to radial deviation. Note that the positive angles are the counterclockwise angle from the positive x-axis according to the right-hand rule; negative angles are the clockwise angle from the positive x-axis. The angular difference between -ve 180° and +ve 180° is “zero”. The curved arrow in the image is only to indicate the direction of wrist motion from ulnar to radial deviation.



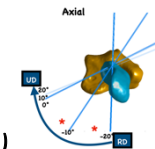
### Orientation of the helical axis of the normal scaphoid (coronal plane)

Table 79 The orientation of the helical axis of motion of the normal scaphoid in the coronal plane during wrist ulnar to radial deviation.

Reference bin (R)	Comparison bin (C)	Number		Mean angle (R)	Mean angle (C)	Median angle (R)	Median angle (C)	<i>p</i> value
		R	C					
20 ° UD	10° UD	22	24	-55.7°	-4.0°	-27.3°	-7.2°	0.238
10° UD	0° (Neutral)	24	29	-4.0°	0.4°	-7.2°	-0.2°	0.075

0° (Neutral)	10° RD	29	27	0.4°	4.5°	-0.2°	2.6°	0.181
10° RD	20° RD	27	19	4.5°	14.5°	2.6°	13.2°	0.134

*Note: The orientation of the helical axis of motion (HAM) of the scaphoid in the coronal plane changed sequentially from a negative to positive direction, as the wrist moved from ulnar to radial deviation. Note that the positive angles are the counterclockwise angle from the positive z-axis according to the right-hand rule; negative angles are the clockwise angle from the positive z-axis. Therefore, the angular difference between -ve 180° and +ve 180° is “zero”.*



### **Orientation of the helical axis of the normal scaphoid (axial plane)**

*Table 80 The orientation of the helical axis of motion of the normal scaphoid in the axial plane during wrist ulnar to radial deviation.*

Reference bin (R)	Comparison bin (C)	Number		Mean angle (R)	Mean angle (C)	Median angle (R)	Median angle (C)	p value
		R	C					
20° UD	10° UD	22	24	87.9°	56.4°	84.6°	52.9°	0.018*
10° UD	0° (Neutral)	24	29	56.4°	27.0°	52.9°	24.5°	<0.001*
0° (Neutral)	10° RD	29	27	27.0°	26.4°	24.5°	20.6°	0.789
10° RD	20° RD	27	19	26.4°	23.6°	20.6°	18.9°	0.765

*Note: The orientation of the helical axis of motion (HAM) of the scaphoid in the axial plane changed sequentially, as the wrist moved from ulnar to radial deviation. Statistically significant changes occurred as the wrist moved from the 20° ulnar deviation to 10° ulnar deviation, and then when the wrist was moving from 10° ulnar deviation and the neutral position. “\*” Indicates statistical significance at 0.05. Note that the positive angles are the counterclockwise angle from the positive - axis according to the right-hand rule; negative angles are the clockwise angle from the positive z-axis.*

#### **3.6.1.2. Normal lunate with wrist ulnar to radial deviation**

The orientation of the HAM of the normal lunate in the 3 anatomical planes is presented in Figure 118. The orientation HAM of the normal lunate changed sequentially with incremental wrist motions from ulnar to radial deviation in sagittal, coronal and axial planes (Table 81 to Table 83). Statistically significant changes occurred at distinct wrist positions in all three planes.

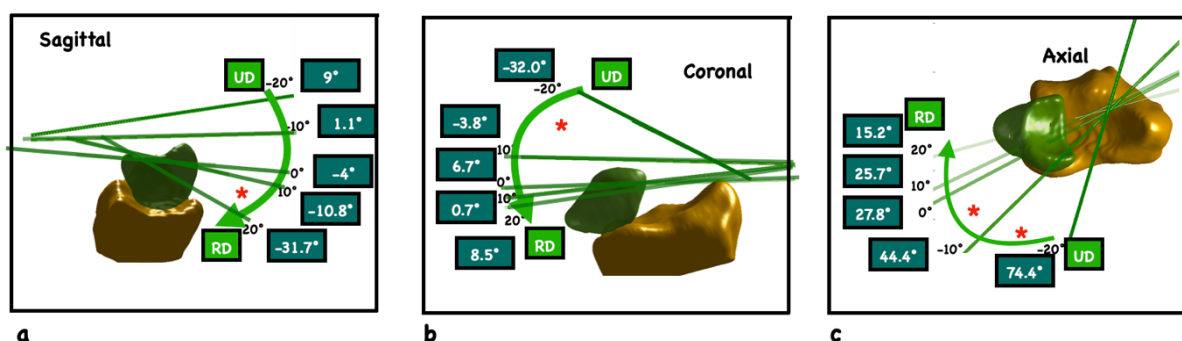


Figure 118 The orientation of the helical axis of motion (HAM) of the normal lunate changed sequentially with incremental wrist motion from ulnar to radial deviation in sagittal, coronal, and axial planes. The straight green lines represent the axis of rotation at corresponding wrist position indicated by the numbers next to them. Wrist ulnar to radial deviation is represented by wrist positions at 10° intervals from -20° ulnar deviation to 20° radial deviation. The significant changes from one position to another occurred in all three planes. “\*” indicates statistical significance at *p* value of 0.05. The curved arrow is only to indicate the direction of wrist ulnar to radial deviation.

#### Orientation of the helical axis of the normal lunate (sagittal plane)

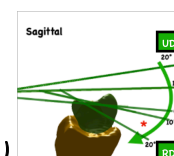
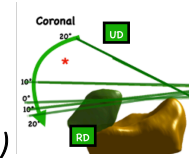


Table 81 The orientation of the helical axis of motion of the normal lunate in the sagittal plane during wrist ulnar to radial deviation.

Reference bin (R)	Comparison bin (C)	Number		Mean angle (R)	Mean angle (C)	Median angle (R)	Median angle (C)	<i>p</i> value
		R	C					
20° UD	10° UD	22	26	9°	1.1°	9.3°	0.5°	0.247
10° UD	0° (Neutral)	26	28	1.1°	-10.8°	0.5°	-10.6°	0.276
0° (Neutral)	10° RD	28	23	-10.8°	-4°	-10.6°	-2.6°	0.473
10° RD	20° RD	23	14	-4°	-31.7°	-2.6°	-35.0°	0.031*

Note: The orientation of the helical axis of motion (HAM) of the normal lunate in the sagittal plane decreased sequentially from positive to negative, as the wrist moved from ulnar to radial deviation. Statistically significant changes occurred as the wrist moved from the 10° radial deviation to 20° radial deviation. “\*” Indicates statistical significance at 0.05.



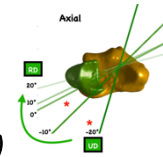


### Orientation of the helical axis of the normal lunate (coronal plane)

Table 82 The orientation of the helical axis of motion of the normal lunate in the coronal plane during wrist ulnar to radial deviation.

Reference bin (R)	Comparison bin (C)	Number		Mean angle (R)	Mean angle (C)	Median angle (R)	Median angle (C)	p value
		R	C					
20° UD	10° UD	22	26	-32.0°	-3.8°	-21.7°	-0.4°	0.001*
10° UD	0° (Neutral)	26	28	-3.8°	6.7°	-0.4°	4.2°	0.586
0° (Neutral)	10° RD	28	23	6.7°	0.7°	4.2°	1.3°	0.331
10° RD	20° RD	23	14	0.7°	8.5°	1.3°	10.7°	0.219

Note: The orientation of the helical axis of motion (HAM) of the normal lunate in the coronal plane increased sequentially from negative to positive, as the wrist moved from ulnar to radial deviation. Statistically significant changes occurred as the wrist moved from the 20° ulnar deviation to 10° ulnar deviation. \* Indicates statistical significance at 0.05



### Orientation of the helical axis of the normal lunate (axial plane)

Table 83 The orientation of the helical axis of motion of the lunate in the axial plane during wrist ulnar to radial deviation.

Reference bin (R)	Comparison bin (C)	Number		Mean angle (R)	Mean angle (C)	Median angle (R)	Median angle (C)	p value
		R	C					
20° UD	10° UD	22	26	74.4°	44.4°	69.4°	39.8°	0.001*
10° UD	0° (Neutral)	26	28	44.4°	27.8°	39.8°	26.3°	0.001*
0° (Neutral)	10° RD	28	23	27.8°	25.7°	26.3°	21.8°	0.331
10° RD	20° RD	23	14	25.7°	15.2°	21.8°	16.0°	0.420

Note: The orientation of the helical axis of motion (HAM) of the normal lunate in the axial plane decreased sequentially, as the wrist moved from ulnar to radial deviation. Statistically significant changes occurred as the wrist moved from the 20° ulnar deviation to 10° ulnar deviation, and then from 10° ulnar deviation to the neutral position. \* Indicates statistical significance at 0.05.

### 3.6.1.3. SLI Scaphoid with wrist ulnar to radial deviation

#### Orientation of the helical axis the SLI scaphoid

The orientation of the HAM of the SLI scaphoid in the 3 anatomical planes is presented in Figure 119. The orientation of the HAM of the SLI scaphoid was similar with the incremental wrist motions from ulnar to radial deviation in sagittal, coronal and axial planes (Table 84 to Table 86). There were no statistically significant changes between the wrist positions in any of the planes.

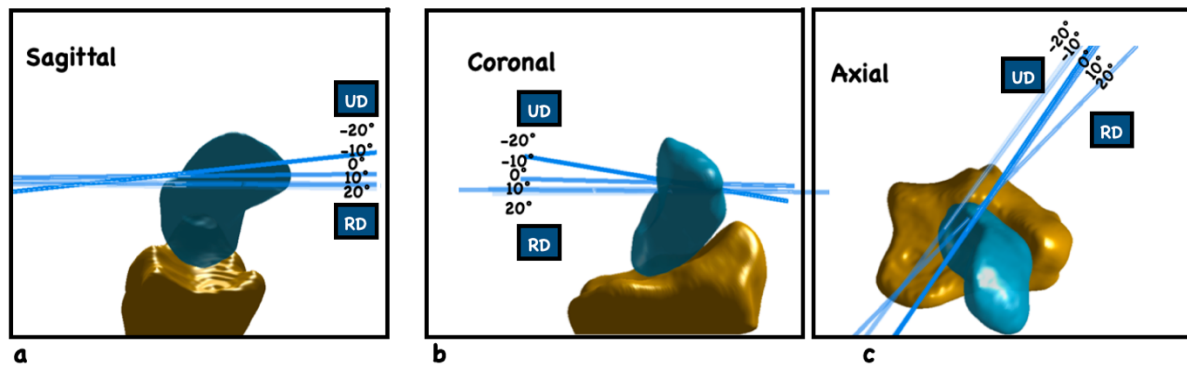
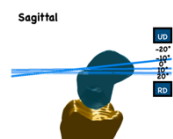


Figure 119 The orientation of the helical axis of motion (HAM) of the SLI scaphoid was similar between the incremental wrist positions from ulnar to radial deviation in sagittal, coronal, and axial planes. Angles indicated are the wrist positions from ulnar to radial deviation. (Comparison with Figure 117)

Table 84 The orientation of the helical axis of motion of the SLI scaphoid in the sagittal plane during wrist ulnar to radial deviation.



Reference bin (R)	Comparison bin (C)	Number		Mean angle (R)	Mean angle (C)	Median angle (R)	Median angle (C)	p value
		R	C					
20 ° UD	10° UD	14	18	12.9°	3.7°	12.1°	1.3°	0.154
10° UD	0° (Neutral)	18	25	3.7°	359.6°	1.3°	2.8°	0.455
0° (Neutral)	10° RD	25	20	-0.4°	-2.0°	2.8°	2.0°	0.894
10° RD	20° RD	20	15	-2.0°	-4.6°	2.0°	-1.5°	0.625

Note: The orientation of the helical axis of motion (HAM) of the SLI scaphoid in the sagittal plane did not change significantly, as the wrist moved from ulnar to radial deviation.

### Orientation of the helical axis the SLI scaphoid (coronal plane)

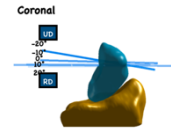


Table 85 The orientation of the helical axis of motion of the SLI scaphoid in the coronal plane during wrist ulnar to radial deviation.

Reference bin (R)	Comparison bin (C)	Number		Mean angle (R)	Mean angle (C)	Median angle (R)	Median angle (C)	p value
		R	C					
20° UD	10° UD	14	18	-5.0°	1.4°	-9.2°	-2.5°	0.154
10° UD	0° (Neutral)	18	25	1.4°	0.1°	-2.5°	-4.7°	0.625
0° (Neutral)	10° RD	25	20	0.1°	-9.7°	-4.7°	-1.9°	0.641
10° RD	20° RD	20	15	-9.7°	-5.7°	-1.9°	2.0°	0.845

Note: The orientation of the helical axis of motion (HAM) of the SLI scaphoid in the coronal plane did not change significantly, as the wrist moved from ulnar to radial deviation.

### Orientation of the helical axis of the SLI scaphoid (axial plane)

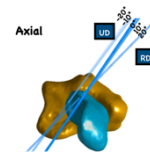


Table 86 The orientation of the helical axis of motion of the SLI scaphoid in the axial plane during wrist ulnar to radial deviation.

Reference bin (R)	Comparison bin (C)	Number		Mean angle (R)	Mean angle (C)	Median angle (R)	Median angle (C)	p value
		R	C					
20° UD	10° UD	14	18	56.4°	54.8°	47.3°	58.1°	0.879
10° UD	0° (Neutral)	18	25	54.8°	45.7°	58.1°	51.6°	0.625
0° (Neutral)	10° RD	25	20	45.7°	53.1°	51.6°	58.1°	0.286
10° RD	20° RD	20	15	53.1°	54.5°	58.1°	59.8°	0.380

Note: The orientation of the helical axis of motion (HAM) of the SLI scaphoid in the axial plane did not change significantly, as the wrist moved from ulnar to radial deviation.

#### 3.6.1.4. SLI lunate with wrist ulnar to radial deviation

The orientation of the HAM of the SLI lunate in the 3 anatomical planes is presented in the Figure 120. The orientation of the HAM of the SLI lunate did change with the incremental wrist positions from ulnar to radial deviation, with statistically significant changes occurring in all three anatomic planes. The changes however were not sequential with the incremental wrist positions in sagittal and coronal planes (Table 87 to Table 89). Sequential change in the angle of HAM was observed only in the axial plane.

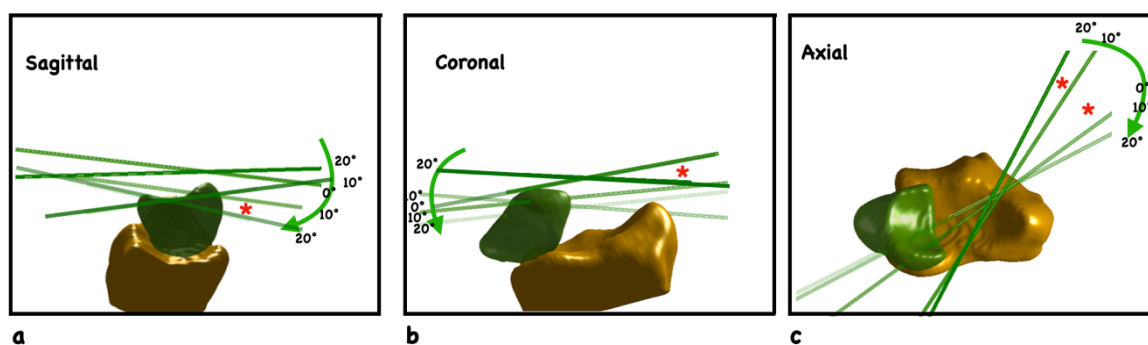
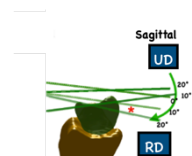


Figure 120 The orientation of the helical axis of motion (HAM) of the SLI lunate did change with the incremental wrist motions from ulnar to radial deviation in sagittal, coronal, and axial planes, but not similar to the normal lunate. Angles indicated are the wrist positions from ulnar to radial deviation. (comparison with Figure 118)

### Orientation of the helical axis of the SLI lunate (sagittal plane)

Table 87 The orientation of the helical axis of motion of the SLI lunate in the sagittal plane during wrist ulnar to radial deviation.



Reference bin (R)	Comparison bin (C)	Number		Mean angle R	Mean angle C	Median angle R	Median angle C	p value
		R	C					
20° UD	10° UD	13	20	2.8°	-6.5°	1.3°	-8.8°	0.019*
10° UD	0° (Neutral)	20	18	-6.5°	-9.1°	-8.8°	-7.9°	1.000
0° (Neutral)	10° RD	18	11	-9.1°	-0.7°	-7.9°	6.6°	0.077
10° RD	20° RD	11	9	-0.7°	-14.7°	6.6°	-11.9°	0.178

Note: The orientation of the helical axis of motion (HAM) of the SLI lunate in the sagittal plane changed, as the wrist moved from ulnar to radial deviation. A sequential pattern of increment or decrement of angles was not evident. Statistically significant changes occur as the wrist moved from the 20° ulnar deviation to 10° ulnar deviation. \* Indicates statistical significance at 0.05.

### Orientation of the helical axis of the SLI lunate (coronal plane)

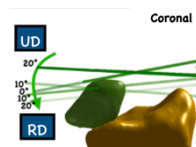


Table 88 The orientation of the helical axis of motion of the SLI lunate in the coronal plane during wrist ulnar to radial deviation.

Reference bin (R)	Comparison bin (C)	Number		Mean angle R	Mean angle C	Median angle R	Median angle C	p value
		R	C					
20 ° UD	10° UD	13	20	-15.1°	10.2°	-4.4°	14.2°	0.101
10° UD	0° (Neutral)	20	18	10.2°	4.4°	14.2°	5.8°	0.516
0° (Neutral)	10° RD	18	11	4.4°	-4.5°	5.8°	-3.2°	0.039*
10° RD	20° RD	11	9	-4.5°	5.3°	-3.2°	6.7°	0.178

Note: The orientation of the helical axis of motion (HAM) of the SLI lunate in the coronal plane changed, as the wrist moved from ulnar to radial deviation. A sequential pattern of increment or decrement of angles was not evident. Statistically significant changes occurred as the wrist moved from the neutral to 10° radial deviation. \* Indicates statistical significance at 0.05.

### Orientation of the helical axis of the SLI lunate (axial plane)

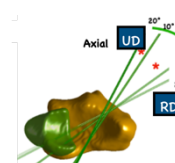


Table 89 The orientation of the helical axis of motion of the SLI lunate in the axial plane during wrist ulnar to radial deviation.

Reference bin (R)	Comparison bin (C)	Number		Mean angle R	Mean angle C	Median angle R	Median angle C	p value
		R	C					
20 ° UD	10° UD	13	20	62.6°	56.6°	60.9°	60.3°	0.829
10° UD	0° (Neutral)	20	18	56.6°	35.9°	60.3°	34.9°	0.001*
0° (Neutral)	10° RD	18	11	35.9°	27.7°	34.9°	28.7°	0.039*
10° RD	20° RD	11	9	27.7°	26.6°	28.7°	26.2°	0.653

Note: The orientation of the helical axis of motion (HAM) of the SLI lunate in the axial plane changed sequentially as the wrist moved from ulnar to radial deviation. The angles sequentially decreased with the wrist motion from ulnar to radial deviation. Statistically significant changes occurred as the wrist moved from 10° ulnar deviation to the neutral position, and then, the neutral position to 10° radial deviation. \* Indicates statistical significance at 0.05.

***The change in the orientation of the helical axis of motion from maximum ulnar deviation to maximum radial deviation***

The orientation of the HAM changed between the wrist positions. The change in the HAM orientation of the scaphoid between the maximum ulnar and maximum radial deviation of the wrist was computed (Table 90). Comparisons were made between the normal and SLI groups in each plane. The change in HAM orientation was significantly more in the normal scaphoid compared to the SLI scaphoid ( $p < 0.001$  for sagittal, coronal, and axial planes).

*Table 90 The change in the orientation of the helical axis of motion (HAM) from maximum ulnar deviation to maximum radial deviation between the normal and SLI scaphoid*

Plane	Normal				SLI				<i>p value</i>
	Mean	Std. Error	Lower CI	Upper CI	Mean	Std. Error	Lower CI	Upper CI	
<b>Sagittal</b>	-30.6°	10.1°	-51.0°	-10.2	8.3°*	9.6°	-11.4°	28.0°	<0.001
<b>Coronal</b>	-70.1°	18.3°	-107.1°	-33.1°	0.7°*	18.1°	-36.5°	37.9°	<0.001
<b>Axial</b>	64.3°	9.0°	46.1°	82.5°	1.8°*	12.9°	-24.7°	28.4°	<0.001

*Note that the change in HAM was significantly different between the normal and SLI wrists. The normal scaphoid had a larger arc of change in the HAM orientation through wrist ulnar to radial deviation. The SLI scaphoid HAM only changed less than 10° in any plane. “\*” indicate statistical significance at a  $p$  value < 0.05.*

Similarly, the change in HAM orientation from maximum ulnar to radial deviation, was significantly more in the normal lunate compared to the SLI lunate ( $p = 0.008$  for sagittal,  $p = 0.004$  for coronal, and  $p < 0.001$  for axial planes).

*Table 91 The change in the orientation of the helical axis of motion (HAM) from maximum ulnar deviation to maximum radial deviation between the normal and SLI lunate*

Plane	Normal				SLI				<i>p value</i>
	Mean	Std. Error	Lower CI	Upper CI	Mean	Std. Error	Lower CI	Upper CI	
<b>Sagittal</b>	-22.8°	11.3°	-45.7°	0.2°	-11.9°*	6.9°	-26.2°	2.4°	0.008*
<b>Coronal</b>	-40.5°	15.7°	-72.3°	-8.7°	-20.4°*	18.3°	-58.7°	17.8°	0.004*
<b>Axial</b>	59.2°	7.5°	44.0°	74.5°	36.0°*	8.7°	17.9°	54.2°	<0.001*

*Note that the change in HAM is significantly different between the normal and SLI wrists. “\*” indicate statistical significance at a  $p$  value < 0.05.*

### 3.6.1.5. Normal scaphoid with wrist extension to flexion

#### *Orientation of the helical axis of the normal scaphoid (sagittal plane)*

The orientation of the HAM of the normal scaphoid did not change significantly in the sagittal plane (Table 92) or the coronal plane (Table 93) during wrist extension to flexion. It was observed that in the axial plane, there was one significant change in the orientation of the HAM (Table 94) between 40° wrist flexion to 50° flexion.

*Table 92 The orientation of the helical axis of motion of the normal scaphoid in the sagittal plane with the wrist moving from extension to flexion.*

Reference bin (R)	Comparison bin (C)	Number		Mean angle (R)	Mean angle (C)	Median angle (R)	Median angle (C)	p value
		R	C					
70 ° Ext	60 ° Ext	4	9	100.5°	89.8°	101.5°	92.5°	0.853
60 ° Ext	50 ° Ext	9	15	89.8°	96.0°	92.5°	94.9°	0.673
50 ° Ext	40 ° Ext	15	13	96.0°	71.4°	94.9°	67.0°	0.256
40 ° Ext	30 ° Ext	13	13	71.4°	82.8°	67.0°	77.3°	0.695
30 ° Ext	20 ° Ext	13	17	82.8°	63.1°	77.3°	45.9°	0.269
20 ° Ext	10 ° Ext	17	14	63.1°	73.9°	45.9°	75.3°	0.576
10 ° Ext	0° (Neutral)	14	18	73.9°	89.1°	75.3°	77.2°	0.910
0° (Neutral)	10 ° Flex	18	11	89.1°	82.4°	77.2°	87.6°	0.316
10 ° Flex	20 ° Flex	11	17	82.4°	72.2°	87.6°	67.4°	0.699
20 ° Flex	30 ° Flex	17	7	72.2°	98.1°	67.4°	116.6°	0.653
30 ° Flex	40 ° Flex	7	12	98.1°	115.0°	116.6°	116.9°	0.764
40 ° Flex	50 ° Flex	12	5	115.0°	117.4°	116.9°	115.2°	0.707
50 ° Flex	60 ° Flex	5	9	117.4°	118.5°	115.2°	114.7°	0.577
60 ° Flex	70 ° Ext	9	5	118.5°	87.9°	114.7°	69.0°	0.577

*Note: The orientation of the helical axis of motion (HAM) of the normal scaphoid in the sagittal plane was not significantly different between wrist positions from extension to flexion.*

### Orientation of the helical axis of the normal scaphoid (coronal plane)

Table 93 The orientation of the helical axis of motion of the normal scaphoid in the coronal plane with the wrist moving from extension to flexion.

Reference bin (R)	Comparison bin (C)	Number		Mean angle (R)	Mean angle (C)	Median angle (R)	Median angle (C)	p value
		R	C					
70 ° Ext	60 ° Ext	4	9	-8.0°	6.8°	-8.0°	6.0°	0.308
60 ° Ext	50 ° Ext	9	15	6.8°	3.1°	6.0°	1.4°	0.673
50 ° Ext	40 ° Ext	15	13	3.1°	6.7°	1.4°	5.8°	0.705
40 ° Ext	30 ° Ext	13	13	6.7°	3.0°	5.8°	2.8°	0.695
30 ° Ext	20 ° Ext	13	17	3.0°	4.3°	2.8°	1.0°	0.713
20 ° Ext	10 ° Ext	17	14	4.3°	2.7°	1.0°	2.6°	0.576
10 ° Ext	0° (Neutral)	14	18	2.7°	6.5°	2.6°	3.3°	0.476
0° (Neutral)	10 ° Flex	18	11	6.5°	4.8°	3.3°	2.3°	0.597
10 ° Flex	20 ° Flex	11	17	4.8°	3.6°	2.3°	3.3°	0.246
20 ° Flex	30 ° Flex	17	7	3.6°	6.6°	3.3°	8.8°	0.178
30 ° Flex	40 ° Flex	7	12	6.6°	4.4°	8.8°	1.6°	0.210
40 ° Flex	50 ° Flex	12	5	4.4°	7.6°	1.6°	6.1°	0.149
50 ° Flex	60 ° Flex	5	9	7.6°	2.9°	6.1°	1.8°	0.094
60 ° Flex	70 ° Ext	9	5	2.9°	-5.6°	1.8°	4.1°	0.577

Note: The orientation of the helical axis of motion (HAM) of the normal scaphoid in the coronal plane was not significantly different between wrist positions from extension to flexion.



### Orientation of the helical axis of the normal scaphoid (axial plane)

Table 94 The orientation of the helical axis of motion of the normal scaphoid in the axial plane with the wrist moving from extension to flexion.

Reference bin (R)	Comparison bin (C)	Number		Mean angle (R)	Mean angle (C)	Median angle (R)	Median angle (C)	p value
		R	C					
70 ° Ext	60 ° Ext	4	9	-6.6°	-4.2°	-12.8°	-2.3°	0.164
60 ° Ext	50 ° Ext	9	15	-4.2°	3.7°	-2.3°	4.7°	0.206
50 ° Ext	40 ° Ext	15	13	3.7°	0.8°	4.7°	2.6°	0.705
40 ° Ext	30 ° Ext	13	13	0.8°	-0.4°	2.6°	-0.3°	0.695
30 ° Ext	20 ° Ext	13	17	-0.4°	0.8°	-0.3°	-0.4°	0.713
20 ° Ext	10 ° Ext	17	14	0.8°	-3.6°	-0.4°	-1.4°	0.376
10 ° Ext	0° (Neutral)	14	18	-3.6°	0.5°	-1.4°	-0.1°	0.918
0° (Neutral)	10 ° Flex	18	11	0.5°	-7.9°	-0.1°	-4.6°	0.597
10 ° Flex	20 ° Flex	11	17	-7.9°	-5.2°	-4.6°	-3.5°	0.699
20 ° Flex	30 ° Flex	17	7	-5.2°	-8.6°	-3.5°	-8.7°	0.653
30 ° Flex	40 ° Flex	7	12	-8.6°	-1.6°	-8.7°	-4.0°	0.515
40 ° Flex	50 ° Flex	12	5	-1.6°	-15.0°	-4.0°	-9.7°	0.005*
50 ° Flex	60 ° Flex	5	9	-15.0°	-8.6°	-9.7°	-10.4°	0.577
60 ° Flex	70 ° Ext	9	5	-8.6°	4.2°	-10.4°	0.1°	0.094

Note: The orientation of the helical axis of motion (HAM) of the normal scaphoid had a significant change when the wrist was moving from 40° to 50° flexion. “\*” Indicates statistical significance at 0.05.

### 3.6.1.6. Normal lunate with wrist extension to flexion

The orientation of the HAM of the normal lunate did not change significantly in sagittal, coronal, or axial planes during wrist extension to flexion (Table 95 to Table 97).

#### *Orientation of the helical axis of the normal lunate (sagittal plane)*

*Table 95 The orientation of the helical axis of motion of the normal lunate in the sagittal plane with the wrist moving from extension to flexion.*

Reference bin (R)	Comparison bin (C)	Number		Mean angle (R)	Mean angle (C)	Median angle (R)	Median angle (C)	p value
		R	C					
70 ° Ext	60 ° Ext	3	7	101.9°	57.3°	111.5°	59.3°	0.490
60 ° Ext	50 ° Ext	7	8	57.3°	92.3°	59.3°	78.5°	0.447
50 ° Ext	40 ° Ext	8	8	92.3°	75.7°	78.5°	67.9°	0.868
40 ° Ext	30 ° Ext	8	9	75.7°	73.1°	67.9°	71.3°	0.819
30 ° Ext	20 ° Ext	9	12	73.1°	95.6°	71.3°	76.4°	0.801
20 ° Ext	10 ° Ext	12	11	95.6°	64.5°	76.4°	66.8°	0.537
10 ° Ext	0° (Neutral)	11	18	64.5°	127.1°	66.8°	130.3°	0.039
0° (Neutral)	10 ° Flex	18	11	127.1°	86.5°	130.3°	89.1°	0.196
10 ° Flex	20 ° Flex	11	17	86.5°	85.6°	89.1°	73.7°	0.699
20 ° Flex	30 ° Flex	17	5	85.6°	77.4°	73.7°	84.3°	0.611
30 ° Flex	40 ° Flex	5	11	77.4°	93.4°	84.3°	100.2°	0.590
40 ° Flex	50 ° Flex	11	5	93.4°	107.1°	100.2°	105.1°	0.106
50 ° Flex	60 ° Flex	5	8	107.1°	102.6°	105.1°	99.6°	0.725
60 ° Flex	70 ° Ext	8	5	102.6°	47.7°	99.6°	48.9°	0.053

*Note: The orientation of the helical axis of motion (HAM) of the normal lunate did not change significantly in the sagittal plane with the wrist motion from extension to flexion.*

### Orientation of the helical axis of the normal lunate (coronal plane)

Table 96 The orientation of the helical axis of motion of the normal lunate in the coronal plane with the wrist moving from extension to flexion.

Reference bin (R)	Comparison bin (C)	Number		Mean angle (R)	Mean angle (C)	Median angle (R)	Median angle (C)	p value
		R	C					
70 ° Ext	60 ° Ext	3	7	37.9°	-11.3°	55.7°	3.2°	0.490
60 ° Ext	50 ° Ext	7	8	-11.3°	-11.9°	3.2°	-3.1°	0.782
50 ° Ext	40 ° Ext	8	8	-11.9°	15.3°	-3.1°	11.3°	1.000
40 ° Ext	30 ° Ext	8	9	15.3°	-15.6°	11.3°	1.0°	0.457
30 ° Ext	20 ° Ext	9	12	-15.6°	-6.0°	1.0°	-3.0°	0.801
20 ° Ext	10 ° Ext	12	11	-6.0°	-1.3°	-3.0°	4.3°	0.292
10 ° Ext	0° (Neutral)	11	18	-1.3°	9.8°	4.3°	8.0°	0.597
0° (Neutral)	10 ° Flex	18	11	9.8°	7.9°	8.0°	11.1°	0.812
10 ° Flex	20 ° Flex	11	17	7.9°	2.1°	11.1°	4.3°	0.246
20 ° Flex	30 ° Flex	17	5	2.1°	5.1°	4.3°	0.9°	0.611
30 ° Flex	40 ° Flex	5	11	5.1°	7.0°	0.9°	0.3°	0.590
40 ° Flex	50 ° Flex	11	5	7.0°	8.2°	0.3°	5.9°	0.590
50 ° Flex	60 ° Flex	5	8	8.2°	-11.6°	5.9°	-6.9°	0.135
60 ° Flex	70 ° Ext	8	5	-11.6°	-13.5°	-6.9°	-11.1°	0.725

Note: The orientation of the helical axis of motion (HAM) of the normal lunate did not change significantly in the coronal plane with the wrist motion.

### Orientation of the helical axis of the normal lunate (axial plane)

Table 97 The orientation of the helical axis of motion of the normal lunate in the axial plane with the wrist moving from extension to flexion.

Reference bin (R)	Comparison bin (C)	Number		Mean angle (R)	Mean angle (C)	Median angle (R)	Median angle (C)	p value
		R	C					
70 ° Ext	60 ° Ext	3	7	2.1°	-15.7°	12.5°	-2.0°	0.490
60 ° Ext	50 ° Ext	7	8	-15.7°	22.5°	-2.0°	24.0°	0.447
50 ° Ext	40 ° Ext	8	8	22.5°	14.0°	24.0°	11.8°	0.046
40 ° Ext	30 ° Ext	8	9	14.0°	-3.9°	11.8°	3.2°	0.457
30 ° Ext	20 ° Ext	9	12	-3.9°	-6.8°	3.2°	-5.2°	0.256
20 ° Ext	10 ° Ext	12	11	-6.8°	-6.2°	-5.2°	0.5°	0.292
10 ° Ext	0° (Neutral)	11	18	-6.2°	-9.1°	0.5°	-9.2°	0.316
0° (Neutral)	10 ° Flex	18	11	-9.1°	-6.5°	-9.2°	-3.8°	0.316
10 ° Flex	20 ° Flex	11	17	-6.5°	-16.2°	-3.8°	-13.4°	0.246
20 ° Flex	30 ° Flex	17	5	-16.2°	-7.2°	-13.4°	-10.9°	0.611
30 ° Flex	40 ° Flex	5	11	-7.2°	-18.1°	-10.9°	-31.8°	0.590
40 ° Flex	50 ° Flex	11	5	-18.1°	-19.9°	-31.8°	-16.4°	0.590
50 ° Flex	60 ° Flex	5	8	-19.9°	-12.9°	-16.4°	-9.6°	0.429
60 ° Flex	70 ° Ext	8	5	-12.9°	-20.3°	-9.6°	-12.5°	0.429

Note: The orientation of the helical axis of motion (HAM) of the normal lunate did not change significantly in the axial plane with the wrist motion.

### 3.6.1.7. SLI scaphoid with wrist extension to flexion

The orientation of the HAM of the SLI scaphoid did not change in the sagittal or the coronal planes during wrist motion from extension to flexion (Table 98, Table 99). In the axial plane, between the wrist positions of 60° to 50° extension (Table 100), there was a significant change in the orientation of the HAM of the SLI scaphoid.

#### *Orientation of the helical axis of the SLI scaphoid (sagittal plane)*

*Table 98 The orientation of the helical axis of motion of the SLI scaphoid in the sagittal plane with the wrist moving from extension to flexion.*

Reference bin (R)	Comparison bin (C)	Number		Mean angle (R)	Mean angle (C)	Median angle (R)	Median angle (C)	<i>p value</i>
		R	C					
60 ° Ext	50 ° Ext	7	8	52.9°	94.8°	56.1°	97.0°	0.072
50 ° Ext	40 ° Ext	8	15	94.8°	72.7°	97.0°	68.2°	0.110
40 ° Ext	30 ° Ext	15	13	72.7°	90.7°	68.2°	78.6°	0.705
30 ° Ext	20 ° Ext	13	18	90.7°	82.4°	78.6°	87.3°	0.605
20 ° Ext	10 ° Ext	18	20	82.4°	77.9°	87.3°	66.5°	0.516
10 ° Ext	0° (Neutral)	20	22	77.9°	80.2°	66.5°	78.1°	0.537
0° (Neutral)	10 ° Flex	22	16	80.2°	99.1°	78.1°	89.8°	0.189
10 ° Flex	20 ° Flex	16	15	99.1°	67.6°	89.8°	69.8°	0.210
20 ° Flex	30 ° Flex	15	13	67.6°	114.0°	69.8°	113.0°	0.256
30 ° Flex	40 ° Flex	13	10	114.0°	125.3°	113.0°	132.9°	0.305
40 ° Flex	50 ° Flex	10	5	125.3°	130.7°	132.9°	133.2°	0.714

*Note: The orientation of the helical axis of motion (HAM) of the SLI scaphoid did not change significantly in the sagittal plane with the wrist motion from extension to flexion.*

### Orientation of the helical axis of the SLI scaphoid (coronal plane)

Table 99 The orientation of the helical axis of motion of the SLI scaphoid in the coronal plane with the wrist moving from extension to flexion.

Reference bin (R)	Comparison bin (C)	Number		Mean angle (R)	Mean angle (C)	Median angle (R)	Median angle (C)	p value
		R	C					
60 ° Ext	50 ° Ext	7	8	5.1°	3.7°	2.5°	4.1°	0.782
50 ° Ext	40 ° Ext	8	15	3.7°	5.7°	4.1°	4.2°	0.879
40 ° Ext	30 ° Ext	15	13	5.7°	6.2°	4.2°	6.8°	0.705
30 ° Ext	20 ° Ext	13	18	6.2°	4.7°	6.8°	3.0°	0.833
20 ° Ext	10 ° Ext	18	20	4.7°	0.9°	3.0°	0.9°	0.516
10 ° Ext	0° (Neutral)	20	22	0.9°	4.5°	0.9°	4.7°	0.064
0° (Neutral)	10 ° Flex	22	16	4.5°	1.1°	4.7°	0.9°	0.051
10 ° Flex	20 ° Flex	16	15	1.1°	1.3°	0.9°	1.3°	0.853
20 ° Flex	30 ° Flex	15	13	1.3°	0.8°	1.3°	1.5°	0.705
30 ° Flex	40 ° Flex	13	10	0.8°	2.9°	1.5°	7.1°	0.133
40 ° Flex	50 ° Flex	10	5	2.9°	13.0°	7.1°	6.1°	0.464

Note: The orientation of the helical axis of motion (HAM) of the SLI scaphoid did not change significantly in the coronal plane with the wrist motion from extension to flexion.

### Orientation of the helical axis of the SLI scaphoid (axial plane)

Table 100 The orientation of the helical axis of motion of the SLI scaphoid in the axial plane with the wrist moving from extension to flexion.

Reference bin (R)	Comparison bin (C)	Number		Mean angle (R)	Mean angle (C)	Median angle (R)	Median angle (C)	p value
		R	C					
60 ° Ext	50 ° Ext	7	8	4.8°	-13.1°	10.2°	-14.7°	0.019*
50 ° Ext	40 ° Ext	8	15	-13.1°	0.4°	-14.7°	-1.1°	0.057
40 ° Ext	30 ° Ext	15	13	0.4°	1.9°	-1.1°	-0.3°	0.705
30 ° Ext	20 ° Ext	13	18	1.9°	-1.1°	-0.3°	-1.3°	0.347
20 ° Ext	10 ° Ext	18	20	-1.1°	0.8°	-1.3°	1.2°	0.516
10 ° Ext	0° (Neutral)	20	22	0.8°	3.9°	1.2°	3.6°	0.537
0° (Neutral)	10 ° Flex	22	16	3.9°	2.2°	3.6°	4.3°	0.855
10 ° Flex	20 ° Flex	16	15	2.2°	6.6°	4.3°	3.3°	0.594
20 ° Flex	30 ° Flex	15	13	6.6°	-5.0°	3.3°	-1.3°	0.058
30 ° Flex	40 ° Flex	13	10	-5.0°	-13.4°	-1.3°	-16.5°	0.305
40 ° Flex	50 ° Flex	10	5	-13.4°	-16.1°	-16.5°	-20.9°	0.464

Note: The orientation of the helical axis of motion (HAM) of the SLI scaphoid changed significantly in the axial plane during extreme extension (60° to 50° extension). “\*” Indicates statistical significance at 0.05.

### 3.6.1.8. SLI lunate with wrist extension to flexion

The orientation of the helical axis of motion (HAM) of the SLI lunate did not change in the sagittal, coronal, or the axial planes during wrist motion from extension to flexion (Table 101, Table 102, Table 103).

#### *Orientation of the helical axis of the SLI lunate (sagittal plane)*

*Table 101 The orientation of the helical axis of motion of the SLI lunate in the sagittal plane with the wrist moving from extension to flexion.*

Reference bin (R)	Comparison bin (C)	Number		Mean angle (R)	Mean angle (C)	Median angle (R)	Median angle (C)	<i>p</i> value
		R	C					
60 ° Ext	50 ° Ext	4	4	95.5°	80.1°	91.9°	79.5°	0.879
50 ° Ext	40 ° Ext	4	5	80.1°	92.4°	79.5°	102.9°	0.764
40 ° Ext	30 ° Ext	5	7	92.4°	125.1°	102.9°	131.1°	0.079
30 ° Ext	20 ° Ext	7	3	125.1°	126.8°	131.1°	144.5°	0.490
20 ° Ext	10 ° Ext	3	3	126.8°	113.6°	144.5°	134.8°	0.414
10 ° Ext	0° (Neutral)	3	10	113.6°	95.0°	134.8°	89.4°	0.612
0° (Neutral)	10 ° Flex	10	10	95.0°	67.2°	89.4°	67.1°	0.074
10 ° Flex	20 ° Flex	10	15	67.2°	95.2°	67.1°	85.1°	0.072
20 ° Flex	30 ° Flex	15	13	95.2°	81.9°	85.1°	86.8°	0.705
30 ° Flex	40 ° Flex	13	10	81.9°	94.4°	86.8°	87.0°	0.855
40 ° Flex	50 ° Flex	10	5	94.4°	116.8°	87.0°	128.7°	0.143

*Note that the orientation of the helical axis of motion (HAM) of the SLI lunate did not change significantly in the sagittal plane with the wrist motion.*



### Orientation of the helical axis of the SLI lunate (coronal plane)

Table 102 The orientation of the helical axis of motion of the SLI lunate in the coronal plane with the wrist moving from extension to flexion.

Reference bin (R)	Comparison bin (C)	Number		Mean angle (R)	Mean angle (C)	Median angle (R)	Median angle (C)	<i>p</i> value
		R	C					
60 ° Ext	50 ° Ext	4	4	-6.4°	0.6°	-4.4°	-0.2°	0.981
50 ° Ext	40 ° Ext	4	5	0.6°	-3.6°	-0.2°	-2.5°	0.764
40 ° Ext	30 ° Ext	5	7	-3.6°	-24.3°	-2.5°	-17.6°	0.079
30 ° Ext	20 ° Ext	7	3	-24.3°	-2.5°	-17.6°	6.3°	0.490
20 ° Ext	10 ° Ext	3	3	-2.5°	1.0°	6.3°	3.9°	0.414
10 ° Ext	0° (Neutral)	3	10	1.0°	1.8°	3.9°	4.1°	0.612
0° (Neutral)	10 ° Flex	10	10	1.8°	1.0°	4.1°	0.4°	0.895
10 ° Flex	20 ° Flex	10	15	1.0°	-0.4°	0.4°	-1.3°	0.513
20 ° Flex	30 ° Flex	15	13	-0.4°	-2.2°	-1.3°	0.5°	0.705
30 ° Flex	40 ° Flex	13	10	-2.2°	0.3°	0.5°	-0.8°	0.855
40 ° Flex	50 ° Flex	10	5	0.3°	10.8°	-0.8°	9.2°	0.143

Note that the orientation of the helical axis of motion (HAM) of the SLI lunate did not change significantly in the coronal plane with the wrist motion.

### Orientation of the helical axis of the SLI lunate (axial plane)

Table 103 The orientation of the helical axis of motion of the SLI lunate in the axial plane with the wrist moving from extension to flexion.

Reference bin (R)	Compariso n bin (C)	Number		Mean angle (R)	Mean angle (C)	Median angle (R)	Median angle (C)	p value
		R	C					
60 ° Ext	50 ° Ext	4	4	44.1°	36.8°	42.1°	37.6°	0.909
50 ° Ext	40 ° Ext	4	5	36.8°	21.5°	37.6°	20.7°	0.294
40 ° Ext	30 ° Ext	5	7	21.5°	28.9°	20.7°	17.1°	0.558
30 ° Ext	20 ° Ext	7	3	28.9°	8.2°	17.1°	9.6°	0.058
20 ° Ext	10 ° Ext	3	3	8.2°	2.4°	9.6°	1.3°	0.414
10 ° Ext	0° (Neutral)	3	10	2.4°	-9.3°	1.3°	-4.8°	0.612
0° (Neutral)	10 ° Flex	10	10	-9.3°	-10.3°	-4.8°	-10.0°	0.371
10 ° Flex	20 ° Flex	10	15	-10.3°	-13.6°	-10.0°	-7.4°	0.870
20 ° Flex	30 ° Flex	15	13	-13.6°	-16.7°	-7.4°	-14.9°	0.256
30 ° Flex	40 ° Flex	13	10	-16.7°	-12.1°	-14.9°	-10.9°	0.133
40 ° Flex	50 ° Flex	10	5	-12.1°	-7.6°	-10.9°	-9.7°	0.714

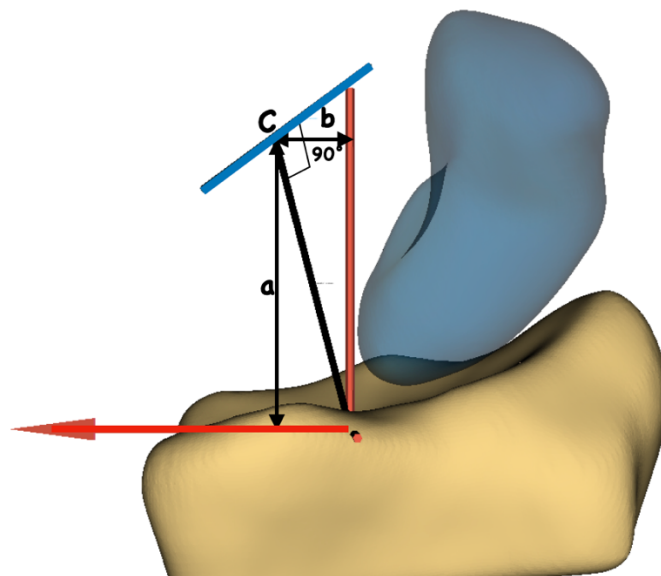
Note that the orientation of the helical axis of motion (HAM) of the SLI lunate did not change significantly in the axial plane with the wrist motion.

### 3.6.2. Position of the helical axis

The detailed results of the position of the HAM is presented in Table 104 to Table 127 at the end of this section, in 3.6.2.9.

#### 3.6.2.1. Normal scaphoid with the wrist ulnar to radial deviation

The position of the HAM was measured with reference to the radius coordinate system (Figure 121). The closest distance between the isocentre of the radius coordinate system and HAM was computed in each direction (radioulnar, dorso-volar and proximodistal). Comparisons were made between the wrist positions and finally the patterns identified were compared between the normal and SLI wrists.



*Figure 121 The position of the helical axis of motion (HAM- indicated by the blue line “C”) of the scaphoid with reference to the radius coordinate system. The double arrows indicate the distance to the HAM from the isocentre of the radius coordinate system in the proximodistal direction (a) and radioulnar direction (b). Similarly, the distance to the HAM was calculated in the dorso-volar direction as well.*

#### *Radioulnar direction*

With the wrist moving from ulnar to radial deviation, the position of the HAM of the normal scaphoid changed to be more radial with reference to the isocentre of the radius coordinate

system (Figure 122, Table 104). There was a statistically significant change as the wrist moved from 20° ulnar deviation to 10° ulnar deviation ( $p = 0.012$ ). As the wrist moved from 10° ulnar deviation to the neutral position again there was statistically significant change in the HAM position ( $p = 0.012$ ).

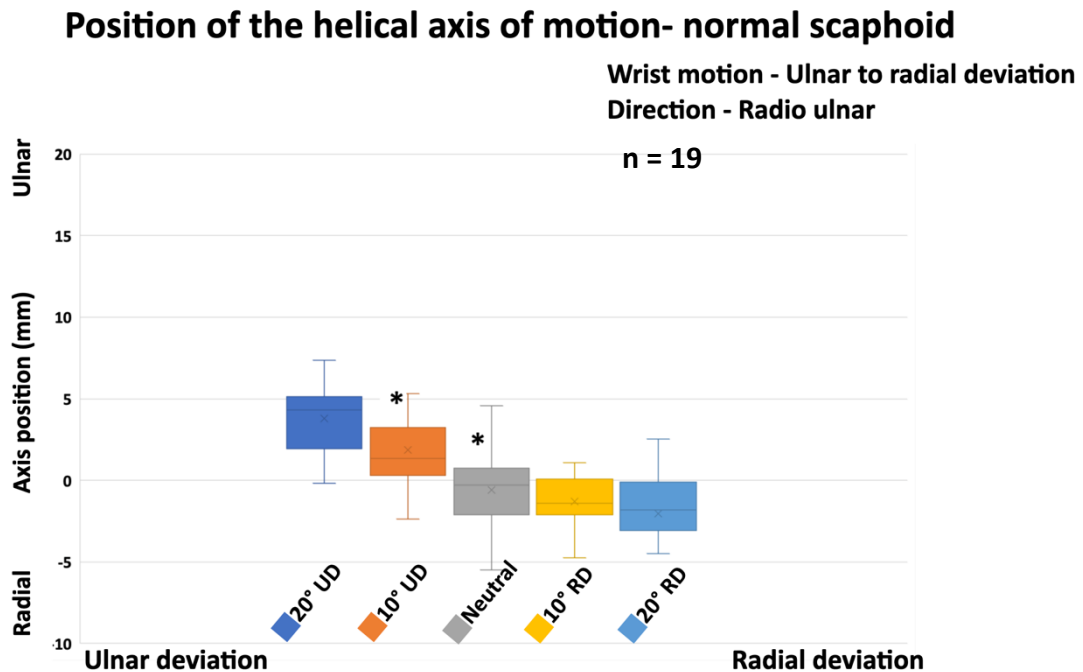


Figure 122 The position of the normal scaphoid helical axis of motion( HAM) in the radioulnar direction. The position of the HAM became more radial with the wrist radial deviation. Note that the “\*” indicate the wrist positions where a statistically significant change in the HAM was observed.

#### *Dorso-volar direction*

As the wrist moved from ulnar to radial deviation, the position of the HAM of the normal scaphoid did not demonstrate a significant change in the dorso volar direction (Figure 123, Table 105).

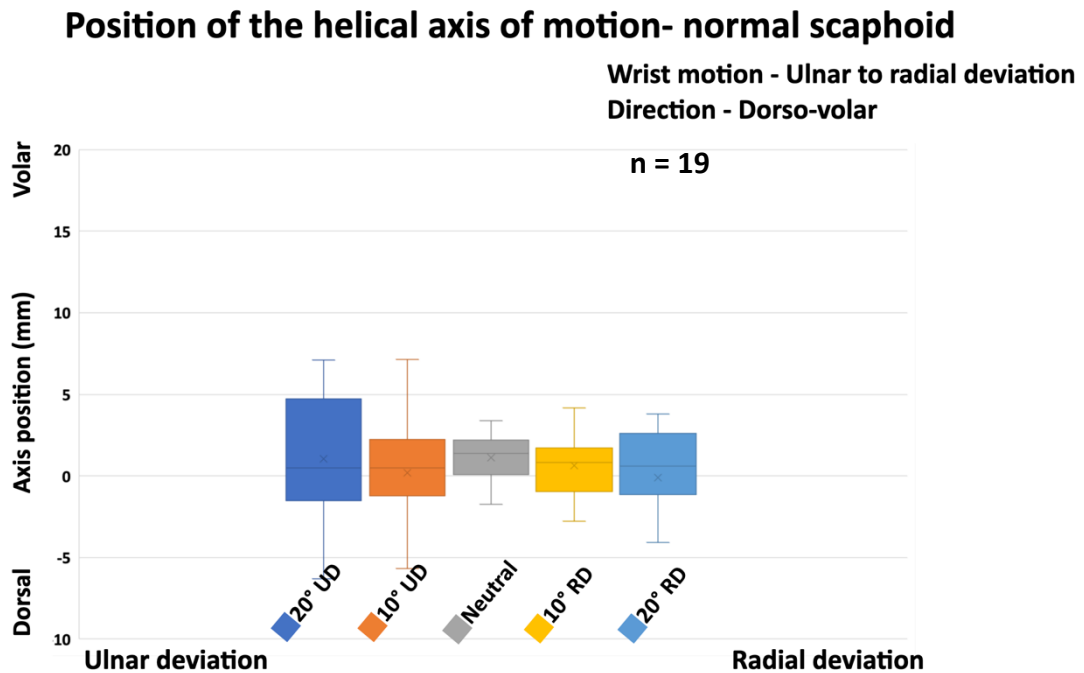


Figure 123 The position of the normal scaphoid helical axis of motion(HAM) in the dorso-volar direction. Note that the HAM did not show significant changes in the dorsovolar direction.

#### Proximo-distal direction

With the wrist moving from ulnar to radial deviation, the position of the HAM of the normal scaphoid became more proximal with reference to the isocentre of the radius coordinate system (Figure 124, Figure 125, Table 106). A statistically significant change was observed from distal to proximal between the wrist position of 10° ulnar deviation to the neutral wrist position.

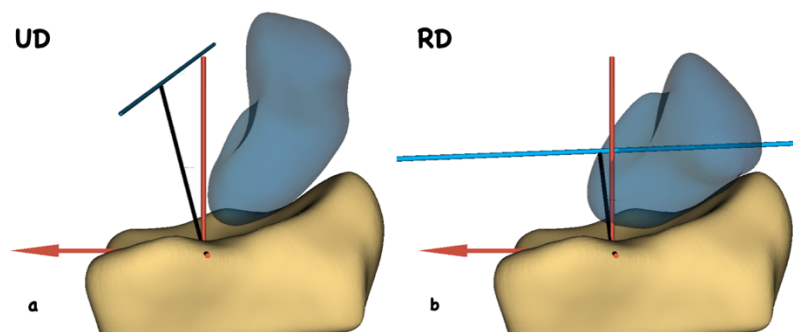


Figure 124 The position of the helical axis of motion (HAM) of the normal scaphoid during a. ulnar (UD) and b. radial deviation (RD) of the wrist. Note the change in position, transitioning from a proximal position in ulnar deviation to a distal position in radial deviation.

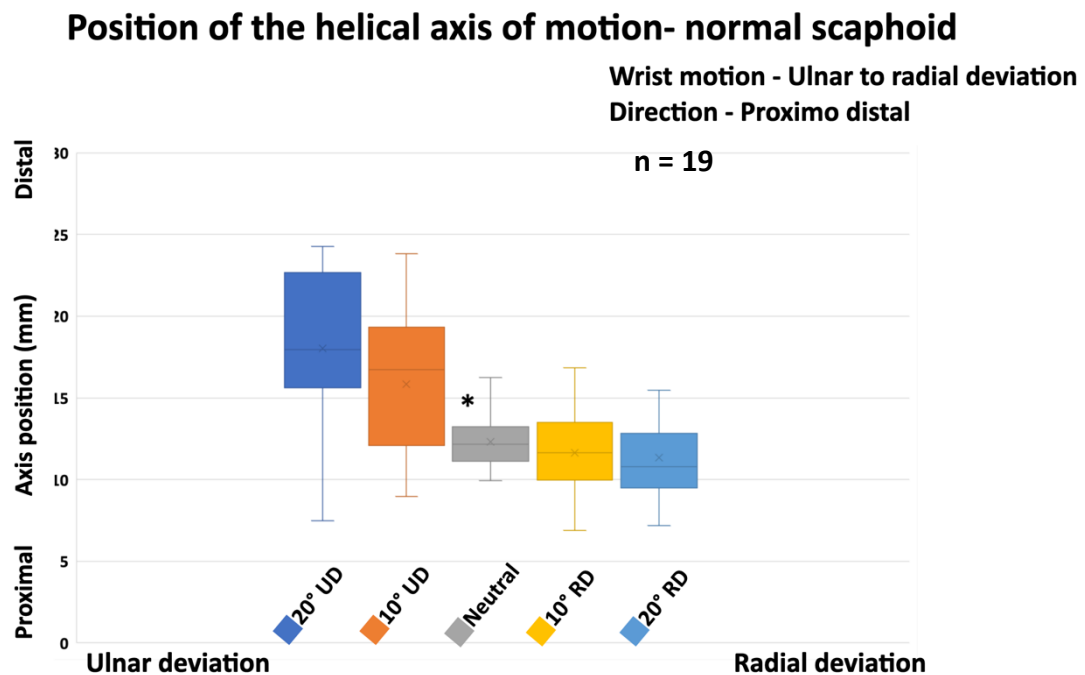


Figure 125 The position of the normal scaphoid helical axis of motion(HAM) in the proximodistal direction. The position of the HAM became more proximal as the wrist moved from the ulnar to radial deviation. “\*” indicates the wrist positions where a statistically significant change in the HAM was observed.

### 3.6.2.2. Normal lunate with the wrist ulnar to radial deviation

#### Radioulnar direction

The position of the HAM of the normal lunate changed to being more radial as the wrist moved from ulnar to radial deviation (Figure 126, Table 107). There was a statistically significant change in the position as the wrist moved from 20° ulnar deviation to 10° ulnar deviation ( $p = 0.002$ ). As the wrist moved from 10° ulnar deviation to the neutral position, again, there was statistically significant change in the position of the helical axis of motion of the normal lunate ( $p < 0.001$ ).

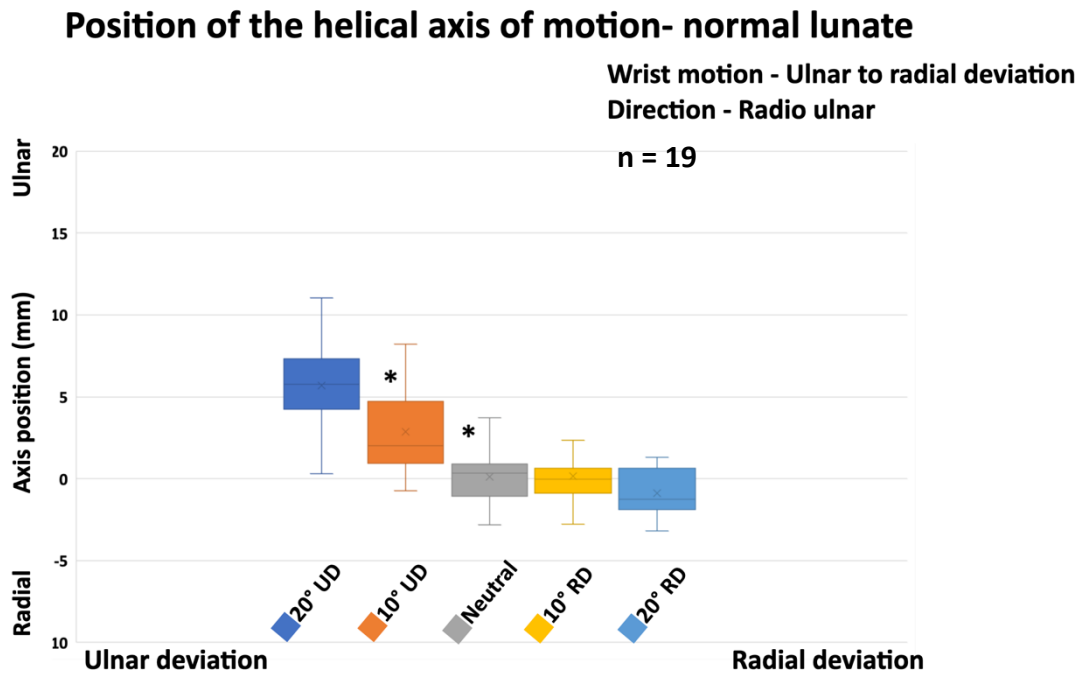


Figure 126 The position of the normal lunate helical axis of motion (HAM), in the radioulnar direction. The position of the HAM became more radial with the wrist radial deviation. “\*” indicate the wrist positions where a statistically significant change in the helical axis of motion was observed.

#### *Dorso-volar direction*

There was a statistically significant change in the position of the HAM of the normal lunate in the dorso-volar direction as the wrist moved from 20° ulnar deviation to 10° ulnar deviation ( $p = 0.023$ ) (Table 108, Figure 127). As the wrist moved from the neutral position to 10° radial deviation, again, there was statistically significant change in the position of the helical axis of motion of the normal lunate ( $p = 0.019$ ).

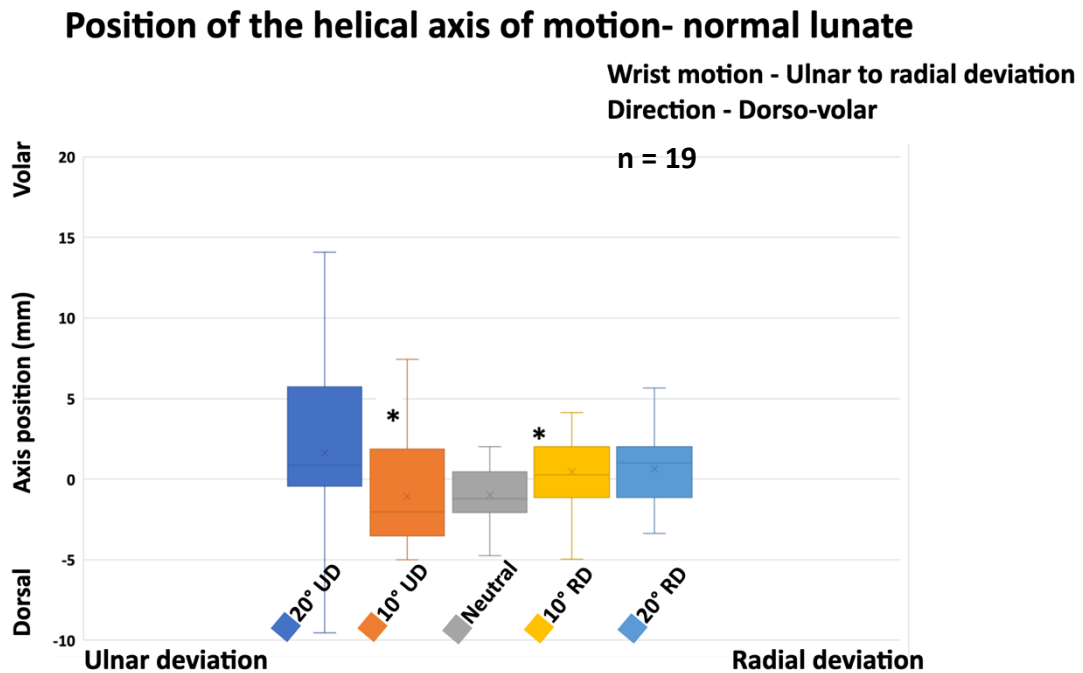


Figure 127 The position of the normal lunate helical axis of motion in the dorso-volar direction. “\*” indicates the wrist positions where a statistically significant change in the helical axis of motion was observed.

#### Proximo-distal direction

With the wrist moving from ulnar to radial deviation, the position of the HAM of the normal lunate changed to being more proximal (Figure 128, Table 109). There was a statistically significant proximal change of the HAM of the normal lunate as the wrist moved from 20° ulnar deviation to 10° ulnar deviation ( $p = 0.019$ ). As the wrist moved from 10° ulnar deviation to neutral position, again, there was statistically significant change in the position of the HAM of the normal lunate ( $p < 0.001$ ).



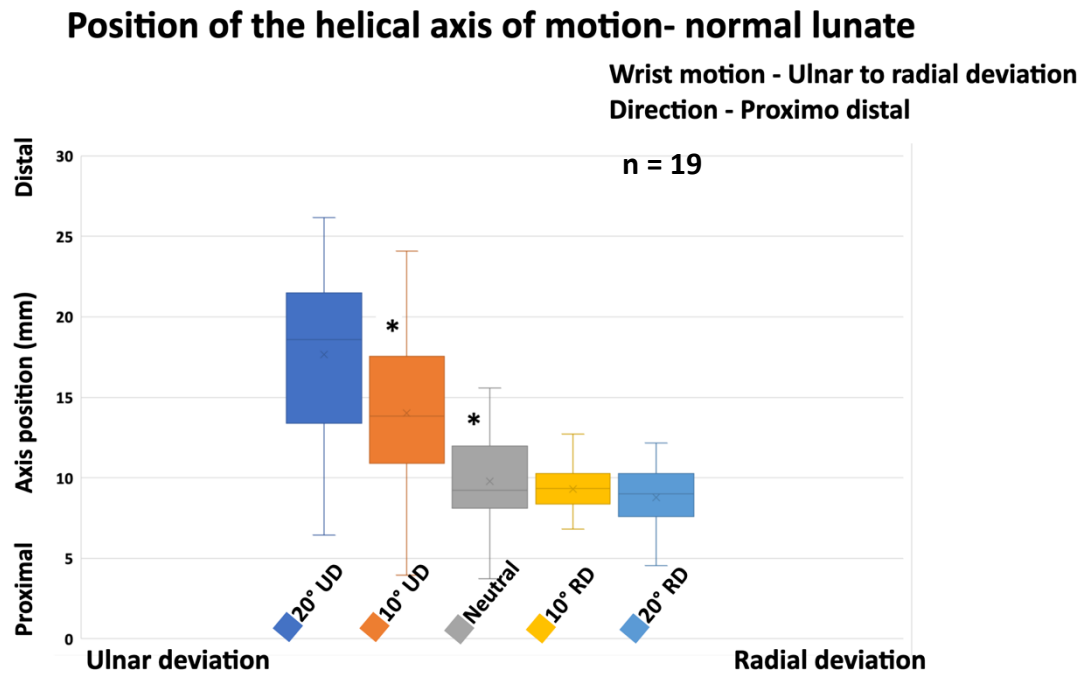


Figure 128 The position of the normal lunate helical axis of motion (HAM) in the proximodistal direction. The position of the HAM became more proximal with the wrist radial deviation. “\*” indicates the wrist positions where a statistically significant change in the HAM was observed.

### 3.6.2.3. SLI Scaphoid with ulnar to radial deviation

With the wrist moving from ulnar to radial deviation there were no statistically significant changes of the HAM position of the SLI scaphoid that occurred between the wrist positions, in any direction (Figure 129 to Figure 131 and Table 110 to Table 112).

## Radioulnar direction

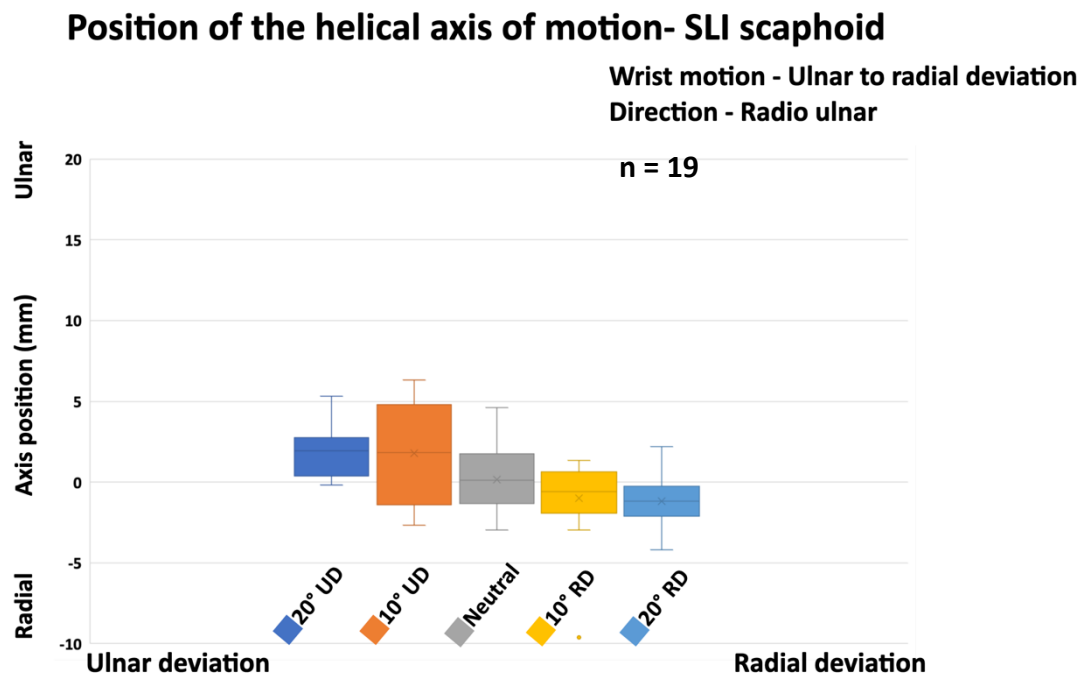


Figure 129 The position of the SLI scaphoid helical axis of motion (HAM), in the radioulnar direction. The position of the HAM became more radial with the wrist radial deviation, but there were no statistically significant changes between the wrist positions.

## Dorso-volar direction

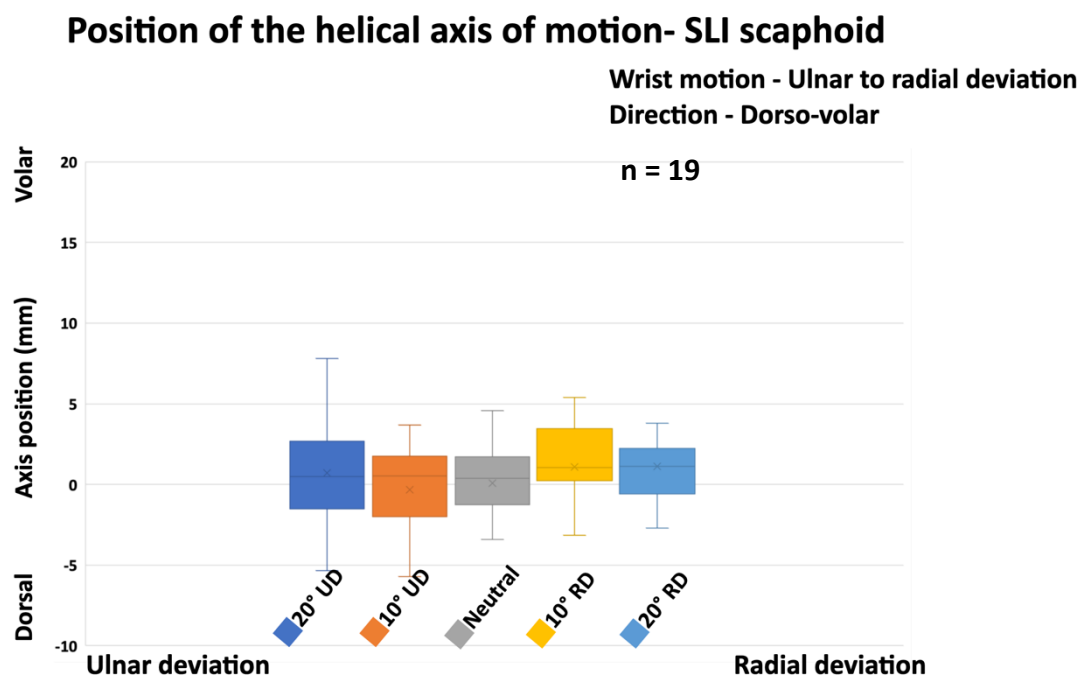


Figure 130 The position of the SLI scaphoid helical axis of motion in the dorso-volar direction. Note that no significant changes occurred in the position of the HAM as the wrist moved from ulnar to radial deviation in the dorso-volar direction.

*Proximo-distal direction*

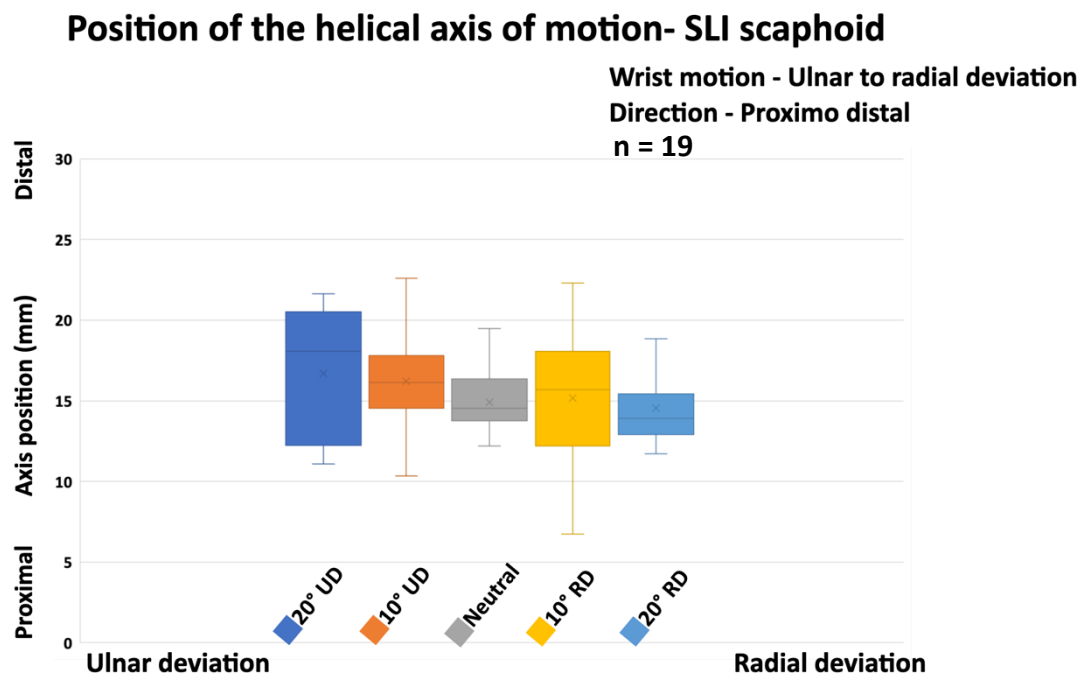


Figure 131 The position of the SLI scaphoid helical axis of motion in the proximodistal direction. Note that no significant changes occurred in the position of the SLI-scaphoid HAM as the wrist moved from ulnar to radial deviation in the proximo-distal direction.

#### 3.6.2.4. SLI lunate with ulnar to radial deviation

With the wrist moving from ulnar to radial deviation the HAM of the SLI lunate changed to be more radial (Figure 132, Table 113). A statistically significant radial change of the helical axis of motion of the SLI lunate occurred between 10° ulnar deviation and the neutral wrist position ( $p = 0.001$ ).

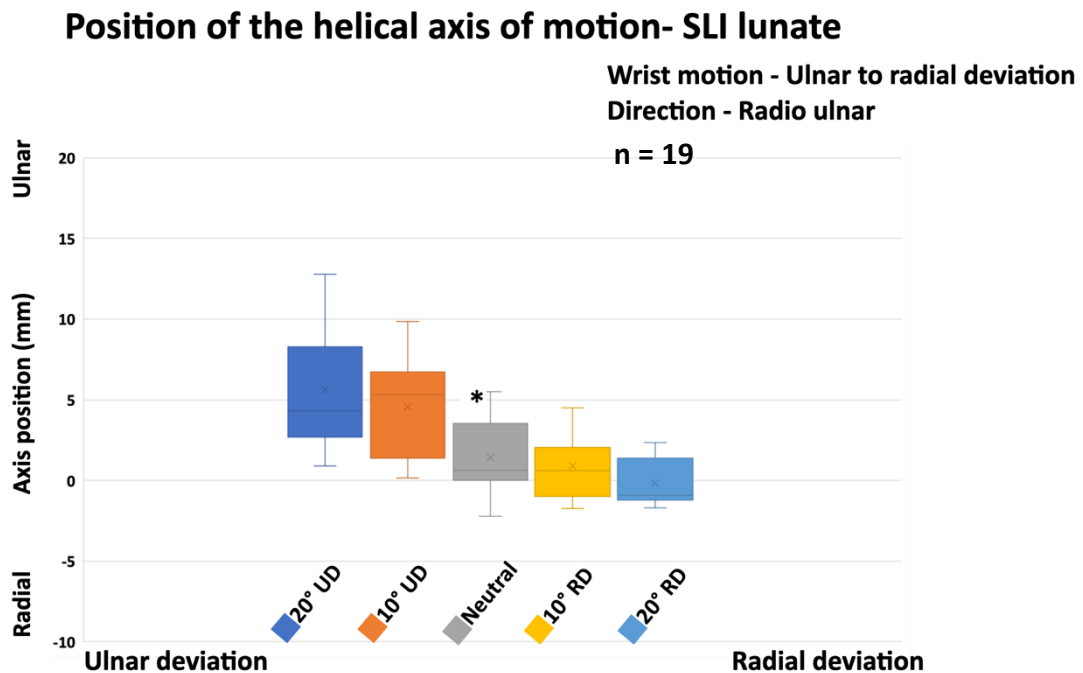


Figure 132 The position of the SLI lunate helical axis of motion, in the radioulnar direction. The position of the HAM of the SLI lunate became more radial with the wrist radial deviation. “\*” indicates the wrist positions where a statistically significant change in the HAM was observed.

#### Dorso-volar direction

With the wrist moving from ulnar to radial deviation the HAM of the SLI lunate changed to be more volar, with high variability at 20° ulnar deviation (Figure 133, Table 114). A statistically significant volar migration of the HAM of the SLI lunate occurred between 20° ulnar deviation to 10° ulnar deviation ( $p = 0.043$ ). In addition, another statistically significant change (volar) of the HAM of the SLI lunate occurred between 10° ulnar deviation and the neutral position of the wrist ( $p = 0.025$ ).

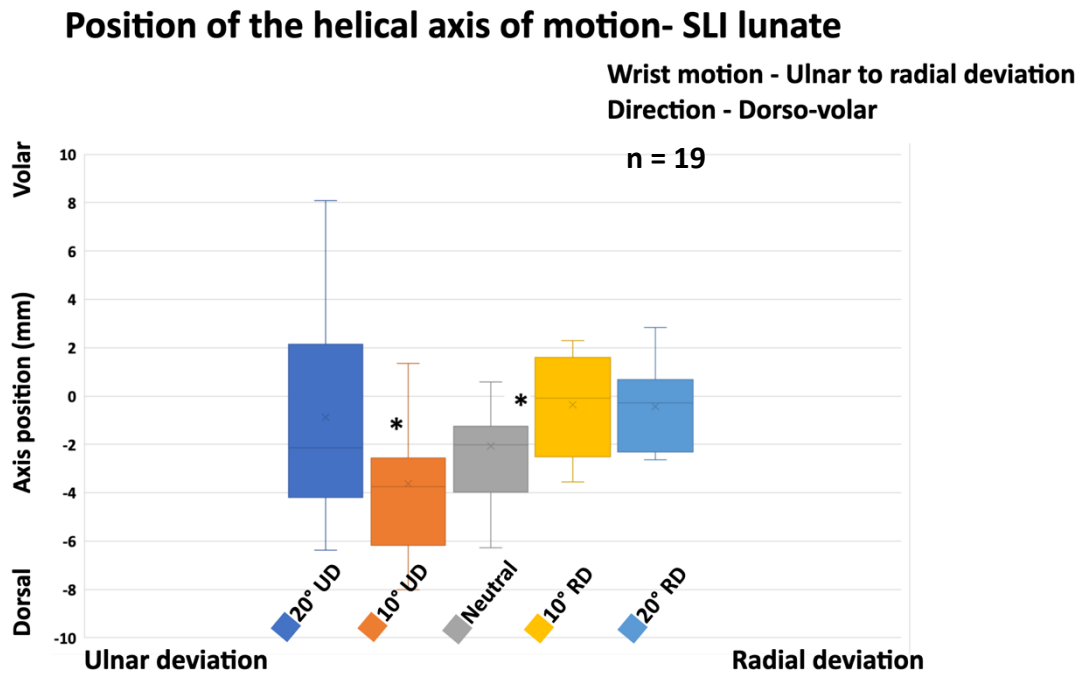


Figure 133 The position of the SLI lunate helical axis of motion during, in the dorso-volar direction. “\*” indicates the wrist positions where a statistically significant change in the HAM was observed.

#### Proximo-distal direction

With the wrist moving from ulnar to radial deviation the HAM of the SLI lunate changed to be more proximal (Figure 134, Table 115). A statistically significant proximal migration of the helical axis of motion of the SLI lunate occurred between 20° ulnar deviation to 10° ulnar deviation ( $p = 0.003$ ).

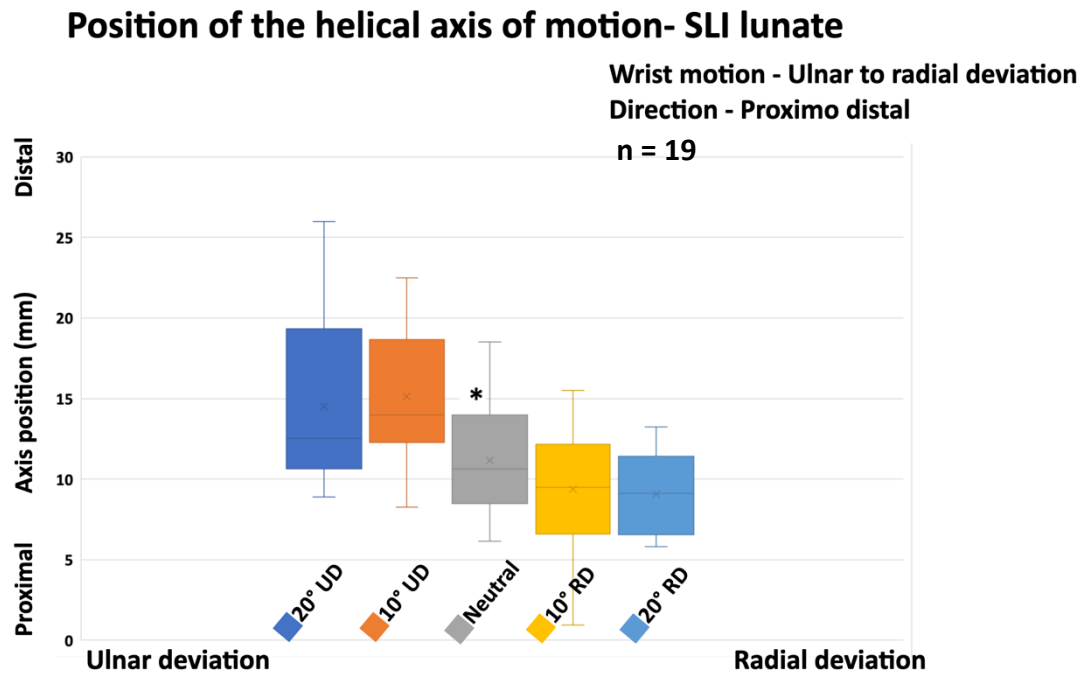


Figure 134 The position of the SLI lunate helical axis of motion in the proximodistal direction. The position of the HAM of the SLI lunate became more proximal with the wrist radial deviation. “\*” indicate the wrist positions where a statistically significant change in the HAM was observed.

### 3.6.2.5. Normal scaphoid with the wrist extension to flexion

With the wrist moving from extension to flexion there were no statistically significant changes of the position of the HAM of the normal scaphoid between the wrist positions, in any plane (Figure 135 to Figure 137 and Table 116 to Table 118).

## Radioulnar direction

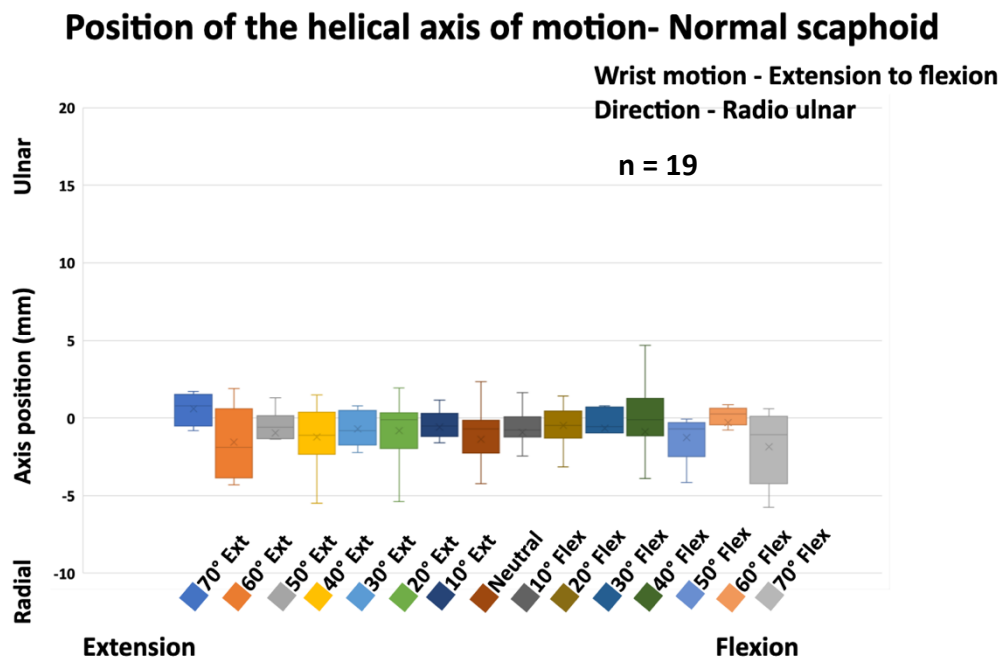


Figure 135 The position of the normal scaphoid helical axis of motion (HAM) during wrist extension to flexion, in the radioulnar direction. The position of the HAM of the normal scaphoid was not different between the wrist positions in radioulnar direction.

## Dorso-volar direction

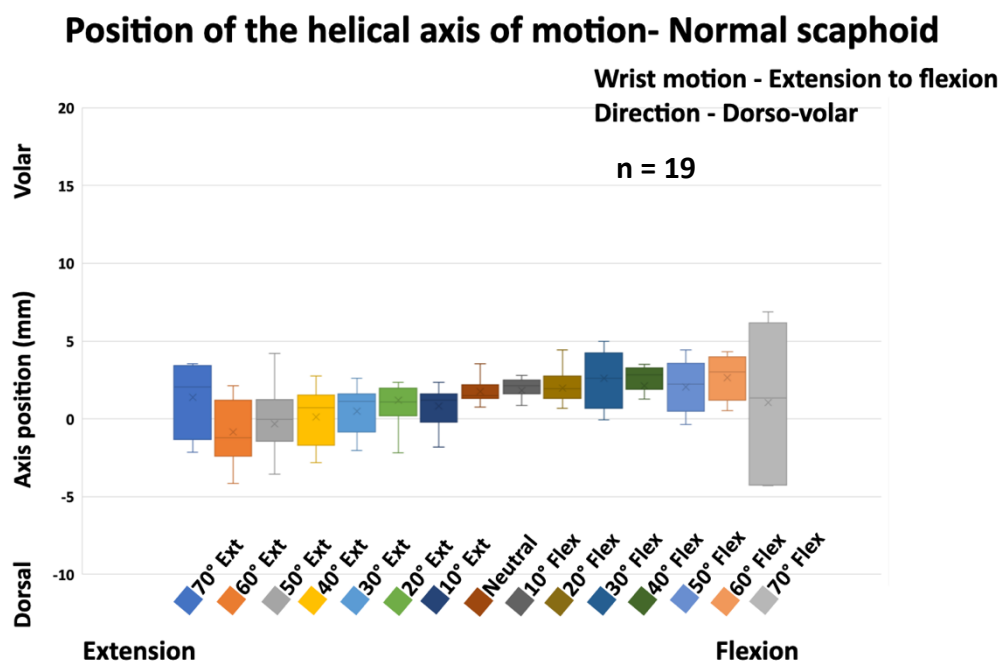


Figure 136 The position of the normal scaphoid helical axis of motion during wrist extension to flexion, in the dorso-volar direction. The position of the HAM of the normal scaphoid was not different between the wrist positions in dorso-volar direction.

#### Proximo-distal direction

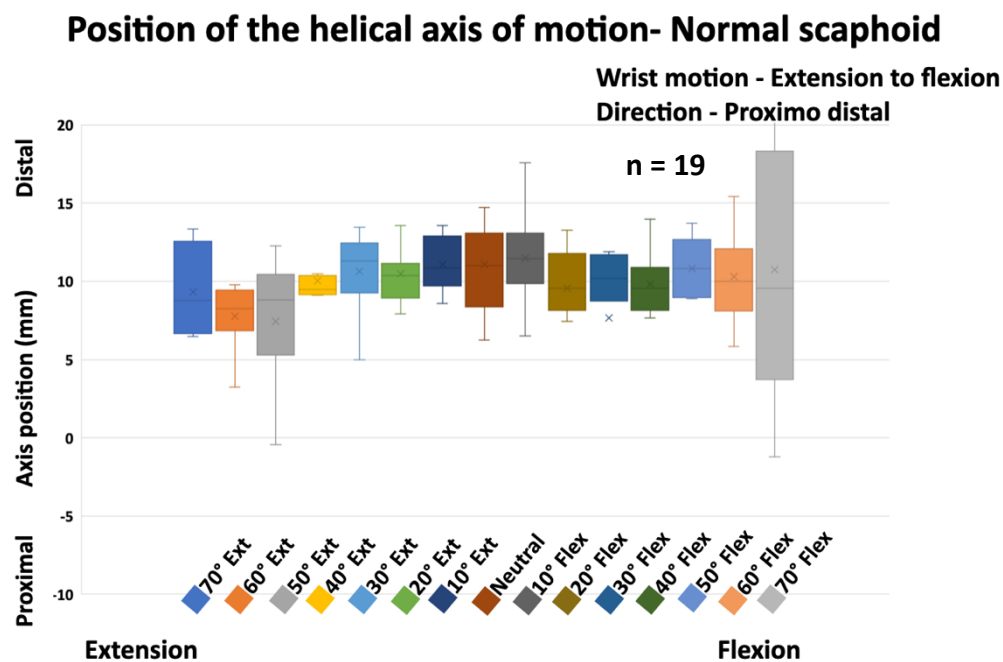


Figure 137 The position of the normal scaphoid helical axis of motion during wrist extension to flexion, in the proximodistal direction. Note that the position of the HAM of the normal scaphoid was not different between the wrist positions in proximodistal direction.

#### 3.6.2.6. Normal lunate with the wrist extension to flexion

##### Radioulnar direction

With the wrist moving from extension to flexion, the position of the HAM of the normal lunate changed significantly between 10° flexion to 20° flexion ( $p = 0.02$ ) (Figure 138, Table 119). The HAM of the normal lunate did not change in the radioulnar plane between the other wrist positions.



## Position of the helical axis of motion- Normal lunate

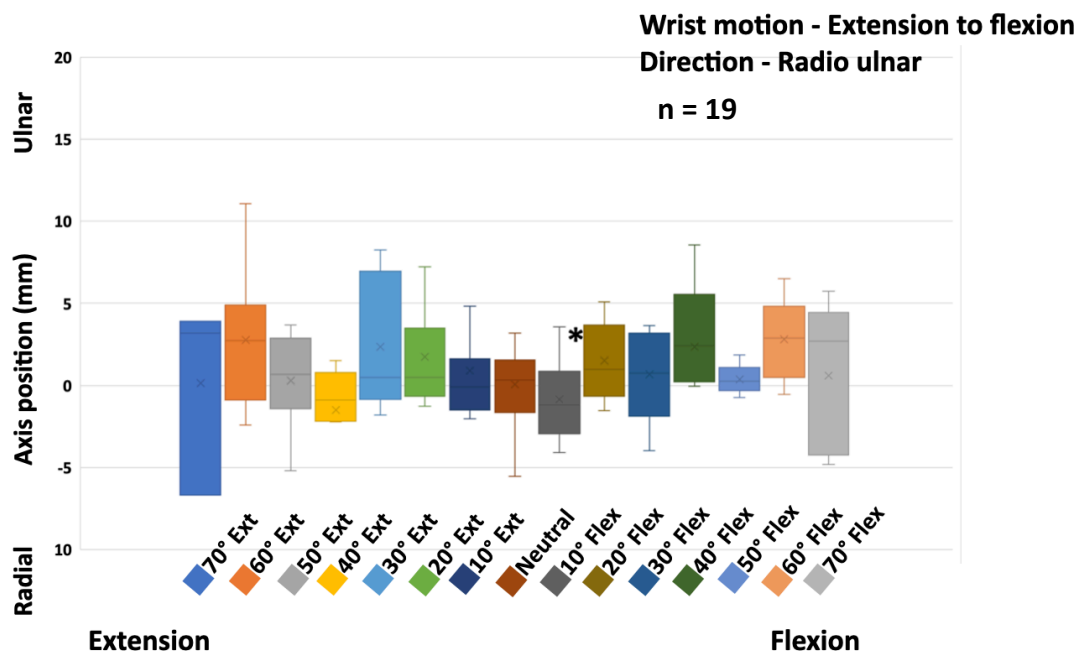


Figure 138 The position of the normal lunate helical axis of motion during wrist extension to flexion, in the radioulnar direction. The only significant change of the HAM of the normal lunate in the radioulnar direction occurred between 10° wrist flexion to 20° wrist flexion. “\*” indicates the wrist positions where a statistically significant change in the HAM was observed.

### Dorso-volar direction

With the wrist moving from extension to flexion there was a statistically significant change of the position of the HAM of the normal lunate that occurred between 10° extension to the neutral position ( $p = 0.035$ ) (Figure 139, Table 120). The HAM of the normal lunate did not change in the dorso-volar plane between the other wrist positions.

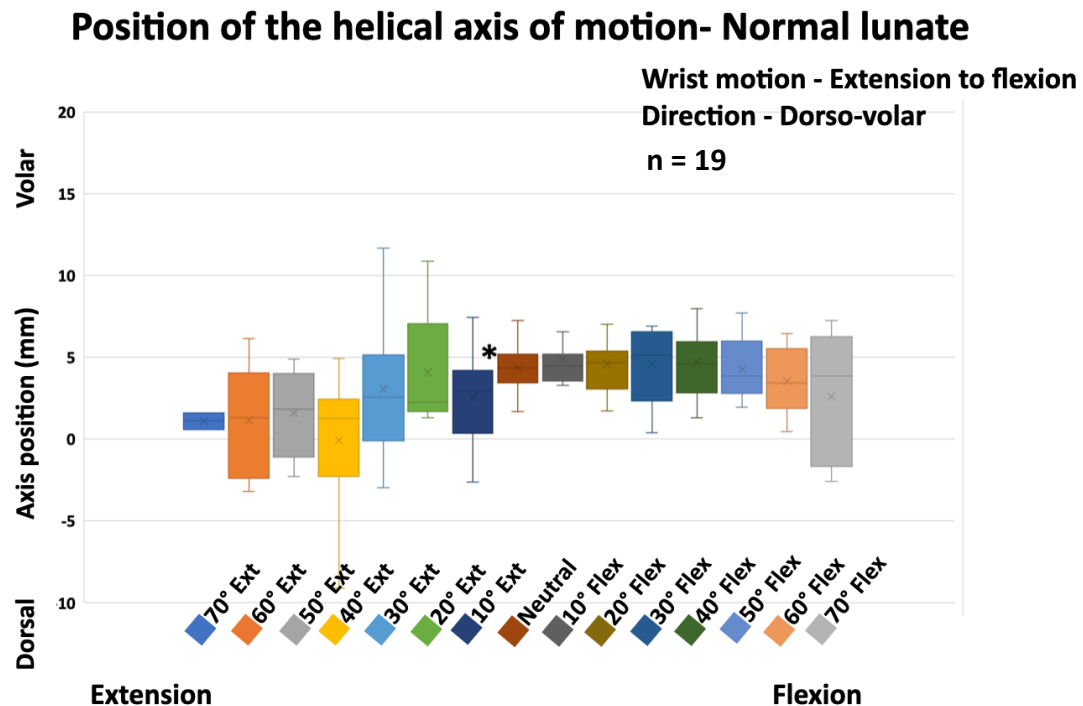


Figure 139 The position of the normal lunate helical axis of motion during wrist extension to flexion, in the dorso-volar direction. Note that the only significant change of the HAM of the normal lunate in the dorso-volar direction occurred between 10° wrist extension to the neutral position. “\*” indicates the wrist positions where a statistically significant change in the HAM was observed.

#### Proximo-distal direction

With the wrist moving from extension to flexion, the position of the HAM of the normal lunate changed to being more distal (Figure 140, Table 121). A statistically significant change occurred 10° flexion to 20° flexion ( $p=0.041$ ). The HAM of the normal lunate did not change in the proximodistal plane between the other wrist positions.

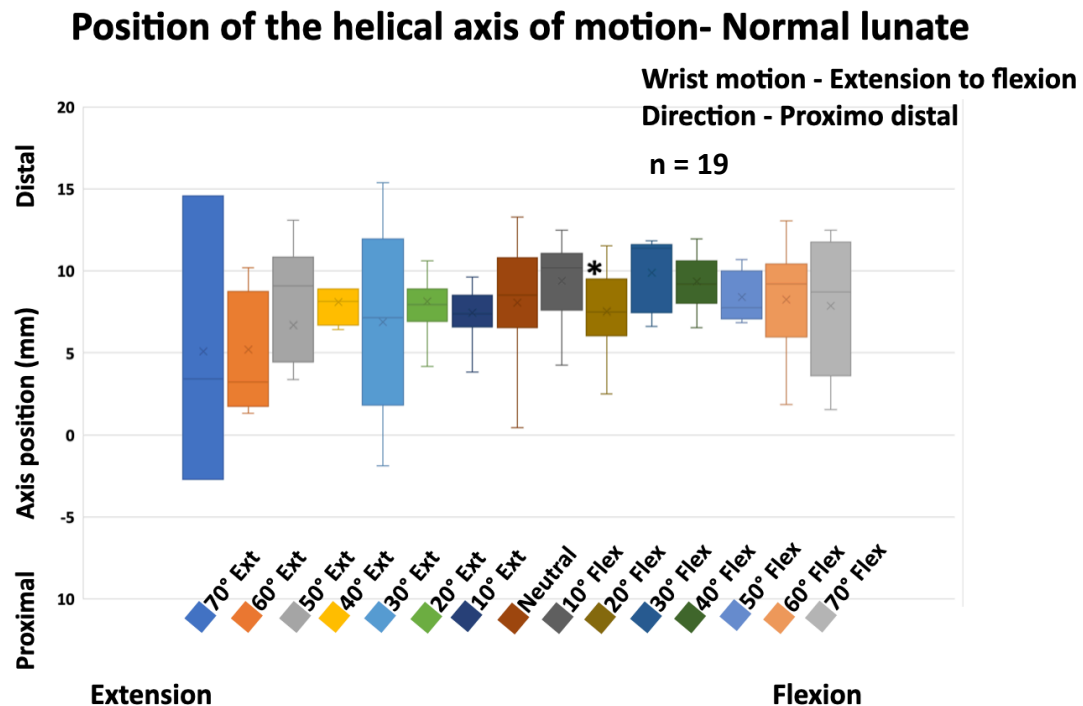


Figure 140 The position of the normal lunate helical axis of motion during wrist extension to flexion, in the proximo distal direction. “\*” indicates the wrist positions where a statistically significant change in the HAM was observed.

### 3.6.2.7. SLI scaphoid with the wrist extension to flexion

With the wrist moving from extension to flexion there were no statistically significant changes in the position of the HAM of the SLI scaphoid in radioulnar or dorso-volar direction (Figure 141, Figure 142 and Table 122, Table 123)

## Radioulnar direction

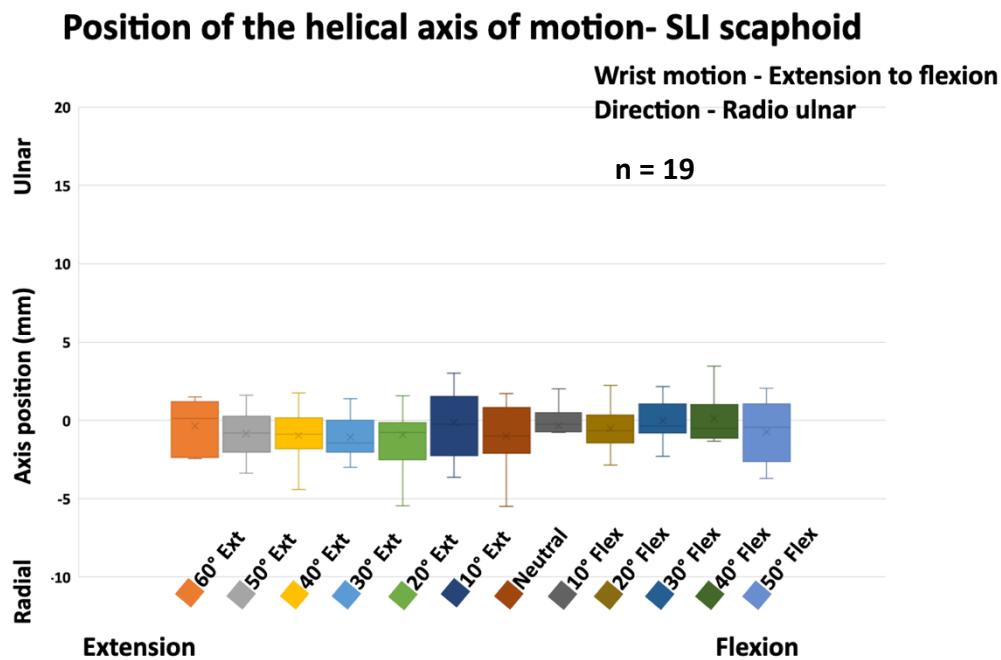


Figure 141 The position of the SLI scaphoid helical axis of motion (HAM) during wrist extension to flexion, in the radioulnar direction. The HAM of the SLI scaphoid did not change significantly between any consecutive wrist position from extension to flexion in the radioulnar direction.

## Dorso-volar direction

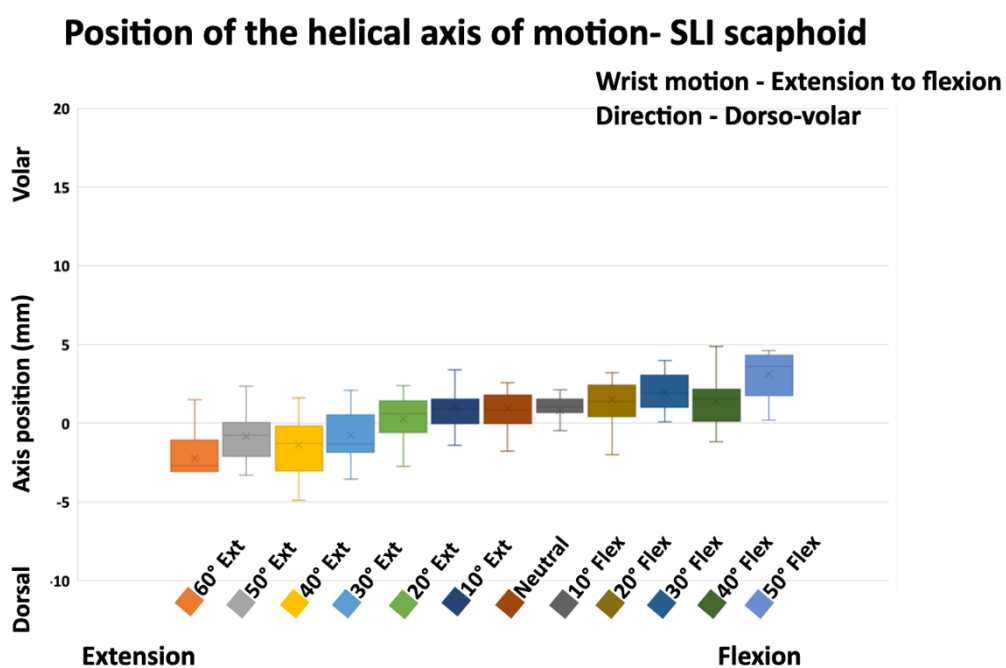


Figure 142 The position of the SLI scaphoid helical axis of motion during wrist extension to flexion, in the dorso-volar direction. The HAM of the SLI scaphoid did not change significantly between any consecutive wrist position from extension to flexion in the dorso-volar direction.

### Proximo-distal direction

With the wrist moving from extension to flexion the helical axis of motion of the SLI scaphoid changed in a proximal direction (Figure 143, Table 124). There were statistically significant changes at 2 stages. The first was observed when the wrist moved from 60° extension to 50° extension ( $p = 0.004$ ). The second significant proximal migration was seen when the wrist moved from 10° flexion to 20° flexion (0.022).

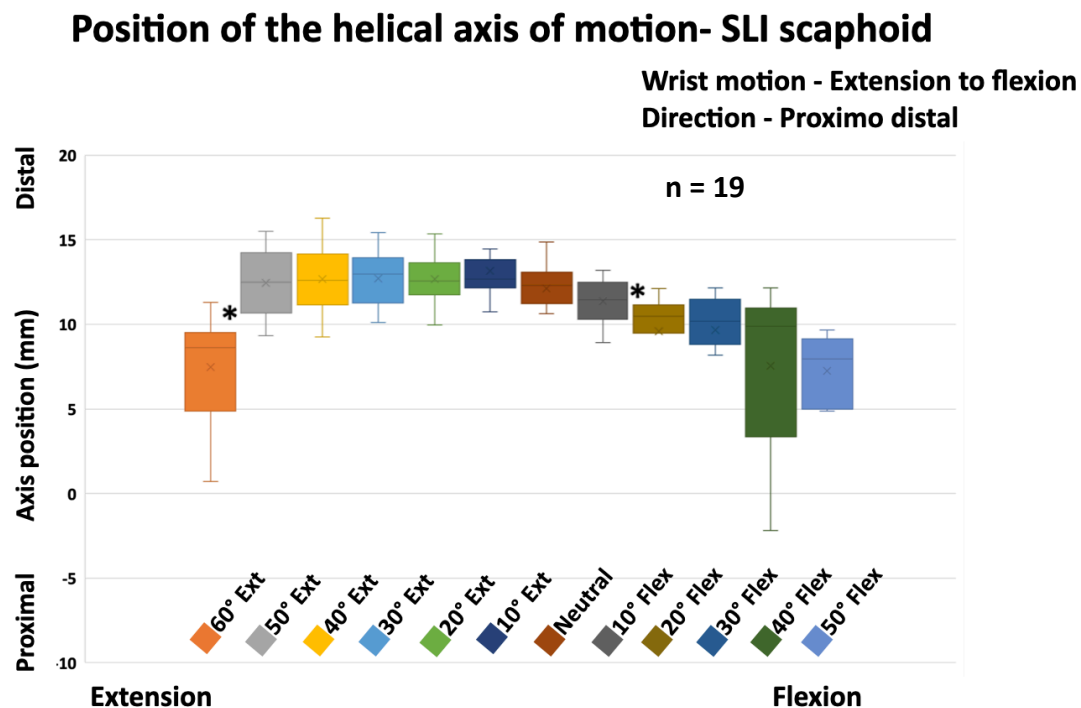


Figure 143 The position of the SLI scaphoid helical axis of motion during wrist extension to flexion, in the proximodistal direction. Note that the significant changes of the HAM of the SLI scaphoid in the proximodistal direction occurred between 60° to 50° wrist extension and between 10° wrist flexion to 20° wrist flexion. “\*” indicate the wrist positions where a statistically significant change in the HAM was observed.

### 3.6.2.8. SLI lunate with the wrist extension to flexion

#### Radioulnar direction

As the wrist moved from extension to flexion, there was no significant radial or ulna change of the position of the helical axis of motion in the SLI lunate (Figure 144, Table 125).

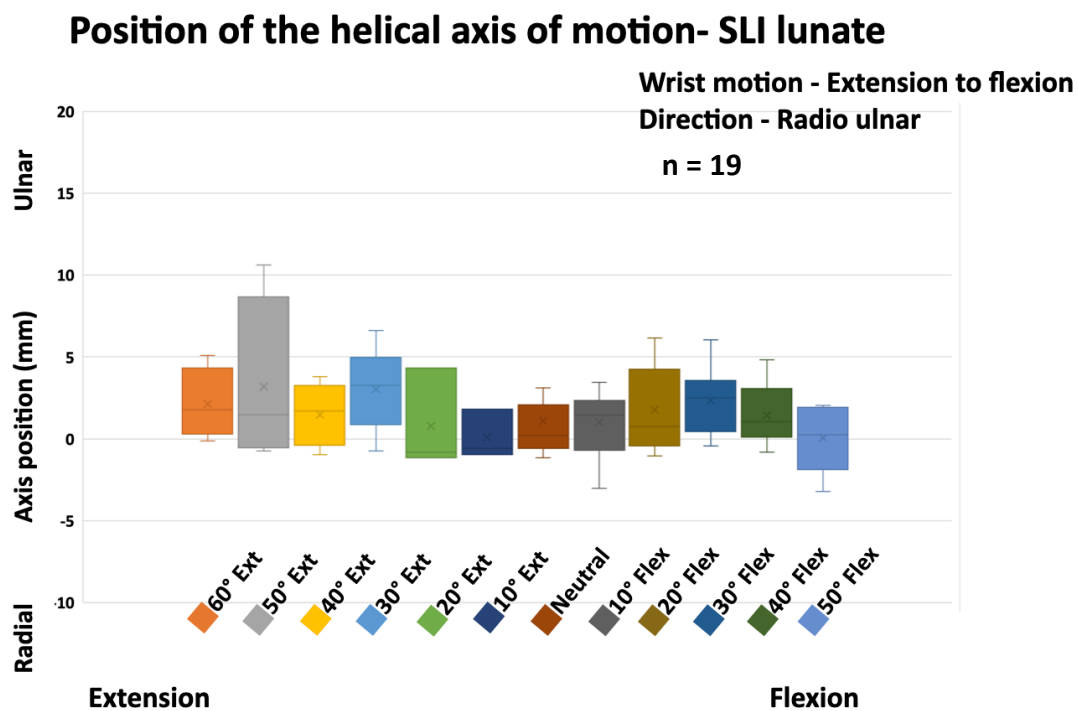


Figure 144 The position of the SLI lunate helical axis of motion during wrist extension to flexion, in the radioulnar direction. Note that there were no significant radial or ulna change of the position of the helical axis of motion in the SLI lunate.

#### Dorso-volar direction

As the wrist moved from extension to flexion, the position of the HAM of the SLI lunate changed to be more volar (Figure 145, Table 126). A statistically significant volar change of the HAM in the SLI lunate occurred when the wrist moved from 40° extension to 30° extension.

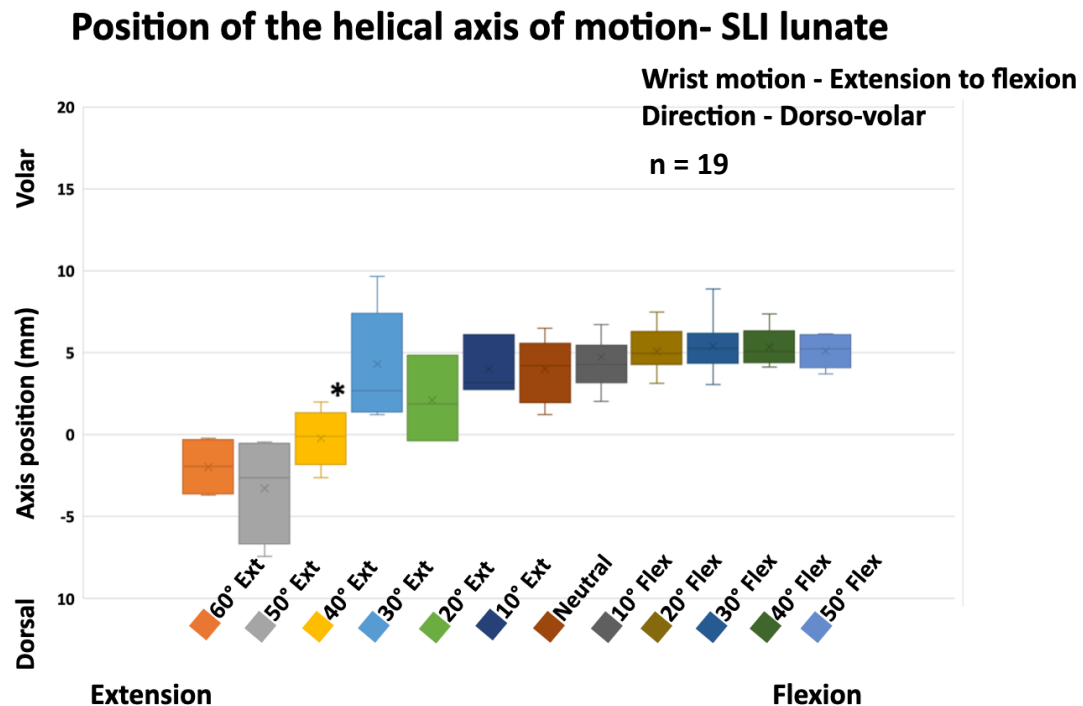


Figure 145 The position of the SLI lunate helical axis of motion (HAM) during wrist extension to flexion, in the dorso-volar direction. The HAM of the SLI lunate changed to be more volar as the wrist moved from extension to flexion. “\*” indicate the wrist positions where a statistically significant change in the HAM was observed.

#### Proximo-distal direction

During wrist extension to flexion, there were no statistically significant proximal or distal changes in the HAM position of the SLI Lunate (Figure 146, Table 127).

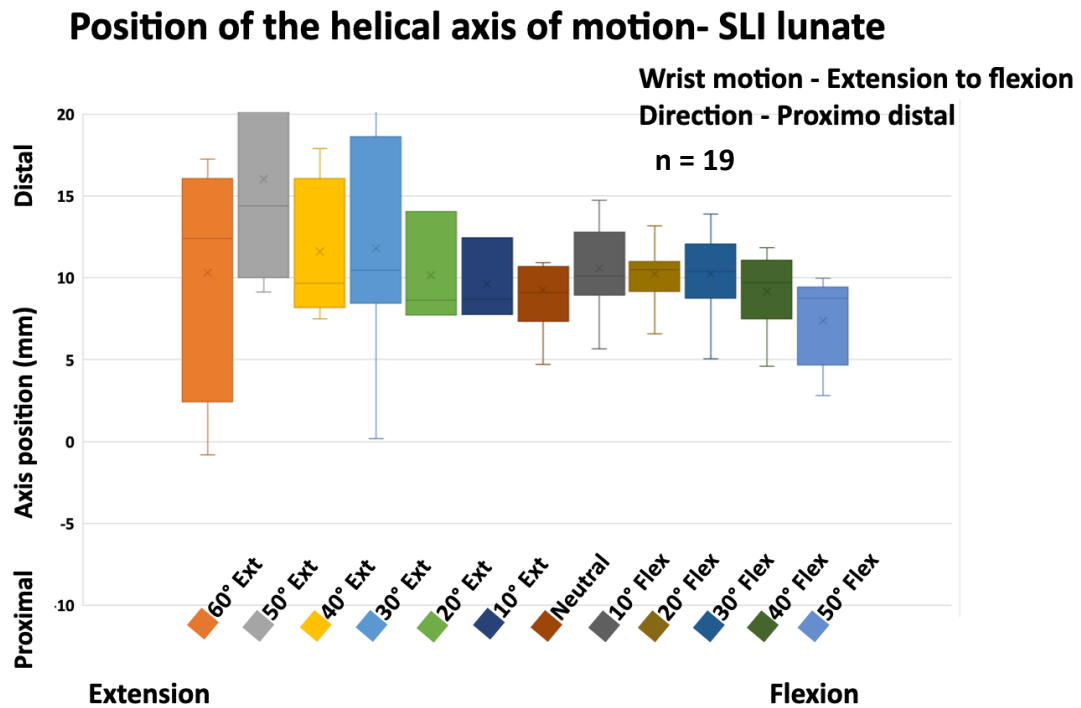


Figure 146 The position of the SLI lunate helical axis of motion (HAM) during wrist extension to flexion, in the proximodistal direction. Note that the HAM of the SLI lunate did not demonstrate any significant changes in the proximodistal direction, as the wrist moved from extension to flexion.



### 3.6.2.9. Position of the helical axis of motion results (Tables)

Table 104 The position of the scaphoid helical axis of motion in the radioulnar direction, during wrist ulnar to radial deviation

Reference bin (R)	Comparison bin (C)	Number		Mann-Whitney U	Wilcoxon W	Z score	Significance
		R	C				
20 ° UD	10° UD	22	24	150.0	450.0	-2.507	0.012*
10° UD	0° (Neutral)	24	29	159.0	594.0	-3.377	<0.001*
0° (Neutral)	10° RD	29	27	323.0	701.0	-1.123	0.261
10° RD	20° RD	27	19	215.0	405.0	-0.926	0.355

\*Indicate statistical significance by the Mann-Whitney U test at a p value of 0.05. The position of the HAM became more radial with the wrist radial deviation.

Table 105 The position of the scaphoid helical axis of motion in the dorso-volar direction, during wrist ulnar to radial deviation

Reference bin (R)	Comparison bin (C)	Number		Mann-Whitney U	Wilcoxon W	Z score	Significance
		R	C				
20 ° UD	10° UD	22	24	240.0	540.0	-0.528	0.598
10° UD	0° (Neutral)	24	29	290.0	590.0	-1.036	0.300
0° (Neutral)	10° RD	29	27	335.0	713.0	-0.926	0.354
10° RD	20° RD	27	19	245.0	435.0	-0.257	0.798

Table 106 The position of the scaphoid helical axis of motion in the proximodistal direction, during wrist ulnar to radial deviation

Reference bin (R)	Comparison bin (C)	Number		Mann-Whitney U	Wilcoxon W	Z score	Significance
		R	C				
20 ° UD	10° UD	22	24	192.0	492.0	-1.583	0.113
10° UD	0° (Neutral)	24	29	180.0	615.0	-3.002	0.003*
0° (Neutral)	10° RD	29	27	309.0	687.0	-1.353	0.176
10° RD	20° RD	27	19	215.0	405.0	-0.926	0.355

\*Indicate statistical significance by the Mann-Whitney U test at a p value of 0.05. The position of the HAM became more proximal with the wrist radial deviation.

Table 107 The position of the lunate helical axis of motion in the radioulnar direction, during wrist ulnar to radial deviation

Reference bin (R)	Comparison bin (C)	Number		Mann-Whitney U	Wilcoxon W	Z score	Significance
		R	C				
20 ° UD	10° UD	22	26	138	489	-3.062	*0.002
10° UD	0° (Neutral)	26	28	129	535	-4.068	*<0.001
0° (Neutral)	10° RD	28	23	316	592	-0.114	0.91
10° RD	20° RD	23	14	106	211	-1.722	0.085

\*Indicate statistical significance by the Mann-Whitney U test at a p value of 0.05. The position of the HAM became more radial with the wrist radial deviation.

Table 108 The position of the lunate helical axis of motion in the dorso-volar direction, during wrist ulnar to radial deviation

Reference bin (R)	Comparison bin (C)	Number		Mann-Whitney U	Wilcoxon W	Z score	Significance
		R	C				
20 ° UD	10° UD	22	26	176	527	-2.276	0.023*
10° UD	0° (Neutral)	26	28	316	667	-0.831	0.406
0° (Neutral)	10° RD	28	23	198	604	-2.347	0.019*
10° RD	20° RD	23	14	142	418	-0.595	0.552

\*Indicate statistical significance by the Mann-Whitney U test at a p value of 0.05

Table 109 The position of the lunate helical axis of motion in the proximodistal direction, during wrist ulnar to radial deviation

Reference bin (R)	Comparison bin (C)	Number		Mann-Whitney U	Wilcoxon W	Z score	Significance
		R	C				
20 ° UD	10° UD	22	26	173	524	-2.338	0.019*
10° UD	0° (Neutral)	26	28	160	566	-3.532	<0.001*
0° (Neutral)	10° RD	28	23	303	579	-0.36	0.719
10° RD	20° RD	23	14	137	242	-0.752	0.452

\*Indicate statistical significance by the Mann-Whitney U test at a p value of 0.05. The position of the HAM became more proximal with the wrist radial deviation.

Table 110 The position of the SLI scaphoid helical axis of motion in the radioulnar direction, during wrist ulnar to radial deviation

Reference bin (R)	Comparison bin (C)	Number		Mann-Whitney U	Wilcoxon W	Z score	Significance
		R	C				
20 ° UD	10° UD	14	18	117	288	-0.342	0.732
10° UD	0° (Neutral)	18	25	152	477	-1.797	0.072
0° (Neutral)	10° RD	25	20	194	404	-1.279	0.201
10° RD	20° RD	20	15	123	243	-0.9	0.368

The position of the HAM became more radial with the wrist radial deviation. There were no statistically significant changes between the wrist positions.

Table 111 The position of the SLI scaphoid helical axis of motion in the dorso-volar direction, during wrist ulnar to radial deviation

Reference bin (R)	Comparison bin (C)	Number		Mann-Whitney U	Wilcoxon W	Z score	Significance
		R	C				
20 ° UD	10° UD	14	18	111	282	-0.57	0.569
10° UD	0° (Neutral)	18	25	210	381	-0.369	0.712
0° (Neutral)	10° RD	25	20	182	507	-1.553	0.12
10° RD	20° RD	20	15	139	259	-0.367	0.714

No significant changes occur in the position of the SLI-scaphoid HAM as the wrist moved from ulnar to radial deviation in the dorso-volar plane.

Table 112 The position of the SLI scaphoid helical axis of motion in the proximodistal direction, during wrist ulnar to radial deviation

Reference bin (R)	Comparison bin (C)	Number		Mann-Whitney U	Wilcoxon W	Z score	Significance
		R	C				
20 ° UD	10° UD	14	18	106	277	-0.76	0.447
10° UD	0° (Neutral)	18	25	158	483	-1.649	0.099
0° (Neutral)	10° RD	25	20	226	551	-0.548	0.584
10° RD	20° RD	20	15	128	248	-0.733	0.463

No significant changes occur in the position of the SLI-scaphoid HAM as the wrist moved from ulnar to radial deviation in the proximo-distal plane.

Table 113 The position of the SLI lunate helical axis of motion in the radioulnar direction, during wrist ulnar to radial deviation

Reference bin (R)	Comparison bin (C)	Number		Mann-Whitney U	Wilcoxon W	Z score	Significance
		R	C				
20° UD	10° UD	13	20	119	329	-0.405	0.685
10° UD	0° (Neutral)	20	18	69	240	-3.245	0.001*
0° (Neutral)	10° RD	18	11	89	155	-0.449	0.653
10° RD	20° RD	11	9	33	78	-1.254	0.21

\*Indicate statistical significance by the Mann-Whitney U test at a p value of 0.05. The position of the HAM of the SLI lunate became more radial with the wrist radial deviation.

Table 114 The position of the SLI lunate helical axis of motion in the dorso-volar direction, during wrist ulnar to radial deviation

Reference bin (R)	Comparison bin (C)	Number		Mann-Whitney U	Wilcoxon W	Z score	Significance
		R	C				
20° UD	10° UD	13	20	75	285	-2.026	0.043*
10° UD	0° (Neutral)	20	18	116	326	-1.871	0.061
0° (Neutral)	10° RD	18	11	49	220	-2.247	0.025*
10° RD	20° RD	11	9	49	94	-0.038	0.97

\*Indicate statistical significance by the Mann-Whitney U test at a p value of 0.05

Table 115 The position of the SLI lunate helical axis of motion in the proximodistal direction, during wrist ulnar to radial deviation

Reference bin (R)	Comparison bin (C)	Number		Mann-Whitney U	Wilcoxon W	Z score	Significance
		R	C				
20° UD	10° UD	13	20	105	196	-0.921	0.357
10° UD	0° (Neutral)	20	18	79	250	-2.953	0.003*
0° (Neutral)	10° RD	18	11	76	142	-1.034	0.301
10° RD	20° RD	11	9	45	90	-0.342	0.732

\*Indicate statistical significance by the Mann-Whitney U test at a p value of 0.05. The position of the HAM of the SLI lunate became more proximal with the wrist radial deviation.

*Table 116 The position of the normal scaphoid helical axis of motion in the radioulnar direction, during wrist extension to flexion*

Reference bin (R)	Comparison bin (C)	Number		Mann- Whitney U	Wilcoxon W	Z score	Significance
		R	C				
70 ° Ext	60 ° Ext	4	9	7	52	-1.697	0.09
60 ° Ext	50 ° Ext	9	15	55	100	-0.745	0.456
50 ° Ext	40 ° Ext	15	13	85	176	-0.576	0.565
40 ° Ext	30 ° Ext	13	13	80	171	-0.231	0.817
30 ° Ext	20 ° Ext	13	17	110	201	-0.021	0.983
20 ° Ext	10 ° Ext	17	14	115	268	-0.159	0.874
10 ° Ext	0° (Neutral)	14	18	102	273	-0.912	0.362
0° (Neutral)	10 ° Flex	18	11	92	263	-0.315	0.753
10 ° Flex	20 ° Flex	11	17	84	150	-0.447	0.655
20 ° Flex	30 ° Flex	17	7	58	211	-0.095	0.924
30 ° Flex	40 ° Flex	7	12	34	62	-0.095	0.499
40 ° Flex	50 ° Flex	12	5	17	32	-1.37	0.171
50 ° Flex	60 ° Flex	5	9	9	24	-1.8	0.072
60 ° Flex	70 ° Ext	9	5	11	26	-1.533	0.125

*The position of the HAM of the normal scaphoid was not different between the wrist positions from extension to flexion in radioulnar direction.*

Table 117 The position of the normal scaphoid helical axis of motion in the dorso-volar direction, during wrist extension to flexion

Reference bin (R)	Comparison bin (C)	Number		Mann- Whitney U	Wilcoxon W	Z score	Significance
		R	C				
70 ° Ext	60 ° Ext	4	9	9	54	-1.389	0.165
60 ° Ext	50 ° Ext	9	15	56	101	-0.686	0.493
50 ° Ext	40 ° Ext	15	13	89	209	-0.392	0.695
40 ° Ext	30 ° Ext	13	13	74	165	-0.538	0.59
30 ° Ext	20 ° Ext	13	17	87	178	-0.984	0.325
20 ° Ext	10 ° Ext	17	14	109	214	-0.397	0.691
10 ° Ext	0° (Neutral)	14	18	74	179	-1.975	0.058
0° (Neutral)	10 ° Flex	18	11	68	239	-1.393	0.164
10 ° Flex	20 ° Flex	11	17	91	244	-0.118	0.906
20 ° Flex	30 ° Flex	17	7	45	198	-0.921	0.357
30 ° Flex	40 ° Flex	7	12	41	119	-0.921	0.933
40 ° Flex	50 ° Flex	12	5	23	38	-0.738	0.461
50 ° Flex	60 ° Flex	5	9	19	34	-0.467	0.641
60 ° Flex	70 ° Ext	9	5	20	35	-0.333	0.739

The position of the HAM of the normal scaphoid wasnot different between the wrist positions from extension to flexion in dorsovolar direction.

*Table 118 The position of the normal scaphoid helical axis of motion in the proximodistal direction, during wrist extension to flexion*

Reference bin (R)	Comparison bin (C)	Number		Mann- Whitney U	Wilcoxon W	Z score	Significance
		R	C				
70 ° Ext	60 ° Ext	4	9	13	58	-0.772	0.44
60 ° Ext	50 ° Ext	9	15	62	107	-0.328	0.743
50 ° Ext	40 ° Ext	15	13	62	182	-1.635	0.102
40 ° Ext	30 ° Ext	13	13	62	153	-1.154	0.249
30 ° Ext	20 ° Ext	13	17	89	242	-0.9	0.368
20 ° Ext	10 ° Ext	17	14	91	244	-1.111	0.266
10 ° Ext	0° (Neutral)	14	18	115	286	-0.418	0.676
0° (Neutral)	10 ° Flex	18	11	89	260	-0.449	0.653
10 ° Flex	20 ° Flex	11	17	60	213	-1.576	0.115
20 ° Flex	30 ° Flex	17	7	59	212	-0.032	0.975
30 ° Flex	40 ° Flex	7	12	36	114	-0.032	0.612
40 ° Flex	50 ° Flex	12	5	21	99	-0.949	0.343
50 ° Flex	60 ° Flex	5	9	22	67	-0.067	0.947
60 ° Flex	70 ° Ext	9	5	19	34	-0.467	0.641

*The position of the HAM of the normal scaphoid were not different between the wrist positions from extension to flexion in proximodistal direction.*

Table 119 The position of the normal lunate helical axis of motion in the radioulnar direction, during wrist extension to flexion

Reference bin (R)	Comparison bin (C)	Number		Mann- Whitney U	Wilcoxon W	Z score	Significance
		R	C				
70 ° Ext	60 ° Ext	3	7	8	14	-0.57	0.569
60 ° Ext	50 ° Ext	7	8	19	55	-1.042	0.298
50 ° Ext	40 ° Ext	8	8	21	57	-1.155	0.248
40 ° Ext	30 ° Ext	8	9	17	53	-1.828	0.068
30 ° Ext	20 ° Ext	9	12	52	130	-0.142	0.887
20 ° Ext	10 ° Ext	12	11	52	118	-0.862	0.389
10 ° Ext	0° (Neutral)	11	18	92	263	-0.315	0.753
0° (Neutral)	10 ° Flex	18	11	78	144	-0.944	0.345
10 ° Flex	20 ° Flex	11	17	44	110	-2.328	0.02*
20 ° Flex	30 ° Flex	17	5	38	53	-0.353	0.724
30 ° Flex	40 ° Flex	5	11	21	36	-0.353	0.462
40 ° Flex	50 ° Flex	11	5	12	27	-1.756	0.079
50 ° Flex	60 ° Flex	5	8	8	23	-1.757	0.079
60 ° Flex	70 ° Ext	8	5	15	30	-0.732	0.464

\*Indicate statistical significance by the Mann-Whitney U test at a p value of 0.05.



Table 120 The position of the normal lunate helical axis of motion in the dorso-volar direction, during wrist extension to flexion

Reference bin (R)	Comparison bin (C)	Number		Mann-Whitney U	Wilcoxon W	Z score	Significance
		R	C				
70 ° Ext	60 ° Ext	3	7	10	16	-0.114	0.909
60 ° Ext	50 ° Ext	7	8	24	52	-0.463	0.643
50 ° Ext	40 ° Ext	8	8	27	63	-0.525	0.6
40 ° Ext	30 ° Ext	8	9	22	58	-1.347	0.178
30 ° Ext	20 ° Ext	9	12	49	94	-0.355	0.722
20 ° Ext	10 ° Ext	12	11	59	125	-0.431	0.667
10 ° Ext	0° (Neutral)	11	18	52	118	-2.112	0.035*
0° (Neutral)	10 ° Flex	18	11	91	262	-0.36	0.719
10 ° Flex	20 ° Flex	11	17	88	241	-0.259	0.796
20 ° Flex	30 ° Flex	17	5	35	188	-0.588	0.557
30 ° Flex	40 ° Flex	5	11	25	91	-0.588	0.777
40 ° Flex	50 ° Flex	11	5	22	37	-0.623	0.533
50 ° Flex	60 ° Flex	5	8	17	53	-0.439	0.661
60 ° Flex	70 ° Ext	8	5	18	33	-0.293	0.77

\*Indicate statistical significance by the Mann-Whitney U test at a p value of 0.05. The only significant change of the HAM of the normal lunate in the dorso-volar direction occurred between 10° wrist extension to the neutral position.

Table 121 The position of the normal lunate helical axis of motion in the proximodistal direction, during wrist extension to flexion

Reference bin (R)	Comparison bin (C)	Number		Mann- Whitney U	Wilcoxon W	Z score	Significance
		R	C				
70 ° Ext	60 ° Ext	3	7	10	38	-0.114	0.909
60 ° Ext	50 ° Ext	7	8	17	45	-1.273	0.203
50 ° Ext	40 ° Ext	8	8	28	64	-0.42	0.674
40 ° Ext	30 ° Ext	8	9	28	73	-0.77	0.441
30 ° Ext	20 ° Ext	9	12	42	87	-0.853	0.394
20 ° Ext	10 ° Ext	12	11	57	123	-0.554	0.58
10 ° Ext	0° (Neutral)	11	18	78	144	-0.944	0.345
0° (Neutral)	10 ° Flex	18	11	73	244	-1.169	0.243
10 ° Flex	20 ° Flex	11	17	50	203	-2.046	0.041*
20 ° Flex	30 ° Flex	17	5	19	172	-1.841	0.066
30 ° Flex	40 ° Flex	5	11	23	89	-1.841	0.61
40 ° Flex	50 ° Flex	11	5	20	35	-0.85	0.396
50 ° Flex	60 ° Flex	5	8	19	34	-0.146	0.884
60 ° Flex	70 ° Ext	8	5	18	33	-0.293	0.77

\*Indicate statistical significance by the Mann-Whitney U test at a p value of 0.05. The only significant change of the HAM of the normal lunate in the proximodistal direction occurred between 10° wrist flexion to 20° wrist flexion.

Table 122 The position of the SLI scaphoid helical axis of motion in the radioulnar direction, during wrist extension to flexion

Reference bin (R)	Comparison bin (C)	Number		Mann- Whitney U	Wilcoxon W	Z score	Significance
		R	C				
60 ° Ext	50 ° Ext	7	8	23	59	-0.579	0.563
50 ° Ext	40 ° Ext	8	15	58	178	-0.129	0.897
40 ° Ext	30 ° Ext	15	13	85	176	-0.576	0.565
30 ° Ext	20 ° Ext	13	18	116	207	-0.04	0.968
20 ° Ext	10 ° Ext	18	20	137	308	-1.257	0.209
10 ° Ext	0° (Neutral)	20	22	165	418	-1.385	0.166
0° (Neutral)	10 ° Flex	22	16	135	388	-1.212	0.225
10 ° Flex	20 ° Flex	16	15	103	223	-0.672	0.502
20 ° Flex	30 ° Flex	15	13	74	194	-1.083	0.279
30 ° Flex	40 ° Flex	13	10	61	116	-1.083	0.804
40 ° Flex	50 ° Flex	10	5	19	34	-0.735	0.462

Note-The HAM of the SLI scaphoid did not change significantly between any consecutive wrist position from extension to flexion in the radioulnar direction.

*Table 123 The position of the SLI scaphoid helical axis of motion in the dorso-volar direction, during wrist extension to flexion*

Reference bin (R)	Comparison bin (C)	Number		Mann- Whitney U	Wilcoxon W	Z score	Significance
		R	C				
60 ° Ext	50 ° Ext	7	8	16	44	-1.389	0.165
50 ° Ext	40 ° Ext	8	15	51	171	-0.581	0.561
40 ° Ext	30 ° Ext	15	13	82	202	-0.714	0.475
30 ° Ext	20 ° Ext	13	18	71	162	-1.841	0.066
20 ° Ext	10 ° Ext	18	20	146	317	-0.994	0.32
10 ° Ext	0° (Neutral)	20	22	218	428	-0.05	0.96
0° (Neutral)	10 ° Flex	22	16	166	419	-0.296	0.767
10 ° Flex	20 ° Flex	16	15	95	231	-0.988	0.323
20 ° Flex	30 ° Flex	15	13	81	201	-0.76	0.447
30 ° Flex	40 ° Flex	13	10	48	103	-0.76	0.292
40 ° Flex	50 ° Flex	10	5	12	67	-1.592	0.111

*The HAM of the SLI scaphoid did not change significantly between any consecutive wrist position from extension to flexion in the dorso-volar direction.*

Table 124 The position of the SLI scaphoid helical axis of motion in the proximodistal direction, during wrist extension to flexion

Reference bin (R)	Comparison bin (C)	Number		Mann-Whitney U	Wilcoxon W	Z score	Significance
		R	C				
60 ° Ext	50 ° Ext	7	8	3	31	-2.893	0.004*
50 ° Ext	40 ° Ext	8	15	58	94	-0.129	0.897
40 ° Ext	30 ° Ext	15	13	97	217	-0.023	0.982
30 ° Ext	20 ° Ext	13	18	114	285	-0.12	0.904
20 ° Ext	10 ° Ext	18	20	167	338	-0.38	0.704
10 ° Ext	0° (Neutral)	20	22	163	416	-1.436	0.151
0° (Neutral)	10 ° Flex	22	16	121	257	-1.626	0.104
10 ° Flex	20 ° Flex	16	15	62	182	-2.293	0.022*
20 ° Flex	30 ° Flex	15	13	96	187	-0.069	0.945
30 ° Flex	40 ° Flex	13	10	56	111	-0.069	0.577
40 ° Flex	50 ° Flex	10	5	19	34	-0.735	0.462

\*Indicate statistical significance by the Mann-Whitney U test at a p value of 0.05. The significant changes of the HAM of the SLI scaphoid in the proximodistal direction occurred between 60° to 50° wrist extension and between 10° wrist flexion to 20° wrist flexion.

Table 125 The position of the SLI lunate helical axis of motion in the radioulnar direction, during wrist extension to flexion

Reference bin (R)	Comparison bin (C)	Number		Mann- Whitney U	Wilcoxon W	Z score	Significance
		R	C				
60 ° Ext	50 ° Ext	4	4	8	18	0	1
50 ° Ext	40 ° Ext	4	5	9	24	-0.245	0.806
40 ° Ext	30 ° Ext	5	7	11	26	-1.056	0.291
30 ° Ext	20 ° Ext	7	3	5	11	-1.254	0.21
20 ° Ext	10 ° Ext	3	3	4	10	-0.218	0.827
10 ° Ext	0° (Neutral)	3	10	12	18	-0.507	0.612
0° (Neutral)	10 ° Flex	10	10	44	99	-0.454	0.65
10 ° Flex	20 ° Flex	10	15	71	126	-0.222	0.824
20 ° Flex	30 ° Flex	15	13	78	198	-0.898	0.369
30 ° Flex	40 ° Flex	13	10	48	103	-0.898	0.292
40 ° Flex	50 ° Flex	10	5	17	32	-0.98	0.327

Note -There were no significant radial or ulna change of the position of the helical axis of motion in the SLI lunate.

Table 126 The position of the SLI lunate helical axis of motion in the dorso-volar direction, during wrist extension to flexion

Reference bin (R)	Comparison bin (C)	Number		Mann- Whitney U	Wilcoxon W	Z score	Significance
		R	C				
60 ° Ext	50 ° Ext	4	4	5	15	-0.866	0.386
50 ° Ext	40 ° Ext	4	5	4	14	-1.47	0.142
40 ° Ext	30 ° Ext	5	7	2	17	-2.517	0.012*
30 ° Ext	20 ° Ext	7	3	6	12	-1.026	0.305
20 ° Ext	10 ° Ext	3	3	2	8	-1.091	0.275
10 ° Ext	0° (Neutral)	3	10	14	20	-0.169	0.866
0° (Neutral)	10 ° Flex	10	10	46	101	-0.302	0.762
10 ° Flex	20 ° Flex	10	15	56	111	-1.054	0.292
20 ° Flex	30 ° Flex	15	13	88	208	-0.438	0.662
30 ° Flex	40 ° Flex	13	10	65	120	-0.438	0.987
40 ° Flex	50 ° Flex	10	5	23	38	-0.245	0.806

\*Indicate statistical significance by the Mann-Whitney U test at a p value of 0.05. The helical axis of motion of the SLI lunate changed to be more volar as the wrist moved from extension to flexion with a significant change occurring at 40° to 30° of flexion.

Table 127 The position of the SLI lunate helical axis of motion in the proximodistal direction, during wrist extension to flexion

Reference bin (R)	Comparison bin (C)	Number		Mann- Whitney U	Wilcoxon W	Z score	Significance
		R	C				
60 ° Ext	50 ° Ext	4	4	6	16	-0.577	0.564
50 ° Ext	40 ° Ext	4	5	6	21	-0.98	0.327
40 ° Ext	30 ° Ext	5	7	15	30	-0.406	0.685
30 ° Ext	20 ° Ext	7	3	8	14	-0.57	0.569
20 ° Ext	10 ° Ext	3	3	4	10	-0.218	0.827
10 ° Ext	0° (Neutral)	3	10	12	67	-0.507	0.612
0° (Neutral)	10 ° Flex	10	10	34	89	-1.209	0.226
10 ° Flex	20 ° Flex	10	15	71	191	-0.222	0.824
20 ° Flex	30 ° Flex	15	13	94	214	-0.161	0.872
30 ° Flex	40 ° Flex	13	10	45	100	-0.161	0.215
40 ° Flex	50 ° Flex	10	5	14	29	-1.347	0.178

The helical axis of motion of the SLI lunate did not demonstrate any significant changes in the proximodistal direction, as the wrist moved from extension to flexion.



### **3.6.3. Important outcome measures-Helical axis of motion**

There were sequential changes in the orientation of the HAM for the normal scaphoid with the incremental wrist positions from ulnar to radial deviation. The changes were significant in the axial plane when the wrist was moving from ulnar deviation to neutral. From neutral to radial deviation there were no significant changes. The normal lunate also had similar changes in helical axis orientation.

In the SLI scaphoid, throughout the range the orientation of the HAM was similar. The SLI lunate did have significant changes in the orientation occurring in all three planes, but they were not restricted to ulnar deviation, but also occurred during radial deviation of the wrist.

The change in the HAM orientation from maximum ulnar to radial deviation was compared between the SLI and the normal wrist. The change was significantly more in the normal scaphoid and the normal lunate than the SLI scaphoid and the SLI lunate in all three planes.

The location of the HAM of the normal scaphoid sequentially moved from ulnar to radial and distal to proximal with the wrist moving from ulnar to radial deviation. Significant position changes were seen when the wrist was moving from ulnar deviation to neutral. The changes in the position of the HAM of the normal lunate also was similar in direction. However, significant changes occurred when the wrist was in radial deviation as well. The SLI scaphoid HAM position did not change significantly during the range of motion. The SLI lunate had the same changes that were observed in the normal lunate, but the magnitude of the change was reduced.

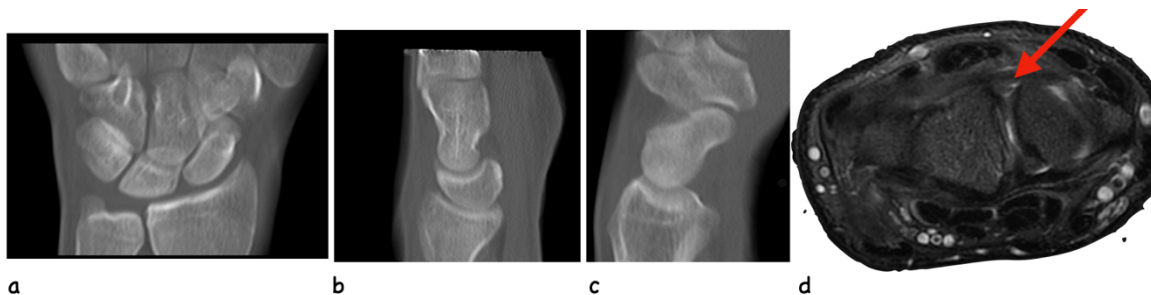
During wrist extension to flexion, there were no significant differences that were identified between the wrist positions in the normal or the SLI wrists. Therefore, comparisons were not made between the normal and SLI groups on the change of position or orientation from maximum extension to maximum flexion.

### 3.7. SPECTRUM OF KINEMATIC CHANGES SEEN IN SLI

In the following section the spectrum of changes that was observed in SLI is presented with examples. A large subgroup analysis was not possible due to inadequate number of cases in each subcategory. Nonetheless, the interesting observations that were noted are presented.

#### ***Case 01 ('Dynamic' SLI)***

The following example is a patient with normal radioscapoid and radiolunate angles and MRI evidence of 'scarring of SLIL' suggestive of partial injury (Figure 147 and Figure 148). Despite the normal radioscapoid and radiolunate angles, this participant had signs of reversal of kinematic pattern of his scaphoid, with greater in-plane motion and less out of plane motion, during wrist radial deviation.



*Figure 147 a, b, c- The neutral wrist position images of the dynamic CT scan of case 01. a. postero anterior view, b. lateral view with the lunate c. lateral view with the scaphoid. d. Axial image of MRI demonstrating possible injury to the scapholunate interosseous ligament (SLIL). Arrow points to the SLIL.*

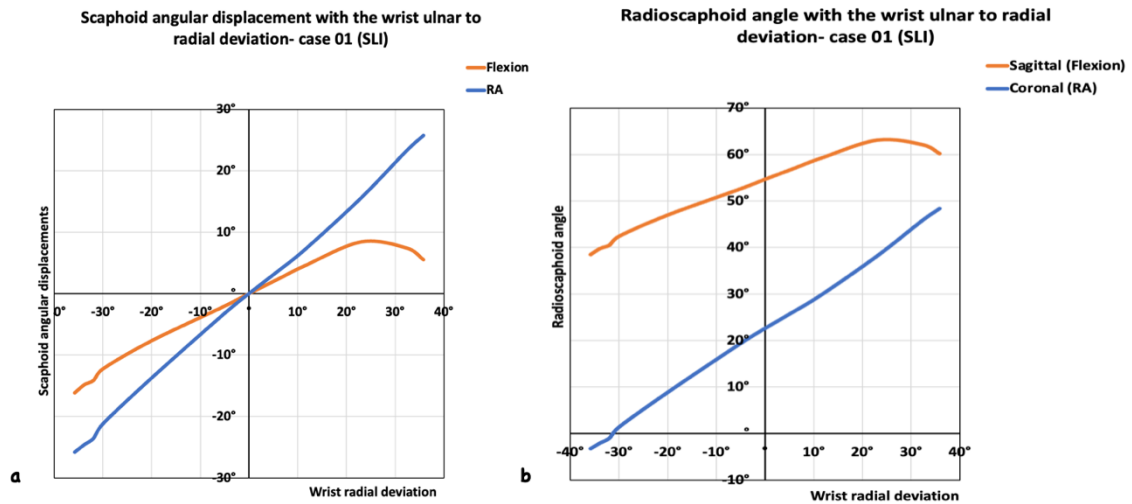


Figure 148 (a) The scaphoid angular displacements (flexion and radial angulation) and (b) the radioscapoid angles of the SLI scaphoid in an example identified as dynamic instability-case 01. Note that when the wrist was in radial deviation, the scaphoid radial angulation was observed to be more than flexion (more in-plane motion and less out-of-plane motion). RA-Radial angulation

### Case 02 ('Static' SLI)

Patients with static SLI also demonstrated the above-mentioned kinematic pattern, where there was more radial angulation of the scaphoid and less flexion, during wrist radial deviation. Case 02 (Figure 149) is an example of 'static' SLI where a clear scapholunate diastasis was visible. The scaphoid flexion and radial angulation during wrist ulnar to radial deviation for case 02 is presented in Figure 150.

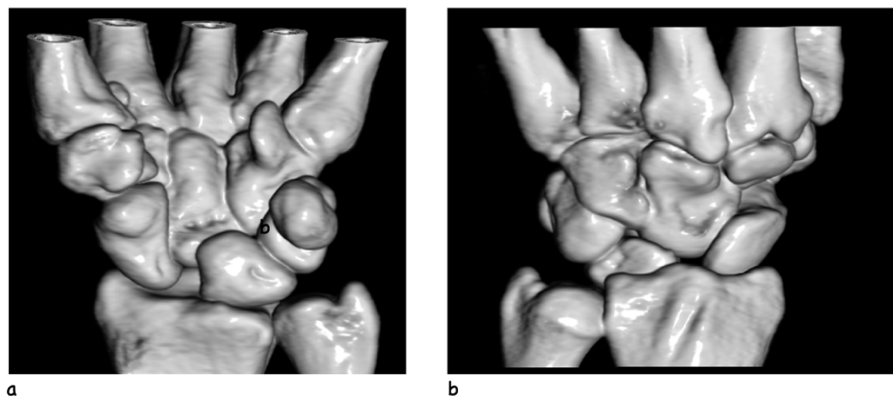


Figure 149 a. anterior and b. posterior views of the dynamic CT scan of the case 02 demonstrating scapholunate diastasis.

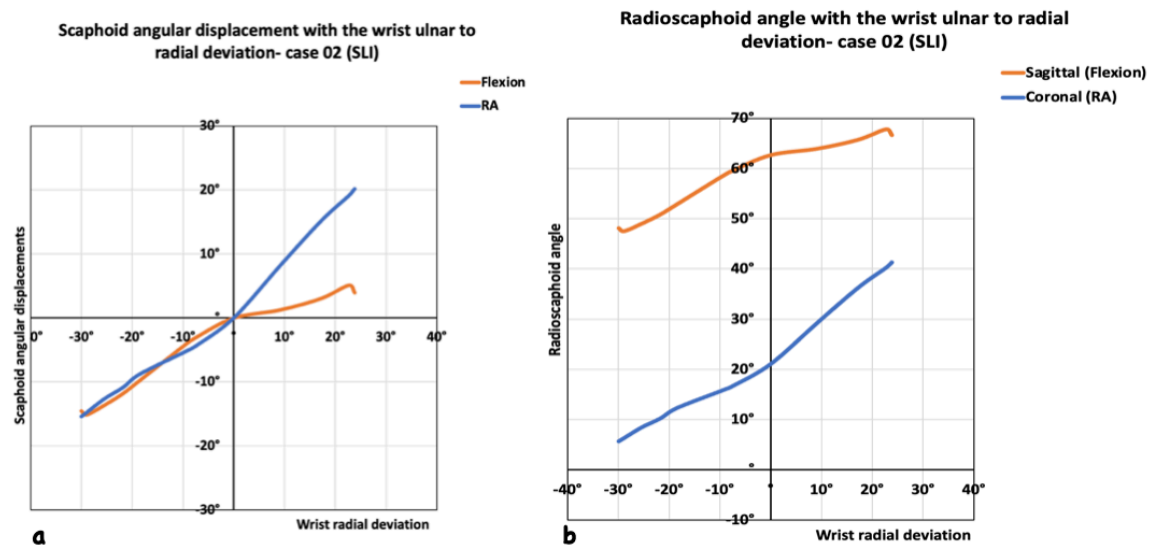


Figure 150 (a)The scaphoid angular displacements (flexion and radial angulation) and (b)the radioscapoid angles of SLI scaphoid in an example identified as static instability (case 02). Note that when the wrist was in radial deviation the scaphoid radial angulation was observed to be more than flexion (more in-plane motion and less out-of-plane motion). RA-Radial angulation

In addition to this reversal of kinematic patterns ‘static’ SLI cases fit in to majority of findings described in the results section.

### Case 03 (SLI with lunate ulnar translocation)

There were three patients with lunate ulnar translocation in this study cohort. Following example is one such case (Figure 151). The ulnar translocation was visible in standard radiography and 3D CT. In addition, it was observed that these patients have an accompanying volar translation of the lunate as well (Figure 152).

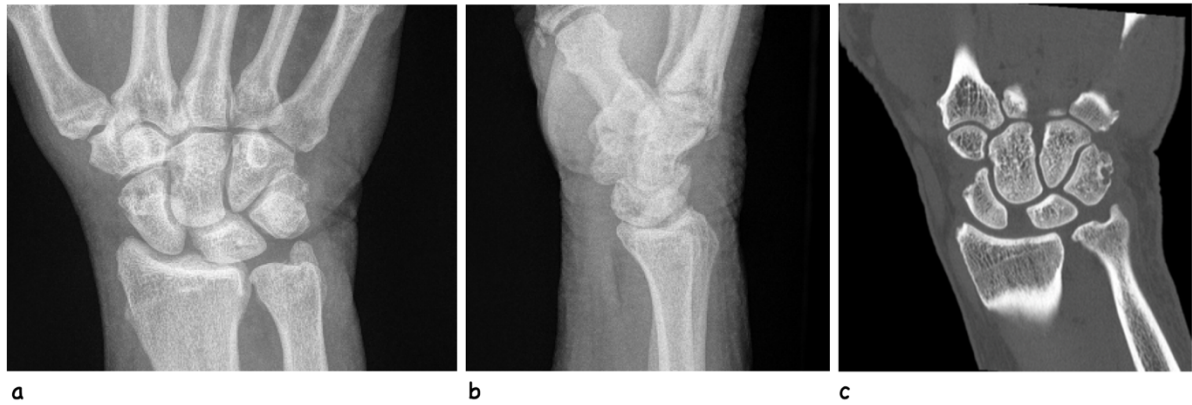


Figure 151 Lunate ulnar translocation (case 03). The lunate uncovering index on X ray was found to be 50 % a. posteroanterior b. lateral radiographs and c. coronal view of the CT scan.

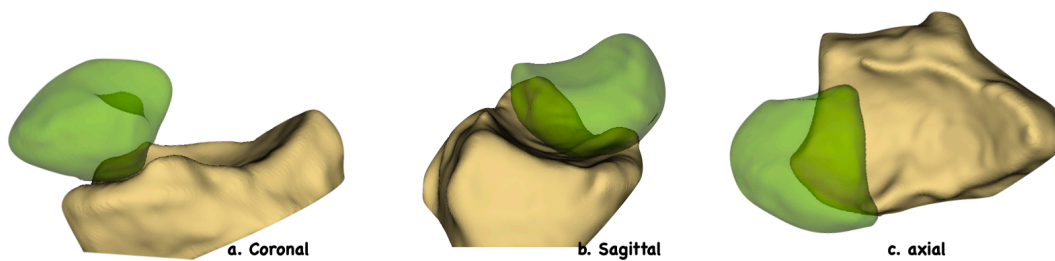


Figure 152 Lunate (case 03) in a. coronal, b. sagittal and c. axial views of the neutral wrist position. Note the volar and ulnar position of the lunate in the axial view, which was not clearly visible on standard radiographs or CT scans.

The lunate centroid position for case 03, with the wrist moving from ulnar to radial deviation is presented in Figure 153. The mean lunate centroid position for the normal and SLI cohorts is also depicted in the same graph for comparison. The lunate centroid of case 03 was volar and ulnar compared to the normal and SLI cohorts. Wrist ulnar to radial deviation was restricted in this patient.

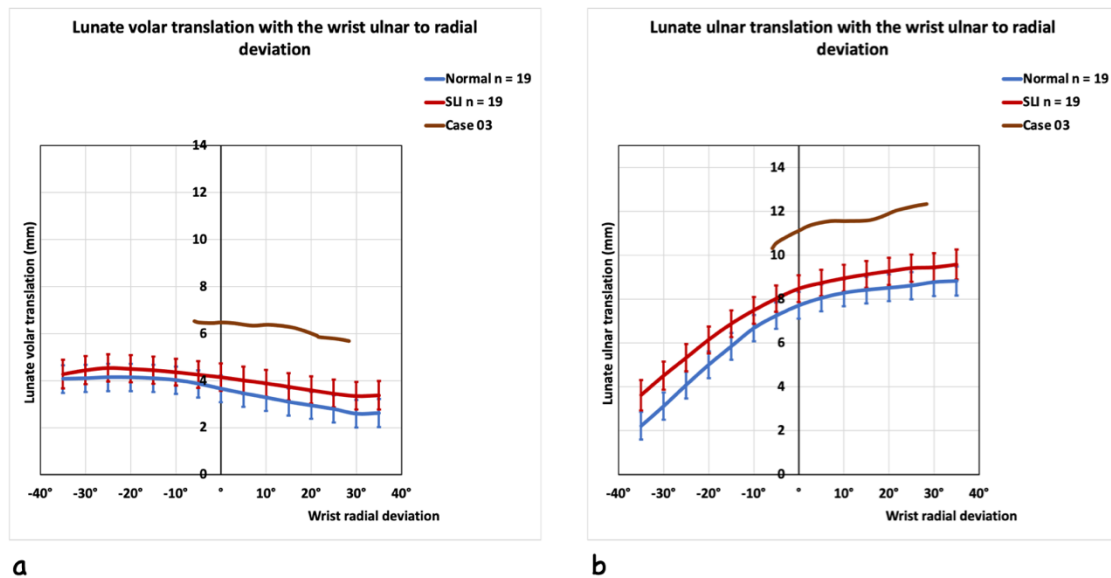


Figure 153 The lunate centroid position with the wrist ulnar to radial deviation. Note that the lunate centroid of case 03 is located volar and ulnar in the background of the normal and SLI cohorts. This patient did have limited range of motion in ulnar to radial deviation.

In addition, the flexion of the lunate of case 03 was markedly restricted from wrist extension to the neutral (Figure 154). The central column flexion occurred through the midcarpal joint until the wrist passed the neutral position (Figure 155). Once the wrist is in flexion, the lunate flexion occurred at the radiocarpal joint.

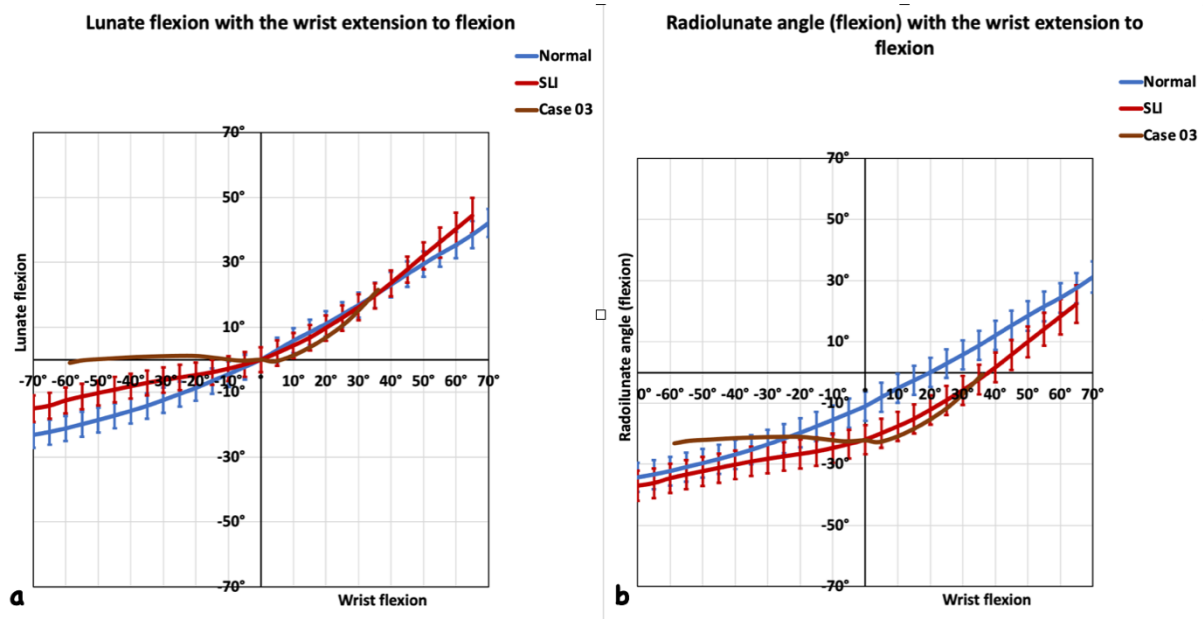


Figure 154 (a) Lunate flexion and (b) the radiolunate angle of case 03, during wrist extension to flexion, in the background of normal and SLI cohorts. Note that the case 03 lunate did not flex, during the wrist movement from extension to the neutral. Compare with Figure 155.

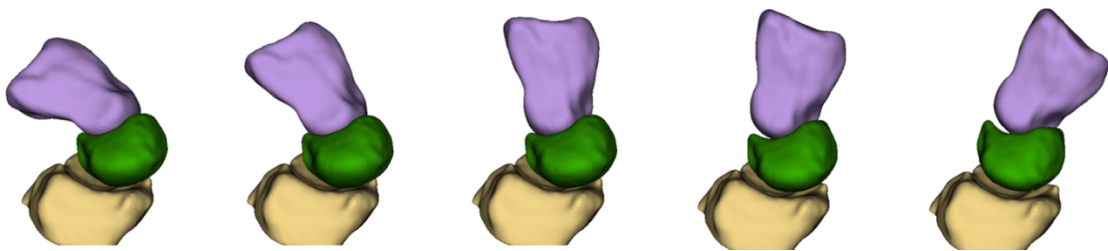
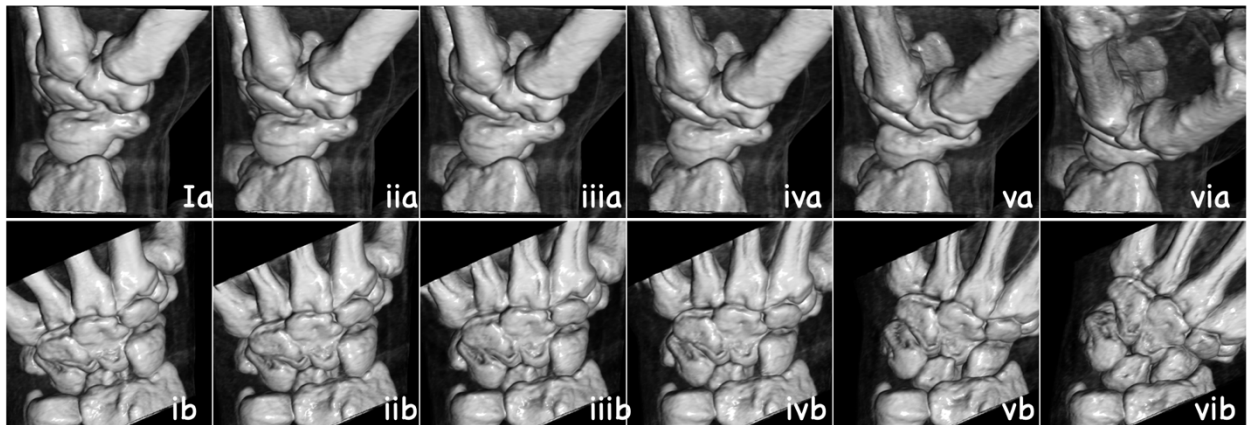


Figure 155 Lunate flexion of case 03, during wrist extension to flexion. Note that the case 03 lunate does not flex, during the wrist movement from extension to the neutral. Lunate flexion occurred once the capitate has moved into flexion.

#### **Case 04 (SLI with scaphoid dorsal subluxation)**

The following patient (case 04) had a clear scaphoid dorsal subluxation. In his 4D CT scan, it was observed that the scaphoid proximal pole was perched at the dorsal rim of the radius during the ulnar deviation of the wrist (Figure 156). Approximately at 10° radial deviation of the wrist, the subluxation reduced.



*Figure 156 The 4D CT images from case 04, with the wrist moving from ulnar to radial deviation. Top row (a)-radial views. Bottom row (b)-dorsal views. In the radial views, note that the scaphoid flexion angle remains relatively unchanged throughout the wrist motion, the proximal pole of the scaphoid is perched at the dorsal rim of the radius in images I a to iv a. As the wrist radially deviated in the images v a to vi a, the proximal pole became contained within the radioscapoid facet. Note the similar findings in the dorsal views and also the dorsal scapholunate gap was less when the wrist was in radial deviation compared to ulnar deviation.*

The graphs for case 03 is presented as Figure 157 and Figure 158. The variability of scaphoid flexion was minimal when the wrist was in ulnar deviation, followed by approximately 5° of extension when the wrist radially deviated 10° from the neutral position (Figure 157a). At 10° radial deviation there was an abrupt change in direction of the scaphoid, where it started to flex. There was continuous radial angulation of the scaphoid as the wrist radially deviated (Figure 157b). The scaphoid centroid was located dorsal (Figure 157c) when the wrist was in ulnar deviation. It continued to move volarly until 10° of wrist radial deviation, until the scaphoid subluxation was reduced. From that point onwards, there was no dorsovolar movement of the scaphoid centroid.



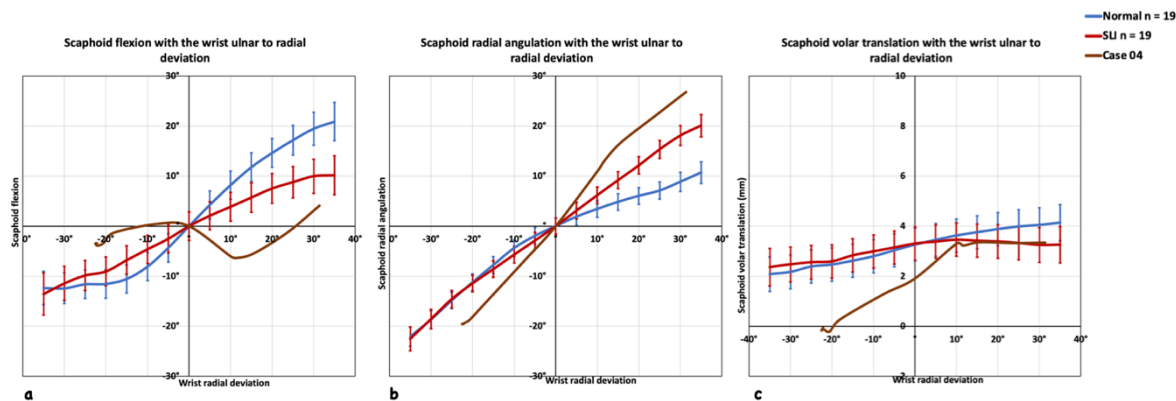


Figure 157 The scaphoid angulations and centroid translation of case 03 with the normal and SLI cohorts in the background. Note the variability in scaphoid flexion (a), increased scaphoid radial angulation (b) and marked dorsal position of the scaphoid centroid until the subluxation was reduced (c). Comparison with Figure 156.

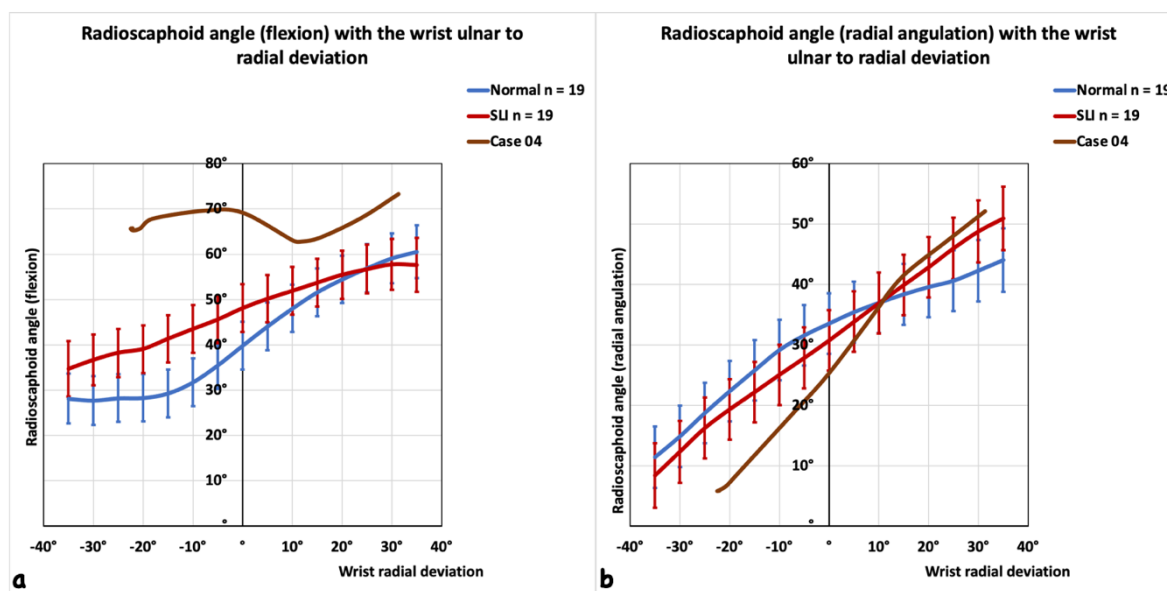
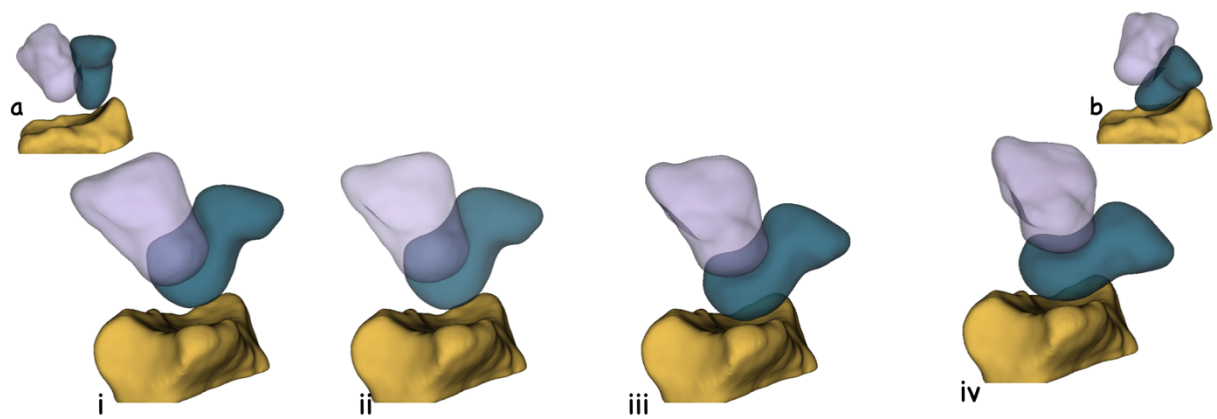


Figure 158 The radioscapoid angles (a. flexion and b. radial angulation) of case 03 with the normal and SLI cohorts in the background. Note the high radioscapoid angle and its' variability (a), increased scaphoid radial angulation (b) Comparison with Figure 156.

Figure 159 is an illustration of scaphoid dorsal subluxation during ulnar deviation of the wrist and how it is contained in the radioscapoid facet when the wrist was in radial deviation.



*Figure 159 Scaphoid dorsal subluxation. Note that with the wrist radial deviation this SLI patient's scaphoid was contained in the radioscapoid fossa. Note an oblique projection was selected for better appreciation of the change in radioscapoid contact. Image 'a' and 'b' are the volar views of the wrist positions depicted in 'i' and 'iv'.*

## CHAPTER 04

### 4. DISCUSSION

Scapholunate instability (SLI) is a dissociative carpal instability that occurs when the scapholunate ligament (SLL) complex is compromised (Linscheid et al., 1972; Mathoulin, 2013). Plain radiographic features of SLI include scapholunate diastasis, scaphoid flexion (Linscheid et al., 1972), proximal scaphoid dorsal subluxation (Chan et al., 2019) and dorsal intercalated segmental instability (DISI) (Linscheid et al., 1972). The 3-dimensional computed tomography (3D-CT) provides a better perspective of the findings and allows an appreciation of the internal rotation of the scaphoid (Garcia-Elias & Lluch, 2017; Omori et al., 2013). 3D-CT also enables the 3D quantification of carpal malalignment in static positions of the wrist.

Malalignment and instability, however, are distinctly different concepts (Garcia-Elias & Lluch, 2017). Garcia Elias reported that the wrist joint is unstable if it is symptomatic, is not able to bear loads, and does not exhibit normal kinematics during any portion of its arc of motion (Garcia-Elias, 1999). Dynamic studies including stress views and dynamic fluoroscopy can accentuate or unmask the instability (Bain et al., 1997). Static imaging only demonstrates the signs of carpal malignment at a particular time point.

Initial research into dynamic changes in SLI was conducted using uniplanar and later biplanar radiography (Garcia-Elias et al., 1989; Ruby et al., 1988). Electromagnetic, optical, and radio-opaque markers have been used to track carpal bones with wrist motion (Bain et al., 2015; Kobayashi, Berger, et al., 1997; Werner et al., 2011). Dynamic tracking of carpal bone motion on cadavers has defined the carpal instability patterns following serial sectioning of carpal ligaments (Short et al., 1995; Short et al., 2007; Werner & Short, 2018). Surgically implanted markers/sensors, limit these studies to be conducted on cadavers. Surgically created ligament injuries in cadavers will respond differently to the traumatic injuries observed in our patients' wrists.

3-D imaging studies combined with marker-less registration techniques have facilitated the in vivo assessment of carpal instabilities (Crisco et al., 2001). 3-D CT-based studies only allow a limited number of static positions to be studied and kinematics in between extrapolated (Best et al., 2019; Crisco et al., 2005). Biplanar video radiography (BVR) and dynamic CT (4D-CT) both overcome these limitations by combining the strengths of 3D CT with marker-less registration and representing true dynamic motion in vivo (Akhbari et al., 2021; R. Carr et al., 2019). BVR has been proven to be accurate in defining in vivo carpal kinematics (Akhbari et al., 2019a, 2019b). However, an inherent limitation is difficulty in the tracking of carpal bones when they overlap (Akhbari et al., 2021). Other concerns with BVR are its limited availability and the time-consuming specialist post-processing assessment.

Dynamic CT offers a unique opportunity to study the in vivo carpal motion, with true movement of the wrist (White et al., 2019). Compared to other techniques, it does not need markers embedded in the carpal bones. Unlike static CT or MRI, has the advantage of capturing the entire motion, rather than a few static positions. Therefore, has the advantage of being able to study the changes during motion, rather than stop-start positions. Unlike biplanar video-radiography (BVR) the output of moving carpal bones created using 4D CT are true 3-D models and do not overlap. Therefore, in the development and study of wrist mechanics, 4D CT is positioned as a unique modality that can assess real patients with different pathologies, throughout motion and with loading.

While 4D CT has been used for in vivo wrist studies investigation in wrist conditions from as early as 2013, the assessments were subjective (Garcia-Elias et al., 2014; Shores et al., 2013). Feasibility and validation of objective quantification of carpal bone displacements were investigated in 2014 (Zhao et al., 2015). The process involves creating surface-rendered models of each carpal bone that can be used to study the carpal postures (Kakar et al., 2016). The radiation dose for a 4D CT scan is 0.231 mSv, which is considered low-dose radiation (R. Carr et al., 2019). Recent 4D CT publications have been directed at improving the diagnostic accuracy of dynamic SL instability (Abou Arab et al., 2018; Athlani et al., 2021; Goelz et al., 2021). Many of these studies focussed on scapholunate diastasis (Abou Arab et al., 2018; Athlani et al., 2020). However, there have been no reports on the 6 degrees of freedom kinematics of the scaphoid and the lunate in SLI compared to the normal wrist in

an in vivo study. Therefore, it was advantageous to use dynamic CT to better understand the in vivo kinematics of SLI, compared to the healthy wrist.

#### **4.1. Validation**

The workflow used in this thesis has been validated and published in multiple previous publications since 2014, not only for the wrist but also for the ankle joint and thumb base (Buzzatti et al., 2018; Mat Jais et al., 2014; Robinson et al., 2021; Wang et al., 2018; Zhao et al., 2015). This included the process of bone segmentation, positioning of the radius or reference bone coordinate system and registration of bone models to calculate Euler's angles, translation, and helical axis of motion.

The above workflow has been adapted from similar studies that used 3D CT to quantify carpal motion, which involves carpal bone segmentation and calculation of displacement (Crisco et al., 1999; Neu et al., 2000; Wolfe et al., 2000). The only conceptual difference was 4D CT was acquired during true wrist motion as a series of 3-dimensional volumes over a period of time. The workflow manages each 3-D volume of the 4D CT scan as a single 3D CT scan consisting of multiple 3D models of the carpal bones, hence, the same post-processing steps can be applied.

The validation studies performed for the current thesis were important to quantify the error rates of the workflow and understand whether it behaves like 3D CT. As 4D CT is low radiation and low resolution, it was a concern that the accuracy and precision of the process could be compromised. Validating the process of segmentation and registration, Zhao et al. reported that the error rates are below 1° for rotation and 1 mm for translations (Zhao et al., 2015).

As part of the current study, a validation process was conducted to assess the feasibility of 4D CT to generate consistent good quality carpal bone segments. Compared to a scaphoid in the first frame (time point zero), all the other segmented scaphoids would be similar at least by 97% as measured using similarity indices. The same results were obtained for the

capitate and the lunate. It is a conclusion of this thesis that it is possible to generate high quality carpal segmentation from 4D CT scans.

Before carpal bone angulations were calculated it was important to define the coordinate system, the radio-ulnar, dorso-volar and proximo distal axes and planes. The guidelines established by the International Society of Biomechanics (ISB) (Wu et al., 2005) were followed, and used them on a partially visualised radius as described in the methodology section and published by de Roo et al. (de Roo et al., 2020). The accuracy of the automatic positioning of the radius coordinate system decreases with the reduction of the visualised radius length in the 4D CT scan (de Roo et al., 2020).

To enable the accuracy of defining the radius coordinate system any 4D CT scans that do not show an adequate length of radius were excluded. There were some scans where, during motion, the radius was almost disappearing from the field of view. Such scans, if at any wrist position the radius was not adequately visualised, were excluded. Every placement of the radius coordinate system was then visually inspected for satisfactory alignment as recommended by (de Roo et al., 2020). Then the aligned partially visualised radius was overlapped with the patient's wrist radiographs, which offered a greater appreciation of the radius length and were aligned in the neutral position and checked for orientation.

Having carefully conducted all these steps and checks, a test and retest assessment of positioning the coordinate system was also conducted. The error rate was worst in the axial plane and was within  $2.1^{\circ}$  ( $\pm 1.48^{\circ}$ ) for angular displacement. The linear displacement error rate was largest along the x-axis and recorded 0.49 mm ( $\pm 0.23$ ) (section 3.1.2). The axial plane rotation represents the internal and external rotation of the carpus. Positioning the coordinate system was not a part of Zhao et al. validation study and most of the other studies. Nonetheless, it is a common problem in every 3D or 4D assessment of the carpus not limited to the radius.

The reason for this problem is that the coordinate systems for every human bone are defined based on anatomical landmarks that can be visually identified and coordinate system can be manually positioned. For instance, the studies on the thumb carpometacarpal joint consider the trapezial coordinate system described by Cooney et al (Cooney et al.,

1981; Goto et al., 2014; Wang et al., 2018) which involves manual positioning of the trapezium coordinate system. The same principle was used for the radius for decades (Goto et al., 2005; Moritomo, Murase, Oka, et al., 2008; Omori et al., 2013). The automatic positioning of the radius coordinate system based on moment of inertia, was used by Crisco et al. (Coburn et al., 2007; Crisco et al., 1999; Crisco et al., 2001). As this depends on automatically identifying the long axis of the radius, the length of the radius that's visible affects the accuracy of the method (de Roo et al., 2020). To increase the reproducibility it was recommended to ensure that there was a satisfactory radial length (de Roo et al., 2020), and to perform manual positioning of the coordinate system if the radius visibility is less than 2 cm.

The third step in the workflow was iterative closest point registration (ICP). This involves matching the carpal bone model in the time point zero with a carpal bone model in a subsequent position, thereby calculating the displacement field. There has been a robust amount of data on using iterative closest point registration to calculate bone displacement since medical image processing was introduced (Maarten Beek et al., 2010; Neu et al., 2000; van de Giessen et al., 2009). A test and retest assessment for ICP registration was also conducted and found that the interclass correlation between repeated observations taken following ICP registration is excellent (0.99) (section 3.1.3).

## **4.2. Patient demographics**

The participants with normal wrists were between the age range of 18- 30 years while the patients with SLI were older (mean age  $36 \pm 13.6$  years). The normal wrist scans were anonymised and archived without any demographic data to comply with the ethics agreement. Therefore, it was not possible to conduct case matching or compare the age or gender distribution to assess if there was a statistically significant difference between the two groups. While this was a limitation of the current thesis, a previous study based on 4D CT has concluded that sex had no influence on carpal kinematics (Brinkhorst et al., 2022). A 3D CT based study has also confirmed once accounted for variation in carpal size, gender does not influence capitate kinematics (Rainbow et al., 2008).

There were no studies that assessed the effect of age in an adult population on carpal kinematics. The healthy participants and SLI patients selected for the current project were all above 18 years of age and had no degenerative changes in the wrist. The further analysis was based on the assumption that, the age does not affect carpal kinematics in a non-arthritic adult population.

4D CT scans of SLI wrists for this project was selected from a database of pathological 4D CT scans maintained at the Flinders Medical Centre. These scans were performed purely for clinical indications. With the existing data from previous researchers stating that the contralateral uninjured wrists were kinematically not normal, it was not justifiable from ethical perspective, to scan the contralateral wrist for clinical reasons. Therefore, pre-existing set of data from Monash University was chosen as the normal control group.

### **4.3. Neutral position of the wrist**

Study 01 confirmed that in the neutral wrist position, the SLI scaphoid was more flexed and internally rotated than the normal scaphoid. Results of study 01 agree with previous studies on the malalignment in the SLI scaphoid (Omori et al., 2013; Ruby et al., 1987; Short et al., 2002b; Werner & Short, 2018). Werner et al. reported that in a cadaveric model, the scaphoid internally rotated less than 4° following the sectioning of SLIL and volar or dorsal carpal ligaments. The mean difference in internal rotation as reported in study 01 of this thesis was 9.8°. It is comparable to the study by Omori et al. that reports SLI scaphoid is 8°(± 4°) internally rotated compared to the normal (Omori et al., 2013).

The findings of the study 01 also confirmed that the lunate in SLI was extended compared to the normal wrist in agreement with previous studies (Linscheid et al., 1972; Omori et al., 2013). The current study did not agree with the supination of the lunate reported by Omori et al (Omori et al., 2013). The potential reason may be that the Omori et al. had a sample size of 3 with grade IV SLI, based on plain radiographs. Therefore, patients represented a higher grade of SLI. The current study had a sample size of 19 SLI wrists, and patients represented the entire spectrum of non-arthritic SLI, which would have added to more variability of lunate axial rotation.





#### 4.4. Radiocarpal kinematics

The focus of Study 01 (2.5) was on three aspects of carpal angulation. Firstly, the 3D radiocarpal angles of the scaphoid and the lunate in the neutral wrist position were computed. Secondly, the angular displacement as a change from the neutral wrist position with the wrist motion was calculated. Then, the radiocarpal angles and centroid positions with wrist motion were calculated.

##### 4.4.1. Radiocarpal angular displacements during wrist motion

Recently there has been multiple 4D CT studies assessing the scaphoid and the lunate angles and scapholunate diastasis (Abou Arab et al., 2018; Rauch et al., 2018; Teixeira et al., 2021). Compared to them, the advantage of the current thesis is that it informs about the objective changes of carpal posture in all 3 planes, during wrist motion.

A study by Rauch et al. (Rauch et al., 2018) reported on the radioscapoid and luno-capitate angles in the sagittal plane during wrist radioulnar deviation using 4D CT. They reported that the change of sagittal plane radioscapoid angle (radioscapoid flexion) observed by two observers were 31° for the normal wrist and 23° (*observer 1*) and 26° (*observer 2*) for the SLI wrist. There was no significant difference between the two groups. Study 01 of this thesis reports values similar to Rauch et al. however, found that SLI scaphoid flexion arc was significantly less than the normal.

According to this thesis, the radioscapoid flexion in ulnar to radial deviation is 33.4° for the normal wrist and 23.6° for the SLI wrist. The study by Rauch et al. only reported on the sagittal plane angles (scaphoid flexion). The current study in-contrast address this limitation by quantifying the change of carpal angles in sagittal, coronal, and axial planes. Study 01 of this thesis also adds that there is an increase in radial angulation of the SLI scaphoid with the wrist radial deviation, which better informs about the 3D kinematic changes of the SLI scaphoid.

While both studies were based on 4D CT, there were some methodological differences. The technique that Rauch et al. used was not a true 3-dimensional analysis, but a multiplanar reconstruction (MPR) slices of 4D CT, with a manually selected longitudinal axis of the scaphoid. 3D models were not created but the longitudinal axis was marked by the observers and tracked through the range of motion. MPRs are generated using 2-dimensional reformatted images that are reconstructed on arbitrary planes from a stack of axial images (Blum et al., 2000). It is reported that the reformatting process can affect the reproducibility with a significant impact on the accuracy of analysis (Capelle et al., 2020; Daggett et al., 2015).

Rauch et al. reported that the reproducibility of the method they used for the luno-capitate angle was 0.79 and the radioscapoid angle was 0.82. It is unclear how the software used in this study calculates the 3-dimensional rotations of carpal bones, however, it is mentioned in the publication as a limitation that due to high 3-dimensional variability, the scapholunate angles could not be calculated. It is my understanding that when MPR reconstructions are arbitrary and user-dependent (Blum et al., 2000), its' ability to capture the 3-dimensional rotations is limited. In the current study, 3D measurements were obtained directly from 3D image reconstructions, which avoids the previously discussed limitations, while maintaining a high level of repeatability (3.1).

Another small but important factor to consider when interpreting Rauch et al.'s findings was that the radius was not aligned to a coordinate system. In these instances, the coordinate system is by default assigned to the coordinate system of the CT scanner, and the carpal angles calculated are compounded by the motion of the forearm and the radius. This increases the error rate, and the error is not systematic as the radius/ forearm motion through the wrist motion is very variable and cannot be quantified without a radius coordinate system. The current study has addressed this limitation by aligning all radii to the coordinate system and also calculating the error rate of such positioning. These methodological limitations are also common to other two 4D CT studies, Abou arab et al. and Teixeira et al. also (Abou Arab et al., 2018; Teixeira et al., 2021). The outcome measures of the latter two studies, however, are different from this thesis.

Another strength of our study in comparison to Rauch et al. was that the longitudinal axis of the scaphoid was automatically calculated on a true 3D model of the scaphoid, that does not depend on observers (Coburn et al., 2007). The current study also reports mean values for the radioscapoid and the radiolunate angles at 5° intervals of wrist motion in all three planes. This true angle is clinically more useful than the total arc of motion. For example, with the results of the study 01, it is possible to inform that the scaphoid was 11.5° extended at 20° ulnar deviation compared to the neutral wrist. It is also 11.4° ulnar angulated and 1.1° internally rotated at 20° ulnar deviation compared to the neutral position. Furthermore, the results in three anatomical planes enable 3-dimensional understanding of the carpal posture during true wrist motion in the normal and SLI wrist in vivo, which is one of the areas with room to improve in the literature.

In a cadaveric study Figueroa et al. also reported that, during wrist radioulnar deviation the flexion of the SLI scaphoid is less than the normal scaphoid (Figueroa et al., 2021). Our findings agree with Figueroa et al.; The current thesis specifically reports that this relative reduction of scaphoid flexion occurs during wrist radial deviation beyond 10°, and not when the wrist is in ulnar deviation.

Study 01 of this thesis also adds that, the reduction of flexion was accompanied by an increase in radial angulation of the SLI scaphoid compared to the normal. While the normal scaphoid externally rotated beyond 10° radial deviation, the SLI scaphoid had significantly less external rotation. This finding on external rotation was however confounded by the values that are within the margin of error of the method. The true significance in axial rotation was observed only beyond 25° of radial deviation.

While direct comparisons of motion between the normal and SLI wrists are important, it is also important to compare the in-plane motion of the scaphoid to its out-of-plane motion. This ratio between in-plane motion and the out-of-plane motion of the scaphoid informs about the net direction of scaphoid motion, and thereby add another important parameter to compare the normal and SLI wrists.

It is well recognised that in the normal wrist, the proximal carpal row moves out-of-plane or into flexion, to allow radial deviation of the distal row (Kobayashi, Berger, et al., 1997; Moritomo, Viegas, Elder, et al., 2000; Neu et al., 2001; Ruby et al., 1988). According to Kobayashi et al. at 15° radial deviation of the wrist, the scaphoid flexed by 8.5° ( $\pm 3^\circ$ ) but radially angulated only 4.2° ( $\pm 2.4^\circ$ ), which is almost 2:1 proportion. The results presented by Brinkhorst et al. in a dynamic CT study also was in accordance with this finding (Brinkhorst et al., 2020). The findings of study 01 of this thesis were in accordance with the previous studies on the normal scaphoid.

With the results of the current study, it can be proposed that with every degree of wrist radial deviation, there was an average of 0.65° of scaphoid flexion; and 0.3° of radial angulation. While the current study confirms what is known on the normal wrist, it adds to the knowledge, that the SLI scaphoid rotated differently. The SLI scaphoid on average radially angulated 0.64° for each degree of wrist radial deviation. Nonetheless, it flexed only 0.29°. This reversal of the magnitudes of the in-plane and out-of-plane motion of the SLI scaphoid, indicates a change in the net direction of scaphoid motion and was detected during wrist radial deviation beyond 10°. The predominant motion of the normal scaphoid in wrist radial deviation was flexion, whereas the predominant motion of the SLI scaphoid in wrist radial deviation was radial angulation.

All these findings can be explained as the scaphoid being dissociated from the lunate and is driven by the distal carpal row into in-plane motion. While this has been theorised for years (Kitay & Wolfe, 2012) there was no in vivo evidence to support that SLI scaphoid had more radial angulation and less flexion with the wrist radial deviation. The reversal of kinematic pattern was one of the fundamental kinematic differences between normal and SLI wrists (3.4.5).

The important point is that SLI creates changes in the direction of scaphoid motion; while maintaining a flexed posture, it radially angulates. It is also important to understand that one of the classic signs of SLI is “flexed scaphoid” but the kinematic change that occurs in SLI is “lack of flexion”. This is one example of malalignment (static position) being different

from instability (unmasked by motion and loading). It is almost paradoxical to say the scaphoid in SLI is “in flexion” but “lacks flexion”.

A possible explanation is that the radial-sided wrist and finger tendons act with the trapezium and trapezoid on the distal pole of the scaphoid, forcing the lateral column to shorten during radial deviation (Figure 160). In the normal wrist, as the radial column shortens, the proximal pole is restrained by the dSL complex. The scaphoid moves into an obligatory flexion, in an out-of-plane motion. In SLI, the proximal pole is ‘unrestrained’ and not linked to the lunate. The scaphoid, therefore, follows the capitate and tends to move in-plane with the distal row during radial deviation.

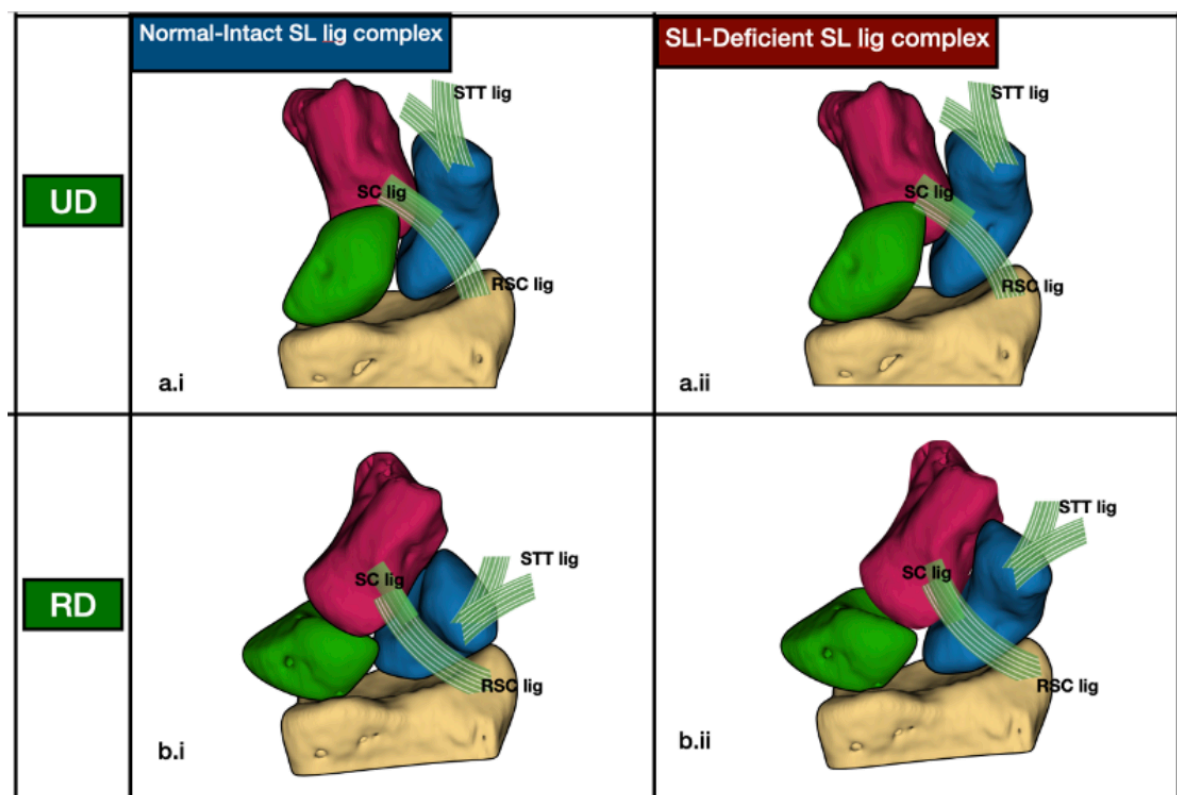


Figure 160 Volar view of the wrist, demonstrating that the SLI scaphoid flexes less than the normal scaphoid. During wrist ulnar to radial deviation the normal scaphoid flexes in an “out-of-plane” motion. (a i and a ii). In contrast in SLI scaphoid, the proximal pole becomes unstable, as the SLL and DIC have been disrupted. As the distal restraints are intact, they provide a deforming force for the scaphoid, leading to less out-of-plane motion and more in-plane motion (b i and b ii). The images shown are examples of normal and SLI wrists.

During wrist extension to flexion, the arc of flexion, or the angular displacement of the SLI scaphoid, was greater than that of the normal scaphoid between the wrist positions of 70°

to 40° extension. A cadaveric study by Figueroa et al. did not find a significant difference in the scaphoid flexion between the normal and SLI deficient wrists during wrist extension to flexion (Figueroa et al., 2021). However, they have not separated the flexion and extension phases of the wrist or compared between a range of wrist positions.

Study 01 of this thesis also reports that the SLI scaphoid flexed less than the normal scaphoid when the wrist was flexing between 50° and 35° of flexion. Therefore, the difference between the SLI scaphoid flexion and the normal scaphoid flexion was influenced by whether the wrist was in a flexed or extended position.

Short et al (Short et al., 2002b) reported following sectioning of SLIL, that the scaphoid flexion arc reduces during wrist flexion-extension. According to Short et al., when the wrist flexed 40°, the normal scaphoid flexed 31.5° and when the wrist extended by 20° the normal scaphoid extended 16.2°. Findings of the current study were similar; with 40° wrist flexion the scaphoid flexion was 31.7° and with 20° wrist extension, the scaphoid extension was 16.0° for the normal wrist. Moojen et al. and Rainbow et al. also have reported similar findings in in-vivo studies based on 3D CT (Moojen, Snel, Ritt, Venema, et al., 2002; Rainbow et al., 2013). According to the study 1 of the current thesis, when the wrist was flexing between 35° to 50° the SLI scaphoid flexion arc was less than the normal, which is in accordance with Short et al. However, the current study does not agree with Short et al. about the findings when the wrist was in extension.

Hence, the results of this thesis were only in partial agreement with the statement that the flexion arc is reduced in SLIL deficient wrist during flexion/ extension. One limitation of the previous studies by Short et al. and Figueroa et al. was that the scaphoid or lunate flexion arc was measured for the entire range of wrist flexion-extension, hence very generalised. Study 01 of the current thesis being a 4D CT study, overcomes that limitation, by presenting scaphoid and lunate displacements for 5° increments of wrist motion.

There are few potential reasons as to why the scaphoid flexes differently when the wrist was flexed and extended. The flexor carpi radialis (FCR) may act as a stabilising force for the scaphoid during the wrist flexion, as it is more at a mechanical advantage. Some researchers

agree on the stabilising function of FCR on scaphoid flexion (Jantea et al., 1994; Linscheid & Dobyns, 2002) however, Salva-Coll and colleagues disagree (Salvà-Coll et al., 2011). They reported that the stabilising function of the FCR is only important in preventing scaphoid pronation and not flexion. The other possible reason is that this phenomenon may be predetermined by the existing radioscapoid angle which is already flexed in SLI. The other potential reason is that the ligaments that connect the scaphoid to the distal row are located volar and have a mechanical advantage to drive the scaphoid when the wrist is in extension.

According to Short et al. with 40° wrist flexion the intact scaphoid radially angulated 2.5° and internally rotated negligibly. With SLIL sectioning they reported significant ulnar angulation of the scaphoid, which was only seen in a limited wrist range of flexion and extension. The ulnar angulation of SLIL deficient scaphoid was not observed with wrist radioulnar deviation. In a subsequent study they reported that when SLIL was sectioned after the RSC, there was a significant ulnar angulation of the scaphoid in the order of 2° to 6° (Short et al., 2005). Data from study 01 were not in accordance with either of these findings. There was 7° of ulnar angulation of the normal scaphoid with 70° wrist flexion in the current study. There was no significant difference between the two groups.

Crisco et al. and Moritomo et al. reported on 3D kinematics of SLI wrists and did not observe such scaphoid ulnar angulation in SLI compared to the normal scaphoid (Crisco et al., 2003; Omori et al., 2013). Another in vivo study on the normal wrist using 4D CT (Brinkhorst et al., 2020) demonstrated that normal scaphoid angulates ulnarly with wrist flexion, which agrees with the results of study 01 but disagrees with Short et al (Short et al., 2005). Moojen et al. also reported that the normal scaphoid angulate ulnarly by 8.3° ( $\pm 1.1^\circ$ ) as the wrist flexed by 60° (Moojen, Snel, Ritt, Kauer, et al., 2002). Hence, current thesis agrees with the available in vivo 3D and 4D studies regarding normal scaphoid angulation in the coronal plane. There was no other published 3D or 4D in vivo studies on SLI during wrist motion to compare our results on scaphoid ulnar angulation.

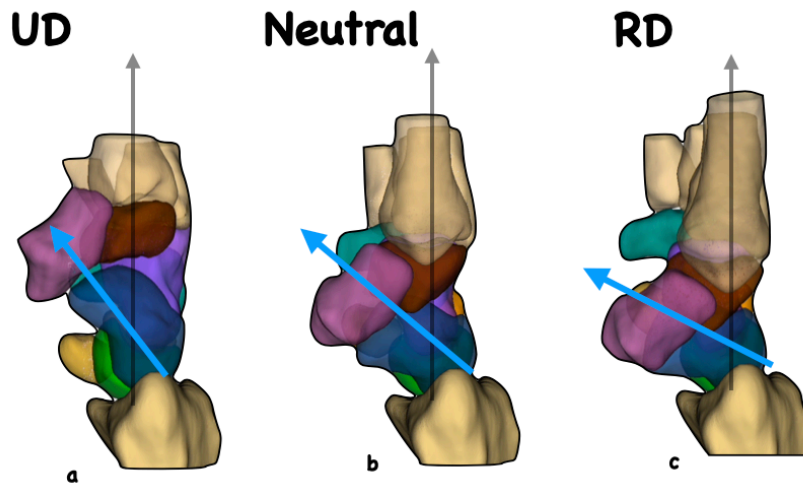
Furthermore, a subsequent sequential sectioning study by Short et al., only found significant ulnar angulation of the scaphoid when STT, SLIL and RSC were all sectioned, and the wrist



cycled through 1000 loading cycles (Short et al., 2007). Even then, it occurred in the range of motion of 20° extension to 20° flexion and 15° ulnar deviation to 5° radial deviation (Short et al., 2007). Unlike their previous studies, SLIL sectioning or added sectioning of STT, SLIL or RSC alone did not generate ulnar angulation of the scaphoid. They also reported that when the 3 ligaments - DIC, DRC and SLIL were all divided, the scaphoid ulnar angulated during wrist ulnar deviation. Also, when DIC and SLIL were divided the scaphoid would ulnar deviate in flexion only. Hence, ulnar angulation of the scaphoid in SLI has not been a consistent finding throughout the studies and appears to change with the combination of ligaments sectioned.

The Lunate in SLI is extended in DISI configuration. There was a lesser flexion arc of the SLI lunate when the wrist moved from ulnar to radial deviation. This is a reduction of angular displacement of the lunate in the sagittal plane. It is likely because, in the normal wrist, the drive for the lunate to flex is imparted from the scaphoid which is connected to the distal row. The out-of-plane motion of the proximal row occurs due to the scaphoid being an oblong bone, positioned obliquely out-of-plane of the distal row causing the entire proximal row to flex (Figure 161).

When observing the lateral projection of the wrist, the distal scaphoid is positioned out-of-plane, as demonstrated in Figure 161. To allow any movement at the distal row, the scaphoid must flex, and move out of the way. The normal scaphoid acts like the 'crank', in a slider crank mechanism, imparting a flexion moment on the proximal row but allowing the distal row to angulate radially.



*Figure 161 The lateral projection of the normal wrist showing the out-of-plane orientation of the scaphoid. a. ulnar deviation (UD) to b. Neutral to c. radial deviation (RD). Throughout the range of motion, the capitate, trapezoid and the metacarpals remain colinear in the sagittal plane. Due to the shape of the trapezoid, the trapezium is strategically positioned volar to the rest of the distal row. The scaphoid is the oblong bone positioned obliquely between the radius and the trapezium. The scaphoid always remains out-of-plane to the distal row. During radioulnar deviation, the flexion of the scaphoid allows the trapezium and the trapezoid complex to angulate radially over the dorsal scaphoid.*

When the scaphoid is disconnected from the proximal row, there is hardly a flexion moment acting on the lunate. The lunate tends to extend into DISI configuration. Cadaveric studies have shown that with every incremental critical ligament sectioning performed after SLIL sectioning, the lunate tended to be more extended. DISI, as defined by a radiolunate angle more than  $15^\circ$ , occurred with the sectioning of SLIL and at least one other critical stabiliser (Pérez et al., 2019).

The lunate also did demonstrate a similar angular displacement change during wrist extension to flexion. When the wrist was moving from  $70^\circ$  extension to  $30^\circ$  flexion, there was less flexion arc in the SLI lunate compared to the normal lunate. This observation occurred in a similar range to where an increased scaphoid flexion was observed. Similar findings have not been reported in previous studies. It appears that during the range between  $70^\circ$  extension to  $40^\circ$  extension, dissociation between the SLI scaphoid and the lunate becomes more apparent, as the scaphoid flexed more together with the distal row,

and the lunate flexed less. Translating this into clinical practice, the wrist range of 70° to 40° extension may be better avoided in rehabilitation programs due to differential flexion between the SLI scaphoid and the lunate.

The current study did not find a significant radial or ulnar angulation of the lunate in SLI. In a cadaveric study Werner et al. reported that following sectioning of the SLIL, DIC and DRC ligaments, the lunate supinated by  $2.7^\circ (\pm 2.3^\circ)$  and  $2.5^\circ (\pm 2.9^\circ)$  during flexion-extension and radioulnar deviation respectively (Werner & Short, 2018). Results of this study O1 confirm that the SLI lunate was  $5.3^\circ$  externally rotated on average compared to the normal lunate, however, this difference was not statistically significant, due to large variability observed. It is likely that clinical cases present a more heterogeneous cohort than discrete sectioning of SLIL, DIC and DRC.

Factors such as carpal morphology (e.g., lunate type) are known to affect carpal kinematics (Bain et al., 2015). The confounding effects of carpal morphology are less important in a cadaveric sequential sectioning study. Because pairwise comparisons are made between the intact and the ligament deficient states, carpal morphology remains the same for control and study groups. In an in vivo study two different cohorts of participants, normal and SLI are compared. While this leads to higher variability because of carpal morphology, in vivo studies remain representative of the real patient population.

Based on the above to further improve research on in vivo carpal kinematics, it may be important that we compare the injured wrist with the uninjured contralateral wrist so that a pairwise comparison is possible. Nonetheless, the caveat to this argument is 'what if the uninjured contralateral wrist is not normal'. Crisco et al. reported carpal postures are not normal in the uninjured contralateral wrist in SLI (Crisco et al., 2003). Hence, the conclusion is that each type of study, cadaveric or in vivo must be interpreted on its own merits. In addition, future 4D CT studies could critically evaluate the kinematics of contralateral uninjured wrist.

In summary, the new findings of study O1 of the current thesis were that there was less flexion and more radial angulation of the SLI scaphoid when the wrist was radially deviating

beyond 10°. The lunate out-of-plane motion was reduced from ulnar to radial deviation of the wrist without an increase in the in-plane motion. There was differential flexion of the scaphoid and the lunate from 70° to 40° of wrist extension.

Comparing scaphoid and the lunate angular displacement data of this thesis with previous studies, two patterns could be identified. The findings of this study agree with previous in vivo studies, but less with cadaveric studies. Secondly, when the current results agree with cadaveric studies, it is mostly in agreement with the findings pertaining to the normal wrist. This could be broadly due to the cadaveric studies having a discrete ligament sectioning sequence which may or may not represent the real patient population. Cadaveric studies with acute ligament sectioning, compare the same wrists, before and after ligament sectioning. Comparing two cohorts of participants, normal and the spectrum of SLI may not be comparable to the cadaveric studies. That could be a potential reason that our results are more in accordance with the in vivo studies than cadaveric studies.

This raises an important question as to whether we should extrapolate cadaveric findings to real-life patients, where the changes are more variable. In clinical practice, it has been observed that it is common for the ligament disruptions to be complete and that adjacent ligaments may have a partial disruption. We need more in vivo studies, to better understand this clinical spectrum.

#### **4.4.2. Radiocarpal angles during wrist motion**

While the angular displacement is important to understand the kinematic changes that occur in SLI, the radiocarpal angles are important from a diagnostic point of view. The knowledge of the radioscapoid angle at a particular wrist position has a diagnostic value so that it can be interpreted even if the wrist is not imaged in the neutral wrist position. Also, it enables understanding the wrist positions where the carpal angles deviate significantly from the normal; hence, avoid such positions in splinting and post-operative rehabilitation.

During wrist extension to flexion, the SLI scaphoid remained flexed compared to the normal scaphoid throughout the range (Figure 162). This has been a consistent finding in other

cadaveric studies on SLI (Padmore et al., 2019; Short et al., 2002b, 2005). Therefore, it can be assumed that if we are interpreting a lateral projection of the wrist, the SLI scaphoid is always flexed compared to the normal scaphoid. For example, the radioscaphoid flexion angle at 50° wrist extension for the normal wrist was 10.2° (5.6°-14.9°) and for the SLI wrist was 21.1° (17.8°-26.5°). The data from study 01 helps identifying a pathological wrist angle in any wrist position from extension to flexion.

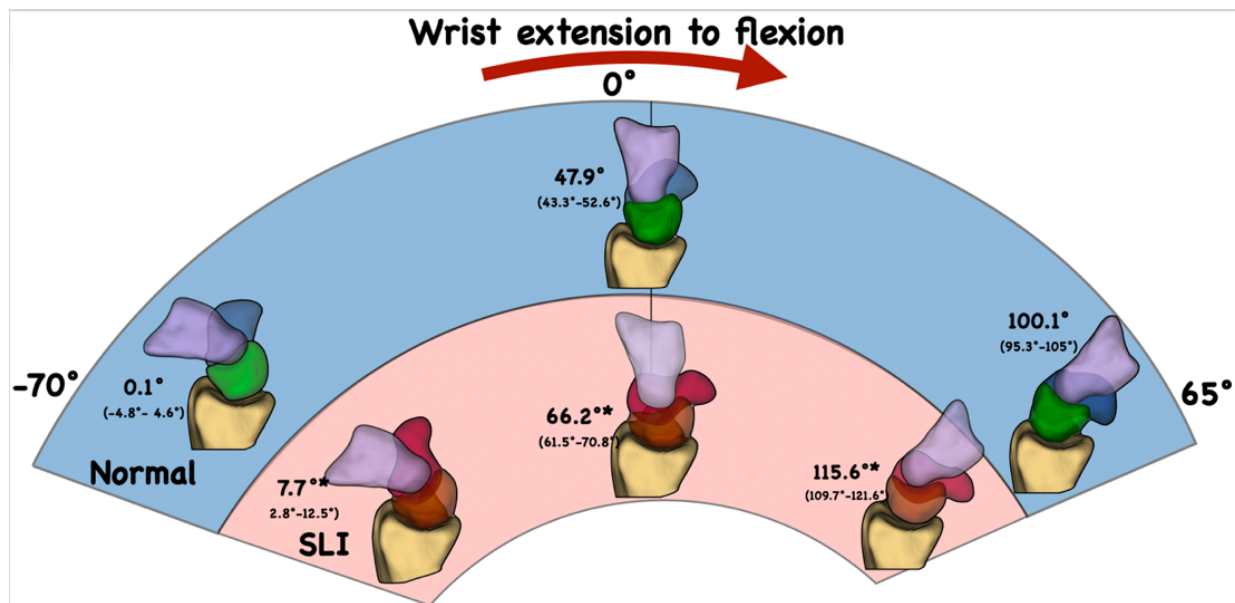


Figure 162 Graphic representation of the radioscapoid angle (flexion) in scapholunate instability (SLI). The radioscapoid angle in SLI remains significantly flexed compared to the normal wrist throughout extension to flexion. Note that “\*” indicates statistical significance at  $p$  value of 0.05 level. The results presented are the mean (95% confidence interval).

The patients’ wrists are often placed in plaster casts in slight wrist extension and imaging conducted are not in the absolute neutral position of the wrist. In a plain lateral radiograph-based study on healthy wrists, Koh et al. assessed the carpal angles every 5° from 20° flexion to 20° extension (Koh et al., 2013). From the neutral position radioscapoid angle of 59.7°, there was on average 4° change in the radioscapoid angle for every 5° of flexion or extension of the wrist. Findings of the current study were similar (neutral position 47.9° and change in flexion 4°). In addition, the current thesis presents data over a larger range of wrist motion, for the normal and SLI scaphoid.

While Koh et al.’s findings provide insight on the normal wrist, the current study adds to that providing data on the change in flexion of the SLI wrist. For every 5° of flexion from 70° wrist extension, the SLI scaphoid on average flexed 4.2° until the neutral position. At the neutral position the SLI radioscapoid flexion angle was 66.2° (61.5°-70.8°). Then from a neutral position to 65° flexion, the SLI radioscapoid angle increased by 3.8° for every 5° wrist flexion (Figure 163).

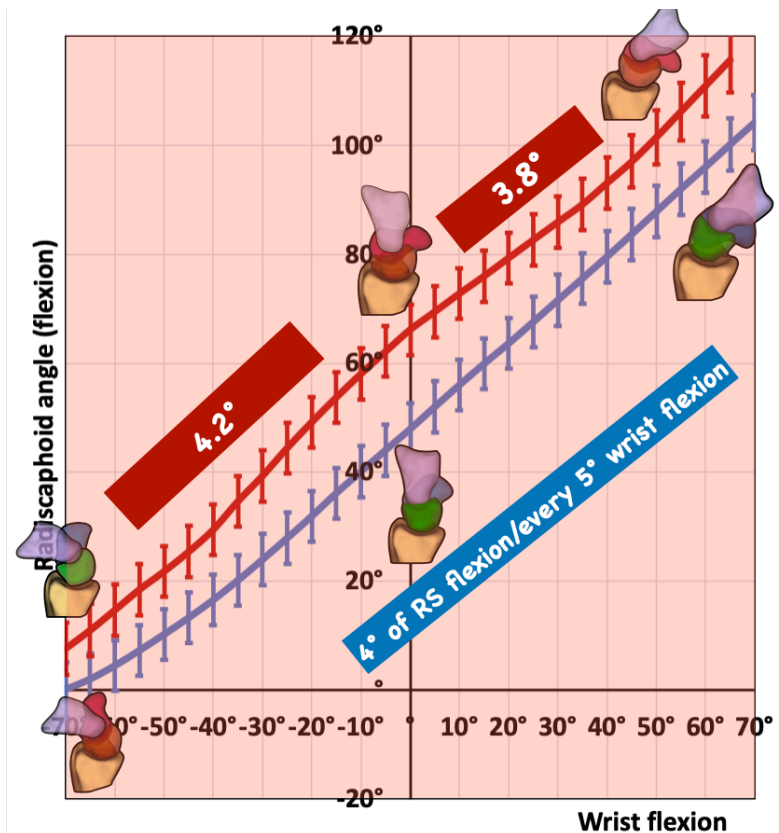
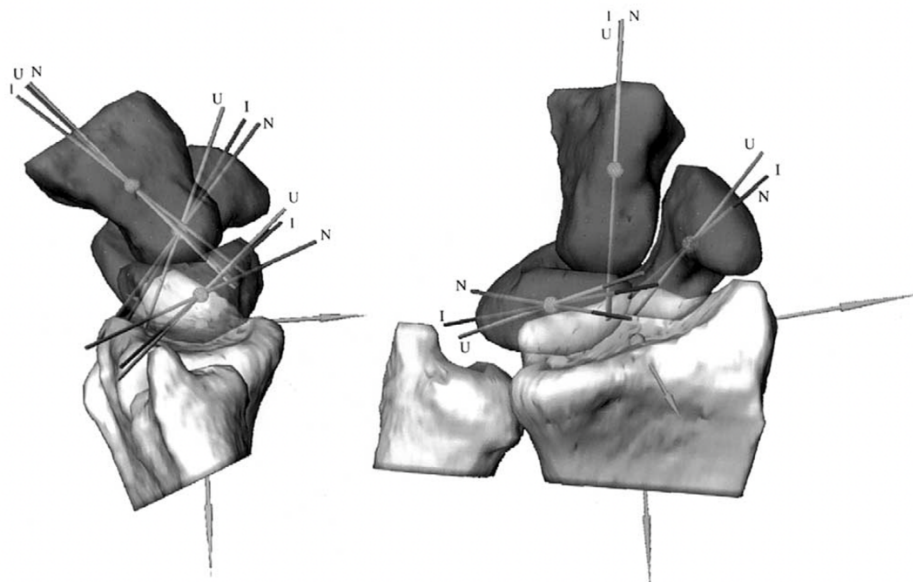


Figure 163 The radioscaphoid angle (flexion) with the wrist extension to flexion (95% confidence intervals are marked by the error bars). Note that the SLI scaphoid remained flexed compared to the normal scaphoid. The normal scaphoid flexed 4° for every 5° of wrist flexion.

In study 01 of this thesis, radiocarpal angles were measured in all three planes, using the principal axis of the carpal bone (scaphoid and the lunate). Measuring radiocarpal angles using Larsen's method was validated only for sagittal plain images (Larsen, Mathiesen, et al., 1991). Although the sagittal plane radioscaphoid angle can reliably be measured on a 3D CT (Lee et al., 2018), the 3-dimensional assessment of the carpal posture was not possible with the volar tangential line. To overcome this limitation, Crisco and Coburn introduced using principal axis-based 3D carpal angles (Coburn et al., 2007; Crisco et al., 2003) (Figure 164). They have validated principal axis-based carpal angles and reported a high correlation value with the clinically measured radiocarpal angles (The coefficient of determination or R<sup>2</sup> value in linear regression has been reported above 0.85 indicating high correlation). Another advantage is that the principal axis based carpal angles are calculated automatically and there is no room for inter or intra observer variability. The only factor that would affect a principal axis based radiocarpal angle would be the carpal morphology. Nonetheless, none of the anatomical landmark or geometry-based method, including Larsen et al. are immune

to variability due to carpal morphology. Therefore, as the technology advances and surgeons are more interested in the 3D configuration of the bone than a single plane angle, the principal axis-based angles provide a reasonable solution.



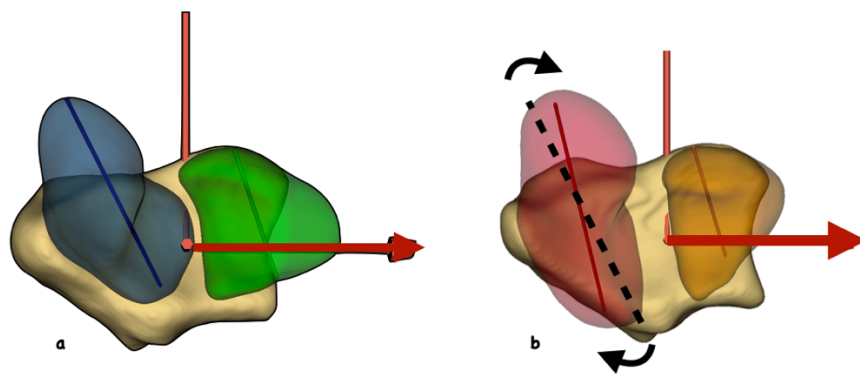
*Figure 164 The average orientations of the first principal inertial axis of the capitate, lunate, and scaphoid of the normal (N), injured (I), and uninjured (U) wrists in an ulnar and palmar view of a normal right wrist. From “Carpal bone postures and motions are abnormal in both wrists of patients with unilateral scapholunate interosseous ligament tears.” by Crisco et al. (2003). J Hand Surg Am, 28(6), 926-937. Copyright [2003] by Elsevier Science & Technology Journals. Reprinted with permission.*

Comparatively less is known about scaphoid (Figure 165) and lunate axial rotation in SLI. Using the principal axis, in the neutral wrist position, the scaphoid in SLI was significantly more internally rotated compared to the normal scaphoid (Figure 165). The mean normal scaphoid internal rotation angle was  $60.4^{\circ} (\pm 9^{\circ})$  and the SLI,  $70.2^{\circ} (\pm 10.7^{\circ})$ . During motion, throughout radioulnar deviation, and extension to flexion, the SLI scaphoid remained internally rotated. This was the only outcome measure that was consistently different in SLI, throughout all wrist motions. Using 3D assessment of the internal rotation, a clear difference between the normal and SLI scaphoid, in any wrist position, and any motion can be observed.

While internal rotation of the scaphoid is potentially a good diagnostic feature for SLI, the other inference is that the wrist is unable to correct the axial malalignment in any position.



The flexed SLI scaphoid would take a position that is not different from the normal in radial deviation; the SLI lunate would be comparable to the normal lunate in the extended wrist or ulnar deviated wrist. However, the internal rotation remains uncorrected throughout. The internal rotation of the scaphoid may be the primary malalignment in the scaphoid, which also highlights the importance of the dorsal scapholunate ligament complex. When the dSLL complex is disrupted the SL interval opens like an “open book” injury (Figure 165) commonly described in relation to pelvic injuries. This open book injury of the proximal row leads to instability of the proximal pole of the scaphoid.



*Figure 165 The internal rotation of the normal scaphoid (a) compared to the SLI scaphoid (b). Note the rotation of the scaphoid(b) in SLI. In addition, the dorsal subluxation of the proximal pole and the radial translation of the SLI scaphoid are also visible in this example. The dashed line is the principal axis of the normal scaphoid imposed on the SLI scaphoid for comparison. Note that the images are from a single representative example.*

The main feature of SLI in the lunate is ‘extension’ in dorsal intercalated segmental instability (DISI) configuration (Linscheid et al., 1972). Results of study 01 revealed that the SLI lunate is significantly extended compared to the normal lunate from the neutral to radial deviation and 20° extension to 60° flexion. There was no significant difference between the SLI lunate and the normal lunate during 70° to 20° extension or the wrist ulnar deviation to neutral wrist position. Therefore, from a diagnostic point of view, the current study reported that the radiolunate angle could distinguish between the normal and SLI wrist, only if the wrist was positioned from neutral to radial deviation and 20° extension to flexion.

The lunate extension in the current study was measured using the principal axis method for use in 3-dimensional models (Coburn et al., 2007; Crisco et al., 2003) and not the clinically

used method as described by Larsen et al (Larsen, Mathiesen, et al., 1991). The principal axis method has been validated to have a high correlation to the radiolunate angle measured using Larsen's method (Coburn et al., 2007; Larsen, Mathiesen, et al., 1991).

### **Carpal paradox**

Static imaging provides the radiolunate (RL) and radioscapoid (RS) angles, but 4D CT enables measuring these angles over a range of wrist motion. The RL and RS angles differed between the normal and SLI wrists at different wrist angles. When measuring the change in angle (angular displacement), it is possible to appreciate that not only the RL or RS angle but also the angular displacement differed between the normal and SLI wrists. The wrist positions where the angular displacement was different between the two groups were not the same as the wrist positions where the radiocarpal angles were different.

The angular displacements of the SLI lunate in the sagittal plane (lunate flexion) differed between the two groups when the wrist was in extension up to 25°. There was no significant difference in lunate flexion when the wrist moved from 20° extension to flexion. The radiolunate angle, however, was significantly different between the normal and the SLI wrist when the wrist was moving from 20° extension to flexion (Figure 166).

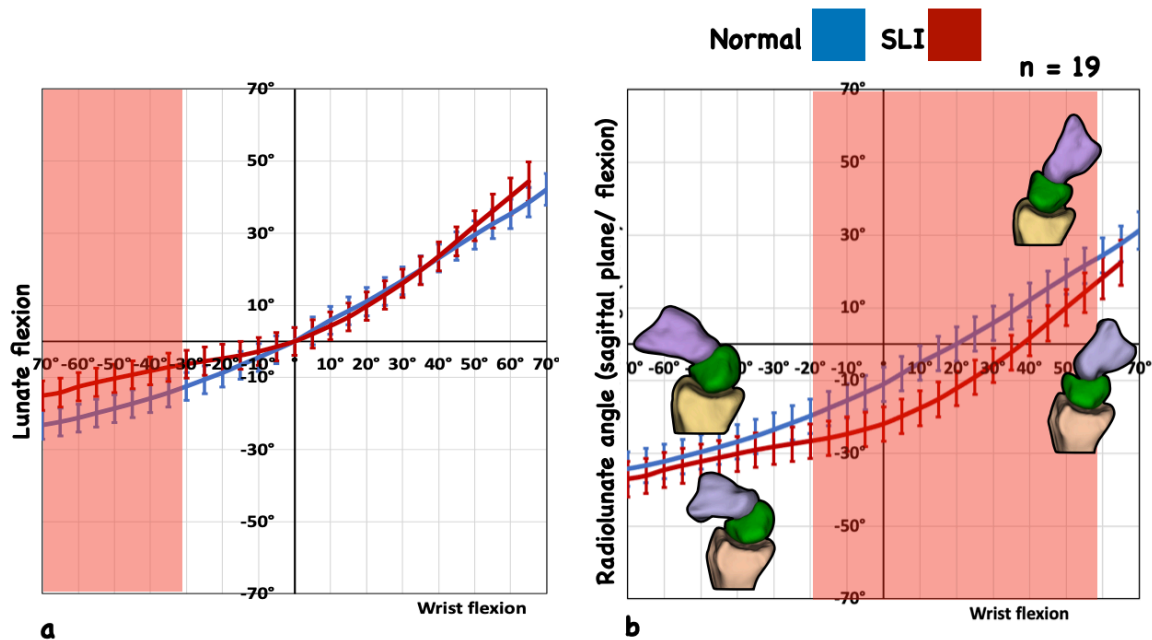


Figure 166 The difference between the lunate flexion and the radiolunate angle. a. Lunate flexion during wrist extension to flexion. A significant difference is observed when the wrist is in extension from 70° to 25°. b. The radiolunate angle is different between the two groups when the wrist is flexing from 20° of extension. The red highlighted zones represent where a statistically significant change was observed between the normal and the SLI lunate. The images of the lunate below the red graph (SLI) represent SLI. The images of the lunate above the blue graph(normal) represent the normal wrist.

This phenomenon is named “the carpal paradox”, where the actual difference in ‘change’ occurred when the wrist was in extension, leading to a measurable difference in radiolunate angle when the wrist is in flexion. It is similar to two athletes competing in a running event, where the speed of the two are different throughout the race, however the winner is selected at the finish line.

This concept is important because, from a diagnostic point of view, the difference of radiolunate angles is important as the wrist moves from 20° extension to flexion. But an intervention to solve the problem must consider that the cause is at the ‘first part of the race’; that is when the wrist is moving from 70° extension to 20° extension. Similar observations were seen with the scaphoid as well (Figure 167).

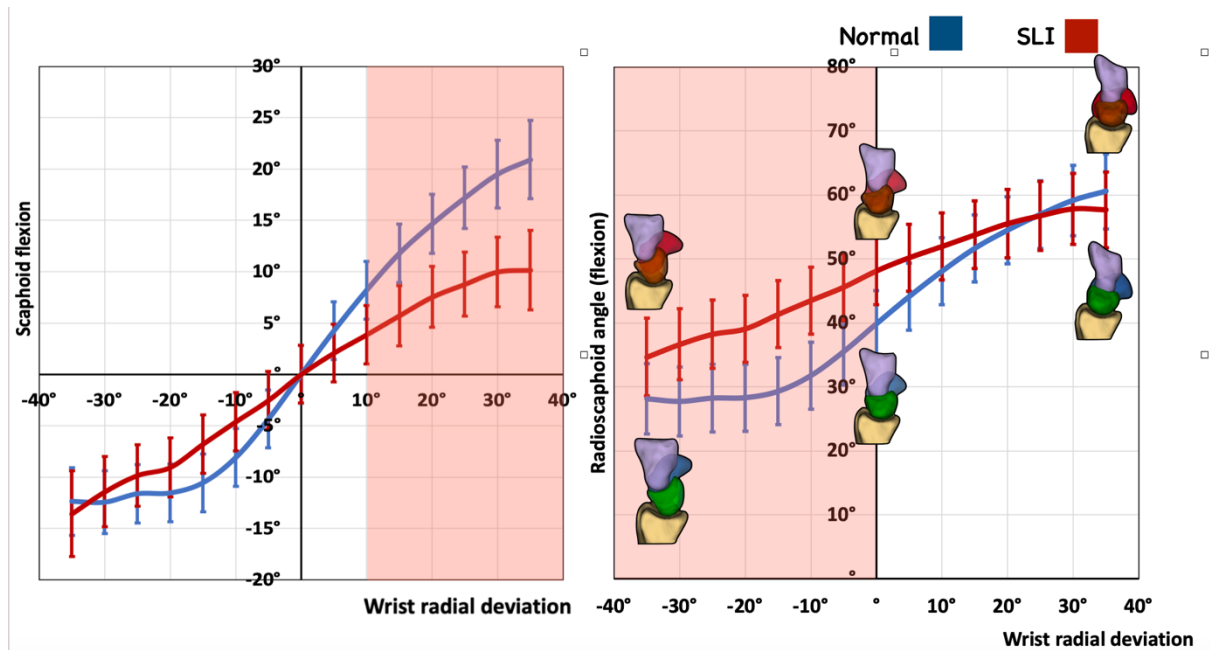


Figure 167 The difference between the scaphoid flexion and the radioscaphoid angle. a. Scaphoid flexion during wrist ulnar to radial deviation. A significant difference was observed when the wrist was radially deviated beyond 10°. b. The radioscaphoid angle was different between the two groups when the was in ulnar deviation to neutral. The red highlighted zones represent where a statistically significant change was observed between the normal and the SLI lunare. The images of the scaphoid above the red graph (SLI) represent SLI. The images of the scaphoid below the blue graph(normal) represent the normal wrist.

#### 4.4.3. Radiocarpal centroid positions

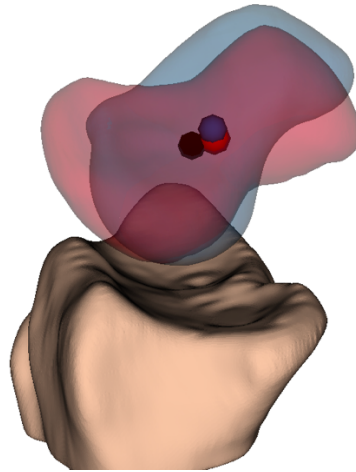
The scaphoid and the lunate centroid positions were compared between the normal and the SLI wrist. In the neutral wrist position, the SLI scaphoid centroid was more radial ( $p = 0.036$ ) and the SLI lunate centroid was more ulnar ( $p = 0.004$ ). The mean difference between the normal and SLI scaphoid centroid positions was 0.8 mm. The mean difference between the normal and SLI lunate centroid position was 1.3 mm. A significant difference in the centroid positions of the scaphoid or the lunate was not observed in the dorso-volar or proximodistal direction.

There are only a few studies that have assessed the in vivo centroid position of the scaphoid and the lunate in SLI (Crisco et al., 2003; Omori et al., 2013). These studies assessed the carpus with the wrist in the neutral position. Werner et al. (Werner et al., 2011) assessed the scaphoid and the lunate centroid translations following ligament sectioning during wrist

motion; however, this was a cadaveric study. In the neutral wrist position, the findings of the current study were in accordance with the results of Omori et al. on the radial translation of the scaphoid in SLI wrists (Omori et al., 2013). Nonetheless, Omori et al. reported that the scaphoid centroid had 4.9 mm radial translation and also a 1.6 mm dorsal translation. Omori's study, selected patients with advanced SLI (grade IV). The number of cases studied was 03. In contrast, the patients in the current study represent the entire spectrum of SLI without arthritic changes, and our selection criteria included 'arthroscopic evidence of scapholunate dissociation'. Current study findings correlate better with Crisco et al. who reported that the inter-centroid distance was 2 mm greater in the SLI wrists (Crisco et al., 2003). Werner et al. also reported a 1.8 mm radial translation of the scaphoid following dorsal SL complex sectioning but did not report a dorsal translation (Werner et al., 2011).

A possible reason for the current study not observing a dorsal translation of the scaphoid centroid is that the 3-dimensional malalignment in SLI is more rotational. The centroid of the scaphoid is in a central location in the oblong bone. Therefore, is likely when the sagittal and axial balance of the scaphoid is disrupted and the scaphoid rotates into flexion and internal rotation in early stages, it rotates around a locus close to the centroid. Therefore, the centroid position remains unchanged in a dorso-volar direction, as the scaphoid flexes in the dorso-volar plane. While the dorsal translation of the scaphoid proximal pole is well recognised in SLI (Chan et al., 2019), it is likely that this is not reflected in the centroid position.

At the stage where the entire scaphoid is subluxated dorsally, indicating that the centroid is also dorsally positioned, it could be a late stage of SLI (Figure 168). The SLI lunate centroid position reported by Omori et al. was 1.6 mm ulnar translated compared to the normal (Omori et al., 2013). Werner et al. reported the SLI lunate centroid was 0.6 mm more ulnar than normal (Werner et al., 2011). Study 01 of this thesis, demonstrated that the SLI lunate position was 1.3 mm ulnar compared to the normal, and confers with the findings of Omori et al. and Werner et al.

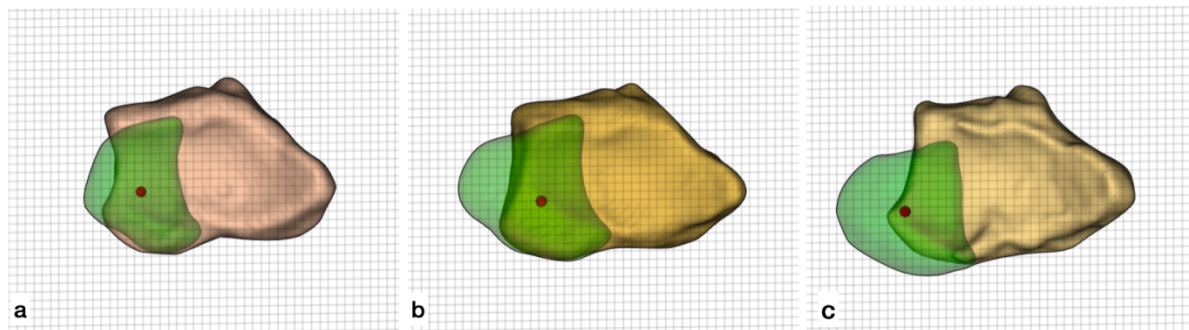


*Figure 168 The mean scaphoid centroid position in the normal wrist (blue) and SLI mean (red) are depicted with a normal scaphoid (blue) and SLI scaphoid (red). Note that the mean normal centroid and the mean SLI centroid are in a similar location in the dorso-volar plane. The scaphoid centroid that demonstrated maximum dorsal position is also depicted in black. Note that the SLI scaphoid is flexed, and the proximal pole is dorsally translated however the dorso-volar position of the centroid is not significantly different.*

Findings of the current study regarding the scaphoid and the lunate centroid position during the wrist motion can be compared with the cadaveric study by Werner et al. (Werner et al., 2011). During extension to the neutral position and from ulnar deviation to the neutral position, the scaphoid centroid was more proximal in SLI compared to the normal. A potential explanation would be that unrestrained scaphoid can be translated proximally in extension and ulnar deviation. The Werner et al. study did not observe this proximal migration.

The SLI scaphoid centroid also remained more radial than the normal scaphoid from the extension to the 15° of flexion. The mean difference between the normal and the SLI scaphoid centroid positions varied between 1.2 to 0.6 mm of radial translation through the range of motion. This conforms to findings by Werner et al., who reported the difference between the intact stage and ligament sectioned stage was 0.5 to 2 mm during flexion and extension. Neither the current study nor Werner et al. reported a change of the scaphoid centroid in the dorso-volar direction.

SLI lunate remained more ulnar compared to the normal lunate from the wrist moving from extreme extension to 55° of flexion and also with 30° to 15° ulnar deviation. There was no significant change in the lunate centroid position in the proximodistal or the dorso-volar directions. This is compatible with the findings of Werner who observed similar changes (Werner et al., 2011). However, in his ligament sectioning of the volar carpal ligaments, he observed that the lunate centroid translated significantly volar during wrist radioulnar deviation. In the current study, volar translation of the lunate centroid position was not a feature seen generally in all the SLI wrists. But in the patients with the ulnar translation of the lunate in our cohort, this volar translation was seen (section 3.7). It is likely that the lunate volar translation occurs in specific cases where lunate stabilisers were injured. It is not a unique feature of SLI in general but a feature of a unique subset of patients (Figure 169-c). As the number of cases were limited (03) a subgroup analysis of this cohort was not conducted.



*Figure 169 Lunate centroid position. a. Normal wrist b. SLI wrist c. A Patient with volar ulnar translocation of the lunate. Note that in image c. the patient with volar ulnar translation of the lunate has the lunate centroid overlapping the volar ulnar corner of the distal radius.*

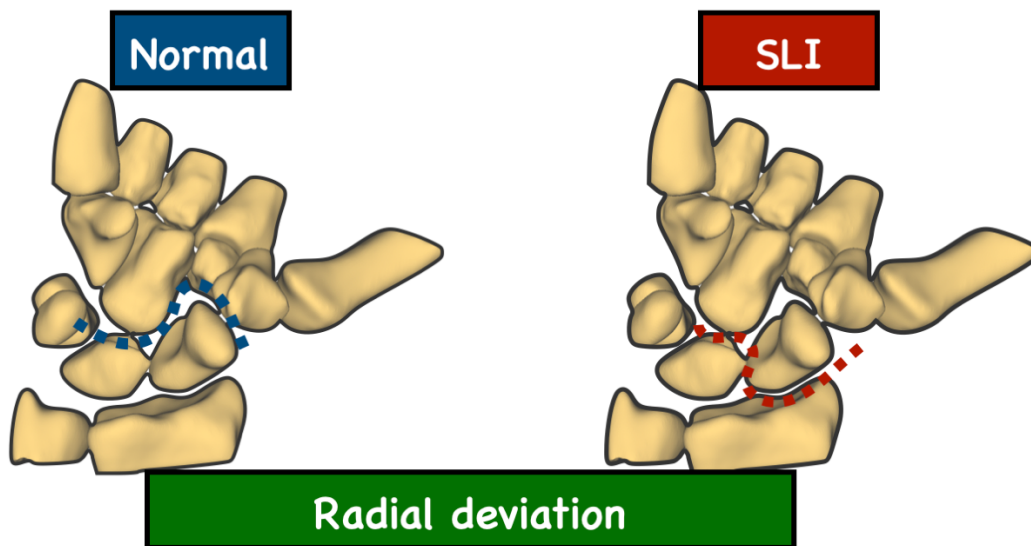
## 4.5. Midcarpal vs. Radiocarpal kinematics

Study 02 of the current thesis evaluated midcarpal kinematics between the normal and the SLI wrists. The radiocarpal and midcarpal joints together create the global wrist motion. Hence, midcarpal kinematics are discussed in comparison to radiocarpal kinematics rather than in isolation.

Midcarpal and radiocarpal kinematics in the normal wrist have been studied using multiple static MRI scans in vivo and in also in cadaveric studies (Kaufmann et al., 2005; Kaufmann et al., 2006; Moritomo et al., 2004, 2006). The midcarpal kinematics of the SLI wrist have not been previously studied. It is important to understand the changes in the radiocarpal and midcarpal articulations that occur during various phases of wrist motion, as they may predict the development of degenerative changes and help choosing reconstruction techniques.

Assessing midcarpal kinematics, study 02 reports that the SLI scaphoid had less midcarpal radial angulation and less midcarpal flexion, when the wrist was radially deviating beyond 10°. In addition, during radial deviation of the SLI wrist, there was more 'radiocarpal radial angulation' of the SLI scaphoid. The dominant articulation where over 50% of the radial angulation occurred for the normal wrist was the scapho-capitate joint. Bain et al. in a cadaveric study reported that in the normal wrist, during radial deviation the midcarpal joint becomes dominant (Bain et al., 2015). Study 02 of the current thesis, while agreeing with Bain et al. on the normal wrist, reports that in the SLI wrist, the motion shifts to the radiocarpal joint during radial deviation. In other words, the radioscapoid joint became the dominant articulation in radial deviation in SLI (Figure 170). This partly supports that SLI is essentially radioscapoid instability.





*Figure 170 The dominant articulation of the radial column in the normal wrist during the wrist radial deviation is the scapho-capitate (midcarpal) joint. The dominant articulation of the radial column in the SLI wrist during the wrist radial deviation is the radioscapoid joint (radiocarpal joint).*

According to our results, over 50% of the motion in the radial column during wrist extension to flexion occurred through the radioscapoid joint for both normal and the SLI wrist. Bain et al. concluded that regardless of the wrist type dominant articulation in the radial column is the radioscapoid joint in flexion, and extension (Bain et al., 2015). Current study agreed with Bain et al. on the normal wrist. In the SLI wrist, the dominant articulation where over 50% of the motion occurred was also the radioscapoid joint. In addition, there was increased radioscapoid motion in the SLI wrist when the wrist was moving from 70° to 40° extension.

Lunate also demonstrated a similar finding when the wrist was moving from 70° to 30° extension. In the normal and the SLI wrists, the luno-capitate joint was the dominant articulation when the wrist was moving from extension to neutral. In the SLI wrist, however there was increased luno-capitate flexion (midcarpal flexion) when the wrist was moving from 70° to 30° flexion, compared to the normal. During extreme extension and extreme flexion, in the SLI wrist, there was a significant increase in luno-capitate internal and external rotation respectively. This was not accompanied by a significant change in the

radiolunate axial rotation. It is likely that the capitate in SLI is internally rotating when the wrist is in extension and externally rotating when the wrist is in flexion.

Previous studies have documented that the proportions of radiolunate motion in extension vary between 52 to 68% (Kaufmann et al., 2006; Moritomo et al., 2006). Bain et al. reported that this changes with the Lunate type; In type I lunate midcarpal extension dominates (predominantly 10:7) and in type 2 lunate radiocarpal extension dominates. One limitation of the current study compared to Bain et al. was that the lunate type was not considered. Nonetheless, considering the normal and SLI cohorts of 19 wrists in each group, compared to 08 normal cadaveric wrists in Bain et al. the current thesis has identified that the carpal motion shifts towards the radioscapoid joint and capito lunate joint in SLI.

Study 02 of the current study also found that there was a significant reduction of out-of-plane scapho-capitate motion in radial deviation beyond 10°, which corresponds to the reduction of out-of-plane motion in the radiocarpal joint. To maintain the collinearity of the “radius-capitate-proximal row axis”, a reduction in the radiocarpal out-of-plane motion must be compensated by a similar reduction of midcarpal out-of-plane motion. In the SLI lunate also, from 35° to 15° ulnar deviation there was less out-of-plane mid-carpal motion, which was also reflected as a reduction in out-of-plane motion in the radio carpal joint. A significant reduction of radiocarpal lunate flexion was observed in SLI in radial deviation. This was accompanied by a reduction in midcarpal flexion, which was not, however, statistically significant.

It is evident that with SLI, the scaphoid motion shifted towards the radiocarpal joint, potentially due to being driven by the distal row and not constrained by the proximal row. This may also explain the development of early radioscapoid arthritis in SLI. Comparatively, the central column motion in SLI tended to shift towards the midcarpal joint especially when the wrist was in extension. This is likely due to the scaphoid failing to impart a flexion moment on the lunate. More importantly, during the wrist range between 70° extension to 40° extension, there was more radioscapoid (radiocarpal) motion and more capito lunate (midcarpal) motion in the SLI wrist compared to the normal. It is likely that during this range of wrist motion the scaphoid and the lunate dissociation is more prominent.

When the wrist was extended the lunate was also extended in both the normal and SLI wrist (Figure 171). In the normal wrist, the scaphoid provides the flexion moment to the lunate, enabling radiolunate flexion. The SLI lunate is dissociated from the scaphoid. Hence, the capitate facilitates the central column flexion. When the wrist is extended, the central column flexion occurs through the capito-lunate joint. Once the capitate is past the neutral position in the sagittal plane, it has a better lever arm to create an effective flexion moment for the SLI lunate, enabling radiolunate flexion. Therefore, it can be observed that the radiolunate angle remains relatively unchanged during wrist extension to neutral; From wrist neutral to flexion, radiolunate flexion occurs.



*Figure 171 A single SLI patient moving the wrist from extension to flexion. The lunate position is outlined. Note that the midcarpal flexion is more when the wrist is in extension, without a significant change in the radiolunate angle. As the wrist moves into flexion the radiolunate angle changes with radiolunate flexion.*

In summary the novel findings of study 02 of the current thesis were that the radioscapoid joint becomes the dominant articulation in radial deviation and when the wrist was moving from 70 to 30° extension. SLI wrist had more midcarpal flexion in the central column. The reduction in midcarpal out-of-plane motion of the scaphoid and the lunate is compensated by a reduction in radiocarpal motion, maintaining the collinearity of the carpus in the sagittal plane.

## 4.6. Helical axis of motion

Position and the orientation of the helical axis of motion (HAM) represent the axis around which each carpal bone rotates. There are reconstruction techniques that have been developed based on maintaining the rotation axis between the scaphoid and the lunate (Rosenwasser et al., 1997; Yao et al., 2016). Nonetheless, some of these techniques of recreating a rigid scapholunate axis were reported to have high complication rates (Aibinder et al., 2019). Therefore, understanding the helical axis of motion may have clinical implications related to surgical reconstruction.

Best et al. studied the HAM for the scaphoid and reported that the scapholunate rotation axis is highly variable and that it is not possible to reconstruct a single rotation axis (Best et al., 2019) (Figure 172). This study by Best et al. was confounded by the fact that multiple wrist positions from multiple different participants were pooled and the HAM was calculated between carpal positions. The axes calculated were for radial and ulnar deviation as one cluster and flexion-extension as another cluster.

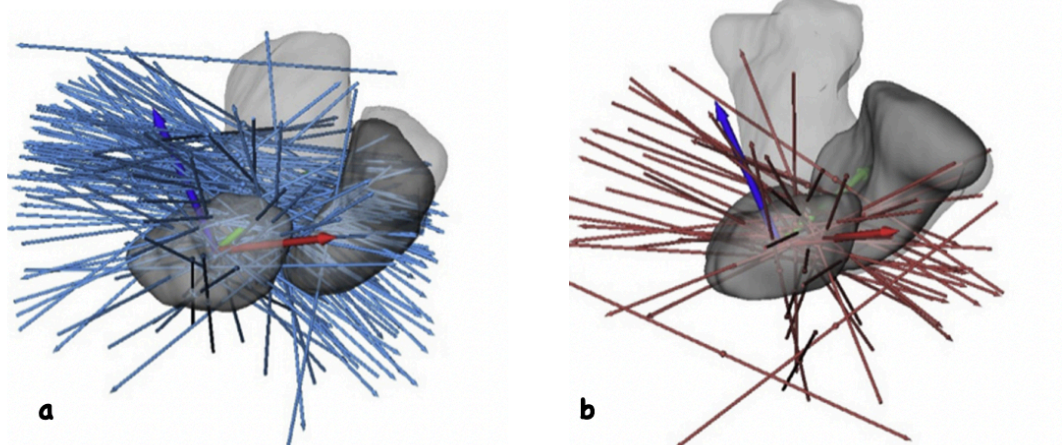
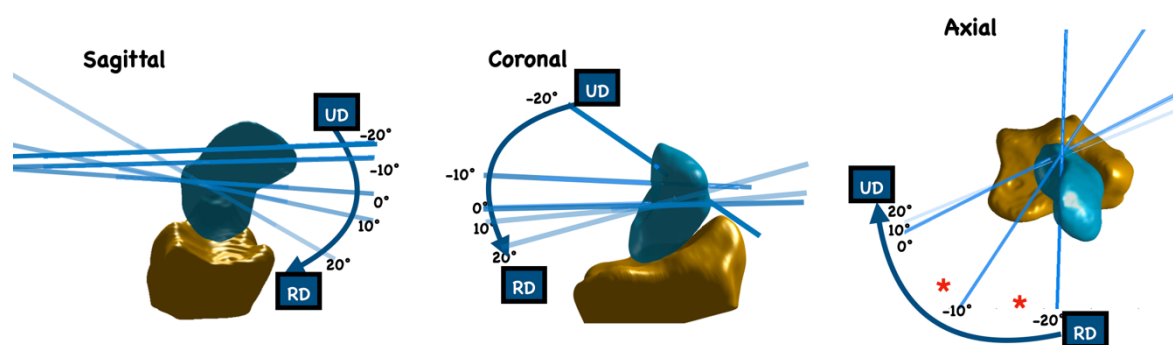


Figure 172 The variability of the orientation of the helical axis of motion (HAM) of the scaphoid relative to the lunate coordinate system. a. wrist flexion extension. b. wrist radioulnar deviation. From “Differences in the Rotation Axes of the Scapholunate Joint During Flexion-Extension and Radial-Ulnar Deviation Motions.” Best, Gordon M et al. (2019). *J Hand Surg Am*, 44(9), 772–778. Copyright [2019] by Elsevier Science & Technology Journals. Reprinted with permission. The marked variability could have been due to the pooling of multiple participants' wrists to calculate the HAM.

To overcome this limitation, in study 03 of this thesis, the HAM of the scaphoid and the lunate relative to the radius is presented, with 10° increments in the wrist position, from extension to flexion and ulnar to radial deviation. When calculating the individual HAM, only the wrist positions within the same individual were studied, without pooling data. Following calculating the HAM for each incremental wrist position for each participant, an average axis for each wrist position was computed. For example, scaphoid HAM of 19 SLI patients for the wrist moving from 20° ulnar deviation to 10° ulnar deviation have been averaged to generate a 'mean HAM': then the same was repeated as the wrist moved from 10° ulnar deviation to the neutral position. Therefore, the findings are representative of a sample mean and the distribution around the mean for a sample size of 19.

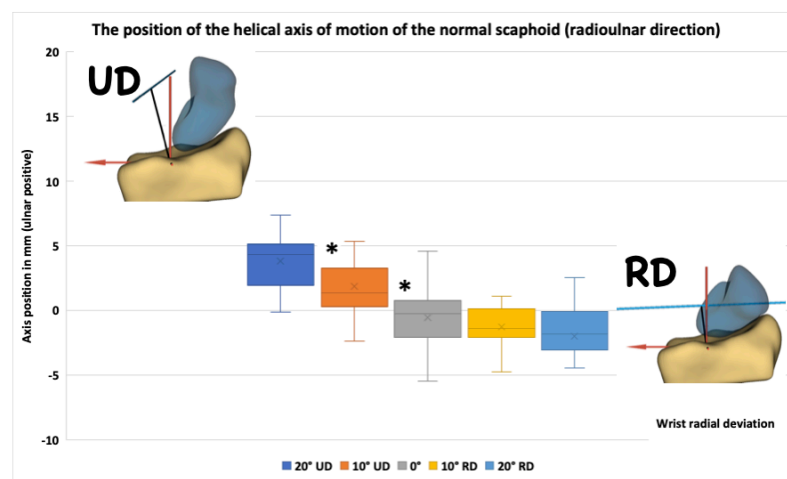
With the wrist moving from extension to flexion there were no significant changes in the position or the orientation of the helical axis. However, in ulnar to radial deviation there were sequential and significant changes in the position and the orientation of the HAM for the scaphoid and the lunate for each incremental wrist position. The orientation of HAM for the normal scaphoid during the wrist ulnar to radial deviation is presented in Figure 173. In each plane, there was a gradual change in the orientation of the HAM as the wrist moved into radial deviation. There were significant differences that occurred with the wrist from 20° ulnar deviation to 10° of ulnar deviation and then also from 10° of ulnar deviation to the neutral position, in the axial plane.



*Figure 173 The orientation of the helical axis of motion (HAM) of the normal scaphoid during the wrist ulnar to radial deviation. The wrist angles are depicted from -20° ulnar deviation to 20° radial deviation. \* Indicate statistically significant difference in orientation between two consecutive positions.*

A similar change was observed with the position of the HAM as well (Figure 174 and Figure 175). As the wrist moved from ulnar to radial deviation, the position of the HAM changed to be more radial and proximal. The significant changes occurred at the wrist positions where the HAM orientation had significant changes as well. HAM helps in understanding the axis around which the scaphoid rotates. It appears from these results, that the axis around which the normal scaphoid rotates, changes in orientation and position with the wrist position.

A possible reason for this behaviour is that the ligamental constraints that are active at each incremental wrist position change, directing the scaphoid to rotate around 'different axes' at each wrist position. It is likely that with the changes in the radial and ulnar deviation wrist positions, the ligamental constraints that act on the scaphoid and the lunate changes, such that the carpal bones rotate or pivot around distinctly different ligamental constraints at each position.



ion

*Figure 174 The position of the helical axis of motion (HAM) of the normal scaphoid during the wrist ulnar to radial deviation in the radioulnar direction. The wrist angles are depicted from -20° ulnar deviation to 20° radial deviation. \* Indicate statistically significant difference in position between two consecutive positions.*

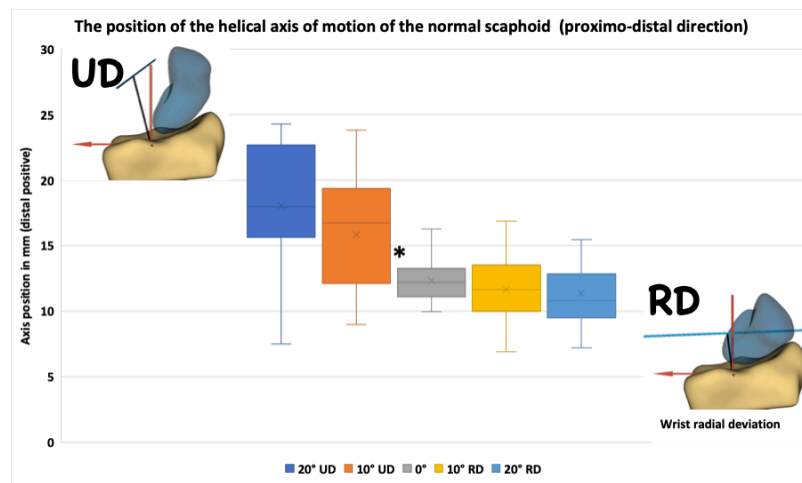


Figure 175 The position of the helical axis of motion (HAM) of the normal scaphoid during the wrist ulnar to radial deviation. The wrist angles are depicted from  $-20^{\circ}$  ulnar deviation to  $20^{\circ}$  radial deviation. \* Indicate statistically significant difference in position between two consecutive wrist positions.

The lunate also was observed to have this sequential pattern of changes in the HAM orientation and position. The pattern of the sequential change in the HAM of scaphoid and the lunate rotation axes were similar (Figure 176). This is the first study that reports on the sequential change in the motion pattern of the scaphoid and the lunate.

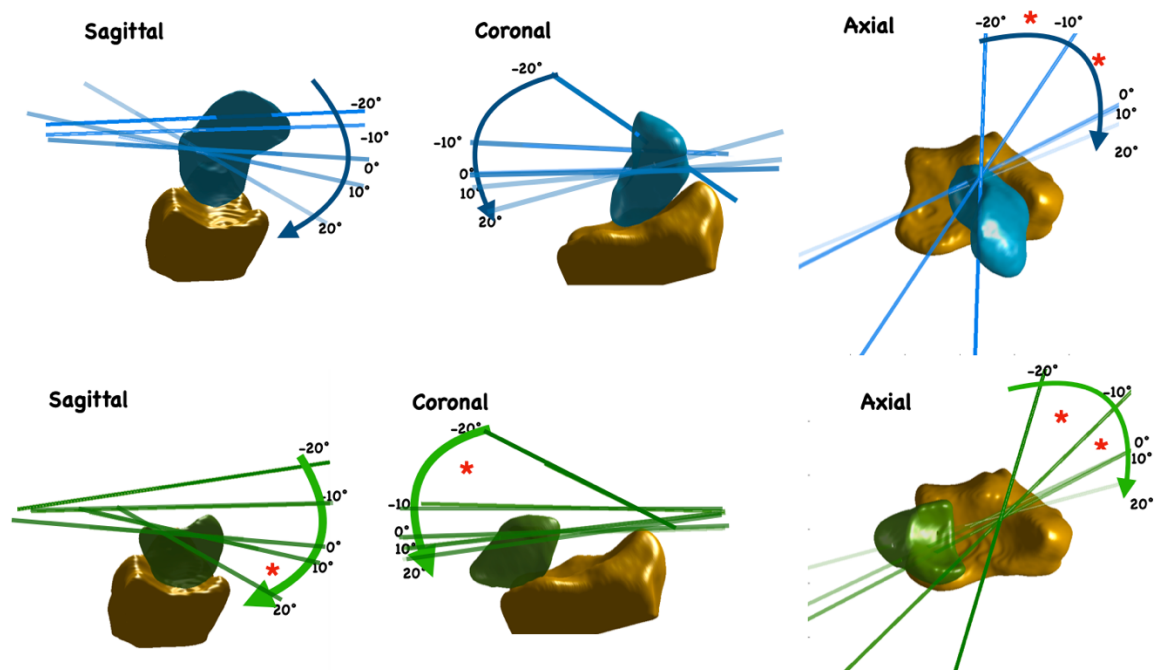


Figure 176 The orientation of the helical axis of motion (HAM) of the normal scaphoid and the lunate during the wrist ulnar to radial deviation. The wrist angles are depicted from  $-20^{\circ}$  ulnar deviation to  $20^{\circ}$  radial

deviation. \* Indicate statistically significant difference in orientation between two consecutive positions. Note that the orientation of the scaphoid HAM and the lunate HAM are similar in three anatomic planes.

In the SLI scaphoid, there were no incremental changes in the orientation or the position of the HAM. The HAM was oriented and positioned similarly in each anatomic plane (Figure 177). There were no statistically significant changes between two consecutive wrist positions. The sequential motion patterns were disrupted. In the normal wrist, the anatomic structures that guide the sequential motion patterns were preserved. In the SLI wrist, anatomic structures that guide the sequential motion patterns were disrupted and the scaphoid HAM remained similar through the motion.

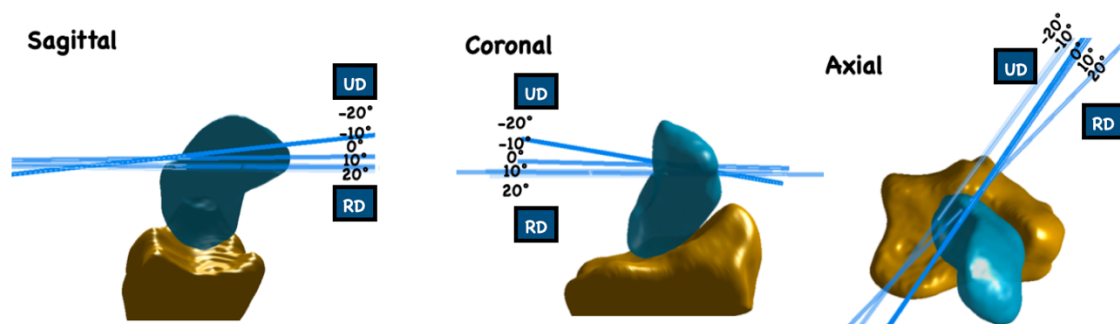


Figure 177 The orientation of the helical axis of motion (HAM) of the SLI scaphoid during the wrist ulnar to radial deviation. The wrist angles are depicted from -20° ulnar deviation to 20° radial deviation. Note that the orientation of the HAM was very similar between the wrist positions.

The other clinical implication of the changing position of the HAM is for designing scapholunate reconstructions. While there were no previous literature to compare findings of the current thesis, similar observations have been made regarding the knee joint (Hollister et al., 1993). Understanding of the knee joint HAM has led to more anatomical ligament reconstructions. It may be possible that SLI reconstruction becomes more anatomical with this advancing knowledge.

Looking at where the HAM exits the normal scaphoid, particularly in radial deviation and extension to flexion, it is clear that the HAM relates to the anatomical footprint of the DIC and SLIL. Studying the incremental wrist motions, the HAM passes through a wider surface area than previously believed (Figure 178). Therefore, a single bundle tendon is unable to



recreate the normal kinematics of the scaphoid. These findings likely favour more anatomical repairs of reattaching the dorsal scapholunate ligament complex to its footprint.

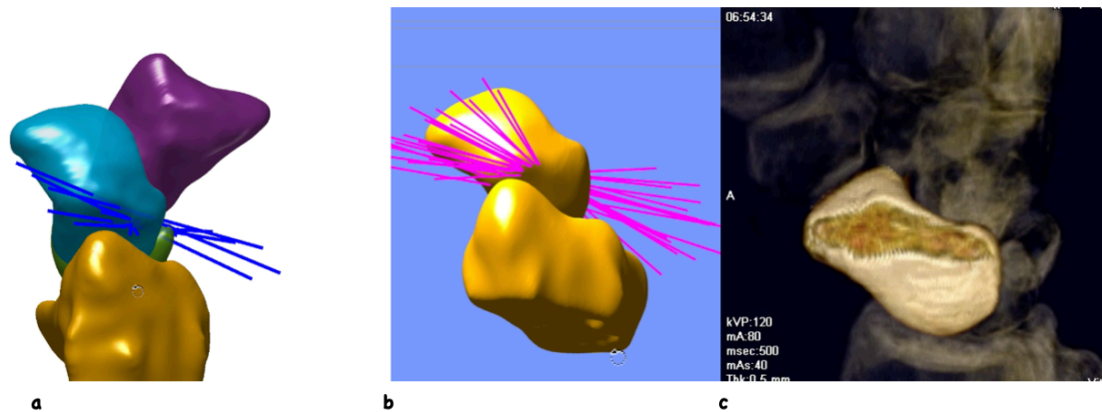


Figure 178 The helical axis of motion (HAM) of the normal scaphoid a. during wrist extension to flexion b. during wrist neutral to radial deviation for one single wrist. c. The footprint of the dorsal scapholunate ligament complex.

A previous study using 4D CT commented that during flexion-extension the axis of rotation passes through the dorsal scaphoid (de Roo, Muurling, et al., 2019) (Figure 179). The limitation of de Roo's study is that their observation was based on one single extreme extension position and a single extreme flexion position, even though they used 4D CT for their study.

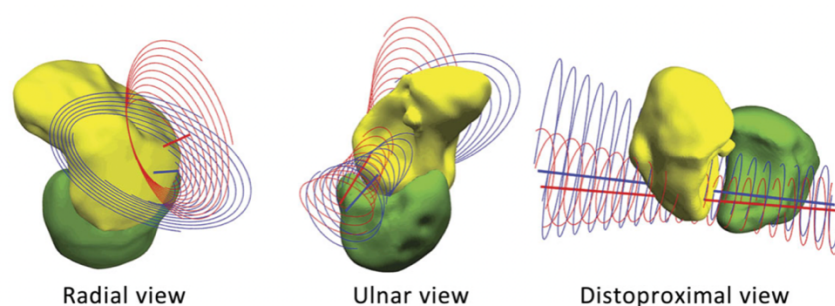


Figure 179 The scapholunate rotation axis in flexion and extension. The blue line is the axis in flexion and the red line is the axis in extension with the 95% confidence ellipse. The axis of rotation was calculated using the displacement from the neutral wrist to the extreme flexion and extreme extension respectively. This is essentially representing a large motion arc using a single axis. From "A four-dimensional-CT study of in vivo

*scapholunate rotation axes: possible implications for scapholunate ligament reconstruction” by de Roo et al., 2019, J Hand Surg Eur Vol, 44(5), 479-487. Copyright [2019] by SAGE Publications Ltd. Journals. Reprinted with permission. Note that the scapholunate rotation axis is the HAM for the scaphoid relative to a coordinate system positioned on the lunate.*

The wrist motion is not one single change in position from extreme radial deviation to neutral, or motion from the neutral to the extreme extension. It consists of multiple small incremental motions that are built into a continuum. If only the neutral position was sampled in the extreme extension, the axis of rotation is invariably a single axis. Dynamic (4D CT) CT is capable of capturing this incremental motion, subjected to its’ temporal resolution or the frame rate. Hence when each step of wrist motion is studied using 4D CT, it is possible to appreciate the change in the position and the orientation of the HAM of carpal bones.

One of the pioneering works on the change in the direction of motion of the scaphoid during the range of motion was published by Craigen and Stanley in 1995. They reported that the scaphoid translates in ulnar deviation and flexes in radial deviation (Craigen & Stanley, 1995). Further developing the concept of Craigen and Stanley, study 03 of the current thesis suggests that the wrist ulnar to radial deviation can be broken down into further small increments, subjected to technical capabilities. In the current study, arbitrary increments of 10° have been used as a solution for not having matched wrist angles. Also, there is evidence that the calculation of HAM becomes unstable below 5° of motion increments, requiring filtering out of such small rotations (Best et al., 2019; de Lange et al., 1990; Woltring et al., 1985). While it was not possible to comment on smaller incremental wrist motions than 10° due to available technical capabilities, as the technology advances, it is likely to be possible to map the smaller changes in rotation axes in future.

In summary the study 03 informs that when the wrist position changes, in every 10° from ulnar to radial deviation the orientation and position of the HAM changes sequentially. It could be due to ligaments or certain bundles of the ligaments being active at certain wrist positions. These can be named ‘sequential ligament restraints’ acting on the carpal bones. In SLI, when some of these restraints are disrupted, the scaphoid moves in a single direction

as indicated by the position and orientation of the HAM. The concept of changing HAM in the normal wrist favours more anatomical repairs in scapholunate instability, rather than single bundle tunnel reconstructions.

#### **4.7. Spectrum of kinematic changes seen in SLI**

Following the literature review, multiple carpal morphological variations that can lead to normal variations in the kinematic patterns were identified. The ligament sectioning studies suggest that various combinations of ligament injuries can lead to different abnormal kinematic features. There was no in vivo study, that reported on the kinematic spectrum of SLI or unique objective diagnostic features. Assessing 4D CT scans of the SLI patient cohort, it was possible to identify unique kinematic pattern in SLI. More importantly, these patterns were objective and quantifiable. A comprehensive subgroup analysis, however, was not possible due to insufficient numbers in each group.

One of the fundamental features of SLI was the reversal of kinematic pattern with greater in- plane and less out of plane motion during wrist radial deviation. A patient with dynamic SLI, despite the normal radioscapoid and radiolunate angles, demonstrated this reversal of kinematic pattern. All patients with static SLI also demonstrated this feature.

While lunate ulnar translocation occurring with SLI has previously been described (Garcia-Elias & Lluch, 2017), a kinematic analysis of this entity has not been published. The current thesis reports that the centroid of the lunate in the patient with ulnar translocation, is volar and ulnar compared to the normal cohort and the other SLI patients. In addition, the lunate in this patient remained extended during wrist extension to neutral. Radiolunate flexion was observed only when the capitate flexed beyond the neutral position. Lunate ulnar translocation occurs only in the presence of multiple carpal ligament injury that includes SLIL, DIC, DRC, volar carpal ligaments (Viegas et al., 1995). While we have not correlated these findings to pathoanatomy, it can be postulated that volar and dorsal restraints of the lunate have been compromised in this situation. These objective findings can be used for future studies for subgroup analysis and to anticipate the requirement for multiple ligament reconstruction in these patients. More importantly, these findings inform the variation of the kinematics in SLI and suggest that one single reconstruction technique will not be suitable for all patients.

The patient with scaphoid dorsal subluxation demonstrated the kinematic changes suggestive of a reduction clunk at 10° of radial deviation. The 'relocation' of the scaphoid was evident in the angular displacement graphs and the centroid translation graphs. While these findings cannot be generalised, the important point is that dynamic CT can be utilised to objectively identify sudden changes in carpal posture presented as clunks.

#### **4.8. Statistics**

All the outcome measures considered in the current study were computed for a sample of 19 SLI patients moving their wrists in ulnar to radial deviation and extension to flexion and compared with a sample of 19 normal wrists. The sample size was dependent on the availability of 4D CT scans. While the sample size was small, the largest 4D CT kinematic study on the uninjured wrist consisted of 20 participants (Brinkhorst et al., 2020). Athlani et al. reported the scapholunate gap using 4D CT, (Athlani et al., 2020) studying 16 SLI patients, 19 participants without SLI and 05 participants where the diagnosis was uncertain. The study by Athlani et al. focussed on the diagnostic accuracy of a single outcome measure, studying the change in the scapholunate gap during wrist radioulnar deviation. Therefore, while the sample size of the current study is small it is similar to the other recent studies, that also have chosen the sample size based on availability.

No previous studies were available reporting on the same outcome measures as the current thesis, using dynamic CT, that could be used to project a power calculation. A post hoc power calculation was an option. However, the recent literature is not in favour of post hoc power analysis as they are decided only by the *p* value (Levine & Ensom, 2001; Onwuegbuzie & Leech, 2004). The confidence intervals are indicated with the *p* values, which is a better indicator of the reliability of the statistical significance.

The wrist ranges of motion and neutral wrist position carpal angles between the two groups were compared using two sample 't-test'. All data was assessed for normality using Shapiro-Wilk test before applying the 't-test'.

The statistical methods used for the dynamic outcome measures in this study were challenging, due to the dynamic nature of data in the study 01,02 and 03. As the patients move their wrists, their wrist angles in each position do not match between participants. This is due to the variability in the range of motion and the patients' speed of moving the wrist. Therefore, when the CT scanner acquires each 3D volume, every patient's wrist was not at the same degree of flexion or extension or radioulnar deviation. Each 3D volume of the CT scan is acquired at a particular time point during the motion, but the wrist angle at this point varies, depending on the rate of the wrist motion, the range of motion and the temporal resolution of the scanner. Therefore, arithmetic averaging cannot be used to calculate a mean value of scaphoid rotation at a particular wrist position.

The interpolation technique on MATLAB R2022<sup>®</sup> was used to overcome this problem similar to previous studies (Brinkhorst et al., 2020; de Roo, Dobbe, et al., 2019; de Roo, Muurling, et al., 2019). To allow for direct comparison across patients, linear interpolation was used to resample the capitate angle every 5° interval using Matlab R2022b (Mathworks, USA). This approach was used in the recent 4D studies referenced above. This was essentially a means of converting the dependent variable (the wrist angle) to a categorical variable preparing for further analysis.

The alternative approach to achieve the same objective was to use binning where all data points around a distinct value are "binned" into a single bin. For example, a wrist angle of 23° ulnar deviation and 18° of ulnar deviation can be binned into a 20° angle. The significance of three outcome measures following binning technique has been calculated as well and found that the results remain the same as with interpolation and binning (Appendix 1.3). This can serve as proof of concepts for future 4D CT studies, that either interpolation or binning can be used in statistical analysis.

Following interpolation, a linear mixed model on IBM SPSS Statistics (Version 27) was used to quantify the statistical significance. A 'Linear mixed model', is a statistical model that has the capability of comparing the two data sets, generated from multiple participants in two groups (normal and SLI) and also considering multiple observations generated for each participant. This has previously been used to compare longitudinal data, specifically carpal

motion patterns (Brinkhorst et al., 2020; "A Model for Longitudinal Data," 2000). The capitate angles were considered the repeated measurements occurring for each participant. There are dependent variables for each repeated measurement of capitate angles, which fits into the concept of longitudinal data belonging to each participant. When capitate angles were considered as repeated measurement, they were correlated according to a first-order autoregressive moving average (ARMA (1,1)) covariance structure similar to Brinkhorst (Brinkhorst et al., 2020) who reported on carpal angulations using 4D CT (described in methodology section ).

The first-order autoregressive moving average (ARMA1) covariance structure posits that capitate angles at similar levels exhibit stronger correlations than those at more distant levels. Concerning within-subject correlations, the GLM incorporates both random intercepts and random slopes for capitate angles. The reason for using ARMA1 was to allow for variations in carpal bone motion patterns and their associations with capitate angles among the study participants. Bonferroni correction was applied within the GLM to adjust the significance level as multiple comparisons were made. The next important step was to assess the goodness of fit of the model selected. This evaluation involved checking the corrected Akaike information criterion and the Bayesian criterion, as well as scrutinizing the distribution of Pearson residuals, which confirmed the statistical model was appropriate.

The results from the position of the HAM in study 03 were first assessed for normality using Shapiro-Wilk test. The sample sizes were variable, and most bins contained sample sizes less than 20, many of which were non-normally distributed. Mann-Whitney U test is a non-parametric test that can be used in such situations, to compare two samples either with small sample size or also non-normally distributed (Hart, 2001; "Mann–Whitney Test," 2008). Therefore, the positions of HAM were compared using Mann-Whitney U test.

For study 03, it was also necessary to calculate the difference between the orientation of the helical axis of the scaphoid between wrist positions. This represented a set of angles arranged around 360° in the x, y and z planes. As the axis is part of “circular data”, it cannot simply be averaged arithmetically, to calculate a mean and a standard deviation. Therefore, statistical analysis of this data has been conducted using the principles of circular statistics.

The direction must be considered. MATLAB Rb2022® has developed a ‘circular statistic toolbox’ which is designed specifically for this purpose (Berens, 2009; Jammalamadaka & SenGupta, 2001). The methods used in this were detailed in the methodology section (2.5.6). While this technique has been widely used in biostatistics and also in other joint kinematics (Abraham & Donahue, 2013; Ippolito et al., 2021; Panagiotopoulou et al., 2017; Turley et al., 2014), to my knowledge this was the first time it has been used for carpal kinematics.

#### **4.9. Limitations**

The limitation of this study includes the small sample size of 19 patients in each group, so it is not possible to do a complete subgroup analysis. In SLI a subgroup analysis is very important in understanding the kinematic spectrum of SLI. The second limitation is that the patient’s wrist motion was not constrained using a restrictive device. The patients were instructed on how to mobilise the wrist, doing ulnar to radial deviation and extension to flexion. Restraining the wrist, would compromise how the patient moved the wrist, and not be a true measure of the patient’s wrist motion.

One of the features of a dynamic CT study when patients are moving their wrists without any restrictive device is that they will not achieve matched wrist angles. For example, 13 normal wrists and 7 SLI wrists reached 70° of extension. Participants naturally have different wrist ranges of motion and move the wrist at different speeds. To minimise this affecting the conclusions, when the p value was less than 0.05 but confidence intervals overlapped, it was highlighted in each graph as this may not be true statistical significance. Alternative would have been capping the end ranges of data, however, in patients with joint ‘instability’ including the end ranges was important. Therefore, decision was made to include all data points and highlight the overlapped confidence intervals.

The direction of motion affects carpal kinematics, and this is referred to as the hysteresis effect (Short et al., 1995). Short et al. reported that the carpal postures are different during



motion from ulnar to radial deviation and radial to ulnar deviation due to the hysteresis effect. While agreeing that this is an important part of a study on carpal kinematics, it was chosen to only study the extension to flexion and ulnar to radial deviation, due to the extensive post-processing required. Wang et al. reported that segmentation of a single thumb carpometacarpal joint through the range of motion takes 120 man-hours (Wang et al., 2018). The scaphoid, lunate and capitate segmentation is not as time-consuming as the trapezium, which is very closely attached to the trapezoid and has an irregular shape. However, it is my experience that the segmentation of one wrist from extension to flexion and ulnar to radial deviation takes at least 12-16 hours.

Another limitation is that kinematics has not been correlated to the carpal morphology. The type of lunate affects carpal kinematics; however, this has not been assessed in the current study. But it is expected to study that in future projects.

## 5. SUMMARY

In the normal wrist, significant alterations in the position and orientation of the HAM took place during ulnar to radial deviation when the wrist was positioned between 20° ulnar deviation and the neutral position. (Figure 180 a, b and c). It is also the same wrist range of motion where maximum out-of-plane motion of the scaphoid occurred (Figure 181 a). Over two thirds of the scaphoid flexion occurred, between the wrist 20° ulnar deviation to 10° radial deviation. This precedes a region of the graph, between 30° to 20° ulnar deviation, which is less steep, where only 5% of the flexion occurred.

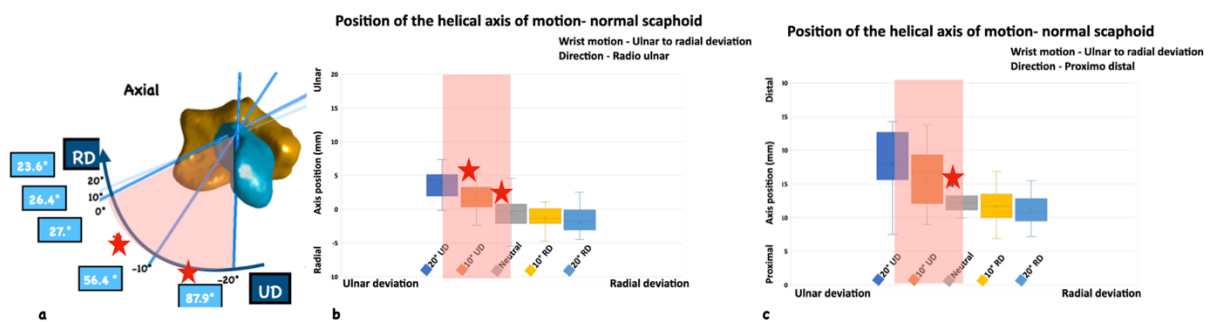


Figure 180 Correlation of the helical axis of motion (HAM) orientation and position of the normal wrist during ulnar to radial deviation. Significant changes in the position and the orientation of the HAM occurred when the wrist moves from 20° of ulnar deviation to the neutral position. a. orientation in the axial plane b. position in the radioulnar direction c. position in the proximo distal direction. The significant changes are indicated by the “\*” and occurred in the shaded zones.

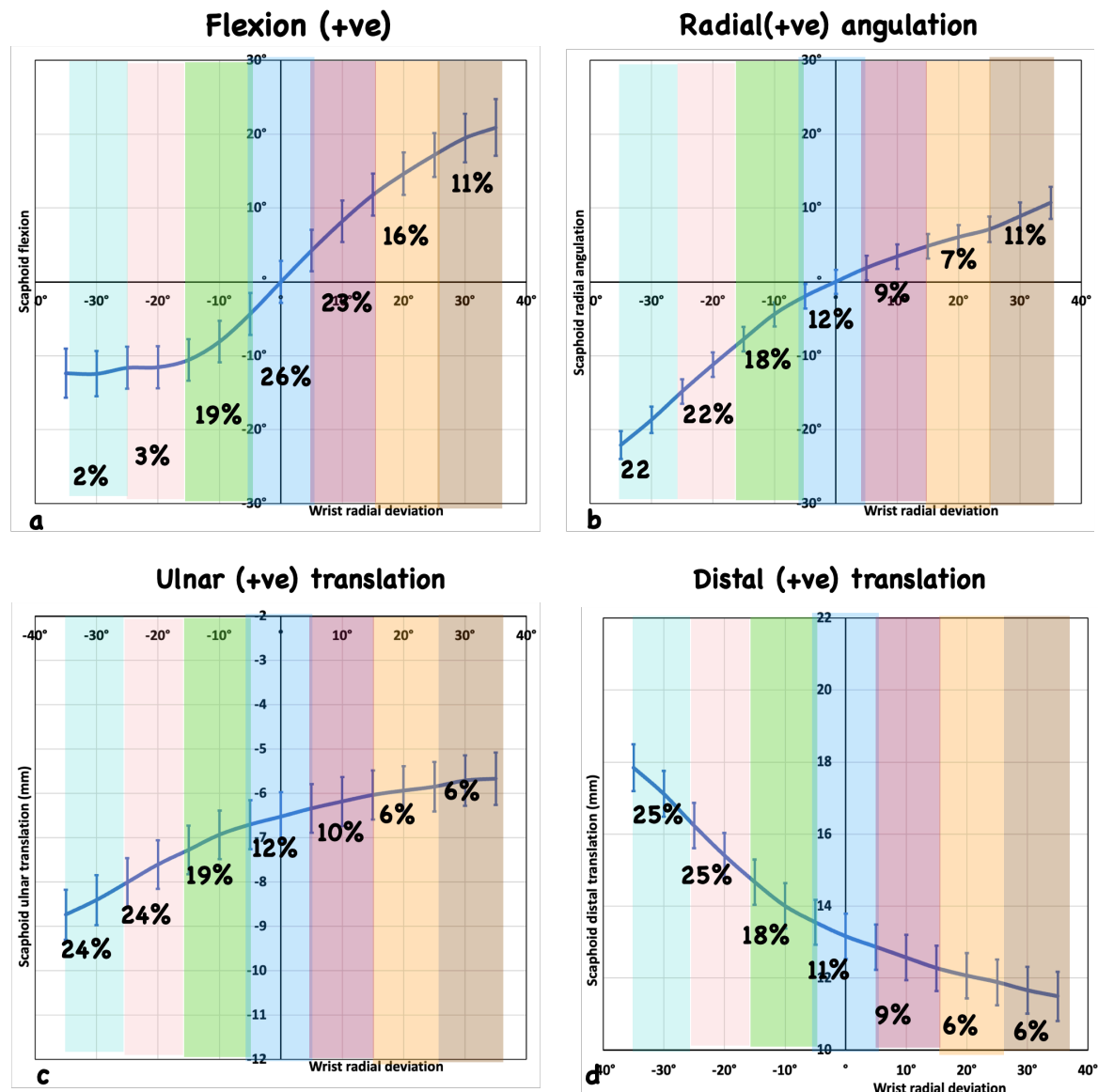


Figure 181 Normal scaphoid angulation and centroid position during the wrist ulnar to radial deviation. a. flexion b. radial angulation c. ulnar translation d. distal translation. The different 10° arcs of wrist motion are highlighted in the different colours. The percentage of motion for each 10° arc is documented in each coloured zone. When the wrist is moving from 30° ulnar deviation to 20° ulnar deviation, the predominant motions of the scaphoid were radial angulation-44%-b), ulnar translation-48%-c) and proximal translation-50%-d) of the centroid. The flexion (a) of the scaphoid predominantly occurred between 10° ulnar to 10° radial deviation (68%). Once the wrist radially deviates beyond 10°, the scaphoid mainly flexed, with less contribution from other 3 motions (b, c, d). Note that the axial rotation and volar translation were not included as there was no identifiable difference in those parameters.

With radial deviation beyond 10°, the scaphoid continued to flex, but there was less radial angulation, ulnar translation, and proximal translation (Figure 181). In SLI, it has been

objectively demonstrated that the change in position and orientation of the helical axis is small and not significantly different between wrist positions (section 3.6.1.3, Figure 182.)

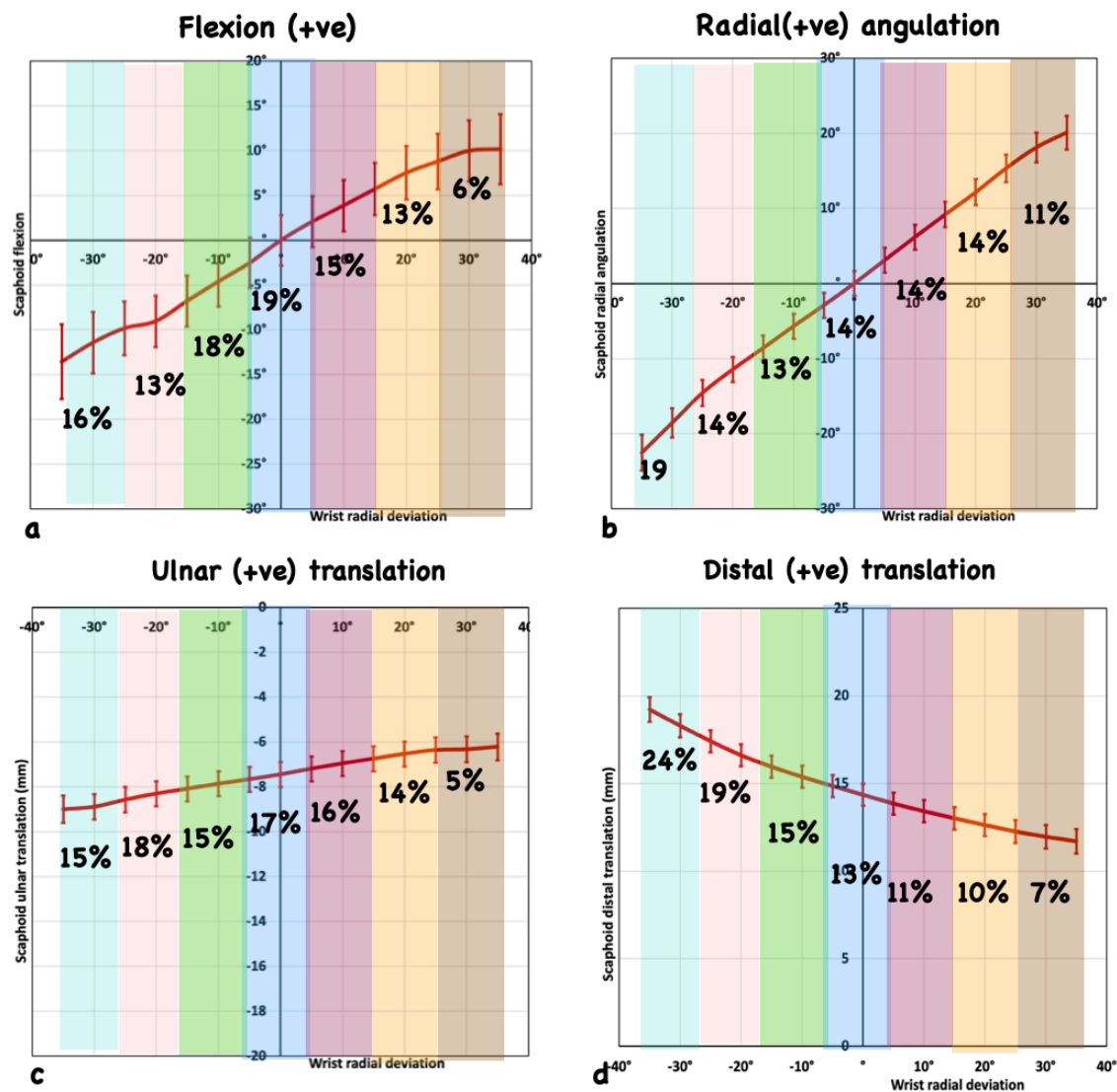


Figure 182 SLI scaphoid angulation and centroid position during the wrist ulnar to radial deviation. a. flexion b. radial angulation c. ulnar translation d. distal translation. The different 10° arcs of wrist motion from ulnar to radial deviation are demonstrated in the different colours. The percentage of motion for each 10° arc is documented in each coloured zone. There was no significant difference identified between the different arcs of motion. As such, each arc of motion has a similar change in percentage of motion. Note that compared to Figure 181 the proportionate motion that occurs in each incremental wrist position is relatively uniform without sequential variations.

When the SLI wrist moves past 10° radial deviation, the distinct kinematic changes of radioscaphoid instability appear, with reduced out-of-plane motion (reduced flexion and external rotation) and increased in-plane motion. This can be explained by the scaphoid being unrestrained by the proximal row and driven by the distal row leading to more radioscaphoid motion and less scapho-capitate motion.

The normal lunate also had a similar range where significant changes in position and orientation of the HAM changed, and the out-of-plane flexion. Even in SLI, the changes that occurred in the lunate were preserved. Nonetheless, the change in the HAM orientation from maximum ulnar to radial deviation in the SLI lunate was significantly less than the normal lunate, in every plane. It confirms that the lunate HAM is affected in SLI, but to a lesser degree.

In addition, the SLI lunate did not show a significant reversal of kinematic changes with wrist radial deviation. The important kinematic change that was observed was a total reduction of out-of-plane motion through the entire range of motion.

The conclusions drawn are that the pathoanatomy of SLI affects a critical range of motion of the wrist. The effects were seen once the wrist is past 10° of radial deviation. The resultant primary changes were seen in the scaphoid as radioscaphoid instability. The reduction in the radiocarpal motion and increase in the midcarpal motion of the lunate, is likely secondary to being unlinked from the scaphoid. A summary of kinematic changes that occur in SLI are presented in Table 128.

*Table 128 Significant outcomes of the scaphoid and lunate angular displacements observed in the SLI wrist compared to the normal.*

Significant outcome measure	UD to Neutral	Neutral to RD	Extension to Neutral	Neutral to flexion
Scaphoid flexion arc	No	Decreased 10° to 35°	Increased 70° to 40°	Decreased 35° to 50°
Scaphoid RA arc	No	Increased 10° to 35°	No	No
Lunate flexion arc	Decreased 30° to 5°	Decreased 10° to 35°	Decreased 70° to 30°	No

*The outcome measures which had a statistically significant difference in the SLI wrist compared to normal wrist is presented. Note that some arcs of motion were increased and some, decreased. When the change was not significant through the entire range, the range where the significant change occurred is mentioned. The changes within the margin of error of the method and changes that occur during less than 10° of wrist motion were not included to avoid over-generalisation. UD- ulnar deviation RD- Radial deviation RA-Radial angulation*

Assessing the changes that occur in the wrist extension to flexion, it is difficult to draw similar conclusions as the proximal and distal rows move in the same plane through the range of motion. However, it was observed that between 70° to 40° wrist extension the scaphoid flexion was very similar to capitate flexion. The ratio between the scaphoid to capitate flexion was above 0.85 (normal scaphoid/capitate is below 0.75) in that wrist range of motion. It is the same range where the SLI lunate flexion was significantly less.

Results from midcarpal assessment confirmed that during the same wrist range, the radial column motion shifted towards the radioscapoid joint, and the central column motion shifted towards the capito-lunate joint, hence worsening the dissociation. A summary of novel findings pertaining to the midcarpal joint in SLI are presented Table 129. Combining the radiocarpal and midcarpal kinematic findings, the current study concluded that in SLI radial column had less midcarpal motion. The central column had greater midcarpal motion when the wrist was moving from 70° to 30° extension. It is apparent that the abnormal kinematic changes are more prominent between 70° to 40° of wrist extension and wrist radial deviation beyond 10°. Hence, these ranges of motion could be avoided in rehabilitation following scapholunate injury.

Table 129 Significant outcomes of the scaphoid and lunate midcarpal angular displacements observed in the SLI wrist compared to the normal.

Significant outcome measure	UD to neutral	Neutral to RD	Extension to neutral	Neutral to flexion
Scapho-capitate flexion	Decreased 30° to 10°	Decreased 10° to 35°	Decreased 70° to 40°	Increased 35° to 50°
Scapho-capitate RA	No	Decreased 10° to 35°	Decreased 70° to 45°	No
Luno-capitate flexion	Decreased 35° to 15°	No	Increased 70° to 30°	No

The outcome measures which had a statistically significant difference in the SLI wrist compared to normal wrist is presented. Note that some arcs of motion were increased and some, decreased. When the change was not significant through the entire range, the range where the significant change occurred is mentioned. The changes within the margin of error of the method and changes that occur during less than 10° of wrist motion were not included to avoid over-generalisation. UD- ulnar deviation RD- Radial deviation RA- Radial angulation

The radio-carpal angulation findings in SLI wrist compared to the normal (3.4), and the wrist motions they occurred are summarised in Table 130.

Table 130 Significant outcomes of the radioscapoid and radiolunate angles and centroid positions observed in the SLI wrist compared to the normal

Significant outcome measure	UD to Neutral	Neutral to RD	Extension to Neutral	Neutral to flexion
Scaphoid flexed	Yes	No	Yes	Yes
Scaphoid internally rotated	Yes	Yes	Yes	Yes
Scaphoid centroid distal	Yes	No	70° to 30°	No
Scaphoid centroid radial	15° to 0°	0° to 5°	Yes	0° to 15°
Lunate extended	No	Yes	20° to 0°	Yes
Lunate centroid ulnar	35° to 15°	No	Yes	Yes

The outcome measures which had a statistically significant difference in the SLI wrist compared to normal wrist is presented. When the change was not significant through the entire range, the range where the significant change occurred is mentioned. The changes within the margin of error of the method and changes that occur

*during less than 10° of wrist motion were not included to avoid over-generalisation. Positive changes are highlighted. UD- ulnar deviation RD- Radial deviation*

Assessing the SLI radiocarpal angles compared to the normal, current thesis has identified that the SLI scaphoid remained flexed throughout wrist extension to flexion, and during wrist ulnar deviation to neutral. The SLI scaphoid was internally rotated in all wrist positions. The SLI scaphoid centroid was radial during the wrist ulnar deviation to neutral and 70° to 30° extension. It was distal during wrist 15° ulnar deviation to 5° radial deviation and 70° extension to 15° flexion.

The diagnostic radiocarpal angles of the SLI lunate, compared to the normal, were radiolunate extension from neutral to 35° radial deviation and from 20° extension to 70° flexion. The SLI lunate centroid was more ulnar during wrist 35° to 15° wrist ulnar deviation and throughout extension to flexion. The important point is that differences were observed in specific wrist positions. Unless the clinician looks for radiolunate extension during neutral wrist position, wrist flexion or radial deviation, it is unlikely to be appreciated. Similar concepts apply for all the above outcome measures presented. These multiple radiocarpal outcome measures can help diagnosis of the SLI compared to the normal. It is specifically in the context that SLI is not a binary diagnosis that can be defined by a single parameter such as scapholunate diastasis.

In summary the current thesis informs about the six degrees of freedom kinematics of the SLI scaphoid and the lunate during motion. Thereby, the current thesis presents outcome measures helpful in diagnosis and understanding 3D kinematics of SLI. Lastly it informs about the HAM, which provides insights into principles of SLI reconstruction.

.



## 6. THE ORIGINAL CONTRIBUTION TO THE LITERATURE

This thesis has contributed to the literature in several ways. Firstly, the thesis presents the six degrees of freedom kinematics of the scaphoid and the lunate in SLI compared to the normal wrist, in vivo. Secondly, this thesis identifies abnormalities of motion distribution in radiocarpal and midcarpal joints in SLI compared to the normal wrist. Finally, the change in the orientation and the position of the helical axis of motion with the wrist position was introduced.

The six degrees of freedom kinematics of the scaphoid and the lunate in SLI is important for diagnosis as well as understanding of the pathomechanics. The radioscapoid angles in three anatomic planes and the centroid positions during wrist motion enable differentiating SLI from the normal wrist, in any wrist position and any anatomic plane. SLI is not a binary diagnosis based on one single parameter. This thesis adds a multitude of factors that can support a diagnosis of SLI.

Structural pathology such as SL ligament injury seen in an MRI or arthroscopy is currently the mainstay of the SLI diagnosis. In other large joints such as knee or shoulder, the diagnosis of instability and surgical decision making is largely supported by clinical demonstration of instability. Complex anatomy of the wrist precludes such clinical assessment. In this context, 4D CT provides a method to assess instability. This thesis objectifies the parameters that can be assessed and used to differentiate between the normal and SLI wrists. It is also likely that objective dynamic abnormalities may help grading of severity, identifying the spectrum of changes, have a prognostic importance and help surgical decision making. These parameters can also be used for subgroup analysis in future.

A summary of abnormal radio-carpal angulation and centroid position findings in SLI compared to the normal wrist are presented in

Table 130 in section 5. While some clinically available current functionalities of picture archives and communication systems (PACS) may not support a 3-dimensional assessment

of the carpus, these values will be diagnostic when used in 3D-supported environments. In addition, the angular displacement of the scaphoid and the lunate, as a change from the neutral wrist position in SLI is also described. This information enables understanding of the kinematics of SLI wrist compared to the normal. Specifically, the scaphoid in SLI had a reversal of kinematic pattern during wrist radial deviation, with more 'in-plane' motion and less 'out-of-plane' motion. The lunate in contrast had less 'out-of-plane' motion throughout ulnar to radial deviation. From wrist 70° to 40° extension the scaphoid and the lunate had differential flexion, worsening the dissociation between them. A summary of such kinematic changes that occur in SLI are presented in Table 128 in section 5.

The motion distribution between the radiocarpal and the midcarpal joints were abnormal in SLI, when the wrist was radially deviating beyond 10° or when the wrist was moving from 70° to 40° extension. A summary of novel findings pertaining to the midcarpal joint in SLI are presented in Table 129 in section 5. These ranges of motion where abnormal kinematic changes unmasked, could be avoided in rehabilitation following scapholunate injury. All these parameters help identifying the wrist as being kinematically abnormal. In the context of not having definite evidence that every case of SLI needs surgical reconstruction, kinematic assessment may help strengthen the decision to offer or not to offer surgery.

Lastly, another novel finding was about the HAM. Identification of the change of the HAM with the wrist position, has not been previously reported. The information in this thesis has defined that the SLI scaphoid has in principle a single axis of rotation through ulnar to radial deviation and extension to flexion. Hence, it is working as a simple hinge, with in-plane motion, throughout wrist motion. However, the normal scaphoid has multiple axis of rotation, which varies, depending upon the motion of the wrist. This provides a unique insight into why the SL ligament complex is so important in the function of the normal wrist. The SL ligament complex enables the sequential and synchronised motions of the scaphoid and the lunate. Once disrupted, the sequential motions of the scaphoid do not occur.

The scaphoid is in a unique position linking the proximal and the distal row. It is able to work as a gear lever to change the gears of the wrist. SL ligament complex is required to restrain and control the proximal scaphoid, and proximal row, without which the distal row dictates

that the motion will be in-plane motion. Without SL ligament complex the wrist will fail to maintain functional stability during motion. The instability is predominantly radioscaphoid; the lunate is malaligned and has reduced motion.

HAM also will inform the decision-making and design of more anatomical SL reconstruction techniques. We may be far from achieving normal wrist kinematics when we reconstruct a single axis. Findings on HAM potentially favours the trend towards anatomical repairs even in delayed presentations, provided the scaphoid and the lunate are reducible. However, a clinical outcome assessment must be conducted before any recommendations are made.

The kinematic aspects and the diagnostic parameters presented in this thesis will help understand some of the mysteries complicating diagnosis, management, and rehabilitation of the SLI wrist.

## 7. FUTURE DIRECTIONS

The future direction of this project includes its clinical translation. Complete clinical translation of this work requires 3D supported PACS systems, where the significant outcome measures proposed in this thesis can be quantified. 3D supported PACS systems are currently available and incorporating 4D CT into this environment as a commercially available software is being researched. While it is currently at research level, each individual finding of this thesis can still be used to support a diagnosis and understand kinematics of SLI.

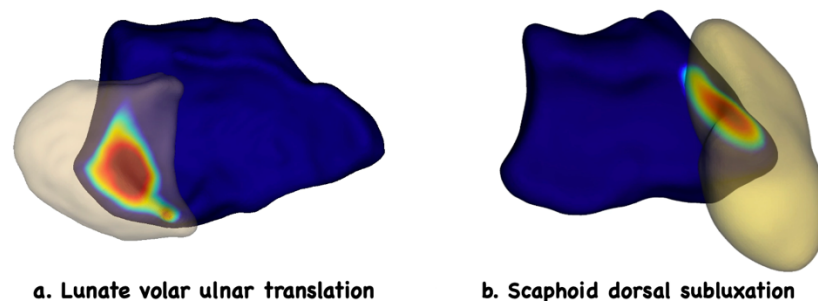
A study on the return motion to better quantify the hysteresis effect has been planned. This needs more efficient post-processing with an automated segmentation process. One challenge was that semiautomatic segmentation was time-consuming. With the low-dose scans, total automation of the segmentation process was not possible due to the resolution. An artificial intelligence/machine learning-based approach can overcome some of these challenges.

The other recommendation based on the challenges is to standardise the wrist motion rate of the patients within the scanner. A timing device/ rhythm control may help in achieving a smoother acceleration and decelerations of wrist motion. As newer CT scanners become available, it will invite modification of the techniques and post-processing. For example, a wider gantry will allow the radius to always be captured within the field, even if the patient mobilises the wrist. This will improve the accuracy of the method, as currently the error rate of this method is mainly due to inadequate length of radius visualisation.

Regardless of the improvements we make with the dynamic CT, low or no radiation options should be considered and developed so dynamic joint imaging can benefit all patient subgroups without excluding children and pregnant patients. Dynamic MRI and 4D ultrasound appear promising in this regard. The important point is that all the concepts and technology presented in this thesis can be applied to dynamic MRI as well.

With an increased sample size, a proper subgroup analysis to comment on the kinematic spectrum will be important. In the literature review 'kinematic spectrum of SLI' has been identified as an area that needs to be addressed. The current thesis provides the framework for this by identifying the objective outcomes that can be quantified and classified and identified unique presentations of SLI. Once adequate patient numbers are collected in the prospective database, a formal subgroup analysis is planned.

In addition, reviewing dart throwers' motion, circumduction, and grip are also other important aspects. The remainder of the carpus, including the STT joint motion and kinematics, and how they relate to scapholunate instability will also be studied. Preliminary work on both these topics has been conducted and it is expected to advance these projects. The carpal instability study is not complete without a kinetic analysis. A study on joint proximity mapping (Figure 183) with wrist motion have been commenced, which will also be addressed in future.



*Figure 183 Joint proximity analysis is a future study that has been planned. a. Joint proximity map of an example of lunate volar ulnar translation b. Joint proximity map of an example of scaphoid dorsal subluxation*

## 8. REFERENCES

- Abe, S., Oka, K., Miyamura, S., Shigi, A., Tanaka, H., Sugamoto, K., Yoshikawa, H., & Murase, T. (2019). Three-Dimensional In Vivo Analysis of Malunited Distal Radius Fractures With Restricted Forearm Rotation. *J Orthop Res*, 37(9), 1881-1891. <https://doi.org/10.1002/jor.24332>
- Abou Arab, W., Rauch, A., Chawki, M. B., Dap, F., Dautel, G., Blum, A., & Gondim Teixeira, P. A. (2018). Scapholunate instability: improved detection with semi-automated kinematic CT analysis during stress maneuvers. *Eur Radiol*, 28(10), 4397-4406. <https://doi.org/10.1007/s00330-018-5430-2>
- Abraham, A. C., & Donahue, T. L. H. (2013). From meniscus to bone: a quantitative evaluation of structure and function of the human meniscal attachments. *Acta biomaterialia*, 9(5), 6322-6329.
- Adler, B. D., Logan, P. M., Janzen, D. L., Favero, K. J., Gropper, P. T., Boyle, J. C., Lawson, I. B., & Connell, D. G. (1996). Extrinsic radiocarpal ligaments: magnetic resonance imaging of normal wrists and scapholunate dissociation. *Can Assoc Radiol J*, 47(6), 417-422.
- Aibinder, W. R., Izadpanah, A., & Elhassan, B. T. (2019). Reduction and Association of the Scaphoid and Lunate: A Functional and Radiographical Outcome Study. *J Wrist Surg*, 8(1), 37-42. <https://doi.org/10.1055/s-0038-1668154>
- Akhbari, B., Morton, A. M., Moore, D. C., & Crisco, J. J. (2021). Biplanar Videoradiography to Study the Wrist and Distal Radioulnar Joints. *J Vis Exp*(168). <https://doi.org/10.3791/62102>
- Akhbari, B., Morton, A. M., Moore, D. C., Weiss, A. C., Wolfe, S. W., & Crisco, J. J. (2019a). Accuracy of biplane videoradiography for quantifying dynamic wrist kinematics. *J Biomech*, 92, 120-125. <https://doi.org/10.1016/j.jbiomech.2019.05.040>
- Apergis, E. (2013). Wrist Anatomy. In *Fracture-Dislocations of the Wrist* (pp. 7-41). Springer Milan. [https://doi.org/10.1007/978-88-470-5328-1\\_2](https://doi.org/10.1007/978-88-470-5328-1_2)
- Athlani, L., Granero, J., Rouizi, K., Hossu, G., Blum, A., Dautel, G., & Teixeira, P. A. G. (2021). Four-Dimensional CT Analysis of Dorsal Intercalated Segment Instability in patients with Suspected Scapholunate Instability. *Journal of Wrist Surgery*, 10(03), 234-240.
- Athlani, L., Rouizi, K., Granero, J., Hossu, G., Blum, A., Dautel, G., & Gondim Teixeira, P. A. (2020). Assessment of scapholunate instability with dynamic computed tomography. *J Hand Surg Eur Vol*, 45(4), 375-382. <https://doi.org/10.1177/1753193419893890>
- Bain, G. I., Clitherow, H. D., Millar, S., Fraysse, F., Costi, J. J., Eng, K., McGuire, D. T., & Thewlis, D. (2015). The effect of lunate morphology on the 3-dimensional kinematics of the carpus. *J Hand Surg Am*, 40(1), 81-89.e81. <https://doi.org/10.1016/j.jhsa.2014.09.019>
- Bain, G. I., Hunt, J., & Mehta, J. A. (1997). Operative fluoroscopy in hand and upper limb surgery. One hundred cases. *J Hand Surg Br*, 22(5), 656-658. [https://doi.org/10.1016/s0266-7681\(97\)80368-3](https://doi.org/10.1016/s0266-7681(97)80368-3)
- Beek, M., Small, C. F., Csongvay, S., Sellens, R. W., Ellis, R. E., & Pichora, D. R. (2004). Wrist Kinematics from Computed Tomography Data. Medical Image Computing and Computer-Assisted Intervention—MICCAI 2004: 7th International Conference, Saint-Malo, France, September 26-29, 2004. Proceedings, Part II 7,

- Beek, M., Small, C. F., Ellis, R. E., Sellens, R. W., & Pichora, D. R. (2010). Bone Alignment Using the Iterative Closest Point Algorithm. *Journal of applied biomechanics*, 26(4), 526-530. <https://doi.org/10.1123/jab.26.4.526>
- Beek, M., Small, C. F., Ellis, R. E., Sellens, R. W., & Pichora, D. R. (2010). Bone alignment using the iterative closest point algorithm. *J Appl Biomech*, 26(4), 526-530. <https://doi.org/10.1123/jab.26.4.526>
- Berens, P. (2009). CircStat: a MATLAB toolbox for circular statistics. *Journal of statistical software*, 31, 1-21.
- Berger, R. A. (1996). The gross and histologic anatomy of the scapholunate interosseous ligament. *J Hand Surg Am*, 21(2), 170-178. [https://doi.org/10.1016/S0363-5023\(96\)80096-7](https://doi.org/10.1016/S0363-5023(96)80096-7)
- Berger, R. A. (1997). The ligaments of the wrist. A current overview of anatomy with considerations of their potential functions. *Hand Clin*, 13(1), 63-82.
- Berger, R. A. (2001). The anatomy of the scaphoid. *Hand Clin*, 17(4), 525-532.
- Berger, R. A., & Bishop, A. T. (1997). A Fiber-Splitting Capsulotomy Technique for Dorsal Exposure of the Wrist. *Techniques in hand & upper extremity surgery*, 1(1). [https://journals.lww.com/techhandsurg/Fulltext/1997/03000/A\\_Fiber\\_Splitting\\_Capsulotomy\\_Technique\\_for\\_Dorsal.2.aspx](https://journals.lww.com/techhandsurg/Fulltext/1997/03000/A_Fiber_Splitting_Capsulotomy_Technique_for_Dorsal.2.aspx)
- Berger, R. A., Blair, W. F., Crowninshield, R. D., & Flatt, A. E. (1982). The scapholunate ligament. *J Hand Surg Am*, 7(1), 87-91. [https://doi.org/10.1016/s0363-5023\(82\)80021-x](https://doi.org/10.1016/s0363-5023(82)80021-x)
- Berger, R. A., Crowninshield, R. D., & Flatt, A. E. (1982). The three-dimensional rotational behaviors of the carpal bones. *Clin Orthop Relat Res*(167), 303-310. <https://www.ncbi.nlm.nih.gov/pubmed/7094476>
- Berger, R. A., Imeada, T., Berglund, L., & An, K. N. (1999). Constraint and material properties of the subregions of the scapholunate interosseous ligament. *J Hand Surg Am*, 24(5), 953-962. <https://doi.org/10.1053/jhsu.1999.0953>
- Besl, P., & McKay, H. D. (1992). A method for registration of 3-D shapes. *IEEE Trans Pattern Anal Mach Intell. Pattern Analysis and Machine Intelligence, IEEE Transactions on*, 14, 239-256. <https://doi.org/10.1109/34.121791>
- Best, G. M., Mack, Z. E., Pichora, D. R., Crisco, J. J., Kamal, R. N., & Rainbow, M. J. (2019). Differences in the Rotation Axes of the Scapholunate Joint During Flexion-Extension and Radial-Ulnar Deviation Motions. *J Hand Surg Am*, 44(9), 772-778. <https://doi.org/10.1016/j.jhsa.2019.05.001>
- Bille, B., Harley, B., & Cohen, H. (2007). A comparison of CT arthrography of the wrist to findings during wrist arthroscopy. *J Hand Surg Am*, 32(6), 834-841. <https://doi.org/10.1016/j.jhsa.2007.04.005>
- Biswas, D., Bible, J. E., Bohan, M., Simpson, A. K., Whang, P. G., & Grauer, J. N. (2009). Radiation exposure from musculoskeletal computerized tomographic scans. *J Bone Joint Surg Am*, 91(8), 1882-1889. <https://doi.org/10.2106/jbjs.H.01199>
- Blevens, A. D., Light, T. R., Jablonsky, W. S., Smith, D. G., Patwardhan, A. G., Guay, M. E., & Woo, T. S. (1989). Radiocarpal articular contact characteristics with scaphoid instability. *J Hand Surg Am*, 14(5), 781-790. [https://doi.org/10.1016/s0363-5023\(89\)80076-0](https://doi.org/10.1016/s0363-5023(89)80076-0)
- Blum, A., Walter, F., Ludwig, T., Zhu, X., & Roland, J. (2000). Multislice CT: principles and new CT-scan applications. *Journal de radiologie*, 81(11), 1597-1614.

- Bond, J. R., & Berquist, T. H. (1991). Radiologic evaluation of hand and wrist motion. *Hand Clin*, 7(1), 113-123.
- Brinkhorst, M., Foumani, M., van Rosmalen, J., Selles, R., Hovius, S., Strackee, S., & Streekstra, G. (2022). Four-dimensional CT analysis of carpal kinematics: An explorative study on the effect of sex and hand-dominance. *Journal of Biomechanics*, 139, 110870. <https://doi.org/10.1016/j.jbiomech.2021.110870>
- Brinkhorst, M., Streekstra, G., van Rosmalen, J., Strackee, S., & Hovius, S. (2020). Effects of axial load on in vivo scaphoid and lunate kinematics using four-dimensional computed tomography. *J Hand Surg Eur Vol*, 45(9), 974-980. <https://doi.org/10.1177/1753193420943400>
- Bryce, T. H. (1896). Certain Points in the Anatomy and Mechanism of the Wrist-Joint Reviewed in the Light of a Series of Rontgen Ray Photographs of the Living Hand. *J Anat Physiol*, 31(Pt 1), 59-79. <https://www.ncbi.nlm.nih.gov/pubmed/17232231>
- Buijze, G. A., Dvinskikh, N. A., Strackee, S. D., Streekstra, G. J., & Blankevoort, L. (2011). Osseous and ligamentous scaphoid anatomy: Part II. Evaluation of ligament morphology using three-dimensional anatomical imaging. *J Hand Surg Am*, 36(12), 1936-1943. <https://doi.org/10.1016/j.jhsa.2011.09.016>
- Buijze, G. A., Lozano-Calderon, S. A., Strackee, S. D., Blankevoort, L., & Jupiter, J. B. (2011). Osseous and ligamentous scaphoid anatomy: Part I. A systematic literature review highlighting controversies. *J Hand Surg Am*, 36(12), 1926-1935. <https://doi.org/10.1016/j.jhsa.2011.09.012>
- Bulstra, A. E. J., Al-Dirini, R. M. A., Turow, A., Oldhoff, M. G. E., Bryant, K., Obdeijn, M. C., Doornberg, J. N., Jaarsma, R. L., & Bain, G. I. (2021). The influence of fracture location and comminution on acute scaphoid fracture displacement: three-dimensional CT analysis. *J Hand Surg Eur Vol*, 46(10), 1072-1080. <https://doi.org/10.1177/17531934211040962>
- Buzzatti, L., Keelson, B., Apperloo, J., Buls, N., Scheerlinck, T., Baeyens, J.-P., Van Gompel, G., De Mey, J., & Cattrysse, E. (2018). Detection of kinematic changes induced by sequential lateral ankle ligament section: a dynamic 4D-CT scan study. European Congress of Radiology (ECR 2018),
- Capelle, C., Devos, P., Caudrelier, C., Verpillat, P., Fourquet, T., Puech, P., Garabedian, C., & Lemaitre, L. (2020). How reproducible are classical and new CT-pelvimetry measurements? *Diagnostic and Interventional Imaging*, 101(2), 79-89.
- Carr, R., MacLean, S., Slavotinek, J., & Bain, G. I. (2019). Four-Dimensional Computed Tomography Scanning for Dynamic Wrist Disorders: Prospective Analysis and Recommendations for Clinical Utility. *Journal of Wrist Surgery*, 8(2), 161-167. <https://doi.org/10.1055/s-0038-1675564>
- Chan, K., Vutescu, E. S., Wolfe, S. W., & Lee, S. K. (2019). Radiographs Detect Dorsal Scaphoid Translation in Scapholunate Dissociation. *J Wrist Surg*, 8(3), 186-191. <https://doi.org/10.1055/s-0038-1677536>
- Chen, J., Tan, J., & Tang, J. B. (2015). Length changes of scapholunate interosseous ligament at different wrist positions: an in vivo 3-dimension image study. *Surg Radiol Anat*, 37(7), 765-772. <https://doi.org/10.1007/s00276-014-1414-3>
- Coburn, J. C., Upal, M. A., & Crisco, J. J. (2007). Coordinate systems for the carpal bones of the wrist. *J Biomech*, 40(1), 203-209. <https://doi.org/10.1016/j.jbiomech.2005.11.015>



- Cooney, W. P., 3rd, Lucca, M. J., Chao, E. Y., & Linscheid, R. L. (1981). The kinesiology of the thumb trapeziometacarpal joint. *J Bone Joint Surg Am*, 63(9), 1371-1381.
- Craigien, M. A., & Stanley, J. K. (1995). Wrist kinematics. Row, column or both? *J Hand Surg Br*, 20(2), 165-170. [https://doi.org/10.1016/s0266-7681\(05\)80044-0](https://doi.org/10.1016/s0266-7681(05)80044-0)
- Crisco, J. J., Coburn, J. C., Moore, D. C., Akelman, E., Weiss, A. P., & Wolfe, S. W. (2005). In vivo radiocarpal kinematics and the dart thrower's motion. *J Bone Joint Surg Am*, 87(12), 2729-2740. <https://doi.org/10.2106/jbjs.D.03058>
- Crisco, J. J., Heard, W. M., Rich, R. R., Paller, D. J., & Wolfe, S. W. (2011). The mechanical axes of the wrist are oriented obliquely to the anatomical axes. *J Bone Joint Surg Am*, 93(2), 169-177. <https://doi.org/10.2106/jbjs.I.01222>
- Crisco, J. J., McGovern, R. D., & Wolfe, S. W. (1999). Noninvasive technique for measuring in vivo three-dimensional carpal bone kinematics. *J Orthop Res*, 17(1), 96-100. <https://doi.org/10.1002/jor.1100170115>
- Crisco, J. J., Pike, S., Hulsizer-Galvin, D. L., Akelman, E., Weiss, A. P., & Wolfe, S. W. (2003). Carpal bone postures and motions are abnormal in both wrists of patients with unilateral scapholunate interosseous ligament tears. *J Hand Surg Am*, 28(6), 926-937. [https://doi.org/10.1016/s0363-5023\(03\)00422-2](https://doi.org/10.1016/s0363-5023(03)00422-2)
- Crisco, J. J., Wolfe, S. W., Neu, C. P., & Pike, S. (2001). Advances in the in vivo measurement of normal and abnormal carpal kinematics. *Orthop Clin North Am*, 32(2), 219-231, vii. [https://doi.org/10.1016/s0030-5898\(05\)70244-3](https://doi.org/10.1016/s0030-5898(05)70244-3)
- Cuénod, P., Charrière, E., & Papaloizos, M. Y. (2002). A mechanical comparison of bone-ligament-bone autografts from the wrist for replacement of the scapholunate ligament. *J Hand Surg Am*, 27(6), 985-990. <https://doi.org/10.1053/jhsu.2002.36514>
- Daggett, M., Werner, B., Collin, P., Gauci, M.-O., Chaoui, J., & Walch, G. (2015). Correlation between glenoid inclination and critical shoulder angle: a radiographic and computed tomography study. *Journal of shoulder and elbow surgery*, 24(12), 1948-1953.
- Daly, B. T., Werner, F. W., Cavallaro, S. M., Tucci, E. R., & Harley, B. J. (2018). Effect of Push-Up Position on Wrist Joint Pressures in the Intact Wrist and Following Scapholunate Interosseous Ligament Sectioning. *J Hand Surg Am*, 43(4), 339-345. <https://doi.org/10.1016/j.jhsa.2017.10.019>
- Daly, L. T., Daly, M. C., Mohamadi, A., & Chen, N. (2020). Chronic Scapholunate Interosseous Ligament Disruption: A Systematic Review and Meta-Analysis of Surgical Treatments. *Hand (N Y)*, 15(1), 27-34. <https://doi.org/10.1177/1558944718787289>
- de Lange, A., Huiskes, R., & Kauer, J. M. (1990). Effects of data smoothing on the reconstruction of helical axis parameters in human joint kinematics. *J Biomech Eng*, 112(2), 107-113. <https://doi.org/10.1115/1.2891160>
- de Lange, A., Kauer, J. M., & Huiskes, R. (1985). Kinematic behavior of the human wrist joint: a roentgen-stereophotogrammetric analysis. *J Orthop Res*, 3(1), 56-64. <https://doi.org/10.1002/jor.1100030107>
- de Roo, M. G. A., Dobbe, J. G. G., Peymani, A., van der Made, A. D., Strackee, S. D., & Streekstra, G. J. (2020). Accuracy of manual and automatic placement of an anatomical coordinate system for the full or partial radius in 3D space. *Scientific Reports*, 10(1), 8114. <https://doi.org/10.1038/s41598-020-65060-7>
- de Roo, M. G. A., Dobbe, J. G. G., van der Horst, C., Streekstra, G. J., & Strackee, S. D. (2019). Carpal kinematic changes after scaphoid nonunion: an in vivo study with four-

- dimensional CT imaging. *J Hand Surg Eur Vol*, 44(10), 1056-1064.  
<https://doi.org/10.1177/1753193419866598>
- de Roo, M. G. A., Muurling, M., Dobbe, J. G. G., Brinkhorst, M. E., Streekstra, G. J., & Strackee, S. D. (2019). A four-dimensional-CT study of in vivo scapholunate rotation axes: possible implications for scapholunate ligament reconstruction. *J Hand Surg Eur Vol*, 44(5), 479-487. <https://doi.org/10.1177/1753193419830924>
- Demehri, S., Hafezi-Nejad, N., Morelli, J. N., Thakur, U., Lifchez, S. D., Means, K. R., Eng, J., & Shores, J. T. (2016). Scapholunate kinematics of asymptomatic wrists in comparison with symptomatic contralateral wrists using four-dimensional CT examinations: initial clinical experience. *Skeletal Radiol*, 45(4), 437-446.  
<https://doi.org/10.1007/s00256-015-2308-0>
- Demehri, S., Hafezi-Nejad, N., Thakur, U., Morelli, J. N., Lifchez, S. D., Means, K. R., & Shores, J. T. (2015). Evaluation of pisotriquetral motion pattern using four-dimensional CT: initial clinical experience in asymptomatic wrists. *Clin Radiol*, 70(12), 1362-1369.  
<https://doi.org/10.1016/j.crad.2015.07.007>
- Destot, E. (2006). The classic: injuries of the wrist: a radiological study. New York, NY: Paul B. Hoeber; 1926. *Clin Orthop Relat Res*, 445, 8-14.  
<https://doi.org/10.1097/01.blo.0000205896.83114.05>
- Dietrich, T. J., Toms, A. P., Cerezal, L., Omoumi, P., Boutin, R. D., Fritz, J., Schmitt, R., Shahabpour, M., Becce, F., & Cotten, A. (2021). Interdisciplinary consensus statements on imaging of scapholunate joint instability. *European Radiology*, 31(12), 9446-9458.
- Dimitris, C., Werner, F. W., Joyce, D. A., & Harley, B. J. (2015). Force in the Scapholunate Interosseous Ligament During Active Wrist Motion. *J Hand Surg Am*, 40(8), 1525-1533. <https://doi.org/10.1016/j.jhsa.2015.04.007>
- Dobbe, J. G. G., de Roo, M. G. A., Visschers, J. C., Strackee, S. D., & Streekstra, G. J. (2019). Evaluation of a Quantitative Method for Carpal Motion Analysis Using Clinical 3-D and 4-D CT Protocols. *IEEE Trans Med Imaging*, 38(4), 1048-1057.  
<https://doi.org/10.1109/tmi.2018.2877503>
- Drain, J., Mehta, S., & Goyal, K. S. (2020). An Analysis of Hamate Morphology Relevant to Hemi-Hamate Arthroplasty. *The Journal of Hand Surgery*, 45(7), 657.e651-657.e656.  
<https://doi.org/https://doi.org/10.1016/j.jhsa.2019.11.009>
- Dreant, N., & Dautel, G. (2003). [Development of a arthroscopic severity score for scapholunate instability]. *Chir Main*, 22(2), 90-94. [https://doi.org/10.1016/s1297-3203\(03\)00018-0](https://doi.org/10.1016/s1297-3203(03)00018-0) (Elaboration d'un score de severite arthroscopique pour les instabilites scapholunaires.)
- Drewniany, J. J., Palmer, A. K., & Flatt, A. E. (1985). The scaphotrapezial ligament complex: an anatomic and biomechanical study. *J Hand Surg Am*, 10(4), 492-498.  
[https://doi.org/10.1016/s0363-5023\(85\)80070-8](https://doi.org/10.1016/s0363-5023(85)80070-8)
- Dunn, M. J., & Johnson, C. (2001). Static scapholunate dissociation: a new reconstruction technique using a volar and dorsal approach in a cadaver model. *J Hand Surg Am*, 26(4), 749-754. <https://doi.org/10.1053/jhsu.2001.26025>
- Easterling, K. J., & Wolfe, S. W. (1994). Scaphoid shift in the uninjured wrist. *J Hand Surg Am*, 19(4), 604-606. [https://doi.org/10.1016/0363-5023\(94\)90265-8](https://doi.org/10.1016/0363-5023(94)90265-8)
- Edirisinghe, Y., Troupis, J. M., Patel, M., Smith, J., & Crossett, M. (2014). Dynamic motion analysis of dart throwers motion visualized through computerized tomography and

- calculation of the axis of rotation. *J Hand Surg Eur Vol*, 39(4), 364-372.  
<https://doi.org/10.1177/1753193413508709>
- Elsaidi, G. A., Ruch, D. S., Kuzma, G. R., & Smith, B. P. (2004). Dorsal wrist ligament insertions stabilize the scapholunate interval: cadaver study. *Clin Orthop Relat Res*(425), 152-157. <https://doi.org/10.1097/01.blo.0000136836.78049.45>
- Fedorov, A., Beichel, R., Kalpathy-Cramer, J., Finet, J., Fillion-Robin, J.-C., Pujol, S., Bauer, C., Jennings, D., Fennessy, F., Sonka, M., Buatti, J., Aylward, S., Miller, J. V., Pieper, S., & Kikinis, R. (2012). 3D Slicer as an image computing platform for the Quantitative Imaging Network. *Magnetic resonance imaging*, 30(9), 1323-1341.  
<https://doi.org/10.1016/j.mri.2012.05.001>
- Figueroa, J., Werner, F. W., Travers, P. M., & Short, W. H. (2021). Carpal Motion in Chronic Geissler IV Scapholunate Interosseous Ligament Wrists. *The Journal of Hand Surgery*, 46(5), 368-376. <https://doi.org/https://doi.org/10.1016/j.jhsa.2020.12.015>
- Fisher, R. (1953). Dispersion on a sphere: Proceedings of the Royal Society of London, Ser. A, v. 217. In.
- Fisk, G. R. (1983). The wrist joint. *Hand*, 15(3), 239-241.  
<https://www.ncbi.nlm.nih.gov/pubmed/6642293>
- Fogg, Q. A. (2004). *Scaphoid variation and an anatomical basis for variable carpal mechanics* [The University of Adelaide].
- Garcia-Elias, M. (1999). Position Statement: Definition of Carpal Instability: The Anatomy and Biomechanics Committee of the International Federation of Societies for Surgery of the Hand. *The Journal of Hand Surgery*, 24(4), 866-867.
- Garcia-Elias, M., Alomar Serrallach, X., & Monill Serra, J. (2014). Dart-throwing motion in patients with scapholunate instability: a dynamic four-dimensional computed tomography study. *J Hand Surg Eur Vol*, 39(4), 346-352.  
<https://doi.org/10.1177/1753193413484630>
- Garcia-Elias, M., Cooney, W. P., An, K. N., Linscheid, R. L., & Chao, E. Y. (1989). Wrist kinematics after limited intercarpal arthrodesis. *J Hand Surg Am*, 14(5), 791-799.  
[https://doi.org/10.1016/s0363-5023\(89\)80077-2](https://doi.org/10.1016/s0363-5023(89)80077-2)
- Garcia-Elias, M., Horii, E., & Berger, R. (1991). Individual carpal bone motion. In *Biomechanics of the wrist joint* (pp. 61-75). Springer.
- Garcia-Elias, M., & Lluch, A. L. (2017). Wrist instabilities, misalignments, and dislocations. *Green's operative hand surgery*. 7th ed. Philadelphia: Elsevier, 418-478.
- Garcia-Elias, M., Lluch, A. L., & Stanley, J. K. (2006). Three-ligament tenodesis for the treatment of scapholunate dissociation: indications and surgical technique. *J Hand Surg Am*, 31(1), 125-134. <https://doi.org/10.1016/j.jhsa.2005.10.011>
- Garg, R., Kraszewski, A. P., Stoecklein, H. H., Syrkin, G., Hillstrom, H. J., Backus, S., Lenhoff, M. L., Wolff, A. L., Crisco, J. J., & Wolfe, S. W. (2014). Wrist kinematic coupling and performance during functional tasks: effects of constrained motion. *J Hand Surg Am*, 39(4), 634-642.e631. <https://doi.org/10.1016/j.jhsa.2013.12.031>
- Geissler, W. B. (2006). [Arthroscopic management of scapholunate instability.]. *Chir Main*, 25S1, S187-S196. <https://doi.org/10.1016/j.main.2006.07.027> (Traitement arthroscopique des instabilites scapholunaires.)
- Geissler, W. B. (2013). Arthroscopic management of scapholunate instability. *J Wrist Surg*, 2(2), 129-135. <https://doi.org/10.1055/s-0033-1343354>

- Gelberman, R. H., Panagis, J. S., Taleisnik, J., & Baumgaertner, M. (1983). The arterial anatomy of the human carpus. Part I: The extraosseous vascularity. *J Hand Surg Am*, 8(4), 367-375. [https://doi.org/10.1016/s0363-5023\(83\)80194-4](https://doi.org/10.1016/s0363-5023(83)80194-4)
- Gheno, R., Buck, F. M., Nico, M. A., Trudell, D. J., & Resnick, D. (2010). Differences between radial and ulnar deviation of the wrist in the study of the intrinsic intercarpal ligaments: magnetic resonance imaging and gross anatomic inspection in cadavers. *Skeletal Radiol*, 39(8), 799-805. <https://doi.org/10.1007/s00256-009-0796-5>
- Goelz, L., Kim, S., Guthoff, C., Eichenauer, F., Eisenschenk, A., Mutze, S., & Asmus, A. (2021). ACTION trial: a prospective study on diagnostic Accuracy of 4D CT for diagnosing Instable Scapholunate Dissociation. *BMC Musculoskelet Disord*, 22(1), 84. <https://doi.org/10.1186/s12891-021-03946-x>
- Gondim Teixeira, P. A., De Verbizier, J., Aptel, S., Wack, M., Dap, F., Dautel, G., & Blum, A. (2016). Posterior Radioscaphoid Angle as a Predictor of Wrist Degenerative Joint Disease in Patients With Scapholunate Ligament Tears. *AJR Am J Roentgenol*, 206(1), 144-150. <https://doi.org/10.2214/ajr.15.14606>
- Goto, A., Leng, S., Sugamoto, K., Cooney, W. P., 3rd, Kakar, S., & Zhao, K. (2014). In vivo pilot study evaluating the thumb carpometacarpal joint during circumduction. *Clin Orthop Relat Res*, 472(4), 1106-1113. <https://doi.org/10.1007/s11999-013-3066-8>
- Goto, A., Moritomo, H., Murase, T., Oka, K., Sugamoto, K., Arimura, T., Masumoto, J., Tamura, S., Yoshikawa, H., & Ochi, T. (2005). In vivo three-dimensional wrist motion analysis using magnetic resonance imaging and volume-based registration. *J Orthop Res*, 23(4), 750-756. <https://doi.org/10.1016/j.orthres.2004.10.001>
- Greditzer, H. G. t., Zeidenberg, J., Kam, C. C., Gray, R. R., Clifford, P. D., Mintz, D. N., & Jose, J. (2016). Optimal detection of scapholunate ligament tears with MRI. *Acta Radiol*, 57(12), 1508-1514. <https://doi.org/10.1177/0284185115626468>
- Hafezi-Nejad, N., Carrino, J. A., Eng, J., Blackmore, C., Shores, J., Lifchez, S. D., Farahani, S. J., & Demehri, S. (2016). Scapholunate Interosseous Ligament Tears: Diagnostic Performance of 1.5 T, 3 T MRI, and MR Arthrography-A Systematic Review and Meta-analysis. *Acad Radiol*, 23(9), 1091-1103. <https://doi.org/10.1016/j.acra.2016.04.006>
- Hagert, E., Garcia-Elias, M., Forsgren, S., & Ljung, B. O. (2007). Immunohistochemical analysis of wrist ligament innervation in relation to their structural composition. *J Hand Surg Am*, 32(1), 30-36. <https://doi.org/10.1016/j.jhsa.2006.10.005>
- Halpenny, D., Courtney, K., & Torreggiani, W. C. (2012). Dynamic four-dimensional 320 section CT and carpal bone injury - a description of a novel technique to diagnose scapholunate instability. *Clin Radiol*, 67(2), 185-187. <https://doi.org/10.1016/j.crad.2011.10.002>
- Hart, A. (2001). Mann-Whitney test is not just a test of medians: differences in spread can be important. *Bmj*, 323(7309), 391-393. <https://doi.org/10.1136/bmj.323.7309.391>
- Harvey, E. J., Hanel, D., Knight, J. B., & Tencer, A. F. (1999). Autograft replacements for the scapholunate ligament: a biomechanical comparison of hand-based autografts. *J Hand Surg Am*, 24(5), 963-967. <https://doi.org/10.1053/jhsu.1999.0963>
- Hendrix, N., Scholten, E., Vernhout, B., Bruijnen, S., Maresch, B., Jong, M. d., Diepstraten, S., Bollen, S., Schalekamp, S., Rooij, M. d., Scholtens, A., Hendrix, W., Samson, T., Ong, L.-L. S., Postma, E., Ginneken, B. v., & Rutten, M. (2021). Development and Validation of a Convolutional Neural Network for Automated Detection of Scaphoid Fractures on Conventional Radiographs. *Radiology: Artificial Intelligence*, 3(4), e200260. <https://doi.org/10.1148/ryai.2021200260>

- Henke, W. (1859). Die bewegungen der Handwurzel. *Z Rat Med*, 7, 27.
- Henrichon, S. S., Foster, B. H., Shaw, C., Bayne, C. O., Szabo, R. M., Chaudhari, A. J., & Boutin, R. D. (2020). Dynamic MRI of the wrist in less than 20 seconds: normal midcarpal motion and reader reliability. *Skeletal Radiol*, 49(2), 241-248. <https://doi.org/10.1007/s00256-019-03266-1>
- Hofstede, D. J., Ritt, M. J., & Bos, K. E. (1999). Tarsal autografts for reconstruction of the scapholunate interosseous ligament: a biomechanical study. *J Hand Surg Am*, 24(5), 968-976. <https://doi.org/10.1053/jhsu.1999.0968>
- Hollister, A. M., Jatana, S., Singh, A. K., Sullivan, W. W., & Lupichuk, A. G. (1993). The axes of rotation of the knee. *Clin Orthop Relat Res*(290), 259-268.
- Horii, E., Garcia-Elias, M., An, K. N., Bishop, A. T., Cooney, W. P., Linscheid, R. L., & Chao, E. Y. (1991). A kinematic study of luno-triquetral dissociations. *J Hand Surg Am*, 16(2), 355-362. [https://doi.org/10.1016/s0363-5023\(10\)80126-1](https://doi.org/10.1016/s0363-5023(10)80126-1)
- Huang, J. I., Thayer, M. K., Paczas, M., Lacey, S. H., & Cooperman, D. R. (2019). Variations in Hook of Hamate Morphology: A Cadaveric Analysis. *The Journal of Hand Surgery*, 44(7), 611.e611-611.e615. <https://doi.org/https://doi.org/10.1016/j.jhsa.2018.08.007>
- Huddleston, H. P., Kurtzman, J. S., Levy, K. H., Connors, K. M., Hayes, W. T., & Koehler, S. M. (2021). Radiocarpal Contact Pressures Are Not Altered after Scapholunate Ligament Tears. *Journal of Wrist Surgery*, 11(03), 250-256.
- Ippolito, G., Serrao, M., Conte, C., Castiglia, S. F., Rucco, F., Bonacci, E., Miscusi, M., Pierelli, F., Bini, F., & Marinozzi, F. (2021). Direct anterior approach for total hip arthroplasty: Hip biomechanics and muscle activation during three walking tasks. *Clinical Biomechanics*, 89, 105454.
- Ishikawa, J., Niebur, G. L., Uchiyama, S., Linscheid, R. L., Minami, A., Kaneda, K., & An, K. N. (1997). Feasibility of using a magnetic tracking device for measuring carpal kinematics. *J Biomech*, 30(11-12), 1183-1186. [https://doi.org/10.1016/s0021-9290\(97\)00097-3](https://doi.org/10.1016/s0021-9290(97)00097-3)
- James, S., Richards, R., & McGrouther, D. (1992). Three-dimensional CT imaging of the wrist: a practical system. *The Journal of Hand Surgery: British & European Volume*, 17(5), 504-506.
- Jammalamadaka, S. R., & SenGupta, A. (2001). *Topics in circular statistics* (Vol. 5). world scientific.
- Jantea, C. L., An, K.-N., Linscheid, R. L., & Cooney, W. (1994). The Role of the Scapho—Trapezial—Trapezoidal Ligament Complex on Scaphoid Kinematics. *Advances in the Biomechanics of the Hand and Wrist*, 345-361.
- Johnson, J. E., Lee, P., McIlff, T. E., Toby, E. B., & Fischer, K. J. (2013). Scapholunate ligament injury adversely alters in vivo wrist joint mechanics: an MRI-based modeling study. *J Orthop Res*, 31(9), 1455-1460. <https://doi.org/10.1002/jor.22365>
- Johnston, J. D., Small, C. F., Bouxsein, M. L., & Pichora, D. R. (2004). Mechanical properties of the scapholunate ligament correlate with bone mineral density measurements of the hand. *J Orthop Res*, 22(4), 867-871. <https://doi.org/10.1016/j.orthres.2003.12.009>
- Kakar, S., Breighner, R. E., Leng, S., McCollough, C. H., Moran, S. L., Berger, R. A., & Zhao, K. D. (2016). The Role of Dynamic (4D) CT in the Detection of Scapholunate Ligament Injury. *J Wrist Surg*, 5(4), 306-310. <https://doi.org/10.1055/s-0035-1570463>



- Kalia, V., Obray, R. W., Filice, R., Fayad, L. M., Murphy, K., & Carrino, J. A. (2009). Functional joint imaging using 256-MDCT: Technical feasibility. *AJR Am J Roentgenol*, 192(6), W295-299. <https://doi.org/10.2214/ajr.08.1793>
- Kaufmann, R., Pfaeffle, J., Blankenhorn, B., Stabile, K., Robertson, D., & Goitz, R. (2005). Kinematics of the midcarpal and radiocarpal joints in radioulnar deviation: an in vitro study. *J Hand Surg Am*, 30(5), 937-942. <https://doi.org/10.1016/j.jhsa.2005.05.016>
- Kaufmann, R. A., Pfaeffle, H. J., Blankenhorn, B. D., Stabile, K., Robertson, D., & Goitz, R. (2006). Kinematics of the midcarpal and radiocarpal joint in flexion and extension: an in vitro study. *J Hand Surg Am*, 31(7), 1142-1148. <https://doi.org/10.1016/j.jhsa.2006.05.002>
- Kawanishi, Y., Moritomo, H., Omokawa, S., Murase, T., Sugamoto, K., & Yoshikawa, H. (2015). In vivo 3-dimensional analysis of stage III Kienbock disease: pattern of carpal deformity and radioscapoid joint congruity. *J Hand Surg Am*, 40(1), 74-80. <https://doi.org/10.1016/j.jhsa.2014.10.035>
- Kichenassamy, S., Kumar, A., Olver, P., Tannenbaum, A., & Yezzi, A. (1995). Gradient flows and geometric active contour models. Proceedings of IEEE International Conference on Computer Vision,
- Kitay, A., & Wolfe, S. W. (2012). Scapholunate instability: current concepts in diagnosis and management. *J Hand Surg Am*, 37(10), 2175-2196. <https://doi.org/10.1016/j.jhsa.2012.07.035>
- Kobayashi, M., Berger, R. A., Nagy, L., Linscheid, R. L., Uchiyama, S., Ritt, M., & An, K. N. (1997). Normal kinematics of carpal bones: a three-dimensional analysis of carpal bone motion relative to the radius. *J Biomech*, 30(8), 787-793. [https://doi.org/10.1016/s0021-9290\(97\)00026-2](https://doi.org/10.1016/s0021-9290(97)00026-2)
- Kobayashi, M., Garcia-Elias, M., Nagy, L., Ritt, M. J., An, K. N., Cooney, W. P., & Linscheid, R. L. (1997). Axial loading induces rotation of the proximal carpal row bones around unique screw-displacement axes. *J Biomech*, 30(11-12), 1165-1167. [https://doi.org/10.1016/s0021-9290\(97\)00080-8](https://doi.org/10.1016/s0021-9290(97)00080-8)
- Koh, K. H., Lee, H. I., Lim, K. S., Seo, J. S., & Park, M. J. (2013). Effect of wrist position on the measurement of carpal indices on the lateral radiograph. *J Hand Surg Eur Vol*, 38(5), 530-541. <https://doi.org/10.1177/1753193412468543>
- Lamas, C., Carrera, A., Proubasta, I., Llusà, M., Majo, J., & Mir, X. (2007). The anatomy and vascularity of the lunate: considerations applied to Kienbock's disease. *Chir Main*, 26(1), 13-20. <https://doi.org/10.1016/j.main.2007.01.001>
- Larsen, C. F., Mathiesen, F. K., & Lindequist, S. (1991). Measurements of carpal bone angles on lateral wrist radiographs. *J Hand Surg Am*, 16(5), 888-893. [https://doi.org/10.1016/s0363-5023\(10\)80156-x](https://doi.org/10.1016/s0363-5023(10)80156-x)
- Larsen, C. F., Stigsby, B., Lindequist, S., Bellstrøm, T., Mathiesen, F. K., & Ipsen, T. (1991). Observer variability in measurements of carpal bone angles on lateral wrist radiographs. *J Hand Surg Am*, 16(5), 893-898. [https://doi.org/10.1016/s0363-5023\(10\)80157-1](https://doi.org/10.1016/s0363-5023(10)80157-1)
- Lee, K. W., Bae, J. Y., Seo, D. K., Kim, S. B., & Lee, H. I. (2018). Measurement of Carpal Alignment Indices Using 3-Dimensional Computed Tomography. *J Hand Surg Am*, 43(8), 771 e771-771 e777. <https://doi.org/10.1016/j.jhsa.2018.01.003>
- Lee, R. K., Griffith, J. F., Ng, A. W., Law, E. K., Tse, W. L., Wong, C. W., & Ho, P. C. (2017). Intrinsic carpal ligaments on MR and multidetector CT arthrography: comparison of

- axial and axial oblique planes. *Eur Radiol*, 27(3), 1277-1285.  
<https://doi.org/10.1007/s00330-016-4436-x>
- Lee, S. K., Park, J., Baskies, M., Forman, R., Yildirim, G., & Walker, P. (2010). Differential strain of the axially loaded scapholunate interosseus ligament. *J Hand Surg Am*, 35(2), 245-251. <https://doi.org/10.1016/j.jhsa.2009.10.031>
- Lendner, N., Wells, E., Lavi, I., Kwok, Y. Y., Ho, P. C., & Wollstein, R. (2019). Utility of the iPhone 4 Gyroscope Application in the Measurement of Wrist Motion. *Hand (N Y)*, 14(3), 352-356. <https://doi.org/10.1177/1558944717730604>
- Leng, S., Zhao, K., Qu, M., An, K. N., Berger, R., & McCollough, C. H. (2011). Dynamic CT technique for assessment of wrist joint instabilities. *Med Phys*, 38 Suppl 1(Suppl 1), S50. <https://doi.org/10.1118/1.3577759>
- Leventhal, E. L., Moore, D. C., Akelman, E., Wolfe, S. W., & Crisco, J. J. (2010). Carpal and forearm kinematics during a simulated hammering task. *J Hand Surg Am*, 35(7), 1097-1104. <https://doi.org/10.1016/j.jhsa.2010.04.021>
- Levine, M., & Ensom, M. H. (2001). Post hoc power analysis: an idea whose time has passed? *Pharmacotherapy: The Journal of Human Pharmacology and Drug Therapy*, 21(4), 405-409.
- Lin, E. C. (2010). Radiation risk from medical imaging. *Mayo Clin Proc*, 85(12), 1142-1146; quiz 1146. <https://doi.org/10.4065/mcp.2010.0260>
- Linscheid, R. L., & Dobyns, J. H. (2002). Dynamic carpal stability. *The Keio journal of medicine*, 51(3), 140-147.
- Linscheid, R. L., Dobyns, J. H., Beabout, J. W., & Bryan, R. S. (1972). Traumatic instability of the wrist. Diagnosis, classification, and pathomechanics. *J Bone Joint Surg Am*, 54(8), 1612-1632.
- Lipton, M., Higgins, C., Farmer, D., & Boyd, D. (1984). Cardiac imaging with a high-speed Cine-CT Scanner: preliminary results. *Radiology*, 152(3), 579-582.
- Logan, S. E., Nowak, M. D., Gould, P. L., & Weeks, P. M. (1986). Biomechanical behavior of the scapholunate ligament. *Biomed Sci Instrum*, 22, 81-85.
- Loisel, F., Wessel, L. E., Morse, K. W., Victoria, C., Meyers, K. N., & Wolfe, S. W. (2021). Is the Dorsal Fiber-Splitting Approach to the Wrist Safe? A Kinematic Analysis and Introduction of the "Window" Approach. *J Hand Surg Am*, 46(12), 1079-1087.  
<https://doi.org/10.1016/j.jhsa.2021.05.029>
- Ma, B., & Ellis, R. E. (2003). Robust registration for computer-integrated orthopedic surgery: laboratory validation and clinical experience. *Medical image analysis*, 7(3), 237-250.
- Mann–Whitney Test. (2008). In *The Concise Encyclopedia of Statistics* (pp. 327-329). Springer New York. [https://doi.org/10.1007/978-0-387-32833-1\\_243](https://doi.org/10.1007/978-0-387-32833-1_243)
- Mardia, K. V., Jupp, P. E., & Mardia, K. (2000). *Directional statistics* (Vol. 2). Wiley Online Library.
- Marghitu, D. B. (2009). *Mechanisms and Robots Analysis with MATLAB®*. Springer Science & Business Media.
- Mat Jais, I. S., Liu, X., An, K. N., & Tay, S. C. (2014). A method for carpal motion hysteresis quantification in 4-dimensional imaging of the wrist. *Med Eng Phys*, 36(12), 1699-1703. <https://doi.org/10.1016/j.medengphy.2014.08.011>
- Mat Jais, I. S., & Tay, S. C. (2017). Kinematic analysis of the scaphoid using gated four-dimensional CT. *Clin Radiol*, 72(9), 794.e791-794.e799.  
<https://doi.org/10.1016/j.crad.2017.04.005>

- Mataliotakis, G., Doukas, M., Kostas, I., Lykissas, M., Batistatou, A., & Beris, A. (2009). Sensory innervation of the subregions of the scapholunate interosseous ligament in relation to their structural composition. *J Hand Surg Am*, 34(8), 1413-1421. <https://doi.org/10.1016/j.jhsa.2009.05.007>
- Mather, R. (2013). CT Dynamics: The Shift from Morphology to Function. *Current Radiology Reports*, 1(1), 64-75. <https://doi.org/10.1007/s40134-012-0004-6>
- Mathoulin, C. L. (2013). From scapholunate interosseus ligament to scapholunate ligament complex. *J Wrist Surg*, 2(2), 98. <https://doi.org/10.1055/s-0033-1341961>
- Mayfield, J. K. (1980). Mechanism of carpal injuries. *Clin Orthop Relat Res*(149), 45-54. <https://www.ncbi.nlm.nih.gov/pubmed/7408319>
- Mayfield, J. K. (1984). Patterns of injury to carpal ligaments. A spectrum. *Clin Orthop Relat Res*(187), 36-42. <https://www.ncbi.nlm.nih.gov/pubmed/6744735>
- Mayfield, J. K., Johnson, R. P., & Kilcoyne, R. K. (1980). Carpal dislocations: pathomechanics and progressive perilunar instability. *J Hand Surg Am*, 5(3), 226-241. [https://doi.org/10.1016/s0363-5023\(80\)80007-4](https://doi.org/10.1016/s0363-5023(80)80007-4)
- McLean, J., Bain, G., Eames, M., Fogg, Q., & Pourgiezis, N. (2006). An Anatomic Study of the Triquetrum–Hamate Joint. *The Journal of Hand Surgery*, 31(4), 601-607. <https://doi.org/https://doi.org/10.1016/j.jhsa.2005.11.007>
- Meade, R. A., Allende, C. A., & Tsai, T. M. (2005). Osteoblastoma of the scaphoid: a case report. *J Surg Orthop Adv*, 14(3), 125-128.
- Meade, T. D., Schneider, L. H., & Cherry, K. (1990). Radiographic analysis of selective ligament sectioning at the carpal scaphoid: a cadaver study. *J Hand Surg Am*, 15(6), 855-862. [https://doi.org/10.1016/0363-5023\(90\)90003-a](https://doi.org/10.1016/0363-5023(90)90003-a)
- Messina, J. C., Van Overstraeten, L., Luchetti, R., Fairplay, T., & Mathoulin, C. L. (2013). The EWAS Classification of Scapholunate Tears: An Anatomical Arthroscopic Study. *J Wrist Surg*, 2(2), 105-109. <https://doi.org/10.1055/s-0033-1345265>
- Mettler, F. A., Jr., Huda, W., Yoshizumi, T. T., & Mahesh, M. (2008). Effective doses in radiology and diagnostic nuclear medicine: a catalog. *Radiology*, 248(1), 254-263. <https://doi.org/10.1148/radiol.2481071451>
- Mettler Jr, F. A., Thomadsen, B. R., Bhargavan, M., Gilley, D. B., Gray, J. E., Lipoti, J. A., McCrohan, J., Yoshizumi, T. T., & Mahesh, M. (2008). Medical radiation exposure in the US in 2006: preliminary results. *Health physics*, 95(5), 502-507.
- Miranda, D. L., Rainbow, M. J., Crisco, J. J., & Fleming, B. C. (2013). Kinematic differences between optical motion capture and biplanar videoradiography during a jump-cut maneuver. *J Biomech*, 46(3), 567-573. <https://doi.org/10.1016/j.jbiomech.2012.09.023>
- Mitsuyasu, H., Patterson, R. M., Shah, M. A., Buford, W. L., Iwamoto, Y., & Viegas, S. F. (2004). The role of the dorsal intercarpal ligament in dynamic and static scapholunate instability. *J Hand Surg Am*, 29(2), 279-288. <https://doi.org/10.1016/j.jhsa.2003.11.004>
- A Model for Longitudinal Data. (2000). In G. Verbeke & G. Molenberghs (Eds.), *Linear Mixed Models for Longitudinal Data* (pp. 19-29). Springer New York. [https://doi.org/10.1007/978-0-387-22775-7\\_3](https://doi.org/10.1007/978-0-387-22775-7_3)
- Moojen, T. M., Snel, J. G., Ritt, M. J., Kauer, J. M., Venema, H. W., & Bos, K. E. (2002). Three-dimensional carpal kinematics in vivo. *Clin Biomech (Bristol, Avon)*, 17(7), 506-514. [https://doi.org/10.1016/s0268-0033\(02\)00038-4](https://doi.org/10.1016/s0268-0033(02)00038-4)



- Moojen, T. M., Snel, J. G., Ritt, M. J., Venema, H. W., Kauer, J. M., & Bos, K. E. (2002). Scaphoid kinematics in vivo. *J Hand Surg Am*, 27(6), 1003-1010. <https://doi.org/10.1053/jhsu.2002.36519>
- Moojen, T. M., Snel, J. G., Ritt, M. J., Venema, H. W., Kauer, J. M., & Bos, K. E. (2003). In vivo analysis of carpal kinematics and comparative review of the literature. *J Hand Surg Am*, 28(1), 81-87. <https://doi.org/10.1053/jhsu.2003.50009>
- Moritomo, H. (2013). Anatomy and clinical relevance of the ulnocarpal ligament. *J Wrist Surg*, 2(2), 186-189. <https://doi.org/10.1055/s-0033-1345023>
- Moritomo, H., Apergis, E. P., Herzberg, G., Werner, F. W., Wolfe, S. W., & Garcia-Elias, M. (2007). 2007 IFSSH committee report of wrist biomechanics committee: biomechanics of the so-called dart-throwing motion of the wrist. *J Hand Surg Am*, 32(9), 1447-1453. <https://doi.org/10.1016/j.jhsa.2007.08.014>
- Moritomo, H., Goto, A., Sato, Y., Sugamoto, K., Murase, T., & Yoshikawa, H. (2003). The triquetrum-hamate joint: an anatomic and in vivo three-dimensional kinematic study. *J Hand Surg Am*, 28(5), 797-805. [https://doi.org/10.1016/s0363-5023\(03\)00259-4](https://doi.org/10.1016/s0363-5023(03)00259-4)
- Moritomo, H., Murase, T., Arimitsu, S., Oka, K., Yoshikawa, H., & Sugamoto, K. (2008). Change in the length of the ulnocarpal ligaments during radiocarpal motion: possible impact on triangular fibrocartilage complex foveal tears. *J Hand Surg Am*, 33(8), 1278-1286. <https://doi.org/10.1016/j.jhsa.2008.04.033>
- Moritomo, H., Murase, T., Goto, A., Oka, K., Sugamoto, K., & Yoshikawa, H. (2004). Capitate-based kinematics of the midcarpal joint during wrist radioulnar deviation: an in vivo three-dimensional motion analysis. *J Hand Surg Am*, 29(4), 668-675. <https://doi.org/10.1016/j.jhsa.2004.04.010>
- Moritomo, H., Murase, T., Goto, A., Oka, K., Sugamoto, K., & Yoshikawa, H. (2006). In vivo three-dimensional kinematics of the midcarpal joint of the wrist. *J Bone Joint Surg Am*, 88(3), 611-621. <https://doi.org/10.2106/jbjs.D.02885>
- Moritomo, H., Murase, T., Oka, K., Tanaka, H., Yoshikawa, H., & Sugamoto, K. (2008). Relationship between the fracture location and the kinematic pattern in scaphoid nonunion. *J Hand Surg Am*, 33(9), 1459-1468. <https://doi.org/10.1016/j.jhsa.2008.05.035>
- Moritomo, H., Viegas, S. F., Elder, K., Nakamura, K., Dasilva, M. F., & Patterson, R. M. (2000). The scaphotrapezio-trapezoidal joint. Part 2: A kinematic study. *J Hand Surg Am*, 25(5), 911-920. <https://doi.org/10.1053/jhsu.2000.8637>
- Moritomo, H., Viegas, S. F., Nakamura, K., Dasilva, M. F., & Patterson, R. M. (2000). The scaphotrapezio-trapezoidal joint. Part 1: An anatomic and radiographic study. *J Hand Surg Am*, 25(5), 899-910. <https://doi.org/10.1053/jhsu.2000.4582>
- Murray, P. M., Palmer, C. G., & Shin, A. Y. (2012). The mechanism of ulnar-sided perilunate instability of the wrist: a cadaveric study and 6 clinical cases. *J Hand Surg Am*, 37(4), 721-728. <https://doi.org/10.1016/j.jhsa.2012.01.015>
- Nagao, S., Patterson, R. M., Buford, W. L., Jr., Andersen, C. R., Shah, M. A., & Viegas, S. F. (2005). Three-dimensional description of ligamentous attachments around the lunate. *J Hand Surg Am*, 30(4), 685-692. <https://doi.org/10.1016/j.jhsa.2005.03.002>
- Nakamura, M., Narita, Y., Sawada, A., Matsugi, K., Nakata, M., Matsuo, Y., Mizowaki, T., & Hiraoka, M. (2009). Impact of motion velocity on four-dimensional target volumes: a phantom study. *Med Phys*, 36(5), 1610-1617. <https://doi.org/10.1118/1.3110073>

- Neo, P. Y., Mat Jais, I. S., Panknin, C., Lau, C. C., Chan, L. P., An, K. N., & Tay, S. C. (2013). Dynamic imaging with dual-source gated Computed Tomography (CT): implications of motion parameters on image quality for wrist imaging. *Med Eng Phys*, 35(12), 1837-1842. <https://doi.org/10.1016/j.medengphys.2013.05.009>
- Neu, C. P., Crisco, J. J., & Wolfe, S. W. (2001). In vivo kinematic behavior of the radio-capitate joint during wrist flexion-extension and radio-ulnar deviation. *J Biomech*, 34(11), 1429-1438. [https://doi.org/10.1016/s0021-9290\(01\)00117-8](https://doi.org/10.1016/s0021-9290(01)00117-8)
- Neu, C. P., McGovern, R. D., & Crisco, J. J. (2000). Kinematic accuracy of three surface registration methods in a three-dimensional wrist bone study. *J Biomech Eng*, 122(5), 528-533. <https://doi.org/10.1115/1.1289992>
- Nikolopoulos, F., Apergis, E., Kefalas, V., Zoubos, A., Soucacos, P., & Papagelopoulos, P. (2011). Biomechanical properties of interosseous proximal carpal row ligaments. *J Orthop Res*, 29(5), 668-671. <https://doi.org/10.1002/jor.21279>
- Nikolopoulos, F. V., Apergis, E. P., Poulilios, A. D., Papagelopoulos, P. J., Zoubos, A. V., & Kefalas, V. A. (2011). Biomechanical properties of the scapholunate ligament and the importance of its portions in the capitate intrusion injury. *Clin Biomech (Bristol, Avon)*, 26(8), 819-823. <https://doi.org/10.1016/j.clinbiomech.2011.04.009>
- Nowak, M. D. (1991). Material Properties of Ligaments. In K.-N. An, R. A. Berger, & W. P. Cooney (Eds.), *Biomechanics of the Wrist Joint* (pp. 139-156). Springer New York. [https://doi.org/10.1007/978-1-4612-3208-7\\_8](https://doi.org/10.1007/978-1-4612-3208-7_8)
- O'Meehan, C. J., Stuart, W., Mamo, V., Stanley, J. K., & Trail, I. A. (2003). The natural history of an untreated isolated scapholunate interosseus ligament injury. *J Hand Surg Br*, 28(4), 307-310. [https://doi.org/10.1016/s0266-7681\(03\)00079-2](https://doi.org/10.1016/s0266-7681(03)00079-2)
- Oki, S., Kaneda, K., Yamada, Y., Yamada, M., Morishige, Y., Harato, K., Matsumura, N., Nagura, T., & Jinzaki, M. (2019). Four-Dimensional CT Analysis Using Sequential 3D-3D Registration. *J Vis Exp*(153). <https://doi.org/10.3791/59857>
- Omori, S., Moritomo, H., Omokawa, S., Murase, T., Sugamoto, K., & Yoshikawa, H. (2013). In vivo 3-dimensional analysis of dorsal intercalated segment instability deformity secondary to scapholunate dissociation: a preliminary report. *J Hand Surg Am*, 38(7), 1346-1355. <https://doi.org/10.1016/j.jhsa.2013.04.004>
- Onwuegbuzie, A. J., & Leech, N. L. (2004). Post hoc power: A concept whose time has come. *Understanding statistics*, 3(4), 201-230.
- Özkan, S., Kheterpal, A., Palmer, W. E., & Chen, N. C. (2019). Dorsal Extrinsic Ligament Injury and Static Scapholunate Diastasis on Magnetic Resonance Imaging Scans. *J Hand Surg Am*, 44(8), 641-648. <https://doi.org/10.1016/j.jhsa.2019.03.003>
- Padmore, C. E., Stoesser, H., Langohr, G. D. G., Johnson, J. A., & Suh, N. (2019). Carpal Kinematics following Sequential Scapholunate Ligament Sectioning. *J Wrist Surg*, 8(2), 124-131. <https://doi.org/10.1055/s-0038-1676865>
- Palmer, A. K., Werner, F. W., Murphy, D., & Glisson, R. (1985). Functional wrist motion: a biomechanical study. *J Hand Surg Am*, 10(1), 39-46. [https://doi.org/10.1016/s0363-5023\(85\)80246-x](https://doi.org/10.1016/s0363-5023(85)80246-x)
- Panagiotopoulou, O., Iriarte-Diaz, J., Wilshin, S., Dechow, P. C., Taylor, A. B., Abraha, H. M., Aljunid, S. F., & Ross, C. F. (2017). In vivo bone strain and finite element modeling of a rhesus macaque mandible during mastication. *Zoology*, 124, 13-29.
- Pang, E. Q., Douglass, N., Behn, A., Winterton, M., Rainbow, M. J., & Kamal, R. N. (2018). Tensile and Torsional Structural Properties of the Native Scapholunate Ligament. *J*

- Hand Surg Am*, 43(9), 864.e861-864.e867.  
<https://doi.org/10.1016/j.jhsa.2018.01.004>
- Panjabi, M., & White, A. A. (1971). A mathematical approach for three-dimensional analysis of the mechanics of the spine. *Journal of Biomechanics*, 4(3), 203-211.  
[https://doi.org/https://doi.org/10.1016/0021-9290\(71\)90005-4](https://doi.org/https://doi.org/10.1016/0021-9290(71)90005-4)
- Panjabi, M. M., Goel, V. K., & Walter, S. D. (1982). Errors in kinematic parameters of a planar joint: guidelines for optimal experimental design. *J Biomech*, 15(7), 537-544.  
[https://doi.org/10.1016/0021-9290\(82\)90007-0](https://doi.org/10.1016/0021-9290(82)90007-0)
- Patterson, R. M., Elder, K. W., Viegas, S. F., & Buford, W. L. (1995). Carpal bone anatomy measured by computer analysis of three-dimensional reconstructions of computed tomography images. *J Hand Surg Am*, 20(6), 923-929.  
[https://doi.org/10.1016/s0363-5023\(05\)80138-8](https://doi.org/10.1016/s0363-5023(05)80138-8)
- Patterson, R. M., Viegas, S. F., Elder, K., & Buford, W. L. (1995). Quantification of anatomic, geometric, and load transfer characteristics of the wrist joint. *Semin Arthroplasty*, 6(1), 13-19.
- Patterson, R. M., Williams, L., Andersen, C. R., Koh, S., & Viegas, S. F. (2007). Carpal kinematics during simulated active and passive motion of the wrist. *J Hand Surg Am*, 32(7), 1013-1019. <https://doi.org/10.1016/j.jhsa.2007.05.004>
- Patterson, R. M., Yazaki, N., Andersen, C. R., & Viegas, S. F. (2013). Prediction of ligament length and carpal diastasis during wrist flexion-extension and after simulated scapholunate instability. *J Hand Surg Am*, 38(3), 509-518.  
<https://doi.org/10.1016/j.jhsa.2012.12.001>
- Payet, E., Bourguignon, D., Auquit-Auckbur, I., Duparc, F., & Dujardin, F. (2015). Radiographic evaluation of a novel horizontal dorsal intercarpal capsulodesis as a treatment of pre-arthritic scapholunate dissociation: a cadaver study. *J Hand Surg Eur Vol*, 40(5), 502-511. <https://doi.org/10.1177/1753193414528094>
- Pelizzari, C. A., Tan, K. K., Levin, D. N., Chen, G. T. Y., & Balter, J. (1991). Interactive 3D patient — image registration. In A. C. F. Colchester & D. J. Hawkes, *Information Processing in Medical Imaging* Berlin, Heidelberg.
- Pérez, A. J., Jethanandani, R. G., Vutescu, E. S., Meyers, K. N., Lee, S. K., & Wolfe, S. W. (2019). Role of Ligament Stabilizers of the Proximal Carpal Row in Preventing Dorsal Intercalated Segment Instability: A Cadaveric Study. *J Bone Joint Surg Am*, 101(15), 1388-1396. <https://doi.org/10.2106/jbjs.18.01419>
- Pietsch, E. (2019). Injuries to the Scapholunate Ligament: How Often do we Miss it? *EC Orthopaedics*, 10, 117-122.
- Rainbow, M. J., Crisco, J. J., Moore, D. C., & Wolfe, S. W. (2008). Gender differences in capitate kinematics are eliminated after accounting for variation in carpal size. *J Biomech Eng*, 130(4), 041003. <https://doi.org/10.1115/1.2913332>
- Rainbow, M. J., Kamal, R. N., Leventhal, E., Akelman, E., Moore, D. C., Wolfe, S. W., & Crisco, J. J. (2013). In vivo kinematics of the scaphoid, lunate, capitate, and third metacarpal in extreme wrist flexion and extension. *J Hand Surg Am*, 38(2), 278-288.  
<https://doi.org/10.1016/j.jhsa.2012.10.035>
- Raja, S., Williams, D., Wolfe, S., Couzens, G., & Ross, M. (2022a). New Concepts in Carpal Instability. In *Wrist and Elbow Arthroscopy with Selected Open Procedures* (pp. 173-185). Springer, Cham. [https://doi.org/10.1007/978-3-030-78881-0\\_14](https://doi.org/10.1007/978-3-030-78881-0_14)

- Rauch, A., Arab, W. A., Dap, F., Dautel, G., Blum, A., & Gondim Teixeira, P. A. (2018). Four-dimensional CT Analysis of Wrist Kinematics during Radioulnar Deviation. *Radiology*, 289(3), 750-758. <https://doi.org/10.1148/radiol.2018180640>
- Repse, S. E., Amis, B., & Troupis, J. M. (2015). Four-dimensional computed tomography and detection of dynamic capitate subluxation. *J Med Imaging Radiat Oncol*, 59(3), 331-335. <https://doi.org/10.1111/1754-9485.12260>
- Ritman, E., Kinsey, J., Robb, R., Harris, L., & Gilbert, B. (1980). Physics and technical considerations in the design of the DSR: a high temporal resolution volume scanner. *American Journal of Roentgenology*, 134(2), 369-374.
- Ritt, M., Stuart, P. R., Berglund, L. J., Berger, R. A., Linscheid, R. L., Cooney, W. P., & An, K. N. (1996). Rotational laxity and stiffness of the radiocarpal joint. *Clinical Biomechanics*, 11(4), 227-232. [https://doi.org/https://doi.org/10.1016/0268-0033\(95\)00074-7](https://doi.org/https://doi.org/10.1016/0268-0033(95)00074-7)
- Ritt, M. J., Linscheid, R. L., Cooney, W. P., 3rd, Berger, R. A., & An, K. N. (1998). The lunotriquetral joint: kinematic effects of sequential ligament sectioning, ligament repair, and arthrodesis. *J Hand Surg Am*, 23(3), 432-445. [https://doi.org/10.1016/s0363-5023\(05\)80461-7](https://doi.org/10.1016/s0363-5023(05)80461-7)
- Robb, R. A. E. (1985). *Three Dimensional Biomedical Imaging* (Vol. olume II (1st ed.)). VCH, New York,. <https://doi.org/https://doi.org/10.1201/9781315121239>
- Robinson, S., Straatman, L., Lee, T.-Y., Suh, N., & Lalone, E. (2021). Evaluation of Four-Dimensional Computed Tomography as a Technique for Quantifying Carpal Motion. *Journal of Biomechanical Engineering*, 143(6). <https://doi.org/10.1115/1.4050129>
- Rohde, R. S., Crisco, J. J., & Wolfe, S. W. (2010). The advantage of throwing the first stone: how understanding the evolutionary demands of Homo sapiens is helping us understand carpal motion. *J Am Acad Orthop Surg*, 18(1), 51-58. <https://doi.org/10.5435/00124635-201001000-00007>
- Rosenwasser, M. P., Miyasajsa, K. C., & Strauch, R. J. (1997). The RASL procedure: reduction and association of the scaphoid and lunate using the Herbert screw. *Tech Hand Up Extrem Surg*, 1(4), 263-272.
- Ruby, L. K. (1992). Wrist biomechanics. *Instr Course Lect*, 41, 25-32.
- Ruby, L. K., An, K. N., Linscheid, R. L., Cooney, W. P., 3rd, & Chao, E. Y. (1987). The effect of scapholunate ligament section on scapholunate motion. *J Hand Surg Am*, 12(5 Pt 1), 767-771. [https://doi.org/10.1016/s0363-5023\(87\)80065-5](https://doi.org/10.1016/s0363-5023(87)80065-5)
- Ruby, L. K., Cooney, W. P., 3rd, An, K. N., Linscheid, R. L., & Chao, E. Y. (1988). Relative motion of selected carpal bones: a kinematic analysis of the normal wrist. *J Hand Surg Am*, 13(1), 1-10. [https://doi.org/10.1016/0363-5023\(88\)90189-x](https://doi.org/10.1016/0363-5023(88)90189-x)
- Ruíz, D. S. M., Murphy, K., & Gailloud, P. (2010). 320-Multidetector row whole-head dynamic subtracted CT angiography and whole-brain CT perfusion before and after carotid artery stenting. *European journal of radiology*, 74(3), 413-419.
- Sagerman, S. D., Hauck, R. M., & Palmer, A. K. (1995). Lunate morphology: can it be predicted with routine x-ray films? *J Hand Surg Am*, 20(1), 38-41. [https://doi.org/10.1016/s0363-5023\(05\)80055-3](https://doi.org/10.1016/s0363-5023(05)80055-3)
- Said, J., Baker, K., Fernandez, L., Komatsu, D. E., Gould, E., & Hurst, L. C. (2018). The Optimal Location to Measure Scapholunate Diastasis on Screening Radiographs. *Hand (N Y)*, 13(6), 671-677. <https://doi.org/10.1177/1558944717729219>
- Salva-Coll, G., Garcia-Elias, M., & Hagert, E. (2013). Scapholunate instability: proprioception and neuromuscular control. *J Wrist Surg*, 2(2), 136-140. <https://doi.org/10.1055/s-0033-1341960>

- Salva-Coll, G., Garcia-Elias, M., Leon-Lopez, M. T., Llusá-Pérez, M., & Rodríguez-Baeza, A. (2011). Effects of forearm muscles on carpal stability. *J Hand Surg Eur Vol*, 36(7), 553-559. <https://doi.org/10.1177/1753193411407671>
- Salvà-Coll, G., Garcia-Elias, M., Llusá-Pérez, M., & Rodríguez-Baeza, A. (2011). The role of the flexor carpi radialis muscle in scapholunate instability. *J Hand Surg Am*, 36(1), 31-36. <https://doi.org/10.1016/j.jhsa.2010.09.023>
- Sandow, M., & Fisher, T. (2020). Anatomical anterior and posterior reconstruction for scapholunate dissociation: preliminary outcome in ten patients. *J Hand Surg Eur Vol*, 45(4), 389-395. <https://doi.org/10.1177/1753193419886536>
- Sandow, M. J. (2015). 3D Dynamic Analysis of the Wrist. *Hand Surg*, 20(3), 366-368. <https://doi.org/10.1142/s0218810415400080>
- Sandow, M. J., Fisher, T. J., Howard, C. Q., & Papas, S. (2014). Unifying model of carpal mechanics based on computationally derived isometric constraints and rules-based motion - the stable central column theory. *J Hand Surg Eur Vol*, 39(4), 353-363. <https://doi.org/10.1177/1753193413505407>
- Savelberg, H. H., Otten, J. D., Kooloos, J. G., Huijskes, R., & Kauer, J. M. (1993). Carpal bone kinematics and ligament lengthening studied for the full range of joint movement. *J Biomech*, 26(12), 1389-1402. [https://doi.org/10.1016/0021-9290\(93\)90090-2](https://doi.org/10.1016/0021-9290(93)90090-2)
- Schimmerl-Metz, S. M., Metz, V. M., Totterman, S. M., Mann, F. A., & Gilula, L. A. (1999). Radiologic measurement of the scapholunate joint: implications of biologic variation in scapholunate joint morphology. *J Hand Surg Am*, 24(6), 1237-1244. <https://doi.org/10.1053/jhsu.1999.1237>
- Sebastian, T. B., Tek, H., Crisco, J. J., & Kimia, B. B. (2003). Segmentation of carpal bones from CT images using skeletally coupled deformable models. *Med Image Anal*, 7(1), 21-45. [https://doi.org/10.1016/s1361-8415\(02\)00065-8](https://doi.org/10.1016/s1361-8415(02)00065-8)
- Sennwald, G. (1987). Anatomical Approach. In *The Wrist: Anatomical and Pathophysiological Approach to Diagnosis and Treatment* (pp. 13-46). Springer Berlin Heidelberg. [https://doi.org/10.1007/978-3-642-71622-5\\_3](https://doi.org/10.1007/978-3-642-71622-5_3)
- Shapeero, L. G., Dye, S. F., Lipton, M. J., Gould, R. G., Galvin, E. G., & Genant, H. K. (1988). Functional dynamics of the knee joint by ultrafast, cine-CT. *Invest Radiol*, 23(2), 118-123. <https://doi.org/10.1097/00004424-198802000-00007>
- Shin, S. S., Moore, D. C., McGovern, R. D., & Weiss, A. P. (1998). Scapholunate ligament reconstruction using a bone-retinaculum-bone autograft: a biomechanic and histologic study. *J Hand Surg Am*, 23(2), 216-221. [https://doi.org/10.1016/s0363-5023\(98\)80116-0](https://doi.org/10.1016/s0363-5023(98)80116-0)
- Shores, J. T., Demehri, S., & Chhabra, A. (2013). Kinematic "4 Dimensional" CT Imaging in the Assessment of Wrist Biomechanics Before and After Surgical Repair. *Eplasty*, 13, e9. <https://www.ncbi.nlm.nih.gov/pubmed/23573338>
- Short, W. H., Werner, F. W., Fortino, M. D., Palmer, A. K., & Mann, K. A. (1995). A dynamic biomechanical study of scapholunate ligament sectioning. *J Hand Surg Am*, 20(6), 986-999. [https://doi.org/10.1016/s0363-5023\(05\)80147-9](https://doi.org/10.1016/s0363-5023(05)80147-9)
- Short, W. H., Werner, F. W., Green, J. K., & Masaoka, S. (2002a). Biomechanical evaluation of ligamentous stabilizers of the scaphoid and lunate. *Journal of Hand Surgery*, 27(6), 991-1002. <https://doi.org/10.1053/jhsu.2002.35878>
- Short, W. H., Werner, F. W., Green, J. K., & Masaoka, S. (2005). Biomechanical evaluation of the ligamentous stabilizers of the scaphoid and lunate: Part II. *J Hand Surg Am*, 30(1), 24-34. <https://doi.org/10.1016/j.jhsa.2004.09.015>



- Short, W. H., Werner, F. W., Green, J. K., Sutton, L. G., & Brutus, J. P. (2007). Biomechanical evaluation of the ligamentous stabilizers of the scaphoid and lunate: part III. *J Hand Surg Am*, 32(3), 297-309. <https://doi.org/10.1016/j.jhsa.2006.10.024>
- Sikora, S. K., Tham, S. K., Harvey, J. N., Garcia-Elias, M., Goldring, T., Rotstein, A. H., & Ek, E. T. (2019). The Twist X-Ray: A Novel Test for Dynamic Scapholunate Instability. *J Wrist Surg*, 8(1), 61-65. <https://doi.org/10.1055/s-0038-1673344>
- Slater, R. R., Jr., Szabo, R. M., Bay, B. K., & Laubach, J. (1999). Dorsal intercarpal ligament capsulodesis for scapholunate dissociation: biomechanical analysis in a cadaver model. *J Hand Surg Am*, 24(2), 232-239. <https://doi.org/10.1053/jhsu.1999.0232>
- Slutsky, D. J. (2013). The Scapholunate Ligament Complex (SLLC). *J Wrist Surg*, 2(2), 97. <https://doi.org/10.1055/s-0033-1343349>
- Snel, J. G., Venema, H. W., Moojen, T. M., Ritt, J. P., Grimbergen, C. A., & den Heeten, G. J. (2000). Quantitative in vivo analysis of the kinematics of carpal bones from three-dimensional CT images using a deformable surface model and a three-dimensional matching technique. *Med Phys*, 27(9), 2037-2047. <https://doi.org/10.1118/1.1289896>
- Sokolow, C., & Saffar, P. (2001). Anatomy and histology of the scapholunate ligament. *Hand Clin*, 17(1), 77-81. <https://www.ncbi.nlm.nih.gov/pubmed/11280161>
- Spoor, C. W. (1984). Explanation, verification and application of helical-axis error propagation formulas. *Human Movement Science*, 3(1), 95-117. [https://doi.org/https://doi.org/10.1016/0167-9457\(84\)90007-1](https://doi.org/https://doi.org/10.1016/0167-9457(84)90007-1)
- Stanford, W., Phelan, J., Kathol, M. H., Rooholamini, S. A., El-Khoury, G. Y., Palutsis, G. R., & Albright, J. P. (1988). Patellofemoral joint motion: evaluation by ultrafast computed tomography. *Skeletal radiology*, 17, 487-492.
- Sulkers, G. S., Schep, N. W., Maas, M., van der Horst, C. M., Goslings, J. C., & Strackee, S. D. (2014). The diagnostic accuracy of wrist cineradiography in diagnosing scapholunate dissociation. *J Hand Surg Eur Vol*, 39(3), 263-271. <https://doi.org/10.1177/1753193413489056>
- Svoboda, S. J., Eglseider, W. A., Jr., & Belkoff, S. M. (1995). Autografts from the foot for reconstruction of the scapholunate interosseous ligament. *J Hand Surg Am*, 20(6), 980-985. [https://doi.org/10.1016/s0363-5023\(05\)80146-7](https://doi.org/10.1016/s0363-5023(05)80146-7)
- Taleisnik, J. (1976). The ligaments of the wrist. *J Hand Surg Am*, 1(2), 110-118. [https://doi.org/10.1016/s0363-5023\(76\)80004-4](https://doi.org/10.1016/s0363-5023(76)80004-4)
- Taleisnik, J., & Kelly, P. J. (1966). The extraosseous and intraosseous blood supply of the scaphoid bone. *J Bone Joint Surg Am*, 48(6), 1125-1137.
- Taneja, A. K., Bredella, M. A., Chang, C. Y., Joseph Simeone, F., Kattapuram, S. V., & Torriani, M. (2013). Extrinsic wrist ligaments: prevalence of injury by magnetic resonance imaging and association with intrinsic ligament tears. *J Comput Assist Tomogr*, 37(5), 783-789. <https://doi.org/10.1097/RCT.0b013e318298aa2a>
- Tang, P., Swart, E., Konopka, G., Raskolnikov, D., & Katcherian, C. (2013). Effect of capitate morphology on contact biomechanics after proximal row carpectomy. *J Hand Surg Am*, 38(7), 1340-1345. <https://doi.org/10.1016/j.jhsa.2013.03.054>
- Tay, S., Primak, A., Fletcher, J., Schmidt, B., An, K., & McCollough, C. (2008). Understanding the relationship of image quality and motion velocity in gated-CT imaging: Preliminary work for 4D musculoskeletal imaging. *JCAT*, 32, 634-639.
- Tay, S. C., Primak, A. N., Fletcher, J. G., Schmidt, B., Amrami, K. K., Berger, R. A., & McCollough, C. H. (2007). Four-dimensional computed tomographic imaging in the

- wrist: proof of feasibility in a cadaveric model. *Skeletal Radiol*, 36(12), 1163-1169. <https://doi.org/10.1007/s00256-007-0374-7>
- Teixeira, P. A. G., Blanc, J. B., Rauch, A., Arab, W. A., Hossu, G., Athlani, L., & Blum, A. (2021). Evaluation of Dorsal Subluxation of the Scaphoid in Patients With Scapholunate Ligament Tears: A 4D CT Study. *AJR Am J Roentgenol*, 216(1), 141-149. <https://doi.org/10.2214/AJR.20.22855>
- Tommasini Carrara de Sambuy, M., Burgess, T. M., Cambon-Binder, A., & Mathoulin, C. L. (2017). The Anatomy of the Dorsal Capsulo-Scapholunate Septum: A Cadaveric Study. *J Wrist Surg*, 6(3), 244-247. <https://doi.org/10.1055/s-0036-1597922>
- Troupis, J. M., & Amis, B. (2013). Four-dimensional computed tomography and trigger lunate syndrome. *J Comput Assist Tomogr*, 37(4), 639-643. <https://doi.org/10.1097/RCT.0b013e31828b68ec>
- Turley, G. A., Griffin, D. R., & Williams, M. A. (2014). Effect of femoral neck modularity upon the prosthetic range of motion in total hip arthroplasty. *Medical & Biological Engineering & Computing*, 52, 685-694.
- Ungi, T., Lasso, A., & Fichtinger, G. (2016). Open-source platforms for navigated image-guided interventions. *Med Image Anal*, 33, 181-186. <https://doi.org/10.1016/j.media.2016.06.011>
- Upal, M. A., Crisco, J. J., Moore, D. C., Sonenblum, S. E., & Wolfe, S. W. (2006). In vivo elongation of the palmar and dorsal scapholunate interosseous ligament. *J Hand Surg Am*, 31(8), 1326-1332. <https://doi.org/10.1016/j.jhsa.2006.06.005>
- van de Giessen, M., Streekstra, G. J., Strackee, S. D., Maas, M., Grimbergen, K. A., van Vliet, L. J., & Vos, F. M. (2009). Constrained registration of the wrist joint. *IEEE Trans Med Imaging*, 28(12), 1861-1869. <https://doi.org/10.1109/TMI.2009.2021432>
- Van Overstraeten, L., & Camus, E. J. (2016). The role of extrinsic ligaments in maintaining carpal stability - A prospective statistical analysis of 85 arthroscopic cases. *Hand Surg Rehabil*, 35(1), 10-15. <https://doi.org/10.1016/j.hansur.2015.09.004>
- Viegas, S. F., Hillman, G. R., Elder, K., Stoner, D., & Patterson, R. M. (1993). Measurement of carpal bone geometry by computer analysis of three-dimensional CT images. *J Hand Surg Am*, 18(2), 341-349. [https://doi.org/10.1016/0363-5023\(93\)90372-a](https://doi.org/10.1016/0363-5023(93)90372-a)
- Viegas, S. F., Patterson, R. M., & Ward, K. (1995). Extrinsic wrist ligaments in the pathomechanics of ulnar translation instability. *J Hand Surg Am*, 20(2), 312-318. [https://doi.org/10.1016/s0363-5023\(05\)80032-2](https://doi.org/10.1016/s0363-5023(05)80032-2)
- Viegas, S. F., Tencer, A. F., Cantrell, J., Chang, M., Clegg, P., Hicks, C., O'Meara, C., & Williamson, J. B. (1987). Load transfer characteristics of the wrist. Part II. Perilunate instability. *J Hand Surg Am*, 12(6), 978-985. [https://doi.org/10.1016/s0363-5023\(87\)80094-1](https://doi.org/10.1016/s0363-5023(87)80094-1)
- Viegas, S. F., Wagner, K., Patterson, R., & Peterson, P. (1990). Medial (hamate) facet of the lunate. *J Hand Surg Am*, 15(4), 564-571. [https://doi.org/10.1016/s0363-5023\(09\)90016-8](https://doi.org/10.1016/s0363-5023(09)90016-8)
- Viegas, S. F., Yamaguchi, S., Boyd, N. L., & Patterson, R. M. (1999). The dorsal ligaments of the wrist: anatomy, mechanical properties, and function. *J Hand Surg Am*, 24(3), 456-468. <https://doi.org/10.1053/jhsu.1999.0456>
- Wang, K. K., Zhang, X., McCombe, D., Ackland, D. C., Ek, E. T., & Tham, S. K. (2018). Quantitative analysis of in-vivo thumb carpometacarpal joint kinematics using four-dimensional computed tomography. *J Hand Surg Eur Vol*, 43(10), 1088-1097. <https://doi.org/10.1177/1753193418789828>

- Waters, M. S., Werner, F. W., Haddad, S. F., McGrattan, M. L., & Short, W. H. (2016). Biomechanical Evaluation of Scaphoid and Lunate Kinematics Following Selective Sectioning of Portions of the Scapholunate Interosseous Ligament. *J Hand Surg Am*, 41(2), 208-213. <https://doi.org/10.1016/j.jhsa.2015.11.009>
- Watson, G. S. (1982). Circular statistics in biology. In: Taylor & Francis.
- Watson, G. S. (1983). *Statistics on spheres*. Wiley, New York, ©1983.
- Watson, H. K., & Ballet, F. L. (1984). The SLAC wrist: scapholunate advanced collapse pattern of degenerative arthritis. *J Hand Surg Am*, 9(3), 358-365. [https://doi.org/10.1016/s0363-5023\(84\)80223-3](https://doi.org/10.1016/s0363-5023(84)80223-3)
- Watson, H. K., Weinzweig, J., & Zeppieri, J. (1997). The natural progression of scaphoid instability. *Hand Clin*, 13(1), 39-49. <https://www.ncbi.nlm.nih.gov/pubmed/9048182>
- Weeks, P. M., Vannier, M. W., Stevens, W. G., Gayou, D., & Gilula, L. A. (1985). Three-dimensional imaging of the wrist. *J Hand Surg Am*, 10(1), 32-39. [https://doi.org/10.1016/s0363-5023\(85\)80245-8](https://doi.org/10.1016/s0363-5023(85)80245-8)
- Weidert, S., Andress, S., Linhart, C., Suero, E. M., Greiner, A., Böcker, W., Kammerlander, C., & Becker, C. A. (2020). 3D printing method for next-day acetabular fracture surgery using a surface filtering pipeline: feasibility and 1-year clinical results. *Int J Comput Assist Radiol Surg*, 15(3), 565-575. <https://doi.org/10.1007/s11548-019-02110-0>
- Werner, F. W. (2021). Design Requirements for Scapholunate Interosseous Ligament Reconstruction. *J Wrist Surg*, 10(6), 484-491. <https://doi.org/10.1055/s-0041-1728802>
- Werner, F. W., Green, J. K., Short, W. H., & Masaoka, S. (2004). Scaphoid and lunate motion during a wrist dart throw motion. *J Hand Surg Am*, 29(3), 418-422. <https://doi.org/10.1016/j.jhsa.2004.01.018>
- Werner, F. W., & Short, W. H. (2018). Carpal Pronation and Supination Changes in the Unstable Wrist. *J Wrist Surg*, 7(4), 298-302. <https://doi.org/10.1055/s-0038-1642615>
- Werner, F. W., Short, W. H., Fortino, M. D., & Palmer, A. K. (1997). The relative contribution of selected carpal bones to global wrist motion during simulated planar and out-of-plane wrist motion. *J Hand Surg Am*, 22(4), 708-713. [https://doi.org/10.1016/s0363-5023\(97\)80133-5](https://doi.org/10.1016/s0363-5023(97)80133-5)
- Werner, F. W., Short, W. H., & Green, J. K. (2005). Changes in patterns of scaphoid and lunate motion during functional arcs of wrist motion induced by ligament division. *J Hand Surg Am*, 30(6), 1156-1160. <https://doi.org/10.1016/j.jhsa.2005.08.005>
- Werner, F. W., Sutton, L. G., Allison, M. A., Gilula, L. A., Short, W. H., & Wollstein, R. (2011). Scaphoid and lunate translation in the intact wrist and following ligament resection: a cadaver study. *J Hand Surg Am*, 36(2), 291-298. <https://doi.org/10.1016/j.jhsa.2010.11.023>
- Wessel, L. E., Kim, J., Morse, K. W., Loisel, F., Koff, M. F., Breighner, R. E., Doty, S. B., & Wolfe, S. W. (2022). The Dorsal Ligament Complex: A Cadaveric, Histology, and Imaging Study. *The Journal of Hand Surgery*, 47(5), 480.e481-480.e489. <https://doi.org/https://doi.org/10.1016/j.jhsa.2021.06.003>
- Wessel, L. E., & Wolfe, S. W. (2023). Scapholunate Instability: Diagnosis and Management - Anatomy, Kinematics, and Clinical Assessment - Part I. *J Hand Surg Am*. <https://doi.org/10.1016/j.jhsa.2023.05.013>
- White, J., Couzens, G., & Jeffery, C. (2019). The use of 4D-CT in assessing wrist kinematics and pathology: a narrative view. *Bone Joint J*, 101-b(11), 1325-1330. <https://doi.org/10.1302/0301-620x.101b11.Bjj-2019-0361.R1>



- Wolfe, S. W., Crisco, J. J., & Katz, L. D. (1997). A non-invasive method for studying in vivo carpal kinematics. *J Hand Surg Br*, 22(2), 147-152. [https://doi.org/10.1016/s0266-7681\(97\)80050-2](https://doi.org/10.1016/s0266-7681(97)80050-2)
- Wolfe, S. W., Neu, C., & Crisco, J. J. (2000). In vivo scaphoid, lunate, and capitate kinematics in flexion and in extension. *J Hand Surg Am*, 25(5), 860-869. <https://doi.org/10.1053/jhsu.2000.9423>
- Woltring, H. J., Huiskes, R., de Lange, A., & Veldpaus, F. E. (1985). Finite centroid and helical axis estimation from noisy landmark measurements in the study of human joint kinematics. *J Biomech*, 18(5), 379-389. [https://doi.org/10.1016/0021-9290\(85\)90293-3](https://doi.org/10.1016/0021-9290(85)90293-3)
- Wu, G., Siegler, S., Allard, P., Kirtley, C., Leardini, A., Rosenbaum, D., Whittle, M., D'Lima, D. D., Cristofolini, L., Witte, H., Schmid, O., & Stokes, I. (2002). ISB recommendation on definitions of joint coordinate system of various joints for the reporting of human joint motion--part I: ankle, hip, and spine. International Society of Biomechanics. *J Biomech*, 35(4), 543-548. [https://doi.org/10.1016/s0021-9290\(01\)00222-6](https://doi.org/10.1016/s0021-9290(01)00222-6)
- Wu, G., van der Helm, F. C., Veeger, H. E., Makhsoos, M., Van Roy, P., Anglin, C., Nagels, J., Karduna, A. R., McQuade, K., Wang, X., Werner, F. W., & Buchholz, B. (2005). ISB recommendation on definitions of joint coordinate systems of various joints for the reporting of human joint motion--Part II: shoulder, elbow, wrist and hand. *J Biomech*, 38(5), 981-992. <https://doi.org/10.1016/j.jbiomech.2004.05.042>
- Yao, J., Zlotolow, D. A., & Lee, S. K. (2016). ScaphoLunate Axis Method. *J Wrist Surg*, 5(1), 59-66. <https://doi.org/10.1055/s-0035-1570744>
- Yazaki, N., Burns, S. T., Morris, R. P., Andersen, C. R., Patterson, R. M., & Viegas, S. F. (2008). Variations of capitate morphology in the wrist. *J Hand Surg Am*, 33(5), 660-666. <https://doi.org/10.1016/j.jhsa.2008.02.002>
- Youm, Y. (1978). Instantaneous center of rotation by least square method. *J Bioeng*, 2(1-2), 129-137.
- Youm, Y., McMurthy, R. Y., Flatt, A. E., & Gillespie, T. E. (1978). Kinematics of the wrist. I. An experimental study of radial-ulnar deviation and flexion-extension. *J Bone Joint Surg Am*, 60(4), 423-431.
- Zar, J. H. (1999). *Biostatistical analysis*. Pearson Education India.
- Zhao, K., Breighner, R., Holmes, D., 3rd, Leng, S., McCollough, C., & An, K. N. (2015). A technique for quantifying wrist motion using four-dimensional computed tomography: approach and validation. *J Biomech Eng*, 137(7), 0745011-0745015. <https://doi.org/10.1115/1.4030405>



